DEVELOPMENTAL DELAY AND INTELLECTUAL DISABILITY

EDITED BY: Santasree Banerjee, Muhammad Ayub, Chen Li and Anjana Munshi

PUBLISHED IN: Frontiers in Genetics and Frontiers in Pediatrics

frontiers Research Topics

frontiers

ISSN 1664-8714
ISBN 978-2-83250-281-5
DOI 10.3389/978-2-83250-281-5

About Frontiers

Frontiers is more than just an open-access publisher of scholarly articles: it is a pioneering approach to the world of academia, radically improving the way scholarly research is managed. The grand vision of Frontiers is a world where all people have an equal opportunity to seek, share and generate knowledge. Frontiers provides immediate and permanent online open access to all its publications, but this alone is not enough to realize our grand goals.

Frontiers Journal Series

The Frontiers Journal Series is a multi-tier and interdisciplinary set of open-access, online journals, promising a paradigm shift from the current review, selection and dissemination processes in academic publishing. All Frontiers journals are driven by researchers for researchers; therefore, they constitute a service to the scholarly community. At the same time, the Frontiers Journal Series operates on a revolutionary invention, the tiered publishing system, initially addressing specific communities of scholars, and gradually climbing up to broader public understanding, thus serving the interests of the lay society, too.

Dedication to Quality

Each Frontiers article is a landmark of the highest quality, thanks to genuinely collaborative interactions between authors and review editors, who include some of the world's best academicians. Research must be certified by peers before entering a stream of knowledge that may eventually reach the public - and shape society; therefore, Frontiers only applies the most rigorous and unbiased reviews.
Frontiers revolutionizes research publishing by freely delivering the most outstanding research, evaluated with no bias from both the academic and social point of view. By applying the most advanced information technologies, Frontiers is catapulting scholarly publishing into a new generation.

What are Frontiers Research Topics?

Frontiers Research Topics are very popular trademarks of the Frontiers Journals Series: they are collections of at least ten articles, all centered on a particular subject. With their unique mix of varied contributions from Original Research to Review Articles, Frontiers Research Topics unify the most influential researchers, the latest key findings and historical advances in a hot research area! Find out more on how to host your own Frontiers Research Topic or contribute to one as an author by contacting the Frontiers Editorial Office: frontiersin.org/about/contact

DEVELOPMENTAL DELAY AND INTELLECTUAL DISABILITY

Topic Editors:
Santasree Banerjee, Beijing Genomics Institute (BGI), China
Muhammad Ayub, Queens University, Canada
Chen Li, Zhejiang University, China
Anjana Munshi, Central University of Punjab, India

Citation: Banerjee, S., Ayub, M., Li, C., Munshi, A., eds. (2022). Developmental Delay and Intellectual Disability. Lausanne: Frontiers Media SA.
doi: 10.3389/978-2-83250-281-5

Table of Contents

frontiers | Frontiers in Genetics

TYPE Editorial
PUBLISHED 08 September 2022
DOI 10.3389/fgene.2022.934815

OPEN ACCESS

EDITED AND REVIEWED BY
Erica E. Davis,
Stanley Manne Children's Research Institute, United States

*CORRESPONDENCE
Santasree Banerjee,
santasree.banerjee@yahoo.com

SPECIALTY SECTION
This article was submitted to Genetics of Common and Rare Diseases, a section of the journal Frontiers in Genetics

RECEIVED 03 May 2022
ACCEPTED 15 August 2022
PUBLISHED 08 September 2022

CITATION
Banerjee S, Munshi A, Li C and Ayub M (2022), Editorial: Developmental delay and intellectual disability.
Front. Genet. 13:934815.
doi: 10.3389/fgene.2022.934815

Editorial: Developmental delay and intellectual disability

Santasree Banerjee[1]*, Anjana Munshi[2], Chen Li[3,4] and Muhammad Ayub[5]

[1]Department of Genetics, College of Basic Medical Sciences, Jilin University, Changchun, China, [2]Department of Human Genetics and Molecular Medicine, School of Health Sciences, Central University of Punjab, Bathinda, India, [3]School of Medicine, Graduate School, Zhejiang University, Hangzhou, China, [4]Zhejiang Provincial Key Laboratory of Genetic and Developmental Disorders, Zhejiang University School of Medicine, Hangzhou, China, [5]Department of Psychiatry, Queens University, Kingston, Ontario, Canada

KEYWORDS

developmental delay, intellectual disabilities, chromosome microarray, whole exome sequencing, novel mutations

Editorial on the Research Topic
Developmental Delay and Intellectual Disability

Intellectual Disability (ID) is characterised by impaired intellectual and adaptive function that starts during the developmental period (Global Research on Developmental Disabilities Collaborators, 2022). It is a lifelong condition and is among the most common neurodevelopmental disorders (Global Research on Developmental Disabilities Collaborators, 2018). Developmental Delay (DD) is a broad term that applies when one or more areas of a child's development are delayed (Global Research on Developmental Disabilities Collaborators, 2018). A disease-causing variant is identified in about half of individuals with DD and ID. Both copy number variants (CNVs) and single nucleotide variants (SNVs) are implicated as major causes of DD and ID (de Ligt et al., 2012; Olusanya and Nair, 2019); more than 130 rare CNVs and SNVs in more than 600 genes have been reported to be associated with this disease spectrum (de Ligt et al., 2012). Previous reports have shown that DD and ID can follow autosomal dominant, autosomal recessive, or X-linked modes of inheritance, as well as making a substantial contribution from *de novo* variants to the molecular aetiology (de Ligt et al., 2012; Black and Lawn, 2018).

Further research into the identification of candidate causal genes will create opportunities to study the molecular mechanisms underlying the disease phenotype and will enable clinicians to make timely and accurate clinical diagnoses (American Psychiatric Association, 2013; Heslop et al., 2014; Black and Lawn, 2018). This will make it possible to group cohorts of cases with similar genetic aetiology and refine their phenotypes including the prognosis and course of the disease. Genetic diagnosis will allow mutational screening in families and make prevention possible through genetic counselling, prenatal, or pre-implantation diagnosis (Tatja et al., 2021).

According to the American Association on Intellectual and Developmental Disabilities, affected individuals with global developmental delay are characterised by a significant delay in the development of motor skills, speech, and cognition, while ID involves deficits in both intellectual function (learning, reasoning, and problem-solving skills) and adaptive function (communication, conceptual, social and practical skills) among children aged 5 years or younger. The global prevalence of DD is 1–3% among children aged 5 years or younger (de Ligt et al., 2012; Olusanya and Nair, 2019). The prevalence of ID is 2.7% and 2.17% among children and adults respectively. In addition, DD patients with *de novo* mutations have a prevalence rate of 1 in 213 to 1 in 448 live-births (American Psychiatric Association, 2013; Heslop et al., 2014; Black and Lawn, 2018; Tatja et al., 2021).

Advances in variant detection technology have evolved in recent years, leading to accelerated causal gene discovery and understanding of genomic lesions in ID/DD cohorts. After preliminary confirmation of the disease through clinical, laboratory and radiological examination, clinicians can order further diagnostic testing, which is influenced by initial findings and availability and access to resources. The range of potential lines of inquiry include but are not limited to: karyotyping to identify gross chromosomal abnormalities; chromosome microarray (CMA) to identify deletions, duplications, loss of heterozygosity, and aneuploidy; and genomic sequencing (target-based sequencing of a gene panel, clinical whole exome sequencing or whole genome sequencing) to identify disease-causing variants (de Ligt et al., 2012; Mefford et al., 2012).

This Research Topic features new causal genes for DD and ID, advances in the mechanistic understanding of previously reported DD and ID genes, and potential therapeutic applications. We received 40 submissions and accepted 21 papers after rigorous peer review (Cerminara et al.; Chen et al.; Deng et al.; Fan et al.; García-Ortiz et al.; Li et al.; Servetti et al.; Smetana et al.; Tao et al.; Wan et al.; Wang et al.; Xiang et al.; Zarate et al.; Zhang et al.; Ali Alghamdi et al.; Binquet et al.; Ha et al.; Li et al.; Rong et al.; Yue et al.; Zhao et al.).

Four publications are based on chromosomal aberrations associated with DD and ID. Deng et al. reported two new cases of chromosome 12q14 deletions and reviewed the published literature (Deng et al.). The authors delineate the genotype-phenotype correlation for 12q interstitial deletions and discuss likely causative genes. Wang et al. reported familial translocation t (2; 4) (q37.3; p16.3) (Wang et al.). They describe a range of complex phenotypes associated with these chromosomal abnormalities. This paper highlights the value of studying extended families for intrafamilial variation in genotypes and associated phenotypes. Smetana et al. reported a case of Xq22.3 deletion associated with Alport syndrome with intellectual disability (ATS-ID, AMME complex; OMIM #300194) with genotype phenotype correlation (Smetana et al.). The deletion is larger in size compared with previously reported cases and includes two additional genes. This may explain a broader phenotype with additional features in the proband. Fan et al. reported a case with deletion of chromosome 7q35-7q36.3, which causes congenital brain dysplasia, DD and ID (Fan et al.). Servetti et al. used an integrated framework to analyse 12 cases of neurodevelopmental disorders with complex phenotypes and suggested that those cases can be explained by multiple mechanisms, including additive effects of multiple CNVs, involving known neurodevelopmental disorder genes and novel candidate genes (Servetti et al.). One study leveraged a consanguineous family with four affected individuals to identify a likely pathogenic homozygous variant in *OSGEP* (Ali Alghamdi et al.). Detailed phenotyping and proteomic analysis are a valuable part of this study (Ali Alghamdi et al.).

Three studies are based on the evaluation of multiple cases. Wan et al. reported six new variants in seven cases and provided phenotype descriptions for MEF2C haploinsufficiency syndrome (MCHS) (Wan et al.). Xiang et al. used whole exome sequencing to investigate 17 patients with unexplained DD and/or ID (Xiang et al.). They used the whole exome data for analysis of CNV, SNV and indels. Seven affected individuals carried a single nucleotide variant or an indel that explained the disease, and three cases carried a disease-associated CNV. Zarate et al. reported two cases of SATB2-Associated Syndrome (Zarate et al.). The clinical symptoms overlapped with mitochondrial disease presentation. The authors recommended considering exome sequencing in suspected cases of mitochondrial disease.

Binquet et al. reported a study that compares the diagnostic yield of trio sequencing in 1,275 cases with the current strategy for fragile X diagnostics, which involves microarray and panel sequencing for 44 genes (Binquet et al.). This is an indication of new avenues in the field that are moving toward reduced costs of sequencing. Garcia-Ortiz et al. examined methylation in blood samples of patients with autism spectrum disorder (ASD) (García-Ortiz et al.). In a case report, Cerminara et al. reported an affected individual with a complex phenotype including ASD and its association with a maternally inherited X-linked missense variant in *HUWE1* and a *de novo* stop variant in *TPH2* (Cerminara et al.).

In a study by Chen et al., maternal uniparental disomy resulted in a homozygous variant in *CNTN2* in an affected individual with unrelated parents (Chen et al.). The predominant phenotype was a focal epilepsy. This gene has been implicated previously in autosomal recessive focal seizures. Tao et al. reported a case of complete maternal uniparental disomy of chromosome 2 with a rare *UNC80* c. 5609-4G>A intronic variant in a Chinese patient with infantile

hypotonia, psychomotor retardation and facial dysmorphology (Tao et al.). Disomy resulted in a homozygous mutation. These two reports reinforce the paradigm of parental disomy causing homozygous disease in outbred populations (Chen et al.; Tao et al.). Two additional papers reported compound heterozygous mutations causing recessive disorders (Yue et al. and Ha et al.) in outbred populations (Ha et al.; Yue et al.).

Li et al. described a case of mosaic Turner syndrome 45, X [56.5%]/46, X, del(Y) (q12) [43.5%] (Li et al.). They used different techniques including FISH and low pass whole genome sequencing to identify the genetic changes. Zhang et al. identified a pathogenic variant in *GRIN1* in a single case and performed further experiments to study the pharmacological impact of the DNA change and rescue mechanisms (Zhang et al.). Zhao et al. described a nonsense variant in *ZNF462* associated with Weiss-Kruszka syndrome-like manifestations (Zhao et al.). Li et al. identified a novel homozygous splice-site variant in a female child with Cohen syndrome (Li et al.). Rong et al. reported a milder phenotype produced by a novel mutation in *SEPSECS* (Rong et al.).

In conclusion, this special issue reports on both CNVs and SNVs associated with DD and ID. In the future, more refined cellular and molecular studies are required to understand the disease mechanisms (Bowling et al., 2017; Karin et al., 2019; Manickam et al., 2021). This collection emphasises the significance of genomic sequencing technology for molecular genetic diagnostics in ID/DD cohorts, thus laying the groundwork for a future Research Topic focused on studies that will identify new candidate genes and disease-causing variants, which in turn will allow us to develop novel therapeutic interventions.

Author contributions

SB wrote the first draft. AM, CL, and MA provided critical comments and editorial suggestions for revisions. All the authors agreed on the submitted version.

Acknowledgments

The guest editors wish to thank all the authors andreviewers for their valuable contributions to this Research Topic. We hope that this collection of articles will interest the livestock science and genetics community.

Conflict of interest

The authors declare that the research was conducted in the absence of any commercial or financial relationships that could be construed as a potential conflict of interest.

Publisher's note

References

American Psychiatric Association (2013). *Diagnostic and statistical manual of mental disorders*. 5th ed. Virginia, United States: American Psychiatric Association.

Black, M. M., and Lawn, J. E. (2018). Early childhood developmental disabilities-data still needed. *Lancet. Glob. Health* 6 (10), e1050–e1051. doi:10.1016/S2214-109X(18)30399-1

Bowling, K. M., Thompson, M. L., Amaral, M. D., Finnila, C. R., Hiatt, S. M., Engel, K. L., et al. (2017). Genomic diagnosis for children with intellectual disability and/or developmental delay. *Genome Med.* 9 (1), 43. doi:10.1186/s13073-017-0433-1

de Ligt, J., Willemsen, M. H., van Bon, B. W., Kleefstra, T., Yntema, H. G., Kroes, T., et al. (2012). Diagnostic exome sequencing in persons with severe intellectual disability. *N. Engl. J. Med.* 367 (20), 1921–1929. doi:10.1056/NEJMoa1206524

Global Research on Developmental Disabilities Collaborators (2022). Accelerating progress on early childhood development for children under 5 years with disabilities by 2030. *Lancet. Glob. Health* 10 (3), e438–e444. doi:10.1016/S2214-109X(21)00488-5

Global Research on Developmental Disabilities Collaborators (2018). Developmental disabilities among children younger than 5 years in 195 countries and territories, 1990-2016: A systematic analysis for the global burden of disease study 2016. *Lancet. Glob. Health* 6 (10), e1100–e1121. doi:10.1016/S2214-109X(18)30309-7

Heslop, P., Blair, P. S., Fleming, P., Hoghton, M., Marriott, A., and Russ, L. (2014). The confidential inquiry into premature deaths of people with intellectual disabilities in the UK: A population-based study. *Lancet* 383 (9920), 889–895. doi:10.1016/S0140-6736(13)62026-7

Karin, K., Takeshi, N., Naoyuki, T., Akihiko, M., Mitsuhiro, K., Ayumi, M., et al. (2019). Gene therapy improves motor and mental function of aromatic l-amino acid decarboxylase deficiency. *Brain* 142 (2), 322–333. doi:10.1093/brain/awy331

Manickam, K., McClain, M. R., Demmer, L. A., Biswas, S., Kearney, H. M., Malinowski, J., et al. (2021). Exome and genome sequencing for pediatric patients with congenital anomalies or intellectual disability: An evidence-based clinical guideline of the American college of medical genetics and genomics (ACMG). *Genet. Med.* 23 (11), 2029–2037. doi:10.1038/s41436-021-01242-6

Mefford, H. C., Batshaw, M. L., and Hoffman, E. P. (2012). Genomics, intellectual disability, and autism. *N. Engl. J. Med.* 366 (8), 733–743. doi:10.1056/NEJMra1114194

Olusanya, B. O., and Nair, M. K. C. (2019). Premature mortality in children with developmental disabilities. *Lancet. Glob. Health* 7 (12), e1601–e1602. doi:10.1016/S2214-109X(19)30419-X

Tatja, H., Marcus, B., Magnus, T., Paul, L., and Agnieszka, B. (2021). Association of intellectual disability with all-cause and cause-specific mortality in Sweden. *JAMA Netw. Open* 4 (6), e2113014. doi:10.1001/jamanetworkopen.2021.13014

frontiers in Genetics

CASE REPORT
published: 18 February 2021
doi: 10.3389/fgene.2021.625564

Case Report: Whole Exome Sequencing Revealed Disease-Causing Variants in Two Genes in a Patient With Autism Spectrum Disorder, Intellectual Disability, Hyperactivity, Sleep and Gastrointestinal Disturbances

Maria Cerminara[1], Giovanni Spirito[2], Livia Pisciotta[1,3], Margherita Squillario[4], Martina Servetti[1,4], Maria Teresa Divizia[4], Margherita Lerone[4], Bianca Berloco[5], Silvia Boeri[5], Lino Nobili[1,5], Diego Vozzi[6], Remo Sanges[2,6], Stefano Gustincich[6†] and Aldamaria Puliti[1,4†]*

[1] Department of Neurosciences, Rehabilitation, Ophthalmology, Genetics, Maternal and Child Health (DiNOGMI), University of Genoa, Genoa, Italy, [2] Neuroscience Area, International School for Advanced Studies (SISSA), Trieste, Italy, [3] Child Neuropsychiatry Unit, Azienda Socio Sanitaria Territoriale Fatebenefratelli Sacco (ASST Fbf Sacco), Milan, Italy, [4] Medical Genetics Unit, Istituto di Ricovero e Cura a Carattere Scientifico (IRCCS) Istituto Giannina Gaslini, Genoa, Italy, [5] Child Neuropsychiatry Unit, Istituto di Ricovero e Cura a Carattere Scientifico (IRCCS) Istituto Giannina Gaslini, Genoa, Italy, [6] Department of Neuroscience and Brain Technologies, Istituto Italiano di Tecnologia, Genoa, Italy

Autism Spectrum Disorder (ASD) refers to a broad range of conditions characterized by difficulties in communication, social interaction and behavior, and may be accompanied by other medical or psychiatric conditions. Patients with ASD and comorbidities are often difficult to diagnose because of the tendency to consider the multiple symptoms as the presentation of a complicated syndromic form. This view influences variant filtering which might ignore causative variants for specific clinical features shown by the patient. Here we report on a male child diagnosed with ASD, showing cognitive and motor impairments, stereotypies, hyperactivity, sleep, and gastrointestinal disturbances. The analysis of whole exome sequencing (WES) data with bioinformatic tools for oligogenic diseases helped us to identify two major previously unreported pathogenetic variants: a maternally inherited missense variant (p.R4122H) in *HUWE1,* an ubiquitin protein ligase associated to X-linked intellectual disability and ASD; and a *de novo* stop variant (p.Q259X) in *TPH2*, encoding the tryptophan hydroxylase 2 enzyme involved in serotonin synthesis and associated with susceptibility to attention deficit-hyperactivity disorder (ADHD). *TPH2*, expressed in central and peripheral nervous tissues, modulates various physiological functions, including gut motility and sleep. To the best of our knowledge, this is the first case presenting with ASD, cognitive impairment, sleep, and gastrointestinal disturbances linked to both *HUWE1* and *TPH2* genes. Our findings could contribute to the existing knowledge on clinical and genetic diagnosis of patients with ASD presentation with comorbidities.

Keywords: autism spectrum disorder, attention deficit disorder and hyperactivity, whole exome sequencing, sleep disturbance, oligenic disease, ORVAL, gut motility disorders

OPEN ACCESS

Edited by:
Chen Li,
Zhejiang University, China

Reviewed by:
Fulya Taylan,
Karolinska Institutet (KI), Sweden
Olivia J. Veatch,
University of Kansas Medical Center, United States

****Correspondence:***
Aldamaria Puliti
apuliti@unige.it

† These authors have contributed equally to this work

Specialty section:
This article was submitted to Genetics of Common and Rare Diseases, a section of the journal Frontiers in Genetics

Received: *03 November 2020*
Accepted: *19 January 2021*
Published: *18 February 2021*

Citation:
Cerminara M, Spirito G, Pisciotta L, Squillario M, Servetti M, Divizia MT, Lerone M, Berloco B, Boeri S, Nobili L, Vozzi D, Sanges R, Gustincich S and Puliti A (2021) Case Report: Whole Exome Sequencing Revealed Disease-Causing Variants in Two Genes in a Patient With Autism Spectrum Disorder, Intellectual Disability, Hyperactivity, Sleep and Gastrointestinal Disturbances. Front. Genet. 12:625564. doi: 10.3389/fgene.2021.625564

INTRODUCTION

Autism spectrum disorder (ASD) is a neurodevelopmental disorder characterized by etiological and clinical heterogeneity, with a frequency around 1% in the general population (Nevison et al., 2018). In the wide picture of ASD, the major clinical manifestations are communicative impairments, difficulties in social interaction, behavior abnormalities. Indeed, ASD patients frequently present with comorbidities, such as intellectual disability (ID) (Postorino et al., 2016), epilepsy (Besag, 2018), sleep or gastrointestinal disturbances (Devnani and Hegde, 2015; Bjorklund et al., 2020; Brooks et al., 2020).

The genetic basis of ASD is deeply heterogeneous implicating different genes, in turn involved in different pathways and biological processes, as those regulating synaptic plasticity, chromatin remodeling, gene transcription, and protein degradation (Bourgeron, 2015). Single nucleotide changes or larger genomic alterations, as copy number variations (CNVs), can be found in ASD cases (Sanders et al., 2015), and recent studies proved that the use of Whole Exome Sequencing (WES) together with CNVs analysis can identify a pathogenetic variant in about 30% of patients (Munnich et al., 2019).

We here report on a male child with ASD and a complex phenotype, who was analyzed by WES with a bioinformatic tool for investigating variants in oligogenic diseases. The results suggest a hypothetical scenario in which two genes (*HUWE1* and *TPH2*) plus 4 possible modifiers could play a role in the patient's phenotype.

METHODS

Clinical Assessment

The clinical assessment of the patient comprised a neurological-behavior examination and evaluation of his sleep and gastrointestinal disturbances as detailed in **Supplementary Material**.

Whole Exome Sequencing

Genomic DNA extraction and subsequent WES and data analysis for affected individual and his parents were carried out by Italian Institute of Technologies (IIT) in Genoa, Italy. Briefly, the exomes were captured using the xGen® Exome Research Panel v1.0 – IDT KIT. Sequences were enriched using the Illumina Nextera Flex For Enrichment KIT. Sequencing was performed on an Illumina NovaSeq 6000 platform (Illumina Inc., CA, USA). The library preparation and its sequencing were performed simultaneously for the parents and the proband using barcode adapters. Alignment of raw paired-end reads to the reference genome (version hg19) was performed with bwa (version 0.7.17) (Li and Durbin, 2010). Duplicated reads were marked with picard (version 2.18.20). Variant discovery was then performed with the GATK4 utility HaplotypeCaller, using the appropriate file containing the coordinates of the sequences targeted by the exome sequencing. Finally all variants were annotated using annovar (databases updated to 27/05/2019) (Wang et al., 2010). The resulting file was used for a manual evaluation of the variants. The sequencing provided a 60x medium coverage.

Variant Prioritization

For the interpretation of variants pathogenicity, we integrated several tools. To unveil the contribution of multiple genes to the patient's phenotype, we used a new platform for the prediction and exploration of candidate disease-causing oligogenic variant combinations (ORVAL, Oligogenic Resource for Variant AnaLysis) following authors recommendations (Renaux et al., 2019). Briefly, we prepared two files: (i) an input file with a list of selected candidate variants and (ii) one file with genes related or possibly related to ASD to be used as "gene panel" file for variant filtering.

The list of candidate variants was obtained by considering the following filtering steps: variants with a frequency below 3% in ExAC/GnomAD v2.11/1000g2015; only exonic, splicing, non-synonymous and stopgain variants with a good coverage were considered; we discarded those variants predicted to be benign or tolerated in PolyPhen and SIFT and retained those with CADD score $\geq$ 20; we also discarded those variants found in more than 1% of in-house controls (i.e., not diagnosed with ASD or any neuropsychiatric disease). Filtering was also based on annotation in public databases as Mouse Genome Database (MGD), OMIM, PubMed, ClinVar. Following this procedure we obtained a list of 71 candidate variants, including both *de novo* and inherited, to be used as input in ORVAL.

The "gene panel" file consisted of genes selected based on three criteria: those related to ASD and present in the SFARI (Simons Foundation Autism Research Initiative) database (August 2020 release); genes with high brain expression, defined as those genes with average log2 RPKM >4.5 in the BrainSpan database (http://www.brainspan.org) (the top 18%) (Miller et al., 2014; Addis et al., 2018) and genes of the KEGG pathways (https://www.genome.jp/kegg) selected for their possible relevance with ASD.

From the output file, a list of possible 23 variants, we kept only those genes/variants characterized by pathogenicity confidence score higher than 99%. These selected genes underwent through a manual revision considering literature and available databases. Briefly, we analyzed all the selected output variants for deleterious prediction through Varsome (Kopanos et al., 2019), we considered the intolerance to loss-of-function variants (pLI) and the deviation of the observed number of missense variants from the expected number (Mis Z-score), as computed by the Exome Aggregation Consortium (ExAC) (http://exac.broadinstitute.org/) (genes with pLI scores of 0.9 or higher are extremely intolerant to heterozygous LoF variation, and thus haploinsufficient; Z-scores of 3.09 or higher indicate intolerance to missense variation) (Lek et al., 2016), we also considered haploinsufficiency on the base of an HIPred_score above 0.5 (Shihab et al., 2017). Finally, a list of 6 variants in 6 genes was obtained.

Selected variants in the candidate genes were all validated by co-segregation analysis using polymerase chain reaction (PCR), and bi-directional Sanger sequencing using the ABI 3730 automated sequencer (Applied Biosystems, Forster City, CA, USA).

Network Analysis of Candidate Genes

To unveil enrichment of annotations of identified genes and known ASD genes, we used GeneCodis4 tool (Tabas-Madrid et al., 2012), as already described (Vaccari et al., 2016). Briefly, a list enclosing all 6 candidate genes, obtained from the ORVAL analysis and that passed our manual inspection, together with all genes present in the SFARI database (August 2020 release) were used as input in GeneCodis4 (total genes = 934). Among the databases of biological knowledge available in GeneCodis4, we focused on the GO Biological Process (BP) domain. In the analysis, the hypergeometric test was applied followed by the false discovery rate correction (FDR) with a cut-off of 5% to determine which annotations were significantly enriched. All genes of the top gene ontology terms, including candidate and SFARI genes, were then projected onto the STRING network (v11) (Szklarczyk et al., 2019). Edges within the STRING network were thresholded at 0.4, according to the authors' recommendation. A graphical representation of the GeneCodis4 and STRING results was obtained by using Cytoscape tool (Shannon et al., 2003).

CASE PRESENTATION

We report on a 5-years old male patient born to non-consanguineous Italian parents. The child came to our attention at the age of 3 years for third level investigations, when he had already performed several clinical assessments and tests at the territorial structures (see the timeline, **Figure 1**). After a thorough medical history and after having viewed and analyzed the clinical documentation, he was diagnosed with ASD even by the help of Autism Diagnostic Observation Schedule (ADOS) and the Autism Diagnostic Interview-Revised (ADI-R). He had developmental delay, absent language, motor impairment, auto and hetero-direct aggressivity, hyperactivity, attentional lability, stereotypes.

In the past, metabolic defects and the main syndromes in differential diagnosis were excluded, Fragile X Syndrome and Prader-Willi/Angelman Syndromes (see timeline, **Figure 1**).

More in details, the clinical assessment of the patient through specific tests showed a low adaptive level for chronological age, prevailing on communication and socialization domains, a deficit on ability of inhibit and self-control inhibition, metacognition, working memory, and ability of organization/planning, problems in the area of withdrawal and isolation, anxiety and depression, somatic complaints, and attentional disturbances, marked impairments on language understanding and production.

By using specific tests (Sleep-CGI-S, Sleep-CGI-I, SDSC) the patient was diagnosed with a moderate sleep disorder. Sleep-CGI-S showed a moderate sleep disorder with marked bedtime resistance, moderate sleep onset delay, moderate difficult to fall asleep, multiple night wakings and family functioning moderately affected. Instead Sleep-CGI-I reported minimal improving in ability to fall asleep, a major improving in bedtime resistance, sleep onset delay, night wakings, and family functioning. At SDSC the results confirmed the mentioned sleep disorders. In particular, the patient has been treated with clonazepam for 2 months and then, until now, with melatonin, that slightly improved his condition (see timeline, **Figure 1**).

Using the Criteria of Rome IV, functional constipation (3 criteria) and functional aerophagia (4 criteria) were diagnosed.

Results obtained from neurological-behavior tests and of sleep evaluation are reported in **Supplementary Table 1**.

RESULTS

Identification of Candidate Genetic Variants

Given the complexity of the patient's phenotype, we suspected a possible genetic basis involving multiple genes. Accordingly, for the identification of candidate variants, we used a bioinformatic tool for the study of oligogenic diseases.

After the bioinformatic analysis of WES data an unreported maternally inherited missense variant affecting the E3 ubiquitin ligase (HECT) domain of *HUWE1* (NM_031407:exon79: c.12 365G>A:p.R4122H), and a *de novo* unreported stop variant in *TPH2* (NM_173353:exon6: c.775C>T:p.Q259X) (see **Figure 2A**, **Table 1**) were identified.

HUWE1 encodes an ubiquitin protein ligase involved in various cellular processes, including synaptogenesis, associated to the Turner type X-linked syndromic cognitive disability (OMIM:309590) and ASD (Moortgat et al., 2018). The *TPH2* gene encodes the tryptophan hydroxylase 2 enzyme involved in serotonin synthesis in central and peripheral nervous tissues. Serotonin modulates various physiological functions, including regulation of gut motility and sleep (Jones et al., 2020). *TPH2* variants are associated to susceptibility to attention deficit-hyperactivity disorder (OMIM:613003) and unipolar depression (OMIM:608516).

The analysis unveiled the presence of additional variants in the following genes, *ALDH5A1, ATG7*, *ITPR3,* and *DIP2C*.

The *ALDH5A1* variant is a rare, maternally inherited stop variant (NM_170740:exon4: c.612G>A:p.Trp204X). *ALDH5A1* encodes the succinic semialdehyde dehydrogenase, implicated in the neurotransmitter GABA catabolism (Chambliss et al., 1995). Homozygous or compound heterozygous mutations in *ALDH5A1* cause the succinic semialdehyde dehydrogenase deficiency (OMIM:271980), a rare complex neurologic disorder mainly characterized by mental retardation and sleep disturbances. By further investigating WES data, we unveiled an additional, paternally inherited, variant in *ALDH5A1* (NM_170740:exon3:c.538C>T:p.His180Tyr). This last variant, present in the general population with a frequency of 0.3154, was considered a hypomorphic variant, leading to a reduction of *ALDH5A1* enzymatic activity of about 20% (Blasi et al., 2002).

The *ITPR3* variant is a paternally inherited, rare missense variant (NM_002224:exon36: c.4862T>C:p.Leu1621Pro). *ITPR3* encodes for the inositol 1,4,5-trisphosphate receptor that transduces many hormonal signals regulating Ca(2+)-dependent processes. To note, the mouse carrying the *tf* spontaneous mutation of the *Itpr3* gene (BTBR T+ Itpr3tf /J strain) has been used as a model of ASD (McFarlane et al., 2008).

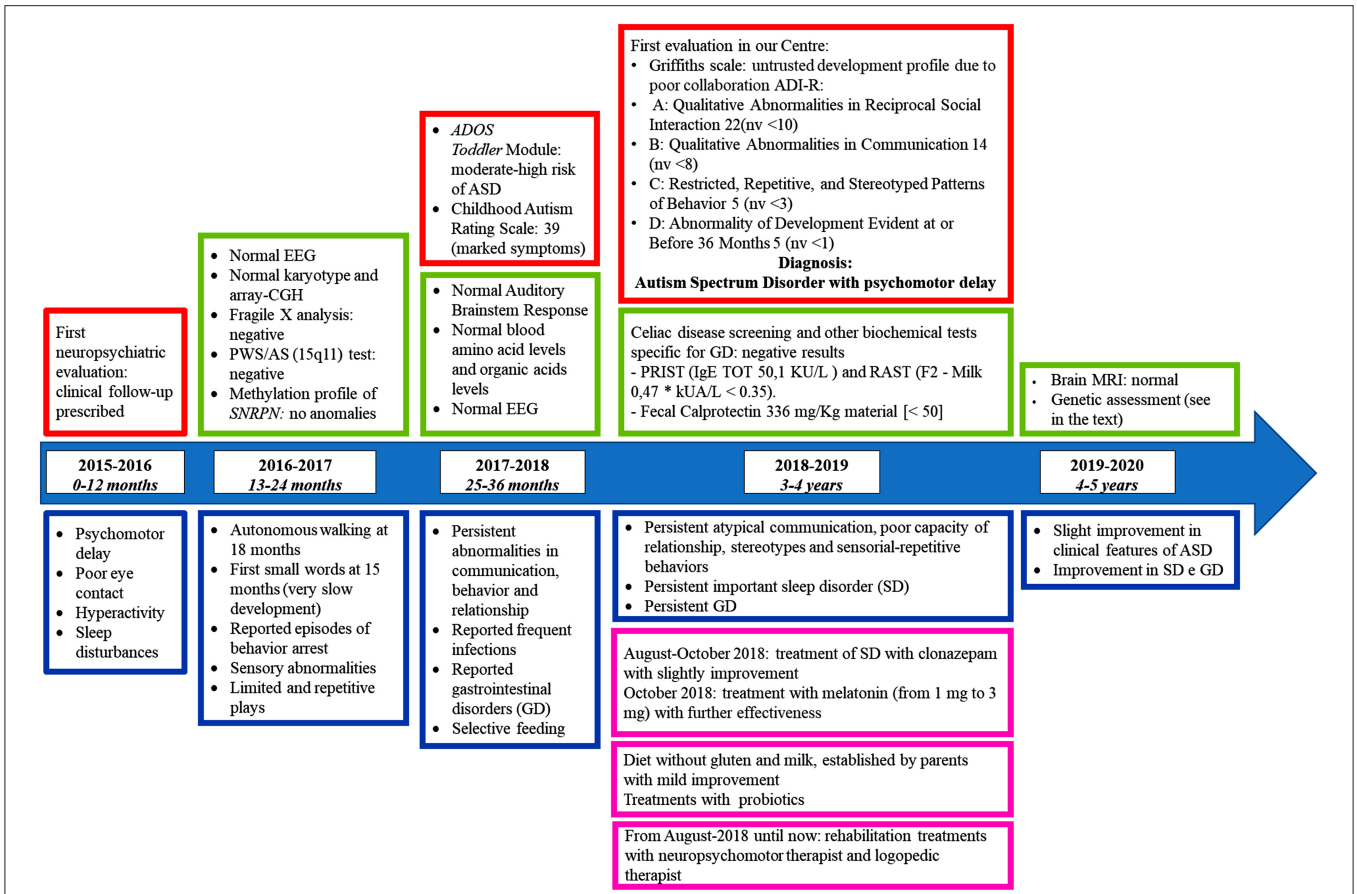

FIGURE 1 | Timeline with patient's relevant clinical data. In this figure main signs and symptoms (blue) shown by the patient, data from his clinical evaluations (red), results of laboratory tests (pink), and treatments (green) are reported. PWS/AS, Prader-Willi Syndrome/Angelman Syndrome; GD, gastro-intestinal disorders; SD, sleep disorders; ADOS, Autism Diagnostic Observation Schedule; ADI-R, Autism Diagnostic Interview-Revised; ASD, Autism Spectrum Disorder; PRIST, Paper Radio Immuno Sorbent Test; RAST, Radio Allergo Sorbent Test; MRI, Magnetic Resonance Imaging; nv, normal value.

The patient showed a maternally inherited unreported missense variant of *DIP2C* (NM_014974:exon7: c.757C>T:p.Arg253Trp). *DIP2C* encodes a member of the disco-interacting protein homolog 2 family, known to regulate several genes and pathways important in neurological functions (Oo et al., 2020). To note, in ASD cases *de novo* loss of function variants were found in *DIP2C*, which is reported in SFARI database as candidate ASD gene (Yuen et al., 2017).

The maternally inherited *ATG7* variant is a rare missense variant (NM_006395:exon12: c.1277C>T:pPro426Leu). *ATG7* encodes an ubiquitin-activating enzyme E1-like protein that mediates membrane fusion in autophagy (Tanida et al., 2001). Autophagy deficiency induced by conditional Atg7 deletion leads to a similar autistic-like behavioral abnormalities in mice (Hui and Tanaka, 2019). *ATG7* plays a role in modulation of dendritic arborization, and synapses elimination during development, mechanisms relevant to the etiology of neurodevelopmental disorders as ASD (Kim et al., 2017).

We investigated the role of the 6 candidate genes in already known ASD-associated biological processes and their possible connection among each other and with other ASD-associated genes reported in SFARI database.

The results indicated that each of the analyzed genes, except *DIP2C*, takes part to at least one process in which other SFARI genes are involved, namely "long term synaptic potentiation," "neurotransmitter catabolic process," "circadian rhythm," "regulation of circadian rhythm," "cell differentiation" (**Figure 2B, Table 2**).

DISCUSSION AND CONCLUSION

ASD is a complex and heterogeneous condition characterized by impaired communication and social interaction, repetitive behaviors, and restricted interests and associated with a range of comorbid conditions. Intellectual disabilities can affect around 50% of ASD cases (Postorino et al., 2016), ADHD is present in about 11% of children and even higher in adult ASD patients (Lugo et al., 2020), and sleep and gastrointestinal disturbances have elevated prevalence in ASD cases compared to controls (Devnani and Hegde, 2015; Bjorklund

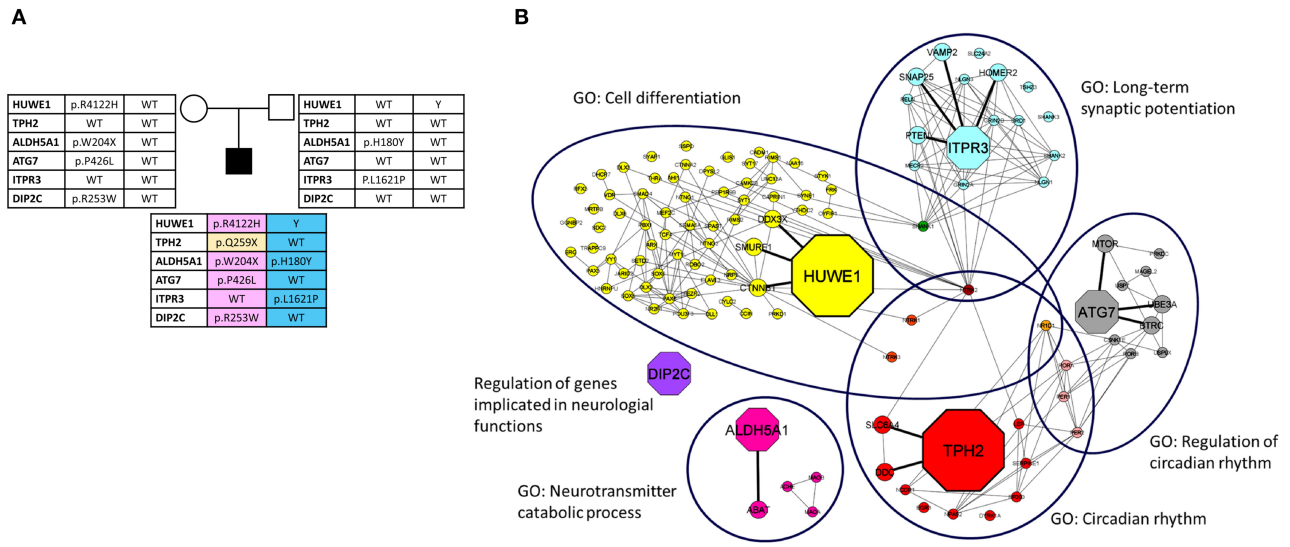

FIGURE 2 | (A) Family's pedigree. Implicated genes and their variants, indicated as amino acid changes, are shown. **(B)** Network analysis. The network depicts the protein-protein interactions (gray lines) revealed by STRING analysis (visualized by Cytoscape tool) on the basis of the enrichment obtained with GeneCodis4 tool. The Figure shows the enriched BP terms clustering the six candidate genes (octagon shape) and the SFARI genes (circle shape). Three candidate genes are also in the SFARI database (*HUWE1, ALDH5A1, DIP2C*). The network has a clear distinction into 6 clusters representing the top six GO-BPs (large ovals).

TABLE 1 | Overview of the variants found in the patient.

Gene	Position	Fnc	RefSeq ID	Variation	GnomAD	1000G	SIFT	Poly-phen2	CADD	dbSNP ID	Var	pLI	Z score	Hapl-insuf
*HUWE1**	X: 53563401	M	NM_031407	c.12365G>A:p.R4122H	NA	NA	D	D	27.7	NA	LP	1	8.87	0.831
TPH2	12: 72366465	Sg	NM_173353	c.775C>T:p.Q259X	NA	NA	–	–	40	NA	VUS	0	1	0.653
ALDH5A1#	6: 24505099	Sg	NM_170740	c.612G>A:p.W204X	0.00004	NA	–	–	41	rs118203982	P	0	0.73	0.505
ALDH5A1#	6:24503590	M	NM_170740	c.538C>T: p.H180Y	0.3105	0.3147	T	B	7.5	rs2760118	B	0	0.73	0.505
ITPR3	6: 33651870	M	NM_002224	c.4862T>C:p.L1621P	0.00001	NA	D	D	29.3	rs1217162248	VUS	0	4.55	0.603
DIP2C°	10: 461811	M	NM_014974	c.757C>T:p.R253W	NA	NA	D	D	34	NA	VUS	1	4.67	0.563
ATG7	3: 11389502	M	NM_006395	c.1277C>T:p.P426L	0.00120	0.0004	D	D	34	rs143545741	VUS	0	1.37	0.652

*Fnc, Function; M, Missense; Sg, Stopgain; NA, not available; D, deleterious; T, tolerated; CADD score, amino acid substitution is predicted damaging if the score is >15; Var, Varsome; VUS, Variant of Uncertain Significance; B, Benign; LP, Likely Pathogenic; P, Pathogenic; GnomAD is referred to GnomAD Exome ALL. *, SFARI gene, syndromic "S"; #, SFARI gene, score 1; °, SFARI gene, score 2.*

et al., 2020). The genetic base of ASD is also heterogeneous, involving at least 102 risk genes (Satterstrom et al., 2020). ASD-associated variants can be rare or more common in the general population. Finally, compensatory mechanisms can tune the major or the minor effect of the variations determining the phenotype present in each subject (Bourgeron, 2015).

In our case, the patient presented ASD associated with intellectual disability, ADHD, sleep, and gastrointestinal disorder. By a deep bioinformatic analysis of WES data we identified *de novo* and inherited variants in six different genes that globally could explain the complex phenotype shown by this patient.

The *HUWE1* p.R4122H variant lies in the HECT domain, known to present an overrepresentation of deleterious variants in patients with X-linked ID (Moortgat et al., 2018). *In vitro* experiments demonstrated that mutations in the HECT domain are likely to impair the gene function (Giles and Grill, 2020). Indeed, certain *HUWE1* variants are present in patients with autism in addition to ID, suggesting *HUWE1* variants could be risk factors for ASD (Giles and Grill, 2020). In the present case, the *HUWE1* variant could account for ID and contribute to ASD together with the other gene candidates. *TPH2* is involved in the synthesis of serotonin, a neurotransmitter with a role in the control of mood, anxiety, sleep-wake regulation and, peripherally, in the modulation of gastrointestinal motility. It has been reported that behavioral symptoms can be associated with gastrointestinal abnormalities in ASD patients, and, in particular, that ASD patients with sleep problems are more likely to have gastrointestinal abnormalities (Maenner et al., 2012; Bjorklund et al., 2020). In this line, we suggest that the *TPH2 de novo* stop variant could account for the hyperactivity, attentional lability, sleep and gastrointestinal disturbances present in this patient.

TABLE 2 | Biological processes associated with genes implicated in the present case and genes reported in the SFARI database.

Annotation	Term	Term genes found	Input size	Term genes	Genes universe	Hyp pval	Hyp pval_adj	Genes
GO:0060291	Long-term synaptic potentiation	17	934	45	18,883	0.0000	0.0000	SLC24A2, SHANK2, NLGN1, VAMP2, SNAP25, PTEN, RELN, NTRK2, MECP2, **ITPR3**, GRIN2B, GRIN2A, SHANK3, DRD1, TSHZ3, NLGN3, SHANK1
GO:0060999	Positive regulation of dendritic spine development	10	934	23	18,883	0.0000	0.0000	ZMYND8, SHANK2, NLGN1, **DLG5**, CDKL5, ITSN1, MTOR, FMR1, SHANK3, SHANK1
GO:0007623	Circadian rhythm	17	934	91	18,883	0.0000	0.0001	NCOR1, NR1D1, PER2, SLC6A4, RORA, PER1, SERPINE1, NTRK3, NTRK2, NTRK1, NPAS2, LEP, **TPH2**, EP300, EGR3, DYRK1A, DDC
GO:0042752	Regulation of circadian rhythm	14	934	66	18,883	0.0000	0.0002	**ATG7**, NR1D1, BTRC, PER2, USP9X, USP7, UBE3A, RORB, RORA, PRKDC, PER1, MTOR, MAGEL2, CSNK1E
GO:0042135	Neurotransmitter catabolic process	5	934	10	18,883	0.0001	0.0021	**ALDH5A1**, ACHE, MAOB, MAOA, ABAT
GO:0030154	Cell differentiation	70	934	1,019	18,883	0.0036	0.0423	CADM1, SYNE1, CYFIP1, SSPO, MYT1L, UNC13A, RIMS1, NTNG1, **HUWE1**, RIMS2, NR1D1, CCIN, SEMA5A, NRP2, CAMK2B, YY1, VDR, THRA, NR2F1, TCF4, SYT1, SPAST, SOX5, SDC2, ROBO2, RFX3, PRKD1, POU3F3, PBX1, PAX6, PAX5, NTRK3, NTRK2, NTRK1, MEF2C, SMAD4, CAPRIN1, JARID2, HNRNPU, FRK, ARX, GLIS1, SYAP1, ERG, PPP1R9B, NTNG2, ELAVL3, TRAPPC9, NAA15, GGNBP2, DPYSL2, YTHDC2, DLX6, DLX3, DLX2, DHCR7, MRTFB, SMURF1, DDX3X, SOX6, STYK1, FEZF2, CYLC2, AHI1, CTNNB1, CTNNA2, SYT17, SHANK1, SETD2, DLL1

Term genes found, number of annotated genes in the reference list; Input size, total number of genes in the input list, including the genes implicated in the present case and the SFARI list genes; Term genes, number of annotated genes in the reference list; Genes universe, total number of human reference genes; Hyp pval, hypergeometric test pValue; Hyp pval_adj, corrected hypergeometric pValue using FDR procedure.

For function and pattern of inheritance, *HUWE1* and *TPH2* could play a major role in the patient's phenotype.

Variants were also identified in *ALDH5A1*, whose absence of activity has been associated to a recessive severe phenotype. In the present case, we could speculate that the stop and the hypomorphic variants leave a quantity of expressed enzyme lower than that expressed by a heterozygous carrier, in this way contributing to the patient's phenotype (Oikonomou et al., 2019; Jones et al., 2020).

Three additional deleterious variants were found, inherited from either patient's healthy mother (*ATG7*, *DIP2C*) or his healthy father (*ITPR3*) suggesting that taken individually, in heterozygosis, these variants do not lead to altered neurodevelopment. Since gene enrichment analysis highlighted they take part to functions notably impaired in ASD, we are unable to exclude they play a role in the patient's phenotype. Rather, they could contribute to the patient's complex phenotype as modifier genes.

To note, increasing findings support an oligogenic model of inheritance for ASD, and combination of inherited and/or *de novo* variants were predicted to range from 2 to 10 (Pickles et al., 1995). However, genetic variants, their connections and how they can act in every single patient, are aspects still largely to be elucidated.

In conclusion, by using an oligogenic approach to the analysis of WES data, we identified a *de novo* stop variant in *TPH2* and one deleterious missense variant in *HUWE1* that could act in a permissive genetic background characterized by deleterious variants in additional four genes. All variants collectively could have a role in the biological processes involved in the pathogenesis of ASD thus contributing to the different features of the patient's phenotype. As this hypothesis is based on the study of a single patient and on variants predicted to be deleterious by bioinformatic analyses, future functional studies are needed to elucidate specific roles of identified genes and variants in the patient's complex phenotype.

DATA AVAILABILITY STATEMENT

Clinical and genetic variant details have been deposited in the Decipher database. Accession number: Patient 421248.

ETHICS STATEMENT

The studies involving human participants were reviewed and approved by the Ethics Committee of the Italian Regione Liguria (P.R. 399REG2017). Written informed consent to participate in this study was provided by the participants' legal guardian/next of kin. Written informed consent was obtained from the individual(s), and minor(s) legal guardian/next of kin, for the publication of data included in this article.

AUTHOR CONTRIBUTIONS

GS, DV, RS, and SG were responsible for whole exome sequencing. MC, MSq, MSe, and AP were responsible for the variant prioritization, oligogenic and network analyses. LP, BB, SB, and LN were in charge of the clinical diagnosis. MD, ML, and AP were in charge of genetic counseling, family recruitment, and ethical procedures. LP and AP wrote the manuscript. All authors gave advises when doing the gene analysis, reviewed the manuscript, and agreed to be accountable for the content of the work.

FUNDING

This research was founded by Italian Ministero della Salute (Project N. RF-2016-02361949 to AP; Cinque per Mille and Ricerca Corrente). This work was developed within the framework of the DINOGMI Department of Excellence (MIUR 2018-2022, legge 232 del 2016).

ACKNOWLEDGMENTS

The authors wish to thank the family and referring nurses of Pediatric Neuropsychiatric Unit for their help and collaboration.

SUPPLEMENTARY MATERIAL

The Supplementary Material for this article can be found online at: https://www.frontiersin.org/articles/10.3389/fgene.2021.625564/full#supplementary-material

REFERENCES

Addis, L., Sproviero, W., Thomas, S. V., Caraballo, R. H., Newhouse, S. J., Gomez, K., et al. (2018). Identification of new risk factors for rolandic epilepsy: CNV at Xp22.31 and alterations at cholinergic synapses. *J. Med. Genet.* 55, 607–616. doi: 10.1136/jmedgenet-2018-105319

Besag, F. M. (2018). Epilepsy in patients with autism: links, risks and treatment challenges. *Neuropsychiatr. Dis. Treat.* 14, 1–10. doi: 10.2147/NDT.S120509

Bjorklund, G., Pivina, L., Dadar, M., Meguid, N. A., Semenova, Y., Anwar, M., et al. (2020). Gastrointestinal alterations in autism spectrum disorder: what do we know? *Neurosci. Biobehav. Rev.* 118, 111–120. doi: 10.1016/j.neubiorev.2020.06.033

Blasi, P., Boyl, P. P., Ledda, M., Novelletto, A., Gibson, K. M., Jakobs, C., et al. (2002). Structure of human succinic semialdehyde dehydrogenase gene: identification of promoter region and alternatively processed isoforms. *Mol. Genet. Metab.* 76, 348–362. doi: 10.1016/s1096-7192(02)00105-1

Bourgeron, T. (2015). From the genetic architecture to synaptic plasticity in autism spectrum disorder. *Nat. Rev. Neurosci.* 16, 551–563. doi: 10.1038/nrn3992

Brooks, J. D., Bronskill, S. E., Fu, L., Saxena, F. E., Arneja, J., Pinzaru, V. B., et al. (2020). Identifying children and youth with autism spectrum disorder in electronic medical records: examining health system utilization and comorbidities. *Autism Res.* 1–11. doi: 10.1002/aur.2419

Chambliss, K. L., Caudle, D. L., Hinson, D. D., Moomaw, C. R., Slaughter, C. A., Jakobs, C., et al. (1995). Molecular cloning of the mature NAD(+)-dependent succinic semialdehyde dehydrogenase from rat and human. cDNA isolation, evolutionary homology, and tissue expression. *J. Biol. Chem.* 270, 461–467. doi: 10.1074/jbc.270.1.461

Devnani, P. A., and Hegde, A. U. (2015). Autism and sleep disorders. *J. Pediatr. Neurosci.* 10, 304–307. doi: 10.4103/1817-1745.174438

Giles, A. C., and Grill, B. (2020). Roles of the HUWE1 ubiquitin ligase in nervous system development, function and disease. *Neural Dev.* 15:6. doi: 10.1186/s13064-020-00143-9

Hui, K. K., and Tanaka, M. (2019). Autophagy links MTOR and GABA signaling in the brain. *Autophagy* 15, 1848–1849. doi: 10.1080/15548627.2019.1637643

Jones, L. A., Sun, E. W., Martin, A. M., and Keating, D. J. (2020). The ever-changing roles of serotonin. *Int. J. Biochem. Cell Biol.* 125:105776. doi: 10.1016/j.biocel.2020.105776

Kim, H. J., Cho, M. H., Shim, W. H., Kim, J. K., Jeon, E. Y., Kim, D. H., et al. (2017). Deficient autophagy in microglia impairs synaptic pruning and causes social behavioral defects. *Mol. Psychiatry* 22, 1576–1584. doi: 10.1038/mp.2016.103

Kopanos, C., Tsiolkas, V., Kouris, A., Chapple, C. E., Albarca Aguilera, M., Meyer, R., et al. (2019). VarSome: the human genomic variant search engine. *Bioinformatics* 35, 1978–1980. doi: 10.1093/bioinformatics/bty897

Lek, M., Karczewski, K. J., Minikel, E. V., Samocha, K. E., Banks, E., Fennell, T., et al. (2016). Analysis of protein-coding genetic variation in 60,706 humans. *Nature* 536, 285–291. doi: 10.1038/nature19057

Li, H., and Durbin, R. (2010). Fast and accurate long-read alignment with Burrows-Wheeler transform. *Bioinformatics* 26, 589–595. doi: 10.1093/bioinformatics/btp698

Lugo, J., Fadeuilhe, C., Gisbert, L., Setien, I., Delgado, M., Corrales, M., et al. (2020). Sleep in adults with autism spectrum disorder and attention deficit/hyperactivity disorder: a systematic review and meta-analysis. *Eur. Neuropsychopharmacol.* 38, 1–24. doi: 10.1016/j.euroneuro.2020.07.004

Maenner, M. J., Arneson, C. L., Levy, S. E., Kirby, R. S., Nicholas, J. S., and Durkin, M. S. (2012). Brief report: association between behavioral features and gastrointestinal problems among children with autism spectrum disorder. *J. Autism Dev. Disord.* 42, 1520–1525. doi: 10.1007/s10803-011-1379-6

McFarlane, H. G., Kusek, G. K., Yang, M., Phoenix, J. L., Bolivar, V. J., and Crawley, J. N. (2008). Autism-like behavioral phenotypes in BTBR T+tf/J mice. *Genes Brain Behav.* 7, 152–163. doi: 10.1111/j.1601-183X.2007.00330.x

Miller, J. A., Ding, S. L., Sunkin, S. M., Smith, K. A., Ng, L., Szafer, A., et al. (2014). Transcriptional landscape of the prenatal human brain. *Nature* 508, 199–206. doi: 10.1038/nature13185

Moortgat, S., Berland, S., Aukrust, I., Maystadt, I., Baker, L., Benoit, V., et al. (2018). HUWE1 variants cause dominant X-linked intellectual disability: a clinical study of 21 patients. *Eur. J. Hum. Genet.* 26, 64–74. doi: 10.1038/s41431-017-0038-6

Munnich, A., Demily, C., Frugere, L., Duwime, C., Malan, V., Barcia, G., et al. (2019). Impact of on-site clinical genetics consultations on diagnostic rate in children and young adults with autism spectrum disorder. *Mol. Autism* 10:33. doi: 10.1186/s13229-019-0284-2

Nevison, C., Blaxill, M., and Zahorodny, W. (2018). California autism prevalence trends from 1931 to 2014 and comparison to national ASD data from IDEA and ADDM. *J. Autism Dev. Disord.* 48, 4103–4117. doi: 10.1007/s10803-018-3670-2

Oikonomou, G., Altermatt, M., Zhang, R. W., Coughlin, G. M., Montz, C., Gradinaru, V., et al. (2019). The serotonergic raphe promote sleep in zebrafish and mice. *Neuron* 103, 686–701 e688. doi: 10.1016/j.neuron.2019.05.038

Oo, Z. M., Adlat, S., Sah, R. K., Myint, M. Z. Z., Hayel, F., Chen, Y., et al. (2020). Brain transcriptome study through CRISPR/Cas9 mediated mouse Dip2c gene knock-out. *Gene* 758:144975. doi: 10.1016/j.gene.2020.144975

Pickles, A., Bolton, P., Macdonald, H., Bailey, A., Le Couteur, A., Sim, C. H., et al. (1995). Latent-class analysis of recurrence risks for complex phenotypes with selection and measurement error: a twin and family history study of autism. *Am. J. Hum. Genet.* 57, 717–726.

Postorino, V., Fatta, L. M., Sanges, V., Giovagnoli, G., De Peppo, L., Vicari, S., et al. (2016). Intellectual disability in Autism Spectrum Disorder: investigation of prevalence in an Italian sample of children and adolescents. *Res. Dev. Disabil.* 48, 193–201. doi: 10.1016/j.ridd.2015.10.020

Renaux, A., Papadimitriou, S., Versbraegen, N., Nachtegael, C., Boutry, S., Nowe, A., et al. (2019). ORVAL: a novel platform for the prediction and exploration of disease-causing oligogenic variant combinations. *Nucleic Acids Res.* 47, W93–W98. doi: 10.1093/nar/gkz,437

Sanders, S. J., He, X., Willsey, A. J., Ercan-Sencicek, A. G., Samocha, K. E., Cicek, A. E., et al. (2015). Insights into Autism Spectrum Disorder genomic architecture and biology from 71 risk loci. *Neuron* 87, 1215–1233. doi: 10.1016/j.neuron.2015.09.016

Satterstrom, F. K., Kosmicki, J. A., Wang, J., Breen, M. S., De Rubeis, S., An, J. Y., et al. (2020). Large-scale exome sequencing study implicates both developmental and functional changes in the neurobiology of autism. *Cell* 180, 568–584 e523. doi: 10.1016/j.cell.2019.12.036

Shannon, P., Markiel, A., Ozier, O., Baliga, N. S., Wang, J. T., Ramage, D., et al. (2003). Cytoscape: a software environment for integrated models of biomolecular interaction networks. *Genome Res.* 13, 2498–2504. doi: 10.1101/gr.1239303

Shihab, H. A., Rogers, M. F., Campbell, C., and Gaunt, T. R. (2017). HIPred: an integrative approach to predicting haploinsufficient genes. *Bioinformatics* 33, 1751–1757. doi: 10.1093/bioinformatics/btx028

Szklarczyk, D., Gable, A. L., Lyon, D., Junge, A., Wyder, S., Huerta-Cepas, J., et al. (2019). STRING v11: protein-protein association networks with increased coverage, supporting functional discovery in genome-wide experimental datasets. *Nucleic Acids Res.* 47, D607–D613. doi: 10.1093/nar/gky1131

Tabas-Madrid, D., Nogales-Cadenas, R., and Pascual-Montano, A. (2012). GeneCodis3: a non-redundant and modular enrichment analysis tool for functional genomics. *Nucleic Acids Res.* 40, W478–W483. doi: 10.1093/nar/gks402

Tanida, I., Tanida-Miyake, E., Ueno, T., and Kominami, E. (2001). The human homolog of Saccharomyces cerevisiae Apg7p is a Protein-activating enzyme for multiple substrates including human Apg12p, GATE-16, GABARAP, and MAP-LC3. *J. Biol. Chem.* 276, 1701–1706. doi: 10.1074/jbc.C000752200

Vaccari, C. M., Tassano, E., Torre, M., Gimelli, S., Divizia, M. T., Romanini, M. V., et al. (2016). Assessment of copy number variations in 120 patients with Poland syndrome. *BMC Med. Genet.* 17:89. doi: 10.1186/s12881-016-0351-x

Wang, K., Li, M., and Hakonarson, H. (2010). ANNOVAR: functional annotation of genetic variants from high-throughput sequencing data. *Nucleic Acids Res.* 38:e164. doi: 10.1093/nar/gkq603

Yuen, R. K. C., Merico, D., Bookman, M., Howe, J. L., Thiruvahindrapuram, B., Patel, R. V., et al. (2017). Whole genome sequencing resource identifies 18 new candidate genes for autism spectrum disorder. *Nat. Neurosci.* 20, 602–611. doi: 10.1038/nn.4524

Conflict of Interest: The authors declare that the research was conducted in the absence of any commercial or financial relationships that could be construed as a potential conflict of interest.

frontiers in Pediatrics

ORIGINAL RESEARCH
published: 20 April 2021
doi: 10.3389/fped.2021.651621

A Novel Homozygous *VPS13B* Splice-Site Mutation Causing the Skipping of Exon 38 in a Chinese Family With Cohen Syndrome

Liangshan Li[1,2†], *Xiangmao Bu*[3†], *Yuhua Ji*[4], *Ping Tan*[5*] *and Shiguo Liu*[1*]

[1] Medical Genetic Department, The Affiliated Hospital of Qingdao University, Qingdao, China, [2] Department of Clinical Laboratory, Medical College of Qingdao University, Qingdao, China, [3] Department of Transfusion, Qingdao Women and Children's Hospital, Qingdao, China, [4] Newborn Disease Screening Centre, Yantai Maternal and Child Health Hospital, Yantai, China, [5] Obstetrical Department, The Affiliated Hospital of Qingdao University, Qingdao, China

Background: Cohen syndrome (CS) is a clinically heterogeneous disorder characterized by extensive phenotypic variation with autosomal recessive inheritance. *VPS13B* was identified to be the disease-causing gene for CS. The objectives of the present study were to screen likely pathogenic mutations of the patient with developmental delay and mental retardation, and to determinate the effect of this splice-site mutation by reverse transcription analysis.

Methods: Whole exome sequencing (WES) in combination with Sanger sequencing were performed to identify the causative mutations of this CS family. Subsequently, the impact of the intronic variant on splicing was analyzed by reverse transcription and the construction of expression vector.

Results: A novel homozygous splice-site mutation (c.6940+1G>T) in the VPS13B gene was identified in this proband. Sanger sequencing analysis of the cDNA demonstrated that the c.6940+1G>T variant could cause the skipping of entire exon 38, resulting in the loss of 208 nucleotides and further give rise to the generation of a premature in-frame stop codon at code 2,247.

Conclusions: The homozygous *VPS13B* splicing variant c.6940+1G>T was co-segregated with the CS phenotypes in this family and was identified to be the cause of CS after comprehensive consideration of the clinical manifestations, genetic analysis and cDNA sequencing result.

Keywords: cohen syndrome, VPS13B, splice-site mutation, mRNA analysis, exon skipping

OPEN ACCESS

Edited by:
Anjana Munshi,
Central University of Punjab, India

Reviewed by:
Velina Guergueltcheva,
Sofiamed University Hospital, Bulgaria
María Eugenia De La Morena-Barrio,
University of Murcia, Spain

***Correspondence:**
Ping Tan
18661807971@163.com
Shiguo Liu
liushiguo2002@126.com

†These authors have contributed equally to this work

Specialty section:
This article was submitted to Genetics of Common and Rare Diseases, a section of the journal Frontiers in Pediatrics

Received: *10 January 2021*
Accepted: *18 March 2021*
Published: *20 April 2021*

Citation:
Li L, Bu X, Ji Y, Tan P and Liu S (2021) A Novel Homozygous VPS13B Splice-Site Mutation Causing the Skipping of Exon 38 in a Chinese Family With Cohen Syndrome. Front. Pediatr. 9:651621. doi: 10.3389/fped.2021.651621

INTRODUCTION

Cohen syndrome (CS) (OMIM 216550), initially described in three patients by Cohen et al., is an uncommon autosomal recessive neurodevelopmental disorder with more than 200 causative mutations in ∼1,000 CS-affected individuals reported to date worldwide (1–3). CS can affect multiple organs and systems including the face, head, eyes, blood system, cardiovascular system, nervous system, and endocrine system (4). CS is relatively common among Finnish population in spite of the low prevalence worldwide (5). Apart from this, CS has also been reported in Indian, Jordanian, Chinese, Saudi, Tunisian, Iranian, German, Syrian, Lebanese, and Pakistani (6–14).

To date, clear phenotype–genotype correlations of CS have not been established yet. Although CS-affected individuals from outside Finland present with variable phenotypes (15), the typical clinical characteristics usually include intellectual disability, short stature, a cheerful disposition, retinal dystrophy, hypotonia, scoliosis, joint laxity, intermittent neutropenia, slender fingers, hyperlinear palms, midchildhood onset truncal obesity and craniofacial dysmorphisms such as microcephaly, thick hair, low hairline, short philtrum, wave-shaped eyes and prominent upper central incisors (1, 16, 17).

Vacuolar protein sorting 13 homolog B (*VPS13B*), also known as *COH1*, was identified to be the disease-causing gene for CS by Kolehmainen et al. (15) and since then, a large number of variants have been detected in CS patients. In addition, *VPS13B* is also responsible for autism spectrum disorders (ASDs) (18). *VPS13B* is localized on chromosome 8 (8q22.2) with 62 exons and encodes a 4022-amino acid transmembrane protein (14). The encoded protein is a Golgi-associated peripheral membrane protein that plays an important role in Golgi integrity and homeostasis, and membrane transport (17, 19), and it belongs to the VPS13 protein family, which are highly conserved in eukaryotic cells (20, 21). Loss-of-function mutations in other *VPS13* family members such as *VPS13A*, *VPS13C,* and *VPS13D* could result in chorea-acanthocytosis (OMIM 200150), rapidly progressive, early-onset autosomal recessive Parkinson's disease (OMIM 616840) and spinocerebellar ataxia, recessive type 4 (OMIM 607317), respectively (22–24).

With the rapid development of high-throughput sequencing technology, next-generation sequencing (NGS) for molecular analysis has enabled patients with inconspicuous clinical symptoms to get timely and accurate diagnosis, which could contribute to improving the quality of life of the patients and facilitating genetic counseling. NGS technology has been routinely available in clinical practice and research due to significant advantages including high efficiency, low cost, and high accuracy (25). Furthermore, it is also worth noting that NGS technology as a powerful tool is increasingly widely used in the identification of pathogenic mutations of rare monogenic disorders and the discovery of novel causative genes of certain diseases.

In the present study, we investigated a pedgree with CS from Shandong province, China and identified a novel homozygous splicing mutation in the VPS13B gene by performing trio-based whole-exome sequencing (WES). In addition, we further determined that the intronic mutation could lead to aberrant mRNA splicing by reverse transcription analysis.

Abbreviations: ACMG, American College of Medical Genetics and Genomics; ACTH, Adrenocorticotropic hormone; ASDs, Autism spectrum disorders; CS, Cohen syndrome; FT3, Free triiodothyronine; FT4, Free thyroxine; GH, Growth hormone; IGF1, Insulin-like growth factor 1; MRI, Magnetic resonance imaging; NCBI, National Center Biotechnology Information; NGS, Next-generation sequencing; PCR, Polymerase chain reaction; TSH, Thyroid stimulating hormone; *VPS13B*, Vacuolar protein sorting 13 homolog B; WES, Whole exome sequencing.

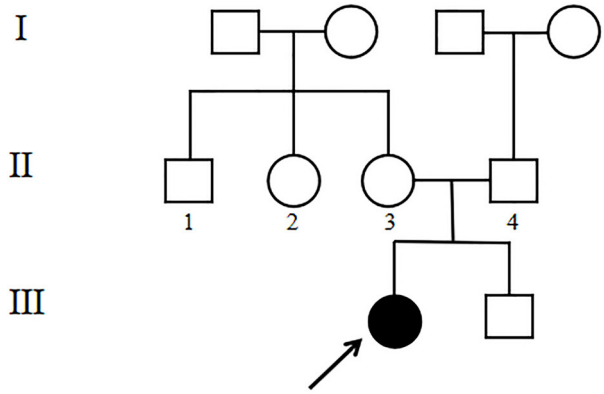

FIGURE 1 | Pedigree of the family with CS. The black arrow denotes the proband.

MATERIALS AND METHODS

Patient

The 4-year-old female proband (III1, **Figure 1**) was the first child of the family born at 40 weeks gestation with a birth weight of 2,600 g from non-consanguineous, healthy parents. There was no significant family history. Other family members including her younger brother (III2, **Figure 1**) did not show any obvious symptoms or signs. This study was approved by the Ethics Committee of the Affiliated Hospital of Qingdao University. Blood samples were collected from the proband and her family members after written informed consent was obtained from the parents.

WES for Mutation Screening

The genomic DNA was isolated from peripheral blood leukocytes of the proband using a DNA extraction kit (TIANGEN, Beijing, China) following the manufacturer's protocol. The DNA was quantified with Nanodrop 2000. The qualified genomic DNA sample was randomly fragmented into 180–250 bp by Covaris S220 sonicator. DNA fragments were end repaired, A-tailed and ligated to adapters on both ends for the preparation of DNA libraries. Adapter-ligated libraries were enriched by polymerase chain reaction (PCR) amplification. A Agilent 64 M liquid phase chip capture system was used to efficiently enrich the whole-exome regions. Exome libraries were enriched in a PCR reaction followed by library quality assessment. Only qualified libraries were sequenced on Illumina NovaSeq platform for paired-end 150 bp reads. The target area coverage was 99.73%, the average sequencing depth was 189.58× and the proportion of average depth of target area >20× was 98.97%.

Sequencing Data Analysis

For raw data, filter reads with adapter contamination, reads with more than 10% of uncertain bases and low quality reads to obtain clean data. Burrows-Wheeler Aligner (BWA) software was used to compare clean reads with reference genome (GRCh37/hg19). Samtools and picard tool were utilized to sort the comparison

results and mark duplicate reads, respectively. Single nucleotide polymorphisms (SNPs) and insertions or deletions (InDels) were determined by the Genome Analysis Toolkit (GATK) software. Subsequently, the SNPs and InDels were annotated by ANNOVAR. Remove synonymous variants and variants with minor allele frequency (MAF) > 1% in at least one of the three available frequency databases 1000 Genomes Project, Exome Aggregation Consortium (ExAC) and esp6500si_all. Finally, the pathogenicity of the variants were predicted by SIFT (https://sift.bii.a-star.edu.sg/), PolyPhen-2 (http://genetics.bwh.harvard.edu/pph2/), MutationTaster (http://www.mutationtaster.org/) and CADD (https://cadd.gs.washington.edu/score).

Sanger Sequencing Validation

The identified variant by WES analysis was confirmed by Sanger sequencing. The genomic DNA was extracted from peripheral blood samples of the proband, her parents, paternal grandparents and maternal grandparents with a DNA extraction kit (TIANGEN, Beijing, China). The partial DNA sequences involving the splicing mutation site were amplified by PCR using primers: forward (5′-TTAATGAGGAGGGAAATTTTGAAGTAC-3′) and reverse (5′-TGGGCAATCTTCAGTTTCATTATAAA-3′). PCR products were analyzed by 1% agarose gel electrophoresis and then were purified and sequenced on an ABI 3730 analyzer (Applied Biosystem). The obtained DNA sequences were compared with the reference sequence on National Center Biotechnology Information (NCBI) website to discover the mutation site.

mRNA Analysis by the Construction of Recombinant Plasmid

Total RNA was extracted from peripheral venous blood of the proband using a Blood RNA Extraction Kit (Takara) according to the manufacturer's instructions. cDNA was prepared from 2 μg total RNA using HiScript® II 1st Strand cDNA Synthesis Kit (+gDNA wiper) (Vazyme). PCR for amplification of the cDNA covering exons 37–41 and partial sequences of exons 36 and 42 of the VPS13B gene was performed with 2×TransStart® FastPfu PCR SuperMix (TransGen Biotech) following primers: forward (5′-CAAGAAAACATGTGGAGAGCTGTT-3′) and reverse (5′-CACTGTCGAAGATACATGTGTGGTT-3′). PCR product was identified by 1% agarose gel electrophoresis followed by the extraction of target cDNA with an agarose gel DNA recovery kit (Solarbio). Subsequently, the recovered PCR product was connected with pEASY®-Blunt E2 Expression Vector. The recombinant plasmid was confirmed by bidirectional sequencing with universal primers: forward (5′-TAATACGACTCACTATAGGG-3′) and reverse (5′-TAGTTATTGCTCAGCGGTGG-3′).

RESULTS

Clinical Phenotypes

On October 30, 2017, when the proband was 1 year and 3 months old, she was admitted to hospital because she was unable to stand or walk independently. Physical examination showed good eye contact, decreased muscle tone in all limbs, active patellar tendon reflex, ankle clonus (–), hyperextended knee and talipes valgus (**Table 1**). Preliminary diagnoses were growth retardation and hypotonia. She could speak "ba" and "ma" at the age of 2 years and was able to walk with an unsteady gait at age 3 years.

TABLE 1 | Summary of clinical findings of the proband.

Clinical phenotypes	Patient (III1)
Developmental delay	+
Intellectual disability	+
Hypotonia	+
Micrognathia	+
Wave-shaped eyes	+
Short philtrum	+
Thick hair	+
Thick eyelashes	+
High myopia	+
Neutropenia	+
Talipes valgus	+
Left coherent palm	+
Hyperlinear palms	+

She was readmitted to hospital due to growth and development retardation, and short stature on May 20, 2020 when she was 3.8 years old. Physical examination: weight 13.4 kg, length 94.7 cm (3rd−10th centile), normal stature, micrognathia, normal limbs and spine, left coherent palm, bipedal varus, unlimited joint movements, no edema in both lower limbs, decreased muscle strength and muscle tension of the limbs, normal bilateral patellar tendon reflexes and bilateral Babinski signs (–) (**Figure 2**; **Table 1**). Laboratory tests: neutrophil count 1.16×10^9/L (Reference value: 1.7–7.7 $\times$ 10^9/L), urine occult blood (±), urine leukocyte (±), cortisol 213.35 nmol/L (Reference value: 118.6–618 nmol/L), adrenocorticotropic hormone (ACTH) 18.00 pg/mL (Reference value: 0–46 pg/mL), free triiodothyronine (FT3) 5.36 pmol/L (Reference value: 3.5–6.5 pmol/L uIU/mL), free thyroxine (FT4) 13.92 pmol/L (Reference value: 11.5–22.7 pmol/L), thyroid stimulating hormone (TSH) 1.722 μIU/mL (Reference value: 0.64–6.27 uIU/mL), insulin-like growth factor 1 (IGF1) 116 μg/L (Reference value: 49–289 μg/L), 25-hydroxyvitamin D 14.31 ng/mL (Reference value: 20–100 μg/L), estradiol 26.66 pmol/L (Reference value: 22–99.1 pmol/L), luteinizing hormone <0.10 mIU/mL (Reference value: 0.2–1.4 mIU/mL), follicle-stimulating hormone 0.52 mIU/mL (Reference value: 0.2–3.8 mIU/mL). The measured growth hormone (GH) values were 0.16, 6.9, 3.0, and 0.16ng/mL, 2.4, 1.9, respectively, at 0, 60, and 90 min on the GH provocation test by oral clonidine and insulin injection with GH peak <10 ng/mL. Blood glucose levels were 5.6 mmol/L, 5.4 mmol/L, 5.5 mmol/L at 0, 60, and 90 min. Plain magnetic resonance imaging (MRI) scan of the pituitary showed no obvious abnormality. Orthotopic radiograph of the left hand revealed that the bone age was equivalent to about 3.5 years of age. No abnormalities were found in hepatobiliary, pancreatic and splenic ultrasound. Abdominal gynecologic

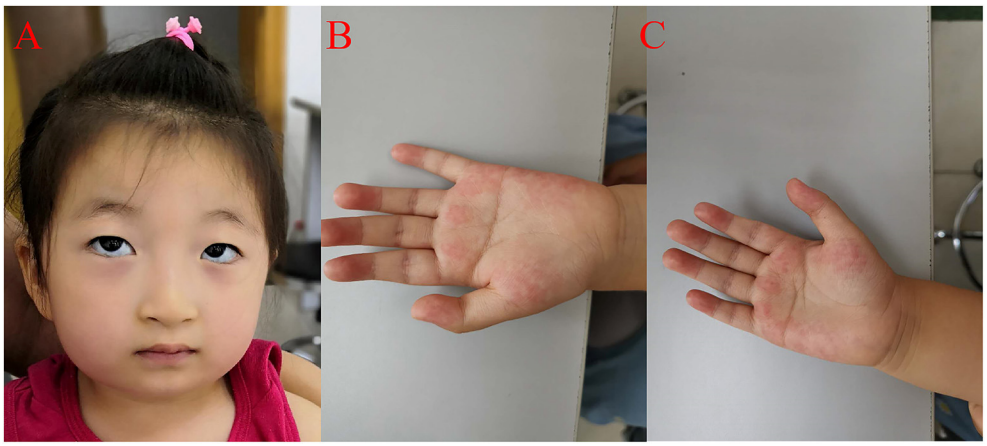

FIGURE 2 | Clinical features of the proband. **(A)** The proband presented with micrognathia, wave-shaped eyes, short philtrum, thick eyelashes and thick hair. **(B)** Left coherent palm with hyperlinearity. **(C)** Hyperlinear right palm.

ultrasound revealed uterus 15*4 cm, left ovary 11*5 cm, and right ovary 14*4cm.

The patient had a normal 46, XX chromosome karyotype and a normal arr (1–22, X)×2 chromosomal microarray. She suffered from intermittent neutropenia with data in different periods shown in **Table 2**. Furthermore, she exhibited mental retardation, wave-shaped eyes, short philtrum, thick hair, thick eyelashes, high myopia (OD −2.10DS −1.19DC*84, OS −3.18DS −2.90DC*74), hyperlinear palms (**Figure 2**; **Table 1**). Genetic testing on this proband was performed for further diagnosis.

Genetic Analysis

WES analysis revealed a novel homozygous splice-site *VPS13B* mutation (c.6940+1G>T, rs202046738) (NM_017890.5) in this proband (III1, **Figures 1, 3A**), which resulted in the first base of intron 38 changed from G to T. Several bioinformatics analysis tools were used to predict the deleteriousness of this splice donor site mutation. MaxEntScan (http://hollywood.mit.edu/burgelab/maxent/Xmaxentscan_scoreseq.html) showed Maximum Entropy Model (MAXENT) 2.14, Maximum Dependence Decomposition Model (MDD) 7.37, First-order Markov Model (MM) 1.73, Weight Matrix Model (WMM) 2.53, with scores of 10.65, 15.88, 10.24, and 11.04, respectively, in wild type. Spliceman (http://fairbrother.biomed.brown.edu/spliceman/index.cgi) revealed a ranking of 59% and Alternative Splice Site Predictor (ASSP) (http://wangcomputing.com/assp/index.html) revealed a score of 5.600 (Donor site cutoff: 4.5). The pathogenicity of the splicing variant was classified as "likely pathogenic" (PVS+PM) according to the American College of Medical Genetics and Genomics (ACMG) guidelines (26) and the frequencies of this mutation were 0.019968% in 1,000 g2015aug_all, 0.01% in gnomAD_exome_EAS, 0.0008% in gnomAD_exome_ALL. Molecular analysis indicated that the homozygous variant was inherited from the unaffected parents (**Figure 3B**). Her maternal grandfather (I1, **Figure 1**) and paternal grandfather (I3, **Figure 1**) were heterozygotes for this variant (**Figure 3B**). However, the maternal grandmother (I2, **Figure 1**) and paternal grandmother (I4, **Figure 1**) did not carry the mutation (**Figure 3C**). In addition, the mutation site was not found in 100 unrelated healthy controls in Shandong, China, either (**Figure 3C**). Therefore, the homozygous genotype was co-segregated with the CS phenotypes in this family.

mRNA Analysis for the VPS13B Splicing Variant

cDNA sequence analysis confirmed that the c.6940+1G>T variant could result in aberrant splicing which caused the skipping of entire exon 38 and abnormal direct joining of exon 37 and exon 39 (**Figure 4**). The skipping of exon 38 led to loss of 208 nucleotides and further gave rise to the generation of a premature in-frame stop codon at code 2247. Presumably, the c.6940+1G>T variant in *VPS13B* is responsible for functional defect of the truncated protein.

DISCUSSION

In this study, we identified a novel homozygous splicing *VPS13B* variant c.6940+1G>T in this proband by high-throughput sequencing analysis, which was inherited from both parents who were non-consanguineous. Furthermore, the mutation frequency was extremely low in different databases, we therefore speculated that the homozygous *VPS13B* variant in this proband may be explained by the founder effect. Although this mutation locus in heterozygous status has been described (27), we reported here a homozygous c.6940+1G>T mutation for the first time to our knowledge. In 2020, Lou et al. also described two CS sisters with heterozygous c.6940+1G>T variant and demonstrated that the splice donor site mutation could result in the entire skipping of exon 38, the clinical features slightly differed from those of our patient (2). The proband in our study also presented with coherent palm with hyperlinearity, which has only been reported in Chinese population to date. The c.6940+1G>T variant was evaluated as "likely pathogenic"

TABLE 2 | Neutrophil counts in different periods.

	2017-11-8	2017-12-17	2019-1-19	2019-7-3	2020-5-20	2020-5-21	2020-6-18
Neutrophil count (Reference value: 1.7–7.7 × 10^9/L)	1.36 × 10^9/L	1.01 × 10^9/L	1.91 × 10^9/L	1.9 × 10^9/L	1.16 × 10^9/L	0.87 × 10^9/L	1.52 × 10^9/L

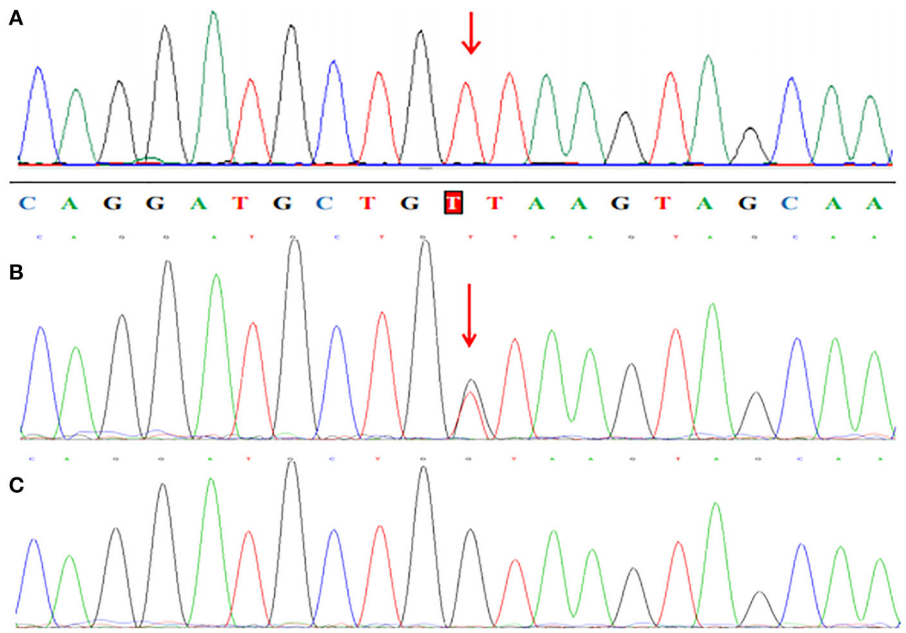

FIGURE 3 | Partial sequence chromatograms of *VPS13B*. The red arrows represent the mutation site. **(A)** Homozygous c.6940+1G>T splice-site mutation. **(B)** Heterozygous c.6940+1G>T splice-site mutation. **(C)** Normal DNA sequence.

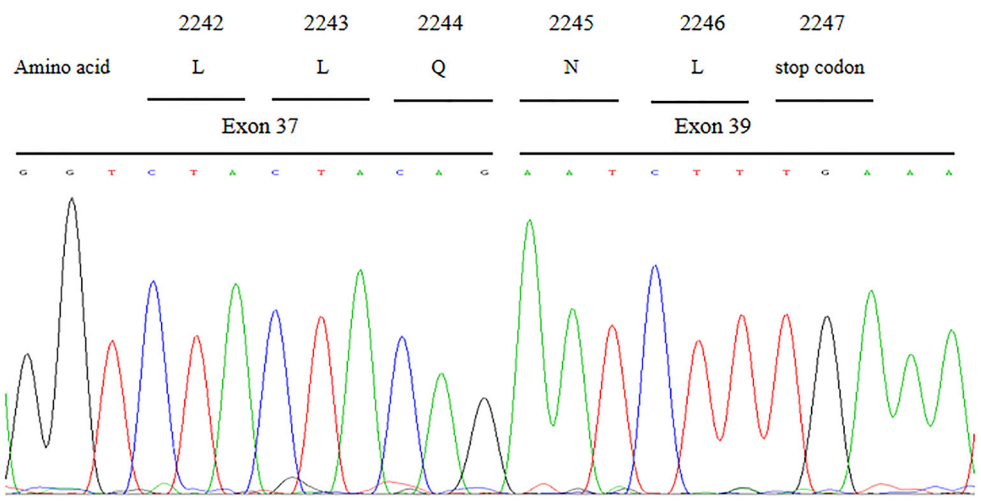

FIGURE 4 | Partial cDNA sequence chromatograms of *VPS13B*. The aberrant splicing resulted in the skipping of entire exon 38 and abnormal direct joining of exon 37 and exon 39, which further gave rise to the generation of a premature in-frame stop codon at code 2,247.

according to the ACMG guideline classification. Genetic analysis showed that her maternal grandfather and paternal grandfather were heterozygous carriers for this mutation, while it was absent in the maternal grandmother and paternal grandmother as well as 100 unrelated, healthy individuals of Chinese origin. Co-segregation analysis suggested that this splice-site mutation was likely responsible for the CS phenotypes in this family. To determine the effect of this *VPS13B* splicing variant, total RNA isolated from venous blood sample was reverse transcribed for the construction of expression vector. Sanger sequencing

analysis of the cDNA covering exons 36–42 of *VPS13B* showed that the homozygous c.6940+1G>T variant could cause the skipping of entire exon 38, which resulted in a premature stop codon producing a truncated VPS13B protein. The homozygous c.6940+1G>T variant in *VPS13B* was identified to be the cause of CS after comprehensive consideration of the clinical manifestations, genetic analysis and cDNA sequencing result.

As a rare autosomal recessive developmental disorder with a broad phenotypic spectrum, CS has been reported in different populations (28). It is characterized by stunted growth, intellectual disability, short philtrum, hypotonia, truncal obesity, overly sociable behavior, early onset and severe myopia, microcephaly, intermittent neutropenia (neutrophil count $<1.5 \times 10^9$/L in children and $<1.8 \times 10^9$/L in adults) (29, 30). The clinical features of the proband in our study were consistent with typical characteristics of CS. The early clinical diagnosis of CS remains challenging and the diagnostic criteria are controversial due to the overlapping features with other disorders and the clinical heterogeneity of CS. The incidence rate of CS may be higher than 1:105,000 because certain clinical symptoms are insignificant during early childhood, which results in CS patients not being diagnosed in a timely manner (31).

CS has been attributed to loss-of-function biallelic mutations in the VPS13B gene. Since the founder mutation c.3348_3349delCT was found in Finnish patients, more than 200 causative mutations have been reported so far in ∼1,000 CS-affected individuals worldwide including non-sense, duplication, missense, splicing, insertion/deletion mutations (7, 15, 17). *VPS13B* maps to chromosome 8q22.2 and encodes six protein isoforms generated by alternative splicing (https://www.uniprot.org/). VPS13B is a transmembrane protein that is associated with vesicle-Mediated sorting, intracellular protein transport, Golgi glycosylation and morphology, and lysosomal–endosomal pathway maintenance (15, 32). VPS13B is widely expressed in brain, blood, small intestine, muscles, placenta, heart, retina, kidney and lung (13, 30).

Rejeb et al. described two cases affected by CS from a non-consanguineous family for the first time in the Tunisian population in 2017 with the clinical features of neutropenia, mental retardation, tapering fingers, thick hair eyebrows and lashes (13). Novel compound heterozygous *VPS13B* mutations c.3582delT/p.A1149fs and c.6295_6296delAT/p.M2124fs were found in the two siblings, which were inherited from the father and the mother, respectively. In 2007, Katzaki et al. identified a deletion variant c.11125delC/p.T3708 fsX61 and a non-sense variant c.11314C>T/p.Q3772X in a male Italian patient with CS who presented with truncal obesity with BMI of 32.2, severe intellectual disability, typical facial gestalt, retinopathy, myopia, joints hyper extensibility, neutropenia and tapering fingers (33). In 2006, six CS cases carrying the same homozygous c.4471G>T/p.Glu1491X in *VPS13B* were reported by Murphy and her colleagues. The patients manifested microcephaly, short philtrum, truncal obesity, developmental delay and prominent central incisors, which were consistent with typical phenotypes of CS (34).

CS is less frequent among Chinese population with only several cases reported to date. In 2019, two CS siblings from Chinese healthy, non-consanguineous parents exhibited mental retardation, speech delay, microcephaly, generalized joint hyper extensibility, hypotonia, thick hair, thick eyebrows, prominent upper central incisors, and hyperlinear palms (14). Hyperlinear palms is an additional phenotypic characteristic of CS only described in Chinese population and the clinical features of our patient have confirmed this. In addition, novel splicing maternal mutation c.3666+1G>T and novel non-sense paternal mutation c.9844A>T/p.K3282X in *VPS13B* were identified in the two siblings by performing WES.

In summary, we identified a novel homozygous splice-site mutation c.6940+1G>T in *VPS13B* by performing WES in a proband with CS. The effect of this splicing variant was confirmed by Sanger sequencing of the cDNA combined with *in silico* analysis that the aberrant splicing led to the skipping of entire exon 38. Family study has revealed that the *VPS13B* variant was co-segregated with the CS phenotypes in this family. Our research demonstrated the pathogenicity of this c.6940+1G>T mutation and made great contributions to the establishment of the genotype–phenotype correlations of CS.

DATA AVAILABILITY STATEMENT

The data presented in the study are deposited in the ClinVar repository, accession number SCV001499947.

ETHICS STATEMENT

This study was approved by the Ethics Committee of the Affiliated Hospital of Qingdao University (QDFY20208902). Written informed consent to participate in this study was provided by the participants' legal guardian/next of kin.

AUTHOR CONTRIBUTIONS

LL conducted the experiments and drafted the manuscript. XB analyzed the data. YJ analyzed and critically reviewed the manuscript. PT drafted the design. SL revised the manuscript. All authors read and approved the final manuscript.

FUNDING

This work was supported by the National Key Research and Development Program of China under Grant no. 2016YFC1000306.

ACKNOWLEDGMENTS

We thank the proband and other contributors for their participation.

REFERENCES

1. Cohen M, Hall B, Smith D, Graham C, Lampert K. A new syndrome with hypotonia, obesity, mental deficiency, and facial, oral, ocular, and limb anomalies. *J Pediatrics.* (1973) 83:280–4. doi: 10.1016/S0022-3476(73)80493-7
2. Lou G, Ke Y, Zhang Y, Liangjie G, Shama S, Qi N, et al. Functional analysis of a compound heterozygous mutation in the vps13b gene in a chinese pedigree with cohen syndrome. *J Mol Neurosci.* (2020). doi: 10.1007/s12031-020-01713-6. [Epub ahead of print].
3. Momtazmanesh S, Rayzan E, Shahkarami S, Rohlfs M, Klein C, Rezaei N. A novel VPS13B mutation in Cohen syndrome: a case report and review of literature. *BMC Med Genet.* (2020) 21:140. doi: 10.1186/s12881-020-01075-1
4. Rodrigues JM, Fernandes HD, Caruthers C, Braddock SR, Knutsen AP. Cohen syndrome: review of the literature. *Cureus.* (2018) 10:e3330. doi: 10.7759/cureus.3330
5. Kivitie-Kallio S, Norio R. Cohen syndrome: essential features, natural history, and heterogeneity. *Am J Med Genet.* (2001) 102:125–35. doi: 10.1002/1096-8628(20010801)102:2<125::AID-AJMG1439>3.0.CO;2-0
6. Alipour N, Salehpour S, Tonekaboni SH, Rostami M, Bahari S, Yassaee V, et al. Mutations in the VPS13B gene in iranian patients with different phenotypes of cohen syndrome. *J Mol Neurosci.* (2020) 70:21–5. doi: 10.1007/s12031-019-01394-w
7. Boschann F, Fischer-Zirnsak B, Wienker TF, Holtgrewe M, Seelow D, Eichhorn B, et al. An intronic splice site alteration in combination with a large deletion affecting VPS13B (COH1) causes Cohen syndrome. *Eur J Med Genet.* (2020) 63:103973. doi: 10.1016/j.ejmg.2020.103973
8. Hashmi JA, Fadhli F, Almatrafi A, Afzal S, Ramzan K, Thiele H, et al. Homozygosity mapping and whole exome sequencing provide exact diagnosis of Cohen syndrome in a Saudi family. *Brain Dev.* (2020) 42:587–93. doi: 10.1016/j.braindev.2020.04.010
9. Kaushik P, Mahajan N, Girimaji SC, Kumar A. Whole exome sequencing identifies a novel homozygous duplication mutation in the VPS13B gene in an indian family with cohen syndrome. *J Mol Neurosci.* (2020) 70:1225–8. doi: 10.1007/s12031-020-01530-x
10. Megarbane A, Slim R, Nurnberg G, Ebermann I, Nurnberg P, Bolz HJ. A novel VPS13B mutation in two brothers with Cohen syndrome, cutis verticis gyrata and sensorineural deafness. *Eur J Hum Genet.* (2009) 17:1076–9. doi: 10.1038/ejhg.2008.273
11. Nasser F, Kurtenbach A, Biskup S, Weidensee S, Kohl S, Zrenner E. Ophthalmic features of retinitis pigmentosa in Cohen syndrome caused by pathogenic variants in the VPS13B gene. *Acta Ophthalmol.* (2020) 98:e316–e21. doi: 10.1111/aos.14255
12. Rafiq MA, Leblond CS, Saqib MA, Vincent AK, Ambalavanan A, Khan FS, et al. Novel VPS13B mutations in three large pakistani cohen syndrome families suggests a baloch variant with autistic-like features. *BMC Med Genet.* (2015) 16:41. doi: 10.1186/s12881-015-0183-0
13. Rejeb I, Jilani H, Elaribi Y, Hizem S, Hila L, Zillahrdt JL, et al. First case report of Cohen syndrome in the Tunisian population caused by VPS13B mutations. *BMC Med Genet.* (2017) 18:134. doi: 10.1186/s12881-017-0493-5
14. Zhao S, Luo Z, Xiao Z, Li L, Zhao R, Yang Y, et al. Case report: two novel VPS13B mutations in a Chinese family with Cohen syndrome and hyperlinear palms. *BMC Med Genet.* (2019) 20:187. doi: 10.1186/s12881-019-0920-x
15. Kolehmainen J, Black GC, Saarinen A, Chandler K, Clayton-Smith J, Traskelin AL, et al. Cohen syndrome is caused by mutations in a novel gene, COH1, encoding a transmembrane protein with a presumed role in vesicle-mediated sorting and intracellular protein transport. *Am J Hum Genet.* (2003) 72:1359–69. doi: 10.1086/375454
16. Enomoto Y, Tsurusaki Y, Yokoi T, Abe-Hatano C, Ida K, Naruto T, et al. CNV analysis using whole exome sequencing identified biallelic CNVs of VPS13B in siblings with intellectual disability. *Eur J Med Genet.* (2020) 63:103610. doi: 10.1016/j.ejmg.2018.12.015
17. Koehler K, Schuelke M, Hell AK, Schittkowski M, Huebner A, Brockmann K. A novel homozygous nonsense mutation of VPS13B associated with previously unreported features of Cohen syndrome. *Am J Med Genet A.* (2020) 182:570–5. doi: 10.1002/ajmg.a.61435
18. Yu TW, Chahrour MH, Coulter ME, Jiralerspong S, Okamura-Ikeda K, Ataman B, et al. Using whole-exome sequencing to identify inherited causes of autism. *Neuron.* (2013) 77:259–73. doi: 10.1016/j.neuron.2012.11.002
19. Seifert W, Kuhnisch J, Maritzen T, Horn D, Haucke V, Hennies HC. Cohen syndrome-associated protein, COH1, is a novel, giant Golgi matrix protein required for Golgi integrity. *J Biol Chem.* (2011) 286:37665–75. doi: 10.1074/jbc.M111.267971
20. Gao M, Yang H. VPS13: A lipid transfer protein making contacts at multiple cellular locations. *J Cell Biol.* (2018) 217:3322–4. doi: 10.1083/jcb.201808151
21. Koh K, Ishiura H, Shimazaki H, Tsutsumiuchi M, Ichinose Y, Nan H, et al. VPS13D-related disorders presenting as a pure and complicated form of hereditary spastic paraplegia. *Mol Genet Genomic Med.* (2020) 8:e1108. doi: 10.1002/mgg3.1108
22. Gauthier J, Meijer IA, Lessel D, Mencacci NE, Krainc D, Hempel M, et al. Recessive mutations in VPS13D cause childhood onset movement disorders. *Ann Neurol.* (2018) 83:1089–95. doi: 10.1002/ana.25204
23. Munoz-Braceras S, Tornero-Ecija AR, Vincent O, Escalante R. VPS13A is closely associated with mitochondria and is required for efficient lysosomal degradation. *Dis Model Mech.* (2019) 12:036681. doi: 10.1242/dmm.036681
24. Seong E, Insolera R, Dulovic M, Kamsteeg EJ, Trinh J, Bruggemann N, et al. Mutations in VPS13D lead to a new recessive ataxia with spasticity and mitochondrial defects. *Ann Neurol.* (2018) 83:1075–88. doi: 10.1002/ana.25220
25. Li L, Ji J, Han M, Xu Y, Zhang X, Liu W, et al. A Novel CD40L mutation associated with X-linked hyper IgM syndrome in a chinese family. *Immunol Invest.* (2020) 49:307–16. doi: 10.1080/08820139.2019.1638397
26. Richards S, Aziz N, Bale S, Bick D, Das S, Gastier-Foster J, et al. Standards and guidelines for the interpretation of sequence variants: a joint consensus recommendation of the American College of Medical Genetics and Genomics and the Association for Molecular Pathology. *Genet Med.* (2015) 17:405–24. doi: 10.1038/gim.2015.30
27. Yang C, Hou M, Li Y, Sun D, Guo Y, Liu P, et al. Gene analysis: a rare gene disease of intellectual deficiency-Cohen syndrome. *Int J Dev Neurosci.* (2018) 68:83–8. doi: 10.1016/j.ijdevneu.2018.05.004
28. Taban M, Memoracion-Peralta DS, Wang H, Al-Gazali LI, Traboulsi EI. Cohen syndrome: report of nine cases and review of the literature, with emphasis on ophthalmic features. *J AAPOS.* (2007) 11:431–7. doi: 10.1016/j.jaapos.2007.01.118
29. Rivera-Brugues N, Albrecht B, Wieczorek D, Schmidt H, Keller T, Gohring I, et al. Cohen syndrome diagnosis using whole genome arrays. *J Med Genet.* (2011) 48:136–40. doi: 10.1136/jmg.2010.082206
30. Seifert W, Holder-Espinasse M, Kuhnisch J, Kahrizi K, Tzschach A, Garshasbi M, et al. Expanded mutational spectrum in Cohen syndrome, tissue expression, and transcript variants of COH1. *Hum Mutat.* (2009) 30:E404–20. doi: 10.1002/humu.20886
31. Dastan J, Chijiwa C, Tang F, Martell S, Qiao Y, Rajcan-Separovic E, et al. Exome sequencing identifies pathogenic variants of VPS13B in a patient with familial 16p11.2 duplication. *BMC Med Genet.* (2016) 17:78. doi: 10.1186/s12881-016-0340-0
32. Duplomb L, Duvet S, Picot D, Jego G, El Chehadeh-Djebbar S, Marle N, et al. Cohen syndrome is associated with major glycosylation defects. *Hum Mol Genet.* (2014) 23:2391–9. doi: 10.1093/hmg/ddt630
33. Katzaki E, Pescucci C, Uliana V, Papa F, Ariani F, Meloni I, et al. Clinical and molecular characterization of Italian patients affected by Cohen syndrome. *J Hum Genet.* (2007) 52:1011–7. doi: 10.1007/s10038-007-0208-4
34. Murphy A, Flanagan O, Dunne K, Lynch S. High prevalence of Cohen syndrome among Irish travellers. *Clin Dysmorph.* (2007) 16:257–9. doi: 10.1097/MCD.0b013e3282742530

Conflict of Interest: The authors declare that the research was conducted in the absence of any commercial or financial relationships that could be construed as a potential conflict of interest.

frontiers in Pediatrics

ORIGINAL RESEARCH
published: 13 May 2021
doi: 10.3389/fped.2021.664449

Genotypes and Phenotypes of MEF2C Haploinsufficiency Syndrome: New Cases and Novel Point Mutations

Lin Wan[1,2], Xinting Liu[1,2], Linyan Hu[2], Huimin Chen[2], Yulin Sun[1,2], Zhichao Li[1,2], Zhenfang Wang[3], Zhi Lin[4], Liping Zou[1,2,5] and Guang Yang[1,2,5]**

[1] Medical School of Chinese People's Liberation Army, Beijing, China, [2] Department of Pediatrics, The First Medical Center, Chinese People's Liberation Army General Hospital, Beijing, China, [3] Department of Rehabilitation, Children Hospital of Shanxi, Taiyuan, China, [4] Department of Pediatrics, Fujian Provincial Hospital, Fuzhou, China, [5] The Second School of Clinical Medicine, Southern Medical University, Guangzhou, China

OPEN ACCESS

Edited by:
Anjana Munshi,
Central University of Punjab, India

Reviewed by:
Catarina M. Quinzii,
Columbia University, United States
Aniefiok John Udoakang,
University of Ghana, Ghana

***Correspondence:**
Guang Yang
yangg301@sina.com
Liping Zou
zouliping21@hotmail.com;
zouliping21@sina.com

Specialty section:
This article was submitted to Genetics of Common and Rare Diseases, a section of the journal Frontiers in Pediatrics

Received: *05 February 2021*
Accepted: *14 April 2021*
Published: *13 May 2021*

Citation:
Wan L, Liu X, Hu L, Chen H, Sun Y, Li Z, Wang Z, Lin Z, Zou L and Yang G (2021) Genotypes and Phenotypes of MEF2C Haploinsufficiency Syndrome: New Cases and Novel Point Mutations. Front. Pediatr. 9:664449. doi: 10.3389/fped.2021.664449

Aim: MEF2C haploinsufficiency syndrome (MCHS) is a severe neurodevelopmental disorder. We describe the clinical phenotypes and genotypes of seven patients with MCHS to enhance the understanding of clinical manifestations and genetic alterations associated with MCHS.

Method: Seven patients (6 females and 1 male, aged between 2 years 5 months and 6 years) who had MEF2C mutations, and their parents underwent trio-based whole-exome sequencing; subsequently, their clinical features were assessed. A literature review of patients with MCHS was performed by searching the PubMed and Online Mendelian Inheritance in Man databases.

Results: Seven mutations were identified, of which six were unreported in the past; of the reported cases, five patients had *de novo* mutations but two had an undefined inheritance pattern. All patients presented delays in developmental milestones, severe intellectual disabilities and lack of speech. Six patients exhibited infantile hypotonia, five patients experienced stereotypic movements and were unable to walk, four patients exhibited poor eye contact indicative of autism and two showed poor performance. While six patients experienced seizure, five among them became seizure free after receiving anti-seizure medicine. Three patients showed a regression in their development, whereas the mothers of two patients exhibited mosaicism but were healthy without any abovementioned symptoms.

Interpretation: Regression was not a common phenomenon but occurred in MCHS. The prognosis of MCHS patients with epilepsy was good, but most patients can achieve a seizure-free status. Healthy people may have low-level mosaicism and carry a pathogenic MEF2C mutation.

Keywords: MEF2C haploinsufficiency syndrome, trio-based whole-exome sequencing, regression, MOSAIC, MEF2C gene mutations

INTRODUCTION

Myocyte enhancer factor 2C (MEF2C) haploinsufficiency syndrome (MCHS) has been attributed to 5q14.3 microdeletions (MIM# 613443, developmental delay, stereotypic movements, epilepsy and/or cerebral malformations) (1) and was defined as any microdeletions of chromosome 5q14.3-5q15 that involved multiple genes (www.omim.org). After identifying similar clinical manifestations in patients with 5q14.3 microdeletion syndrome, the smallest common deletion regions were found to only contain the MEF2C gene (2). The MEF2C gene located in the 5q14.3 region is a member of the MEF2 transcription factor family; it regulates the number of excitatory synapses, dendrite morphology, and post-synaptic dendrite differentiation (3–5).

Haploinsufficiency of MEF2C was recognized as the pathogenic mechanism, in that patients with deletion, truncation, or missense mutation of this gene present with similar yet distinct phenotypes (6). To date, 23 patients have been reported to have pathogenic and likely pathogenic MEF2C variants or microdeletions without an involvement of other contiguous or distant genes (1, 6–14). Typical clinical characteristics include severe global developmental delay accompanied by absent speech, limited walking, seizures, and stereotypic movements (15). Here we have described a new cohort of seven patients with MEF2C point mutations, discussed their clinical features and reported six novel mutations as well as reviewed previous data of patients having pathogenic or likely pathogenic MEF2C variants or MEF2C microdeletions without the involvement of other contiguous or distant genes, which facilitated us to further clarify MCHS genotypes and phenotypes.

METHOD

Seven patients with confirmed MEF2C mutations who also had developmental delay, stereotypic movements or epilepsy were enrolled from the First Medical Center of PLA General Hospital, Fujian Provincial Hospital, and Children's Hospital of Shanxi. Detailed clinical information was collected including clinical manifestations, history of epilepsy, previous development status, family history, physical examination, treatments, and findings from electroencephalogram (EEG) and magnetic resonance imaging (MRI). Genomic DNA was extracted from peripheral blood leukocytes of the patients and their parents for trio-based whole-exome sequencing (Trio-WES). In accordance with the requirements of Research Ethics Board at First Medical Center of PLA General Hospital, informed consent was obtained from the patients' parents.

Trio-WES was performed for patients and their parents. One microgram of genomic DNA extracted from blood leukocytes was used for targeted exon enrichment on a NovaSeq 6000 instrument (Illumina, San Diego, CA, USA) according to the manufacturer's recommendations for paired-end 150-bp reads. Raw data were processed as previously described. Sequence Alignment/Map format files were aligned to a human genome reference sequence (GRCh38/hg18) using BWA (Burrows–Wheeler Aligner; v0.6.7), and potential duplicate paired-end reads were removed using Picard 1.109. Indel realignment and base quality score recalibration were performed using the Genome Analysis Toolkit (GATK; v3.3-0). Variants with a quality score of >30 and an alignment quality score of >20 were annotated with SeattleSeq SNP Annotation (http://snp.gs.washington.edu/ SeattleSeqAnnotation141/). Rare variants present at a frequency of >1% in dbSNP 138 and the NHLBI GO Exome Sequencing Project or those present in local exomes of unaffected individuals were excluded. Variant prioritization focused on *de novo* heterozygous mutations and compound heterozygotes or hemizygotes affecting the coding sequence (missense, non-sense, and splice-site variants and coding indels). Candidate variants were inspected with the Integrative Genomics Viewer (https://www.broadinstitute.org/igv/) and confirmed by performing Sanger sequencing. Sequence variants were numbered starting from the first base of the ATG codon based on the numbering pattern of reference sequences. Variants were named using the Alamut 2.6.1 software (Interactive Biosoftware, Rouen, France) by following the Human Genome Variation Society nomenclature. The variation was searched across the Human Gene Mutation Database (http://www.hgmd.cf.ac.uk/ac/index.php), Genome Aggregation Database (http://gnomad.broadinstitute.org/about), NCBI Clinvar (https://www.ncbi.nlm.nih.gov/clinvar/) and Gene4Denovo (http://www.genemed.tech/gene4denovo/). SIFT, Polyphen-2, CADD, M-CAP, FATHMM, MutationTaster, Mutation Assessor and dbscSNV were used to predict mutations. On the basis of the results obtained from the abovementioned experiments, the pathogenicity of these mutations was determined in accordance with the American College of Medical Genetics (ACMG) clinical variant interpretation guidelines.

Abbreviations: EEG, electroencephalogram; MCHS, MEF2C haploinsufficiency syndrome; MRI, magnetic resonance imaging; Trio-WES, trio-based whole-exome sequencing.

RESULTS

Clinical Profiles

All the seven patients were born to unrelated Han Chinese parents through normal pregnancies.

Patient 1 is a 5-year-old girl, who was observed to have severe hypotonia in her infancy and developmental delay. She was incapable of lifting her head when she was 7-month-old as well as was incapable of sitting by herself and had trouble imitating speech or actions when she was 1-year-old. By the age of 14 months, she was found to lack the ability to maintain eye contact and displayed head-shaking, hand-clapping and hand-wringing as well as bruxism. While she exhibited purposeful hand use, she presented recurrent, febrile or non-febrile, generalized tonic-clonic seizures at the age of 18 months. After receiving treatment with Levetiracetam (LEV) at 20 months, she achieved seizure-free status at the age of 2 years. At the age of 18 months and 2 years, the findings of her EEG tests revealed spike-and-slow waves with bilateral temporal involvement. Her MRI findings at the age of 14 months indicated a widened subarachnoid space (**Table 1**).

Patient 2 is a female who is currently 5 years 9 months old. She exhibited a delay in achieving some developmental milestones,

TABLE 1 | Clinical phenotype of patients with MEF2C gene mutation.

No.	P1	P2	P3	P4	P5	P6	P7
Age	**5 years**	**5 years 9 months**	**4 years 4 months**	**2 years 10 months**	**6 years**	**2 years 7 months**	**2 years 5 months**
Sex	F	F	F	F	F	M	F
Genetic defect	c.9A>T, (p.Arg3Ser)	c.78delT, (p.Phe26Leufs*3)	c.833_834insTT, (p.Leu278Phefs*1)	c.55-2(1VS2)A>G	C.44G>C, (p.R15P)	c.1A>G, (p.Met1Val)	c.3G>A, (p.Met1?)
Origin	Unknown	*De novo*	*De novo*	*De novo*	*De novo*	*De novo*	Unknown
Variation type	Missense	Frameshift	Frameshift	Splice site	Missense	Affecting the translation initiation site	Affecting the translation initiation site
Febrile seizure	+	+	+	+	-	+	-
Seizure type	Recurrent FS, GTC	Recurrent FS, GTC	Recurrent FS, absence	Recurrent FS, dystonic	GTC, IS	Recurrent FS, GTC	-
Age of seizure onset (months)	1.5 years	10 months	8 months	11 months	6 months	9 months	NA
ASM	LEV	LEV, OXC	LEV, VPA	OXC	VGB, LEV, VPA	VPA, OXC, TPM	NA
ASM response	Seizure free	Seizure free	Seizure free	Seizure free	Seizure free	No response	NA
Stereotypic movements	+	+	+	+	-	-	+
Poor hand skills	-	-	-	-	+	-	+
Delays in milestones	+	+	+	+	+	+	+
Independent sitting/age	1 year	1 year	8–9 months	1 year	-	9 months but regressed	2 years
Independent walking/age (months)	-	2 years	2 years	-	-	-	-
Infantile dystonia	Hypotonia	-	Hypotonia	Hypotonia	Hypotonia	Hypotonia	Hypotonia
Speech	-	-	-	-	-	-	-
Regression	-	+	-	+	-	+	-
Poor eye contact/autistic features	+	-	+	-	+	-	+
MRI	Frontal subarachnoid space enlargement	Normal	Delayed myelination	Normal	Delayed myelination	Small splenium of callosum	Normal
EEG	Bilateral temporal spike-slow waves	Bilateral temporal and occipital spike-slow waves	Generalized sharp-slow waves	Normal	Hypsarrhythmia	Left temporal and occipital slow waves	Left occipital 2–3 Hz sharp-slow waves in sleep

FS, febrile seizure; GS, generalized seizures; GTC, generalized tonic-clonic seizures; IS, infantile spasms; LEV, levetiracetam; NA, not available; OXC, oxcarbazepine; PB, phenobarbital; PS, partial seizure; TPM, topiramate; VGB, vigabatrin; VPA, valproic acid; WMH, white matter hyperintensity.

such as head lifting at 4 months, independent sitting at 1 year and independent walking at 2 years. She could say "baba," or "mama" at the age of 1 year but exhibited regression in development with subsequent instances of only unconscious articulation. Nevertheless, she possessed non-verbal communication skills. Hand clapping was observed at 8 months. She displayed good eye contact as well as a purposeful hand use. She presented recurrent, febrile or non-febrile, generalized tonic-clonic seizures at 10 months; after being treated with LEV at the age of 15 months, she achieved a seizure-free status. Her seizure, which was characterized as a generalized tonic seizure without fever, relapsed at the age of 3 years and was treated with valproate (VPA) and LEV. She achieved a seizure-free status when she was 3.5 years old. EEG (15 months) findings revealed spike-and-slow waves with bilateral temporal and occipital involvement. MRI findings at the age of 10 months were normal (**Table 1**).

Patient 3 is a female who is currently 4 years 4 months old. She showed some signs of developmental delay, such as lifting her head at the age of 5 months, sitting independently at the age of 9 months, and walking at the age of 2 years; she also did not exhibit any non-verbal communication skills and could not imitate actions or babble. Poor eye contact was observed at the age of 8 months. Hand clapping and hand wringing were observed when she was 1 year 6 months old. She demonstrated purposeful hand use, and at the age of 8 months, she experienced recurrent, febrile or non-febrile, generalized

tonic-clonic seizures. She presented with status epilepticus, which later became absence status epilepticus at the age of 3 years 2 months. At this time, she was started on LEV medication but showed no response to it; subsequently, VPA was added to the treatment strategy at the age of 3 years 6 months, and the patient finally achieved a seizure-free status at the age of 4 years. Her EEG tests at the age of 15 months demonstrated sharp-slow synthetical waves at the left central and left parietal-frontal regions. EEG showed generalized sharp-slow waves and MRI findings indicated delayed myelination in the periventricular area at the age of 3 years 2 months (**Table 1**).

Patient 4 is a female who is currently 2 years 10 months old. Developmental delay was observed with regard to lifting of her head only at the age of 7 months and the ability to sit independently only at the age of 1 year; she also did not have the ability to walk independently and did not display any non-verbal communication skills. Although she could say the words "baba" or "mama" at the age of 2 years, she displayed a regression in development and only showed signs of unconscious articulation subsequently. Poor eye contact, head shaking, hand clapping, hand wringing, and bruxism were observed at the age of 1 year 3 months. Purposeful hand use was presented and retained. She experienced recurrent, febrile or non-febrile, generalized tonic-clonic seizures at the age of 11 months. Dystonic seizure occurred at 14 months. LEV was administered at the age of 16 months and the patient achieved seizure-free status at the age of 2.5 years. Her EEG (15 months and 2.5 years) and MRI (3 year) findings revealed normal findings (**Table 1**).

Patient 5 is a female who is currently aged 6 years; she was observed to have severe hypotonia at infancy and exhibited developmental delay. She could lift her head at 4 months but has not been able to sit or walk independently; she also did not display any non-verbal communication skills and was unable to imitate or babble. Poor eye contact was observed at 5 months. She did not exhibit purposeful hand usage. She presented generalized tonic-clonic seizure at the age of 6 months, which was treated with VPA; the patient responded positively to this treatment at the age of 7 months. However, seizure, which was characterized as spasms and of the tonic-clonic type, recurred at 1 year and 7 months; adrenocorticotropic hormone was used to treat this did not produce a positive outcome. Subsequently, vigabatrin, LEV and VPA were used for treatment; this treatment had a positive effect, and the patient achieved seizure-free status at the age of 2 years 7 months. Her EEG test revealed spike-slow waves with bilateral occipital involvement at the age of 6 months and hypsarrhythmia at 2 years of age. MRI scans taken at the age of 2 years showed delayed myelination in the periventricular region (**Table 1**).

Patient 6 is a male who is currently 2 years 7 months old. He was observed to have severe hypotonia in his infancy and developmental delay. He was incapable of lifting his head at the age of 5 months but could sit independently at 9 months; however, he exhibited a regression in development and was unable to walk independently. He also did not show any non-verbal communication skills and was unable to imitate or babble. Poor eye contact, head shaking, hand clapping and hand wringing were observed at the age of 1 year and 6 months. The patient displayed purposeful hand usage. He also presented recurrent, febrile or non-febrile, generalized tonic-clonic seizures at the age of 9 months. Topiramate, VPA and LEV were used but none of them showed a positive effect; this treatment was withdrawn at the age of 2 years. At present, the patient's daily seizures have been characterized as myoclonic. EEG findings obtained at the age of 10 months revealed spike-slow waves with bilateral-central-frontal involvement. MRI scans taken at the age of 15 months showed developmental malformation of the corpus callosum (**Table 1**).

Patient 7 is a female who is currently 2 years 5 months old. She experienced severe hypotonia at infancy and was observed to have developmental delay. She was incapable of both lifting her head at the age of 7 months and sitting independently at the age of 2 years; she was also unable to walk independently, demonstrated no non-verbal communication skills, and was unable to imitate or babble. Poor eye contact as well as head-shaking and hand-clapping behavior were observed at the age of 1 year. She did not display purposeful hand usage. She did not experience seizure. EEG test conducted at the age of 2 years revealed 2–3 Hz sharp-slow waves at the left parietal-occipital region. MRI scans taken at the age of 14 months showed malformation of the corpus callosum, delayed myelination and leukomalacia in the periventricular region (**Table 1**).

Sequencing Analysis of Trio-WES Tests

Trio-WES revealed two ambiguously inherited (P1, c.9A>T, p.Arg3Ser, P1's mother, c.9A>T, mosaic, 10/119; P7, c.3G>A, p.Met1, P7's mother, c.9A>T, mosaic, 8/113) and five *de novo* [P2, c.78delT, p.Phe26Leufs*3; P3, c.833_834insTT, p.Leu278 Phefs*1; P4, c.55-2 (1VS2) A>G; P5, c.44G>C, p.Arg15Pro; P6, c.1A>G, p.Met1Val] heterozygous mutations in the MEF2C gene. All these mutations were searched across the databases mentioned in the section Methods; because P2 and P3 mutations lead to the formation of a truncated protein, the other five mutations were assessed using the mutation prediction tools mentioned previously. Subsequently, the clinical implications and considerations for evaluating *in silico* algorithms that can be used along with the clinical variant interpretation guidelines established by the American College of Medical Genetics were investigated; five mutations were classified as pathogenetic, two mutations were considered to be likely pathogenic (more details see **Supplementary Table 1**).

DISCUSSION

In cases where the gene is abnormally expressed owing to mutation or deletion and a lower level of protein is produced; therefore, insufficient material for maintaining normal cellular physiological functions leads to MCHS (1). Patients with MCHS often exhibit delayed developmental milestones, severe intellectual disabilities, limited or absent speech, seizures, hypotonia, limited walking abilities, and stereotypic movements (12).

All seven patients in our cohort presented delays in developmental milestones, severe intellectual disabilities, and absent speech. Six patients exhibited infantile hypotonia and

five cases showed stereotypic movements; these symptoms were also common in the 23 patients reported previously (100, 100, 95.7, 78.2, and 73.9%) (1, 6–14). Four cases in our cohort had poor eye contact, indicative of autism, while two cases showed poor hand skills. Of the 23 patients in the previous study (1, 6–14), 18 were evaluated for autism-related manifestations and 13 of these patients reported autism-like manifestation; furthermore, 14 of the 23 patients were evaluated for hand function of whom 5 were reported to have poor hand skills. The results of our study are consistent with the proportion of these two manifestations reported in previous studies. Brain MRI scans revealed abnormalities in five cases, similar to those reported previously (12); however, the manifestations were varied and included delayed myelination, frontal subarachnoid space enlargement, and corpus callosum dysgenesis. Wang et al. (13) noted that MCHS was more common in females than in males, but the same pattern was observed in our cohort. It is worth noting that in our study, five patients were unable to work, which is significantly higher than the proportion reported in the literature. However, at present, we cannot comment on whether the children in our cohort may acquire the ability to work in the future.

Six patients experienced seizure, including five with onset at infancy, which was consistent with the proportion reported in previous studies; 18 patients of the 23 patients analyzed were found to experience seizures, and 12 of those patients showed onset when they were <1-year-old (8, 12). Febrile seizures were very common in our cohort (5/7); similarly, three out of five patients described by Wang et al. had febrile convulsions (13). Previous descriptions of seizure outcome in such patients are limited as only seven patients had described the response to antiseizure medicine (ASM). Six achieved seizure-free status, and one patient showed partial response (1, 8, 11, 13, 14). At present in our cohort, six patients received ASM and only one patient experienced refractory epilepsy. Seizures experienced by the other five patients were effectively controlled, including the case with infantile spasm, which is a severe form of epilepsy. Most patients with epilepsy and MCHS exhibited good responses to ASM and achieved a seizure-free status. There does not seem to be a significant difference between the choice of ASM and treatment outcome.

Regression has only been described in two patients with MCHS (1, 13). Contrary to the reports found in the literature, three patients (P2, P4, and P6) in our cohort also showed clinical regression. Zweier et al. concluded that the loss of MEF2C function in humans can significantly reduce the gene expressions levels of MeCP2 and CDKL5, and MEF2C mutations reduce synergistic reactivation of the E-box promoter of MeCP2 and CDKL5 (15). MeCP2 is the pathogenic gene responsible for Rett syndrome (16), and the stereotypical loss of motor and language skills and developmental delay encountered in autism were also observed in patients with Rett syndrome; this result overlaps with MCHS and causes some difficulties in MCHS diagnosis. However, delayed early life development may help distinguish between the two conditions.

Sixteen MEF2C point mutations were previously described (1, 7–9, 11–14). Seven patients in our cohort had MEF2C point mutations, including six novel mutations. Specifically, two variants (c.3G>A, p.Met1?; c.1A>G, p.Met1Val) affecting the translation initiation site had not been described in previous studies. On reviewing previous studies as well as our cohort, we found an interesting phenomenon: patients with intragenic deletions seemed more likely to be ambulatory than the patients with point mutations in MEF2C (6/7 vs. 9/23). This contradicts with the observations reported by Wang et al.; however, we need to investigate more cases to support our hypothesis. Variants affecting the translation initiation site have not yet been reported. Patients 6 and 7 in our study were affected by this type of point mutation, but they exhibited different clinical phenotypes. P6 showed persistent drug-resistant epilepsy and developmental regression, whereas P7 did not.

The human MEF2C protein consists of six core structural domains, including MADS (MCM1, agamous, deficiens, serum response factor), myocyte enhancer factor 2 (MEF2), HJURP-C (Holliday junction recognition protein C-terminal), transcriptional activation domain 1 (TAD1), transcriptional activation domain 2 (TAD2) and a nuclear localization signal (NLS). The MADS domain contains 56 amino acids, while the MEF2 domain spans amino acids 57–86. The HJURP-C domain consisting of 29 amino acids was adjacent to the MEF2 domain and followed by two transcriptional activation domains (TAD1 and TAD2), which are responsible for activating transcription. The NLS domain (nuclear localization signal) is located at the C-terminus of MEF2C, which controls nuclear translocation of the protein. The MADS and MEF2C domains mediate dimerization and DNA binding, and the other domains act as transcriptional activators (17). The reported mutation sites (including those in our study) do not have a specific distribution within the structural domains, and there are no obvious phenotypes indicating mutation sites in hot spots (**Figure 1**). Among our small cohort, there was no obvious correlation between clinical phenotype and mutation sites across different domains.

To date, only 30 patients with MEF2C point mutations, including the 7 cases described here, have been identified (1, 6, 7, 9, 11–14), which limited our ability to analyze correlations. There was no obvious genotype–phenotype correlation after classification, suggesting that more clinical cases are needed for conducting further analyses. All mutations reported in the published papers were *de novo*, and two of the seven patients (P1 and P7) in our cohort had mutations whose inheritance pattern remains unclear, with their mothers having low-level mosaicism (mother of P1: 10/119; mother of P7: 8/113). MCHS was previously considered to be an autosomal dominant disease, and healthy mosaicism has not yet been reported. To our knowledge, this is the first description of such a phenomenon, which leads us to speculate that a low-level mosaicism does not cause MCHS.

This was a small cohort study, so we cannot draw firm conclusions about the phenotypic–genotypic associations. Similarly, owing to technical reasons and the subjects' refusal to undergo further studies, we could not further analyze

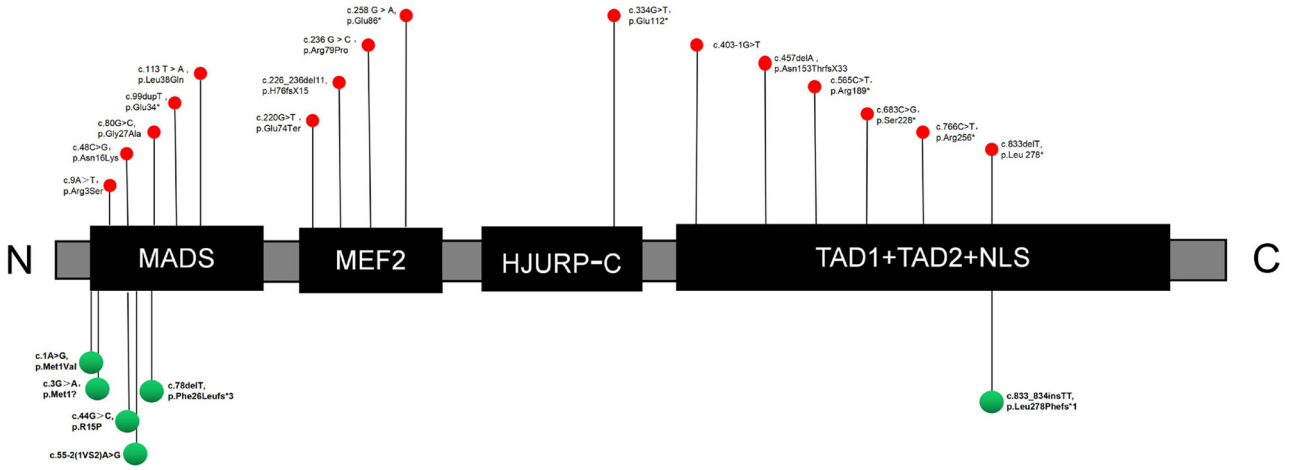

FIGURE 1 | Sites of mutations in the MEF2C protein. Red and green indicate reported mutations and novel mutations detected in this study, respectively. C, C-terminus; N, N-terminus; MADS, MCM1, agamous, deficiens, serum response factor; MEF2, myocyte enhancer factor 2; HJURP-C, Holliday junction recognition protein C-terminal; NLS, nuclear location signal; TAD, transcriptional activation domain.

the genetic patterns of the two cases; however, we suspect that the patients inherited the mutated gene from the mother in both instances as their mothers carried the same mutation.

CONCLUSION

We described six novel MEF2C gene mutations. Although the clinical manifestations of MCHS are diverse, common features include global developmental delay, impaired language function, seizure, stereotyped behavior, infantile hypothermia, and abnormal brain MRI findings. Although regression was not a common phenomenon, it was reported to occur occasionally. Currently, it has been difficult to establish a clear genotype-phenotype relationship in MCHS, which should be the focus of future research. Although patients with MCHS often experience seizures during the early stages of their life, most patients eventually achieve a seizure-free status. People without any MCHS symptoms may also have low-level mosaicism and carry the pathogenic MEF2C mutation that can be passed on to their offspring.

DATA AVAILABILITY STATEMENT

The data presented in the study are deposited in the China National Genebank repository, accession number is CNP0001827.

ETHICS STATEMENT

The studies involving human participants were reviewed and approved by Ethics Committee of the PLA General Hospital. Written informed consent to participate in this study was provided by the participants' legal guardian/next of kin.

AUTHOR CONTRIBUTIONS

LW and GY wrote the first draft of this manuscript. LZ and GY contributed to study conception and design. All authors helped revise the manuscript with regard to important intellectual content.

FUNDING

This research was funded by the National Natural Science Foundation of China (Reference: 81671279) and the Medical Big Data and Artificial Intelligence Research and Development Project of the Chinese PLA General Hospital (Reference: 2019MBD-004).

SUPPLEMENTARY MATERIAL

The Supplementary Material for this article can be found online at: https://www.frontiersin.org/articles/10.3389/fped.2021.664449/full#supplementary-material

REFERENCES

1. Le Meur N, Holder-Espinasse M, Jaillard S, Goldenberg A, Joriot S, Amati-Bonneau P, et al. MEF2C haploinsufficiency caused by either microdeletion of the 5q14.3 region or mutation is responsible for severe mental retardation with stereotypic movements, epilepsy and/or cerebral malformations. *J Med Genet*. (2010) 47:22–9. doi: 10.1136/jmg.2009.069732
2. Novara F, Beri S, Giorda R, Ortibus E, Nageshappa S, Darra F, et al. Refining the phenotype associated with MEF2C haploinsufficiency. *Clin Genet*. (2010) 78:471–7. doi: 10.1111/j.1399-0004.2010.01413.x

3. Shalizi A, Gaudillière B, Yuan Z, Stegmüller J, Shirogane T, Ge Q, et al. A calcium-regulated MEF2 sumoylation switch controls postsynaptic differentiation. *Science*. (2006) 311:1012–7. doi: 10.1126/science.1122513
4. Barbosa AC, Kim MS, Ertunc M, Adachi M, Nelson ED, McAnally J, et al. MEF2C, a transcription factor that facilitates learning and memory by negative regulation of synapse numbers and function. *Proc Natl Acad Sci USA*. (2008) 105:9391–6. doi: 10.1073/pnas.0802679105
5. Li Z, McKercher SR, Cui J, Nie Z, Soussou W, Roberts AJ, et al. Myocyte enhancer factor 2C as a neurogenic and antiapoptotic transcription factor in murine embryonic stem cells. *J Neurosci*. (2008) 28:6557–68. doi: 10.1523/JNEUROSCI.0134-08.2008
6. Srivastava S, Cohen JS, Vernon H, Barañano K, McClellan R, Jamal L, et al. Clinical whole exome sequencing in child neurology practice. *Ann Neurol*. (2014) 76:473–83. doi: 10.1002/ana.24251
7. Zweier M, Gregor A, Zweier C, Engels H, Sticht H, Wohlleber E, et al. Mutations in MEF2C from the 5q14.3q15 microdeletion syndrome region are a frequent cause of severe mental retardation and diminish MECP2 and CDKL5 expression. *Hum Mutat*. (2010) 31:722–33. doi: 10.1002/humu.21253
8. Bienvenu T, Diebold B, Chelly J, Isidor B. Refining the phenotype associated with MEF2C point mutations. *Neurogenetics*. (2013) 14:71–5. doi: 10.1007/s10048-012-0344-7
9. Paciorkowski AR, Traylor RN, Rosenfeld JA, Hoover JM, Harris CJ, Winter S, et al. MEF2C Haploinsufficiency features consistent hyperkinesis, variable epilepsy, and has a role in dorsal and ventral neuronal developmental pathways. *Neurogenetics*. (2013) 14:99–111. doi: 10.1007/s10048-013-0356-y
10. Tanteles GA, Alexandrou A, Evangelidou P, Gavatha M, Anastasiadou V, Sismani C. Partial MEF2C deletion in a Cypriot patient with severe intellectual disability and a jugular fossa malformation: review of the literature. *Am J Med Genet A*. (2015) 167A:664–9. doi: 10.1002/ajmg.a.36945
11. Rocha H, Sampaio M, Rocha R, Fernandes S, Leão M. MEF2C haploinsufficiency syndrome: report of a new MEF2C mutation and review. *Eur J Med Genet*. (2016) 59:478–82. doi: 10.1016/j.ejmg.2016.05.017
12. Vrečar I, Innes J, Jones EA, Kingston H, Reardon W, Kerr B, et al. Further clinical delineation of the MEF2C haploinsufficiency syndrome: report on new cases and literature review of severe neurodevelopmental disorders presenting with seizures, absent speech, and involuntary movements. *J Pediatr Genet*. (2017) 6:129–41. doi: 10.1055/s-0037-1601335
13. Wang J, Zhang Q, Chen Y, Yu S, Wu X, Bao X, et al. Novel MEF2C point mutations in Chinese patients with Rett (-like) syndrome or non-syndromic intellectual disability: insights into genotype-phenotype correlation. *BMC Med Genet*. (2018) 19:191. doi: 10.1186/s12881-018-0699-1
14. Borlot F, Whitney R, Cohn RD, Weiss SK. MEF2C-related epilepsy: delineating the phenotypic spectrum from a novel mutation and literature review. *Seizure*. (2019) 67:86–90. doi: 10.1016/j.seizure.2019.03.015
15. Zweier M, Rauch A. The MEF2C-related and 5q14.3q15 microdeletion syndrome. *Mol Syndromol*. (2012) 2:164–70. doi: 10.1159/000337496
16. Sandweiss AJ, Brandt VL, Zoghbi HY. Advances in understanding of Rett syndrome and MECP2 duplication syndrome: prospects for future therapies. *Lancet Neurol*. (2020) 19:689–98. doi: 10.1016/S1474-4422(20)30217-9
17. Dong C, Yang XZ, Zhang CY, Liu YY, Zhou RB, Cheng QD, et al. Myocyte enhancer factor 2C and its directly-interacting proteins: a review. *Prog Biophys Mol Biol*. (2017) 126:22–30. doi: 10.1016/j.pbiomolbio.2017.02.002

Conflict of Interest: The authors declare that the research was conducted in the absence of any commercial or financial relationships that could be construed as a potential conflict of interest.

frontiers in Genetics

CASE REPORT
published: 21 June 2021
doi: 10.3389/fgene.2021.692087

Case Report: *SATB2*-Associated Syndrome Overlapping With Clinical Mitochondrial Disease Presentation: Report of Two Cases

Yuri A. Zarate[1], Hilary J. Vernon[2], Katherine A. Bosanko[1], Praveen K. Ramani[3], Murat Gokden[4], Karin Writzl[5], Marija Meznaric[6], Tina Vipotnik Vesnaver[7], Raghu Ramakrishnaiah[8] and Damjan Osredkar[9]*

[1] Section of Genetics and Metabolism, University of Arkansas for Medical Sciences, Little Rock, AR, United States, [2] Department of Genetics, Johns Hopkins University School of Medicine, Baltimore, MD, United States, [3] Department of Pediatric Neurology, University of Arkansas for Medical Sciences, Little Rock, AR, United States, [4] Department of Pathology, University of Arkansas for Medical Sciences, Little Rock, AR, United States, [5] Clinical Institute of Medical Genetics, University Medical Centre Ljubljana, Ljubljana, Slovenia, [6] Faculty of Medicine, Institute of Anatomy, University of Ljubljana, Ljubljana, Slovenia, [7] Department of Radiology, University Medical Centre Ljubljana, Ljubljana, Slovenia, [8] Division of Neuroradiology and Pediatric Radiology, University of Arkansas for Medical Sciences, Little Rock, AR, United States, [9] Department of Pediatric Neurology, University Children's Hospital, University Medical Centre Ljubljana, Ljubljana, Slovenia

OPEN ACCESS

Edited by:
Muhammad Ayub, Queens University, Canada

Reviewed by:
Emanuela Bottani, University of Verona, Italy
Qifei Li, Boston Children's Hospital and Harvard Medical School, United States

***Correspondence:**
Yuri A. Zarate
yazarate@uams.edu

Specialty section:
This article was submitted to Genetics of Common and Rare Diseases, a section of the journal Frontiers in Genetics

Received: *07 April 2021*
Accepted: *14 May 2021*
Published: *21 June 2021*

Citation:
Zarate YA, Vernon HJ, Bosanko KA, Ramani PK, Gokden M, Writzl K, Meznaric M, Vipotnik Vesnaver T, Ramakrishnaiah R and Osredkar D (2021) Case Report: SATB2-Associated Syndrome Overlapping With Clinical Mitochondrial Disease Presentation: Report of Two Cases. Front. Genet. 12:692087. doi: 10.3389/fgene.2021.692087

SATB2-associated syndrome (SAS) is an autosomal dominant neurogenetic multisystemic disorder. We describe two individuals with global developmental delay and hypotonia who underwent an extensive evaluation to rule out an underlying mitochondrial disorder before their eventual diagnosis of SAS. Although the strict application of the clinical mitochondrial disease score only led to the designation of "possible" mitochondrial disorder for these two individuals, other documented abnormalities included nonspecific neuroimaging findings on magnetic resonance imaging and magnetic resonance spectroscopy, decreased complex I activity on muscle biopsy for patient 2, and variation in the size and relative proportion of types of muscle fibers in the muscle biopsies that were aligned with mitochondrial diseases. SAS should be in the differential diagnoses of mitochondrial disorders, and broad-spectrum diagnostic tests such as exome sequencing need to be considered early in the evaluation process of undiagnosed neurodevelopmental disorders.

Keywords: *SATB2*, glass syndrome, mitochondrial disease, muscle biopsy, *SATB2*-Associated syndrome

INTRODUCTION

Mitochondrial diseases are a heterogeneous group of clinical disorders due to deficiency of the respiratory chain. While primary mitochondrial disease (PMD) refers to disorders whose underlying genetic cause directly impairs the composition or function of the electron respiratory chain, secondary mitochondrial dysfunction (SMD), by contrast, refers to any abnormal mitochondrial function other than PMD (Falk, 2010). A broad variety of disorders and pathologic processes can result in SMD including myopathies and muscular dystrophies, other genetic disorders, chromosomal abnormalities, neurodegenerative disorders, inborn errors of metabolism, and autism spectrum disorders (ASDs), among others (Falk, 2010; Niyazov et al., 2016; Frye, 2020).

Phenotypically, whether PMD or SMD, mitochondrial disorders are typically characterized by a broad clinical spectrum often involving multiple organs such as skeletal muscles, brain, heart, liver, kidney, or endocrine glands (Bianchi et al., 2003). With overlapping clinical phenotypes being caused by alterations in several different genes and mutations in the same mitochondrial disease gene leading to different phenotypes, the diagnosis of mitochondrial disease is often challenging. Most diagnostic algorithms include a combination of clinical, biochemical, neuroradiologic, and genetic data (Parikh et al., 2015; Witters et al., 2018).

SATB2-associated syndrome (SAS; Glass syndrome, OMIM 612313) is an autosomal dominant neurogenetic multisystemic disorder caused by variants in *SATB2* at 2q33.1 (Zarate et al., 2019). Clinical features of SAS include developmental delay with severe speech delay, hypotonia, palate and dental abnormalities, behavioral difficulties, seizures, and skeletal anomalies (Zarate and Fish, 2017). Individuals with SAS are also often found to have nonspecific abnormalities on neuroimaging such as delayed myelination or abnormal white matter hyperintensities [T2/fluid-attenuated inversion recovery (FLAIR)] (Lewis et al., 2020). Here, we report two individuals with SAS who were extensively examined for a possible mitochondrial disorder before their molecular testing that confirmed an alteration in *SATB2*. Given the described overlapping clinical phenotypes between mitochondrial diseases and SAS, particularly early in life, we conclude that SAS should be considered in the differential diagnosis of individuals undergoing evaluation for mitochondrial dysfunction.

MATERIALS AND METHODS

Participants were recruited into the SAS clinical registry through a referral by a treating clinician, a facilitated inquiry by the testing laboratory, direct contact by a caregiver, or via the SAS support group. Individuals with a molecularly confirmed diagnosis of SAS were eligible for the study. Medical records including laboratory results were reviewed.

Molecular Investigations

Patient 1

Initially, targeted exome sequencing (ES) was performed using next-generation sequencing on the isolated DNA sample. The fragmentation and enrichment of the isolated DNA sample were performed according to the protocol Illumina TruSight One, with subsequent sequencing on Illumina MiSeq (Illumina Inc., San Diego, CA). After duplicates were removed, the alignment of reads to UCSC hg19 reference assembly was done using BWA algorithm (v0.6.3), and variant calling was done using GATK framework (v2.8). Proband whole ES was performed as previously described (Bergant et al., 2018). The pathogenic variant was confirmed by Sanger sequencing in the proband. Parental testing was performed on blood-derived DNA by Sanger sequencing. Reanalysis of the initial clinical ES data revealed that the *SATB2* variant was missed because of low coverage. The analysis of the mitochondrial genome was performed using next-generation sequencing of the source DNA sample. Variant calling was performed using HaplotypeCaller in GATK v 2.8. The analysis of variants detected in the mitochondrial genome was performed using MITOMASTER tool [with Cambridge Reference Sequence (rCRS)] and MitoSeek.

Patient 2

Trio ES was performed according to standard procedures (Retterer et al., 2016). The entire mitochondrial genome was amplified and sequenced using solid-state sequencing by synthesis process. DNA sequence was assembled and analyzed in comparison to rCRS.

Biochemical and Histological Investigations

Muscle biopsies were processed by a standard battery of histological, histochemical, and immunohistochemical investigations (Dubowitz and Sewry, 2007). For both individuals, oxidative phosphorylation enzymology activities (complex I, II, III, and IV) were tested in a mitochondrial preparation that was immediately isolated from skeletal muscle with enzymatic activities normalized for citrate synthase activity (Bugiani et al., 2004). For patient 1, analysis for the expression of myosin heavy-chain isoforms with quantitative analysis of muscle fiber diameters and an immunohistochemical analysis for the expression of laminin α2 (antibodies reacting with fragments 80 and 300 kDa of laminin) was also conducted (Sewry, 2000).

CASE PRESENTATIONS

Patient 1 (SATB2-214)

The patient was born at 39 weeks' gestation with birth weight of 3.55 kg (66th centile), length of 53 cm (95th centile), and head circumference of 35 cm (66th centile). Prenatally, his mother received escitalopram during the first 8 weeks of gestation. Family history was significant for a maternal uncle with epilepsy. At 2 months, he was noted to have decreased eye contact, and an ophthalmology evaluation showed strabismus with horizontal nystagmus. At 8 months, he was noted to have hypotonia. He walked at 27 months, and by 36 months of age, he displayed global developmental delay and was receiving all therapies. He said his first word at 6 years of age. Psychological testing at 6 years 10 months of age (Bayley scales of infant development III) revealed cognitive development equal to age appropriate achievements of 23 months.

At 8 months, his initial metabolic laboratories were largely unremarkable (**Table 1**). Brain magnetic resonance imaging (MRI) at 14 months showed patchy areas of higher intensity signal on T2 and FLAIR sequences in the deep white matter bilaterally. Magnetic resonance spectroscopy (MRS) showed various regions with high choline with normal *N*-acetylaspartate (NAA)/creatinine ratio. At 21 months of age, muscle biopsy revealed no morphological abnormalities of the mitochondria and normal respiratory enzyme activity (**Supplementary Figure 1**). Morphometry showed slight hypotrophy of both types 1 and 2 myofibers, but normal variability coefficients of muscle fiber diameters. Repeat brain MRI at 49 months showed abnormal high signal in the deep white

TABLE 1 | Clinical characteristics of two individuals with *SATB2*-associated syndrome.

	Patient 1 (SATB2-214)	**Patient 2 (SATB2-79)**
Gender	Male	Male
Mutation (DNA)	c.1165C>T	c.1515delT
Substitution (protein)	p.(Arg389Cys)	p.(Phe505Leufs*41)
Inheritance	*De novo*	*De novo*
Age at last examination	7 years	19 years
Clinical		
Developmental delay	Global, severe	Global, severe
Hypotonia	Yes	Yes
Growth retardation	No	Early in infancy
Epilepsy	No	Single febrile seizure
Testing		
Brain MRI (age)	Delayed myelination; increased T2 and FLAIR signal in deep white matter (14 and 49 months)	Delayed myelination, increased T2 signal in the periatrial white matter, mild ventricular dilatation, and anterior thinning of corpus callosum (1, 2, and 4 years)
Brain MRS (age)	Slightly elevated lipid peak (49 months)	Slight decrease in N-acetylaspartate (18 months)
Muscle biopsy (age)	Mild hypotrophy of fast and slow twitch muscle fibers; no morphological mitochondrial changes (21 months)	Occasional atrophic appearing type I and neural cell adhesion molecule positive myofibers (4 years)
Respiratory chain findings	Normal	Abnormal; decreased complex I, complex I + III, and complex II + III activity
Plasma amino acids	At 8 months, alanine 1.3× above normal	Unremarkable
Urine organic acids	Unremarkable	Unremarkable
Urine amino acids	N/A	Unremarkable
Carnitine	Normal	Normal
Lactate	Normal	Normal
Pyruvate	Normal	Normal
Creatine phosphokinase	N/A	Normal
Cerebrospinal fluid lactate	Normal	Normal
Mitochondrial DNA (muscle)	Negative	Negative
Mitochondrial DNA (blood)	Negative	Negative
Mitochondrial disease criteria (points)		
Muscular	1 (Motor developmental delay)	1 (Motor developmental delay)
Neurological	2 (Developmental delay, speech delay)	2 (Developmental delay, speech delay)
Multisystem	0	1 (Growth delay early)
Metabolic	0	0
Imaging	0	0
Total points (clinical, metabolic, imaging)	3/8 (Possible)	4/8 (Possible)
Morphology	0	0
Total mitochondrial disease criteria (MDC) score	3/12	4/12

matter temporally, parietally, and occipitally (**Figures 1A,B**) with a largely unremarkable MRS (reported as subtle peak of lipids and α-glutamate, **Figure 1C**). At 4 years of age, targeted ES was normal. Sequencing of the mitochondrial genome from muscle- and blood-derived DNA was normal. At 7 years, whole ES revealed a pathogenic variant in *SATB2* (NM_001172509.1), c.1165C>T, and p.(Arg389Cys). The variant was not found in DNA derived from parental lymphocytes.

Patient 2 (SATB2-79)

This individual was previously reported as part of a large cohort study with no detailed clinical information provided (Zarate et al., 2019). He was born at 36 weeks' gestation weighing 2.94 kg (70th centile) and 53.3 cm long (98th centile). Pregnancy was complicated by preterm labor at 28 weeks of age, and family history was noncontributory. He had a significant delay in his motor milestones, sitting by 11 months and walking at 21 months. Speech delay was noticeable during the second year of life but with little progression over time. From early infancy, he was a poor feeder and was diagnosed with failure to thrive necessitating a gastrostomy feeding tube (G-tube), which was placed at 2 years of age. He had a single febrile seizure at 3 years of age. Starting in childhood, the patient exhibited behavioral problems including self-stimulatory behaviors, hoarding, and other obsessive–compulsive behaviors. He was diagnosed with ASD. On his most recent evaluation at 19

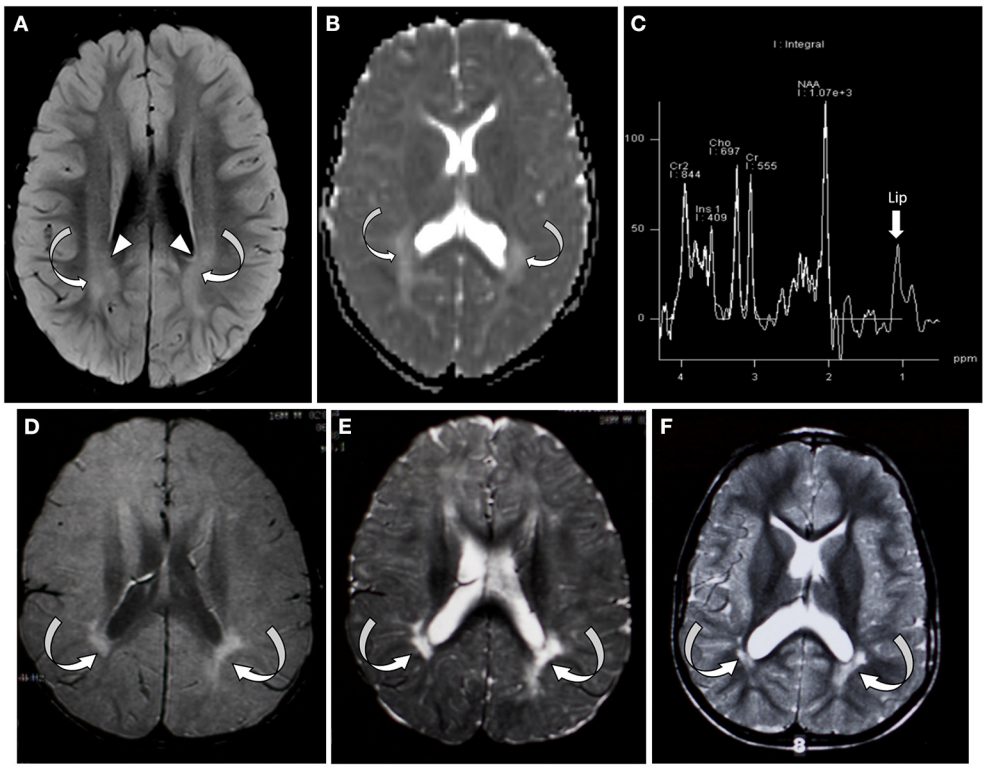

FIGURE 1 | Brain MRI/MRS from patient 1 **(A–C)** and patient 2 **(D–F)**. **(A)** Axial FLAIR sequence at the level of the lateral ventricle and centrum semiovale at 4 years of age showing bilateral symmetric areas of amorphous hyperintensity (curved arrows) within the periventricular white matter. Notice the hyperintensity is seen extending up to the ventricular margin (arrowhead). **(B)** Apparent diffusion coefficient map of the brain through the lateral ventricles showing areas of hyperintensity suggestive of facilitated diffusion (absent diffusion restriction/curved arrows). **(C)** Single-voxel MRI spectroscopy with the voxel placed over the white matter showed slightly elevated lipid peak (arrow). **(D–F)** Axial FLAIR and axial T2 images through the centrum semiovale and ventricles performed at 1, 2, and 4 years of age, respectively. Arrows indicate bilateral periventricular white matter thinning and hyperintensity, predominantly in the periatrial region.

years of age, he had severe intellectual disability and intermittent aggressive behaviors. Dysmorphic features included widely spaced incisors, retrognathia, a high-arched palate, bilateral fifth finger clinodactyly, and a left-sided supernumerary nipple. His parents reported limited oral intake, and most nutrition was obtained from G-tube feedings. At 21 years of age, treatment with antipsychotic medication was initiated for aggressive behavior.

The patient underwent an extensive genetic and metabolic evaluation during childhood (**Table 1**). Brain MRI scans obtained during childhood showed delayed myelination with increased T2 signal in the periatrial white matter, mild ventricular dilation, and anterior thinning of the corpus callosum (**Figures 1D–F**). MRS showed a slight decrease in NAA. The patient had a quadriceps muscle biopsy at 4 years 10 months of age, which showed occasional atrophic-appearing type I myofibers (**Figure 2A**) and occasional neural cell adhesion molecule (NCAM)–positive muscle fibers (**Figure 2B**). Oxidative phosphorylation enzymology revealed decreased complex I activity, decreased complex I + III activity, and decreased complex II + III activity. Individual testing of complex III and IV showed normal activity. Based on these results, he was diagnosed with oxidative phosphorylation disease with complex I defect. He was treated with various vitamin supplements including coenzyme Q10 and levocarnitine for a few years with no significant improvements noted. Genetic testing at 19 years of age included a normal single-nucleotide polymorphism array, normal transferrin electrophoresis, and normal Angelman/Prader-Willi syndrome methylation testing. Clinical trio-ES revealed a *de novo* pathogenic variant in *SATB2* (NM_015265.3):c.1515delT, p.(Phe505Leufs*41). No pathogenic variants were identified in the blood- or muscle-derived mitochondrial DNA. Hearing evaluation, ophthalmologic examination, echocardiogram, and electroencephalogram were normal.

DISCUSSION AND CONCLUSION

Mitochondrial diseases with respiratory chain dysfunction are characterized by a broad phenotype. While skeletal muscles and brain are the most commonly affected tissues, other organs and tissues such as heart, liver, kidney, and endocrine glands may also be involved (Falk, 2010). Clinical manifestations can include hypotonia, gross and/or fine motor delay, seizures, growth retardation, and behavioral difficulties in the autism-spectrum range that may present at any age (Witters et al., 2018). Similarly, SAS can present with any of these overlapping neurodevelopmental features early in life (Zarate et al., 2018). Indeed, according to a recent review of the SAS phenotype, besides the universal presence

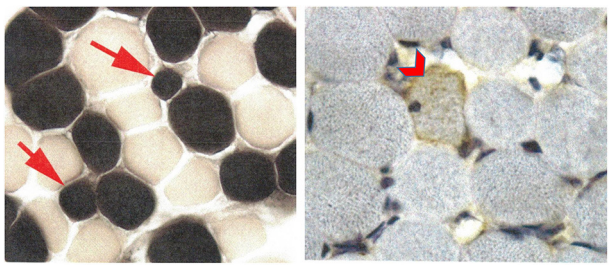

FIGURE 2 | Patient 2 muscle biopsy. ATPase reaction at pH 4.3 shows a few, but not all, type 1 myofibers to be atrophic (arrows) without angulated contours. Neural cell adhesion molecule (NCAM) is weakly positive in a rare myofiber (chevron) without evidence of myopathic or neurogenic changes.

of developmental delay, hypotonia, growth retardation, and seizures are present in 59, 31, and 20% of individuals, respectively (Zarate et al., 2019). We here describe two unrelated individuals with SAS who, because of the clinical phenotypic overlap, were investigated for a presumed mitochondrial disease before their final diagnosis was made. Patient 1 had the most commonly reported single-nucleotide variant in SAS (Arg389Cys), whereas patient 2 had a unique truncating variant (Phe505Leufs*41). In retrospect, both cases had an overall phenotype that was consistent with SAS. To our knowledge, this is the first report of individuals with SAS that describes detailed muscle histology and enzymology, as well as brain MRS.

The strict application of the mitochondrial disease score (clinical, metabolic, and imaging) led to the designation of "possible" mitochondrial disorder (Witters et al., 2018) for the individuals described in this report. While one individual had documented abnormal respiratory chain complex activity, the other had nonspecific abnormalities with no clear evidence of mitochondrial disease. Some overlapping phenotypic features with mitochondrial disorders are worth mentioning. First, on neuroimaging, as seen in the two individuals from this report, individuals with SAS have nonspecific abnormalities such as delayed myelination (62%) or abnormal white matter hyperintensities (T2/FLAIR) (48%) (Lewis et al., 2020). In mitochondrial disorders, signal abnormalities and hyperintensities are often seen but tend to be bilateral, symmetrical, and with predominant involvement of the basal ganglia and brainstem (Falk, 2010; de Beaurepaire et al., 2018). Second, while neither of the individuals described in this report had a lactate peak, patient 2 did have a slight decrease in NAA on MRS. The most common metabolic brain abnormalities identified in mitochondrial diseases on MRS include a variable decrease in NAA and accumulation of lactate in brain (Bianchi et al., 2003). Third, muscle respiratory chain studies for patient 2 revealed decreased complex I activity. Isolated deficiency of complex I is the most commonly identified biochemical defect in childhood-onset mitochondrial disease (Fassone and Rahman, 2012). Lastly, variation in the size and relative proportion of the type of muscle fibers (along with NCAM expression), as seen in the muscle biopsies of the individuals described here, have been reported in patients with various mitochondrial respiratory chain dysfunctions (Enns et al., 2005).

Accounting for ∼0.3% of individuals with unexplained developmental delay/intellectual disability, pathogenic variants in *SATB2* are one of the most common causes of syndromic intellectual disability (Deciphering Developmental Disorders, 2017; Zarate et al., 2017). Mitochondrial diseases, on the other hand, are the most frequent neurometabolic disease with an estimated incidence of ∼1/5,000 births (Witters et al., 2018). Therefore, it is possible that an individual with SAS could also have a mitochondrial disease. For the two individuals here described, pathogenic variants in mitochondrial (from muscle and blood) or nuclear (from blood) encoded respiratory chain proteins were ruled out. The subtle phenotypic overlap including the abnormal respiratory chain finding in patient 2 could be an indication of an SMD. It is known that individuals with nonsyndromic ASD or with genetic disorders associated with ASD but not classically associated with mitochondrial disease (such as Down syndrome, Rett syndrome, or Phelan-McDermid syndrome) can have mitochondrial dysfunction and respond to mitochondrial interventions (Niyazov et al., 2016; Frye, 2020). The lack of documented improvement to such treatment in patient 2 could be reflective of the well-known variable response to these interventions, the predominant SAS phenotype, or the absence of a mitochondrial dysfunction amenable to correction.

In summary, we present two individuals with SAS with early-onset neurodevelopmental phenotypes. In addition to some overlapping signs and symptoms also seen in mitochondrial diseases, both individuals had nonspecific findings on neuroimaging and muscle histology that are sometimes seen in mitochondrial disorders. While both individuals were only in the "possible" mitochondrial disorder category, other more distinctive findings such as lactate abnormalities on plasma, cerebrospinal fluid, or MRS could have been missed because of episodic nature of those findings. The possibility of an SMD in SAS would need a larger cohort of individuals evaluated systematically who would undergo dedicated testing to be confirmed. In the interim, we propose that SAS should be in the differential diagnoses of mitochondrial disorders, and broad-spectrum diagnostic tests such as ES should be considered early in the evaluation process of undiagnosed neurodevelopmental disorders.

DATA AVAILABILITY STATEMENT

The datasets for this article are not publicly available due to concerns regarding participant/patient anonymity. Requests to access the datasets should be directed to the corresponding author.

ETHICS STATEMENT

The studies involving human participants were reviewed and approved by Institutional Review Board of the University of Arkansas for Medical Sciences. Written informed consent to participate in this study was provided by the participants' legal

guardian/next of kin. Written informed consent was obtained from the individual(s), and minor(s)' legal guardian/next of kin, for the publication of any potentially identifiable images or data included in this article.

AUTHOR CONTRIBUTIONS

YZ analyzed and interpreted the data, prepared, and corrected the manuscript. HV, KB, PR, MG, RR, DO, TV, MM, and KW interpreted the data and were involved in the revision of this manuscript. All authors read and approved the final manuscript.

SUPPLEMENTARY MATERIAL

The Supplementary Material for this article can be found online at: https://www.frontiersin.org/articles/10.3389/fgene.2021.692087/full#supplementary-material

REFERENCES

Bergant, G., Maver, A., Lovrecic, L., Cuturilo, G., Hodzic, A., and Peterlin, B. (2018). Comprehensive use of extended exome analysis improves diagnostic yield in rare disease: a retrospective survey in 1,059 cases. *Genet. Med*. 2. 20, 303–312. doi: 10.10381038/gim.2m.0172017.142

Bianchi, M. C., Tosetti, M., Battini, R., Manca, M. L., Mancuso, M., Cioni, G., et al. (2003). Proton MR spectroscopy of mitochondrial diseases: analysis of brain metabolic abnormalities and their possible diagnostic relevance. *AJNR Am. J. Neuroradiol*. 2. 24, 1958, 1958–1966.

Bugiani, M., Invernizzi, F., Alberio, S., Briem, E., Lamantea, E., Carrara, F., et al. (2004). Clinical and molecular findings in children with complex I deficiency. *Biochim. Biophys. Acta* 1. 659,1659, 136–147. doi: 10.10161016/j.bbabio.2o.0042004.09.006

de Beaurepaire, I., Grévent, D., Rio, M., Desguerre, I., de Lonlay, P., Levy, R., et al. (2018). High predictive value of brain MRI imaging in primary mitochondrial respiratory chain deficiency. *J. Med. Genet*. 5. 55, 378–383. doi: 10.11361136/jmedgenet-20172017-105094105094

Deciphering Developmental Disorders, S. (2017). Prevalence and architecture of de novonovo mutations in developmental disorders. *Nature* 5. 542, 433–438. doi: 10.10381038/nature2e21062

Dubowitz, V., and Sewry, C. A. (2007). "Histological and histochemical stains and reactions," in *Muscle Biopsy A Practical Approach, 3rd edn*, ed. V. Dubowitz. (China: Saunders Elsevier), 21–39.

Enns, G. M., Hoppel, C. L., DeArmond, S. J., Schelley, S., Bass, N., Weisiger, K., et al. (2005). Relationship of primary mitochondrial respiratory chain dysfunction to fiber type abnormalities in skeletal muscle. *Clin. Genet*. 6. 68, 337–348. doi: 10.11111111/j.1j.3991399-00040004.20052005.0049900499.x

Falk, M. J. (2010). Neurodevelopmental manifestations of mitochondrial disease. *J. Dev. Behav. Pediatr*. 3. 31, 610–621. doi: 10.10971097/DBP.0P.b0b013e3e3181e1ef4f42c2c1

Fassone, E., and Rahman, S. (2012). Complex I deficiency: clinical features, biochemistry and molecular genetics. *J. Med. Genet*. 4. 49, 578–590. doi: 10.11361136/jmedgenet-20122012-101159101159

Frye, R. E. (2020). Mitochondrial dysfunction in autism spectrum disorder: u: Unique abnormalities and targeted treatments. *Semin. Pediatr. Neurol*. 3. 35:1008, 100829. doi: 10.10161016/j.spen.2n.0202020.100829100829

Lewis, H., Samanta, D., Orsell, J. L., Bosanko, K. A., Rowellwell, A., Jones, M., et al. (2020). Epilepsy and electroencephalographic abnormalities in SATB2B2-associated syndrome. *Pediatr. Neurol*. 112, 94–100. doi: 10.10161016/j.pediatrneurol.2l.0202020.04.006

Niyazov, D. M., Kahler, S. G., and Frye, R. E. (2016). Primary mitochondrial disease and secondSecondary mitochondrial dysfunction: i: Importance of distinction for diagnosis and treatment. *Mol. Syndromol*. 7. 7, 122–137. doi: 10.11591159/000446586000446586

Parikh, S., Goldstein, A., Koenig, M. K., Scaglia, F., Enns, G. M., Saneto, R., et al. (2015). Diagnosis and management of mitochondrial disease: a consensus statement from the Mitochondrial Medicine Society. *Genet. Med*. 1. 17, 689–701. doi: 10.10381038/gim.2m.0142014.177

Retterer, K., Juusola, J., Cho, M. T., Vitazka, P., Millan, F., Gibellini, F., et al. (2016). Clinical application of whole-exome sequencing across clinical indications. *Genet. Med*. 1. 18, 696–704. doi: 10.10381038/gim.2m.0152015.148

Sewry, C. A. (2000). Immunocytochemical analysis of human muscular dystrophy. *Microsc. Res. Tech*. 4. 48, 142–154. doi: 10.10021002/(SICI)10971097-00290029(2000020120000201/15)48:3/4<142::::AID-JEMT3T3>3.0.CO;2-92-9

Witters, P., Saada, A., Honzik, T., Tesarova, M., Kleinle, S., Horvath, R., et al. (2018). Revisiting mitochondrial diagnostic criteria in the new era of genomics. *Genet. Med*. 2. 20, 444–451. doi: 10.10381038/gim.2m.0172017.125

Zarate, Y. A., Bosanko, K. A., Caffrey, A. R., Bernstein, J. A., Martin, D. M., Williams, M. S., et al. (2019). Mutation update for the SATB2B2 gene. *Hum. Mutat*. 4. 40, 1013, 1013–10291029. doi: 10.10021002/humu.2u.377123771

Zarate, Y. A., and Fish, J. L. (2017). SATB2B2-associated syndrome: M: Mechanisms, phenotype, and practical recommendations. *Am. J. Med. Genet. A* 1. 173, 327–337. doi: 10.10021002/ajmg.a.3a.802238022

Zarate, Y. A., Kalsner, L., Basinger, A., Jones, J. R., Li, C., Szybowska, M., et al. (2017). Genotype and phenotype in 12 additional individuals with SATB2B2-associated syndrome. *Clin. Genet*. 9. 92, 423–429. doi: 10.11111111/cge.1e.298212982

Zarate, Y. A., Smith-Hicks, C. L., Greene, C., Abbott, M. A., Siu, V. M., Calhoun, A., et al. (2018). Natural history and genotype-phenotype correlations in 72 individuals with SATB2B2-associated syndrome. *Am. J. Med. Genet. A* 1. 176, 925–935. doi: 10.10021002/ajmg.a.3a.863038630

Conflict of Interest: The authors declare that the research was conducted in the absence of any commercial or financial relationships that could be construed as a potential conflict of interest.

frontiers in Genetics

ORIGINAL RESEARCH
published: 03 August 2021
doi: 10.3389/fgene.2021.694312

OPEN ACCESS

Edited by:
Chen Li,
Zhejiang University, China

Reviewed by:
Yi Shiau Ng,
Wellcome Trust Centre for Mitochondrial Research (WT), United Kingdom
Saumel Ahmadi,
Washington University in St. Louis, United States

***Correspondence:**
Hongjie Yuan
hyuan@emory.edu
Xiuhua Bozarth
Xiuhua.Bozarth@seattlechildrens.org

†Present address:
Jin Zhang,
Department of Neurology, The First Hospital of Shanxi Medical University, Taiyuan, China
Weiting Tang,
Department of Neurology, Xiangya Hospital, Central South University, Changsha, China
Ding Liu,
Department of Neurology, Xiangya Second Hospital, Central South University, Changsha, China
Wenshu XiangWei,
Department of Pediatrics and Pediatric Epilepsy Center, Peking University First Hospital, Beijing, China

‡*These authors have contributed equally to this work*

Specialty section:
This article was submitted to Genetics of Common and Rare Diseases, a section of the journal Frontiers in Genetics

Received: *12 April 2021*
Accepted: *21 June 2021*
Published: *03 August 2021*

Citation:
Zhang J, Tang W, Bhatia NK, Xu Y, Paudyal N, Liu D, Kim S, Song R, XiangWei W, Shaulsky G, Myers SJ, Dobyns W, Jayaraman V, Traynelis SF, Yuan H and Bozarth X (2021) A de novo GRIN1 Variant Associated With Myoclonus and Developmental Delay: From Molecular Mechanism to Rescue Pharmacology. Front. Genet. 12:694312. doi: 10.3389/fgene.2021.694312

A *de novo GRIN1* Variant Associated With Myoclonus and Developmental Delay: From Molecular Mechanism to Rescue Pharmacology

Jin Zhang[1†‡], Weiting Tang[1†‡], Nidhi K. Bhatia[2], Yuchen Xu[1,3], Nabina Paudyal[2], Ding Liu[1†], Sukhan Kim[1,4], Rui Song[1,3], Wenshu XiangWei[1†], Gil Shaulsky[1], Scott J. Myers[1,4], William Dobyns[5], Vasanthi Jayaraman[2], Stephen F. Traynelis[1,4], Hongjie Yuan[1,4*] and Xiuhua Bozarth[5,6*]

[1] Department of Pharmacology and Chemical Biology, Emory University School of Medicine, Atlanta, GA, United States, [2] Department of Biochemistry and Molecular Biology, The University of Texas Health Science Center, Houston, TX, United States, [3] Department of Neurology, Xiangya Hospital, Central South University, Changsha, China, [4] Center for Functional Evaluation of Rare Variants (CFERV), Emory University School of Medicine, Atlanta, GA, United States, [5] Center for Integrative Brain Research, Seattle Children's Research Institute, Seattle, WA, United States, [6] Division of Pediatric Neurology, Department of Neurology, Seattle Children's Hospital, University of Washington, Seattle, WA, United States

N-Methyl-D-aspartate receptors (NMDARs) are highly expressed in brain and play important roles in neurodevelopment and various neuropathologic conditions. Here, we describe a new phenotype in an individual associated with a novel *de novo* deleterious variant in *GRIN1* (c.1595C>A, p.Pro532His). The clinical phenotype is characterized with developmental encephalopathy, striking stimulus-sensitive myoclonus, and frontal lobe and frontal white matter hypoplasia, with no apparent seizures detected. NMDARs that contained the P532H within the glycine-binding domain of GluN1 with either the GluN2A or GluN2B subunits were evaluated for changes in their pharmacological and biophysical properties, which surprisingly revealed only modest changes in glycine potency but a significant decrease in glutamate potency, an increase in sensitivity to endogenous zinc inhibition, a decrease in response to maximally effective concentrations of agonists, a shortened synaptic-like response time course, a decreased channel open probability, and a reduced receptor cell surface expression. Molecule dynamics simulations suggested that the variant can lead to additional interactions across the dimer interface in the agonist-binding domains, resulting in a more open GluN2 agonist-binding domain cleft, which was also confirmed by single-molecule fluorescence resonance energy transfer measurements. Based on the functional deficits identified, several positive modulators were evaluated to explore potential rescue pharmacology.

Keywords: NMDAR, GluN1, channelopathy, intellectual disability, movement disorder, positive modulators, molecular dynamics, translational study

Abbreviations: ABD, agonist-binding domain; β-lac, beta-lactamase; CTD, cytosolic carboxyl terminal domain; FRET, fluorescence resonance energy transfer; LoF, loss-of-function; MD, molecular dynamics; MTSEA, 2-aminoethyl methanethiosulfonate hydrobromide; NGS, next-generation sequencing; NMDAR, *N*-methyl-D-aspartate receptor; NTD (as well as ATD), amino terminal domain; P_{OPEN}, channel open probability; TEVC, two-electrode voltage clamp; TMD, transmembrane domains (M1–M4).

INTRODUCTION

N-Methyl-D-aspartate receptors are ligand-gated ionotropic glutamatergic receptors that mediate excitatory synaptic transmission in the central nervous system and play an important role in brain development. NMDARs are a multimeric complex of two GluN1 subunits (encoded by the *GRIN1* gene) and two GluN2 subunits (encoded by *GRIN2A-D*) (Traynelis et al., 2010; Hansen et al., 2021). GluN1 is expressed in virtually all brain regions throughout development (Akazawa et al., 1994). All NMDAR GluN subunits share a similar architecture that includes an extracellular amino terminal domain (NTD, also known as ATD), a bi-lobed extracellular agonist binding domain (ABD), a transmembrane domain (TMD containing M1, M2, M3, and M4), and an intracellular carboxyl terminal domain (CTD). Activation of NMDARs requires both glycine binding to the GluN1 subunit and glutamate binding to the GluN2 subunit. NMDARs play critical roles in normal brain function, such as neural development, synaptic plasticity, learning, memory, and motor function.

N-Methyl-D-aspartate receptors have been implicated in various neurological disorders including Parkinson's, Alzheimer's, Huntington's diseases, as well as in epilepsy and schizophrenia (Traynelis et al., 2010; Paoletti et al., 2013; Hansen et al., 2021). Furthermore, genetic variation in the genes (*GRIN*) encoding the GluN subunits have been associated with a wide range of neurologic and neuropsychiatric disorders (Burnashev and Szepetowski, 2015; Yuan et al., 2015; Hu et al., 2016; XiangWei et al., 2018; Myers et al., 2019; Camp and Yuan, 2020). In addition, heterozygous pathogenic variants in the G*RIN1* gene have been identified in patients with autosomal dominant encephalopathy, seizures, microcephaly, movement disorders, and severe intellectual disability (Hamdan et al., 2011; Tarabeux et al., 2011; Epi4K Consortium et al., 2013; Iossifov et al., 2014; Redin et al., 2014; Farwell et al., 2015; Ohba et al., 2015; Zhu et al., 2015; Bosch et al., 2016; Halvardson et al., 2016; Helbig et al., 2016; Lelieveld et al., 2016; Lemke et al., 2016; Retterer et al., 2016; Vanderver et al., 2016; Chen et al., 2017a; Rossi et al., 2017; Zehavi et al., 2017; Fry et al., 2018; Li et al., 2019).

Here, we describe the clinical phenotype of a patient with a novel *de novo GRIN1* variant, evaluate the functional and structural influence of the variant, and explore potential rescue pharmacology to rectify the altered function. We show that this GluN1 variant produces changes in GluN2 conformation and function that result in a loss of function. These actions likely reflect the location of Pro532 at the interface of the GluN1 and GluN2 ABDs as confirmed by MD simulations and single-molecule fluorescence resonance energy transfer (smFRET) measurements.

MATERIALS AND METHODS

Ethics, Consent, and Permissions

Written informed consent was obtained from the parent of the patient reported. This study was approved by the Medical Ethics Committee and the Institutional Review Boards of Seattle Children's Hospital, University of Washington (IRB: #13291). All clinical data of this study were analyzed anonymously. All functional studies were performed according to the guidelines of Emory University and The University of Texas Health Science Center.

Patient and Diagnostic Workup

We evaluated a female patient with a new clinical phenotype with a novel *de novo* deleterious variant in *GRIN1* (c.1595C>A, p.Pro532His), who is from a large Caucasian family. A three generation pedigree was taken including proband and two full siblings of proband, biological parents and six uncles and aunts, four grandparents and nine grand uncles and aunts, and eight great grandparents. Her parents are nonconsanguineous. One younger sister and three brothers are healthy. One of her brothers has healthy children. There is a distant maternal relative with Down syndrome who died. There is a maternal family history of hemochromatosis. The patient's father is 44 years old and in good health. He is 6 ft 1 in. tall. He has a healthy brother and sister, and his brother has a daughter with some hearing loss and minor anomalies but otherwise normal cognitive function. A brother of her father died in infancy of unknown cause. Clinical data was collected *via* electronic medical record review. Diagnostic workup, including karyotype, a chromosome microarray, metabolic testing (plasma amino and urine organic acids, serum lactate, serum pyruvate, oligosaccharides, acylcarnitine profile, and glycosylation), and a skin biopsy study for electron microscopy, were performed. Trio-whole exome sequencing (proband and biological parents) was performed at GeneDx. The Web resource gnomAD was used to search for *GRIN1*gene variants.

Molecular Biology and *Xenopus laevis* Oocyte Injections

We utilized cDNA for wild-type human NMDA receptor GluN1-1a (hereafter GluN1; NCBI NM_007327/NP_015566), GluN2A (NCBI NM_000833/NP_000824), and GluN2B (NCBI NM_000834/NP_000825) subunits subcloned into the plasmid vector pCI-neo (Promega, Madison, WI, United States). The mutant GluN1 cDNA was generated by site-directed mutagenesis using the QuikChange protocol (Stratagene, La Jolla, CA, United States) and cRNA was synthesized *in vitro* from a linearized cDNA template according to manufacturer instructions (mMessage mMachine; Ambion, Austin, TX, United States) (Chen et al., 2017b). *Xenopus laevis* oocytes were prepared (XiangWei et al., 2019) from commercially available ovaries (Xenopus One Inc., Dexter, MI, United States); 5–10 ng of total cRNA in 50 nl of RNase-free water was injected into each oocyte using a microinjector (Drummond Nanoject II) with a ratio of 1:2 for GluN1:GluN2. Injected oocytes were stored at 15–17°C in Barth's solution as previously described (Chen et al., 2017b).

Two-Electrode Voltage-Clamp Current Recordings From *Xenopus* Oocytes

Two-electrode voltage-clamp (TEVC) recordings from *Xenopus* oocytes were performed as previously described (Chen et al., 2017b). The recording solution contained 90 mM NaCl, 1 mM

KCl, 10 mM HEPES, 0.5 mM $BaCl_2$, and 0.01 mM EDTA (23°C, pH 7.4 unless otherwise stated). The membrane potential was held at −40 or −60 mV. The amplitudes at each agonist concentration were fitted with

$$Response\ (\%) = 100/(1 + (EC_{50}/[agonist])^N) \quad (1)$$

where EC_{50} is the concentration that produces a half maximal response, [*agonist*] is the concentration of glutamate, glycine, or other agonists, and N is the Hill slope. Concentration–response curves were recorded for NMDAR current response as activated by maximally effective concentrations of glutamate and glycine, with coapplication of variable concentrations of negative allosteric modulators Mg^{2+} or Zn^{2+} (Zn^{2+} buffered with tricine) (Traynelis et al., 1998). The current response amplitudes were fitted with:

$$Response\ (\%) = (100 - minimum)/ (1 + ([modulator]/IC_{50})^N) + minimum \quad (2)$$

where *minimum* is the residual response in saturating concentration of the negative modulator (Mg^{2+} or Zn^{2+}), IC_{50} is the concentration of the modulator that produces a half-maximal inhibition, and N is the Hill slope.

The channel open probability (P_{OPEN}) was calculated from the degree of potentiation produced when maximally effective glutamate and glycine are coapplied with 200 μM MTSEA (Toronto Research Chemicals) (Yuan et al., 2005) according to

$$P_{OPEN} = (\gamma_{MTSEA}/\gamma_{CONTROL}) \times (1/potentiation) \quad (3)$$

where γ is the channel chord conductance for GluN1/GluN2A before and after MTSEA modification (Yuan et al., 2005) and *potentiation* is the ratio of current after MTSEA to that observed before MTSEA.

All recording solutions for 24(S)-hydroxycholesterol, pregnenolone sulfate, and tobramycin were supplemented with 0.02% cremophor.

Whole-Cell Voltage-Clamp Current Recordings From Mammalian Cells

HEK293 cells (ATCC CRL-1573) were transiently cotransfected as previously described (Chen et al., 2017b) with plasmid cDNAs encoding wild-type human GluN1/GluN2A/GFP, GluN1/GluN2B/GFP, or the variant GluN1-P532H/GluN2A/GFP, or GluN1-P532H/GluN2B/GFP. The ratio of transfected cDNAs was 1:1:5 when co-expressed with GluN2A and 1:1:1 when co-expressed with GluN2B. Following an 18–24-h transfection, whole-cell voltage-clamp current recordings were made (Chen et al., 2017b; Ogden et al., 2017) with an extracellular solution containing 150 mM NaCl, 3 mM KCl, 10 mM HEPES, 0.01 mM EDTA, 0.5 mM $CaCl_2$, and 11 mM D-mannitol, with the pH adjusted to 7.4 by addition of NaOH (23°C). The recording electrodes were filled with an internal solution that contained 110 mM D-gluconic acid, 110 mM CsOH, 30 mM CsCl, 5 mM HEPES, 4 mM NaCl, 0.5 mM $CaCl_2$, 2 mM $MgCl_2$, 5 mM BAPTA, 2 mM Na-ATP, and 0.3 mM Na-GTP adjusted to pH 7.35 with CsOH; the osmolality was adjusted to 300–310 mOsmol kg^{-1} using CsCl or water. The current responses to external application of glutamate (1,000 μM) and glycine (1 to 100 μM) were recorded using an Axopatch 200B patch-clamp amplifier (Molecular Devices) with the holding potential of −60 mV. The current responses were filtered at 8 kHz (−3 dB, 8 pole Bessel filter, frequency devices) and digitized at 20 kHz using a Digidata 1440A and Axon Instruments software (Molecular Devices, Sunnyvale, CA, United States).

Beta-Lactamase (β-Lactamase) Reporter Assay From Mammalian Cells

HEK293 cells were plated in 96-well plates and transiently transfected with cDNA encoding WT β-lactamase (β-lac)-GluN1 or β-lac-GluN1-P532H with either WT GluN2A or WT GluN2B using Fugene6 (Promega) (Swanger et al., 2016). The background absorbance was determined by the cells treated with Fugene6 only. A negative control for surface β-lac activity was determined in cells that were not transfected with GluN2A and GluN2B cDNA. Eight wells were transfected for each condition, and the levels of surface and total β-lactamase were measured in four wells each. After 24 h transfection, the cells were washed with Hank's balanced salt solution (HBSS) supplemented with 10 mM HEPES, and then 100 μl of a 100-μM nitrocefin (Millipore, Burlington, MA, United States) solution in HBSS with HEPES was added to each well to allow the measurement of surface activity (Swanger et al., 2016). In separate wells, the cells were lysed by a 30-min incubation in 50 μl H_2O prior to the addition of 50 μl of 200 μM nitrocefin to determine total activity. The absorbance was read on a microplate reader (SpectraMax M2) at 486 nm once every minute for 30 min (30°C). The rate of increase in absorbance was determined from the slope of the linear regression.

MD Simulation Methods

The dimer structure of GluN1/GluN2A bound to glycine and glutamate (PBD ID 5H8Q) was taken from the Protein Data Bank for MD simulation. Two simulation systems (wild-type and P532H variant) were prepared. The PSFGEN module of the Visual Molecular Dynamics Simulation software (VMD) was used for building missing residues and hydrogen atoms to the protein structure followed by protein solvation and ionization (Humphrey et al., 1996; Gullingsrud et al., 2006). First, the protein was placed in the water box of size 97 × 90 × 105 Å, with around 24,372 TIP3P water molecules and six chloride ions for charge neutralization (Humphrey et al., 1996; Gullingsrud et al., 2006). Total atoms in the simulation box ranged from 82,006 to 82,009. Each system was subjected to conjugate gradient energy minimization for 5,000 steps by applying restraint force of spring constant 4 kcal/mol/Å2 on the heavy atoms of protein and on the residues interacting with the ligands glutamate and glycine. The system was then equilibrated for 5 ns using 1 fs time step and gradually the restraint force constant was decreased to zero. Following system equilibration, 300 ns production was performed using 2 fs time step under constant NTP ensemble. NTP ensemble refers to constant number of particles

(N), constant pressure of 1 bar controlled by Nose-Hoover Langevin piston and constant temperature at 310 K controlled by the Langevin thermostat. Particle mesh Ewald (PME) (York et al., 1993) method was applied for calculating long-range electrostatic interactions and SHAKE restraint was used on covalent bonds involving hydrogen atoms. Smooth switching of small-range nonbonded interaction was done between 10 and 12 Å with pair list cut-off updates on 14 Å. NAMD 2.12 (Phillips et al., 2005) program was used for performing the simulation. CHARMM36 force field (Best et al., 2012), with cMAP dihedral correction was used for the protein. The CHARMM general force field (CGENFF) was used for ligands (Vanommeslaeghe et al., 2010). Simulations were submitted at Stampede2 cluster of Texas Advancing Computing Center (TACC). MD trajectories were analyzed using TCL scripts, VMD software and python Matplotlib (Hunter, 2007).

smFRET Methods

Cysteine-light constructs of human GluN1 wild type, GluN1-P532H variant, and GluN2 were generated by mutating nondisulphide-bonded extracellular cysteines (Cys15, Cys22 in GluN1 and Cys231, Cys399, and Cys460 in GluN2) to serines, and cysteines were introduced at positions 502 and 701 in the GluN2A cysteine-light construct to measure conformational changes across ABD of GluN2. All the mutations were confirmed by Sanger sequencing (Genewiz). HEK293 cells were transiently cotransfected with the plasmids harboring cDNAs encoding GluN1/GluN2A (1:3; 10 μg of total cDNA per 10 cm dish) or the variant GluN1-P532H/GluN2A with the FRET mutations mentioned above. Transfections were performed the day before the smFRET experiment using JetPRIME transfection reagent (polyplus). On the day of experiment, i.e., 24 h post-transfection, the cells were labeled with donor and acceptor fluorophore and the sample was prepared as described previously (Dolino et al., 2017; Litwin et al., 2019; Durham et al., 2020).

For smFRET slide preparation, we used the same protocol as described previously (Durham et al., 2020). To selectively pull down the NMDA receptors onto the slide, we used biotinylated anti-mouse antibody bound to the streptavidin-coated slide followed by anti-NMDAR1 antibody (ab64572, Abcam). After antibody treatment, the slide was treated with bovine serum albumin and then with lysate of HEK293 cells expressing the modified NMDA FRET construct. The slide was then flushed with oxygen scavenging buffer containing (3.3% (*w*/*w*) glucose, 3 units/ml pyranose oxidase, 0.001% (*w*/*w*) catalase, 1 mM ascorbic acid, and 1 mM methyl viologen, in 1× imaging buffer (Durham et al., 2020), containing 1 mM glutamate and 1 mM glycine. smFRET data was acquired using a custom-built Pico-Quant MicroTime 200 Fluorescence Lifetime Microscope (Picoquant). Pulsed interleaved excitation was used and donor excitation was at 532 nm (LDH-D-TA-530) and acceptor at 637 nm (LDH-D-C-640, Picoquant). SPAD photodiodes (SPCM CD3516H; Excelitas Technologies) were used to detect the photons emitted from the sample and emission filters [550 nm (FF01-582/64; AHF) and 650 nm (2XH690/70; AHF)] were also used. For data analysis, we used molecules showing single acceptor and donor photobleaching step in addition to anticorrelation between acceptor and donor to ensure that the data was from a single-molecule showing FRET. FRET efficiencies were calculated using donor and acceptor intensities using the Forster equation (detailed description provided in Cooper et al., 2015; Litwin et al., 2019; Durham et al., 2020). Numbers of conformational states were estimated using step transition and state identification (STaSI).

Assessment of Synaptic and Nonsynaptic Charge Transfer

The relative change in synaptic and non-synaptic charge transfer was evaluated as a ratio to the WT receptors by the following equations (Swanger et al., 2016; Li et al., 2019):

$$R_{AGONIST} = 1/(1 + (EC_{50}/[agonist])^{N}) \quad (4)$$

$$Charge\ transfer_{Synaptic} = \tau_{wMUT}/\tau_{wWT} \times P_{MUT}/P_{WT} \times Surf_{MUT}/Surf_{WT} \times R_{GLY} \times R_{GLU,\ Synaptic} \times Mg_{MUT}/Mg_{WT} \quad (5)$$

$$Charge\ transfer_{Non-synaptic} = P_{MUT}/P_{WT} \times Surf_{MUT}/Surf_{WT} \times R_{GLY} \times R_{GLU,\ Non\ Synaptic} \times Mg_{MUT}/Mg_{WT} \quad (6)$$

where [glutamate] is 1×10^{-3} M for $R_{GLU,Synaptic}$ and 1×10^{-7} M for $R_{GLU,Non-synaptic}$, [glycine] is 3×10^{-6} M, and N is the Hill slope. t_w is the weighted constant for deactivation time course, P is the channel open probability, *Surf* is cell surface protein levels, *Mg* is percentage inhibition by 1 mM Mg^{2+} (V_{HOLD} −60 mV), R_{GLY} and R_{GLU} are relative response to a given concentration of glutamate or glycine. The τ_w, *P*, *Surf*, and *Mg* for the variant were calculated as a ratio to the WT receptors.

All data are given as mean with the 95% confidence intervals. Statistical significance was set to $p < 0.05$ and assessed by an unpaired Student's *t*-test. The number of independent experiments was represented by *n*. Samples sizes were determined *a priori* from power analysis for an effect size of 1–2 (Gpower) and were 6–17 to ensure at least 0.8 power with $\alpha = 0.05$. All compounds and agents were purchased from Sigma-Aldrich (St. Louis, MO, United States) unless stated otherwise.

RESULTS

Clinical Phenotypes

The patient was born at full term by C-section due to breech presentation with maternal age of 26 years and paternal age of 34 years. The pregnancy was complicated by decreased fetal movement at 6 months of gestation. Parents are nonconsanguineous Caucasian. Birth weight was 7 lbs, and length was 20 in. Birth occipital frontal circumference (OFC) was not available but was 52.7 cm at the age of 10 years (65 percentile). There is no family history of developmental impairment in the three-generation pedigree. The patient had some tongue thrusting at birth but was able to breast feed, fix, and follow. She had head lag which was noted when she was 3 months

old. However, by the age of 3 months, the patient lost these previously acquired skills, developed difficulties with feeding, increased irritability in infancy, and required G-tube placement at the age of 4 years. She could hold her head up at age 12 years in sitting position. Her weight ranged from 25% to 32% from age 3 months to 4 years, then increased after the G-tube placement to 50% from age 6 to 8 years, then gradually decreased to less than 3% at the age of 13 years. Her height ranged from 50% to 80% from age 3 months to 8 years, then gradually drop to less than 3% by the age of 13 years.

The patient had severe gastroesophageal reflux and scoliosis, as well as progressive contractures, mostly of her legs. She has mild to moderate equinus contractures of the feet. Knee contractures were at 45° to 90°. Her gross motor function was classified as (GMFCS) V. She has a left thoracolumbar scoliosis at 80° from T8 to L4. The patient had spasticity in all extremities. The patient has not had confirmed seizures. EEG at the age of 5 years showed diffuse slowing. The ophthalmological evaluation at 3 months of age showed normal visual evoked potential and normal dilated fundi examination. The patient has profound developmental delay and intellectual disability. She is nonverbal, does not make eye contact, and has no sign or other forms of language. She has remained non-mobile and her gross motor function classification system (GMFCS) Level V. She is G-tube dependent at the age of 16–18 years. The patient has marked brachycephaly, midface (maxillary) hypoplasia, and mildly protuberant ears. The patient has low normal muscle bulk and mildly increased tone in the arms and moderate to severe increased tone in the legs. The patient has very frequent stimulus-sensitive myoclonic jerks. The patient did not have a muscle biopsy. The EEG monitoring captured the myoclonus with no EEG correlation, suggesting subcortical origin. Brain MRI at 3 months and about 5 years of age showed enlarged extra axial space, best seen over the frontal lobes with some mildly enlarged sulci (**Figure 1A**). Her corpus callosum was mildly thin. The brainstem, cerebellum, and posterior fossa appeared normal, and there was no polymicrogyria detected (**Figure 1A**).

Diagnostic Workup

Karyotype and a chromosome microarray were normal. Metabolic testing was normal, including plasma amino and urine organic acids, serum lactate, serum pyruvate, oligosaccharides, acylcarnitine profile, and glycosylation. The patient had a skin biopsy study for electron microscopy with normal results. The whole-exome sequencing was performed by GeneDx, which identified a *de novo*, heterozygous variant p.Pro532His, c.1595C>A, in exon 11 in the *GRIN1* gene (NM_007327) (**Figure 1B**). The GluN1-P532H variant has not been reported previously. This variant was interpreted as likely pathogenic by GeneDx. The variant was not observed in healthy populations in the gnomAD database[1] (evaluated on March 3, 2021) and in about 6,400 individuals of European and African American ancestry in the NHLBI Exome Sequencing Project.

[1]http://gnomad.broadinstitute.org/

Pharmacological Properties of GluN1-P532H Receptor Complex

The residue Pro532 is located in the S1 region of the ABD (**Figures 1C–E**), which harbors the binding pocket for the coagonist glycine. This proline is conserved in GluN1 through all vertebral species and across all human GluN2 subunits (**Figure 1D**), suggesting a potential important role in channel function. NMDAR complexes with wild-type (WT) GluN1 subunit or variant GluN1-Pro532His were coexpressed with either wild-type GluN2A or GluN2B subunits. The electrophysiological properties of these receptor complexes were compared by determining the potency of endogenous agonists and modulators. Since the residue at which this missense variation occurred is located in the GluN1 ABD, which fully encodes the glycine-binding pocket, we first assessed the effects on glycine potency. The concentration of agonist that produces a half-maximal current response (EC_{50}) was determined by measuring the response to a range of glycine concentrations coapplied with a maximally effective concentration of glutamate (1,000 μM) onto NMDARs expressed in oocyte using TEVC (V_{HOLD}: −40 mV). The GluN1-P532H receptors showed only minimal effects on glycine potency, with an EC_{50} value for GluN1-P532H/GluN2A of 2.0 μM compared with 1.8 μM for WT GluN1/GluN2A. The EC_{50} value for GluN1-P532H/GluN2B was 0.34 μM, slightly lower than 0.45 μM found for WT GluN1/GluN2B (**Figures 2A,B** and **Table 1**), indicating this variant may have a modest effect on glycine potency. We subsequently evaluated glutamate potency on GluN1-P532H-containing NMDARs in the presence of maximally effective concentration of glycine (100 μM). Unexpectedly, GluN1-P532H-containing receptors significantly decreased glutamate potency, increasing EC_{50} values by 16-fold for GluN1-P532H/GluN2A (EC_{50}: 105 μM) compared with GluN1/GluN2A (6.4 μM) and 43-fold for GluN1-P532H/GluN2B (EC_{50}: 82 μM) compared with WT GluN1/GluN2B) (1.9 μM; $p < 0.01$, unpaired *t*-test; **Figures 2C,D** and **Table 1**). These data suggest that activation of variant receptors requires higher concentrations of glutamate.

It is well known that NMDAR function can be regulated by a set of endogenous negative allosteric modulators, including Mg^{2+}, protons, and Zn^{2+} (Traynelis et al., 2010). We therefore evaluated the effects of GluN1-P532H on the sensitivity of the NMDAR to these modulators. The concentration–response curves for Mg^{2+} inhibition at −60 mV showed a comparable potency for GluN1-P532H/GluN2A with an IC_{50} value of 22 μM compared with 19 μM of WT GluN1/GluN2A. The IC_{50} value for GluN1-P532H/GluN2B was 35 μM, which was similar to 38 μM for WT GluN1/GluN2B ($p = 0.99$ and 0.88, unpaired *t*-test; **Figures 2E,F** and **Table 1**). Determination of the concentration–response relationship of Zn^{2+} revealed a modest increase in Zn^{2+} sensitivity in GluN1-P532H/GluN2A by almost twofold, with IC_{50} values decreasing from 8.5 nM for WT GluN1/GluN2A to 4.1 nM for GluN1-P532H/GluN2A ($p < 0.05$, unpaired *t*-test; **Figure 2G** and **Table 1**). The GluN1-P532H receptor showed no change in proton sensitivity, assessed by comparison of NMDAR-mediated current amplitude recorded at pH 6.8 with

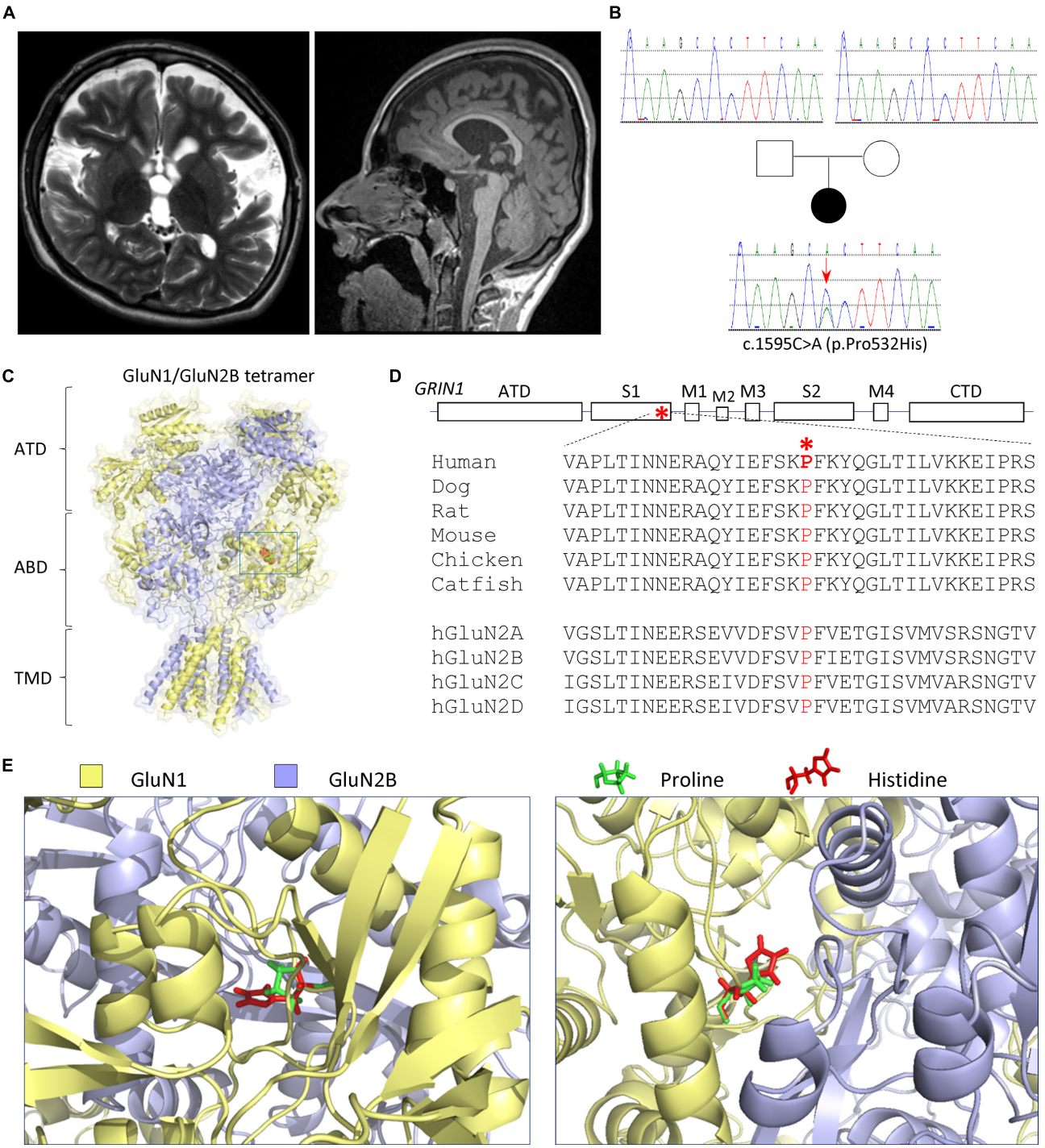

FIGURE 1 | Patient and variant information. **(A)** Brain MRI (*left panel*: coronal T2; *right panel*: sagittal T1) at 5 years old showed thin corpus callosum, diffuse volume loss, enlarged lateral and third ventricles, and enlarged extra axial space, best seen over the frontal lobes with mild enlarged sulci. The brainstem, cerebellum, and posterior fossa appeared normal (*right panel*). **(B)** Pedigree and genotypes of a *de novo GRIN1* (NM_007327) variant c.1595C>A (p.Pro532His). **(C–E)** The variation is located in the agonist-binding domain S1 highlighted in RED in a space-filled homology model of human GluN1/GluN2B receptor (Li et al., 2016; Chen et al., 2017b) built from the rat GluN1/GluN2B crystallographic data (PDB: 4PE5) (Karakas and Furukawa, 2014; Lee et al., 2014). **(C)** Schematic topology of a GluN1 subunit, where the position of the Pro532His is marked with a box and expanded below. NTD (also known as ATD) denotes the amino terminal domain, S1 and S2 interact to form the agonist-binding domain (ABD), M1–4 are the transmembrane domains, and CTD is the carboxyl terminal domain. **(D)** The proline residue at position 532 is highly conserved across vertebrate species and all GluN2 subunits. **(E)** The location in the agonist-binding domain S1 is expanded to show the position of the proline (in green) and variant histidine (in red). The *left panel* provides a side view, and the *right panel* provides a top view.

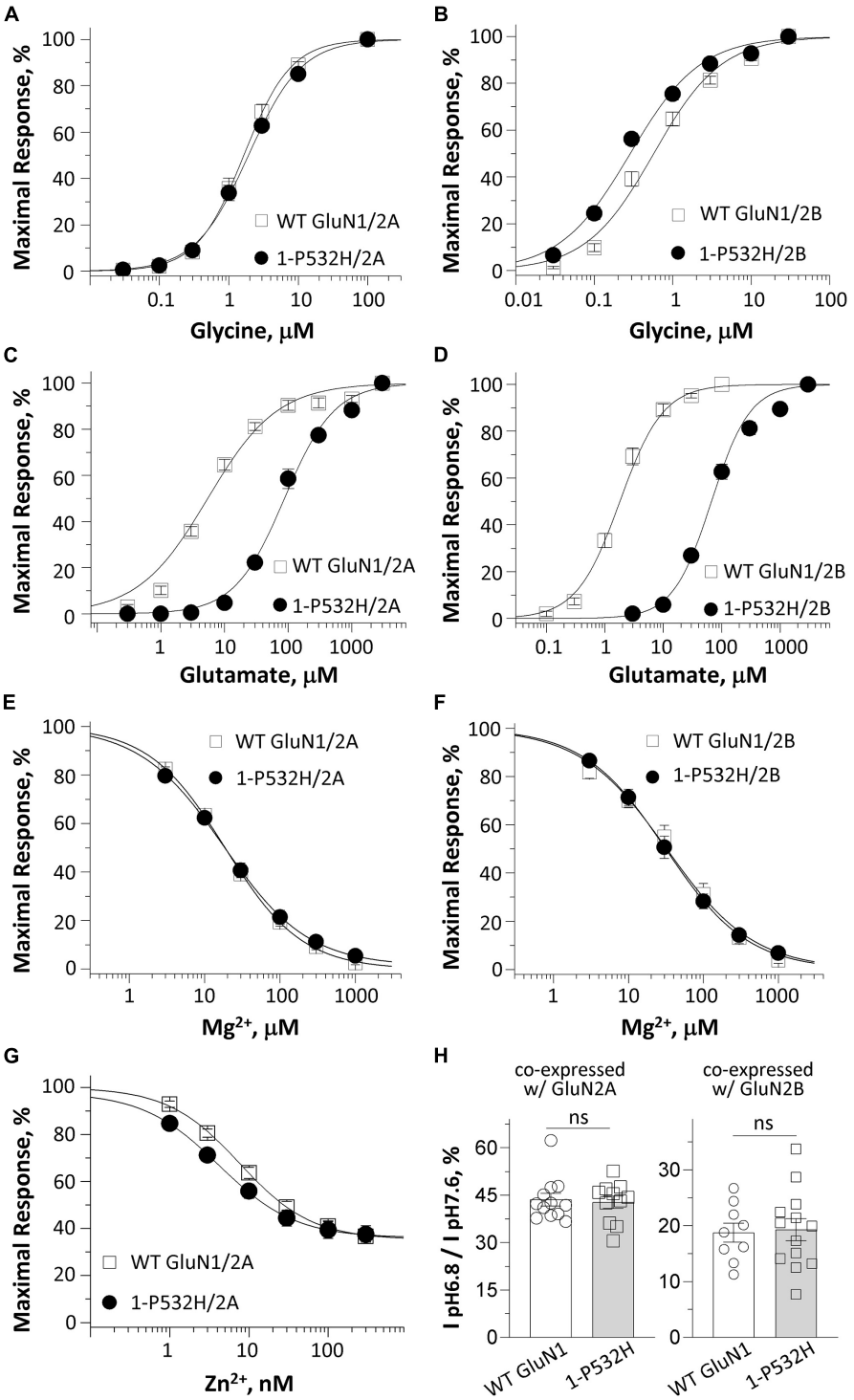

FIGURE 2 | Effects of GluN1-P532H variant on agonist potency and sensitivity to negative endogenous modulators. **(A–D)** Composite concentration–response curves determined by TEVC recordings from *Xenopus* oocytes are shown for WT GluN1 or GluN1-P532H coexpressed with GluN2A (*left panels*) or GluN2B (*right panels*). Glycine (in the presence of 1,000 μM glutamate; **A,B**) and glutamate (in the presence of 100 μM glycine; **C,D**) concentration-effect curves showed that the GluN1-P532H variant has reduced glutamate potency (increased EC_{50} values; see **Table 1**) with a mild or no change in glycine potency. **(E,F)** Concentration–response curves for WT GluN1 and GluN1-P532H coexpressed with GluN2A **(E)** and GluN2B **(F)** receptors at a holding potential of –60 mV revealed no change in inhibition by extracellular Mg^{2+}. **(G)** Composite inhibitory concentration–response curves for Zn^{2+} at a holding potential of –20 mV showed enhanced inhibition by Zn^{2+} (decreased IC_{50} values, see **Table 1**). **(H)** Percentage of current at pH 6.8 compared with pH 7.6 in the GluN1-P532H/GluN2A receptors (*left panel*) and GluN1-P532H/GluN2B receptors (*right panel*) indicated the variant has no effect on proton sensitivity.

TABLE 1 | Summary of functional properties of GluN1-P532H-containing receptors.

Parameters	Cells	Coexpressed with GluN2A		Coexpressed with GluN2B	
		WT GluN1	GluN1-P532H	WT GluN1	GluN1-P532H
Glutamate EC_{50} [μM] (n)	Oocytes	6.4 (5.2, 7.5) (27)	105 (85, 126) (26)*	1.9 (1.4, 2.4) (12)	82 (62, 102) (20)*
Glycine, EC_{50} [μM] (n)		1.8 (1.4, 2.1) (11)	2.0 (1.6, 2.4) (12)	0.45 (0.35, 0.54) (19)	0.34 (0.24, 0.44) (16)
Mg, IC_{50} [μM] (n)$^{\xi}$		19 (16, 22) (16)	22 (13, 30) (14)	38 (23, 52) (7)	35 (22, 48) (7)
pH, %6.8/7.6 (n)$^{\gamma}$		44% (40%, 47%) (12)	43% (39%, 46%) (11)	19% (16%, 22%) (9)	19% (16%, 23%) (13)
Zinc, IC_{50} [nM] (n)$^{\phi}$		8.5 (6.8, 10) (12)	4.1 (3.0, 5.2) (12)*	NA	NA
% Inhibition by 300 nM zinc		63% (59%, 68%) (12)	62% (55%, 70%) (12)	NA	NA
Amplitude (peak, pA/pF)	HEK cells	144 (71, 216)	47 (17, 78)	59 (23, 94)	48 (22, 74)
Amplitude (SS, pA/pF)		109 (56, 162)	40 (17, 63)	49 (21, 77)	42 (19, 64)
I_{SS}/I_{PEAK}, 1 mM glutamate		0.77 (0.74, 0.79)	0.88 (0.82, 0.93)*	0.88 (0.82, 0.94)	0.86 (0.79, 0.92)
10%–90% rise time (ms), 1 mM glutamate		6.0 (4.7, 7.3)	14 (10, 17)*	12 (9.4, 15)	13 (11, 15)
τ_{FAST} deactivation (ms), 1 mM glutamate		48 (33, 62)	21 (13, 28)*	536 (468, 605)	24 (19, 28)*
τ_{SLOW} deactivation (ms), 1 mM glutamate		268 (83, 454)	189 (29, 351)	2,045 (1172, 2917)	218 (55, 381)*
%τ_{FAST} deactivation, 1 mM glutamate		64%	91%	77%	74%
τ_{W} deactivation (ms), 1 mM glutamate		66 (54, 77)	26 (20, 31)*	821 (723, 918)	37 (30, 43)*
Charge transfer, pA × ms/pF		8,598	1,085	50,028	1,743
N		7	7	7	8
I_{SS}/I_{PEAK}, 1 μM glycine	HEK cells	0.37 (0.24, 0.50)	0.50 (0.35, 0.65)	NA	NA
τ_{FAST} desensitization (ms), 1 μM glycine		326 (90, 562)	102 (30, 174)	NA	NA
τ_{SLOW} desensitization (ms), 1 μM glycine		1481 (322, 2639)	1961 (791, 3031)	NA	NA
%τ_{FAST} desensitization (ms), 1 μM glycine		53%	57%	NA	NA
τ_{W} desensitization (ms), 1 μM glycine		757 (374, 1141)	1041 (206, 1877)	NA	NA
I_{SS}/I_{PEAK}, 30 μM glycine		0.43 (0.26, 0.59)	0.71 (0.54, 0.87)	NA	NA
τ_{FAST} desensitization (ms), 30 μM glycine		652 (425, 878)	1423 (627, 2218)	NA	NA
τ_{SLOW} desensitization (ms), 30 μM glycine		1943 (783, 3104)	2817 (893, 4741)	NA	NA
%τ_{FAST} desensitization (ms), 30 μM glycine		68%	67%	NA	NA
τ_{W} desensitization (ms), 30 μM glycine		974 (667, 1282)	1898 (882, 2915)	NA	NA
N		11	10	NA	NA
%Potentiation by MTSEA$^{\#}$	Oocytes	326% (267%, 385%)	804% (679%, 929%)	NA	NA
P_{OPEN} (from MTSEA)		0.26 (0.22, 0.30)	0.11 (0.09, 0.11)*	NA	NA
N		41	34	NA	NA
Surface/total ratio (β-lac)	HEK cells	100%	64% (55%, 74%)*	100%	67% (43%, 90%)*
Total protein % of WT (β-lac)		100%	110% (95%, 125%)	100%	193% (106%, 280%)*
N		5	5	7	7
Synaptic charge transfer		1.0	0.22	NA	NA
Nonsynaptic charge transfer		1.0	0.004	NA	NA

The data were expressed as mean (−95% CI, +95% CI) (n); CI, confidence interval; (n) is the number of oocytes or HEK cells.
**$p < 0.05$ indicated when the 95% confidence intervals of the datasets for the variant receptors do not overlap with the wild-type receptors.*
$^{\xi}$Holding potential was −60 mV.
$^{\gamma}$Percentage of the current at pH 6.8 compared with that at pH 7.6.
$^{\phi}$Holding potential was −20 mV.
*$^{\#}$Evaluated by TEVC recordings on Xenopus oocytes, see the Section "Materials and Methods" and **Figure 3**.*
NA, not available.

that recorded at pH 7.6 when coexpressed with either GluN2A or GluN2B (**Figure 2H** and **Table 1**).

Taken together, these data suggested that GluN1-P532H may reduce excitatory drive as a result of the decreased activation of glutamate (reduced potency) and the enhanced inhibition by endogenous zinc. They also reveal the unexpected effect of a variant located in the GluN1 glycine-binding domain on glutamate EC_{50}, the binding site for which resides in the GluN2 subunit.

Biophysical Properties and Cell Expression of GluN1-Pro532His Receptor Complex

The deactivation response time course following rapid removal of agonist (e.g., glutamate) from NMDARs has been proposed to determine the time-course of the NMDAR component of the excitatory postsynaptic current (EPSC) (Lester et al., 1990). To evaluate the influence of GluN1-P532H on the deactivation

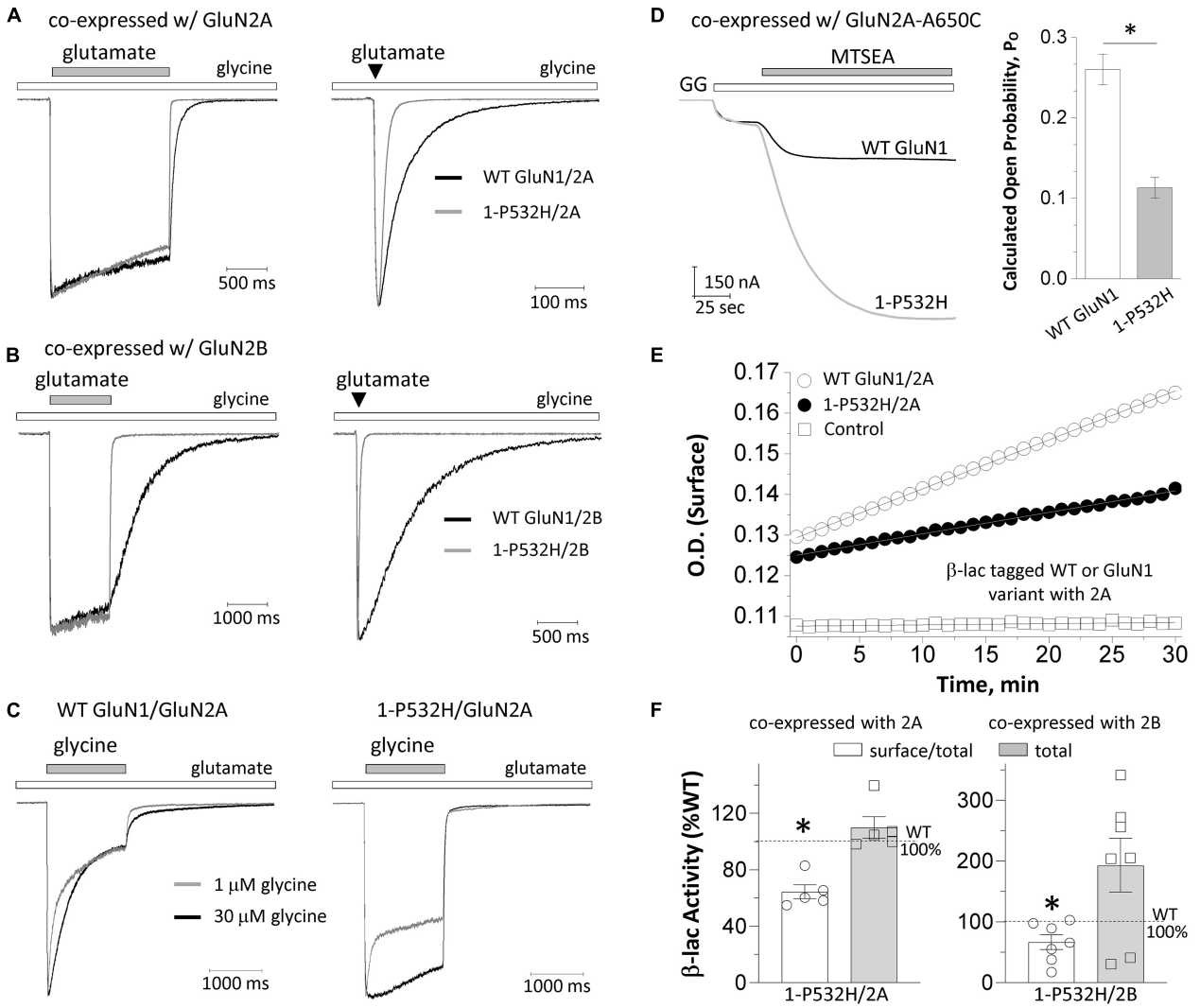

FIGURE 3 | Effects of GluN1-P532H variant on receptor biophysical properties and cell surface trafficking. **(A,B)** The current response was obtained from whole cell voltage clamp recordings at a holding potential of –60 mV from HEK293 cells that were transiently transfected with GluN1-P532H/GluN2A **(A)** or GluN1-P532H/GluN2B **(B)**. The current amplitude generated by a prolonged application (1.5 s; *left panels*) and a brief application (5 ms; *right panels*) of 1,000 μM glutamate in the presence of 100 μM glycine was normalized to that for wild-type receptors to compare response time course, and indicated a shortened synaptic-like response time course for variant NMDARs. **(C)** The current response generated from HEK cells that were transfected with WT GluN1/GluN2A (*left panel*) and GluN1-P532H/GluN2A (*right panel*) by a prolonged application (1.5 s) of two concentrations of glycine (1 μM in *gray*; 30 μM in *black*) in the presence of 1,000 μM glutamate was normalized to compare response time course and desensitization. **(D)** The channel open probability was evaluated by measuring the degree of MTSEA (200 μM; closed bar) potentiation using TEVC recordings from *Xenopus* oocytes expressing the WT GluN1 (black) or the variant GluN1-P532H (gray) coexpressed with GluN2A-A650C at a holding potential of –40 mV and activated by 1,000 μM glutamate and 100 μM of glycine (GG, open bar). The GluN1-P532H-containing receptors showed an increased potentiation compared with the WT, reflecting a reduced channel open probability (see **Table 1**). **(E)** Representative plots of nitrocefin absorbance (optical density, OD) as a function of time are shown for HEK293 cells expressing WT β-lac-GluN1 or β-lac-GluN1-P532H coexpressed with GluN2A. **(F)** The slopes of OD versus time course in minutes were averaged (n = 5–7 independent experiments) and presented as percentages of WT for the ratio of surface/total. Data are expressed as mean ± SEM and were analyzed by unpaired Student's t-test (*$p < 0.05$, compared with the corresponding WT surface/total ratio).

time course, we measured the current response time course following glutamate removal using a rapid solution exchange system. Current responses to prolonged application of glutamate (1.5 s, 1,000 μM) were recorded under whole-cell voltage clamp from transiently transfected HEK293 cells expressing WT GluN1/GluN2A, GluN1-P532H/GluN2A, WT GluN1/GluN2B, or GluN1-P532H/GluN2B. GluN1-P532H significantly decreased glutamate deactivation time course, which could be described by two exponential components with a weighted time constant (τw) of 26 ms for GluN1-P532H/GluN2A compared with 66 ms for WT GluN1/GluN2A. Weighted time constant for deactivation was 37 ms for GluN1-P532H compared with 821 ms for WT GluN1/GluN2B ($p < 0.01$, unpaired t-test; **Figures 3A,B** *left panels* and **Table 1**). To mimic synaptic events, we also recorded

the current response time course while briefly moving the transfected HEK cell into the agonist solution for 5 ms (brief application). Similar to the prolonged (1.5 s) application of glutamate, GluN1-P532H/GluN2A had a faster deactivation time course with a τ_W of 18 ms compared with 61 ms for WT GluN1/GluN2A. Similarly, GluN1-P532H/GluN2B had a faster deactivation time course with τ_W of 28 ms compared with 704 ms for WT GluN1/GluN2B (**Figures 3A,B** *right panels*). These data suggest that the variant GluN1-P532H-containing NMDARs have a faster deactivation response time course, and therefore will likely produce brief synaptic currents.

There is a negative allosteric coupling between glycine and glutamate binding such that when glutamate first binds to the receptor, there is a decrease in affinity for glycine. If glycine is present at subsaturating levels, glutamate binding can produce a slowly decreasing current because glycine unbinds as the system relaxes to a new equilibrium. This glycine-dependent relaxation in current has been referred to as glycine-dependent desensitization (Mayer et al., 1989; Benveniste et al., 1990). To evaluate whether the variant influences glycine-dependent desensitization, we recorded current responses to prolonged application of two concentrations of glycine (1 and 30 μM; 1.5 s) in the presence of 1,000 μM glutamate under whole-cell voltage clamp from HEK cells transfected with WT GluN1/GluN2A and GluN1-P532H/GluN2A. GluN1-P532H variant-containing NMDA receptors showed a diminished desensitization to high concentration of glycine ($p < 0.01$, unpaired *t*-test; **Figure 3C** and **Table 1**), while the fast component to desensitization in a subsaturating concentration of glycine appears to be retained in the variant receptors. These data suggest that GluN1-P532H does not eliminate glycine-dependent desensitization.

To assess the effects of the GluN1-P532H variant on single-channel open probability, we measured the degree by which covalent modification of an M3 residue by MTSEA potentiates NMDARs with a cysteine mutation in GluN2A M3 SYTANLAAF gating region (GluN2A-A650C); covalent modification by MTSEA of this residue locks the channels open (Jones et al., 2002; Yuan et al., 2005). We calculated the channel open probability based on the degree of MTSEA potentiation of the NMDAR response to maximally effective agonists (1,000 μM glutamate and 100 μM glycine) in TEVC oocytes recordings (V_{HOLD}: −40 mV; **Figure 3D**). The MTSEA-mediated current increase is reciprocally related to the channel open probability prior to MTSEA application (see the section "Materials and Methods"). These MTSEA-derived estimations indicated that channel open probability for GluN1-P532H/GluN2A decreased by 2.6-fold from 0.26 ($n = 41$) for WT GluN1/GluN2A to 0.11 ($n = 34$) ($p < 0.01$, unpaired *t*-test; **Figure 3D** and **Table 1**).

To evaluate whether the variant influences receptor cell surface expression, we measured the cell surface protein level and total protein level using a reporter assay in which β-lac was fused to the extracellular NTD of WT GluN1 (β-lac-GluN1) and the variant (β-lac-GluN1-P532H). The β-lac-GluN1 fusion protein was coexpressed with WT GluN2A or WT GluN2B in HEK293 cells. The level of surface receptor expression was determined by the β-lac cleavage of the cell-impermeable chromogenic substrate nitrocefin in the extracellular solution (Lam et al., 2013; Swanger et al., 2016). When coexpressed with WT GluN2A or WT GluN2B, the GluN1-P532H variant showed a significant decrease of surface-to-total protein level, compared with WT GluN1 receptors (GluN1-P532H/GluN2A: 64% of WT, GluN1-P532H/GluN2B: 67% of WT; $p < 0.05$; **Figures 3E,F** and **Table 1**). However, the variant when coexpressed with GluN2B showed a tendency to have higher total protein levels (total: 193% of WT; $p = 0.06$; **Figure 3F** and **Table 1**). These data suggest that the GluN1-P532H variant has a significant influence on surface expression. This may involve alterations in receptor assembly, as have been noted for mutations at other interdomain GluN1 residues (Farina et al., 2011).

To evaluate the net impact of GluN1-P532H variant on receptor function, we estimated the functional consequence of all measured changes of multiple parameters that resulted from this variant on synaptic and nonsynaptic charge transfer to wild-type receptors (Swanger et al., 2016; Li et al., 2019). This calculation indicated that the GluN1-P532H variant reduces synaptic and nonsynaptic charge transfer by 4.5- and 250-fold, respectively (**Table 1**). Overall, these data suggested that GluN1-P532H is a LoF variant and may induce NMDAR hypofunction as a result of a shortened synaptic response time course, a decreased channel open probability, and a reduced receptor cell surface expression levels.

Effects of GluN1-P532H Variant on Agonist-Binding Domain Cleft Distance

To investigate the structural effects of GluN1-P532H mutation, we performed MD simulation using the structure of the dimeric glycine and glutamate-binding domains of human NMDA (GluN1/GluN2A) receptor (PDB ID 5H8Q) (**Figure 4A**). Snap shots of the wild-type and mutant protein structure in the MD simulation trajectories are shown in **Figure 4B**. The structures show that the histidine in the mutant protein at site 532 in GluN1 is within 2.6 Å of the hydroxyl group of threonine 748 on the lower lobe of GluN2A. Consistent with the interaction across the dimer, there is a motion of the lower lobe of GluN2A ABD toward the GluN1 ABD and an opening of GluN2 ABD cleft as seen in the distance between the Cα atoms of sites Q503 and M701 (**Figure 4C**). No significant changes are observed in the glycine-binding cleft between wild-type and GluN1-P532H mutant, as seen in the Cα atom distance between sites Ser507 and Thr701 (**Figure 4D**). The changes in the ABD clefts are consistent with the functional measurements that show reduced glutamate potency but only slight changes in the glycine potency between the mutant and wild-type GluN1/GluN2A receptors.

To confirm the results from the MD simulations showing a more open GluN2 glutamate-binding domain cleft in the GluN1-P532H mutant, we investigated the distance across the ABD cleft in the GluN2 subunit using smFRET. **Figures 4E,F** depicts the normalized cumulative histograms generated from efficiency traces of 25–30 molecules for the wild-type and GluN1-P532H bound to glutamate and glycine. Concatenated FRET efficiency traces showing the population of the different FRET states shown in the smFRET histograms are provided

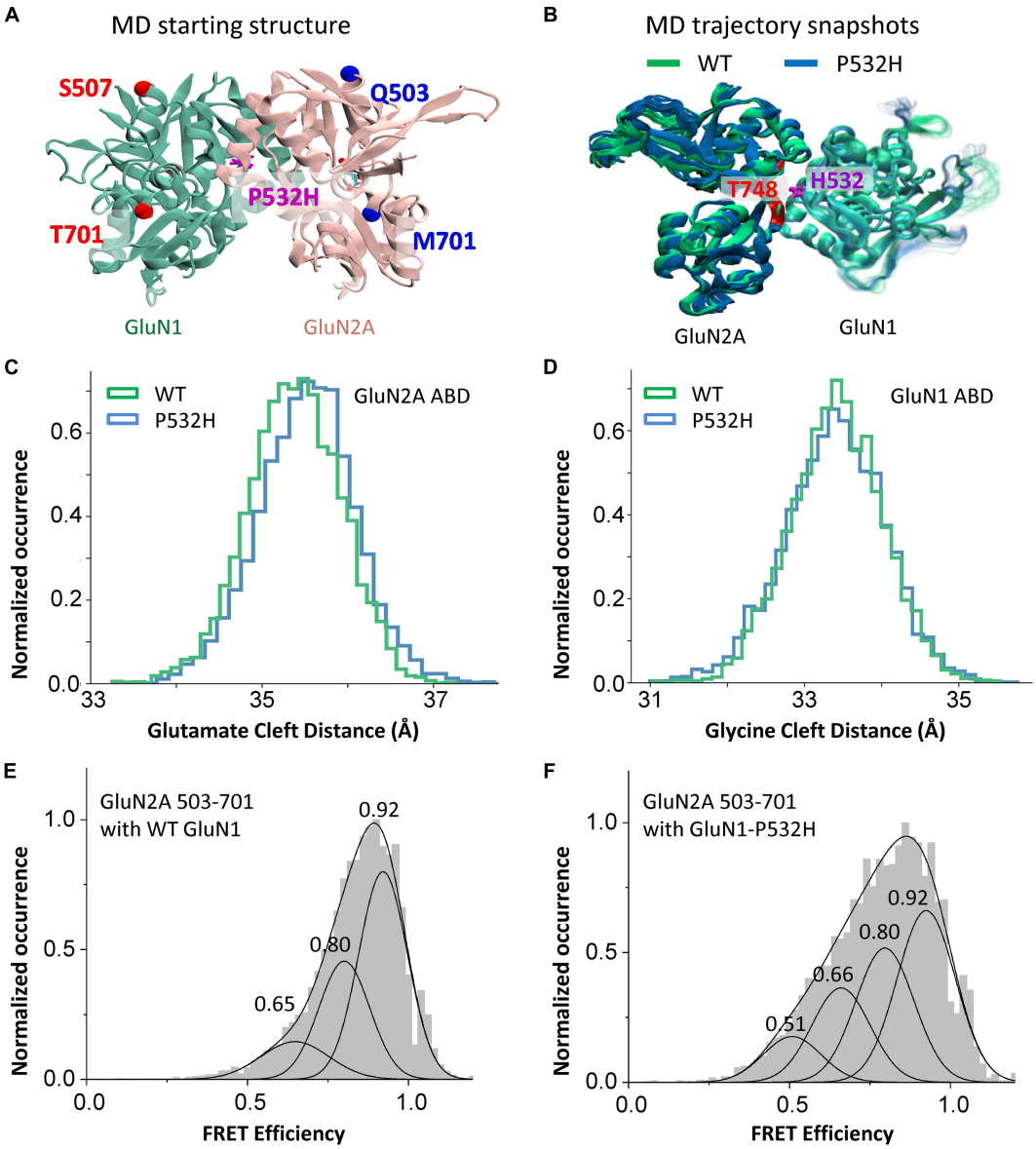

FIGURE 4 | Effects of GluN1-P532H variant on agonist-binding domain cleft distance. **(A)** Agonist-binding domain (ABD) dimer, GluN1 (green) and GluN2A (rose), used for MD simulation showing sites for measuring distances. **(B)** Structures from MD trajectory taken from 150 to 300 ns of simulations for wild-type (green) and GluN1-P532H variant (blue). Each frame in the figure represents the conformation of every 7.5 ns simulation time. **(C,D)** Histogram of distance measurement between the Cα atoms of sites Gln503 and Met701 in GluN2A **(C)** and Ser507 and Thr701 in GluN1 **(D)**, as seen in the MD simulation. **(E,F)** Normalized cumulative single-molecule FRET efficiency histograms depicting changes across the cleft (between sites 503 and 731) of glutamate-binding domain of GluN2A subunit in wild-type **(E)** and GluN1-P532H **(F)** bound to glutamate and glycine. The FRET efficiency states estimated by Gaussian fitting are listed and are shown in FRET efficiency traces in **Supplementary Figures 1–5**.

in the **Supplementary Figures 1–5**. The smFRET histograms show a shift in the population to lower FRET states in the GluN1-P532H mutant as compared with wild-type receptor. The low FRET states correspond to longer distances across the agonist-binding cleft, and hence more open cleft states, confirming the MD simulations. The more open cleft state is consistent with the decrease in glutamate potency observed in receptors containing the GluN1-P532H mutant relative to the wild-type protein.

Positive Allosteric Modulators Enhance Response of GluN1-Pro532His NMDARs

We tested whether the NMDAR hypofunction caused by GluN1-P532H variants can be rectified by a set of positive allosteric modulators (PAMs) and coagonists (Tang et al., 2020). 24(S)-Hydroxycholesterol [24(S)HC], an endogenous cholesterol metabolite in the brain, can enhance the current response of NMDARs (Linsenbardt et al., 2014; Wilding et al., 2016).

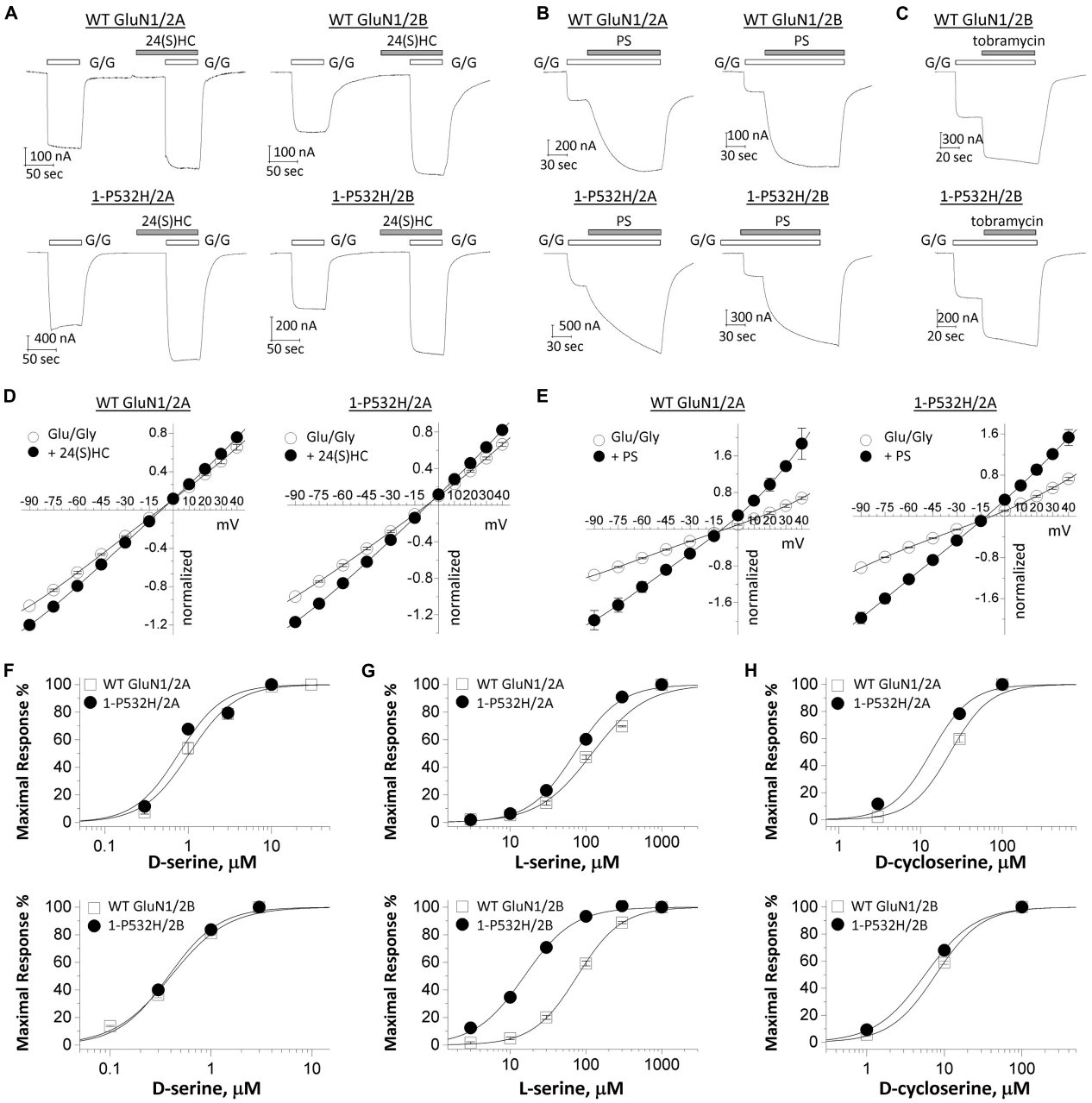

FIGURE 5 | Effects of positive allosteric modulators on loss-of-function GluN1-P532H variant. **(A–C)** Representative traces of current recordings using two electrode voltage clamp (TEVC) recordings (V_{HOLD}: –40 mV) from *Xenopus* oocytes showing effects of 10 μM 24(S)-hydroxycholesterol [24(S)HC], 100 μM pregnenolone sulfate (PS), and 300 μM tobramycin on WT GluN1(*upper panels*) and GluN1-P532H variant (*lower panels*) when coexpressed with GluN2A or GluN2B. G/G: 1,000 μM glutamate/100 μM glycine. **(D,E)** Current-voltage relationships for WT GluN1 (*left panels*) and GluN1-P532H variant (*right panels*) when coexpressed with GluN2A are shown for the current response to maximally effective concentrations of the agonists (Glu/Gly: 1,000 μM glutamate and 100 μM glycine; open circle) and in the agonists supplemented with 10 μM 24(S)-hydroxycholesterol (filled circle; **D**) and 100 μM pregnenolone sulfate (PS) (filled circle; **E**). Data are the mean ± SEM. All data points were normalized to the current response by agonists (Glu/Gly) at –90 mV. The measured voltage at –60 and +30 mV is given in **Table 2**. **(F–H)** Concentration–response curves for coagonists D-serine **(F)**, L-serine **(G)**, and D-cycloserine **(H)** on WT and GluN1-P532H variant when coexpressed with GluN2A (*upper panels*) or GluN2B (*lower panels*) in the presence of 1 mM glutamate were determined from TEVC (V_{HOLD}: –40 mV).

Pregnenolone sulfate (PS) can enhance neuronal NMDAR with selectivity for GluN2A- and GluN2B (Wu et al., 1991; Ceccon et al., 2001; Malayev et al., 2002; Horak et al., 2004). Tobramycin, an aminoglycoside antibiotic, can selectively potentiate GluN2B-containing NMDAR function (Swanger et al., 2016). **Figures 5A–C** shows that all three PAMs significantly potentiate the current response to maximally effective agonists (1 mM glutamate and 100 μM glycine) for both

TABLE 2 | Summary of rescue pharmacology.

Parameters	Coexpressed with GluN2A		Coexpressed with GluN2B	
	WT GluN1	GluN1-P532H	WT GluN1	GluN1-P532H
$I_{(24(S)HC)}/I_{(control)}$ % (*n*)	122% (110%, 134%) (8)	125% (114%, 136%) (10)	162% (154%, 169%) (7)	159% (142%, 176%) (12)
$I_{(PS)}/I_{(control)}$ % (*n*)	315% (186%, 445%) (7)	260% (213%, 307%) (10)	382% (324%, 441%) (7)	331% (268%, 393%) (15)
$I_{(tobramycin)}/I_{(control)}$ % (*n*)	NA	NA	199% (181%, 216%) (7)	189% (179%, 198%) (10)
$I_{(24(S)HC)}/I_{(control)}$, −60 mV (*n*)	1.2 (1.1, 1.3) (5)	1.3 (1.2, 1.4) (9)	NA	NA
$I_{(24(S)HC)}/I_{(control)}$, +30 mV (*n*)	1.2 (1.1, 1.2) (5)	1.2 (1.1, 1.4) (9)	NA	NA
$I_{(PS)}/I_{(control)}$, −60 mV (*n*)	1.6 (1.4, 1.8) (6)	2.0 (1.8, 2.2) (6)	NA	NA
$I_{(PS)}/I_{(control)}$, +30 mV (*n*)	2.2 (1.0, 3.3) (6)	2.2 (1.6, 2.7) (6)	NA	NA
D-Serine, EC_{50} [μM] (*n*)	1.1 (0.90, 1.2) (7)	0.79 (0.70, 0.88) (10)*	0.42 (0.37, 0.46) (9)	0.39 (0.33, 0.46) (14)
L-Serine, EC_{50} [μM] (*n*)	180 (169, 191) (6)	79 (68, 90) (9)*	82 (74, 91) (7)	18 (17, 19) (12)*
D-Cycloserine, EC_{50} [μM] (*n*)	28 (26, 30) (10)	12 (11, 13) (10)*	6.4 (5.1, 7.6) (8)	5.8 (4.7, 6.9) (11)

The data were generated by TEVC recordings on Xenopus oocytes (V_{HOLD}: −40 mV, unless otherwise stated) and expressed as mean (−95% CI, +95% CI) (n); CI, confidence interval; (n) is the number of oocytes.

**$p < 0.05$ indicated when the 95% confidence intervals of the datasets for the variant receptors do not overlap with the wild-type receptors.*

NA, not available.

wild-type and GluN1-P532H-containing NMDARs (**Table 2**). We evaluated the potentiation by these three PAMs over a range of holding potentials (−90 to 40 mV) in the absence of extracellular Mg^{2+}. **Figures 5D,E** shows the current-voltage relationships for NMDAR current responses to a maximally effective concentration of agonists coapplied with the indicated concentrations of each PAMs. We observed similar potentiating effects for coapplication of these PAMs for NMDARs that contained either WT or GluN1-P532H at both negative and positive holding potentials (**Figures 5D,E** and **Table 2**). In addition, three coagonists at glycine site, D-serine, L-serine, and D-cycloserine, were evaluated. These three coagonists showed a similar potency for WT and variant GluN1-P532H-containing NMDARs, with the exception of L-serine at GluN1-P532H/GluN2B (**Figures 5F–H** and **Table 2**). This result suggests that these PAMs and coagonists might enhance the current response caused by the LoF variant.

DISCUSSION

In this study, we report one patient who presented with early onset severe encephalopathy, and striking stimulus-induced myoclonus due to a *de novo* pathogenic variant in the *GRIN1* gene. Recent studies have reported over 20 patients and 26 pathogenic variants in the *GRIN1* gene (Hamdan et al., 2011; Tarabeux et al., 2011; Epi4K Consortium et al., 2013; Iossifov et al., 2014; Redin et al., 2014; Farwell et al., 2015; Ohba et al., 2015; Zhu et al., 2015; Bosch et al., 2016; Halvardson et al., 2016; Helbig et al., 2016; Lelieveld et al., 2016; Lemke et al., 2016; Retterer et al., 2016; Vanderver et al., 2016; Chen et al., 2017a; Rossi et al., 2017; Zehavi et al., 2017; Fry et al., 2018; Li et al., 2019). Phenotypes associated with *de novo GRIN1* pathogenic variants include severe early onset psychomotor delay in all reported patients and epilepsies in up to 70% of these patients (Hansen et al., 2021). Dyskinetic movement disorders were reported in some of the patients including chorea, dystonia, oculogyric crisis, and nonspecific stereotypic movements (Lemke et al., 2016). Fry et al. (2018) recently reported *de novo* pathogenic variants in the *GRIN1* gene in 11 patients with extensive bilateral polymicrogyria. The patient described here has striking stimulus-induced myoclonus, which was not previously reported. Brain MRI in this patient showed mild volume loss with enlarged extra axial space, best seen over the frontal lobes, mildly enlarged sulci, and thinned corpus callosum, which is similar with some reported cases with *GRIN1* variants (Lemke et al., 2016). This patient has *de novo GRIN1* missense variant (c.1595C>A, p.Pro532His) that changes a proline residue at 532, which is conserved through all vertebrate species and across all other GluN subunits. Furthermore, this position is also invariant in the healthy population for *GRIN1*, *GRIN2A*, and *GRIN2B*, indicating it plays a potentially important role in channel function. This analysis is consistent with the functional variation likely being deleterious. The Pro residue at which the variant is located is in the ABD for glycine in the GluN1 subunit. Surprisingly, instead of altering the glycine potency, our functional evaluation indicated that NMDARs containing GluN1-P532H showed a significant and marked decrease in glutamate potency, even though the glutamate-binding pocket resides in the GluN2 subunit.

The ABD is formed by two discontinuous protein segments (S1 and S2), which together form an upper (D1) and a lower (D2) lobe of a bilobed clamshell-like domain (Traynelis et al., 2010). The GluN1 and GluN2 ABDs form a heterodimeric complex in full-length proteins, and multiple crystallographic studies have identified interactions between the GluN1-glycine-binding domain and GluN2-glutamate-binding domain. There are three sites of interaction (Furukawa et al., 2005), several of which appear to play a role in controlling the rate of receptor deactivation. Interestingly, the residue Pro532 is located in Site-II (Furukawa et al., 2005), suggesting the variant-induced reduction in glutamate potency may be mediated by the heterodimer interaction between GluN1 and GluN2 subunits. MD simulations performed on the mutant protein showed that the mutation leads to histidine on GluN1 residing within hydrogen bonding distance with Thr748 on lower lobe of GluN2 and an opening of the GluN2 ABD cleft. This opening was also confirmed

by smFRET measurements. Consistent with the stabilization of a more open glutamate-binding domain cleft, activation of the variant receptors requires 15-fold higher concentrations of glutamate when coexpressed with GluN2A and 43-fold higher concentrations of glutamate when coexpressed with GluN2B. In addition, the variant-containing NMDAR complexes also showed an increase in sensitivity to endogenous Zn^{2+} inhibition (more inhibition), a reduction of current responses to maximally effective concentrations of coagonists, a decreased channel open probability, a shortened synaptic-like response time course, and a reduced cell surface expression levels, suggesting a shortened time course of the NMDAR component of the EPSC at synapses that utilize GluN1/GluN2A or GluN1/GluN2B. Therefore, GluN1-P532H is a LoF variant and may underlie certain features of the patient's clinical phenotypes, raising the possibility that mitigation of the functional deficits by a set of NMDAR-positive allosteric modulators might rescue the variant's consequences.

In summary, our study suggests that the novel *de novo GRIN1* variant (Pro532His) decreases NMDAR function and is associated with profound psychomotor impairment and striking stimulus-induced myoclonus without epilepsy. Evaluation of positive allosteric modulators raises the possibility to use these compounds as a strategy to partially rectify some functional deficits of the LoF variant, which might be clinically beneficial.

DATA AVAILABILITY STATEMENT

The datasets for this article are not publicly available due to concerns regarding participant/patient anonymity. Requests to access the datasets should be directed to the corresponding author.

ETHICS STATEMENT

The studies involving human participants were reviewed and approved by the Medical Ethics Committee and the Institutional Review Boards of Seattle Children's Hospital, University of Washington. Written informed consent to participate in this study was provided by the participants' legal guardian/next of kin. Written informed consent was obtained from the individual(s), and minor(s)' legal guardian/next of kin, for the publication of any potentially identifiable data included in this article.

AUTHOR CONTRIBUTIONS

ST, HY, SM, VJ, and XB designed the experiments and wrote the manuscript. XB and WD collected clinical information and evaluation and assessment of whole-exome sequencing. JZ, WT, YX, DL, SK, SM, WX, GS, and HY performed biological experiments and analyzed biological data. NP performed MD simulations. NB performed smFRET measurements. VJ designed the MD simulation and smFRET experiments. All authors discussed the results and implications and commented on the manuscript.

FUNDING

This work was supported by NIH—the Eunice Kennedy Shriver National Institute of Child Health and Human Development (NICHD) (HY, grant R01HD082373), by the NIH—National Institute of Neurologic Disorders and Stroke (NINDS) (ST, grants R35NS111619), by Austin Purpose (ST), by Emory-Xiangya Exchange Program (YX and RS), by NIH—National Institute of General Medical Sciences (NIGMS) (VJ, grant R35GM122528), and by HAMBP Fellowship NIH grant (NP, T32GM008280). The content is solely the responsibility of the authors and does not necessarily represent the official views of the funding agencies.

ACKNOWLEDGMENTS

The authors thank Jing Zhang, Nana Liu, and Phoung Le for technical support, and Sage Therapeutics Inc. for supplying the 24(S)-hydroxycholesterol.

SUPPLEMENTARY MATERIAL

The Supplementary Material for this article can be found online at: https://www.frontiersin.org/articles/10.3389/fgene.2021.694312/full#supplementary-material

Supplementary Figure 1 | Concatenated Fret efficiency traces corresponding to the conformational changes across the cleft of glutamate-binding domain of GluN2 subunit in wild-type and GluN1-P532H variant bound to glutamate and glycine.

Supplementary Figure 2 | Single-molecule representative traces measuring changes across the cleft of glutamate-binding domain of GluN2 subunit in the wild-type receptor bound to glutamate and glycine_Part-1.

Supplementary Figure 3 | Single-molecule representative traces measuring changes across the cleft of glutamate-binding domain of GluN2 subunit in the wild-type receptor bound to glutamate and glycine_Part-2.

Supplementary Figure 4 | Single-molecule representative traces measuring changes across the cleft of glutamate-binding domain of GluN2 subunit in the GluN1-P532H variant bound to glutamate and glycine_Part-1.

Supplementary Figure 5 | Single-molecule representative traces measuring changes across the cleft of glutamate-binding domain of GluN2 subunit in the GluN1-P532H variant bound to glutamate and glycine_Part-2.

REFERENCES

Akazawa, C., Shigemoto, R., Bessho, Y., Nakanishi, S., and Mizuno, N. (1994). Differential expression of five N-methyl-D-aspartate receptor subunit mRNAs in the cerebellum of developing and adult rats. *J. Comp. Neurol.* 347, 150–160. doi: 10.1002/cne.903470112

Benveniste, M., Clements, J., Vyklicky, L. Jr., and Mayer, M. L. (1990). A kinetic analysis of the modulation of N-methyl-D-aspartic acid receptors by glycine in mouse cultured hippocampal neurones. *J. Physiol.* 428, 333–357. doi: 10.1113/jphysiol.1990.sp018215

Best, R. B., Zhu, X., Shim, J., Lopes, P. E., Mittal, J., Feig, M., et al. (2012). Optimization of the additive CHARMM all-atom protein force field targeting

improved sampling of the backbone phi, psi and side-chain chi(1) and chi(2) dihedral angles. *J. Chem. Theory Comput.* 8, 3257–3273. doi: 10.1021/ct300400x

Bosch, D. G., Boonstra, F. N., De Leeuw, N., Pfundt, R., Nillesen, W. M., De Ligt, J., et al. (2016). Novel genetic causes for cerebral visual impairment. *Eur. J. Hum. Genet.* 24, 660–665. doi: 10.1038/ejhg.2015.186

Burnashev, N., and Szepetowski, P. (2015). NMDA receptor subunit mutations in neurodevelopmental disorders. *Curr. Opin. Pharmacol.* 20, 73–82. doi: 10.1016/j.coph.2014.11.008

Camp, C. R., and Yuan, H. (2020). GRIN2D/GluN2D NMDA receptor: unique features and its contribution to pediatric developmental and epileptic encephalopathy. *Eur. J. Paediatr. Neurol.* 24, 89–99. doi: 10.1016/j.ejpn.2019.12.007

Ceccon, M., Rumbaugh, G., and Vicini, S. (2001). Distinct effect of pregnenolone sulfate on NMDA receptor subtypes. *Neuropharmacology* 40, 491–500. doi: 10.1016/s0028-3908(00)00197-0

Chen, W., Shieh, C., Swanger, S. A., Tankovic, A., Au, M., Mcguire, M., et al. (2017a). GRIN1 mutation associated with intellectual disability alters NMDA receptor trafficking and function. *J. Hum. Genet.* 62, 589–597. doi: 10.1038/jhg.2017.19

Chen, W., Tankovic, A., Burger, P. B., Kusumoto, H., Traynelis, S. F., and Yuan, H. (2017b). Functional evaluation of a de novo GRIN2A mutation identified in a patient with profound global developmental delay and refractory epilepsy. *Mol. Pharmacol.* 91, 317–330. doi: 10.1124/mol.116.106781

Cooper, D. R., Dolino, D. M., Jaurich, H., Shuang, B., Ramaswamy, S., Nurik, C. E., et al. (2015). Conformational transitions in the glycine-bound GluN1 NMDA receptor LBD via single-molecule FRET. *Biophys. J.* 109, 66–75. doi: 10.1016/j.bpj.2015.05.025

Dolino, D. M., Chatterjee, S., Maclean, D. M., Flatebo, C., Bishop, L. D. C., Shaikh, S. A., et al. (2017). The structure-energy landscape of NMDA receptor gating. *Nat. Chem. Biol.* 13, 1232–1238. doi: 10.1038/nchembio.2487

Durham, R. J., Paudyal, N., Carrillo, E., Bhatia, N. K., Maclean, D. M., Berka, V., et al. (2020). Conformational spread and dynamics in allostery of NMDA receptors. *Proc. Natl. Acad. Sci. U.S.A.* 117, 3839–3847. doi: 10.1073/pnas.1910950117

Epi4K Consortium, Epilepsy Phenome/Genome Project, Allen, A. S., Berkovic, S. F., Cossette, P., Delanty, N., et al. (2013). De novo mutations in epileptic encephalopathies. *Nature* 501, 217–221. doi: 10.1038/nature12439

Farina, A. N., Blain, K. Y., Maruo, T., Kwiatkowski, W., Choe, S., and Nakagawa, T. (2011). Separation of domain contacts is required for heterotetrameric assembly of functional NMDA receptors. *J. Neurosci.* 31, 3565–3579. doi: 10.1523/jneurosci.6041-10.2011

Farwell, K. D., Shahmirzadi, L., El-Khechen, D., Powis, Z., Chao, E. C., Tippin Davis, B., et al. (2015). Enhanced utility of family-centered diagnostic exome sequencing with inheritance model-based analysis: results from 500 unselected families with undiagnosed genetic conditions. *Genet. Med.* 17, 578–586. doi: 10.1038/gim.2014.154

Fry, A. E., Fawcett, K. A., Zelnik, N., Yuan, H., Thompson, B. A. N., Shemer-Meiri, L., et al. (2018). De novo mutations in GRIN1 cause extensive bilateral polymicrogyria. *Brain* 141, 698–712.

Furukawa, H., Singh, S. K., Mancusso, R., and Gouaux, E. (2005). Subunit arrangement and function in NMDA receptors. *Nature* 438, 185–192. doi: 10.1038/nature04089

Gullingsrud, J., Kim, C., Taylor, S. S., and McCammon, J. A. (2006). Dynamic binding of PKA regulatory subunit RI alpha. *Structure* 14, 141–149. doi: 10.1016/j.str.2005.09.019

Halvardson, J., Zhao, J. J., Zaghlool, A., Wentzel, C., Georgii-Hemming, P., Mansson, E., et al. (2016). Mutations in HECW2 are associated with intellectual disability and epilepsy. *J. Med. Genet.* 53, 697–704.

Hamdan, F. F., Gauthier, J., Araki, Y., Lin, D. T., Yoshizawa, Y., Higashi, K., et al. (2011). Excess of de novo deleterious mutations in genes associated with glutamatergic systems in nonsyndromic intellectual disability. *Am. J. Hum. Genet.* 88, 306–316. doi: 10.1016/j.ajhg.2011.02.001

Hansen, K. B., Bowie, D., Furukawa, H., Menniti, F. S., Sobolevsky, A. I., Swanson, G. T., Swanger, S. A., et al. (2021). Structure, function, and pharmacology of glutamate receptor ion channels. *Pharmacol. Rev.* 73, 1–200. doi: 10.1124/pharmrev.120.000131

Helbig, K. L., Farwell Hagman, K. D., Shinde, D. N., Mroske, C., Powis, Z., Li, S., et al. (2016). Diagnostic exome sequencing provides a molecular diagnosis for a significant proportion of patients with epilepsy. *Genet. Med.* 18, 898–905. doi: 10.1038/gim.2015.186

Horak, M., Vlcek, K., Petrovic, M., Chodounska, H., and Vyklicky, L. Jr. (2004). Molecular mechanism of pregnenolone sulfate action at NR1/NR2B receptors. *J. Neurosci.* 24, 10318–10325. doi: 10.1523/jneurosci.2099-04.2004

Hu, C., Chen, W., Myers, S. J., Yuan, H., and Traynelis, S. F. (2016). Human GRIN2B variants in neurodevelopmental disorders. *J. Pharmacol. Sci.* 132, 115–121. doi: 10.1016/j.jphs.2016.10.002

Humphrey, W., Dalke, A., and Schulten, K. (1996). VMD: visual molecular dynamics. *J. Mol. Graph.* 14, 33–38, 27–38.

Hunter, J. D. (2007). Matplotlib: a 2D graphics environment. *Comput. Sci. Eng.* 9, 90–95. doi: 10.1109/mcse.2007.55

Iossifov, I., O'Roak, B. J., Sanders, S. J., Ronemus, M., Krumm, N., Levy, D., et al. (2014). The contribution of de novo coding mutations to autism spectrum disorder. *Nature* 515, 216–221.

Jones, K. S., Vandongen, H. M., and Vandongen, A. M. (2002). The NMDA receptor M3 segment is a conserved transduction element coupling ligand binding to channel opening. *J. Neurosci.* 22, 2044–2053. doi: 10.1523/jneurosci.22-06-02044.2002

Karakas, E., and Furukawa, H. (2014). Crystal structure of a heterotetrameric NMDA receptor ion channel. *Science* 344, 992–997. doi: 10.1126/science.1251915

Lam, V. M., Beerepoot, P., Angers, S., and Salahpour, A. (2013). A novel assay for measurement of membrane-protein surface expression using a beta-lactamase. *Traffic* 14, 778–784. doi: 10.1111/tra.12073

Lee, C. H., Lu, W., Michel, J. C., Goehring, A., Du, J., Song, X., et al. (2014). NMDA receptor structures reveal subunit arrangement and pore architecture. *Nature* 511, 191–197. doi: 10.1038/nature13548

Lelieveld, S. H., Reijnders, M. R., Pfundt, R., Yntema, H. G., Kamsteeg, E. J., De Vries, P., et al. (2016). Meta-analysis of 2,104 trios provides support for 10 new genes for intellectual disability. *Nat. Neurosci.* 19, 1194–1196. doi: 10.1038/nn.4352

Lemke, J. R., Geider, K., Helbig, K. L., Heyne, H. O., Schutz, H., Hentschel, J., et al. (2016). Delineating the GRIN1 phenotypic spectrum: a distinct genetic NMDA receptor encephalopathy. *Neurology* 86, 2171–2178. doi: 10.1212/wnl.0000000000002740

Lester, R. A., Clements, J. D., Westbrook, G. L., and Jahr, C. E. (1990). Channel kinetics determine the time course of NMDA receptor-mediated synaptic currents. *Nature* 346, 565–567. doi: 10.1038/346565a0

Li, D., Yuan, H., Ortiz-Gonzalez, X. R., Marsh, E. D., Tian, L., McCormick, E. M., et al. (2016). GRIN2D recurrent de novo dominant mutation causes a severe epileptic encephalopathy treatable with NMDA receptor channel blockers. *Am. J. Hum. Genet.* 99, 802–816. doi: 10.1016/j.ajhg.2016.07.013

Li, J., Zhang, J., Tang, W., Mizu, R. K., Kusumoto, H., Xiangwei, W., et al. (2019). De novo GRIN variants in NMDA receptor M2 channel pore-forming loop are associated with neurological diseases. *Hum. Mutat.* 40, 2393–2413. doi: 10.1002/humu.23895

Linsenbardt, A. J., Taylor, A., Emnett, C. M., Doherty, J. J., Krishnan, K., Covey, D. F., et al. (2014). Different oxysterols have opposing actions at N-methyl-D-aspartate receptors. *Neuropharmacology* 85, 232–242. doi: 10.1016/j.neuropharm.2014.05.027

Litwin, D. B., Durham, R. J., and Jayaraman, V. (2019). Single-molecule FRET methods to study glutamate receptors. *Methods Mol. Biol.* 1941, 3–16. doi: 10.1007/978-1-4939-9077-1_1

Malayev, A., Gibbs, T. T., and Farb, D. H. (2002). Inhibition of the NMDA response by pregnenolone sulphate reveals subtype selective modulation of NMDA receptors by sulphated steroids. *Br. J. Pharmacol.* 135, 901–909. doi: 10.1038/sj.bjp.0704543

Mayer, M. L., Vyklicky, L. Jr., and Clements, J. (1989). Regulation of NMDA receptor desensitization in mouse hippocampal neurons by glycine. *Nature* 338, 425–427. doi: 10.1038/338425a0

Myers, S. J., Yuan, H., Kang, J. Q., Tan, F. C. K., Traynelis, S. F., and Low, C. M. (2019). Distinct roles of GRIN2A and GRIN2B variants in neurological conditions. *F1000Research* 8:F1000 Faculty Rev-1940.

Ogden, K. K., Chen, W., Swanger, S. A., Mcdaniel, M. J., Fan, L. Z., Hu, C., et al. (2017). Molecular mechanism of disease-associated mutations in the pre-M1 helix of NMDA receptors and potential rescue pharmacology. *PLoS Genet.* 13:e1006536. doi: 10.1371/journal.pgen.1006536

Ohba, C., Shiina, M., Tohyama, J., Haginoya, K., Lerman-Sagie, T., Okamoto, N., et al. (2015). GRIN1 mutations cause encephalopathy with infantile-onset epilepsy, and hyperkinetic and stereotyped movement disorders. *Epilepsia* 56, 841–848. doi: 10.1111/epi.12987

Paoletti, P., Bellone, C., and Zhou, Q. (2013). NMDA receptor subunit diversity: impact on receptor properties, synaptic plasticity and disease. *Nat. Rev. Neurosci.* 14, 383–400. doi: 10.1038/nrn3504

Phillips, J. C., Braun, R., Wang, W., Gumbart, J., Tajkhorshid, E., Villa, E., et al. (2005). Scalable molecular dynamics with NAMD. *J. Comput. Chem.* 26, 1781–1802.

Redin, C., Gerard, B., Lauer, J., Herenger, Y., Muller, J., Quartier, A., et al. (2014). Efficient strategy for the molecular diagnosis of intellectual disability using targeted high-throughput sequencing. *J. Med. Genet.* 51, 724–736.

Retterer, K., Juusola, J., Cho, M. T., Vitazka, P., Millan, F., Gibellini, F., et al. (2016). Clinical application of whole-exome sequencing across clinical indications. *Genet. Med.* 18, 696–704.

Rossi, M., Chatron, N., Labalme, A., Ville, D., Carneiro, M., Edery, P., et al. (2017). Novel homozygous missense variant of GRIN1 in two sibs with intellectual disability and autistic features without epilepsy. *Eur. J. Hum. Genet.* 25, 376–380. doi: 10.1038/ejhg.2016.163

Swanger, S. A., Chen, W., Wells, G., Burger, P. B., Tankovic, A., Bhattacharya, S., et al. (2016). Mechanistic insight into NMDA receptor dysregulation by rare variants in the GluN2A and GluN2B agonist binding domains. *Am. J. Hum. Genet.* 99, 1261–1280. doi: 10.1016/j.ajhg.2016.10.002

Tang, W., Liu, D., Traynelis, S. F., and Yuan, H. (2020). Positive allosteric modulators that target NMDA receptors rectify loss-of-function GRIN variants associated with neurological and neuropsychiatric disorders. *Neuropharmacology* 177:108247. doi: 10.1016/j.neuropharm.2020.108247

Tarabeux, J., Kebir, O., Gauthier, J., Hamdan, F. F., Xiong, L., Piton, A., et al. (2011). Rare mutations in N-methyl-D-aspartate glutamate receptors in autism spectrum disorders and schizophrenia. *Transl. Psychiatry* 1:e55. doi: 10.1038/tp.2011.52

Traynelis, S. F., Burgess, M. F., Zheng, F., Lyuboslavsky, P., and Powers, J. L. (1998). Control of voltage-independent zinc inhibition of NMDA receptors by the NR1 subunit. *J. Neurosci.* 18, 6163–6175. doi: 10.1523/jneurosci.18-16-06163.1998

Traynelis, S. F., Wollmuth, L. P., Mcbain, C. J., Menniti, F. S., Vance, K. M., Ogden, K. K., et al. (2010). Glutamate receptor ion channels: structure, regulation, and function. *Pharmacol. Rev.* 62, 405–496.

Vanderver, A., Simons, C., Helman, G., Crawford, J., Wolf, N. I., Bernard, G., et al. (2016). Whole exome sequencing in patients with white matter abnormalities. *Ann. Neurol.* 79, 1031–1037.

Vanommeslaeghe, K., Hatcher, E., Acharya, C., Kundu, S., Zhong, S., Shim, J., et al. (2010). CHARMM general force field: a force field for drug-like molecules compatible with the CHARMM all-atom additive biological force fields. *J. Comput. Chem.* 31, 671–690.

Wilding, T. J., Lopez, M. N., and Huettner, J. E. (2016). Chimeric glutamate receptor subunits reveal the transmembrane domain is sufficient for NMDA receptor pore properties but some positive allosteric modulators require additional domains. *J. Neurosci.* 36, 8815–8825. doi: 10.1523/jneurosci.0345-16.2016

Wu, F. S., Gibbs, T. T., and Farb, D. H. (1991). Pregnenolone sulfate: a positive allosteric modulator at the N-methyl-D-aspartate receptor. *Mol. Pharmacol.* 40, 333–336.

XiangWei, W., Jiang, Y., and Yuan, H. (2018). De novo mutations and rare variants occurring in NMDA receptors. *Curr. Opin. Physiol.* 2, 27–35. doi: 10.1016/j.cophys.2017.12.013

XiangWei, W., Kannan, V., Xu, Y., Kosobucki, G. J., Schulien, A. J., Kusumoto, H., et al. (2019). Heterogeneous clinical and functional features of GRIN2D-related developmental and epileptic encephalopathy. *Brain* 142, 3009–3027. doi: 10.1093/brain/awz232

York, D. M., Darden, T. A., Pedersen, L. G., and Anderson, M. W. (1993). Molecular dynamics simulation of HIV-1 protease in a crystalline environment and in solution. *Biochemistry* 32, 1443–1453. doi: 10.1021/bi00057a007

Yuan, H., Erreger, K., Dravid, S. M., and Traynelis, S. F. (2005). Conserved structural and functional control of N-methyl-D-aspartate receptor gating by transmembrane domain M3. *J. Biol. Chem.* 280, 29708–29716. doi: 10.1074/jbc.m414215200

Yuan, H., Low, C. M., Moody, O. A., Jenkins, A., and Traynelis, S. F. (2015). Ionotropic GABA and glutamate receptor mutations and human neurologic diseases. *Mol. Pharmacol.* 88, 203–217. doi: 10.1124/mol.115.097998

Zehavi, Y., Mandel, H., Zehavi, A., Rashid, M. A., Straussberg, R., Jabur, B., et al. (2017). De novo GRIN1 mutations: an emerging cause of severe early infantile encephalopathy. *Eur. J. Med. Genet.* 60, 317–320. doi: 10.1016/j.ejmg.2017.04.001

Zhu, X., Petrovski, S., Xie, P., Ruzzo, E. K., Lu, Y. F., McSweeney, K. M., et al. (2015). Whole-exome sequencing in undiagnosed genetic diseases: interpreting 119 trios. *Genet. Med.* 17, 774–781. doi: 10.1038/gim.2014.191

Conflict of Interest: HY is PI on a research grant from Sage Therapeutics to Emory University School of Medicine. ST is PI on research grants from Janssen and Biogen to Emory University School of Medicine, is a member of the SAB for Sage Therapeutics and Eumentis, Inc., is co-founder of NeurOp Inc. and Agrithera Inc., and receives royalties for software. ST and HY are co-inventors on Emory-owned Intellectual Property that includes allosteric modulators of NMDA receptor function. SM owns shares in NeurOp. Inc.

The remaining authors declare that the research was conducted in the absence of any commercial or financial relationships that could be construed as a potential conflict of interest.

Publisher's Note: All claims expressed in this article are solely those of the authors and do not necessarily represent those of their affiliated organizations, or those of the publisher, the editors and the reviewers. Any product that may be evaluated in this article, or claim that may be made by its manufacturer, is not guaranteed or endorsed by the publisher.

frontiers in Genetics

CASE REPORT
published: 01 September 2021
doi: 10.3389/fgene.2021.716874

Case Report: Two New Cases of Chromosome 12q14 Deletions and Review of the Literature

Ruizhi Deng†, *Melysia T. McCalman*†, *Thomas P. Bossuyt and Tahsin Stefan Barakat**

Department of Clinical Genetics, Erasmus MC University Medical Center, Rotterdam, Netherlands

Interstitial deletions on the long arm of chromosome 12 (12q deletions) are rare, and are associated with intellectual disability, developmental delay, failure to thrive and congenital anomalies. The precise genotype-phenotype correlations of different deletions has not been completely resolved. Ascertaining individuals with overlapping deletions and complex phenotypes may help to identify causative genes and improve understanding of 12q deletion syndromes. We here describe two individuals with non-overlapping 12q14 deletions encountered at our clinical genetics outpatient clinic and perform a review of all previously published interstitial 12q deletions to further delineate genotype-phenotype correlations. Both individuals presented with a neurodevelopmental disorder with various degrees of intellectual disability, failure to thrive and dysmorphic features. Previously, larger deletions overlapping large parts of the deletions encountered in both individuals have been described. Whereas, individual 1 seems to fit into the previously described phenotypic spectrum of the 12q14 microdeletion syndrome, individual 2 displays more severe neurological symptoms, which are likely caused by haploinsufficiency of the BAF complex member *SMARCC2*, which is included in the deletion. We furthermore perform a review of all previously published interstitial 12q deletions which we found to cluster amongst 5 regions on chromosome 12, to further delineate genotype-phenotype correlations, and we discuss likely disease relevant genes for each of these deletion clusters. Together, this expands knowledge on deletions on chromosome 12q which might facilitate patient counseling. Also, it illustrates that re-analysis of previously described microdeletions syndromes in the next generation sequencing era can be useful to delineate genotype-phenotype correlations and identify disease relevant genes in individuals with neurodevelopmental disorders.

Keywords: chromosome, deletion 12q, clinical genetics, reverse phenotyping, BAFopathies, SMARCC2

OPEN ACCESS

Edited by:
Santasree Banerjee,
Beijing Genomics Institute (BGI), China

Reviewed by:
Ankita Patel,
Quest Diagnostics, United States
David Chitayat,
University of Toronto, Canada
Dhanya Lakshmi Narayanan,
Kasturba Hospital, India
Sarah Vergult,
Ghent University, Belgium

***Correspondence:**
Tahsin Stefan Barakat
t.barakat@erasmusmc.nl

†*These authors have contributed equally to this work*

Specialty section:
This article was submitted to Genetics of Common and Rare Diseases, a section of the journal Frontiers in Genetics

Received: *29 May 2021*
Accepted: *02 August 2021*
Published: *01 September 2021*

Citation:
Deng R, McCalman MT, Bossuyt TP and Barakat TS (2021) Case Report: Two New Cases of Chromosome 12q14 Deletions and Review of the Literature. Front. Genet. 12:716874. doi: 10.3389/fgene.2021.716874

INTRODUCTION

Interstitial deletions of chromosome 12q are rare, often *de novo* occuring, chromosome abnormalities. Various studies described phenotypes of different 12q deletions, including developmental delay, intellectual disability, growth retardation and dysmorphic features (Rauen et al., 2002; Miyake et al., 2004; James et al., 2005; Menten et al., 2007; Niyazov et al., 2007; Adam et al., 2010; Lynch et al., 2011; Vergult et al., 2011; Al-Maawali et al., 2014; Carlsen et al., 2015; De Crescenzo et al., 2015; Cano et al., 2016; Labonne et al., 2016; Alesi et al., 2019; Uehara et al., 2019),

but an in-depth overview of all published cases to determine genotype-phenotype correlations and to identify candidate disease-causing genes for most of these microdeletion syndromes is lacking.

We here describe two new cases encountered in our clinic presenting with different, non-overlapping interstitial deletions of chromosome 12q14. The combined deleted region of both cases largely overlaps with previously reported larger deletions (Buysse et al., 2009; Lynch et al., 2011; Nso-Roca et al., 2014; Mc Cormack et al., 2015). The major phenotypical differences identified in both affected individuals triggered us to perform a review of all previously published cases of chromosome 12q14 deletions and 12q deletion in general, with the goal to delineate a phenotype-genotype correlation that would allow improved prediction of clinical phenotypes.

A total of 69 individuals, with various overlapping 12q deletions, were identified in literature, with deletions located across five clusters, with one or several small region of overlap (SROs). Of these, 27 individuals were found with deletions in 12q14. We discuss their phenotypes and the likely disease causing genes of these deletions in the context of the deletions encountered in the two individuals that we describe.

METHODS

Patient Recruitment

Patients were recruited during their routine visits of the outpatient clinic of the Clinical Genetics Department of the Erasmus MC, Rotterdam, The Netherlands. Written informed consent was obtained from the legal guardians for publication of anonymized medical data and clinical photographs.

Review Strategy

We searched Pubmed (last assessed: May 2021) for papers describing patients with chromosome 12q deletions, focusing on reports in English and available to the library of the Erasmus MC, and extended our search to papers mentioned in the reference lists of identified papers. We excluded papers that only focused on somatic deletions (e.g., in tumor cells) or papers reporting complex rearrangements and translocations. Identified patients from literature were grouped according to the cytogenetic location of their deletions, and reported symptoms were collected and counted for each group. All genetic coordinates are given in genome build hg19.

Gene Expression and Probability of Loss-Of-Function Intolerance Analysis

Publically available RNA-seq data from different brain regions and other fetal tissues were collected from the ENCODE project (Consortium, 2012), accession numbers and details are given in **Supplementary Table 8**. Gene expression levels were normalized based on fragments per kilobase of transcript per million mapped reads (FPKM). pLI scores were downloaded from the gnomAD website (https://gnomad.broadinstitute.org/downloads). Gene expression levels and pLI score were plotted using R packages.

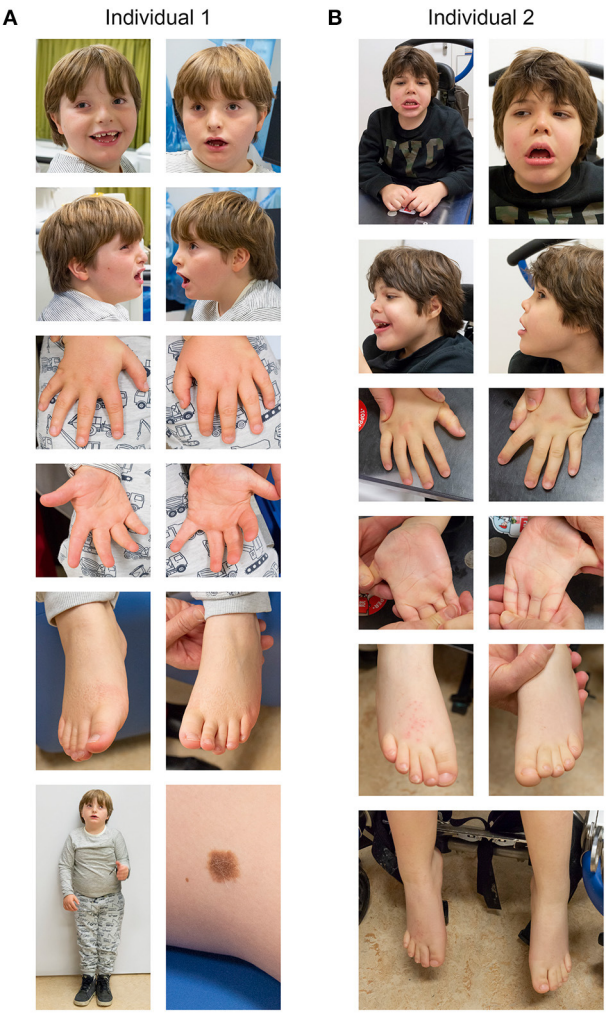

FIGURE 1 | Clinical photographs of individual 1 **(A)** and individual 2 **(B)**. See text for details.

RESULTS

Individual 1

Individual 1 is a 7-year-old male, presenting with developmental delay, moderate intellectual disability and growth retardation (**Figure 1**). He was the third child of non-consanguineous Dutch parents, born at 36 weeks of gestation, with a birth weight of 1,945 gram (<p3), head circumference of 31.5 cm (p42) and a good start (APGAR 9 and 9 at 1 and 5 min, respectively). Family history was negative for developmental delay or congenital anomalies. Pregnancy was conceived through *in vitro* fertilization (IVF) (his older brother was the product of a fertilized egg conceived during the same IVF cycle and is healthy) and was complicated with recurrent vaginal bleeding and placental insufficiency, with IUGR noticed at 20 weeks of gestation. Screening for TORCHES and routine karyotyping were normal. Frequent airway infections complicated the first year but improved over time, after which psychomotor delay, failure to thrive and dysmorphic features

were noticed. He started independent walking at the age of 3 years, with a pronounced exorotation of the legs, requiring orthopedic shoes. First words started around 4 years of age, and at the last investigation at 7 years of age, speech development is severely delayed although progressive with only a few understandable words, requiring special education. His language perception and non-verbal skills are more developed. His tested IQ was 50 (SON-IQ). He reacts very sensitive to sounds, and cannot tolerate crowded places or sudden changes of regularities in his daily activities, indicative of an autism spectrum disorder. Other behavioral issues include occasional temper tantrums when unable to express himself, hyperphagia and incontinence. Physical examination at age of 7 years showed a short stature [110 cm (−3.44 SD)], with normal weight [31 kg (+1.6 SD)] and head circumference of 52.5 cm (+0.15 SD). Outer and inner canthal distance were increased [OCD: 10 cm (>p97); ICD: 3.5 cm (>p97)] with interpupillary distance in the normal range [IPD: 5.5 cm (>p50)]. Neurological examination was normal except a low muscular tone and clumpsy gait. Other findings included upslanting palpebral fissures, a broad nasal bridge, with midfacial hypoplasia, an open mouth posture, with small irregular implanted teeth, a single café-aut-lait spot on the back and a large naevus on the left upper leg which was present since birth (**Figure 1A**). Previous ultrasound studies of heart and kidneys were normal. Imaging studies of the hips showed coxae valgea antetorta, without signs of osteopoikilosis. A SNP-array identified a *de novo* 4.4 Mb deletion on chromosome 12q14.2-q15 [arr 12q14.2q15 (64,899,031–69,328,844)1×]. This deletion includes 24 protein coding genes including the genes *LEMD3* and *HMGA2*, and overlaps with a region previously linked to a chromosome 12q14 deletion syndrome (Menten et al., 2007).

Individual 2

Individual 2 is a 7-year-old male with pronounced psychomotor retardation, severe intellectual disability and failure to thrive (**Figure 1**). He was born after an uneventful pregnancy as the second child to non-consanguineous Dutch parents at 35 + 6 weeks of gestation, with a birth weight of 2,380 gram (p10) and an uncomplicated start of life directly after birth. Family history was negative for developmental delay or congenital anomalies. Feeding difficulties required hospital admission for the first week of life. At 3 months of age developmental delay was first noticed, and at the age of 9 month hypotonia and dysmorphic features were observed. Recurrent airway infections required continuous cotrimoxazol treatment. Independent sitting skills were acquired at 3 years of age, but ambulation, speech, or toilet training never developed. A number of surgical interventions were required due to recurrent hip and knee luxation and flexion contractures. Currently he is wheel chair bound, has no signs of regression and requires PEG feeding. Communication occurs via a language computer aid and pictograms. There is a social smiling with occasional temper tantrums, and more recently involuntary movements. Physical examination at the age of 7 years showed a length of 118 cm (−2.27 SD), weight of 23 kg (−0.99 SD) and head circumference of 52 cm (−0.21 SD); Inner and outer canthal distance were 3 cm (<p75) and 9.5 cm (>p97), respectively. Neurological examination showed pyramidal and extrapyramidal signs, including involuntary movements of the head, trunk and upper extremities. He makes sounds and seems to understand simple instructions to a certain degree. Other findings included a coarse facial appearance with upslanting palpebral fissures, epicanthal folds, a broad nasal bridge, upturned nose, an open mouth posture with widely spaced teeth in the lower jaw and high-arched palate, bilateral simian crease, bilateral 2–3 toe syndactyly and retractile testis. An initial ventricular septum defect closed spontaneously. Brain MRI imaging showed widened central and peripheral liquor spaces. Cerebrospinal fluid analysis and EEG were normal. SNP-array identified a *de novo* 7.3 Mb deletion of chromosome 12q13.2q14.2 [arr 12q13.2q14.2 (56,554,154–63,870,277) × 1]. This deletion includes 73 genes, including *SMARCC2,* and is partially overlapping with previously described deletions in 12q13.3q14.2 (Buysse et al., 2009; Lynch et al., 2011; Nso-Roca et al., 2014; Mc Cormack et al., 2015).

LITERATURE REVIEW OF CHROMOSOME 12q DELETIONS

Both patients differ in their clinical phenotype. Whereas, individual 1 is more mildly affected and is able to walk and has a limited ability to speak, individual 2 is more severely affected, with lack of independent ambulation and speech. Both individuals have a short stature, failure to thrive and a few shared dysmorphic features (**Figure 1**), but clear differences in their phenotype manifest. As both deletions encountered in these individuals were non-overlapping but having breakpoints in proximity (e.g., within ∼1 Mb), and previously a number of deletions were described that encompass large parts of both deletions (Buysse et al., 2009; Lynch et al., 2011; Nso-Roca et al., 2014; Mc Cormack et al., 2015), we set out to review the literature to identify likely genes involved in the phenotypic differences and to further delineate the genotype-phenotype correlation associated with chromosome 12q deletions in general. We found 69 published individuals with 12q deletions and their clinical phenotypes (**Supplementary Table 1**). Overlapping deletions clustered in 5 regions at 12q11q13.1, 12q13q15, 12q13.3q23.1, 12q21.1q23.2, and 12q22q24.33 (**Figure 2**). We here focus on the cluster at 12q13q15, which includes the two deletions encountered in individual 1 and 2, and discuss the other clusters in more detail in the **Supplemental Material** and **Supplementary Tables 4–7**.

Individual 1 Fits the Spectrum of 12q13q15 Deletions Encompassing the 12q14 Microdeletion Syndrome

Twenty-seven individuals (14 females, and 13 males) with overlapping deletions located within 12q13q15 have been previously reported with varying degrees of global developmental delay/intellectual disability, growth retardation and short stature as the main phenotype (Menten et al., 2007; Buysse et al., 2009; Mari et al., 2009; Spengler et al., 2010; Lynch et al., 2011; Alyaqoub et al., 2012; Bibb et al., 2012; Takenouchi et al., 2012;

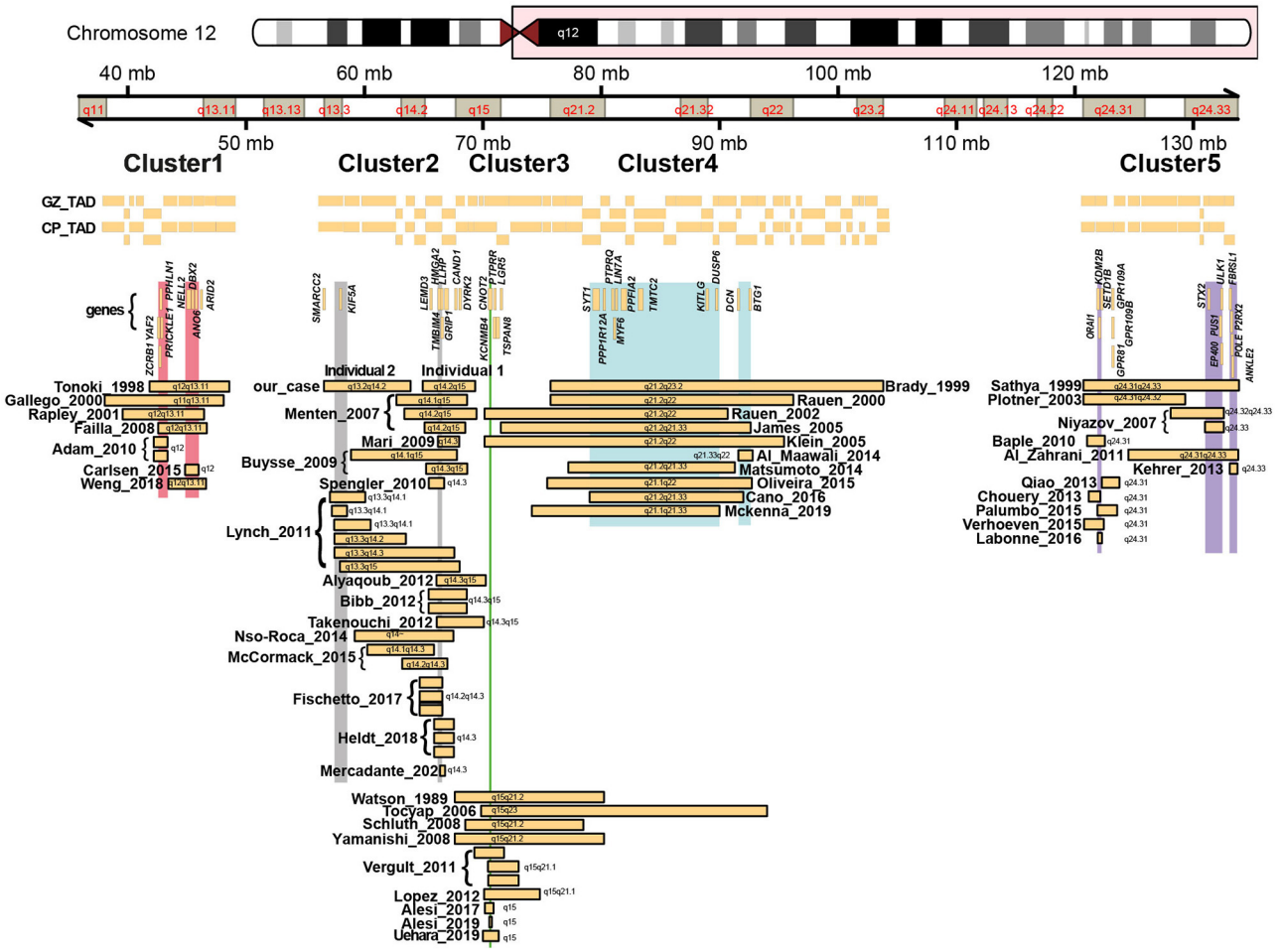

FIGURE 2 | Schematic overview of all previously reported deletions along chromosome 12q, with chromosome ideograms and bands indicated. Horizontal bars represent identified deletions that cluster amongst 5 regions, with names and years referring to the first author and year of publication from the studies in which these deletions were described. Also indicated are topological associated domains (Won et al., 2016) identified from chromatin conformation capture analysis of the germinal zone (GZ) and cortical plate (CP) from human fetal brain. Vertical bars represent small regions of overlaps shared between the different deletions. Genes discussed in the main text or in the **Supplemental Materials** are indicated.

Fischetto et al., 2017; Heldt et al., 2018; Mercadante et al., 2020; **Figure 3**, **Supplementary Table 2**).

The deletion encountered in individual 1 overlaps with 22 reported deletions which have been associated with a 12q14 microdeletion syndrome (Menten et al., 2007; Buysse et al., 2009; Mari et al., 2009; Spengler et al., 2010; Lynch et al., 2011; Alyaqoub et al., 2012; Bibb et al., 2012; Takenouchi et al., 2012; Nso-Roca et al., 2014; Mc Cormack et al., 2015; Fischetto et al., 2017; Heldt et al., 2018; Mercadante et al., 2020), and the boundaries largely overlap with seven of these previously published deletions (Menten et al., 2007; Buysse et al., 2009; Bibb et al., 2012; Takenouchi et al., 2012), with an SRO located in 12q14.3. Menten et al. described three individuals, with a core phenotype of mild intellectual disability, low birth weight with failure to thrive in early infancy, proportionate short stature and osteopoikilosis (the latter is in combination with multiple subcutaneous nevi or nodules also known as Buschke-Ollendorf syndrome) (Hellemans et al., 2004). Dysmorphic features between the three individuals were not consistent, and included synophrys, mild hypertelorism, broad and high nasal bridge, micrognathia, maxillary overbite, round face with deep-set eyes, bushy eyebrows, thin lips, and a triangular face with widely spaced eyes. In a follow-up study, two additional individuals with overlapping deletions were described (Buysse et al., 2009), that presented with a similar phenotype. Interestingly, in that report, also an intragenic deletion of *HMGA2* was found in a boy with proportionate short stature, and this deletion segregated with this phenotype in this family, indicating that *HMGA2* is responsible for the short stature seen in individuals with 12q14 deletions. His neurodevelopment was normal (Buysse et al., 2009). Bibb et al. reported a mother and a daughter sharing a deletion in this region (Bibb et al., 2012). The daughter presented with failure to thrive, hypertelorism, upturned nose, mild micronathia, and clinodactyly, and was suspected of Silver-Russel syndrome. She

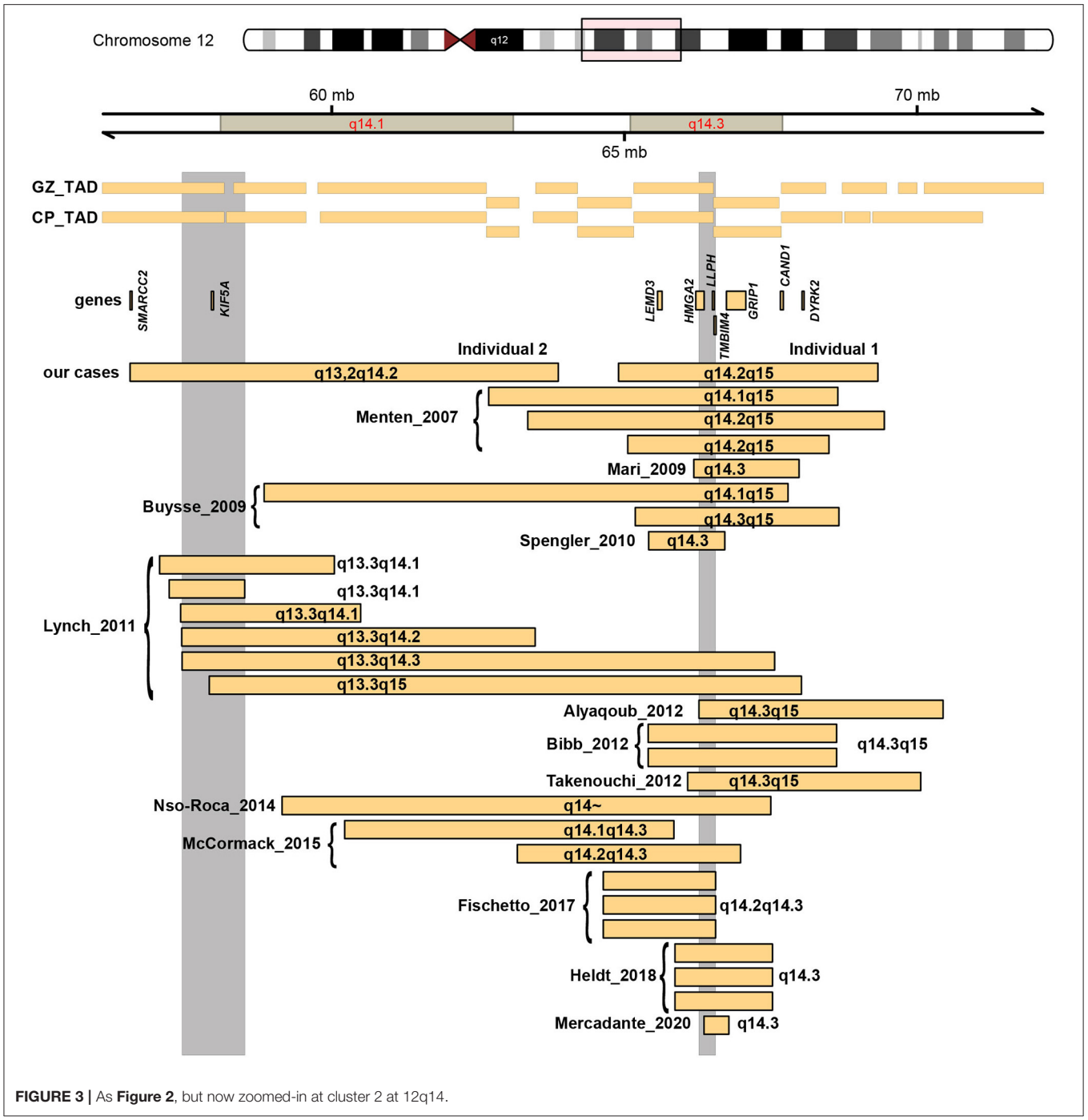

FIGURE 3 | As **Figure 2**, but now zoomed-in at cluster 2 at 12q14.

also had physical and language delays, mild intellectual disability, behavioral problems, and sleep disturbance. The mother also presented early in life with failure to thrive, a short stature, mild language delay, microcephaly, a café aut lait spot, mild clinodactyly, upslanting palpebral fissures, and osteopoikilosis. The individual described by Takenouchi et al. showed failure to thrive, short stature, no relative macrocephaly, and surprisingly an appropriate psychomotor development at 29 month of age without autism (Takenouchi et al., 2012). Lynch et al. described 6 additional cases with 12q14 deletions, of whom only two shared the SRO in 12q14.3 (Lynch et al., 2011). Both deletions were larger than the one found in individual 1 in this report. Both individuals had failure to thrive, one individual displayed moderate developmental delay and expressive speech delay, whereas the second individual had severe developmental delay, with autism and absence of speech.

Taken together, the phenotype of moderate developmental delay and failure to thrive of individual 1 seems to fit well to

the spectrum previously described for similar range deletions, although osteopoikilosis has not yet been noticed in this individual. The key features of failure to thrive, short stature and osteopoikilosis found in 12q14 deletions seem by current day's knowledge to be explained by haploinsufficiency of *HMGA2* and *LEMD3*, respectively.

HMGA2, located at band 12q14.3, encodes an architectural transcription factor, and is a critical component of the enhanceosome. Based on studies performed after the reports on the various 12q14 deletions, *HMGA2* has now been implicated as one of the causes of Silver-Russel syndrome (OMIM #618908), which is characterized by intrauterine growth retardation, postnatal feeding difficulties and growth failure, with dysmorphic features including a relative macrocephaly at birth and a triangular face with prominent forehead. Support for *HMGA2* being implicated in growth originally came from GWAS studies (Weedon et al., 2007) and mouse models (Zhou et al., 1995). In the 12q14 deletions discussed above *HMGA2* was hypothesized to be causal for failure to thrive and short statures (Menten et al., 2007; Buysse et al., 2009; Bibb et al., 2012; Takenouchi et al., 2012). Mari et al. (2009), Heldt et al. (2018), and Mercadante et al. (2020) described individuals with a clinical phenotype reminiscent to Silver-Russel syndrome, with deletions that included *HMGA2* and a limited number of additional genes (Mari et al., 2009; Heldt et al., 2018; Mercadante et al., 2020). Smaller genetic alterations, solely affecting *HMGA2*, including a 7bp deletion that affects splicing (De Crescenzo et al., 2015), a 7.3Kb deletion of exon 1 and 2 (Leszinski et al., 2018), other small deletions (Buysse et al., 2009), and missense and truncating variants have subsequently been found in Silver-Russel syndrome like cases (Abi Habib et al., 2018; Hübner et al., 2020), pinpointing *HMGA2* as the causative gene. In agreement with this, all cases with a deletion encompassing this gene have a short stature (Zhou et al., 1995; Weedon et al., 2007; Buysse et al., 2009; Alyaqoub et al., 2012; **Supplementary Table 2**).

Osteopoikilosis is linked to loss-of-function of *LEMD3* (Hellemans et al., 2004; Mumm et al., 2007; Zhang et al., 2009), a gene encoding a LEM-domain containing protein that functions to antagonize BMP and transforming growth factor-beta signaling (Hellemans et al., 2004). Six of the twenty-seven individuals from literature with deletions in this cluster had osteopoikilosis and in all 6 cases LEMD3 was deleted. However, LEMD3 was deleted in 16 out of the 27 cases, and in the remaining cases with LEMD3 deletion, including the case described herein, no osteopoikilosis was reported at the moment of investigation (**Supplementary Table 2**). It is unknown whether those cases later on developed this condition.

Interestingly, the neurodevelopmental phenotypes associated with deletions of 12q14 cannot be explained by haploinsufficiency of either *HMGA2* or *LEMD3* alone, as individuals that only have gene specific alterations either showed normal development (Buysse et al., 2009; Leszinski et al., 2018; Hübner et al., 2020), or only mild delay (Mercadante et al., 2020). Psychomotor retardation is also rarely encountered in Silver-Russel syndrome. This indicates that neurodevelopmental delay, observed in most cases of 12q14 deletions, might be caused by other genes in or outside the SRO. The minimal SRO overlapping with the deletion found in individual 1 is 281,741 bp, and next to *HMGA2* contains the genes *LLPH* and *TMBIM4*. Both have not yet been associated with human disease. *LLPH* encodes an intrinsically disordered protein predicted to function in the nucleolus, possibly as a molecular hub for protein-protein interactions (Yu et al., 2016). *TMBIM4* is a highly conserved Golgi membrane protein that inhibits apoptosis and promotes Ca(2+) release from intracellular stores (Saraiva et al., 2013). Both genes however have a low pLI score (Karczewski et al., 2020), making it unlikely that haploinsufficiency of these genes causes a human disorder.

A frequently discussed candidate gene for the neurodevelopmental phenotypes, outside of the SRO is *GRIP1*. *GRIP1*, encodes a Glutamate-receptor interacting protein 1 that is widely expressed in brain and involved in glutamergic synapse transmission. It has been reported to function in modulating long-term synaptic depression in the cerebellum (Takamiya et al., 2008; Alyaqoub et al., 2012). Bi-allelic variants in *GRIP1* were found to segregate with Fraser syndrome which is characterized by cryptophthalmos, syndactyly, and abnormalities of the respiratory and urogenital tract (Van Haelst et al., 2008; Vogel et al., 2012). *GRIP1* has been suggested as a candidate gene for developmental delay and learning difficulties observed in 12q14 deletions (Menten et al., 2007; Dória et al., 2020). However, as *GRIP1* is not deleted in all individuals (18 out of 27 in this cluster) with neurodevelopmental delay in this cluster (**Supplementary Table 2**), the individual described by Takenouchi et al. did not display psychomotor retardation despite *GRIP1* deletion and multiple heterozygous loss-of-function variants are found in healthy controls from gnomAD (pLI = 0.50828) (Karczewski et al., 2020), it seems unlikely that *GRIP1* is implicated in neurodevelopmental delay in 12q14 deletions.

The precise genetic cause of neurodevelopmental delay in 12q14 deletion thus remains to be determined. Within the genes covered by the deletion of individual 1, *CAND1* and *DYRK2* have a high pLI score (pLI = 1.0 and pLI = 0.99751, respectively), indicating that they could be susceptible to haploinsufficiency. Both genes are expressed in brain, and are each deleted in 11 and 5 cases, respectively, making them interesting candidate genes to explore further in future studies.

The More Severe Clinical Phenotype of Individual 2 Is Likely Explained by Haploinsufficiency of SMARCC2

Whereas, individual 1 is well-explained by the deletion and the spectrum of phenotypes associated with the 12q14 microdeletion syndrome, individual 2 is more severely affected than what has been described for individuals with other large deletions in this region (Buysse et al., 2009; Lynch et al., 2011; Nso-Roca et al., 2014; Mc Cormack et al., 2015). As mentioned above, the individuals with the largest deletions described by Lynch et al. (2011) that overlap with the SRO in 12q14, presented with moderate to severe developmental delay, but both individuals achieved independent walking. Individual 4 of Lynch et al. (2011) which harbors a deletion that overlaps large parts of the deleted

region in individual 2 from this report, displayed more severe delay and autism, but developed the use of single words and was reported to be extremely active. Also the other three cases of Lynch et al. (2011) were reported to be moderately delayed, with speech delay and absence of speech in one individual, but also acquired independent ambulation. Similar, the largest deletions described by Buysse et al. (2009) is milder affected and able to use many words. The individual described by Nso-Roca had learning problems, besides failure to thrive, and the individual described by Mc Cormack in which the deletion did not contain *HMGA2*, had relative macrocephaly and autism, wild mild delayed gross and fine motor skills and language delay showing encouraging improvements in all aspects of development over time. The 6 cases described by Lynch et al. (2011) possibly point to another SRO at 12q13.3q14.1, containing 34 genes (**Supplementary Table 3**), which overlaps with the deletion found in individual 2, which covers 73 genes.

To further understand the more severe phenotype of individual 2, we manually assessed all 73 genes included in the deletion searching for known phenotypes, determined their pLI scores and assessed whether there was evidence of expression of these genes in fetal human tissues including brain (**Figure 4**). We found 19 genes with a pLI > 0.9, indicating that they are intolerant for loss-of-function and could thus be involved in causing a phenotype, when deleted on a single allele. These genes included protein coding genes previously not associated with human disorders or with unclear associations, including *LRP1*, *R3HDM2*, *ANKRD52*, *BAZ2A*, *R3HDM2*, *USP15*, *MBD6*, *AGAP2*, *DCTN2*, and the two OMIM genes *KIF5A* and *SMARCC2*. *KIF5A* (OMIM #604187) is associated with a autosomal dominant form of hereditary spastic paraplegia, with lower limb spasticity, and hyperreflexia, and variable involvement of the upper limbs beginning in childhood or young adulthood. A complicated phenotype with other neurological symptoms can also be observed in individuals with *KIF5A* variants, and genotype-phenotype correlations seem to depend on the *KIF5A* domain in which a variant is found (De Boer et al., 2021). Most of the variants encountered are missense variants, possibly pointing to a dominant-negative mechanism. Although *KIF5A* could possibly explain spasticity in individual 2, the fact that this gene is also deleted in other more mildly affected cases with deletions of the SRO at 12q13.3q14.1, make it less likely that KIF5A could explain the more severe phenotype of individual 2.

In contrast, based on this analysis, *SMARCC2* appeared as a likely disease implicated gene. *SMARCC2* is a member of the BRG1-associated factor (BAF) chromatin-remodeling complex that plays an essential role in the regulation of gene expression and higher-order chromatin organization by modulating the nucleosome and changing chromatin accessibility (Alfert et al., 2019). Aberrations of complex members result in BAFopathies, that present with syndromic neurodevelopmental disorder, including Coffin-Siris syndrome and Nicolaides-Baraitser syndrome. Recently *de novo* variants in *SMARCC2* were found to cause a syndrome with intellectual disability and developmental delay (Machol et al., 2019) (OMIM #618362). Machol et al. (2019 described 15 unrelated individuals with mild to severe intellectual disability, developmental delay with pronounced speech delay with 7 individuals lacking language, behavioral abnormalities, growth retardation in 6 individuals, feeding difficulties in 8 individuals, muscle tone abnormalities including hypotonia and spasticity in 13 individuals, and movement disorders found in two individuals. Behavioral problems included aggression and self-injurious behavior, hyperactivity, hypersensitivity to touch, sleep disturbances, and obsessive and rigid behavior. Dysmorphic features included hypertrichosis, thick eyebrows/prominent supra-orbital ridges, thin upper or thick lower vermillion and upturned nose, suggesting overlap with Coffin-Siris and Nicolaides-Baraitser syndromes. Encountered *SMARCC2* variants included both missense variants and protein truncating alterations, including splice site alterations. To our knowledge, no whole gene deletion of *SMARCC2* has previously been described, but given the overlap in phenotypes (including severe intellectual disability, absence of speech, muscle tone abnormalities, movement disorders and overlap in dysmorphic features) and the loss-of-function mechanism for some of the variants reported by Machol et al., we propose that *SMARCC2* is the most likely disease causing gene in individual 2. Additional genes contained in the deletion and with impact on the phenotype which have not been identified yet cannot be ruled out.

DISCUSSION

We report two individuals with previously undescribed interstitial deletions at 12q14. In their diverse phenotype they triggered a review of all previously described chromosome 12q deletion. Whereas, we find that the phenotype of individual 1 is compatible to what has previously been described for the 12q14 microdeletion syndrome (Menten et al., 2007), individual 2 is more severely affected. This difference in phenotype seems to be caused by haploinsufficiency of the BAF chromatin remodeling complex member *SMARCC2*, which has recently been implicated in a neurodevelopmental disorder with overlaps to Coffin-Siris syndrome (Machol et al., 2019) (OMIM #618362). To our knowledge, individual 2 is the first case of a whole gene deletion of *SMARCC2*, thereby expanding the disease causing molecular spectrum of this recently identified syndrome. As other BAFopathies are characterized by complex specific DNA-methylation signatures (Aref-Eshghi et al., 2018), it will be interesting to investigate whether such an epi-signature can also be determined for pathogenic *SMARCC2* variants, and whether an identical signature would be obtained in individual 2, which would further support the diagnosis. The case of individual 2, and also the review of the other deletion clusters amongst chromosome 12q, illustrate that a regular re-interpretation of previously diagnosed microdeletions can be useful to gain new insights in the mechanisms leading to disease phenotypes in the affected individuals. In the case of individual 2, the initial diagnosis of a 12q13.2q14.2 deletion was made years before *SMARCC2* was identified as a disease gene. Similarly, re-interpretation and additional fine mapping of previously suggested microdeletion syndromes at 12q15 and 12q24.31

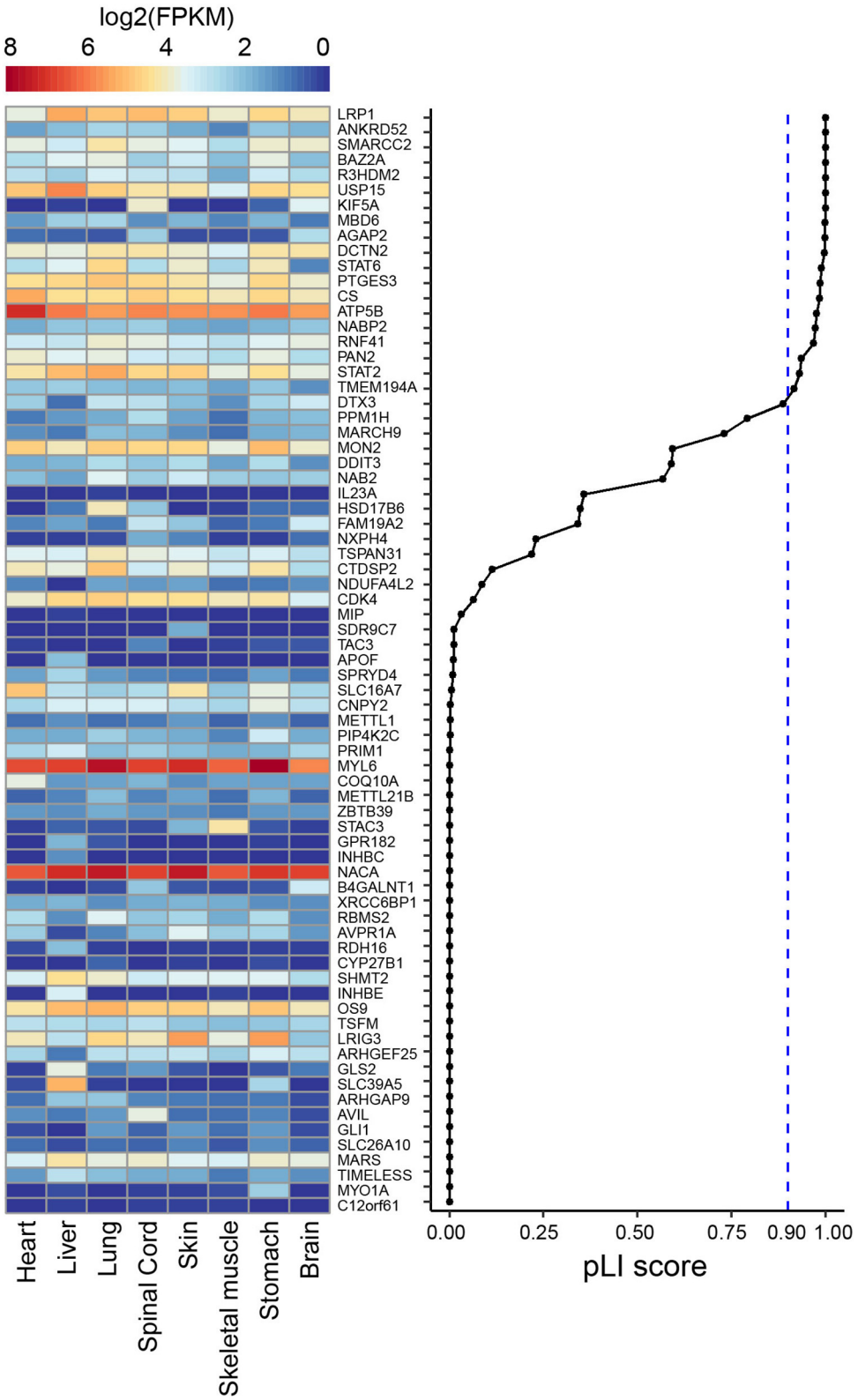

FIGURE 4 | Heat map showing publically available gene expression data (in $\log_2$ FPKM) amongst 8 human fetal tissues from ENCODE for the 73 genes that are included in the deletion found in individual 2. Genes are ranked according to their pLI score from gnomAD (Karczewski et al., 2020).

has now led to the conclusions that most of the phenotypes associated with these microdeletion syndromes are caused by alterations of the genes *CNOT2* (Alesi et al., 2017) and *SETD1B* (Weerts et al., 2021), respectively. It is expected that further progress in genetics, cell biology and personalized medicine will advance options to influence the phenotypes by gene-specific or pathway driven therapeutics. It is thus remains crucial to identify disease causing genes in previously diagnosed microdeletion cases. We suggest that a long term follow-up of patients with microdeletions can be helpful for this and can also improve the genetic counseling in these cases.

DATA AVAILABILITY STATEMENT

Publicly available datasets were analyzed in this study. This data can be found at: ENCODE project (see **Supplementary Table 8**).

ETHICS STATEMENT

Ethical review and approval was not required for the study on human participants in accordance with the local legislation and institutional requirements. Written informed consent to participate in this study was provided by the participants' legal guardian/next of kin. Written informed consent was obtained from the minor(s)' legal guardian/next of kin for the publication of any potentially identifiable images or data included in this article.

AUTHOR CONTRIBUTIONS

MM performed the initial literature review. RD performed bioinformatics analysis, literature review and wrote parts of the manuscript, and was supported by TPB. TSB conceived the study, performed clinical investigations, and wrote the manuscript together with RD. All authors contributed to the article and approved the submitted version.

FUNDING

RD was supported by a China Scholarship Council (CSC) Ph.D. Fellowship (201906300026) for her Ph.D. studies at the Erasmus Medical Center, Rotterdam, the Netherlands. MM acknowledges direct support from Stichting 12q. TSB lab was supported by the Netherlands Organization for Scientific Research (ZonMW Veni, grant 91617021), a NARSAD Young Investigator Grant from the Brain & Behavior Research Foundation, an Erasmus MC Fellowship 2017, and Erasmus MC Human Disease Model Award 2018.

ACKNOWLEDGMENTS

We are grateful to the patients and families who participated in this study and would like to thank Stichting 12q (https://stichting12q.nl/) for supporting this work. We thank Soheil Yousefi (Erasmus MC Rotterdam) with help on RNA-seq data analysis.

SUPPLEMENTARY MATERIAL

The Supplementary Material for this article can be found online at: https://www.frontiersin.org/articles/10.3389/fgene.2021.716874/full#supplementary-material

Supplementary Figure 1 | As **Figure 2**, but now zoomed-in at cluster 1.

Supplementary Figure 2 | As **Figure 2**, but now zoomed-in at cluster 3.

Supplementary Figure 3 | As **Figure 2**, but now zoomed-in at cluster 4.

Supplementary Figure 4 | As **Figure 2**, but now zoomed-in at cluster 5.

Supplementary Table 1 | Summary of reported 12q deletions.

Supplementary Table 2 | Summary of overlapping clinical features of 27 reported individuals with deletions at 12q13q15 (12q14). a, G-banding; b, BAC; c, array-CGH; d, SNP-array.

Supplementary Table 3 | Genes included in SROs.

Supplementary Table 4 | Summary of clinical features of 8 reported individuals with deletions at 12q11.1q13.1. a, G-banding; b, BAC; c, array-CGH; d, SNP-array.

Supplementary Table 5 | Summary of overlapping clinical features of 11 reported probands with deletions at 12q13.3q23.1. a, G-banding; b, BAC; c, array-CGH; d, SNP-array; e, Microsatellite Marker Analysis.

Supplementary Table 6 | Summary of overlapping clinical features of 10 reported individuals with deletions at 12q21.1q23.2. a, G-banding; b, BAC; c, array-CGH; d, SNP-array.

Supplementary Table 7.1 | Summary of overlapping clinical features of 13 reported individuals with deletions at 12q22q24.33. a, G-banding; b, BAC; c, array-CGH; d, SNP-array.

Supplementary Table 7.2 | Summary of overlapping clinical features of 7 reported individuals with deletions at 12q24.31.

Supplementary Table 7.3 | Summary of overlapping clinical features of 7 reported individuals with deletions at 12q24.31.

Supplementary Table 8 | Public data used.

REFERENCES

Abi Habib, W., Brioude, F., Edouard, T., Bennett, J. T., Lienhardt-Roussie, A., Tixier, F., et al. (2018). Genetic disruption of the oncogenic HMGA2-PLAG1-IGF2 pathway causes fetal growth restriction. *Genet. Med*. 20, 250–258. doi: 10.1038/gim.2017.105

Adam, M. P., Mehta, A., Knight, L., Hall, D. E., and Rossi, M. R. (2010). A family with a 1.17 Mb deletion of 12q12: refining genotype-phenotype correlation. *Am. J. Med. Genet. A* 152a, 2394–2398. doi: 10.1002/ajmg.a.33570

Alesi, V., Loddo, S., Cal,ì, F., Orlando, V., Genovese, S., Ferretti, D., et al. (2019). A heterozygous, intragenic deletion of CNOT2 recapitulates the phenotype of 12q15 deletion syndrome. *Am. J. Med. Genet. A* 179, 1615–1621. doi: 10.1002/ajmg.a.61217

Alesi, V., Loddo, S., Grispo, M., Riccio, S., Montella, A. C., Dallapiccola, B., et al. (2017). Reassessment of the 12q15 deletion syndrome critical region. *Eur. J. Med. Genet*. 60, 220–223. doi: 10.1016/j.ejmg.2017.01.009

Alfert, A., Moreno, N., and Kerl, K. (2019). The BAF complex in development and disease. *Epigenet. Chrom.* 12:19. doi: 10.1186/s13072-019-0264-y

Al-Maawali, A., Marshall, C. R., Scherer, S. W., Dupuis, L., Mendoza-Londono, R., and Stavropoulos, D. J. (2014). Clinical characteristics in patients with interstitial deletions of chromosome region 12q21-q22 and identification of a critical region associated with keratosis pilaris. *Am. J. Med. Genet. A* 164a, 796–800. doi: 10.1002/ajmg.a.36356

Alyaqoub, F., Pyatt, R. E., Bailes, A., Brock, A., Deeg, C., Mckinney, A., et al. (2012). 12q14 microdeletion associated with HMGA2 gene disruption and growth restriction. *Am. J. Med. Genet. A* 158a, 2925–2930. doi: 10.1002/ajmg.a.35610

Aref-Eshghi, E., Bend, E. G., Hood, R. L., Schenkel, L. C., Carere, D. A., Chakrabarti, R., et al. (2018). BAFopathies' DNA methylation epi-signatures demonstrate diagnostic utility and functional continuum of coffin-siris and nicolaides-baraitser syndromes. *Nat. Commun.* 9:4885. doi: 10.1038/s41467-018-07193-y

Bibb, A. L., Rosenfeld, J. A., and Weaver, D. D. (2012). Report of a mother and daughter with the 12q14 microdeletion syndrome. *Am. J. Med. Genet. A* 158a, 417–422. doi: 10.1002/ajmg.a.34397

Buysse, K., Reardon, W., Mehta, L., Costa, T., Fagerstrom, C., Kingsbury, D. J., et al. (2009). The 12q14 microdeletion syndrome: additional patients and further evidence that HMGA2 is an important genetic determinant for human height. *Eur. J. Med. Genet.* 52, 101–107. doi: 10.1016/j.ejmg.2009.03.001

Cano, M., Trapasso, J., Trapasso, T., and Matalon, R. (2016). 12 q deletion with oculodentodigital dysplasia -like phenotype. *Clin. Case Rep. Rev.* 2, 387–390. doi: 10.15761/CCRR.1000224

Carlsen, E., Frengen, E., Fannemel, M., and Misceo, D. (2015). Haploinsufficiency of ANO6, NELL2 and DBX2 in a boy with intellectual disability and growth delay. *Am. J. Med. Genet. A* 167a, 1890–1896. doi: 10.1002/ajmg.a.37079

Consortium, E. P. (2012). An integrated encyclopedia of DNA elements in the human genome. *Nature* 489, 57–74. doi: 10.1038/nature11247

De Boer, E. M. J., Van Rheenen, W., Goedee, H. S., Kamsteeg, E. J., Brilstra, E. H., Veldink, J. H., et al. (2021). Genotype-phenotype correlations of KIF5A stalk domain variants. *Amyotroph. Lateral Scler. Frontotemporal Degener.* doi: 10.1080/21678421.2021.1907412. [Epub ahead of print].

De Crescenzo, A., Citro, V., Freschi, A., Sparago, A., Palumbo, O., Cubellis, M. V., et al. (2015). A splicing mutation of the HMGA2 gene is associated with silver-russell syndrome phenotype. *J. Hum. Genet.* 60, 287–293. doi: 10.1038/jhg.2015.29

Dória, S., Alves, D., Pinho, M. J., Pinto, J., and Leão, M. (2020). 12q14 microduplication: a new clinical entity reciprocal to the microdeletion syndrome? *BMC Med. Genomics* 13:2. doi: 10.1186/s12920-019-0653-x

Fischetto, R., Palumbo, O., Ortolani, F., Palumbo, P., Leone, M. P., Causio, F. A., et al. (2017). Clinical and molecular characterization of a second family with the 12q14 microdeletion syndrome and review of the literature. *Am. J. Med. Genet. A* 173, 1922–1930. doi: 10.1002/ajmg.a.38253

Heldt, F., Wallaschek, H., Ripperger, T., Morlot, S., Illig, T., Eggermann, T., et al. (2018). 12q14 microdeletion syndrome: a family with short stature and silver-russell syndrome (SRS)-like phenotype and review of the literature. *Eur. J. Med. Genet.* 61, 421–427. doi: 10.1016/j.ejmg.2018.02.010

Hellemans, J., Preobrazhenska, O., Willaert, A., Debeer, P., Verdonk, P. C., Costa, T., et al. (2004). Loss-of-function mutations in LEMD3 result in osteopoikilosis, buschke-ollendorff syndrome and melorheostosis. *Nat. Genet.* 36, 1213–1218. doi: 10.1038/ng1453

Hübner, C. T., Meyer, R., Kenawy, A., Ambrozaityte, L., Matuleviciene, A., Kraft, F., et al. (2020). HMGA2 variants in silver-russell syndrome: homozygous and heterozygous occurrence. *J. Clin. Endocrinol. Metab.* 105:dgaa273. doi: 10.1210/clinem/dgaa273

James, P. A., Oei, P., Ng, D., Kannu, P., and Aftimos, S. (2005). Another case of interstitial del(12) involving the proposed cardio-facio-cutaneous candidate region. *Am. J. Med. Genet. A* 136, 12–16. doi: 10.1002/ajmg.a.30693

Karczewski, K. J., Francioli, L. C., Tiao, G., Cummings, B. B., Alföldi, J., Wang, Q., et al. (2020). The mutational constraint spectrum quantified from variation in 141,456 humans. *Nature* 581, 434–443. doi: 10.1038/s41586-020-2308-7

Labonne, J. D., Lee, K. H., Iwase, S., Kong, I. K., Diamond, M. P., Layman, L. C., et al. (2016). An atypical 12q24.31 microdeletion implicates six genes including a histone demethylase KDM2B and a histone methyltransferase SETD1B in syndromic intellectual disability. *Hum. Genet.* 135, 757–771. doi: 10.1007/s00439-016-1668-4

Leszinski, G. S., Warncke, K., Hoefele, J., and Wagner, M. (2018). A case report and review of the literature indicate that HMGA2 should be added as a disease gene for Silver-Russell syndrome. *Gene* 663, 110–114. doi: 10.1016/j.gene.2018.04.027

Lynch, S. A., Foulds, N., Thuresson, A.-C., Collins, A. L., Annerén, G., Hedberg, B.-O., et al. (2011). The 12q14 microdeletion syndrome: six new cases confirming the role of HMGA2 in growth. *Euro. J. Hum. Genet.* 19, 534–539. doi: 10.1038/ejhg.2010.215

Machol, K., Rousseau, J., Ehresmann, S., Garcia, T., Nguyen, T. T. M., Spillmann, R. C., et al. (2019). Expanding the spectrum of BAF-related disorders: *de novo* variants in SMARCC2 cause a syndrome with intellectual disability and developmental delay. *Am. J. Hum. Genet.* 104, 164–178. doi: 10.1016/j.ajhg.2018.11.007

Mari, F., Hermanns, P., Giovannucci-Uzielli, M. L., Galluzzi, F., Scott, D., Lee, B., et al. (2009). Refinement of the 12q14 microdeletion syndrome: primordial dwarfism and developmental delay with or without osteopoikilosis. *Eur. J. Hum. Genet.* 17, 1141–1147. doi: 10.1038/ejhg.2009.27

Mc Cormack, A., Sharpe, C., Gregersen, N., Smith, W., Hayes, I., George, A. M., et al. (2015). 12q14 Microdeletions: additional case series with confirmation of a macrocephaly region. *Case Rep. Genet.* 2015:192071. doi: 10.1155/2015/192071

Menten, B., Buysse, K., Zahir, F., Hellemans, J., Hamilton, S. J., Costa, T., et al. (2007). Osteopoikilosis, short stature and mental retardation as key features of a new microdeletion syndrome on 12q14. *J. Med. Genet.* 44, 264–268. doi: 10.1136/jmg.2006.047860

Mercadante, F., Buse, M., Salzano, E., Fragapane, T., Palazzo, D., Malacarne, M., et al. (2020). 12q14.3 microdeletion involving HMGA2 gene cause a Silver-Russell syndrome-like phenotype: a case report and review of the literature. *Ital. J. Pediatr.* 46:108. doi: 10.1186/s13052-020-00866-9

Miyake, N., Tonoki, H., Gallego, M., Harada, N., Shimokawa, O., Yoshiura, K., et al. (2004). Phenotype-genotype correlation in two patients with 12q proximal deletion. *J. Hum. Genet.* 49, 282–284. doi: 10.1007/s10038-004-0144-5

Mumm, S., Wenkert, D., Zhang, X., Mcalister, W. H., Mier, R. J., and Whyte, M. P. (2007). Deactivating germline mutations in LEMD3 cause osteopoikilosis and buschke-ollendorff syndrome, but not sporadic melorheostosis. *J. Bone Miner. Res.* 22, 243–250. doi: 10.1359/jbmr.061102

Niyazov, D. M., Nawaz, Z., Justice, A. N., Toriello, H. V., Martin, C. L., and Adam, M. P. (2007). Genotype/phenotype correlations in two patients with 12q subtelomere deletions. *Am. J. Med. Genet. A* 143a, 2700–2705. doi: 10.1002/ajmg.a.32005

Nso-Roca, A. P., Marco, F. C., Ricote, J. M., and Ruiz, M. J. (2014). Endocrinological anomalies in a patient with 12q14 microdeletion syndrome. Completing phenotype of this exceptional short stature condition. *J. Pediatr. Endocrinol. Metab.* 27, 539–543. doi: 10.1515/jpem-2013-0239

Rauen, K. A., Albertson, D. G., Pinkel, D., and Cotter, P. D. (2002). Additional patient with del(12)(q21.2q22): further evidence for a candidate region for cardio-facio-cutaneous syndrome? *Am. J. Med. Genet.* 110, 51–56. doi: 10.1002/ajmg.10478

Saraiva, N., Prole, D. L., Carrara, G., Johnson, B. F., Taylor, C. W., Parsons, M., et al. (2013). hGAAP promotes cell adhesion and migration via the stimulation of store-operated Ca2+ entry and calpain 2. *J. Cell Biol.* 202, 699–713. doi: 10.1083/jcb.201301016

Spengler, S., Schonherr, N., Binder, G., Wollmann, H. A., Fricke-Otto, S., Muhlenberg, R., et al. (2010). Submicroscopic chromosomal imbalances in idiopathic silver-russell syndrome (SRS): the SRS phenotype overlaps with the 12q14 microdeletion syndrome. *J. Med. Genet.* 47, 356–360. doi: 10.1136/jmg.2009.070052

Takamiya, K., Mao, L., Huganir, R. L., and Linden, D. J. (2008). The glutamate receptor-interacting protein family of GluR2-binding proteins is required for long-term synaptic depression expression in cerebellar purkinje cells. *J. Neurosci.* 28, 5752–5755. doi: 10.1523/JNEUROSCI.0654-08.2008

Takenouchi, T., Enomoto, K., Nishida, T., Torii, C., Okazaki, T., Takahashi, T., et al. (2012). 12q14 microdeletion syndrome and short stature with or without relative macrocephaly. *Am. J. Med. Genet. A* 158a, 2542–2544. doi: 10.1002/ajmg.a.35527

Uehara, T., Takenouchi, T., Yamaguchi, Y., Daimon, Y., Suzuki, H., Sakaguchi, Y., et al. (2019). CNOT2 as the critical gene for phenotypes of 12q15 microdeletion syndrome. *Am. J. Med. Genet. A* 179, 659–662. doi: 10.1002/ajmg.a.61068

Van Haelst, M. M., Maiburg, M., Baujat, G., Jadeja, S., Monti, E., Bland, E., et al. (2008). Molecular study of 33 families with fraser syndrome

new data and mutation review. *Am. J. Med. Genet. A* 146a, 2252–2257. doi: 10.1002/ajmg.a.32440

Vergult, S., Krgovic, D., Loeys, B., Lyonnet, S., Lieden, A., Anderlid, B. M., et al. (2011). Nasal speech and hypothyroidism are common hallmarks of 12q15 microdeletions. *Eur. J. Hum. Genet.* 19, 1032–1037. doi: 10.1038/ejhg.2011.67

Vogel, M. J., Van Zon, P., Brueton, L., Gijzen, M., Van Tuil, M. C., Cox, P., et al. (2012). Mutations in GRIP1 cause fraser syndrome. *J. Med. Genet.* 49, 303–306. doi: 10.1136/jmedgenet-2011-100590

Weedon, M. N., Lettre, G., Freathy, R. M., Lindgren, C. M., Voight, B. F., Perry, J. R., et al. (2007). A common variant of HMGA2 is associated with adult and childhood height in the general population. *Nat. Genet.* 39, 1245–1250. doi: 10.1038/ng2121

Weerts, M. J. A., Lanko, K., Guzmán-Vega, F. J., Jackson, A., Ramakrishnan, R., Cardona-Londoño, K. J., et al. (2021). Delineating the molecular and phenotypic spectrum of the SETD1B-related syndrome. *Genet. Med.* doi: 10.1038/s41436-021-01246-2. [Epub ahead of print].

Won, H., De La Torre-Ubieta, L., Stein, J. L., Parikshak, N. N., Huang, J., Opland, C. K., et al. (2016). Chromosome conformation elucidates regulatory relationships in developing human brain. *Nature* 538, 523–527. doi: 10.1038/nature19847

Yu, N. K., Kim, H. F., Shim, J., Kim, S., Kim, D. W., Kwak, C., et al. (2016). A transducible nuclear/nucleolar protein, mLLP, regulates neuronal morphogenesis and synaptic transmission. *Sci. Rep.* 6:22892. doi: 10.1038/srep22892

Zhang, Y., Castori, M., Ferranti, G., Paradisi, M., and Wordsworth, B. P. (2009). Novel and recurrent germline LEMD3 mutations causing Buschke-Ollendorff syndrome and osteopoikilosis but not isolated melorheostosis. *Clin. Genet.* 75, 556–561. doi: 10.1111/j.1399-0004.2009.01177.x

Zhou, X., Benson, K. F., Ashar, H. R., and Chada, K. (1995). Mutation responsible for the mouse pygmy phenotype in the developmentally regulated factor HMGI-C. *Nature* 376, 771–774. doi: 10.1038/376771a0

Conflict of Interest: The authors declare that the research was conducted in the absence of any commercial or financial relationships that could be construed as a potential conflict of interest.

Publisher's Note: All claims expressed in this article are solely those of the authors and do not necessarily represent those of their affiliated organizations, or those of the publisher, the editors and the reviewers. Any product that may be evaluated in this article, or claim that may be made by its manufacturer, is not guaranteed or endorsed by the publisher.

frontiers in Genetics

CASE REPORT
published: 14 September 2021
doi: 10.3389/fgene.2021.747422

Case Report: Complete Maternal Uniparental Disomy of Chromosome 2 With a Novel *UNC80* Splicing Variant c.5609-4G> A in a Chinese Patient With Infantile Hypotonia With Psychomotor Retardation and Characteristic Facies 2

*Yilun Tao[1], Dong Han[1], Yiju Wei[2], Lihong Wang[3], Wenxia Song[4] and Xiaoze Li[1]**

[1]Medical Genetic Center, Changzhi Maternal and Child Health Care Hospital, Changzhi, China, [2]Department of Pediatrics, Penn State Health Hershey Medical Center, Penn State College of Medicine, Hershey, PA, United States, [3]Department of Pediatrics, Changzhi Maternal and Child Health Care Hospital, Changzhi, China, [4]Obstetrics Department, Changzhi Maternal and Child Health Care Hospital, Changzhi, China

OPEN ACCESS

Edited by:
Santasree Banerjee,
Beijing Genomics Institute (BGI), China

Reviewed by:
Keiko Matsubara,
National Center for Child Health and Development (NCCHD), Japan
Mohammad Faghihi,
Express Gene Molecular Diagnostics Laboratory, United States

***Correspondence:**
Xiaoze Li
lixiaoze520@126.com

Specialty section:
This article was submitted to Genetics of Common and Rare Diseases, a section of the journal Frontiers in Genetics

Received: 26 July 2021
Accepted: 02 September 2021
Published: 14 September 2021

Citation:
Tao Y, Han D, Wei Y, Wang L, Song W and Li X (2021) Case Report: Complete Maternal Uniparental Disomy of Chromosome 2 With a Novel UNC80 Splicing Variant c.5609-4G> A in a Chinese Patient With Infantile Hypotonia With Psychomotor Retardation and Characteristic Facies 2. Front. Genet. 12:747422. doi: 10.3389/fgene.2021.747422

Background: Infantile hypotonia with psychomotor retardation and characteristic facies 2 (IHPRF2) is a rare autosomal recessive neurodevelopmental disorder caused by mutations in the *UNC80* gene. It is characterized by severe global developmental delay, poor or absent speech and absent or limited walking abilities. The current study explored a case of a Chinese patient with IHPRF2 caused by a novel splicing variant of *UNC80*.

Case Report: The proband is a 8-year-old Chinese male manifested with global developmental delay, severe truncal hypotonia, absent speech and intellectual disability. SNP array analysis revealed a uniparental isodisomy of the entire chromosome 2 [UPD(2)] in the proband. Whole exome sequencing (WES) subsequently identified a novel mutation c.5609-4G>A in the *UNC80* gene, which was inherited from his mother and was confirmed by Sanger sequencing, indicating that UPD(2) was of maternal origin.

Conclusion: A novel *UNC80* homozygous splicing variant c.5609-4G>A associated with maternal UPD(2) was identified. These findings indicate that UPD poses a high risk of autosomal recessive diseases, and provides information on the variant spectrum for *UNC80*. Our findings elucidate on understanding of the genotype-phenotype associations that occur in IHPRF2 patients.

Keywords: maternal uniparental disomy, chromosome 2, UNC80 gene, SNP array, whole exome sequencing

INTRODUCTION

Infantile hypotonia with psychomotor retardation and characteristic facies 2 (IHPRF2, MIM 616801) is a rare autosomal recessive neurodevelopmental disorder with onset at birth or in early infancy (Shamseldin et al., 2016). It is a phenotypically heterogeneous disease characterized by severe global developmental delay, hypotonia, facial dysmorphism, intellectual disability, poor or absent speech and lack of or limited walking abilities (Perez et al., 2016; Shamseldin et al., 2016; He et al., 2018). The first case of IHPRF2 was reported in Bedouin families in 2016 (Perez et al., 2016). It has previously been reported that IHPRF2 is caused by homozygous or compound heterozygous mutation in *UNC80* gene (MIM 612636) (Lu et al., 2010).

The *UNC80* gene is located on chromosome 2 and comprises of 64 exons. *UNC80* gene encodes a subunit of the non-selective sodium leak channel (NALCN) complex, consisting of 3,258 amino acids (Lu et al., 2010). This channel complex is a voltage-insensitive and nonselective sodium-leak channel, which is predominantly expressed in the brain and plays an important role in the establishment and maintenance of resting membrane potentials in neuron (Lu et al., 2007; Zhang et al., 2021). Proteins expressed from the *UNC80* gene interacts with NALCN and acts as a scaffold protein for UNC79 (Lu et al., 2010; Wie et al., 2020). Recessive loss-of-function biallelic pathogenic variants of *UNC80* cause UNC80 deficiency, which can result in dysfunctional NALCN complex leading to severe pathological phenotypes (Valkanas et al., 2016; Wie et al., 2020).

Uniparental disomy (UPD), a rare case that was first reported in 1980, occurs when a chromosome pair is derived from the same parent in a disomic cell with a balanced karyotype (Engel 1980). The prevalence of UPD ranges from 1 in 2000 to 1 in 5,000 people (Robinson, 2000; Liehr, 2010; Nakka et al., 2019). UPDs can cause clinical abnormalities, resulting in an aberrant dosage of imprinting genes or homozygosity of variants for recessive phenotypes (Yamazawa et al., 2010). Maternal and paternal UPDs have been reported in almost every human chromosome (Nakka et al., 2019). However, maternal UPD of chromosome 2 [UPD(2)mat] with a homozygous pathogenic variant in *UNC80* has not been previously reported.

We report a case of IHPRF2 with a novel homozygous splicing variant c.5609-4G>A of *UNC80* gene arising from UPD(2)mat, which expands on the disease spectrum associated with *UNC80* mutations. In addition, previous genotypes and phenotypes of patients with IHPRF2 were reviewed, to help in understanding the genotype-phenotype relationship of *UNC80*.

MATERIALS AND METHODS

Case Report

The proband is an 8-year-old male born as the sole child of healthy and non-consanguineous Chinese parents. The mother did not report any history of exposure to teratogenic pathogens or drugs during gestation. Birth weight of the child was 3,150 g (25th percentile), birth length was 51 cm (75th percentile), and occipitofrontal circumference (OFC) was 36 cm (>95th percentile) on week 39 of gestation. He has been suffering from severe hypotonia and feeding difficulty since birth. The proband was able to grasp at 6 months and could sit at 9 months. At 13 months of age, the patient was admitted to Beijing Children's Hospital affiliated to Capital Medical University for astasia, development delay and failure to thrive with feeding difficulty. He manifested dystonia in the extremities, with complete inability to stand up and walk. He could not speak, even simple words such as "baba" and "mama". Electroencephalograph (EEG) analysis did not reveal any abnormalities, whereas brain magnetic resonance imaging (MRI) showed bilateral dilation of lateral ventricles, periventricular leukomalacia and delayed myelination. No definite diagnosis existed to that time, and he did not undergo any adjuvant therapy. At the age of five, he presented to our hospital for severe psychomotor development. On examination, he had severe intellectual disability, hypotonia, strabismus and esotropia. He was unable to speak or communicate. He was able to walk with some aid but exhibited poor balance and he could not jump on one foot. In addition, the subject suffered from constipation. Facial dysmorphisms included a triangular face, microcephaly, low-set posterior rotated ears, and a thin and tented upper lip. He had long and slender fingers. His height, weight and head circumference were 107 cm (14th percentile), 15.5 kg (4th percentile) and 47.1 cm (<1st percentile), respectively.

In this family, we identified only one patient (proband) and proband's father and mother is normal. We therefore used SNP array analysis and whole genome sequencing to search for any evidence of the disease.

SNP Array Analysis

A DNA sample (250 ng) was extracted from the peripheral blood of the patient and was hybridized using an Affymetrix CytoScan® 750K array kit (Affymetrix, Inc., Santa Clara, CA, United States) according to the manufacturer's protocol. The SNP array data was analyzed for the presence of copy number variations (CNVs) using Affymetrix Chromosome Analysis Suite (ChAS) Software version 3.3. Pathogenicity of CNVs was evaluated based on published literature and public databases, including DGV (http://dgv.tcag.ca/dgv/app/home), Clingen (https://www.clinicalgenome.org/), DECIPHER (https://decipher.sanger.ac.uk/) and OMIM (https://www.omim.org/). This analysis was performed in accordance with the American College of Medical Genetics and Genomics (ACMG) and the Clinical Genome Resource (ClinGen) 2020 guidelines (Riggs et al., 2020).

Whole-Exome Sequencing

Peripheral blood sample of the patient was collected. Genomic DNA was extracted using a QIAamp DNA Mini Kit (Qiagen, China), according to the manufacturer's instructions. DNA library preparation was performed following Illumina protocols, which included end repair, adapter ligation and PCR enrichment. The amplified DNA was then captured using Whole Exome Capture Kit (MyGenostics Inc, Beijing, China). Biotinylated capture probes were designed to tile all exons

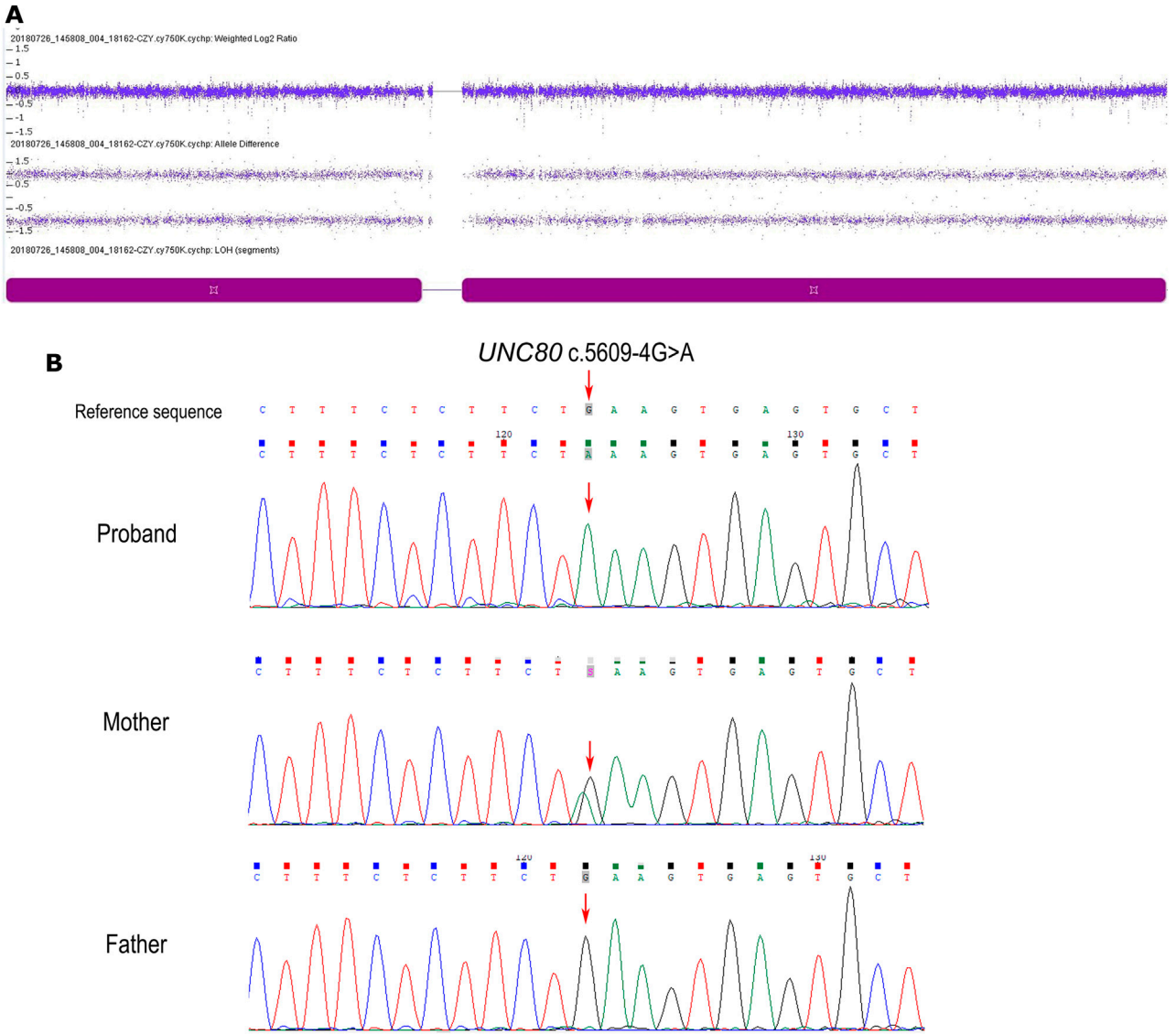

FIGURE 1 | (A) Single nucleotide polymorphism microarray (SNP array, Affymetrix Cytoscan 750k) profiles of chromosome 2 in the patient. The dark purple block indicates complete UPD in chromosome 2, with two allele difference tracks where the plot has a line at + 1 and −1. **(B)** Sequence electropherogram of the c.5609-4G> A variation showing (arrow) the homozygous mutation in the patient, the heterozygous genotype in his mother, and wild-type in his father.

without repeated regions. The enriched libraries were sequenced for paired-end reads of 150 bp using the Illumina HiSeq X Ten platform.

The bioinformatics analyses were carried out utilizing established methods with some modifications (Zheng et al., 2018; Dai et al., 2019; Han et al., 2020; Zhang et al., 2020). After sequencing, clean reads were aligned to the UCSC hg19 human reference genome using the Burrows-Wheeler Alignment tool. Duplicated reads were removed using the Picard tool (http://broadinstitute.github.io/picard). The variants of SNP and small insertions or deletions (InDel) were detected by GATK HaplotypeCaller, then using GATK VariantFiltration to filter variant. The identified variants were then annotated using ANNOVAR. The variants with frequencies less than 0.05 in the normal population database were screened out, including the 1,000 Genomes, Exome Aggregation Consortium (ExAC), GnomAD and Inhouse database (MyGenostics Inc, Beijing, China). In addition, the identified variants were predicted using Mutation Taster (MT), Sorting Intolerant From Tolerant (SIFT), PolyPhen-2 (PP2) and Genomic Evolutionary Rate Profiling (GERP++), dbscSNV, SPIDEX, SPliceAI. Classification of variants (pathogenic, likely pathogenic, VUS and likely benign and benign) has been done according to the variant interpretation guidelines of American College of Medical Genetics and Genomics (Richards et al., 2015). Finally, we compared the variants found in patient and his parents. The function of the variant and their correlation with the disease phenotype was done by previously published articles and OMIM database.

Sanger Sequencing

Candidate variable sites were confirmed by Sanger sequencing for the patient and his parents. The primers are as follows: F 5′- CAA CGAAGAGAACAAACACCTACG -3′, R 5′- TATTGGAGG GCATTGAGTTGC-3. The reference sequence NM_032,504 of *UNC80* was used. Target sequences were sequenced on an ABI 3730 genetic analyzer (Applied Biosystems, Foster City Carlsbad, CA, United States) and identified using Chromas 2.6.5 (Technelysium Pty Ltd, Australia).

RESULTS

Genome-wide SNP array analysis did not reveal any clinically significant copy number variations. However, it revealed an absence of heterozygosity (AOH) across the entire chromosome 2 (**Figure 1A**). There was no disease-related imprinting gene located on chromosome 2, therefore, whole exome sequencing (WES) of the patient was subsequently performed. A novel homozygous variant c.5609-4G> A in *UNC80* was detected in the proband, which was only present in his mother as a heterozygous trait and was absent in the father (**Figure 1B**). This contradiction to Mendelian inheritance indicates that the AOH originated from maternal UPD. The variant c.5609-4G> A was located on intron 35, -4 bp to exon 36 splice acceptor site of the *UNC80* gene. This variant has not been previously reported and was absent on the 1,000 Genome Project, the ExAC, the gnomAD database or our inhouse database. Furthermore, it has not been reported in HGMD. *In silico* analysis by MutationTaster and regSNP-intron showed that the variant may have an impact on pre-mRNA splicing (the score was 0.96 and 0.37), whereas SPliceAI indicated a prediction that is in total disagreement. Samples were not available for reanalysis, therefore, RT-PCR was not performed to explore the effect of splicing. Based on ACMG guidelines, the c.5609-4G>A variant was classified as variant of uncertain clinical significance (PM2). The diagnosis of IHPRF2 was confirmed by molecular and clinical findings.

DISCUSSION

The current study reports a case of an IHPRF2 patient with global developmental delay, truncal hypotonia, intellectual disability, and absent speech. A novel *UNC80* homozygous splicing variant c.5609-4G> A originating from UPD(2)mat was identified, which has not been previously reported, and was absent in the general population. Bioinformatics analysis showed that the variant might be involved in splicing modulation. Similar variants, which lead to protein truncation have been previously reported (Anna and Monika, 2018; Li et al., 2019; Śmigiel et al., 2020). And *in vitro* cytology experiments have demonstrated that loss-of-function mutations in *UNC80* are associated with IHPRF2 (Valkanas et al., 2016; Wie et al., 2020). Clinical presentation of the patient showed that he had IHPRF2. These findings indicate that the variant c.5609-4G> A is associated with pathogenesis of IHPRF2. However, further functional studies are needed to validate the pathogenicity of this variant.

The potential harmful effects of UPD include imprinted gene diseases, or activation of recessive pathogenic genes. Maternal and paternal UPD2, with normal phenotypes, have been reported previously, indicating the absence of genomic imprinting effects in UPD2 (Keller et al., 2009; Ou et al., 2013; Zhou et al., 2017; Zhang et al., 2019). Single conventional SNP-array analysis did not provide a conclusive diagnosis for the patient, therefore, an integrated approach is needed to determine the underlying genetic cause. This limitation has hindered genetic counseling for the family. Homozygosity of the *UNC80* c.5609-4G>A variant resulted from UPD, thus the recurrence risk for IHPRF2 in this family is significantly reduced compared to a 25% risk expected when both parents are carriers of a *UNC80* pathogenic variant. These findings indicate that UPD is a possible cause of autosomal recessive diseases and should be noticed, especially when patients have large chromosome segments of AOH or a rare homozygous pathogenic variant.

Comprehensive clinical and genetic analysis of 39 reported cases of IHPRF2 (including the present case) from 23 families are summarized in **Supplementary Table S1**. A total of 29 distinct *UNC80* variants were identified from these patients (**Supplementary Table S2**). These variants included thirteen nonsense, eight missense, four frameshifts, three splice-site and one deletion. Approximately 65.5% (19/29) of the variants were nonsense, frameshift or splicing variants, indicating that loss of function is the mechanism behind the cause of IHPRF2 by *UNC80* variants. Variants were unevenly distributed throughout the *UNC80* gene (**Figure 2**), but were mainly concentrated in the exons (26/29, 89.66%). Twenty-three variants were observed once or twice, indicating high genetic heterogeneity among IHPRF2 patients. However, approximately 50% of the alleles in IHPRF2 patients were contributed by only 6 variants including p. Arg51*, p. Arg174*, p. Val189Met, c.601-1G>A, p. Thr561Arg fs*33 and p. Arg1265*. Almost all of the 6 variants were identified in the homozygous state in pedigrees with at least 2 patients. Only three genetically diagnosed IHPRF2 patients with compound heterozygous variants were reported from the Chinese population, and they possessed six variants including c.1447C>A, c.3719G>A, c.4926_4937del, c.4963C>T, c.8818C>T, and 8385C>G (Yang et al., 2017; He et al., 2018). These findings did not show a specific hotspot variant, indicating that most IHPRF2 patients in China do not undergo genetic testing.

Genotypes among the 23 genetically diagnosed families were highly heterogeneous, with each family presenting with a unique genotype. Only one variant, c.520C>T (p.Arg174*), was observed in 2 different families. This finding can be attributed to complex phenotypic heterogeneity of IHPRF2. Among the 39 genetically diagnosed patients, 29 (74.36%) presented with homozygous genotypes. Most patients were associated with consanguineous marriages (27/29, 93.10%), which explains why IHPRF2 is highly prevalent in Mediterranean and Arabic populations.

The 39 patients presented with intellectual disability, global developmental delay, absent or very poor speech and dyskinesias. Most patients had facial dysmorphisms including triangular face

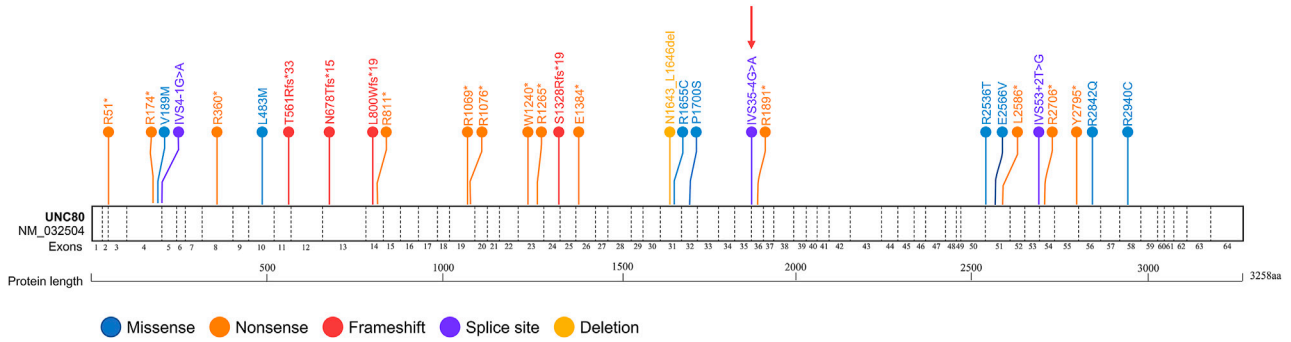

FIGURE 2 | Reported variants in the *UNC80* gene. Structure of *UNC80* gene is shown, along with the 29 previously reported variants. The variant found in the current study is indicated by a red arrow.

TABLE 1 | Clinical features of IHPRF2 patients.

Clinical feature		**Frequency in reported affected individuals with pathogenic *UNC80* variants**			
		N/N	**M/M**	**Total**	**This study**
Neurodevelopmental and behavioral	Profound intellectual disability	26/26 (100%)	7/7 (100%)	34/34 (100%)	+
	Seizures	11/29 (37.93%)	5/7 (71.43%)	16/37 (43.24%)	–
	Feeding difficulties	16/19 (84.21%)	2/3 (66.67%)	18/23 (78.26%)	+
	Absent or very poor speech	27/27 (100%)	7/7 (100%)	34/34 (100%)	+
	Dyskinesias	23/23 (100%)	4/4 (100%)	28/28 (100%)	+
	hypotonia	27/29 (93.10%)	7/7 (100%)	35/37 (94.59%)	+
	Inability to walk independently	12/13 (92.31%)	3/4 (75%)	16/18 (88.89%)	+
	Abnormal brain MRI	12/25 (48%)	1/4 (25%)	13/30 (43.33%)	+
	Abnormal EEG	15/25 (60%)	5/5 (100%)	20/31 (64.52%)	–
Ophthalmologic	Strabismus	22/27 (81.48%)	1/3 (33.33%)	24/31 (77.42%)	+
	Esotropia	11/12 (91.67%)	1/2 (50%)	11/13 (84.62%)	+
Growth	Normal birth parameters	18/22 (81.82%)	5/6 (83.33%)	24/29 (82.67%)	+
	Height < 3rd Percentile	15/18 (83.33%)	2/6 (33.33%)	18/25 (72%)	+
	Weight < 3rd Percentile	16/19 (84.21%)	3/6 (50%)	20/25 (80%)	–
	Severe global developmental delay	30/30 (100%)	7/7 (100%)	38/38 (100%)	+
	IUGR	9/12 (75%)		9/13 (69.23%)	–
Nonspecific facial features	Triangular face	26/29 (89.66%)	4/5 (80%)	31/35 (88.57%)	+
	Micrognathia	6/12 (50%)		7/13 (53.85%)	–
	Microcephaly	20/28 (71.43%)	3/6 (50%)	24/35 (68.57%)	+
	High forehead	8/9 (88.89%)		8/9 (88.89%)	–
	Frontal bossing	8/12 (66.67%)		9/13 (69.23%)	–
	Short and smooth philtrum	9/12 (75%)		9/13 (69.23%)	–
	Low set posterior rotated ears	9/12 (75%)		9/13 (69.23%)	+
	Nystagmus	1/7 (14.29%)	0/3 (0%)	1/10 (10%)	–
	Prominent nasal bridge	10/13 (76.92%)		10/14 (76.92%)	–
	Thin upper lip	16/20 (80%)	0/2 (0%)	16/22 (72.73%)	+
	Tented upper lip	7/8 (87.50%)		7/8 (87.50%)	+
Musculoskeletal	Tapering fingers	21/23 (91.30%)		21/24 (87.50%)	+
	Clubfeet	6/11 (54.55%)		6/11 (54.55%)	–
	Scoliosis	10/14 (71.43%)	1/3 (33.33%)	11/18 (61.11%)	–
	Contractures	10/24 (41.67%)		10/24 (41.67%)	–
Gastrointestinal	Constipation	13/14 (92.86%)	2/3 (66.67%)	15/20 (75%)	+

M, missense allele; N, null allele, null alleles were defined as those containing frameshift, splice-site and/or nonsense variants.

(31/35), strabismus (24/31), microcephaly (24/35), thin upper lip (16/22), prominent nasal bridge (10/14), short and smooth philtrum (9/13), frontal bossing (9/13), low set posterior rotated ears (9/13) and high forehead (8/9). Other common phenotypes included hypotonia (35/37), tapering fingers (21/24), birth length less than 3rd percentile (20/25), feeding difficulties (17/23), constipation (15/20), and esotropia (11/13). In addition, other neurodevelopmental abnormalities including seizures, abnormal EEG, abnormal brain MRI, and inability to walk independently were observed in 43.24% (16/37), 64.52% (20/31), 43.33% (13/30), and 83.33% (15/18) of IHPRF2 patients, respectively.

In this study, null *UNC80* alleles were defined as those containing frameshift, splice-site, and/or nonsense mutations. Patients were split into two groups with different genotypes including: (i) N/N (null/null) (n = 30) and (ii) M/M (missense/missense) (n = 8). One individual with genotype of M/N (missense/null) was excluded. Incidences of most phenotypes of the individuals with genotype "N/N" werelarger compared to that of the "M/M" group (**Table 1**), indicating a relatively poor survival in patients with null variants. However, there was no significant difference observed between the two groups which can be attributed to the small sample size, challenges in phenotypic assessment, and other modifying factors that influence IHPRF2 phenotypes. In this study, the patient exhibited a homozygous splice site variant and was grouped in the "N/N" genotype class. He had been unwell since birth, and presented with severe congenital nervous system anomalies as well as global developmental delay. Seizures were not observed, and there was no way to verify that seizures may have actually ever occurred and were not captured. The patient presented with typical clinical manifestations of IHPRF2 and relatively poor prognosis, which can be associated with the null variant.

In summary, a novel splicing variant, c.5609-4G>A in *UNC80* was identified in the current study. This finding elucidatesn on genetic variants that cause IHPRF2. The review section describes all known *UNC80* variants, thus provides a basis for exploring genotype-phenotype correlations of IHPRF2. The findings of this current study indicate the importance of genetic testing in identifying the underlying molecular cause of the IHPRF2 disease and in providing adequate genetic counseling on possible recurrence risks.

DATA AVAILABILITY STATEMENT

The datasets presented in this study can be found in online repositories. The names of the repository/repositories and accession number(s) can be found below: NCBI SRA BioProject, accession no: PRJNA757139.

ETHICS STATEMENT

The studies involving human participants were reviewed and approved by Changzhi Maternal and Child Health Care Hospital. Written informed consent to participate in this study was provided by the participants' legal guardian/next of kin. Written informed consent was obtained from the individual(s), and minor(s)' legal guardian/next of kin, for the publication of any potentially identifiable images or data included in this article.

AUTHOR CONTRIBUTIONS

YT conceived and designed the experiment, conducted genetic data acquisition and interpretation, reviewed the published cases and wrote the manuscript. DH performed the experiment and patient follow-up. YW conducted the bioinformatics analysis and revised the manuscript. WS and LW performed in patient management. XL supervised the study. All authors have read and approved the final manuscript.

ACKNOWLEDGMENTS

We are grateful to the patient and his family in our research. We also express our gratitude to all the pediatricians that were involved in this study.

SUPPLEMENTARY MATERIAL

The Supplementary Material for this article can be found online at: https://www.frontiersin.org/articles/10.3389/fgene.2021.747422/full#supplementary-material

REFERENCES

Anna, A., and Monika, G. (2018). Splicing Mutations in Human Genetic Disorders: Examples, Detection, and Confirmation. *J. Appl. Genet.* 59, 253–268. doi:10.1007/s13353-018-0444-7

Dai, Y., Liang, S., Dong, X., Zhao, Y., Ren, H., Guan, Y., et al. (2019). Whole Exome Sequencing Identified a Novel DAG1 Mutation in a Patient with Rare, Mild and Late Age of Onset Muscular Dystrophy-Dystroglycanopathy. *J. Cel. Mol. Med.* 23, 811–818. doi:10.1111/jcmm.13979

Han, P., Wei, G., Cai, K., Xiang, X., Deng, W. P., Li, Y. B., et al. (2020). Identification and Functional Characterization of Mutations in LPL Gene Causing Severe Hypertriglyceridaemia and Acute Pancreatitis. *J. Cel. Mol. Med.* 24, 1286–1299. doi:10.1111/jcmm.14768

He, Y., Ji, X., Yan, H., Ye, X., Liu, Y., Wei, W., et al. (2018). Biallelic UNC80 Mutations Caused Infantile Hypotonia with Psychomotor Retardation and Characteristic Facies 2 in Two Chinese Patients with Variable Phenotypes. *Gene.* 660, 13–17. doi:10.1016/j.gene.2018.03.063

Keller, M. C., McRae, A. F., McGaughran, J. M., Visscher, P. M., Martin, N. G., and Montgomery, G. W. (2009). Non-pathological Paternal Isodisomy of Chromosome 2 Detected from a Genome-wide SNP Scan. *Am. J. Med. Genet.* 149A, 1823–1826. doi:10.1002/ajmg.a.32973

Li, L., Cao, Y., Zhao, F., Mao, B., Ren, X., Wang, Y., et al. (2019). Validation and Classification of Atypical Splicing Variants Associated with Osteogenesis Imperfecta. *Front. Genet.* 10, 979. doi:10.3389/fgene.2019.00979

Liehr, T. (2010). Cytogenetic Contribution to Uniparental Disomy (UPD). *Mol. Cytogenet.* 3, 8. doi:10.1186/1755-8166-3-8

Lu, B., Su, Y., Das, S., Liu, J., Xia, J., and Ren, D. (2007). The Neuronal Channel NALCN Contributes Resting Sodium Permeability and Is Required for normal Respiratory Rhythm. *Cell.* 129, 371–383. doi:10.1016/j.cell.2007.02.041

Lu, B., Zhang, Q., Wang, H., Wang, Y., Nakayama, M., and Ren, D. (2010). Extracellular Calcium Controls Background Current and Neuronal Excitability via an UNC79-UNC80-NALCN Cation Channel Complex. *Neuron.* 68, 488–499. doi:10.1016/j.neuron.2010.09.014

Nakka, P., Pattillo Smith, S., O'Donnell-Luria, A. H., McManus, K. F., Mountain, J. L., Ramachandran, S., et al. (2019). Characterization of Prevalence and Health Consequences of Uniparental Disomy in Four Million Individuals from the General Population. *Am. J. Hum. Genet.* 105, 921–932. doi:10.1016/j.ajhg.2019.09.016

Ou, X., Liu, C., Chen, S., Yu, J., Zhang, Y., Liu, S., et al. (2013). Complete Paternal Uniparental Isodisomy for Chromosome 2 Revealed in a Parentage Testing Case. *Transfusion.* 53, 1266–1269. doi:10.1111/j.1537-2995.2012.03863.x

Perez, Y., Kadir, R., Volodarsky, M., Noyman, I., Flusser, H., Shorer, Z., et al. (2016). UNC80mutation Causes a Syndrome of Hypotonia, Severe Intellectual Disability, Dyskinesia and Dysmorphism, Similar to that Caused by Mutations in its Interacting Cation channelNALCN. *J. Med. Genet.* 53, 397–402. doi:10.1136/jmedgenet-2015-103352

Richards, S., Aziz, N., Aziz, N., Bale, S., Bick, D., Das, S., et al. (2015). Standards and Guidelines for the Interpretation of Sequence Variants: a Joint Consensus Recommendation of the American College of Medical Genetics and Genomics and the Association for Molecular Pathology. *Genet. Med.* 17, 405–423. doi:10.1038/gim.2015.30

Riggs, E. R., Andersen, E. F., Cherry, A. M., Kantarci, S., Kearney, H., Patel, A., et al. (2020). Technical Standards for the Interpretation and Reporting of Constitutional Copy-Number Variants: a Joint Consensus Recommendation of the American College of Medical Genetics and Genomics (ACMG) and the Clinical Genome Resource (ClinGen). *Genet. Med.* 22, 245–257. doi:10.1038/s41436-019-0686-8

Robinson, W. P. (2000). Mechanisms Leading to Uniparental Disomy and Their Clinical Consequences. *Bioessays.* 22, 452–459. doi:10.1002/(sici)1521-1878(200005)22:5<452:aid-bies7>3.0.co;2-k

Shamseldin, H. E., Faqeih, E., Alasmari, A., Zaki, M. S., Gleeson, J. G., and Alkuraya, F. S. (2016). Mutations in UNC80, Encoding Part of the UNC79-UNC80-NALCN Channel Complex, Cause Autosomal-Recessive Severe Infantile Encephalopathy. *Am. J. Hum. Genet.* 98, 210–215. doi:10.1016/j.ajhg.2015.11.013

Śmigiel, R., Biela, M., Szmyd, K., Błoch, M., Szmida, E., Skiba, P., et al. (2020). Rapid Whole-Exome Sequencing as a Diagnostic Tool in a Neonatal/Pediatric Intensive Care Unit. *J. Clin. Med.* 9, 2220. doi:10.3390/jcm9072220

Valkanas, E., Schaffer, K., Dunham, C., Maduro, V., du Souich, C., Rupps, R., et al. (2016). Phenotypic Evolution of UNC80 Loss of Function. *Am. J. Med. Genet.* 170, 3106–3114. doi:10.1002/ajmg.a.37929

Wie, J., Bharthur, A., Bharthur, A., Wolfgang, M., Narayanan, V., Ramsey, K., et al. (2020). Intellectual Disability-Associated UNC80 Mutations Reveal Inter-subunit Interaction and Dendritic Function of the NALCN Channel Complex. *Nat. Commun.* 11, 3351. doi:10.1038/s41467-020-17105-8

Yamazawa, K., Ogata, T., and Ferguson-Smith, A. C. (2010). Uniparental Disomy and Human Disease: an Overview. *Am. J. Med. Genet.* 154C, 329–334. doi:10.1002/ajmg.c.30270

Yang, X., Pan, G., Li, W. H., Zhang, L. M., Wu, B. B., Wang, H. J., et al. (2017). Analysis of Gene Mutation of Early Onset Epileptic Spasm with Unknown Reason. *Zhonghua Er Ke Za Zhi.* 55, 813–817. doi:10.3760/cma.j.issn.0578-1310.2017.11.004

Zhang, D., Zhao, W., Liu, J., Ou, M., Liang, P., Li, J., et al. (2021). Sodium Leak Channel Contributes to Neuronal Sensitization in Neuropathic Pain. *Prog. Neurobiol.* 202, 102041. doi:10.1016/j.pneurobio.2021.102041

Zhang, R., Chen, S., Han, P., Chen, F., Kuang, S., Meng, Z., et al. (2020). Whole Exome Sequencing Identified a Homozygous Novel Variant in CEP290 Gene Causes Meckel Syndrome. *J. Cel. Mol. Med.* 24, 1906–1916. doi:10.1111/jcmm.14887

Zhang, X., Ding, Z., He, R., Qi, J., Zhang, Z., and Cui, B. (2019). Complete Paternal Uniparental Disomy of Chromosome 2 in an Asian Female Identified by Short Tandem Repeats and Whole Genome Sequencing. *Cytogenet. Genome Res.* 157, 197–202. doi:10.1159/000499893

Zheng, Y., Xu, J., Liang, S., Lin, D., and Banerjee, S. (2018). Whole Exome Sequencing Identified a Novel Heterozygous Mutation in HMBS Gene in a Chinese Patient with Acute Intermittent Porphyria with Rare Type of Mild Anemia. *Front. Genet.* 9, 129. doi:10.3389/fgene.2018.00129

Zhou, S., Wang, H., Wang, Q. K., Wang, P., Wang, F., and Xu, C. (2017). Loss of Heterozygosity Detected at Three Short Tandem Repeat Locus Commonly Used for Human DNA Identification in a Case of Paternity Testing. *Leg. Med.* 24, 7–11. doi:10.1016/j.legalmed.2016.11.001

Conflict of Interest: The authors declare that the research was conducted in the absence of any commercial or financial relationships that could be construed as a potential conflict of interest.

Publisher's Note: All claims expressed in this article are solely those of the authors and do not necessarily represent those of their affiliated organizations, or those of the publisher, the editors and the reviewers. Any product that may be evaluated in this article, or claim that may be made by its manufacturer, is not guaranteed or endorsed by the publisher.

frontiers in Genetics

ORIGINAL RESEARCH
published: 21 September 2021
doi: 10.3389/fgene.2021.732002

Neurodevelopmental Disorders in Patients With Complex Phenotypes and Potential Complex Genetic Basis Involving Non-Coding Genes, and Double CNVs

*Martina Servetti[1,2†], Livia Pisciotta[1,3†], Elisa Tassano[4], Maria Cerminara[1], Lino Nobili[1,5], Silvia Boeri[1,5], Giulia Rosti[1], Margherita Lerone[2], Maria Teresa Divizia[2], Patrizia Ronchetto[4] and Aldamaria Puliti[1,2]**

[1]Department of Neurosciences, Rehabilitation, Ophthalmology, Genetics, Maternal and Child Health (DiNOGMI), University of Genoa, Genoa, Italy, [2]Medical Genetics Unit, IRCCS Istituto Giannina Gaslini, Genoa, Italy, [3]Child Neuropsychiatry Unit, ASST Fatebenefratelli Sacco, Milano, Italy, [4]Human Genetics Laboratory, IRCCS Istituto Giannina Gaslini, Genoa, Italy, [5]Child Neuropsychiatry Unit, Istituto Giannina Gaslini, Genoa, Italy

OPEN ACCESS

Edited by:
Anjana Munshi,
Central University of Punjab, India

Reviewed by:
Patrick May,
University of Luxembourg, Luxembourg
Gavin R. Oliver,
Mayo Clinic, United States

***Correspondence:**
Aldamaria Puliti
apuliti@unige.it

†These authors have contributed equally to this work

Specialty section:
This article was submitted to Genetics of Common and Rare Diseases, a section of the journal Frontiers in Genetics

Received: 28 June 2021
Accepted: 03 September 2021
Published: 21 September 2021

Citation:
Servetti M, Pisciotta L, Tassano E, Cerminara M, Nobili L, Boeri S, Rosti G, Lerone M, Divizia MT, Ronchetto P and Puliti A (2021) Neurodevelopmental Disorders in Patients With Complex Phenotypes and Potential Complex Genetic Basis Involving Non-Coding Genes, and Double CNVs. Front. Genet. 12:732002. doi: 10.3389/fgene.2021.732002

Neurodevelopmental disorders (NDDs) are a heterogeneous class of brain diseases, with a complex genetic basis estimated to account for up to 50% of cases. Nevertheless, genetic diagnostic yield is about 20%. Array-comparative genomic hybridization (array-CGH) is an established first-level diagnostic test able to detect pathogenic copy number variants (CNVs), however, most identified variants remain of uncertain significance (VUS). Failure of interpretation of VUSs may depend on various factors, including complexity of clinical phenotypes and inconsistency of genotype-phenotype correlations. Indeed, although most NDD-associated CNVs are *de novo*, transmission from unaffected parents to affected children of CNVs with high risk for NDDs has been observed. Moreover, variability of genetic components overlapped by CNVs, such as long non-coding genes, genomic regions with long-range effects, and additive effects of multiple CNVs can make CNV interpretation challenging. We report on 12 patients with complex phenotypes possibly explained by complex genetic mechanisms, including involvement of antisense genes and boundaries of topologically associating domains. Eight among the 12 patients carried two CNVs, either *de novo* or inherited, respectively, by each of their healthy parents, that could additively contribute to the patients' phenotype. CNVs overlapped either known NDD-associated or novel candidate genes (*PTPRD*, *BUD13*, *GLRA3, MIR4465, ABHD4,* and *WSCD2*). Bioinformatic enrichment analyses showed that genes overlapped by the co-occurring CNVs have synergistic roles in biological processes fundamental in neurodevelopment. Double CNVs could concur in producing deleterious effects, according to a two-hit model, thus explaining the patients' phenotypes and the incomplete penetrance, and variable expressivity, associated with the single variants. Overall, our findings could contribute to the knowledge on clinical and genetic diagnosis of complex forms of NDD.

Keywords: variants of uncertain significance, long non-coding genes, antisense gene, oligogenic disease, array-CGH, additive effect, microdeletion, microduplication

INTRODUCTION

Neurodevelopmental disorders (NDDs) are a heterogeneous class of conditions involving the brain, including intellectual disability and autism spectrum disorder (ASD), that affect about 1–3% of children (Miller et al., 2010). The genetics of NDDs is complex and include copy number variants (CNVs) and deleterious variants in single genes (Coe et al., 2019).

Nowadays new technologies, such as whole exome (WES) and whole genome sequencing (WGS), have become more efficient and inexpensive such that it is ongoing a debate for choosing the proper first-tier diagnostic test (Srivastava et al., 2019; Alvarez-Mora et al., 2021; Arteche-Lopez et al., 2021).

Despite of that, the detection of CNVs by the array comparative genomic hybridization (array-CGH) continues to be widely used as a first-tier test, resulting in an average diagnostic yield between 15 and 20% (Miller et al., 2010). Interpretation of CNVs is complex and, despite the use of standard classification guides (Riggs et al., 2020), most identified variants remain of uncertain significance (VUS).

Failure of interpretation of VUSs may depend on different factors, including poor annotation of protein-coding genes, lack of functional information for untranslated expressed genes or for genomic intergenic regions overlapped by the CNVs. The observation of inconsistent genotype-phenotype correlations also complicates CNV interpretation. Although most NDD causative CNVs are *de novo*, increasing evidence indicates that CNVs with high risk for NDDs show incomplete penetrance since transmission from unaffected parents to affected children has been observed. Possible explanation for the observed inconsistency of genotype-phenotype correlation may involve complex interactions of potentially pathogenic CNVs with additional/secondary CNVs, or single nucleotide variants, that could act together to determine a disease state (Velinov, 2019). According to this hypothesis, additive effects of CNVs were for instance reported in probands carrying 16p11.2 deletions and secondary CNVs that disrupt genes associated with autism and/or intellectual disability (Girirajan et al., 2010; Duyzend et al., 2016).

The goal of this study was to clarify the contribution of microdeletions and microduplications identified, by array-CGH diagnostic test, in 12 patients with complex NDD phenotype using multiple bioinformatics resources and the synergistic effort of a team of neuropsychiatrists and geneticists.

We found potential pathogenic variants in novel candidate genes for neurodevelopmental disorders. Furthermore, CNV-mediated double-hit mechanisms seem to play a relevant role in the complex forms of neurodevelopmental disorders affecting our patients. Indeed, these co-occurring hits involved already known NDD-associated genes or hypothetical novel NDD candidate genes enriched for pathways or biological processes known to be implicated in neurodevelopment.

METHODS

Clinical Assessment

The clinical assessment of the patients comprised a thorough medical history also attentive to investigating systemic symptoms and sleep, neurological-behaviour examination, developmental/cognitive assessment, and basic metabolic screening. Prior to array-CGH analysis, all patients were first evaluated by using different genetic tests for the common genetic causes of NDDs, including karyotype analysis, and tests for Fragile X syndrome. Written informed consent was obtained from the patient's parents or legal representative. This study was reviewed and approved by the Ethics Committee of the Italian Regione Liguria (R. P. 001/2019).

CNV Detection and Annotation

Array-CGH analysis was performed on DNA samples, extracted from peripheral blood, using a whole-genome 180 K Agilent array with ~13 Kb overall median probe spacing (Human Genome CGH Microarray, Agilent Technologies, Santa Clara, CA, USA). Data were analyzed using Agilent CytoGenomics and genomic positions reported according to the human genome assembly (GRCh37/hg19). All detected CNVs were tested for inheritance by hybridization of the parental DNA with the same array platform. *De novo* CNVs were confirmed either by FISH analysis or by quantitative real-time PCR as already reported (Vaccari et al., 2014; Tassano et al., 2015). To assess the clinical significance of the detected CNVs, we used several tools. Aberration segments were reviewed using GRCh37 hg19 of UCSC Genome Browser (http://genome.ucsc.edu/index.html). We annotated all detected CNVs and CNV-encompassed genes across public databases: Genomic Variants Database (DGV) (http://dgv.tcag.ca/dgv/app/home), DECIPHER (https://decipher.sanger.ac.uk/), Clinical Genome Resource (ClinGen) (https://clinicalgenome.org/), the Online Mendelian Inheritance in Man (OMIM) (http://www.omim.org), Simons Foundation Autism Research Initiative (SFARI) database (https://gene.sfari.org/), databases of mouse models (Mouse Genome Informatics, MGI) (http://www.informatics.jax.org). Literature mining was also performed. We considered only variants present in <0.1% of control individuals. We checked CNVs for the presence of dosage-sensitive genes (haploinsufficiency/triple sensitivity score) by using Clinical Genome Resource (ClinGen) consortium resource (https://dosage.clinicalgenome.org/). We also considered probability of intolerance to loss-of-function (LoF) variants (pLI) as reported in the Genome Aggregation Database (gnomAD, (https://gnomad.broadinstitute.org/). Genes with pLI scores of 0.9 or higher are extremely intolerant to heterozygous LoF variation, and thus haploinsufficient (Lek et al., 2016).

We then investigated deleted/duplicated regions for encompassing topologically associating domains (TADs), or their boundaries (TDBs), using Hi-C (http://3dgenome.fsm.northwestern.edu/). Indeed, TADs data from genome-wide higher order chromatin interaction data in human embryonic stem cells (h-ESC), h-ESC derived neural progenitor cells (H1NPC) (Dixon et al., 2015), and brain cortex (Schmitt et al., 2016), were downloaded (http://chromosome.sdsc.edu/mouse/download.html) (see **Supplementary file**) and mapped to hg19 coordinates using the UCSC browser. We then investigated identified CNV-genes, not previously associated with genetic diseases, for relevance to NDDs by considering different

criteria: expression in the brain; reported mutations in the mouse associated with a neurodevelopmental phenotype; interaction with genes known to be associated with a neurodevelopmental disorder. To identify CNV disrupted genes with high brain expression, we used the BrainSpan database (http://www.brainspan.org/static/download.html) (Huckins et al., 2019) and extracted the list of genes with average log2 RPKM >4.5 (the top 18%), as also reported (Addis et al., 2018; Cerminara et al., 2021). We further investigated brain expression of genes at single gene isoforms using GTEx data (https://www.gtexportal.org/home/). We searched for gene-specific mouse models presenting a neurodevelopmental phenotype using MGI database. CNV-genes coding for microRNAs (miRNAs) were further investigated to detect the presence, among their possible targets, of any genes known to be associated with NDDs (**Supplementary file**) or to be involved in brain development and/or function by using miRDB (http://mirdb.org/), Target Scan (http://www.targetscan.org/vert_72/) and DIANA TOOLS (http://diana.imis.athena-innovation.gr/DianaTools/index.php).

Network Analysis of Candidate Genes

We used GeneCodis4 (Tabas-Madrid et al., 2012) to unveil enrichment of annotations, as already reported (Cerminara et al., 2021). Briefly, all the genes obtained from either duplicated or deleted regions were used as input in GeneCodis4 together with known NDD-associated genes, as those related to ASD and reported in SFARI database and those reported in OMIM as associated with intellectual disability (see **Supplementary file**). This tool allows the classification of genes according to their putative biological function by screening the Gene Ontology (GO), OMIM, Panther, and KEGG Pathways. In the analysis, the hypergeometric test was applied followed by the false discovery rate correction (FDR) with a cut-off of 5% to determine which annotations were significantly enriched. For GO analysis, various hierarchical levels of the annotation data structure were used. All genes of the top gene ontology terms, including candidate and known NDD genes, were then projected onto the STRING network (v11) (Szklarczyk et al., 2019). Edges within the STRING network were thresholded at 0.4, according to the authors' recommendation. A graphical representation of the GeneCodis4 and STRING results was obtained by using Cytoscape tool (Shannon et al., 2003).

Pathogenicity Evaluation and Graphical Representation of CNVs

To evaluate the pathogenicity of variants we focused on the following criteria: 1) patients with multiple CNVs, enclosing NDD genes, which could have additive effects on the patients' phenotype on the basis of results from gene enrichment and protein-protein interactions analyses; 2) patients with CNVs encompassing regions that control the expression of known NDD genes, including those with potential long-range effects; 3) patients whose CNVs encompass genes not yet reported as NDD-associated, but whose expression profile and function suggest a possible involvement in the disease, when at least another patient is reported with a similar CNV and phenotype in publically available databases. Results of this analysis were graphically reported using UCSC and specific Custom Tracks. In particular we used RefSeq Curated for gene representation and OMIM genes to underline genes already associated with disease. Decipher track was manually modified; we selected patients with CNVs similar to those of our patients, that is either deletions or duplications according to those found in our patients and overlapping approximately the same region and genes. We selected Decipher CNVs only if their related patients had a NDD phenotype (we kept out patients for whom we had no information about their phenotype). The CNVs thus selected were further investigated for being present in the same patient with other secondary CNVs overlapping additional NDD genes, and in this case reported in figures (marked with letters). Developmental Delay case track includes manually selected CNVs similar in size and gene content to those of our cases; we proceeded analogously also for Developmental Delay Control CNVs. A track reporting SFARI genes was added to underline the presence of a known ASD associated gene in the genomic region shown in figures. Brain-expressed gene track represents genes with a prevalent expression in the brain according to the BrainSpan data processed as detailed above, useful to highlight possible new NDD candidate genes.

RESULTS

Clinical Presentation of Patients

The 12 patients we report were all born to non-consanguineous parents. After clinical evaluation and follow up, the employment of specific tests and instruments, all subjects showed a complex phenotype, each of them characterized by different neurological features and other associated impairments and comorbidities. The main clinical features were represented by a variable degree of intellectual disability, in three cases associated with a diagnosed ASD, and epilepsy. Language disorder, self-aggressive behaviours and sleep disturbances could be also observed (see **Table 1**).

Additive Effects of CNVs Involving Known NDD Genes

Four patients presented with two CNVs, overlapping known NDD genes, and inherited, respectively, by each of their healthy parents. We thought that in these cases, CNVs could additively contribute to the patient's phenotype (**Table 2**).

The first case, IGGAC13, is a male patient with a maternal deletion of chromosome 7 involving *CNTNAP2* and a paternal deletion of chromosome 11 involving *LRRC4C* (**Figures 1A,B**). Both genes are present in the SFARI database. Few CNVs are reported to overlap these two genes in control individuals and in NDD patients according to Developmental Cases and Decipher databases. Of note, NDD patients reported in Decipher and represented in **Figure 1** carried one additional CNV involving other NDD-associated genes. Indeed, a case has been previously reported with two deleterious variants, one of which disrupting *LRRC4C* and one affecting another SFARI-reported gene *DPP6*

TABLE 1 | Clinical features.

Patient ID	ASD	ID	Other NDDs	Neurological signs/disorders	Others	Results of other laboratory tests
IGGAC01	NO	ID	Language disorder, Coordination disorder, Atypical behaviours, Attention disorder and Hyperactivity, Self-aggressive behaviours	Hypotonia Epilepsy, Sleep disturbances	Gastrointestinal disorders, dysphagia and selective feeding	Normal blood amino acid and organic acids levels Fragile X analysis: negative
IGGAC04	NO	ID	NO	Hypotonia and Epilepsy	Prenatal gastrointestinal perforation	Normal blood amino acid, organic acids levels, acylcarnitine profile, guanidinoacetic acid Karyotype, Fragile X analysis: negative
IGGAC06	YES	ID	NO	Sleep disturbances	Congenital lymphedema	Normal blood amino acid and organic acids levels Karyotype, Fragile X analysis: negative
IGGAC07	NO	ID	Atypical behaviours, Attention disorder and Hyperactivity	NO	NO	Findings of the amniocentesis
IGGAC08	NO	Borderline	Language disorder, Attention disorder and Hyperactivity	NO	Growth defect	Normal blood amino acid and organic acids levels Fragile X analysis: negative
IGGAC10	NO	ID	NO	Epilepsy	NO	Normal blood amino acid and organic acids levels Fragile X analysis: negative
IGGAC13	YES	ID	NO	Epilepsy	NO	Normal blood amino acid and organic acids levels Karyotype, Fragile X analysis: negative
IGGAC14	NO	ID	Learning disorder and Aggressivity	Chiari I malformation and Mild skull base abnormality	NO	Normal blood amino acid and organic acids levels Karyotype, Fragile X analysis: negative
IGGAC15*	NO	Borderline	Psychomotor delay and mild Atypical behaviours	NO	NO	Fragile X analysis: negative
IGGAC16*	NO	ID	Hyperactivity	Sleep disturbances	NO	Fragile X analysis: negative
IGGAC023	YES	ID	NO	Enuresis	NO	Normal blood amino acid and organic acids levels Karyotype, Fragile X analysis: negative
IGGAC024	NO	ID	Language disorder and Hyperactivity	NO	Growth defect, Brain midline defects	Normal blood amino acid and organic acids levels Karyotype, Fragile X analysis: negative

*ASD, autism spectrum disorder; ID, intellectual disability. * Brother and sister.*

(Maussion et al., 2017). The two variants, as in our case, were inherited one from the mother and one from the father, both unaffected.

CNTNAP2 encodes a member of the neurexin family which functions in the nervous system as cell adhesion molecule. *LRRC4C* (NGL1) is a specific binding partner for netrin G1, which is a member of the netrin family of axon guidance molecules. In fact, both molecules, *CNTNAP2* and *LRRC4C,* are implicated in synapse formation (Um and Ko, 2017). We hypothesized that, while half dosage of each of these two molecules is compatible with a normal development, half dosage of both genes can impair synapse correct development and function. In fact, gene enrichment and String analysis showed that both genes are members of the KEGG cell adhesion molecule pathway and interact with other known NDD genes (**Figure 1C**; **Supplementary Table S1**).

The second case is a male patient (IGGAC14) that inherited from his healthy father a deletion of chromosome 17 encompassing a SFARI gene, *DNAH17,* and its antisense gene

TABLE 2 | Overview of the CNVs found in the patients.

Patient ID	Gender	CNV coordinates (hg19)	Minimal region (Kb)	del/dup	Inh	Total genes (RefSeqAll)	Candidate genes
IGGAC13	M	7:146464283-146532437	68	del	mat	1	*CNTNAP2*
		11:40303114-40694847	392	del	pat	1	*LRRC4C*
IGGAC14	M	17:76419867-76548866	129	del	pat	3	*DNAH17*
		X:561527-908212	347	dup	mat	1	*SHOX*
IGGAC15[a]	M	15:22765628-23208901	443	del	mat	6	*NIPA1,CYFIP1,TUBGCP5,NIPA2*
		6:33337684-33669083	331	dup	*de novo*	13	*SYNGAP1*
IGGAC16[a]	F	15:22765628-23208901	443	del	mat	6	*NIPA1,CYFIP1,TUBGCP5,NIPA2*
		6:33337684-33669083	331	dup	*de novo*	13	*SYNGAP1*
		16:6371455-6568176	197	del	pat	1	*RBFOX1*
IGGAC07	M	12:108487109-108896252	409	dup	mat	3	*WSCD2*
		14:22360671-23120435	760	dup	*de novo*	5	*ABHD4*
		22:22998284-23643223	645	dup	mat	8	*GNAZ*
IGGAC10	M	3:123113523-123997093	884	dup	pat	9	*ADCY5*
		6:86338564-86413285	75	del	mat	4	*SYNCRIP*
IGGAC06	M	9:10286927-11086155	799	del	mat	2	*PTPRD*
		11:116182875-116677043	494	del	not mat	4	*BUD13*
IGGAC08	M	4:175734964-175934265	199	del	mat	3	*GLRA3*
		6:140767462-141008265	241	del	*de novo*	1	*MIR4465*
		10:134289353-134917702	628	dup	*de novo*	9	*INPP5A*
IGGAC04	M	5:88232587-90181774	1,949	del	*de novo*	9	*MEF2C-AS1* and *ADGVR1*
IGGAC01	F	16:8969984-10078802	1,109	dup	*de novo*	6	*USP7* and *GRIN2A*
IGGAC24	M	19:55948706-56471996	523	dup	*de novo*	24	*SHISA7*
IGGAC23	M	10:125121038-127119447	1,998	dup	*de novo*	13	*CTBP2*

[a]*Brother and sister.*

DNAH17-AS1. *DNAH17* encodes a heavy chain associated with axonemal dynein, a member of microtubule-associated motor protein complexes. From his healthy mother, the patient inherited a duplication involving *SHOX* on chromosome X (**Figure 2**), also reported in the SFARI database**.** *SHOX* belongs to the paired homeobox family and is located in the pseudoautosomal region 1 (PAR1) of X and Y chromosomes. Enrichment of *SHOX* microduplications in NDD cases, particularly in those with ASD, has been described (Tropeano et al., 2016). Gene enrichment evidenced a function of *SHOX* in the regulation of transcription by RNA polymerase II, and of *DNAH17* in microtubule-based movement, two important biological processes in neurodevelopment disorder (**Figure 2**; **Supplementary Table S1**). As shown in **Figure 2A**, other patients with NDD phenotype are reported in Decipher database to have duplications of *SHOX* and a secondary CNV involving neurodevelopmental genes. Indeed, a chromosome 17 deletion similar to that of our patient was reported in Decipher database in a case with NDD phenotype having a secondary CNV also overlapping developmental genes (**Figure 2B**).

We observed a family with two affected siblings, a male (IGGAC15) and a female (IGGAC16), showing discordant phenotypes. They inherited from their unaffected mother a deletion encompassing a syndromic region at 15q11.2 (**Figure 3A**). The siblings also shared a duplication involving the SFARI gene *SYNGAP1* (**Figure 3B**). Of note, the *SYNGAP1* duplication was not observed in parents, at least in their blood-extracted DNA, thus leading to suppose mosaicism in either father or mother. Patient IGGAC16 also inherited a paternal, recurrent deletion involving the SFARI gene *RBFOX1* (**Figure 3C**). Interestingly, loss of function variants of *SYNGAP1* have been identified in patients with ASD and intellectual disability with or without epilepsy. However, to the best of our knowledge, no cases with duplication or gain of function variants have been reported so far. Overexpression of SynGAP was reported to block neurite outgrowth by a mechanism that involves Ras-like GTPase cascade (Tomoda et al., 2004), to produce a depression of AMPAR-mediated excitatory postsynaptic currents in neurons (Rumbaugh et al., 2006), and to regulate decreasing and increasing miniature excitatory synaptic currents in hippocampal neurons (McMahon et al., 2012). In fact, some phenotypic differences between the two siblings were observed. The male patient showed a mild phenotype characterized by a borderline cognitive functioning associated with atypical behaviours and psychomotor delay in early infancy, his sister had a more complex phenotype with mild cognitive impairment, irregular sleep rhythms, hyperactivity, coordination, and language

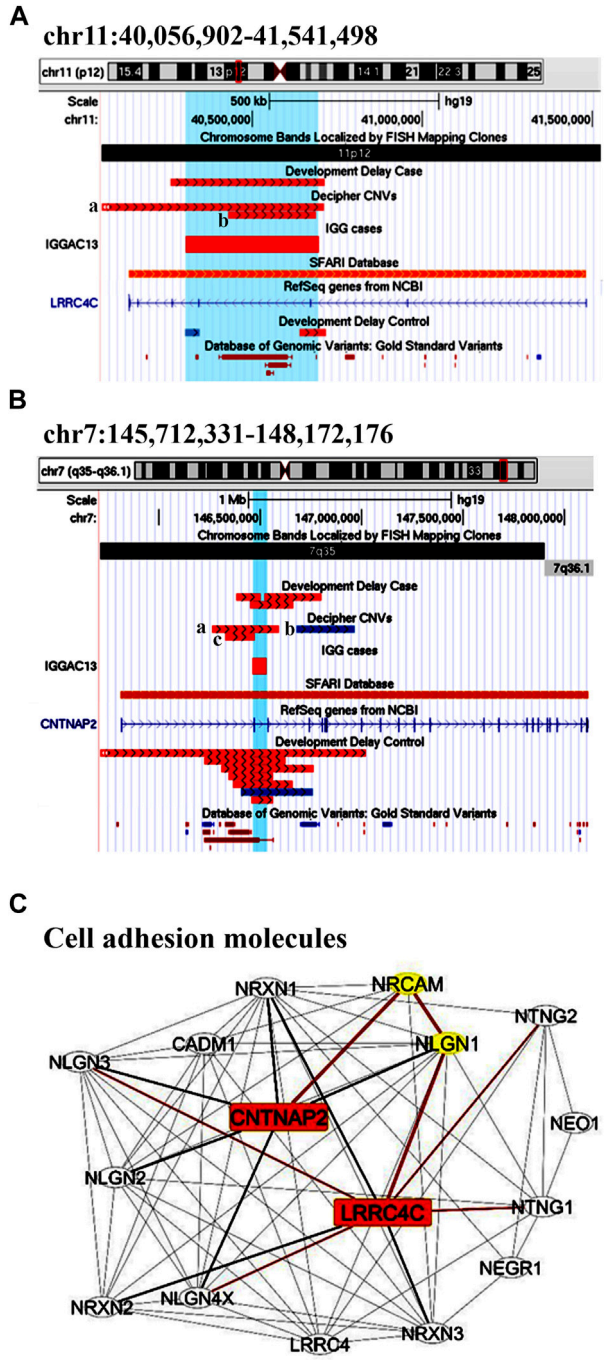

FIGURE 1 | Additive effects between *CNTNAP2* and *LRRC4C* in patient IGGAC13. **(A)** Screenshots of chromosome 11 region overlapping the deletion of patient IGGAC13 (red bar IGGAC13, chr11:40,303,114-40,694,847). Decipher CNVs (a: deletion in patient 282991; b: deletion in patient 276911). **(B)** Screenshots of chromosome 7 region overlapping the deletion of patient IGGAC13 (red bar IGGAC13, chr7:146,464,283-146,532,437). Decipher CNVs (a: deletion in patient 319381; b: intragenic duplication in patient 255117; c: deletion in patient 250646). Only Decipher patients with additional CNVs that overlap neurodevelopmental genes were selected and reported in the figure. **(C)** The network depicts the protein-protein interactions (grey lines), experimentally determined interaction (red lines) and co-expression (bold black lines) of the KEGG pathway "Cell

(*Continued*)

disorders. We could speculate that the two CNVs shared by the two siblings can explain the phenotypic features shared by both of them, while the third CNV could have worsened the phenotype of the female patient.

Addictive Effects of CNVs Involving Potential Novel Candidate Genes and New Pathogenic Mechanisms

Four patients reported double CNVs involving genes or genomic regions not yet described as NDD-associated but that could act in concert, similarly to the four cases described above, with a potential impact on the patients' phenotype (**Table 2**).

The first case (IGGAC06) carried a maternal deletion of chromosome 9 and a non-maternal deletion of chromosome 11; as genetic analysis of the patient's father was not available, we cannot determine if the chromosome 11 deletion was *de novo* or paternally inherited (**Figures 4A,C**). The chromosome 9 deletion encompassed *PTPRD*, which encodes a protein-tyrosine phosphatase receptor, and *PTPRD-AS2*, a long non-coding RNA (lncRNA) gene known as *PTPRD* antisense RNA 2 (head-to-head) predicted to make expression of mRNA more stable and thus enhancing *PTPRD* protein production. Thus, a reduced expression of *PTPRD* can be hypothesized because of the deletion of the first two untranslated exons of the gene and of *PTPRD-AS2*. A total of 7 deletions encompassing exonic regions of *PTPRD* are reported in controls, while several CNVs and, in particular, 16 deletions and one intragenic duplication involving coding regions of the gene are present among cases in Developmental Delay and Decipher databases with NDD phenotypes. Five among Decipher cases have an additional CNV involving brain expressed genes that, analogously to those reported in patient IGGAC06, could have an additive effect in causing patient's phenotype. Interestingly, *PTPRD* is predicted to be intolerant to loss of function variants (pLI = 1) and to haploinsufficiency mechanisms (score = 0.75; value above 0.5 are predicted to be haploinsufficient) (Shihab et al., 2017). *PTPRD* has a role in synaptic adhesion and synapse organization and can bidirectionally induce pre- and postsynaptic differentiation of neurons by trans-synaptically binding to interleukin-1 receptor accessory protein (*IL1RAP*) (Yoshida et al., 2012; Yamagata et al., 2015). In the mouse, *PTPRD* was shown to regulate neurogenesis (Tomita et al., 2020) and mice lacking *PTPRD* showed impaired learning with enhanced hippocampal long-term potentiation (Uetani et al., 2000), thus suggesting a role for *PTPRD* in neurodevelopmental disorders. In OMIM database, *PTPRD* is not associated with a disorder, and its implication in human disease is still to be completely clarified. Homozygous deletions of *PTPRD* were observed in a patient with intellectual disability and trigonocephaly (Choucair et al., 2015)

FIGURE 1 | adhesion molecule," revealed by STRING analysis on the basis of enrichment obtained with GeneCodis4, and visualized by Cytoscape tool. The Figure shows the clustering of the candidate genes with other known NDD genes. In yellow the interacting molecules directly linking the two candidate genes to each other.

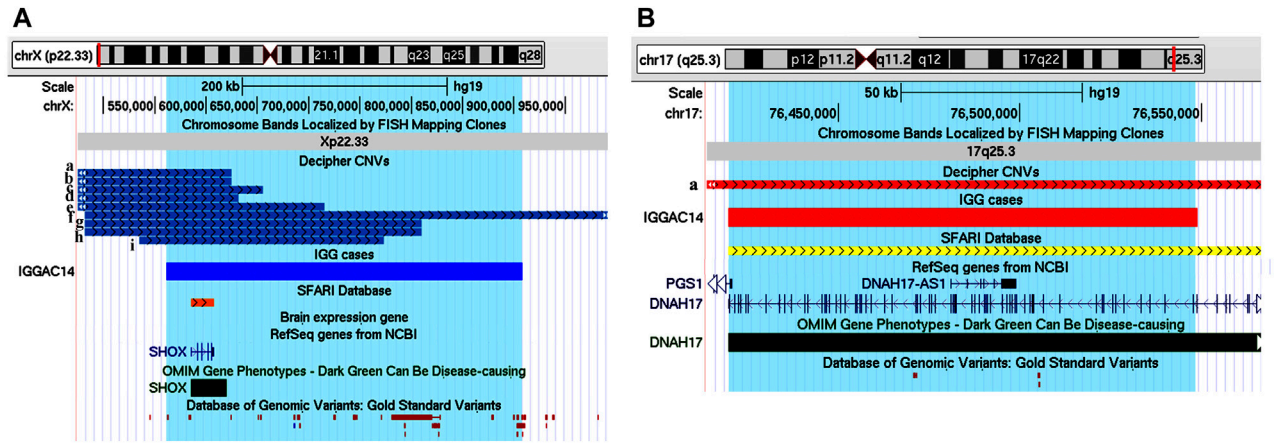

FIGURE 2 | Additive effects between *SHOX* and *DNAH17* in patient IGGAC14. **(A)** Screenshot of chromosome X region overlapping the duplication of patient IGGAC14 (blue bar, chrX:561,527-908,212). Duplications in Decipher database (a: patient 259967; b: patient 367079; c: patient 380394; d: patient 284815; e: patient 289670; f: patient 322776; g: patient 367150; h: patient 279033; i: patient 353723). **(B)** Screenshot of chromosome 17 region encompassing the deletion of patient IGGAC14 (red bar, chr17:76,419,867-76,548,866). Deletions in Decipher database (a: patient 289758).

and his family members carrying the same deletions were reported to be unaffected. Instead, a heterozygous *de novo* splicing variant of the gene was reported in a girl with moderate nonsyndromic developmental delay (Yan et al., 2019). Furthermore, genetic studies showed an oligogenic association of *PTPRD* variants with obsessive-compulsive disorder (Mattheisen et al., 2015) and with restless leg syndrome (Schormair et al., 2008). Overall, results from various genetic studies are consistent with both major/oligogenic and modest/polygenic contributions of common and rare *PTPRD* variations in neurological, behavioural, and neurodevelopmental disorders (Uhl and Martinez, 2019). Gene enrichment and String analysis showed *PTPRD* interacting with many NDD genes playing a role in synaptic membrane adhesion and neuronal development (**Figure 4B**; **Supplementary Table S1**).

The chromosome 11 deletion encompassed *BUD13,* which encodes a component of the retention and splicing (RES) complex of the spliceosomal complex. In zebrafish, the lack of *BUD13* caused defects in intron splicing specifically in genes with neurodevelopmental regulatory functions, thus resulting in a decrease of differentiated neurons and brain developmental defects (Fernandez et al., 2018). GeneCodis analysis showed an enrichment of *BUD13* with various NDD genes in the GeneOntology category of mRNA splicing, via spliceosome, a biological process with an important role in neurodevelopment (**Figure 4D**, **Supplementary Table S1**).

Patient IGGAC08 has a complex phenotype mainly characterized by language disorder, hyperactivity, learning difficulties, borderline cognitive level, motor skill impairment, and short stature (**Table 1**). His mother also had school difficulties and showed dyslexia in childhood. Mother and son share a deletion of chromosome 4q34.1 encompassing *GLRA3* which encodes the alpha-3 subunit of the neuronal glycine receptor, a ligand-gated ion channel. In addition, patient IGGAC08 had a *de novo* deletion involving *hsa-mir-4465* and a *de novo* duplication including *INPP5A* (**Table 2** and **Figures 5A–C**). *GLRA3* receptors are expressed in spinal cord, brainstem, hippocampus, amygdala, striatum, and cortex. The glycine receptor is a glycoprotein composed of 5 subunits, three α and two β subunits. The alpha subunits bind the glycine ligand while the beta subunits bind to gephyrin, a cytosolic protein required for a regulated synaptic aggregation and clustering of these receptors.

Gephyrin has functional links with several synaptic proteins, mutations of which have been reported in various neurodevelopmental disorders (Choii and Ko, 2015; Kim et al., 2021). Half dosage of *GLRA3* may contribute to impair gephyrin-mediated aggregation and post-synaptic clustering.

Loss of *PTEN*, a SFARI gene, can cause postsynaptic and presynaptic changes in excitatory and inhibitory connectivity. *In vitro* analyses have recently demonstrated that a miRNA (microRNA-301a) can downregulate *PTEN* after glycine receptor activation (Chen et al., 2016). Tao et al. (2019) showed that *miR-4465* significantly inhibited the expression of *PTEN*, upregulated phosphorylated AKT and ultimately inhibited autophagy by activating mTOR in HEK293, HeLa, and SH-SY5Y cells (Tao et al., 2019). Half dosage of *hsa-mir-4465* in our patient is expected to cause upregulation of *PTEN,* contributing to postsynaptic impairment. MiRNAs are important regulators of brain development and neuronal function, and have been associated with a variety of nervous system diseases, including ASD (Cheng et al., 2018; Wu et al., 2020).

In mice, the deletion of *Inpp5a* causes perinatal lethality in 90% of the homozygous mutants, early onset ataxia and relatively small stature in surviving mutants. Heterozygotes do not exhibit obvious motor coordination impairment unless challenged in motor skill test (Yang et al., 2015). *Inpp5a* is a downstream effector of signalling from mGlu1 receptor, one of the two members of group I metabotropic glutamate receptors, that

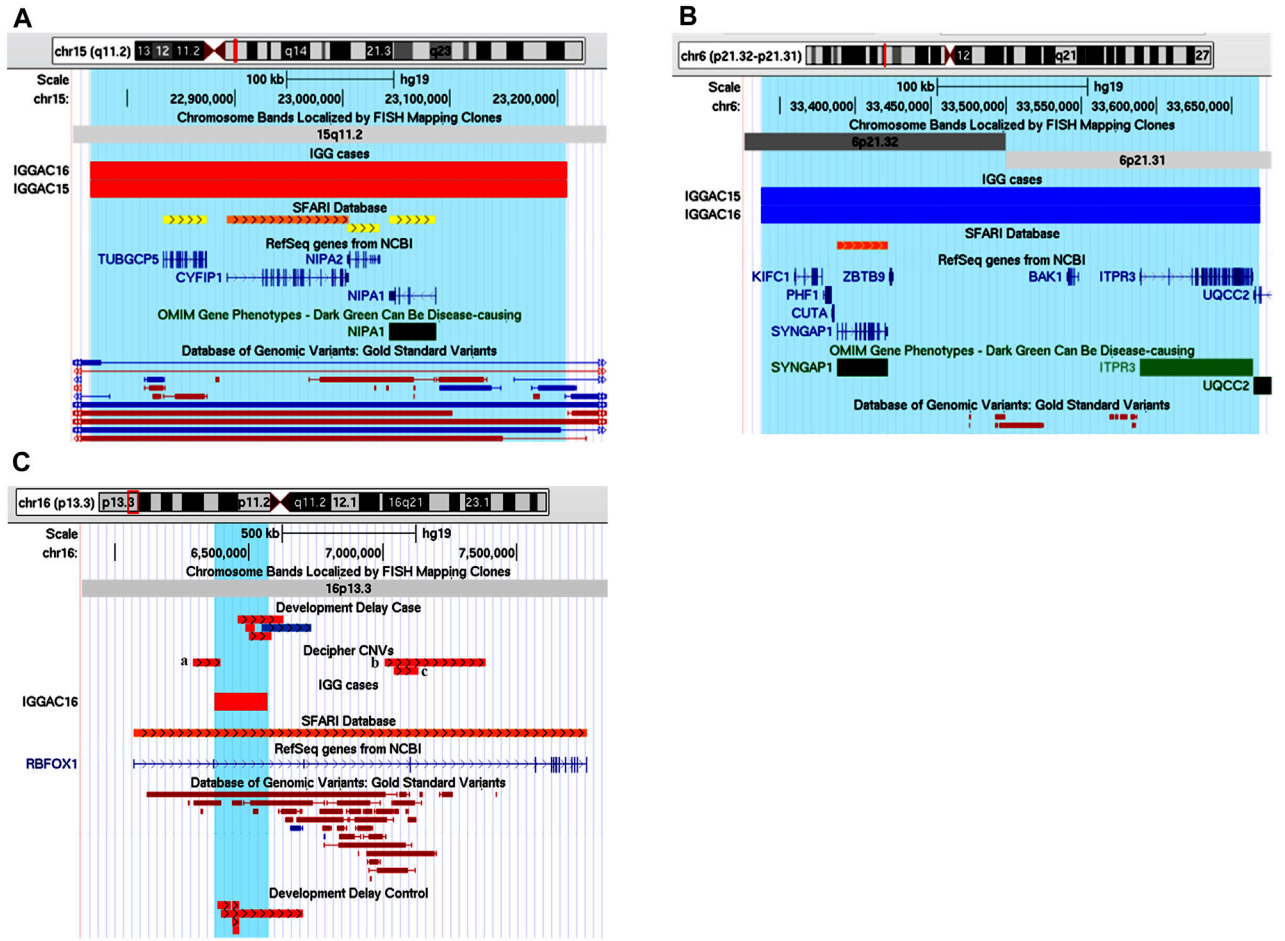

FIGURE 3 | Additive effects in a familial case, siblings IGGAC15 and IGGAC16. **(A)** Screenshot of chromosome 15 region encompassing the deletion shared by the two siblings (red bars, chr15:22,765,628-23,208,901). **(B)** Screenshot of chromosome 6 region encompassing the duplication shared by the two siblings (blue bars, chr6:33,337,684-33,669,083). **(C)** Screenshot of chromosome 16 region encompassing the deletion of patient IGGAC16 (red bar, chr16:6,371,455-6,568,176). Deletions reported in Decipher patients (a: patient 283262; b: patient 327250; c: patient 403649).

regulates synaptic plasticity, particularly in cerebellar Purkinje cells. The mGlu1 receptor activity needs to be fine-tuned and balanced for normal motor coordination. Alteration of expression, either enhancement or decrease, of group 1 mGlu metabotropic receptors in mice is known to alter their activity, which results in defects of motor coordination (Rossi et al., 2013; Bossi et al., 2018). The deletion of *INPP5A* in this patient may be in part responsible for his impairment in motor skills.

IGGAC10 patient showed a complex phenotype mainly characterized by intellectual disability and epilepsy (**Table 1**). He carried a maternal deletion encompassing *SYNCRIP* and a paternal duplication involving the upstream regulatory genomic region of *ADCY5*. Both CNVs overlap a TDB between two flanking TADs described in different tissues, including brain cortex, which could also contribute to dysregulating the expression of implicated genes (**Figures 6A,B**).

SYNCRIP encodes the synaptotagmin-binding cytoplasmic RNA-interacting protein, a member of the cellular heterogeneous nuclear ribonucleoprotein (hnRNP) family that plays a role in multiple aspects of mRNA maturation. Missense and truncating variants of *SYNCRIP* were found in ASD patients with more severe phenotypes (Guo et al., 2019) and in patients with severe non-syndromic sporadic intellectual disability (Rauch et al., 2012), respectively. *ADCY5* encodes a member of the membrane-bound adenylyl cyclase enzymes which mediate G-protein-coupled receptor signalling through the synthesis of the second messenger cAMP. According to SFARI database, missense and frameshift variants of *ADCY5* have been reported in ASD patients. Gain of function variants of *ADCY5* have been associated with a broad range of movement disorders, most notably chorea, dystonia and myoclonus (Vijiaratnam et al., 2019).

Thus, the two CNVs could cause, by a mechanism also implicating a modification of chromatin conformation, a dysregulation of both *SYNCRIP* and *ADCY5* contributing to the complex phenotype observed in this patient.

IGGAC07 patient carried a *de novo* duplication of chromosome 14, and two maternally inherited duplications of

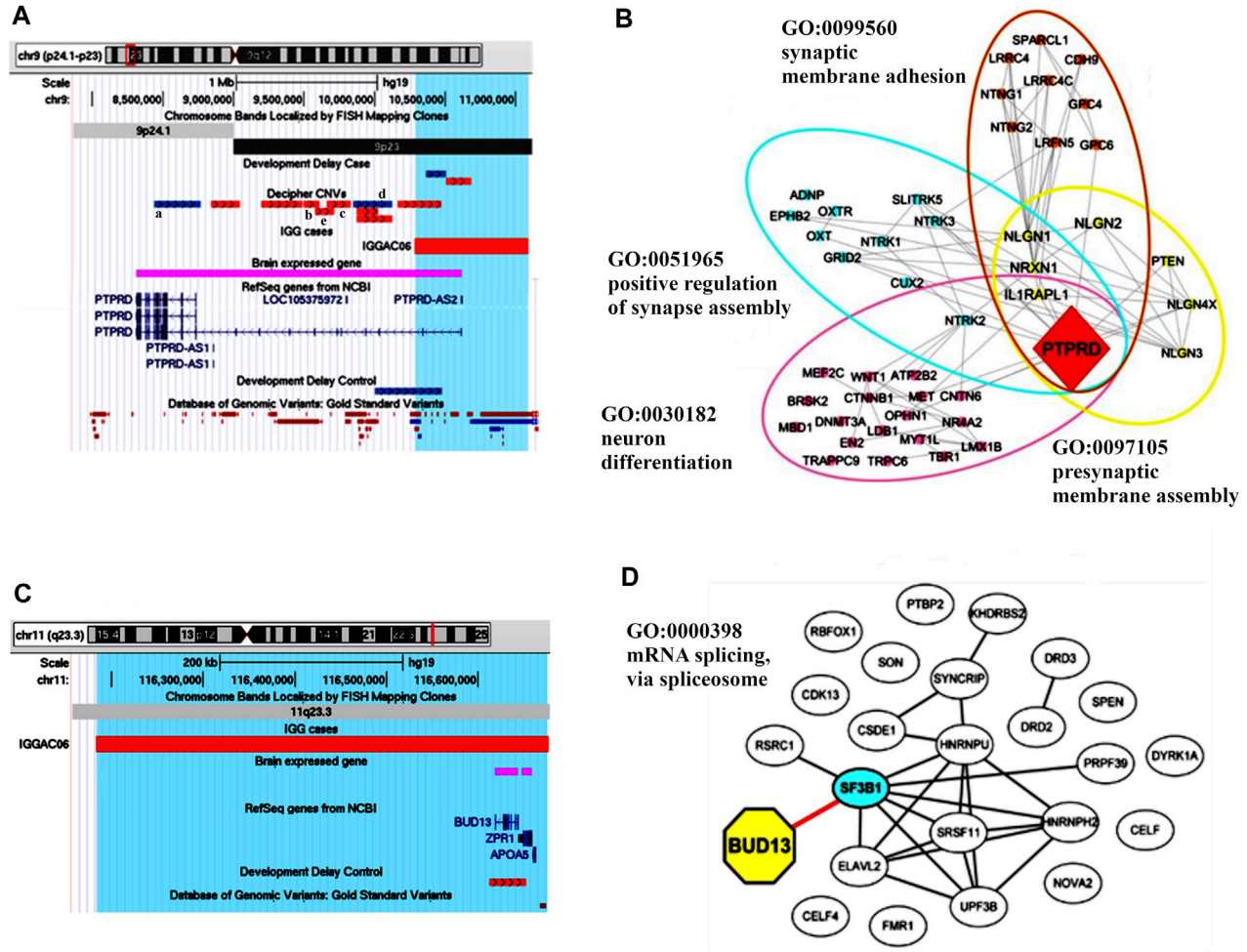

FIGURE 4 | Additive effects between *PTPRD* and *BUD13* in patient IGGAC06. **(A)** Screenshot of chromosome 9 region overlapping the deletion of patient IGGAC06 (red bar, chr9:10,286,927-11,086,155). Decipher CNVs (a: intragenic duplication in patient 333436; b: deletion in patient 412118; c: deletion in patient 337260; d: intragenic duplication in patient 260089 and e: deletion in patient 279686). **(B)** The network depicts the protein-protein interactions (grey lines) revealed by STRING analysis (visualized by Cytoscape tool) on the basis of the enrichment obtained with GeneCodis4 tool. The Figure shows the enriched GO terms clustering the candidate gene *PTPRD* and known NDD genes. **(C)** Screenshot of chromosome 11 region overlapping the deletion of patient IGGAC06 (red bar, chr11: 116,182,875-116,677,043). **(D)** The network depicts the protein-protein interactions (grey lines) and experimentally determined interaction with a SFARI gene (red line) revealed by STRING analysis (visualized by Cytoscape tool) on the basis of the GO term "mRNA splicing *via* spliceosome". The network indicates a direct interaction of *BUD13* with the known NDD gene *SF3B1*.

chromosome 12 and chromosome 22, respectively (**Table 2**; **Figures 7 A–C**).

Interestingly, chromosome 14 duplication encompassed *ABHD4*, a gene recently shown to be involved in developmental anoikis, a mechanism of cell death in the prenatal brain preventing from survival of misplaced cells (Laszlo et al., 2020). Indeed, *ABHD4* is involved in N-acylethanolamine biosynthesis, including the endocannabinoid molecule anandamide which has various physiological functions such as the regulation of synaptic plasticity and apoptosis. *ABHD4* expression is tightly controlled spatially and temporally in the developing brain and a misregulation of its expression due to the duplication could contribute to the patient's phenotype. Duplications encompassing *ABHD4* were annotated in only one control individual, while various cases were reported both in Decipher and in Developmental Delay databases with duplications larger than that observed in our patient and a smaller one sharing with our patient *ABHD4* duplication.

The maternal duplication on chromosome 22 involved a region with triplosensitivity including *GNAZ*, the Guanine Nucleotide-binding protein (G protein) Alpha Z polypeptide encoding gene. In this region, many duplications are reported in both Decipher and Developmental Delay databases, most of them extending over the short region containing *GNAZ*. Only a total of 4 control individuals are reported in either Developmental Delay Control or in DGV databases with duplications overlapping the *GNAZ* gene. *GNAZ* is a member of the Gαi

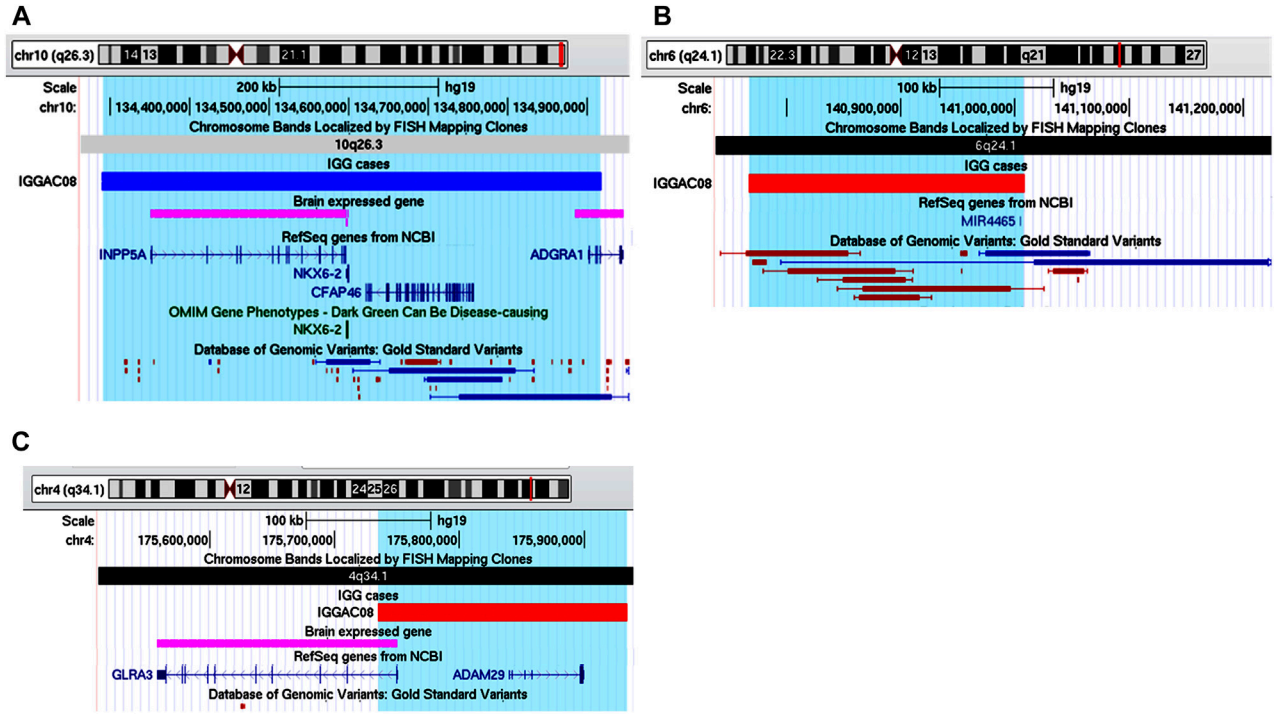

FIGURE 5 | Additive effects of *INPP5A*, *MIR4465* and *GLRA3* in patient IGGAC08. **(A)** Screenshot of chromosome 10 region encompassing the duplication of patient IGGAC08 (blue bar, chr10:134,289,353-134,917,702). **(B)** Screenshot of chromosome 6 region encompassing the deletion of patient IGGAC08 (red bar, chr6:140,767,462-141,008,265). **(C)** Screenshot of chromosome 4 region encompassing the deletion of patient IGGAC08 (red bar, chr4:175,734,964-175,934,265).

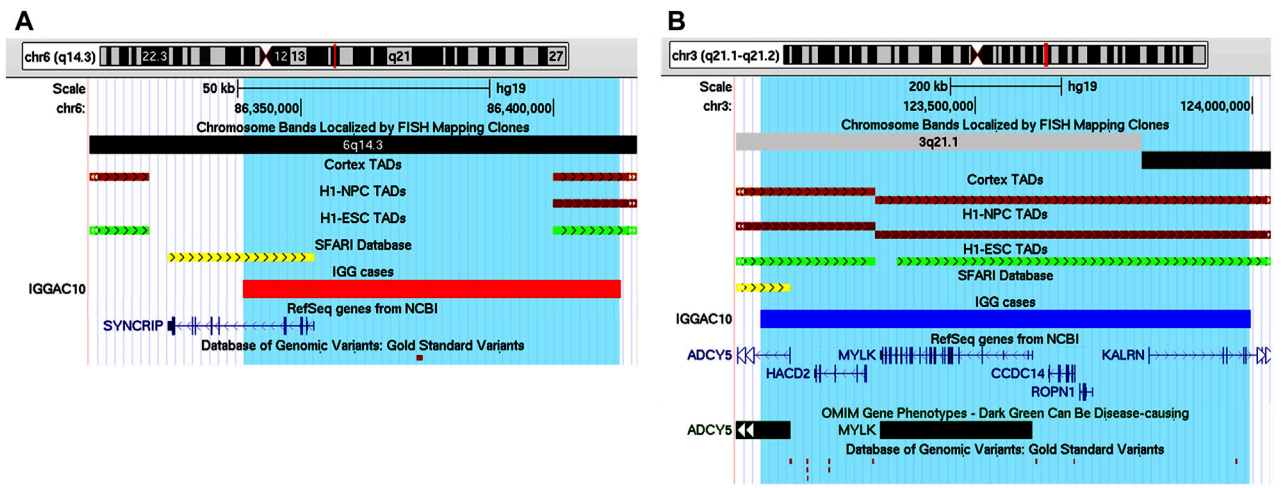

FIGURE 6 | Additive effects between *SYNCRIP* and *ADCY5* in patient IGGAC10. **(A)** Screenshot of chromosome 6 region encompassing the deletion of patient IGGAC10 (red bar, chr6:86,338,564-86,413,285). TADs from Cortex, H1NPC and h-ESC cells. **(B)** Screenshot of chromosome 3 region encompassing the duplication of patient IGGAC10 (blue bar, chr3:123,113,523-123,997,093). TADs from Cortex, H1NPC and h-ESC cells.

subfamily of heterotrimeric G proteins, and couples to G-protein-coupled receptors triggering important pathways in neuronal development (Hultman et al., 2014). The duplication of chromosome 12 entirely encompassed *WSCD2*, which encodes a WSC Domain-containing protein with a still unclear function. Interestingly, genome wide association analyses found significant results for variants in *WSCD2* in patients with psychiatric disorders (Lo et al., 2017). Finally, we could hypothesise that all the *de novo* and the inherited duplications could have jointly contributed to the NDD phenotype of patient IGGCA07.

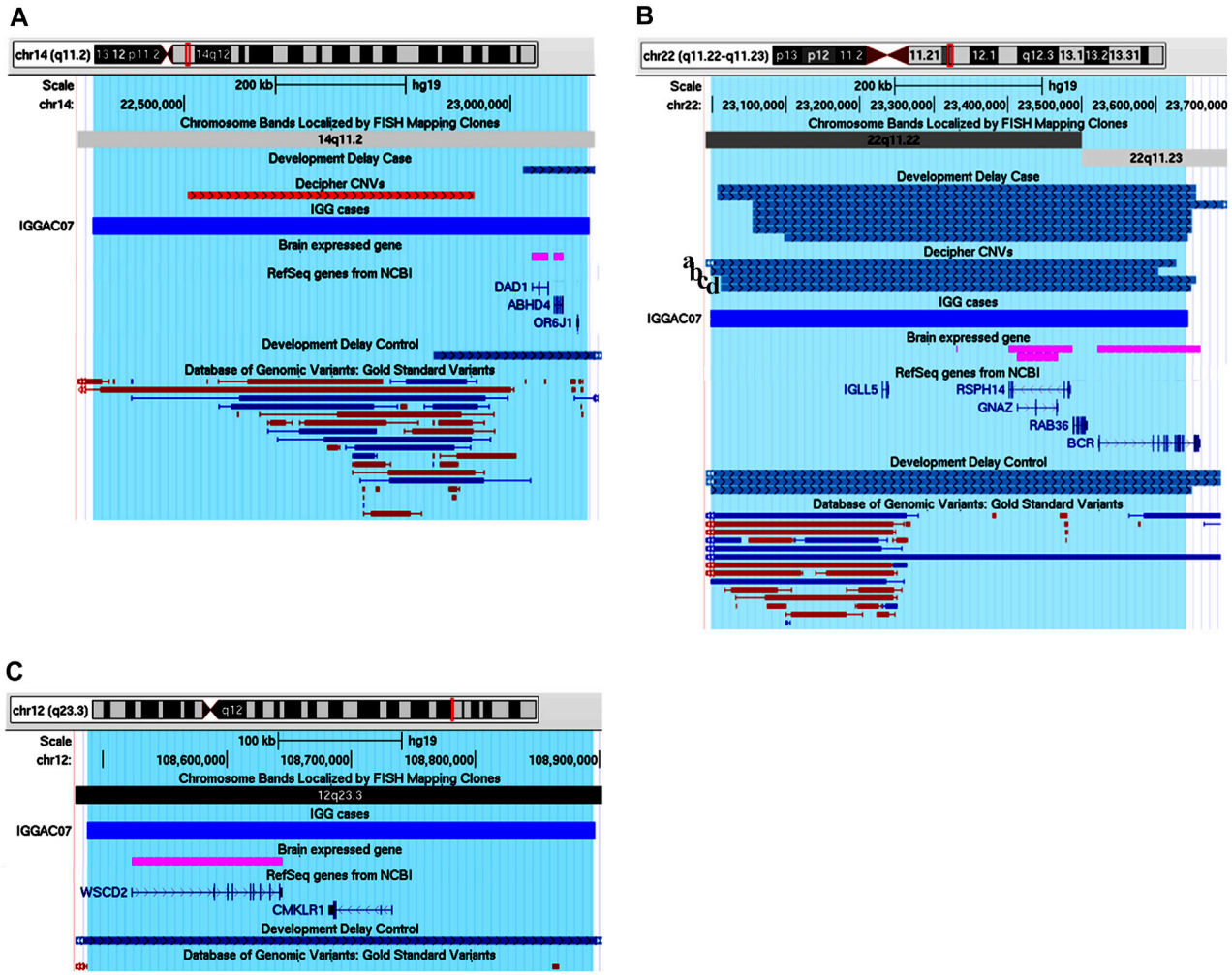

FIGURE 7 | Additive effects of *ABHD4*, *GNAZ* and *WSCD2* in patient IGGAC07. **(A)** Screenshot of chromosome 14 region encompassing the duplication of patient IGGAC07 (blue bar, chr14:22,360,671-23,120,435). Brain-expressed genes (see *Methods*). **(B)** Screenshot of chromosome 22 overlapping the duplication of patient IGGAC07 (blue bar, chr22:22,998,284-23,643,223). Duplications in Decipher database (a: patient 251352; b: patient 286708; c: patient 301091; d: patient 288064). Brain-expressed genes (see *Methods*). **(C)** Screenshot of chromosome 12 overlapping the duplication of patient IGGAC07 (blue bar, chr12:108,487,109-108,896,252). Brain-expressed genes (see *Methods*).

CNV-Mediated Complex Pathogenic Mechanisms

We found 4 patients with CNVs that could affect expression of NDD genes throughout an indirect and/or long-range effect (**Table 1** and **Table 2**).

One case (IGGAC04) presented with very severe psychomotor delay, hypotonia, and epilepsy (**Table 1**), carrying a *de novo* heterozygous deletion of chromosome 5 (**Figure 8A**). This deletion encompasses 6 genes, two of them expressed in the nervous system: *MEF2C-AS1,* which encodes a lncRNA annotated as antisense RNA of *MEF2C*, and *ADGRV1,* which encodes a member of the G-protein-coupled receptor superfamily associated with familial febrile seizures and Usher syndrome 2 (OMIM 602851). *MEF2C* (myocyte enhancer factor-2, OMIM 600662) is a transcription factor playing a role during development, mostly in myogenesis and neurogenesis. *MEF2C* haploinsufficiency has been shown to be responsible for severe cognitive deficit with stereotyped movements, epilepsy, and/or cerebral malformations (Le Meur et al., 2010). It has been recently demonstrated that, during myogenic differentiation a lncRNA, the *OIP5-AS1*, through its complementarity with *MEF2C* 3′UTR, enhances *MEF2C* mRNA stability thus promoting *MEF2C* expression and ultimately enhancing myogenesis (Yang et al., 2020). We hypothesized that during neurogenesis, analogously to *OIP5-AS1*, *MEF2C-AS1* could enhance *MEF2C* mRNA stability and promote *MEF2C* expression and neurogenesis. In this view, the heterozygous deletion observed in patient IGGAC04 could reduce the expression of *MEF2C-AS1* causing a decrease of *MEF2C*, thus interfering with neuronal differentiation and contributing to the patient's phenotype. Although as a consequence of *MEF2C-AS1* deletion a gene loss-

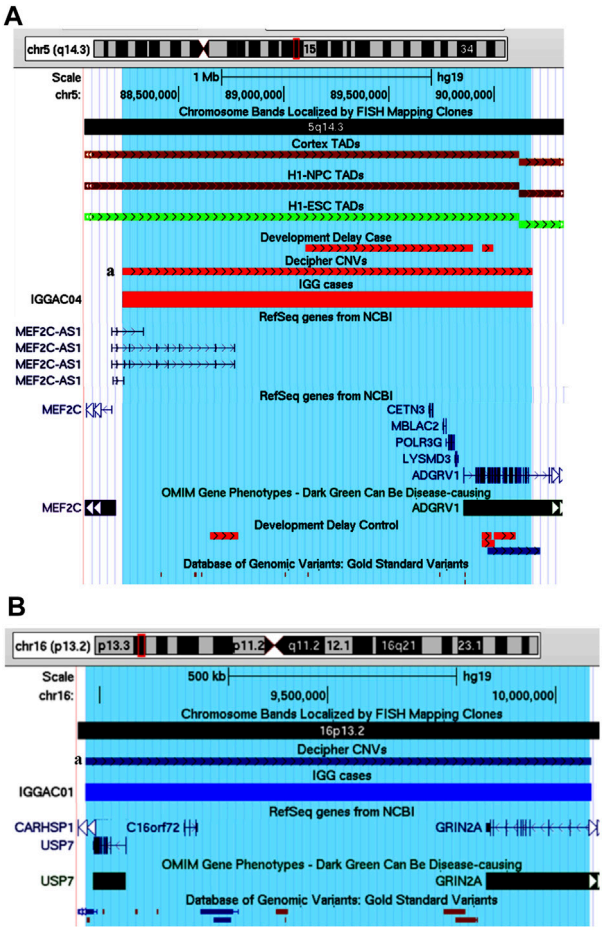

FIGURE 8 | Potential candidate genes and pathogenetic mechanisms in patient IGGAC04 and IGGAC01. **(A)** Screenshot of chromosome 5 region overlapping the deletion of patient IGGAC4 (red bar, chr5:88,232,587-90,181,774). Decipher CNVs (a: deletion in patient 251716). TADs from Cortex, H1NPC and h-ESC cells. **(B)** Screenshot of chromosome 16 region overlapping the duplication of patient IGGAC01 (blue bar, chr16:8,969,984-10,078,802). Decipher CNVs (a: duplication in patient 382832).

of-function is likely, functional experiments would be required to exclude some compensatory mechanisms, as up-regulation of the healthy allele. The deletion of *ADGRV1* could be responsible for the epilepsy phenotype. Of note, we found one patient in the Decipher database (Patient 251716) carrying a deletion overlapping the one of our patient and having similar clinical features characterized by intellectual disability, muscular hypotonia, and seizures. No deletions overlapping the same region were present among controls (Developmental Delay and DGV Controls). The chromosome 5 region deleted in these patients overlaps a TDB described in different tissues, including those relevant for neurodevelopment (e.g., Cortex), according to their relative Hi-C maps (**Figure 8A**), which could further complicate the fine regulation of expression of the overlapped genes, including *MEF2C-AS*.

One case (IGGAC01) showed a complex phenotype mostly characterized by psychomotor delay, autistic features, hypotonia, epilepsy, gastrointestinal and sleep disturbances (**Table 1**), and carried a *de novo* heterozygous duplication of chromosome 16 (**Figure 8B**). The duplication involved, in particular, two OMIM reported genes, *USP7,* encoding the Ubiquitin Specific Peptidase 7, and *GRIN2A*, encoding the NR2 subunit of the N-methyl-D-aspartate (NMDA) glutamate receptor. *USP7* has been shown to regulate the ubiquitination of a variety of proteins with functions in different biological processes as oxidative stress response, histone modification and regulation of chromatin remodelling (Khoronenkova et al., 2011). Deletions, truncating and missense variants of *USP7* have been associated with the Hao-Fountain syndrome (OMIM 616863), characterized by speech delay, autistic spectrum disorder, attention-deficit hyperactivity disorder, sleep disturbances and gastroesophageal reflux disease (Fountain et al., 2019). All these clinical features are present in our case who has the complete duplication of *USP7*. Notably, in syndromic forms of ASD, duplications in addition to deletions of *USP7* have been reported (Sanders et al., 2011), thus supporting the idea of dosage sensitivity, with both low and high *USP7* expression causing imbalances of neuronal homeostasis. The duplication present in patient IGGAC01 partially overlapped *GRIN2A*. Truncating as well as missense, activating variants of *GRIN2A* have been associated with an idiopathic form of focal epilepsy, EEG continuous spike-and-wave during sleep (CSWS), and speech disorder (OMIM 245570) (Lemke et al., 2013) whose clinical aspects are present in our patient. Different molecular alterations of NMDA receptor subunits seem to result in a deleterious dysregulation of NMDA receptor function (Balu and Coyle, 2011). Although the effect of partial duplications on gene function are not easily predictable, some clinical features of the IGGAC01 patient suggested the occurrence of a dysregulation of *GRIN2A* that could have contributed to the patient's phenotype. Of note, a patient with phenotype resembling that of patient IGGAC01 was reported in Decipher database with a similar duplication, including both *USP7* and *GRIN2A* (**Figure 8B**). We thus hypothesised that the phenotype of these two patients could result from the impairment of both *USP7* and *GRIN2A*.

IGGAC24 had a *de novo* duplication of chromosome 19 that encompasses various genes, 11 of which are expressed in the brain. The duplication also overlaps a TDB described in the brain cortex and other different tissues, which could contribute to dysregulating gene expression of implicated genes (**Figure 9A** and **Table 1**). Attempting to prioritize enclosed genes and define possible candidate genes, we performed a gene enrichment analysis as described above (see *Methods*). Two genes emerged for their functions known to play a role in neurodevelopmental disorders, namely *SHISA7* and *U2AF2*. Indeed, in Decipher at least one NDD case with a duplication that partially overlaps the TDB and the *SHISA7* gene (Patient 338729) was reported while no similar duplications, implicating brain-expressed genes, were reported among controls. We focused on *SHISA7*, a transmembrane protein that interacts with GABAA receptors (Han et al., 2019) and, by acting as auxiliary protein for the trafficking of AMPA receptors, regulates synaptic plasticity (Schmitz et al., 2017). Notably, spine loss has been observed in *SHISA7* knockout mice and in wild type mice with *SHISA7* overexpression (Schmitz et al., 2017; von Engelhardt, 2019).

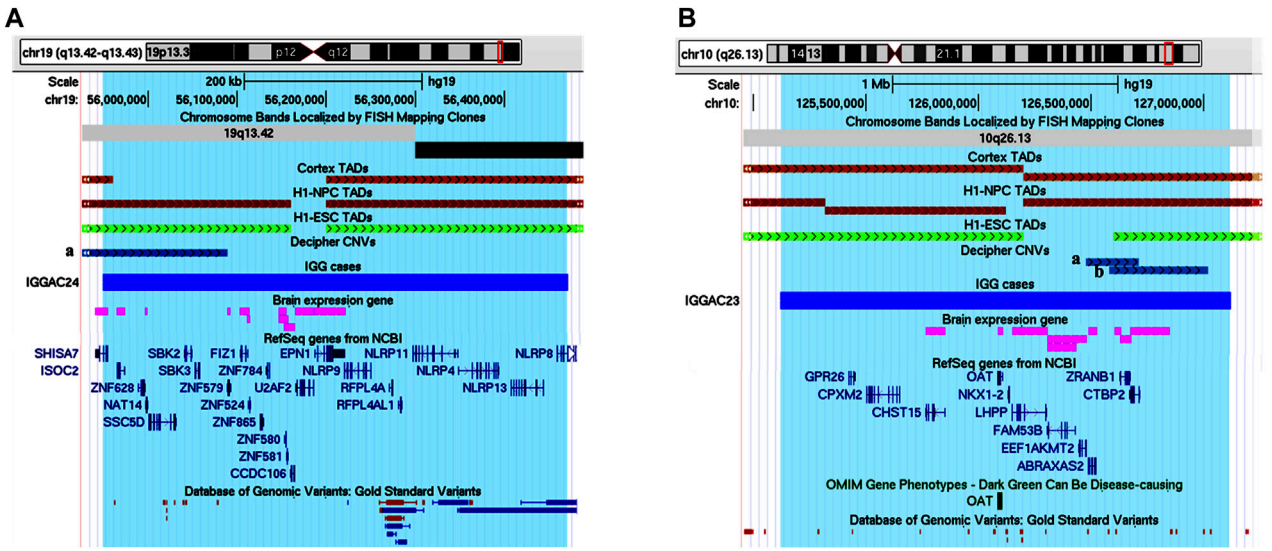

FIGURE 9 | Duplications of topological domain boundaries (TDBs) potentially involved in the phenotype of patient IGGAC24 and patient IGGAC23. **(A)** Screenshot of chromosome 19 region encompassing the duplication of patient IGGAC24 (blue bar, chr19:55,948,706-56,471,996). TADs from Cortex, H1NPC and h-ESC cells. Brain-expressed genes (see *Methods*). Decipher patient with reported duplication (a. patient 338729) **(B)** Screenshot of chromosome 10 region encompassing the duplication of patient IGGAC23 (blue bar, chr10:125,121,038-127,119,447). Brain-expressed genes (see *Methods*). Decipher patients with reported duplications (a: patient 283429, b: patient 378968).

Thus, we hypothesised that the duplication could cause a dysregulation of *SHISA7* expression, possibly also by altering chromatin conformation, and ultimately causing a dysregulation of synaptic plasticity.

Patient IGGAC23 showed a *de novo* duplication of chromosome 10 overlapping 7 brain-expressed genes and a TDB described in the brain cortex and other tissues (**Figure 9B** and **Table 1**). After gene enrichment analysis of these 7 genes with known NDD genes, one emerged as the most interesting, *CTBP2*. This gene produces two alternative transcripts for two different proteins, one of them is a component of specialized synapses (ribbon synapses) and the other one is a negative regulator of transcription. *CTBP2* knock-out mice present a neurological phenotype characterized by abnormalities of brain development. A recent study reported that the overexpression of *CTBP2* inhibits neuronal differentiation (Zhang et al., 2020). Of note, while no duplications similar to that of this patient were reported among controls, in Decipher a patient with autistic behaviour and a duplication shorter than the one of patient IGGC23, but still enclosing *CTBP2*, was reported. Thus, the duplication present in patient IGGAC23 could have caused overexpression and/or dysregulated expression of overlapped genes, among which *CTBP2*, whose overexpression has already been associated with impaired neuronal defects.

DISCUSSION AND CONCLUSION

In the frame of identifying the most likely genes and genetic mechanisms underlying complex phenotypes in neurodevelopmental disorders, and to better interpret CNV causal effects in complex cases, we performed a detailed analysis of both clinical features and CNVs of 12 patients.

In particular, we analyzed patients' CNVs in the light of information on gene expression, gene function, and chromatin organization features of involved genomic regions. Then we assessed the presence of potential deleterious CNVs acting in concert in the same patients, according to a two-hit model emerging from the recent literature as a possible pathogenetic mechanism with important roles in neurodevelopmental disorders.

Four patients reported with a complex phenotype, i.e. not referable to a known syndromic neurodevelopmental disorder, carried a CNV that can possibly have indirect deleterious effects on neuronal expressed genes and finally on their phenotype. In one case, a deletion encompassed *MEF2C-AS1*, the antisense gene of a known NDD-associated gene, *MEF2C*. Involvement of antisense genes in NDDs has been rarely reported so far. One example is represented by *PTCHD1-AS*, the antisense-gene of the NDD-associated gene *PTCHD1*. In fact, although the molecular function of *PTCHD1-AS* is still to be clearly elucidated, it has been demonstrated that its disruption diminished miniature excitatory postsynaptic current frequency in iPSC-derived neurons from subjects with ASD, thus supporting a role for this long noncoding RNA in the etiology of ASD (Ross et al., 2020). Interest on regulatory elements of gene expressions, like lncRNA and regulatory enhancer elements, and their involvement in brain disorders has been recently increased and new tools have been applicated for their detection, as those implicated in ASD and Schizofrenia (Piluso et al., 2019; Alinejad-Rokny et al., 2020).

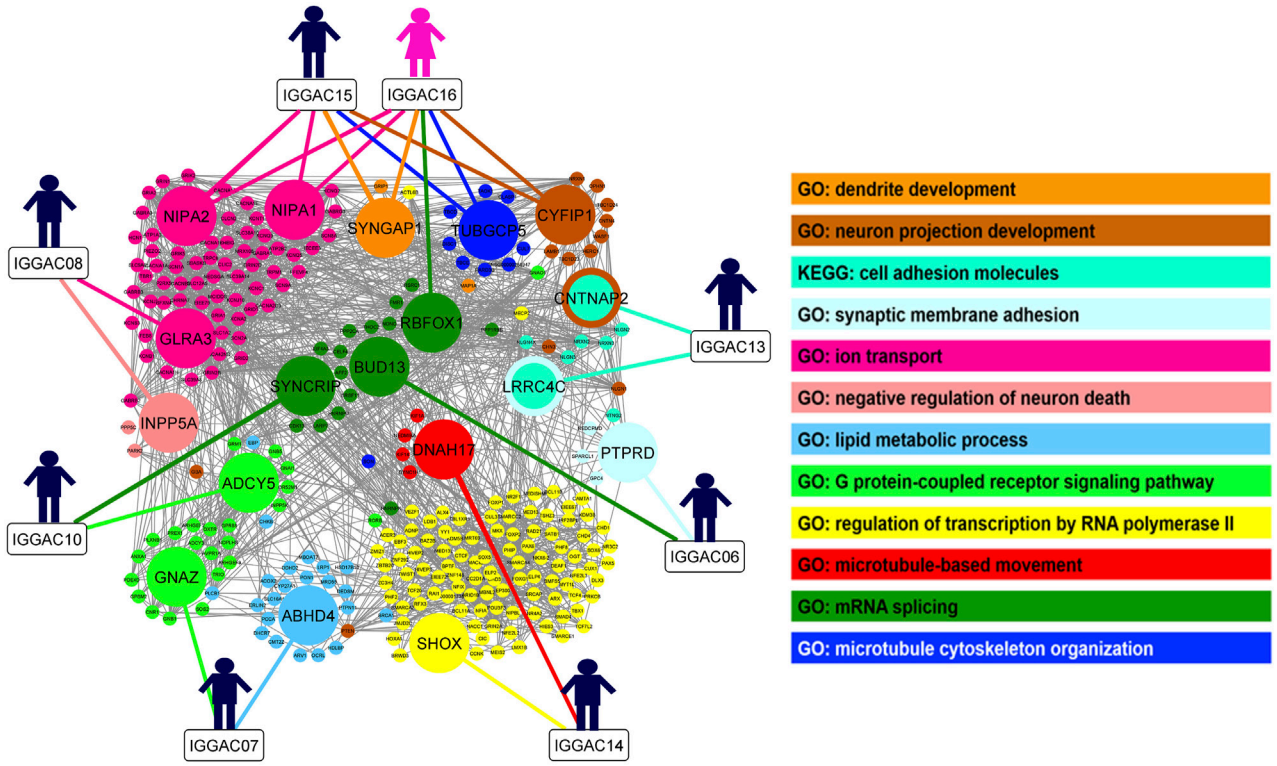

FIGURE 10 | Overview of biological processes and pathways involved in patients with CNV-genes acting according to double-hit model. The network depicts the protein-protein interactions (grey lines) revealed by STRING analysis (visualized by Cytoscape tool) on the basis of the enrichment obtained with GeneCodis4 tool. The Figure shows the enriched BP terms and KEGG pathways clustering the CNV-genes of the eight patients with known NDD genes (SFARI reported genes with score 1/2 and OMIM genes correlated to NDDs). The analysis shows that all eight patients have CNV-overlapped genes involved in two known NDD-associated biological processes, except patient IGGAC13, for whom the two implicated genes appeared in the same KEGG pathway. GO terms "neuron projection development", "synaptic membrane adhesion", "ion trasport", "G-protein-coupled receptor signalling pathway" and "mRNA splicing" are shared by at least two different patients.

Deletions and duplications may overlap TDBs between two flanking topological associated domains causing a dysregulation of chromatin organization and, in turn, a dysregulation of implicated genes which ultimately affects the patient's phenotype. So far, implication of CNVs in TAD boundaries have been rarely investigated in NDDs (Di Gregorio et al., 2017; Melo et al., 2020). Chromatin conformation domains can be different in various cells and tissues, and we were aware that effects of deletions and duplications deduced on the basis of TDBs data reported in databases have to be considered hypothetical, deserving further experimental validation. To tentatively achieve a more reliable data analysis of our patients, we considered only TDBs reported in more than one tissue, assuming that they could possibly represent a chromatin feature common to many tissues, including brain areas involved by NDDs. All our four cases have a CNV encompassing a TDB between two flanking topologically associated domains described in at least three tissues which could have played a role in NDD phenotype, such as brain cortex (Schmitt et al., 2016) and human embryonic stem cell-derived neurons (Dixon et al., 2015).

One important finding emerging from this evaluation of diagnostic array-CGH results is the presence of co-occurring CNVs that, according to the two-hit model, could have contributed to the patients' phenotype.

In eight patients, we found two CNVs overlapping either known NDD genes and/or genes with potential roles in neurodevelopment. In three patients, we found one *de novo* and one variant inherited from unaffected parents, the remaining five patients inherited one CNV from each of their unaffected parents. In three out of eight cases, namely IGGAC06, IGGAC07, and IGGAC08, involved genes have not yet been associated with disease and we presented data in favor of their implication in neurodevelopmental disorders. Indeed, we searched the Decipher database for cases with one CNV corresponding to that presented by our patients and a secondary CNV, involving genes with a role in neurodevelopment. We found some cases, reported in the figures, that further support the hypothesis that identified co-occurring CNVs in our patients act additively causing deleterious phenotypes according to a two-hit model.

In order to gain insight into possible interaction among genes implicated in the CNVs co-occurring in the same patient and to evaluate whether these genes share molecular functions or biological processes, we performed gene enrichment and protein-protein interaction analyses (**Figure 10**;

Supplementary Table S1). We also tested interaction with other known NDD associated genes, which helped to better define the role of new candidate genes in important neurodevelopmental pathways and biological processes. In one case, IGGAC13, the two major implicated genes, i.e., *CNTNAP2* and *LRRC4C*, interact with each other through *NRXN1* and with other NDD-associated genes and have a common function in the KEGG cell adhesion molecule pathway (**Figure 1**). In all the other cases, genes affected by co-occurring CNVs do not seem to directly interact, but they have a role in important, although distinct, biological processes that together contribute to proper brain development (**Figure 10**). We thus hypothesized that, in all these cases, the double-hit mechanism by affecting two pathways/biological processes finally determines an impairment of neurological development.

As observable in **Figure 10**, couple of patients have genes involved in the same pathway/biological process and one additional gene dealing with another biological process. As an example, both IGGAC06 and IGGAC10 have one CNV each involving a different gene but with a common function in mRNA splicing, and each of the two patients has an additional CNV involving one gene with a role, respectively, in synaptic membrane adhesion and in G-coupled receptor signaling, two fundamental functions of synapse.

Of note, co-occurring secondary CNVs overlapping NDD genes were also found in patients with syndromic or recurrent gene-specific CNVs, which could modulate penetrance and/or severity of the disease. This phenomenon is well exemplified by the case of two siblings, IGGAC15 and IGGAC16, who shared two CNVs overlapping known NDD genes, including an already described deletion of chromosome 15 with reduced penetrance (Cox and Butler, 2015). In addition to these two CNVs, patient IGGAC16 also carried a deletion of chromosome 16 implicating *RBFOX1*, a known NDD gene, also described with reduced penetrance (Lal et al., 2013). Patient IGGAC16, the one of the two siblings who carried a total of three CNVs, exhibited a more complex phenotype compared to her brother.

Overall, our genetic analysis allowed to unveil candidate genes and to infer some synergistic and complex mechanisms that could origin the neurodevelopmental disorder in these patients. However, novel candidate genes and genes affected by co-occurring CNVs although individually associated with NDD biological processes, require further functional analyses to understand their potential interactions and ultimately to clarify their contribution to patient phenotypes.

Variability and complexity of genetic components make the functional validation of NDD genes and pathogenic mechanisms a challenge. Validation of hypothesised mechanisms in one patient can represent a research project by itself. Concerning the present cases, we could consider different levels of validation starting from verifying the effect of a CNV on expression of the implicated genes in induced neurons (iN) that could be obtained from patients' fibroblasts. With this approach we could evaluate the effects of deletions of antisense or miRNA genes on the expression of their specific targets (as for patient IGGAC4 and IGGAC8) or of CNV involving TDB boundaries on implicated genes (as for patient IGGAC10). A further level of investigation is represented by the analysis of morphology and connections of iNs, usefull to investigate impairment of cell adhesion molecules, as for the case IGGAC13. Patient-derived iN could be used to evaluate defects on RNA splicing as in the case of IGGAC6 patient. To evaluate the effects of more complex genetic mechanisms on brain development and on behaviour, a further level of validation can be represented by studies with animal models, as mice. Indeed, as mice with double/multiple heterozygous variants can be obtained (Bossi et al., 2018), the synergistic effects of multiple variants could be also evaluated. In this view, and as mouse models for both *LRRC4C* and *CNTNAP2* genes are available, it could be interesting to obtain a mouse strain carrying heterozygous, loss of function mutations in both genes, thus mimicking the genotype of patient IGGAC13.

Our findings further support the hypothesis that double-hit mechanisms, involving inherited and *de novo* CNVs, could synergistically cause, or modulate, the neurodevelopmental phenotype. Indeed, the co-occurrence of pathogenic variants has also been observed after analysing the CNVs together with the results of whole exome sequencing, underlining the importance of the genetic background for the penetrance of a deleterious variant (Pizzo et al., 2019).

Recently reported data indicate that, in NDDs, WES analyses have diagnostic yields of about 36% while chromosomal microarray analysis of less than 20% (Srivastava et al., 2019; Savatt and Myers, 2021). As variants causing NDDs can be CNVs or single nucleotide variants (SNVs), isolated or even combined, the genetic diagnostic approach has to take into consideration methods able to detect both type of variants. Indeed, several clinical laboratories are now incorporating CNV calling into WES and are able to detect multi-exon deletions and duplications (Savatt and Myers, 2021).

WGS, by definition, detects more comprehensively all classes of genetic variants and, as cost decreases, will eventually supersede WES and chromosomal array analyses in clinical testing algorithms over time.

Finally, our work describes a possible integrated framework of investigation of CNVs based on publically available resources of genomic annotations and bioinformatic analyses to prioritize candidate genes and infer pathogenic mechanisms. This approach could be used for interpretation of those CNVs that, after a first level analysis, remains of uncertain significance.

Indeed, it would be interesting to test these patients by WES to check for single nucleotide variants which, according to multi-hit model, could further contribute to their phenotype.

DATA AVAILABILITY STATEMENT

The datasets presented in this study can be found in online repositories. Clinical and genetic variant details have been deposited in the Decipher database with the following accession numbers: 433116 (IGGAC01); 433118 (IGGAC04); 433122 (IGGAC06); 433123 (IGGAC07); 433125 (IGGAC08); 433130 (IGGAC10); 433133 (IGGAC13); 433135 (IGGAC14); 433138 (IGGAC15); 433139 (IGGAC16); 433172 (IGGAC23); 433173 (IGGAC24).

ETHICS STATEMENT

The studies involving human participants were reviewed and approved by Ethics Committee of the Italian Regione Liguria (R.P. 001/2019). Written informed consent to participate in this study was provided by the participants' legal guardian/next of kin.

AUTHOR CONTRIBUTIONS

MS, LP, and AP participated in the design of the study. PR and ET were responsible for array-CGH experiments. PR, MC, and AP performed some array-CGH validation experiments. ML, MD, GR, LP, SB, and LN collected all clinical phenotypes and MS managed the database of clinical and CNVs data. MS, LP, MC, and AP participated in data analysis and interpretation. MS, LP, and AP wrote the manuscript. All authors critically revised the manuscript and agreed to be accountable for the content of the work.

FUNDING

Funding for this research was provided by Italian Ministero della Salute (Project N. RF-2016-02361949 to AP; "Cinque per Mille" and Ricerca Corrente). This work was developed within the framework of the DINOGMI Department of Excellence (MIUR 2018-2022, legge 232 del 2016).

ACKNOWLEDGMENTS

The authors wish to thank all families and referring nurses of Child Neuropsychiatric Unit for their help and collaboration.

SUPPLEMENTARY MATERIAL

The Supplementary Material for this article can be found online at: https://www.frontiersin.org/articles/10.3389/fgene.2021.732002/full#supplementary-material

REFERENCES

Addis, L., Sproviero, W., Thomas, S. V., Caraballo, R. H., Newhouse, S. J., Gomez, K., et al. (2018). Identification of New Risk Factors for Rolandic Epilepsy: CNV at Xp22.31 and Alterations at Cholinergic Synapses. *J. Med. Genet.* 55 (9), 607–616. doi:10.1136/jmedgenet-2018-105319

Alinejad-Rokny, H., Heng, J. I. T., and Forrest, A. R. R. (2020). Brain-Enriched Coding and Long Non-coding RNA Genes Are Overrepresented in Recurrent Neurodevelopmental Disorder CNVs. *Cel Rep.* 33 (4), 108307. doi:10.1016/j.celrep.2020.108307

Alvarez-Mora, M. I., Corominas, J., Gilissen, C., Sanchez, A., Madrigal, I., and Rodriguez-Revenga, L. (2021). Novel Compound Heterozygous Mutation in TRAPPC9 Gene: The Relevance of Whole Genome Sequencing. *Genes* 12 (4), 557. doi:10.3390/genes12040557

Arteche-López, A., Gómez Rodríguez, M. J., Sánchez Calvin, M. T., Quesada-Espinosa, J. F., Lezana Rosales, J. M., Palma Milla, C., et al. (2021). Towards a Change in the Diagnostic Algorithm of Autism Spectrum Disorders: Evidence Supporting Whole Exome Sequencing as a First-Tier Test. *Genes* 12 (4), 560. doi:10.3390/genes12040560

Balu, D. T., and Coyle, J. T. (2011). Glutamate Receptor Composition of the post-synaptic Density Is Altered in Genetic Mouse Models of NMDA Receptor Hypo- and Hyperfunction. *Brain Res.* 1392, 1–7. doi:10.1016/j.brainres.2011.03.051

Bossi, S., Musante, I., Bonfiglio, T., Bonifacino, T., Emionite, L., Cerminara, M., et al. (2018). Genetic Inactivation of mGlu5 Receptor Improves Motor Coordination in the Grm1 Mouse Model of SCAR13 Ataxia. *Neurobiol. Dis.* 109 (Pt A), 44–53. doi:10.1016/j.nbd.2017.10.001

Cerminara, M., Spirito, G., Pisciotta, L., Squillario, M., Servetti, M., Divizia, M. T., et al. (2021). Case Report: Whole Exome Sequencing Revealed Disease-Causing Variants in Two Genes in a Patient with Autism Spectrum Disorder, Intellectual Disability, Hyperactivity, Sleep and Gastrointestinal Disturbances. *Front. Genet.* 12, 625564. doi:10.3389/fgene.2021.625564

Chen, J., Zhuang, Y., Zhang, Z.-F., Wang, S., Jin, P., He, C., et al. (2016). Glycine Confers Neuroprotection through microRNA-301a/PTEN Signaling. *Mol. Brain* 9 (1), 59. doi:10.1186/s13041-016-0241-3

Cheng, Y., Wang, Z.-M., Tan, W., Wang, X., Li, Y., Bai, B., et al. (2018). Partial Loss of Psychiatric Risk Gene Mir137 in Mice Causes Repetitive Behavior and Impairs Sociability and Learning via Increased Pde10a. *Nat. Neurosci.* 21 (12), 1689–1703. doi:10.1038/s41593-018-0261-7

Choii, G., and Ko, J. (2015). Gephyrin: a central GABAergic Synapse Organizer. *Exp. Mol. Med.* 47, e158. doi:10.1038/emm.2015.5

Choucair, N., Mignon-Ravix, C., Cacciagli, P., Abou Ghoch, J., Fawaz, A., Mégarbané, A., et al. (2015). Evidence that Homozygous PTPRD Gene Microdeletion Causes Trigonocephaly, Hearing Loss, and Intellectual Disability. *Mol. Cytogenet.* 8, 39. doi:10.1186/s13039-015-0149-0

Coe, B. P., Stessman, H. A. F., Sulovari, A., Geisheker, M. R., Bakken, T. E., Lake, A. M., et al. (2019). Neurodevelopmental Disease Genes Implicated by De Novo Mutation and Copy Number Variation Morbidity. *Nat. Genet.* 51 (1), 106–116. doi:10.1038/s41588-018-0288-4

Cox, D., and Butler, M. (2015). The 15q11.2 BP1-BP2 Microdeletion Syndrome: a Review. *Ijms* 16 (2), 4068–4082. doi:10.3390/ijms16024068

Di Gregorio, E., Riberi, E., Belligni, E. F., Biamino, E., Spielmann, M., Ala, U., et al. (2017). Copy Number Variants Analysis in a Cohort of Isolated and Syndromic Developmental Delay/intellectual Disability Reveals Novel Genomic Disorders, Position Effects and Candidate Disease Genes. *Clin. Genet.* 92 (4), 415–422. doi:10.1111/cge.13009

Dixon, J. R., Jung, I., Selvaraj, S., Shen, Y., Antosiewicz-Bourget, J. E., Lee, A. Y., et al. (2015). Chromatin Architecture Reorganization during Stem Cell Differentiation. *Nature* 518 (7539), 331–336. doi:10.1038/nature14222

Duyzend, M. H., Nuttle, X., Coe, B. P., Baker, C., Nickerson, D. A., Bernier, R., et al. (2016). Maternal Modifiers and Parent-Of-Origin Bias of the Autism-Associated 16p11.2 CNV. *Am. J. Hum. Genet.* 98 (1), 45–57. doi:10.1016/j.ajhg.2015.11.017

Fernandez, J. P., Moreno-Mateos, M. A., Gohr, A., Miao, L., Chan, S. H., Irimia, M., et al. (2018). RES Complex Is Associated with Intron Definition and Required for Zebrafish Early Embryogenesis. *Plos Genet.* 14 (7), e1007473. doi:10.1371/journal.pgen.1007473

Fountain, M. D., Oleson, D. S., Rech, M. E., Segebrecht, L., Hunter, J. V., McCarthy, J. M., et al. (2019). Pathogenic Variants in USP7 Cause a Neurodevelopmental Disorder with Speech Delays, Altered Behavior, and Neurologic Anomalies. *Genet. Med.* 21 (8), 1797–1807. doi:10.1038/s41436-019-0433-1

Girirajan, S., Rosenfeld, J. A., Cooper, G. M., Antonacci, F., Siswara, P., Itsara, A., et al. (2010). A Recurrent 16p12.1 Microdeletion Supports a Two-Hit Model for Severe Developmental Delay. *Nat. Genet.* 42 (3), 203–209. doi:10.1038/ng.534

Guo, H., Duyzend, M. H., Duyzend, M. H., Coe, B. P., Baker, C., Hoekzema, K., et al. (2019). Genome Sequencing Identifies Multiple Deleterious Variants in Autism Patients with More Severe Phenotypes. *Genet. Med.* 21 (7), 1611–1620. doi:10.1038/s41436-018-0380-2

Han, W., Li, J., Pelkey, K. A., Pandey, S., Chen, X., Wang, Y.-X., et al. (2019). Shisa7 Is a GABAA Receptor Auxiliary Subunit Controlling Benzodiazepine Actions. *Science* 366 (6462), 246–250. doi:10.1126/science.aax5719

Huckins, L. M., Dobbyn, A., Dobbyn, A., Ruderfer, D. M., Hoffman, G., Wang, W., et al. (2019). Gene Expression Imputation across Multiple Brain Regions

Provides Insights into Schizophrenia Risk. *Nat. Genet.* 51 (4), 659–674. doi:10.1038/s41588-019-0364-4

Hultman, R., Kumari, U., Michel, N., and Casey, P. J. (2014). Gαz Regulates BDNF-Induction of Axon Growth in Cortical Neurons. *Mol. Cell Neurosci.* 58, 53–61. doi:10.1016/j.mcn.2013.12.004

Khoronenkova, S. V., DianovaII, Parsons, J. L., and Dianov, G. L. (2011). USP7/HAUSP Stimulates Repair of Oxidative DNA Lesions. *Nucleic Acids Res.* 39 (7), 2604–2609. doi:10.1093/nar/gkq1210

Kim, S., Kang, M., Park, D., Lee, A.-R., Betz, H., Ko, J., et al. (2021). Impaired Formation of High-Order Gephyrin Oligomers Underlies Gephyrin Dysfunction-Associated Pathologies. *iScience* 24 (2), 102037. doi:10.1016/j.isci.2021.102037

Lal, D., Trucks, H., Møller, R. S., Hjalgrim, H., Koeleman, B. P. C., de Kovel, C. G. F., et al. (2013). Rare Exonic Deletions of theRBFOX1gene Increase Risk of Idiopathic Generalized Epilepsy. *Epilepsia* 54 (2), 265–271. doi:10.1111/epi.12084

László, Z. I., Lele, Z., Zöldi, M., Miczán, V., Mógor, F., Simon, G. M., et al. (2020). ABHD4-dependent Developmental Anoikis Safeguards the Embryonic Brain. *Nat. Commun.* 11 (1), 4363. doi:10.1038/s41467-020-18175-4

Le Meur, N., Holder-Espinasse, M., Jaillard, S., Goldenberg, A., Joriot, S., Amati-Bonneau, P., et al. (2010). MEF2C Haploinsufficiency Caused by Either Microdeletion of the 5q14.3 Region or Mutation Is Responsible for Severe Mental Retardation with Stereotypic Movements, Epilepsy And/or Cerebral Malformations. *J. Med. Genet.* 47 (1), 22–29. doi:10.1136/jmg.2009.069732

Lek, M., Karczewski, K. J., Minikel, E. V., Samocha, K. E., Banks, E., Fennell, T., et al. (2016). Analysis of Protein-Coding Genetic Variation in 60,706 Humans. *Nature* 536 (7616), 285–291. doi:10.1038/nature19057

Lemke, J. R., Lal, D., Reinthaler, E. M., Steiner, I., Nothnagel, M., Alber, M., et al. (2013). Mutations in GRIN2A Cause Idiopathic Focal Epilepsy with Rolandic Spikes. *Nat. Genet.* 45 (9), 1067–1072. doi:10.1038/ng.2728

Lo, M.-T., Hinds, D. A., Tung, J. Y., Franz, C., Fan, C.-C., Wang, Y., et al. (2017). Genome-wide Analyses for Personality Traits Identify Six Genomic Loci and Show Correlations with Psychiatric Disorders. *Nat. Genet.* 49 (1), 152–156. doi:10.1038/ng.3736

Mattheisen, M., Samuels, J. F., Wang, Y., Greenberg, B. D., Fyer, A. J., McCracken, J. T., et al. (2015). Genome-wide Association Study in Obsessive-Compulsive Disorder: Results from the OCGAS. *Mol. Psychiatry* 20 (3), 337–344. doi:10.1038/mp.2014.43

Maussion, G., Cruceanu, C., Rosenfeld, J. A., Bell, S. C., Jollant, F., Szatkiewicz, J., et al. (2017). Implication of LRRC4C and DPP6 in Neurodevelopmental Disorders. *Am. J. Med. Genet.* 173 (2), 395–406. doi:10.1002/ajmg.a.38021

McMahon, A. C., Barnett, M. W., O'Leary, T. S., Stoney, P. N., Collins, M. O., Papadia, S., et al. (2012). SynGAP Isoforms Exert Opposing Effects on Synaptic Strength. *Nat. Commun.* 3, 900. doi:10.1038/ncomms1900

Melo, U. S., Schöpflin, R., Acuna-Hidalgo, R., Mensah, M. A., Fischer-Zirnsak, B., Holtgrewe, M., et al. (2020). Hi-C Identifies Complex Genomic Rearrangements and TAD-Shuffling in Developmental Diseases. *Am. J. Hum. Genet.* 106 (6), 872–884. doi:10.1016/j.ajhg.2020.04.016

Miller, D. T., Adam, M. P., Aradhya, S., Biesecker, L. G., Brothman, A. R., Carter, N. P., et al. (2010). Consensus Statement: Chromosomal Microarray Is a First-Tier Clinical Diagnostic Test for Individuals with Developmental Disabilities or Congenital Anomalies. *Am. J. Hum. Genet.* 86 (5), 749–764. doi:10.1016/j.ajhg.2010.04.006

Piluso, G., Monteleone, P., Galderisi, S., Giugliano, T., Bertolino, A., Rocca, P., et al. (2019). Assessment of De Novo Copy-Number Variations in Italian Patients with Schizophrenia: Detection of Putative Mutations Involving Regulatory Enhancer Elements. *World J. Biol. Psychiatry* 20 (2), 126–136. doi:10.1080/15622975.2017.1395072

Pizzo, L., Jensen, M., Polyak, A., Rosenfeld, J. A., Mannik, K., Krishnan, A., et al. (2019). Rare Variants in the Genetic Background Modulate Cognitive and Developmental Phenotypes in Individuals Carrying Disease-Associated Variants. *Genet. Med.* 21 (4), 816–825. doi:10.1038/s41436-018-0266-3

Rauch, A., Wieczorek, D., Graf, E., Wieland, T., Endele, S., Schwarzmayr, T., et al. (2012). Range of Genetic Mutations Associated with Severe Non-syndromic Sporadic Intellectual Disability: an Exome Sequencing Study. *The Lancet* 380 (9854), 1674–1682. doi:10.1016/S0140-6736(12)61480-9

Riggs, E. R., Andersen, E. F., Cherry, A. M., Kantarci, S., Kearney, H., Patel, A., et al. (2020). Technical Standards for the Interpretation and Reporting of Constitutional Copy-Number Variants: a Joint Consensus Recommendation of the American College of Medical Genetics and Genomics (ACMG) and the Clinical Genome Resource (ClinGen). *Genet. Med.* 22 (2), 245–257. doi:10.1038/s41436-019-0686-8

Ross, P. J., Zhang, W.-B., Mok, R. S. F., Zaslavsky, K., Deneault, E., D'Abate, L., et al. (2020). Synaptic Dysfunction in Human Neurons with Autism-Associated Deletions in PTCHD1-AS. *Biol. Psychiatry* 87 (2), 139–149. doi:10.1016/j.biopsych.2019.07.014

Rossi, P. I. A., Musante, I., Summa, M., Pittaluga, A., Emionite, L., Ikehata, M., et al. (2013). Compensatory Molecular and Functional Mechanisms in Nervous System of the Grm1crv4 Mouse Lacking the mGlu1 Receptor: A Model for Motor Coordination Deficits. *Cereb. Cortex* 23 (9), 2179–2189. doi:10.1093/cercor/bhs200

Rumbaugh, G., Adams, J. P., Kim, J. H., and Huganir, R. L. (2006). SynGAP Regulates Synaptic Strength and Mitogen-Activated Protein Kinases in Cultured Neurons. *Proc. Natl. Acad. Sci.* 103 (12), 4344–4351. doi:10.1073/pnas.0600084103

Sanders, S. J., Ercan-Sencicek, A. G., Hus, V., Luo, R., Murtha, M. T., Moreno-De-Luca, D., et al. (2011). Multiple Recurrent De Novo CNVs, Including Duplications of the 7q11.23 Williams Syndrome Region, Are Strongly Associated with Autism. *Neuron* 70 (5), 863–885. doi:10.1016/j.neuron.2011.05.002

Savatt, J. M., and Myers, S. M. (2021). Genetic Testing in Neurodevelopmental Disorders. *Front. Pediatr.* 9, 526779. doi:10.3389/fped.2021.526779

Schmitt, A. D., Hu, M., and Ren, B. (2016). Genome-wide Mapping and Analysis of Chromosome Architecture. *Nat. Rev. Mol. Cel Biol.* 17 (12), 743–755. doi:10.1038/nrm.2016.104

Schmitz, L. J. M., Klaassen, R. V., Ruiperez-Alonso, M., Zamri, A. E., Stroeder, J., Rao-Ruiz, P., et al. (2017). The AMPA Receptor-Associated Protein Shisa7 Regulates Hippocampal Synaptic Function and Contextual Memory. *Elife* 6. doi:10.7554/eLife.24192

Schormair, B., Kemlink, D., Roeske, D., Eckstein, G., Xiong, L., Lichtner, P., et al. (2008). PTPRD (Protein Tyrosine Phosphatase Receptor Type delta) Is Associated with Restless Legs Syndrome. *Nat. Genet.* 40 (8), 946–948. doi:10.1038/ng.190

Shannon, P., Markiel, A., Ozier, O., Baliga, N. S., Wang, J. T., Ramage, D., et al. (2003). Cytoscape: a Software Environment for Integrated Models of Biomolecular Interaction Networks. *Genome Res.* 13 (11), 2498–2504. doi:10.1101/gr.1239303

Shihab, H. A., Rogers, M. F., Campbell, C., and Gaunt, T. R. (2017). HIPred: an Integrative Approach to Predicting Haploinsufficient Genes. *Bioinformatics* 33 (12), btx028–1757. doi:10.1093/bioinformatics/btx028

Srivastava, S., Love-Nichols, J. A., Love-Nichols, J. A., Dies, K. A., Ledbetter, D. H., Martin, C. L., et al. (2019). Meta-analysis and Multidisciplinary Consensus Statement: Exome Sequencing Is a First-Tier Clinical Diagnostic Test for Individuals with Neurodevelopmental Disorders. *Genet. Med.* 21 (11), 2413–2421. doi:10.1038/s41436-019-0554-6

Szklarczyk, D., Gable, A. L., Lyon, D., Junge, A., Wyder, S., Huerta-Cepas, J., et al. (2019). STRING V11: Protein-Protein Association Networks with Increased Coverage, Supporting Functional Discovery in Genome-wide Experimental Datasets. *Nucleic Acids Res.* 47 (D1), D607–D613. doi:10.1093/nar/gky1131

Tabas-Madrid, D., Nogales-Cadenas, R., and Pascual-Montano, A. (2012). GeneCodis3: a Non-redundant and Modular Enrichment Analysis Tool for Functional Genomics. *Nucleic Acids Res.* 40, W478–W483. doi:10.1093/nar/gks402

Tao, Z., Feng, C., Mao, C., Ren, J., Tai, Y., Guo, H., et al. (2019). MiR-4465 Directly Targets PTEN to Inhibit AKT/mTOR Pathway-Mediated Autophagy. *Cell Stress and Chaperones* 24 (1), 105–113. doi:10.1007/s12192-018-0946-6

Tassano, E., Gimelli, S., Divizia, M. T., Lerone, M., Vaccari, C., Puliti, A., et al. (2015). Thrombocytopenia-absent Radius (TAR) Syndrome Due to Compound Inheritance for a 1q21.1 Microdeletion and a Low-Frequency Noncoding RBM8A SNP: a New Familial Case. *Mol. Cytogenet.* 8, 87. doi:10.1186/s13039-015-0188-6

Tomita, H., Cornejo, F., Aranda-Pino, B., Woodard, C. L., Rioseco, C. C., Neel, B. G., et al. (2020). The Protein Tyrosine Phosphatase Receptor Delta Regulates Developmental Neurogenesis. *Cel Rep.* 30 (1), 215–228. e215. doi:10.1016/j.celrep.2019.11.033

Tomoda, T., Kim, J. H., Zhan, C., and Hatten, M. E. (2004). Role of Unc51.1 and its Binding Partners in CNS Axon Outgrowth. *Genes Development* 18 (5), 541–558. doi:10.1101/gad.1151204

Tropeano, M., Howley, D., Gazzellone, M. J., Wilson, C. E., Ahn, J. W., Stavropoulos, D. J., et al. (2016). Microduplications at the pseudoautosomalSHOXlocus in Autism Spectrum Disorders and Related Neurodevelopmental Conditions. *J. Med. Genet.* 53 (8), 536–547. doi:10.1136/jmedgenet-2015-103621

Uetani, N., Kato, K., Ogura, H., Mizuno, K., Kawano, K., Mikoshiba, K., et al. (2000). Impaired Learning with Enhanced Hippocampal Long-Term Potentiation in PTPdelta-Deficient Mice. *EMBO J.* 19 (12), 2775–2785. doi:10.1093/emboj/19.12.2775

Uhl, G. R., and Martinez, M. J. (2019). PTPRD: Neurobiology, Genetics, and Initial Pharmacology of a Pleiotropic Contributor to Brain Phenotypes. *Ann. N.Y. Acad. Sci.* 1451 (1), 112–129. doi:10.1111/nyas.14002

Um, J. W., and Ko, J. (2017). Neural Glycosylphosphatidylinositol-Anchored Proteins in Synaptic Specification. *Trends Cel Biol.* 27 (12), 931–945. doi:10.1016/j.tcb.2017.06.007

Vaccari, C. M., Romanini, M. V., Musante, I., Tassano, E., Gimelli, S., Divizia, M. T., et al. (2014). De Novo deletion of Chromosome 11q12.3 in Monozygotic Twins Affected by Poland Syndrome. *BMC Med. Genet.* 15, 63. doi:10.1186/1471-2350-15-63

Velinov, M. (2019). Genomic Copy Number Variations in the Autism Clinic-Work in Progress. *Front. Cell. Neurosci.* 13, 57. doi:10.3389/fncel.2019.00057

Vijiaratnam, N., Bhatia, K. P., Lang, A. E., Raskind, W. H., and Espay, A. J. (2019). ADCY5-Related Dyskinesia: Improving Clinical Detection of an Evolving Disorder. *Mov Disord. Clin. Pract.* 6 (7), 512–520. doi:10.1002/mdc3.12816

von Engelhardt, J. (2019). AMPA Receptor Auxiliary Proteins of the CKAMP Family. *Ijms* 20 (6), 1460. doi:10.3390/ijms20061460

Wu, X., Li, W., and Zheng, Y. (2020). Recent Progress on Relevant microRNAs in Autism Spectrum Disorders. *Ijms* 21 (16), 5904. doi:10.3390/ijms21165904

Yamagata, A., Yoshida, T., Sato, Y., Goto-Ito, S., Uemura, T., Maeda, A., et al. (2015). Mechanisms of Splicing-dependent Trans-synaptic Adhesion by PTPδ-IL1RAPL1/IL-1RAcP for Synaptic Differentiation. *Nat. Commun.* 6, 6926. doi:10.1038/ncomms7926

Yan, H., Shi, Z., Wu, Y., Xiao, J., Gu, Q., Yang, Y., et al. (2019). Targeted Next Generation Sequencing in 112 Chinese Patients with Intellectual Disability/developmental Delay: Novel Mutations and Candidate Gene. *BMC Med. Genet.* 20 (1), 80. doi:10.1186/s12881-019-0794-y

Yang, A. W., Sachs, A. J., and Nystuen, A. M. (2015). Deletion of Inpp5a Causes Ataxia and Cerebellar Degeneration in Mice. *Neurogenetics* 16 (4), 277–285. doi:10.1007/s10048-015-0450-4

Yang, J.-H., Chang, M.-W., Pandey, P. R., Tsitsipatis, D., Yang, X., Martindale, J. L., et al. (2020). Interaction of OIP5-AS1 with MEF2C mRNA Promotes Myogenic Gene Expression. *Nucleic Acids Res.* 48 (22), 12943–12956. doi:10.1093/nar/gkaa1151

Yoshida, T., Shiroshima, T., Lee, S.-J., Yasumura, M., Uemura, T., Chen, X., et al. (2012). Interleukin-1 Receptor Accessory Protein Organizes Neuronal Synaptogenesis as a Cell Adhesion Molecule. *J. Neurosci.* 32 (8), 2588–2600. doi:10.1523/JNEUROSCI.4637-11.2012

Zhang, L., Zhang, X., Zhang, Y., Xu, N., Wang, J., Zhu, Y., et al. (2020). Brn4 Promotes the Differentiation of Radial Glial Cells into Neurons by Inhibiting CtBP2. *Life Sci.* 254, 116866. doi:10.1016/j.lfs.2019.116866

Conflict of Interest: The authors declare that the research was conducted in the absence of any commercial or financial relationships that could be construed as a potential conflict of interest.

Publisher's Note: All claims expressed in this article are solely those of the authors and do not necessarily represent those of their affiliated organizations, or those of the publisher, the editors and the reviewers. Any product that may be evaluated in this article, or claim that may be made by its manufacturer, is not guaranteed or endorsed by the publisher.

frontiers in Pediatrics

ORIGINAL RESEARCH
published: 05 October 2021
doi: 10.3389/fped.2021.685310

Analysis of Global and Local DNA Methylation Patterns in Blood Samples of Patients With Autism Spectrum Disorder

María Victoria García-Ortiz[1,2,3†], *María José de la Torre-Aguilar*[1,4†], *Teresa Morales-Ruiz*[1,2,3], *Antonio Gómez-Fernández*[1,4], *Katherine Flores-Rojas*[1,5,6], *Mercedes Gil-Campos*[1,5,6*], *Pilar Martin-Borreguero*[1,7], *Rafael R. Ariza*[1,2,3], *Teresa Roldán-Arjona*[1,2,3] *and Juan Luis Perez-Navero*[1,4,8]

[1] Maimónides Biomedical Research Institute of Córdoba (IMIBIC), Córdoba, Spain, [2] Department of Genetics, University of Córdoba, Córdoba, Spain, [3] Reina Sofía University Hospital, Córdoba, Spain, [4] Department of Pediatrics, Reina Sofia University Hospital, University of Córdoba, Córdoba, Spain, [5] Pediatric Metabolism Unit, Reina Sofia University Hospital, University of Córdoba, Córdoba, Spain, [6] Physiopathology of Obesity and Nutrition Networking Biomedical Research Center (CIBEROBN), Córdoba, Spain, [7] Department of Child and Adolescent Clinical Psychiatry and Psychology, Reina Sofia University Hospital, Córdoba, Spain, [8] Biomedical Research Center–Rare Diseases (CIBERER), Carlos III Health Institute, Madrid, Spain

OPEN ACCESS

Edited by:
Chen Li,
Zhejiang University, China

Reviewed by:
Maud de Dieuleveult,
Assistance Publique Hopitaux de Paris, France
Maria Paola Lombardi,
University of Amsterdam, Netherlands

***Correspondence:**
Mercedes Gil-Campos
mercedes_gil_campos@yahoo.es

[†] *These authors have contributed equally to this work*

Specialty section:
This article was submitted to Genetics of Common and Rare Diseases, a section of the journal Frontiers in Pediatrics

Received: *24 March 2021*
Accepted: *06 September 2021*
Published: *05 October 2021*

Citation:
García-Ortiz MV, Torre-Aguilar MJ, Morales-Ruiz T, Gómez-Fernández A, Flores-Rojas K, Gil-Campos M, Martin-Borreguero P, Ariza RR, Roldán-Arjona T and Perez-Navero JL (2021) Analysis of Global and Local DNA Methylation Patterns in Blood Samples of Patients With Autism Spectrum Disorder. Front. Pediatr. 9:685310. doi: 10.3389/fped.2021.685310

The goal of this investigation was to determine whether there are alterations in DNA methylation patterns in children with autism spectrum disorder (ASD).

Material and Methods: Controlled prospective observational case-control study. Within the ASD group, children were sub-classified based on the presence (AMR subgroup) or absence (ANMR subgroup) of neurodevelopmental regression during the first 2 years of life. We analyzed the global levels of DNA methylation, reflected in *LINE-1*, and the local DNA methylation pattern in two candidate genes, Neural Cell Adhesion Molecule (NCAM1) and Nerve Growth Factor (NGF) that, according to our previous studies, might be associated to an increased risk for ASD. For this purpose, we utilized blood samples from pediatric patients with ASD ($n = 53$) and their corresponding controls ($n = 45$).

Results: We observed a slight decrease in methylation levels of *LINE-1* in the ASD group, compared to the control group. One of the CpG in *LINE-1* (GenBank accession no.X58075, nucleotide position 329) was the main responsible for such reduction, highly significant in the ASD subgroup of children with AMR ($p < 0.05$). Furthermore, we detected higher *NCAM1* methylation levels in ASD children, compared to healthy children ($p < 0.001$). The data, moreover, showed higher *NGF* methylation levels in the AMR subgroup, compared to the control group and the ANMR subgroup. These results are consistent with our prior study, in which lower plasma levels of *NCAM1* and higher levels of *NGF* were found in the ANMR subgroup, compared to the subgroup that comprised neurotypically developing children.

Conclusions: We have provided new clues about the epigenetic changes that occur in ASD, and suggest two potential epigenetic biomarkers that would facilitate the diagnosis of the disorder. We similarly present with evidence of a clear differentiation in DNA methylation between the ASD subgroups, with or without mental regression.

Keywords: autism spectrum disorder, neurodevelopmental regression, DNA methylation patterns, NCAM, NGF

INTRODUCTION

Autism spectrum disorder (ASD) is a severe neurodevelopmental disorder featuring variable but pronounced deficits in communication and social interaction, and is associated to multiple genetic risk factors (1, 2). Environmental (viral infection, parental age, diet) and epigenetic factors (DNA methylation, histone modification and microRNA) would act on some predisposing genetic factors (3). However, although epigenetic mechanisms, transcriptome profiles, and environmental factors have been suggested to be implicated, no clear pathogenesis mechanisms have been yet identified in ASD (4–12).

One of the best-known epigenetic marks is the 5-methylcytosine (5-mC), generated by the methylation at C5 of cytosine in symmetric CG contexts. A high proportion of regulatory regions, such as promoters and enhancers, contains areas with high density of CpG dinucleotides (called "CpG islands") that are usually unmethylated, and whose methylation is generally associated to transcriptional silencing (13). Extensive experimental evidence supports that DNA methylation is a crucial step during brain development, and plays a key role in processes including synaptic plasticity, learning, memory, or cognitive decline (14).

Unlike mutations, epigenetic changes are potentially reversible, which has opened new pathways in the study of some diseases. Nowadays, it is accepted that ASD has a strong epigenetic component (14–19). Several genome-wide studies revealed multiple alterations in DNA methylation patterns in the brains of ASD individuals (20, 21). The largest meta-analysis study using peripheral blood samples from about 800 autistic individuals revealed that 55 of examined CpG sites were associated to ASD (22). Nevertheless, the main regions analyzed in these studies are the CpG islands of the protein coding regions, whereas DNA methylation in the genomic non-coding regions, which are often implicated in genetic regulation pathways, has not yet been examined. On the other hand, a significant fraction of the mutations associated to an increased risk of ASD affects transcriptional factors or chromatin-modifying proteins (23). Genetic mutations of the MECP2 gene related to autism spectrum disorders have been recently identified (4). MECP2 is a master epigenetic regulator that exhibits high levels of expression in the brain. However, a reduced expression of MECP2, associated to hypermethylation of its promoter, has been described in the frontal cortex of patients with ASD (8). Understanding the epigenetic changes involved in ASD can also help to identify subgroups of patients, allowing a better stratification for the implementation of pharmacological and/or behavioral therapies.

Long interspersed element-1 (*LINE-1*) is an autonomous transposable element that makes up roughly 17% of the human genome where it remains active (24). It is possible for retrotransposition of *LINE-1* into a new position of the genome to cause duplication, deletion, or insertion at the target site, triggering genomic instability and changes in gene expression (25). Although the process by which *LINE-1* transcription and retrotransposition is regulated remains indeterminate, mounting evidence propose that epigenetic pathways, such as DNA methylation and histone modifications, are implicated in the retrotransposition of *LINE-1* and could have an impact on the target genes expression (26). There have been reports of altered DNA methylation levels and patterns of CpG residues in *LINE-1* promoter regions in many diseases, including ASD (22, 26).

Other authors have posited that both a proinflammatory condition and an alteration in adhesion molecules in the early stages of neurodevelopment may play a role in the pathophysiology of ASD. Our group has recently published a study on the plasma levels of particular adhesion molecules and growth factors in patients with ASD compared to healthy children. When sub-classifying according to the presence or absence of neurodevelopmental regression in children with ASD, lower plasma levels of the Neural Cell Adhesion Molecule (NCAM1) and higher levels of Nerve Growth Factor (NGF) were observed in the subgroup of autistic children without mental regression, compared to the levels obtained in the mental regression subgroup and the control group (27).

Based on evidence of close implication of loci-specific DNA methylation in the pathophysiology of neurological disorders including ASD (20, 21), and previous demonstration of an association between the epigenetic regulation of *LINE-1* and its effects in ASD pathobiology (26), the present study aims to compare global methylation levels in blood samples of pediatric patients with ASD and healthy children, and to examine the DNA methylation status of *NCAM1* and *NGF, two* genes that we have previously shown to be deregulated in autistic spectrum disorder. Here, we report the results of a global and local DNA methylation analysis from a pediatric sample with ASD compared to normally developing children.

MATERIALS AND METHODS

Subjects

This was a controlled prospective observational case-control study. The patients with ASD were recruited from the Department of Child and Adolescent Clinical Psychiatry and

Psychology at the Reina Sofia University Hospital. Some of the patients (those aged 2–3) were assimilated into the study at the time of their ASD diagnosis, while the older patients (those aged 3–6) were selected from among children who had already been given diagnoses at the same unit. The diagnosis of ASD was based on the clinical judgment of professionals specializing in identifying the unique developmental profile associated with subjects with ASD. The diagnoses were based on the information obtained from semi-structured clinical development interviews, and psychological and behavioral tests that have been internationally acknowledged to be reliable and valid for this purpose. Two clinical psychologists, a psychiatrist and an occupational therapist with extensive clinical experience and training in diagnostic tests for research in ASD performed the diagnoses, employing the criteria established in DSM-5 (28). In addition, two pediatricians reviewed the subjects' medical histories and conducted an examination of all the children.

Children with ASD presenting with other known neurological, metabolic or genetic diagnoses were excluded from the study, and the same applied to children undergoing medical treatments for autism-related behavioral comorbidities that might interfere with the results, such as sedatives, muscle relaxants or similar. In addition, a control group of normally developing children was recruited, matched to the ASD group in terms of gender and age.

Within the ASD group, children were sub-classified based on the presence or absence of neurodevelopmental regression occurring during the first 2 years of life. This was assessed by means of a five-item questionnaire in accordance with the guide used by the ADI-R clinical interview for the evaluation of this process (29). Children with ASD who obtained a score equal to or greater than three were included in the mental regression subgroup (AMR: Autism Mental Regression), while those with a score inferior to this cut-off value were included in the non-mental regression subgroup (ANMR: Autism Non-Mental Regression) (27).

The study was approved by the Clinical Research and Bioethics Committee at the Reina Sofia University Hospital, conforming to the fundamental principles established in the Declaration of Helsinki (latest version 2013), supplemented by the Declaration of Taipei (2016).

Standardized Diagnostic Measurements and Assessment of ASD Severity

All the cases of ASD were selected after carrying out the Checklist for Autism in Toddlers (M-CHAT). Subsequently, a comprehensive clinical history of each child was taken. The Autism Diagnostic Observation Schedule, Second Edition (ADOS-2), was used in cases of suspected ASD. Each of the following tests was also administered: the Autism Diagnostic Interview-revised (ADI-R), the Pervasive Developmental Disorders Behavior Inventory™ (PDDBI), the Childhood Autism Rating Scale test (CARS), the Battelle Developmental test, and the Strengths and Difficulties Questionnaire (SDQ). These tests enabled the clinical team to diagnose ASD with more certainty.

None of the ASD cases selected for the present study exhibited any other associated pathology (seizures, or other neurological, metabolic or genetic diseases). Each patient was clinically assessed with complementary explorations. The children also underwent a genetic study (karyotype and microarrays) to detect secondary or syndromic ASD. None of the patients required medication to treat behavioral disorders or aggression.

Sample Collection, DNA Extraction and Bisulfite Treatment of the DNA

After overnight fasting, peripheral whole blood samples were collected from participants *via* antecubital vein into 6-ml blood collection tubes containing EDTA. After centrifugation at 3,500 g for 10 min, plasma was divided into aliquots and processed within 2 h from sampling, and then frozen at −80°C until analysis. Blood count and a general biochemical analysis were performed to confirm the absence of other diseases.

Genomic DNA was extracted from 2 mL of plasma with the QIAamp DNA Blood kit (QIAGEN), following the manufacture's protocol, and quantified in a NanoDrop ND-1,000 spectrophotometer (Nano-Drop Technologies). Bisulfite conversion of isolated DNA (500 ng) was performed with the EZ DNA Methylation Gold Kit (Zymo Research), according to the manufacturer's instructions.

PCR and Pyrosequencing

Utilizing the Immolase DNA Polymerase (Bioline) 50 ng of bisulfite, converted DNA were added to the PCR reaction, following the manufacturer's recommendations. **Table 1** shows the forward and reverse primer sequences for each gene. The PCR product was subjected to agarose gel electrophoresis to test for the presence of a single PCR product. 15 μL of the verified biotinylated PCR product was used for each sequencing assay. DNA pyrosequencing was performed in a PyroMark Q24 instrument (Qiagen), following the manufacturer's guidelines, and subsequent methylation analysis was determined with the PyroMark Q24 Software (Qiagen). Sequencing primers for each gene are listed in **Table 1**. In the light of the literature (30–33) and recent results from this group of children (27), two loci previously linked to ASD (*NCAM1* and *NGF*) were selected for methylation analysis. Primers for *NCAM1* were designed to amplify a 3′UTR region (UCSC region chr11:112,965,249–112,965,403) that included CpG positions for which changes in methylation levels have been previously described (34). Primers for *NGF* were obtained from Qiagen to amplify a region at the 5′UTR, near the non-transcribed first exon of the gene (UCSC region chr1:115,880,563–115,880,774) (**Table 1**).

Statistical Analysis

The sample size for this study was determined based on the most relevant genome-wide and local DNA methylation studies on ASD using published data results (18, 24, 26). GraphPad Prism 6 Software was used to perform the statistical analyses. The data are expressed as mean ± SD (95% confidence intervals), median (IQR) or absolute (relative frequencies). For data that fit a normal distribution (Shapiro-Wilk normality test) *t*-tests were used. For data not normally distributed, the non-parametric

TABLE 1 | List of primers used for pyrosequencing.

Gene	Primer	Sequence (5′-3′)	Length (bp)	Accession no. (Gene ID)	Annealing T_m (°C)
LINE-1	Forward	TTTTGAGTTAGGTGTGGGATATA	146	NM_019079 (54596)	50
	Reverse	[BTN] AAAATCAAAAAATTCCCTTTC			
	Sequencing	AGTTAGGTGTGGGATATAG			
NCAM1	Forward	TATTTTTGTGTTTTTTTGGGGGTTAGATTA	154	NM_181351 (4684)	55
	Reverse	[BTN] CCCAACTATACAATCTTCTCTACTTCAT			
	Sequencing	GGGGTTAGATTATTTTTTGAT			
NGF	Forward	Hs_NGF_01_PM PyroMark CpG assay (PM00002618)	211	NM_002506 (4803)	58
	Reverse				
	Sequencing				

LINE-1, Long interspersed element-1; NCAM1, Neural Cell Adhesion Molecule; NGF, Nerve Growth Factor.

Mann-Whitney test were applied. Categorical variables were evaluated using the χ^2-test or the Fisher exact test. To assess the methylation differences between healthy control group and ASD subgroups, in CpG positions together or individually, unpaired *t*-test and two-way ANOVA model with Tukey's HSD *post-hoc* tests were used Correlations between methylation levels and the scores obtained from the various tests performed were carried out using the Spearman's p (rho). Receiver operating characteristics (ROC) analysis was conducted to calculate the area under the curve (AUC). All the tests were two-tailed, and a $p < 0.05$ was considered statistically significant.

RESULTS

Global Methylation Analysis in Autism Spectrum Disorder

Fifty-four children with ASD and 45 healthy children were included in the study. The principal demographic and test results for the diagnosis are shown in **Table 2**. Within the ASD group, there were 20 children with AMR and 33 with ANMR; one child could not be classified in these subgroups because he was adopted and there was no previous clinical information.

Because *LINE-1* retrotransposon represents a considerable portion of the human genome, the methylation level of *LINE-1* reflects the global DNA methylation status (24). To determine whether global methylation levels were altered in ASD, 53 blood samples from children with ASD and 45 from the control group were drawn to isolate to gDNA. Bisulfite pyrosequencing was performed analyzing 5 CpG positions of the repetitive element *LINE-1*. Three samples from ASD patients gave inconclusive results, so they were removed from the *LINE-1* methylation analysis. Methylation of *LINE-1* was slightly reduced in the group of children with ASD compared to the control group (73.45 ± 0.43 vs. 74.56 ± 0.45) (**Figures 1A,C**). When each studied CpG of the *LINE-1* fragment was analyzed separately, position 2 (GenBank accession no.X58075, nucleotide position 329, complementary strand) was the main responsible for the observed decrease in *LINE-1* methylation levels in the ASD group (**Figure 1B** and **Table 3**). Moreover, when analysis was performed with patients with AMR and AMNR, methylation levels of CpG 2 from *LINE-1* in the AMR subgroup was significantly lower (71.16 ± 0.60), compared to the healthy control group (72.98 ± 0.52) (**Figure 1D** and **Table 3**). Although methylation levels at position 2 of *LINE-1* in the ANMR subgroup were also lower than in the control group, this difference was not statistically significant.

TABLE 2 | Demographic and anthropometric data in children with autism spectrum disorders compared to controls.

		ASD (n:50)	Control (n:45)	*p*
Age (months)		43.76 ± 11,2	48.81 ± 18.33	0.117
Gender (male)		41 (82%)	38 (84%)	0.472
Weight (kg)		16.97 ± 3.51	17.06 ± 4.5	0.951
Battelle test	AMR	47.05 ± 10.33		0.002
	ANMR	60.96 ± 13.29		
CARS test	AMR	35.9 ± 8.12		0.009
	ANMR	30.6 ± 6.11		
PDBBI test	AMR	53.93 ± 10.39		0.023
	ANMR	46.13 ± 10.47		

ASD, autism spectrum disorders; AMR, autism mental regression; ANMR, autism non-mental regression; PDDBI, Pervasive Developmental Disorders Behavior Inventory; CARS, Childhood Autism Rating Scale.

As expected from slight changes in *LINE-1* methylation levels, no clinical correlations were observed between the methylation status of *LINE-1* and any of the tests performed to evaluate the diagnosis, severity, and the regressive aspects of the disorder (**Supplementary Table 4**).

Methylation Status Analysis of *NCAM1* and *NGF* in ASD

DNA methylation status was analyzed for each gene (**Figures 2A**, **3A**), both in the ASD group and in the subgroups ANMR and AMR separately. Pyrosequencing results showed a significant increase in *NCAM1* methylation levels in the ASD children and in each subgroup, ANMR and AMR, compared to healthy children (**Figures 2B,D** and **Table 4**). Specifically, 70% of ASD individuals presented *NCAM1* methylation levels above the mean, with no distinction

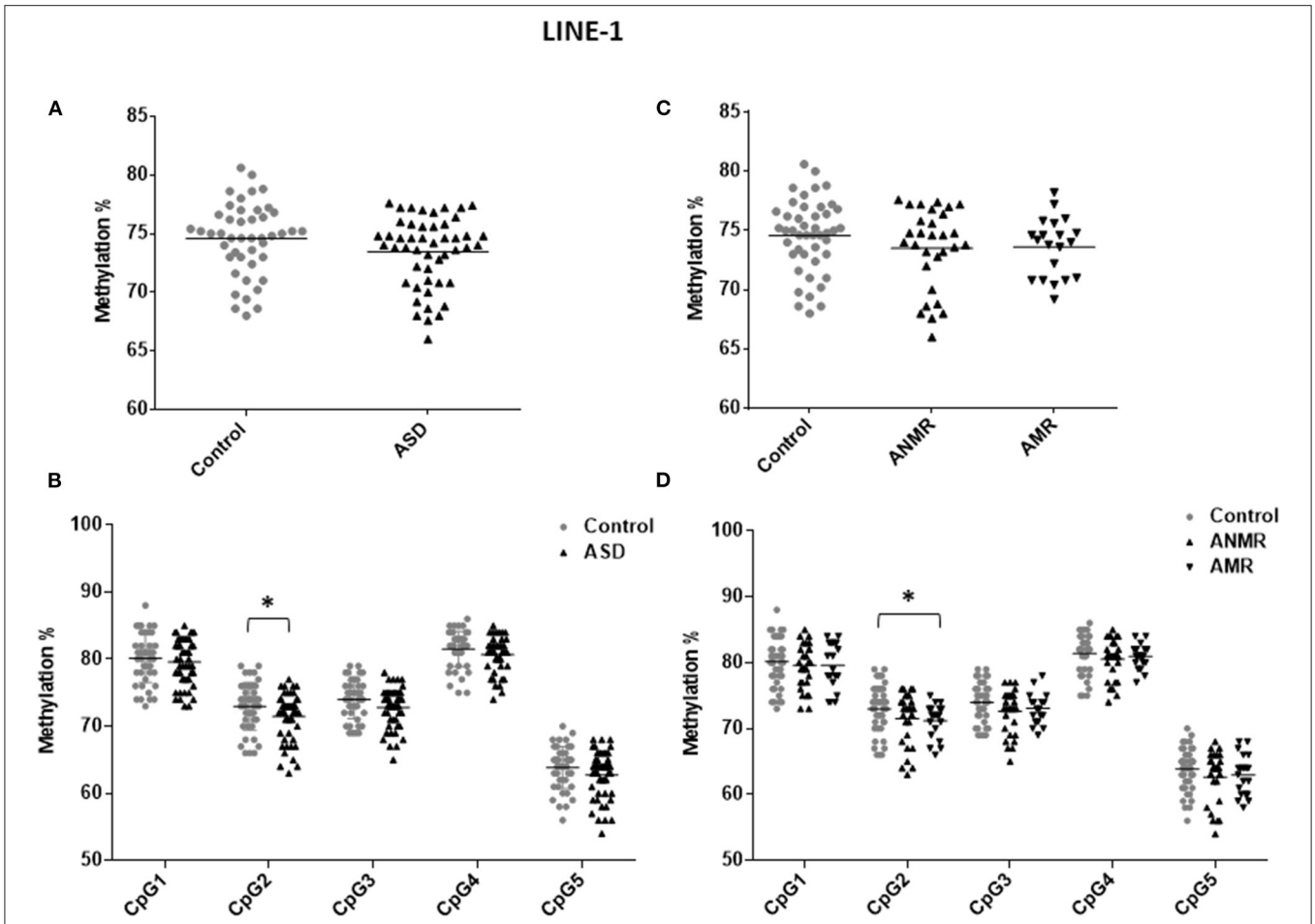

FIGURE 1 | Scatter plot showing comparisons of methylation status of LINE-1 in children with autism spectrum disorders (ASD) compared to controls. **(A,B)** Methylation levels and differentially methylated sites (CpG1–CpG5) in the LINE-1 sequence in ASD group and healthy control group. **(C,D)** Methylation levels and differentially methylated sites in the LINE-1 sequence in ASD group subdivided as follows: ANMR (non-mental regression group), AMR (mental regression group), and a healthy control group. The dark bars represent the mean values of each group. Asterisks indicate statistically significant differences (*$P \leq 0.05$) compared to control group.

TABLE 3 | Pyrosequencing results of LINE-1 showing percent change in methylation in ASD group, ANMR and AMR subgroups compared to healthy control group.

	LINE-1					
	Control vs. ASD		Control vs. ANMR		Control vs. AMR	
	Percent change in methylation	*p*-value	Percent change in methylation	*p*-value	Percent change in methylation	*p*-value
All CpG	1.11	0.078	1.06	0.16	0.95	0.15
CpG site 1	0.56	0.49	0.55	0.51	0.56	0.62
CpG site 2	**1.49***	0.05	1.49	0.15	**1.82***	0.03
CpG site 3	1.15	0.08	1.34	0.13	0.88	0.23
CpG site 4	0.81	0.06	0.84	0.10	0.42	0.15
CpG site 5	1.07	0.17	1.19	0.28	0.89	0.24

*ASD, autism spectrum disorders; AMR, autism mental regression; ANMR, autism non-mental regression. *$P \leq 0.05$ with statistically significant changes highlighted in bold.*

between AMR and ANMR. In the control group of healthy individuals, only 42% had higher-than-mean *NCAM1* methylation levels. In addition, CpG 1 in *NCAM1* (UCSC location chr11:112,965,292) was the position that suffered this notable increase in methylation, especially in the AMR subgroup (**Figures 2C,E**).

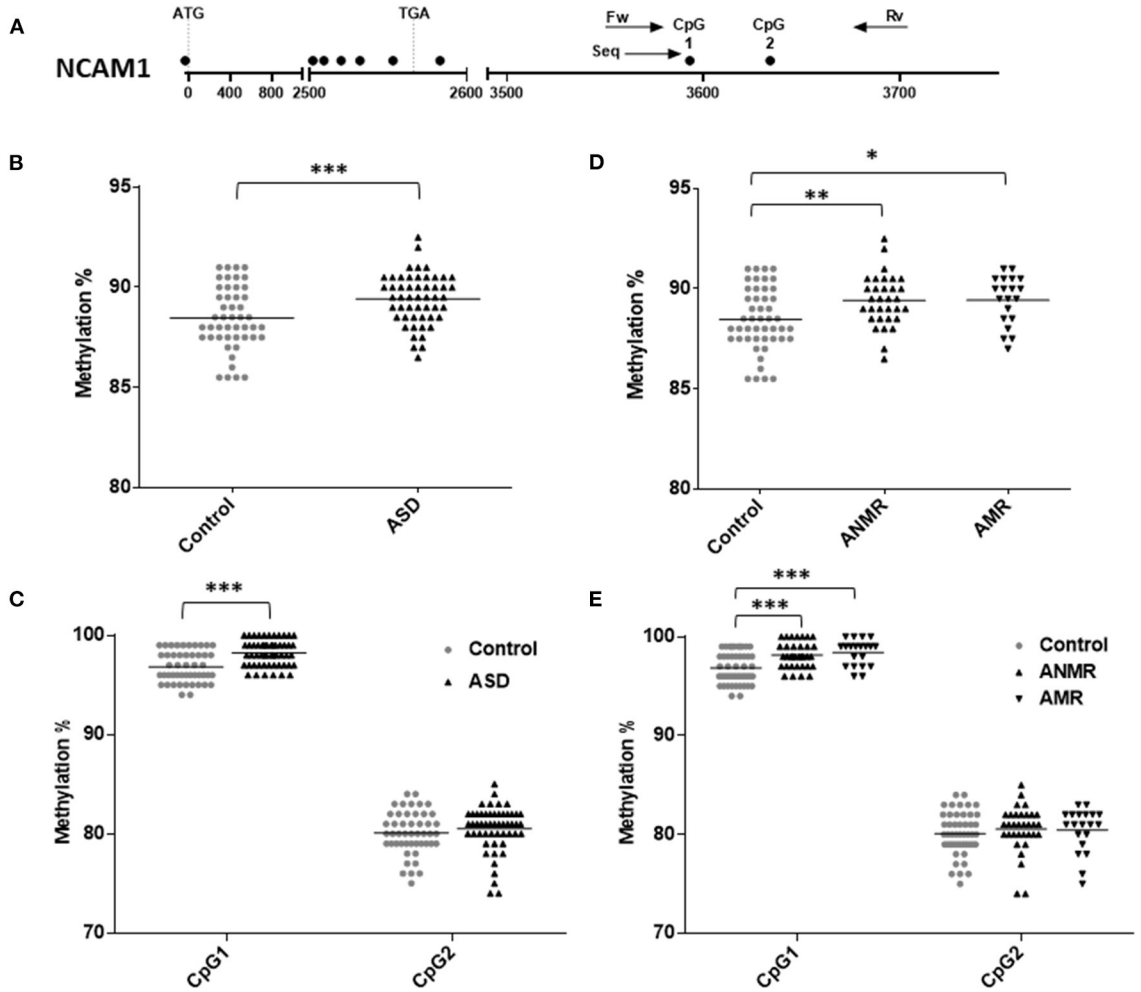

FIGURE 2 | Scatter plot showing comparisons of methylation status of *NCAM1* in children with autism spectrum disorders (ASD) compared to controls. **(A)** Schematic diagram of analyzed gene. Each circle represents a CpG dinucleotide. Position of ATG and TGA codon are indicated. Arrows show the location of pyrosequencing primers. **(B,C)** Methylation levels and differentially methylated sites (CpG1 and CpG2) in the *NCAM1* gene in ASD group and healthy control group. **(D,E)** Methylation levels and differentially methylated sites in the *NCAM1* gene in ASD group subdivided as follows: ANMR (non-mental regression group), AMR (mental regression group), and a healthy control group. The dark bars represent the mean values of each group. Asterisks indicate statistically significant differences (*$P < 0.05$; **$P < 0.01$; ***$P < 0.001$) compared to control group.

TABLE 4 | Pyrosequencing results of NCAM1 showing percent change in methylation in ASD group, ANMR and AMR subgroups compared to healthy control group.

	NCAM1					
	Control vs. ASD		**Control vs. ANMR**		**Control vs. AMR**	
	Percent change in methylation	***p*-value**	**Percent change in methylation**	***p*-value**	**Percent change in methylation**	***p*-value**
All CpG	**−0.96*****	0.0009	**−0.96****	0.005	**−0.97***	0.016
CpG site 1	**−1.41*****	<0.0001	**−1.31*****	0.0003	**−1.57*****	0.0002
CpG site 2	−0.43	0.16	−0.46	0.19	−0.37	0.34

*ASD, autism spectrum disorders; AMR, autism mental regression; ANMR, autism non-mental regression; NCAM1, Neural Cell Adhesion Molecule. *P ≤ 0.05; **P < 0.01; ***P < 0.001 with statistically significant changes highlighted in bold.*

On the other hand, no differences were observed in the levels of *NGF* methylation between the ASD group and the healthy group (**Figure 3B**). Concretely, lower-than-mean levels of *NGF* methylation were detected in 47% of children diagnosed with ASD and in 53% of neurotypically developing children. Within the ASD group, the AMR subgroup had higher-than-mean

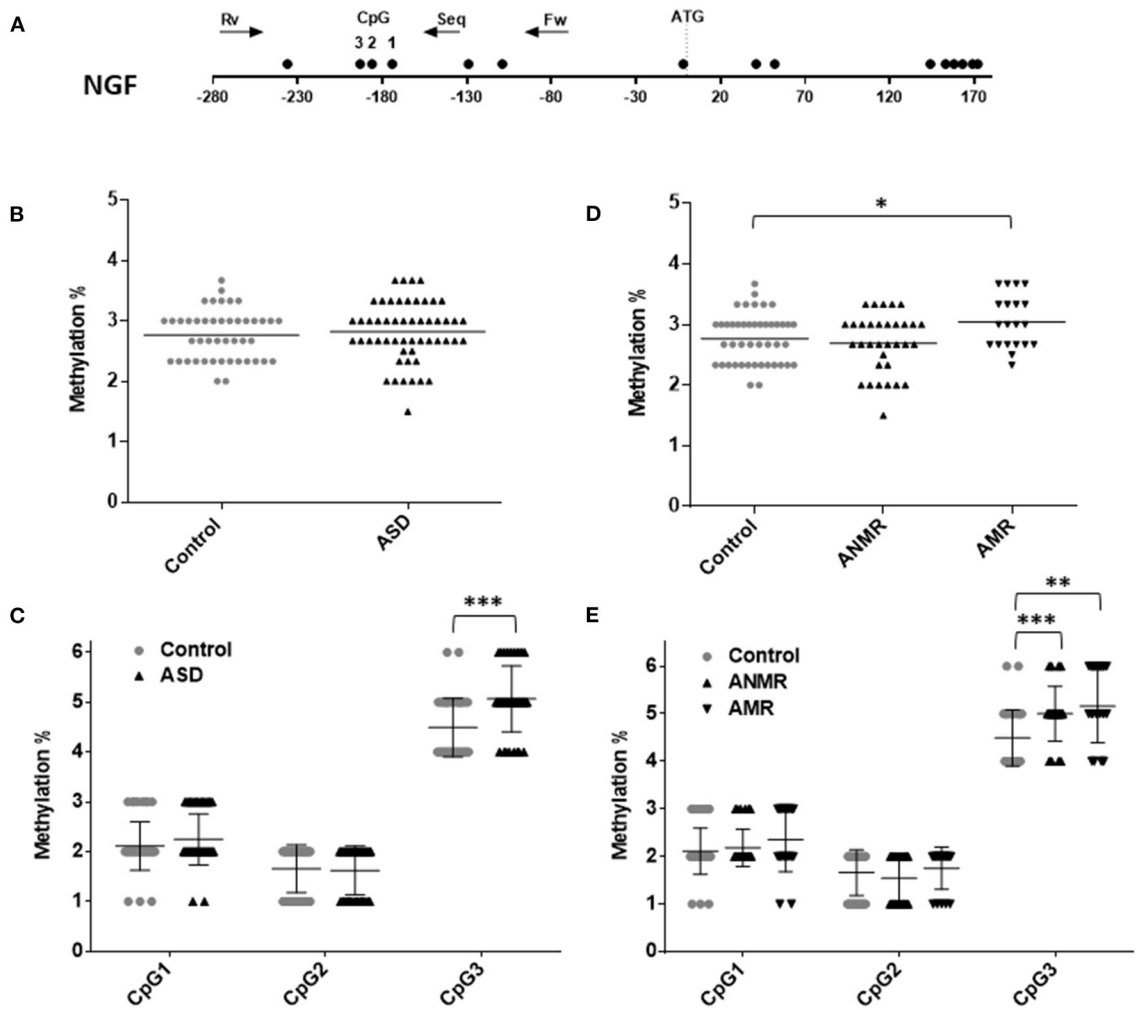

FIGURE 3 | Scatter plot showing comparisons of methylation status of *NGF* in children with autism spectrum disorders (ASD) compared to controls. **(A)** Schematic diagram of analyzed gene. Each circle represents a CpG dinucleotide. Position of ATG codon is indicated. Arrows show the location of pyrosequencing primers. **(B,C)** Methylation levels and differentially methylated sites (CpG 1, 2, and 3) in the *NGF* gene in ASD group and healthy control group. **(D,E)** Methylation levels and differentially methylated sites in the *NGF* gene in ASD group subdivided as follows: ANMR (non-mental regression group), AMR (mental regression group), and a healthy control group. The dark bars represent the mean values of each group. Asterisks indicate statistically significant differences ($^{*}P < 0.05$; $^{**}P < 0.01$; $^{***}P < 0.001$) compared to control group.

NGF methylation levels than both the ANMR subgroup and the normally developing children (**Figure 3D**). Methylation analysis of each CpG revealed that the CpG at position 3 of the analyzed region (UCSC location chr1: 115,880,705) showed a higher level of methylation in children diagnosed with ASD, with or without mental regression (**Figures 3C,E** and **Table 5**).

In the ROC curve, the AUC was calculated to explore differences in *LINE-1*, *NCAM1* and/or *NGF* methylation between ASD and healthy status (**Figure 4**). The AUC for *NCAM1* was 0.67 ($p = 0.02$). However, for *LINE-1* and *NGF*, the values resulted not optimal to discriminate between ASD and healthy conditions.

DISCUSSION

In the present work we report results from a global and local DNA methylation analysis of a pediatric sample with ASD compared to a normally developing children subgroup. ASD is a neurodevelopmental disorder that presumably affects multiple areas of the brain, including the frontal, temporal, and occipital cortex, as well as the cerebellum. Since brain tissue cannot be collected from live individuals, a more accessible tissue sample has been suggested, such as peripheral blood. High correlations have been found between methylation levels of specific genes in the blood and brain regions in children with neurodevelopmental disorders and controls (6, 35, 36).

TABLE 5 | Pyrosequencing results of NGF showing percent change in methylation in ASD group, ANMR and AMR subgroups compared to healthy control group.

	NGF					
	Control vs. ASD		Control vs. ANMR		Control vs. AMR	
	Percent change in methylation	*p*-value	Percent change in methylation	*p*-value	Percent change in methylation	*p*-value
All CpG	−0.05	0.20	0.04	0.81	**−0.28****	0.029
CpG site 1	−0.13	0.21	−0.07	0.61	−0.24	0.09
CpG site 2	0.04	0.83	0.11	0.35	−0.09	0.57
CpG site 3	**−0.49*****	0.0004	**−0.51**	0.0008***	**−0.67****	0.001

*ASD, autism spectrum disorders; AMR, autism mental regression; ANMR, autism non-mental regression; NGF, Nerve Growth Factor. *P ≤ 0.05; **P < 0.01; ***P < 0.001 with statistically significant changes highlighted bold.*

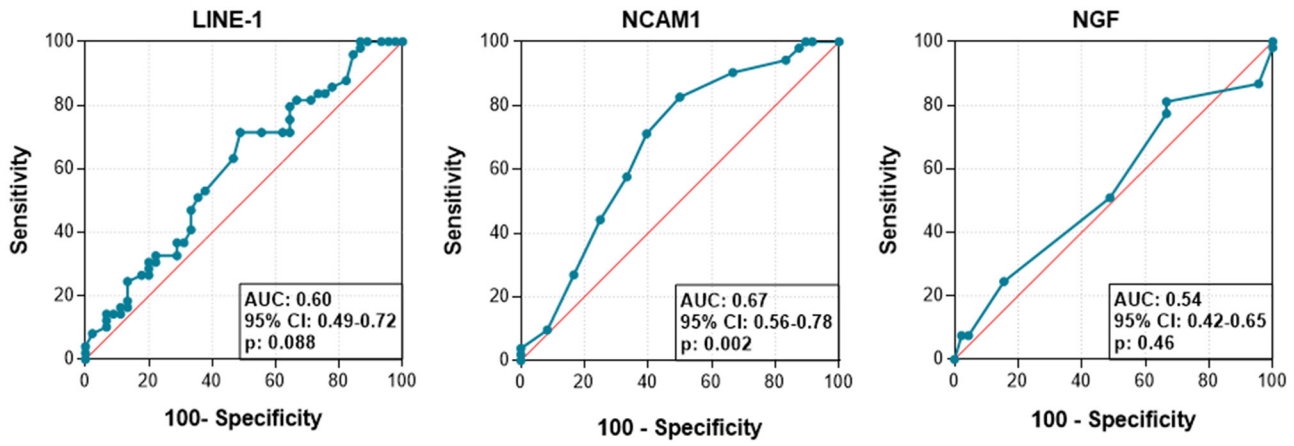

FIGURE 4 | Receiver operator characteristic curves (ROC) and area under the curve (AUC) values to differentiate ASD from healthy condition according to the methylation status of each target.

DNA methylation in non-coding regions, including *LINE-1* retrotransposons, which constitutes a substantial portion of the human genome, has been very little investigated in the context of ASD. The first report of an increase in *LINE-1* expression in the autism cerebellum was published by Shpyleva et al. (34). These authors carried out a methylated DNA immunoprecipitation (MeDIP) analysis of cytosine-5 methylation in *LINE-1*, obtaining a downward trend of *LINE-1* methylation in ASD, although this difference was not statistically significant, possibly due to heterogeneity within the ASD population. However, they also observed significantly less binding of repressive MeCP2 and histone H3K9me3 to *LINE-1* sequences in the autistic cerebellum, suggesting that relaxation of epigenetic repression may have aided in increased expression. Moreover, since the results were obtained from postmortem brain samples, it could not be determined whether these observations were functionally related to the etiology or pathophysiology of autism.

A recent study with 36 ASD subjects and 20 unaffected individuals showed that the *LINE-1* methylation levels were significantly reduced in ASD individuals with severe language impairment and were inversely correlated with the transcript level (37). Nevertheless, this study was carried out using lymphoblastoid cell lines derived from peripheral mononuclear cells. Here, we report an analysis of *LINE-1* methylation status using blood samples from 50 ASD patients and 45 control individuals. Our results show a slight decrease in the levels of *LINE-1* methylation in the ASD group, compared to the normal neurodevelopmental healthy group, with the following mean values: 73.5% in ASD and 74.2% in controls. Although these differences in the pattern of *LINE-1* methylation between the ASD group and the control group are not statistically significant, they are higher than those observed in relevant studies also carried out by pyrosequencing in other neurodegenerative diseases. In this regard, Bollati et al. (38) evaluated methylation of *ALU*, *LINE-1* (same CpGs fragment than in the present study), and *SAT-α* sequences in blood samples from 43 patients with Alzheimer's disease (AD) and 38 healthy donors. *LINE-1* methylation increased in AD patients, compared to healthy volunteers, obtaining the following mean methylation values: AD 83.6% and volunteers 83.1% (*p*-value: 0.05).

Furthermore, our study focused on a *LINE-1* fragment containing 5 CpG positions for analysis. Remarkably, we observed a statistically significant decrease in methylation levels at position 2 of the *LINE-1* analyzed fragment, which is then

reflected in the subgroup of children with mental regression. Thus, while the mean CpG 2 methylation value of *LINE-1* in healthy controls is 72.97%, it falls to 71.15% in the subgroup of AMR children (*p*-value: 0.047). This result should be interpreted as a strong indicator for expanding the *LINE-1* study region. Therefore, a more in-depth future study of *LINE-1* methylation patterns in patients with ASD and healthy controls with an enlarged analyzed region is needed.

Quantification of DNA methylation in candidate gene promoters using different samples (blood, specific regions in post-mortem brain) from patients with ASD has identified differentially methylated regions (DMR) in OXTR, SHANK3, UBE3A, and MECP2 at CpG sites of specific promoters (5–9). Increasing evidence suggests that growth factors modulate motor, emotional and cognitive functions, which may account for the clinical manifestations of several disorders (39). NGF belongs to the neurotrophin family and is considered a key regulator of the development, differentiation, survival and regeneration of nerve cells. NGF is present mainly in highly functional brain regions. Previous studies from our group of the same cohort of ASD children as this study, as well as other groups of children with this disorder, have shown increased levels of *NGF* in children with ASD (27). Moreover, in this disorder, different subgroups considering the presence or absence of neurodevelopmental regression have been reported (40, 41). Our results seem to support these notions, since we found different *NGF* methylation patterns in both subgroups, AMR and ANMR. In this regard, approximately half of both children diagnosed with ASD (47%) and typically developing children (53%) have lower-than-mean levels of *NGF* methylation.

These results are consistent with those previously observed by our group, in which *NGF* was detected in <50% of the children with ASD and typically developing children (27). More specifically, while only 39% of the ANMR subgroup showed increased levels of *NGF* methylation, this value rose to more than 60% in the AMR subgroup, suggesting a possible higher expression of *NGF* in the first subgroup. This is precisely what we showed in our previously published results, using samples from the same individuals, where the ANMR subgroup exhibited higher *NGF* levels than the typically developing children (27), making even more plausible the suggestion that these observations might indicate a disturbance in neuronal development, and pointing to *NGF* as a possible biomarker in autism disorder.

NCAM1 is a glycoprotein mainly expressed on the surface of nerve cells, in the central and peripheral nervous tissue of vertebrates, and acts as an adhesion molecule between cells and their extracellular environment (14, 41). It plays a critical role in the developmental and plasticity pathways of the nervous system (8). *NCAM1* may accumulate in presynaptic and postsynaptic membranes and it has been associated with behavioral phenotypes in ASD children (42). Changes in DNA methylation have not yet been described at the *NCAM1* level. In the present study, we reported that when compared to the typically developing children subgroup, higher levels of *NCAM1* methylation were observed in children with ASD, without differentiation between the AMR and the ANMR subgroups. Interestingly, and in agreement with these data, our previous studies found lower plasma levels of *NCAM1* in the same subgroup of ASD children without neurodevelopmental regression, compared to the levels in the subgroup of typically developing children (27). *NCAM1* could be suggested as a possible biomarker, capable of contributing to the diagnostic process of the autistic disorder.

In conclusion, given the high heterogeneity in ASD, it is essential to know the biological factors that trigger this disorder to understand the behavioral variability of the patients. Identification of epigenetic biomarkers based on changes in DNA methylation could help to clarify the pathophysiology of autism, facilitating its diagnosis and prognosis. To date, a consensus has not yet been generated on the gene's specific methylation signature for autism. In this study, we provide new clues about the epigenetic changes that occur in the autistic disorders as well as a clear differentiation in DNA methylation between the ASD subgroups, according to the presence or absence of mental regression. Thus, we have reported a differentially methylated CpG position in the *LINE-1* retrotransposon between healthy children and children with ASD. In addition, we have pointed two candidate genes, *NGF* and *NCAM1*, as potential epigenetic biomarkers that would facilitate the diagnosis of the disorder. Finally, the findings of this study are in line with previous research and reinforce our understanding of this disorder. However, we consider that further investigation is necessary in this line of research.

DATA AVAILABILITY STATEMENT

The raw data supporting the conclusions of this article will be made available by the authors, without undue reservation.

ETHICS STATEMENT

The studies involving human participants were reviewed and approved by Ethics Committee of Investigation of Cordoba. Written informed consent to participate in this study was provided by the participants' legal guardian/next of kin.

AUTHOR CONTRIBUTIONS

MVG-O, TM-R, MT-A, TR-A, RRA, and JP-N were involved in planning and supervised the work. AG-F, KF-R, PM-B, and MT-A processed the clinical data. MVG-O and TM-R processed the experimental data and performed the analysis. MVG-O, TR-A, MG-C, MT-A, and JP-N drafted the manuscript. All authors discussed the results and commented on the manuscript.

SUPPLEMENTARY MATERIAL

The Supplementary Material for this article can be found online at: https://www.frontiersin.org/articles/10.3389/fped.2021.685310/full#supplementary-material

REFERENCES

1. Menezo YJ, Elder K, Dale B. Link between increased prevalence of autism spectrum disorder syndromes and oxidative stress, DNA methylation, and imprinting: the impact of the environment. *JAMA Pediatr.* (2015) 169:1066–7. doi: 10.1001/jamapediatrics.2015.2125
2. Fombonne E. Epidemiology of autistic disorder and other pervasive developmental disorders. *J Clin Psychiatry.* (2005) 66(Suppl. 10):3–8.
3. Yoon SH, Choi J, Lee WJ, Do JT. Genetic and epigenetic etiology underlying autism spectrum disorder. *J Clin Med.* (2020) 9:966. doi: 10.3390/jcm9040966
4. Wen Z, Cheng TL, Li GZ, Wen Z, Cheng TL, Li GZ, et al. Identification of autism-related MECP2 mutations by whole-exome sequencing and functional validation. *Mol Autism.* (2017) 8:43. doi: 10.1186/s13229-017-0157-5
5. Elagoz Yuksel M, Yuceturk B, Faruk Karatas O, Ozen M, Dogangun B. The altered promoter methylation of oxytocin receptor gene in autism. *J Neurogenet.* (2016) 30:280–4. doi: 10.1080/01677063.2016.1202951
6. Gregory SG, Connelly JJ, Towers AJ, Johnson J, Biscocho D, Markunas CA, et al. Genomic and epigenetic evidence for oxytocin receptor deficiency in autism. *BMC Med.* (2009) 7:62. doi: 10.1186/1741-7015-7-62
7. Jiang YH, Sahoo T, Michaelis RC, Bercovich D, Bressler J, Kashork CD, et al. A mixed epigenetic/genetic model for oligogenic inheritance of autism with a limited role for UBE3A. *Am J Med Genet A.* (2004) 131:1–10. doi: 10.1002/ajmg.a.30297
8. Nagarajan RP, Hogart AR, Gwye Y, Martin MR, LaSalle JM. Reduced MeCP2 expression is frequent in autism frontal cortex and correlates with aberrant MECP2 promoter methylation. *Epigenetics.* (2006) 1:e1–11. doi: 10.4161/epi.1.4.3514
9. Zhu L, Wang X, Li XL, Towers A, Cao X, Wang P, et al. Epigenetic dysregulation of SHANK3 in brain tissues from individuals with autism spectrum disorders. *Hum Mol Genet.* (2014) 23:1563–78. doi: 10.1093/hmg/ddt547
10. Tremblay MW, Jiang YH. DNA methylation and susceptibility to autism spectrum disorder. *Annu Rev Med.* (2019) 27:151–66. doi: 10.1146/annurev-med-120417-091431
11. Bailey A, Le Couteur A, Gottesman I, Bolton P, Simonoff E, Yuzda E, et al. Autism as a strongly genetic disorder: evidence from a British twin study. *Psychol Med.* (1995) 25:63–77. doi: 10.1017/S0033291700028099
12. Goldberg AD, Allis CD, Bernstein E. Epigenetics: a landscape takes shape. *Cell.* (2007) 23:635–8. doi: 10.1016/j.cell.2007.02.006
13. Jones PA. Functions of DNA methylation: islands, start sites, gene bodies and beyond. *Nat Rev Genet.* (2012) 29:484–92. doi: 10.1038/nrg3230
14. Vogel Ciernia A, LaSalle J. The landscape of DNA methylation amid a perfect storm of autism aetiologies. *Nat Rev Neurosci.* (2016) 17:411–23. doi: 10.1038/nrn.2016.41
15. Grayson DR, Guidotti A. Merging data from genetic and epigenetic approaches to better understand autistic spectrum disorder. *Epigenomics.* (2016) 8:85–104. doi: 10.2217/epi.15.92
16. Keil KP, Lein PJ. DNA methylation: a mechanism linking environmental chemical exposures to risk of autism spectrum disorders. *Environ Epigenet.* (2016) 2:dvv012. doi: 10.1093/eep/dvv012
17. Loke YJ, Hannan AJ, Craig JM. The role of epigenetic change in autism spectrum disorders. *Front Neurol.* (2015) 26:107. doi: 10.3389/fneur.2015.00107
18. Siu MT, Weksberg R. Epigenetics of autism spectrum disorder. *Adv Exp Med Biol.* (2017) 978:63–90. doi: 10.1007/978-3-319-53889-1_4
19. Wiśniowiecka-Kowalnik B, Nowakowska BA. Genetics and epigenetics of autism spectrum disorder-current evidence in the field. *J Appl Genet.* (2019) 60:37–47. doi: 10.1007/s13353-018-00480-w
20. Ladd-Acosta C, Hansen KD, Briem E, Fallin MD, Kaufmann WE, Feinberg AP. Common DNA methylation alterations in multiple brain regions in autism. *Mol Psychiatry.* (2014) 19:862–71. doi: 10.1038/mp.2013.114
21. Andrews SV, Ellis SE, Bakulski KM, Sheppard B, Croen LA, Hertz-Picciotto I, et al. Cross-tissue integration of genetic and epigenetic data offers insight into autism spectrum disorder. *Nat Commun.* (2017) 24:1011. doi: 10.1101/091330
22. Andrews SV, Sheppard B, Windham GC, Schieve LA, Schendel DE, Croen LA, et al. Case-control meta-analysis of blood DNA methylation and autism spectrum disorder. *Mol Autism.* (2018) 28:40. doi: 10.1101/320622
23. De Rubeis S, He X, Goldberg AP, Poultney CS, Samocha K, Cicek AE, et al. Synaptic, transcriptional and chromatin genes disrupted in autism. *Nature.* (2014) 13:209–15. doi: 10.1038/nature13772
24. Cordaux R, Batzer MA. The impact of retrotransposons on human genome evolution. *Nat Rev Genet.* (2009) 10:691–703. doi: 10.1038/nrg2640
25. Han JS, Szak ST, Boeke JD. Transcriptional disruption by the L1 retrotransposon and implications for mammalian transcriptomes. *Nature.* (2004) 20:268–74. doi: 10.1038/nature02536
26. Kitkumthorn N, Mutirangura A. Long interspersed nuclear element-1 hypomethylation in cancer: biology and clinical applications. *Clin Epigenetics.* (2011) 2:315–30. doi: 10.1007/s13148-011-0032-8
27. Gomez-Fernandez A, de la Torre-Aguilar MJ, Gil-Campos M, Flores-Rojas K, Cruz-Rico MD, Martin-Borreguero P, et al. Children with autism spectrum disorder with regression exhibit a different profile in plasma cytokines and adhesion molecules compared to children without such regression. *Front Pediatr.* (2018) 26:264. doi: 10.3389/fped.2018.00264
28. APA. *DSM-V.* (2013). Available online at: http://www.dsm5.org/Pages/Default.aspx
29. Beck CR, Garcia-Perez JL, Badge RM, Moran JV. LINE-1 elements in structural variation and disease. *Annu Rev Genomics Hum Genet.* (2011) 12:187–215. doi: 10.1146/annurev-genom-082509-141802
30. Plioplys AV, Hemmens SE, Regan CM. Expression of a neural cell adhesion molecule serum fragment is depressed in autism. *J Neuropsychiatry Clin Neurosci.* (1990) 2:413–7. doi: 10.1176/jnp.2.4.413
31. Purcell AE, Rocco MM, Lenhart JA, Hyder K, Zimmerman AW, Pevsner J. Assessment of neural cell adhesion molecule (NCAM) in autistic serum and postmortem brain. *J Autism Dev Disord.* (2001) 31:183–94. doi: 10.1023/A:1010751232295
32. Guney E, Ceylan MF, Kara M, Tekin N, Goker Z, Senses Dinc G, et al. Serum nerve growth factor (NGF) levels in children with attention deficit/hyperactivity disorder (ADHD). *Neurosci Lett.* (2014) 7:107–11. doi: 10.1016/j.neulet.2013.12.026
33. Anton L, Brown AG, Bartolomei MS, Elovitz MA. Differential methylation of genes associated with cell adhesion in preeclamptic placentas. *PLoS ONE.* (2014) 25:e100148. doi: 10.1371/journal.pone.0100148
34. Shpyleva S, Melnyk S, Pavliv O, Pogribny I, Jill James S. Overexpression of LINE-1 retrotransposons in autism brain. *Mol Neurobiol.* (2018) 55:1740–9. doi: 10.1007/s12035-017-0421-x
35. Murphy BC, O'Reilly RL, Singh SM. Site-specific cytosine methylation in S-COMT promoter in 31 brain regions with implications for studies involving schizophrenia. *Am J Med Genet B Neuropsychiatr Genet.* (2005) 5:37–42. doi: 10.1002/ajmg.b.30134
36. Kaminsky Z, Tochigi M, Jia P, Pal M, Mill J, Kwan A, et al. A multi-tissue analysis identifies HLA complex group 9 gene methylation differences in bipolar disorder. *Mol Psychiatry.* (2012) 17:728–40. doi: 10.1038/mp.2011.64
37. Tangsuwansri C, Saeliw T, Thongkorn S, Chonchaiya W, Suphapeetiporn K, Mutirangura A, et al. Investigation of epigenetic regulatory networks associated with autism spectrum disorder (ASD) by integrated global LINE-1 methylation and gene expression profiling analyses. *PLoS ONE.* (2018) 23:13:e0201071. doi: 10.1371/journal.pone.0201071
38. Bollati V, Galimberti D, Pergoli L, Dalla Valle E, Barretta F, Cortini F, et al. DNA methylation in repetitive elements and Alzheimer disease. *Brain Behav Immun.* (2011) 25:1078–83. doi: 10.1016/j.bbi.2011.01.017
39. Galvez-Contreras AY, Campos-Ordonez T, Gonzalez-Castaneda RE, Gonzalez-Perez O. Alterations of growth factors in autism and attention-deficit/hyperactivity disorder. *Front Psychiatry.* (2017) 8:126. doi: 10.3389/fpsyt.2017.00126
40. Kern JK, Geier DA, Geier MR. Evaluation of regression in autism spectrum disorder based on parental reports. *N Am J Med Sci.* (2014) 6:41–7. doi: 10.4103/1947-2714.125867
41. Xi CY, Hua TY, Zhao YJ, Liu XM. Characteristics of developmental regression in autistic children. *Zhongguo Dang Dai Er Ke Za Zhi.* (2010) 12:781–3.
42. Yang X, Zou M, Pang X, Liang S, Sun C, Wang J, et al. The association between NCAM1 levels and behavioral phenotypes in children with autism spectrum disorder. *Behav Brain Res.* (2019) 1:234–8. doi: 10.1016/j.bbr.2018.11.012

Conflict of Interest: The authors declare that the research was conducted in the absence of any commercial or financial relationships that could be construed as a potential conflict of interest.

Publisher's Note: All claims expressed in this article are solely those of the authors and do not necessarily represent those of their affiliated organizations, or those of the publisher, the editors and the reviewers. Any product that may be evaluated in this article, or claim that may be made by its manufacturer, is not guaranteed or endorsed by the publisher.

frontiers in Genetics

CASE REPORT
published: 08 October 2021
doi: 10.3389/fgene.2021.743833

Case Report: A Case of Epileptic Disorder Associated With a Novel *CNTN2* Frameshift Variant in Homozygosity due to Maternal Uniparental Disomy

Wenjie Chen[1,2†], *Fei Chen*[3], *Yiping Shen*[3,4,5,6*†], *Zhixian Yang*[7] *and Jiong Qin*[1*†]

[1]Department of Paediatrics, Peking University People's Hospital, Beijing, China, [2]Department of Neurology, Guangzhou Women and Children's Medical Center, Guangzhou, China, [3]The Maternal and Child Health Care Hospital of Guangxi Zhuang Autonomous Region, Guangxi Birth Defects Prevention and Control Institute, Guangxi, China, [4]Department of Medical Genetics, Shanghai Children's Medical Center, Shanghai Jiao Tong University School of Medicine, Shanghai, China, [5]Division of Genetics and Genomics, Boston Children's Hospital, Boston, MA, United States, [6]Department of Neurology, Harvard Medical School, Boston, MA, United States, [7]Department of Pediatrics, Peking University First Hospital, Beijing, China

Background: Contactin 2, encoded by *CNTN2* on chromosome 1q32.1, is a neural-specific glycoprotein and plays important roles in neurodevelopment. A deleterious homozygous variant in the *CNTN2* gene was previously reported to cause autosomal recessive cortical myoclonic tremor and epilepsy. Since then, there has been no further report confirming the association of *CNTN2* and epilepsy. Here, we reported one new case, who presented with epilepsy, carrying a novel homozygous frameshift variant in *CNTN2*. The clinical and genetic features of the patient were reviewed.

Case presentation: The male patient presented with preschool age-of-onset neurodevelopmental impairment and focal seizures of temporal origin, and responded to valproate. A trio-whole exome sequencing revealed a novel homozygous frameshift variant in *CNTN2* (c.2873_c.2874delCT, p.Thr958Thrfs). The patient's mother was a heterozygous carrier while his father was wild-type; they were both unaffected and non-consanguineous. Further study revealed that maternal uniparental disomy (1q32.1) unmasked the heterozygous variant of *CNTN2* in the proband.

Conclusions: This case enhanced the gene–disease relationship between *CNTN2* and epilepsy, which will help to further understand this emerging disorder.

Keywords: *CNTN2*, epilepsy, uniparental disomy (UPD), neurodevelopmental disorder (NDD), genotype-phenotype correlation

OPEN ACCESS

Edited by:
Prof. Anjana Munshi,
Central University of Punjab, India

Reviewed by:
Thomas Liehr,
Friedrich Schiller University Jena, Germany
Liang-Liang Fan,
Central South University, China

***Correspondence:**
Jiong Qin
qinjiong@pkuph.edu.cn
Yiping Shen
yiping.shen@childrens.harvard.edu

†***ORCID**:*
Wenjie Chen
orcid.org/0000-0001-9884-2270
Jiong Qin
orcid.org/0000-0002-9109-3286
Yiping Shen
orcid.org/0000-0001-5820-0839

Specialty section:
This article was submitted to Genetics of Common and Rare Diseases, a section of the journal Frontiers in Genetics

Received: *19 July 2021*
Accepted: *08 September 2021*
Published: *08 October 2021*

Citation:
Chen W, Chen F, Shen Y, Yang Z and Qin J (2021) Case Report: A Case of Epileptic Disorder Associated With a Novel CNTN2 *Frameshift Variant in Homozygosity due to Maternal Uniparental Disomy. Front. Genet. 12:743833. doi: 10.3389/fgene.2021.743833*

BACKGROUND

One deleterious homozygous mutation in the contactin two gene (*CNTN2*) was previously reported to be associated with epilepsy, familial adult myoclonic, 5 (FAME5, OMIM 615400) (Stogmann et al., 2013). The reported patients were from a consanguineous Egyptian family. He presented with early adolescence onset focal epilepsy which responded well to carbamazepine treatment. Myoclonus developed soon after seizure; he also presented with neuropsychiatric symptoms and borderline

cognitive level. However, controversy exists about the diagnosis of "familial cortical myoclonic tremor with epilepsy" (FCMTE) that Stogmann et al. established in the report (Striano et al., 2013). Striano et al. have challenged about the nature of tremors that Stogmann et al. described as cortical origin. In addition, Striano et al. also inquired the difference of inheritance pattern presenting in the family compared with the previous patients with FCMTE (Striano et al., 2013).

Given the small number of mutations and lack of phenotypic information, the relationship between *CNTN2* and epileptic disorder is of limited support at this time. Reporting of additional case can further enhance the causal relationship and better understand the genotypic and phenotypic spectra. Herein, we presented a Chinese patient with cognitive and behavior deficit, neuropsychiatric disorders, and pediatric epilepsy of temporal origin, who carried a novel homozygous frameshift variant p.Thr958Thrfs in *CNTN2* gene. Moreover, we also reported an unusual inheritance of the *CNTN2* variant involving maternal uniparental disomy (UPD).

CASE PRESENTATION

The 7-year-old boy was born at full term by cesarean section; his parents were healthy and non-consanguineous Chinese Han. The parents denied any family history of neurologic disease. The boy had his first attack of generalized tonic-clonic seizure at the age of 5 years. Seizures lasted for 4–5 min and 2–3 times per month at initiation.

Levetiracetam (LEV) was given 4 months later after the first seizure and seizure was free. However, 3 months later, seizure was recurrent and was refractory to control even with the highest dose of LEV (50 mg/kg/day). Since then, seizure became frequent and focal seizure types evolved including 1) attacks with presentation of fear or panic followed by a scared scream, hand holding and scratching, foot pedaling, then loss of awareness, followed by swallow and eye blink that lasted for 30–90 s, which occurred up to 6–7 attacks per day; and 2) pause in activity, gazing, then loss of awareness, followed by swallow or jerking of left facial muscle that lasted for 10 s to 1 min, several times a day. Oxcarbazepine (OXC, 30 mg/kg/day) was added 6 months later, yet it was still ineffective.

He had a history of development delay before seizure onset, mainly presenting in learning ability, and seizures had been exacerbating his poor academic performance based on the description of his parents. On examination at the age of 7 years, his cognitive function was impaired at mild-moderate level, including learning difficulties, memory deficits, hyperactivity, and attention deficit, and could not handle well with schoolwork. In addition, he also behaved aggressively and impulsively. The previous VEEG showed left temporal-PG1-frontal interictal epileptiform discharges, ictal suggesting temporal and frontal lobe origin. Brain MRI revealed no abnormality. We prescript valproate (VPA) to the patient and ordered a trio-exome sequencing.

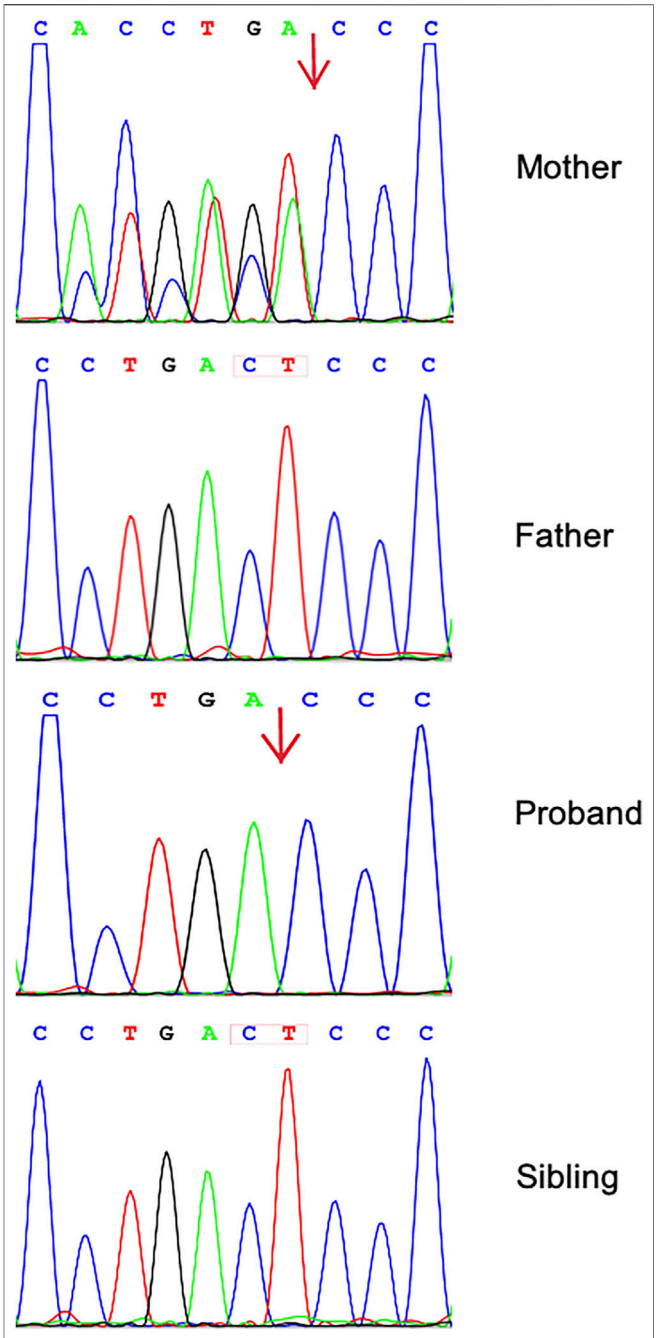

FIGURE 1 | Sequence analysis of *CNTN2* gene from the family. Chromatograms showing that the mother is heterozygous for c.2873_c.2874delCT (p.Thr958Thrfs*17). The proband shows a homozygosity of the mutation; his father and little brother have wild-type sequence.

SEQUENCING METHODS

Genomic DNA was extracted from peripheral blood samples of the proband and his parents. We planned a proband–parent trio approach. Exome data processing, variant calling, and variant annotation were performed by the Chigene Translational Medicine Research Center (Beijing, China) as a clinical service. For whole-exome sequencing (WES), sequencing library was created by Agilent SureSelect Human All Exon V6 Kit (Agilent Technologies, Santa Clara, CA) in accordance with

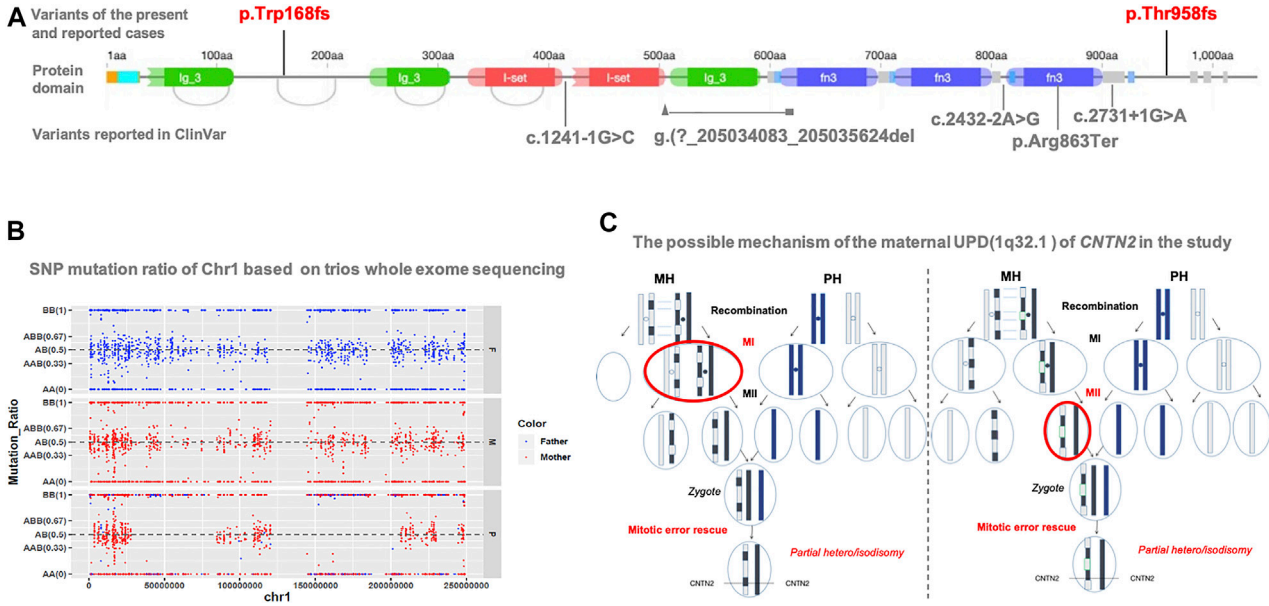

FIGURE 2 | (**A**) Protein structure of CNTN2 and localization of variants reported in the present study, previous literature (red), and ClinVar database (gray). This present variant (red: c.2873_c.2874delCT, p.T958Tfs*17) is in the second last exon but within the last 50aa. There is only one publication (NM_005076.5: c.504del, p.Trp168fs) reported with FAME5. Another five reported loss-of-function variants in ClinVar lack detailed clinical information. The origin graph of protein domain is cited from DECIPHER (https://www.deciphergenomics.org/). **(B)** SNP analysis reveals the altered regions on chromosome 1, including maternal heterodisomy at chr1: 1-26488019, chr1: 79411951-150123132, and chr1:206230986-249250621; and maternal isodisomy at chr1: 26488019-49511248, chr1: 50957509-79411951, and chr1: 150123132-206230986 (**C**) Based on the results of SNP analysis, the possible mechanism that results in the mixture pattern of uniparental disomy (UPD) is recombination of maternal homologs (MH) before Meiosis I, then LEFT: chromosome segregation error at Meiosis I (MI), or RIGHT: chromosome segregation error at Meiosis II (MII), and then a rescuing segregation error in the zygote. For simplicity, we only show the chromatid of chromosome pair for UPD with partial hetero/isodisomy. Paternal homologs (PH).

the manufacturer's protocol. The prepared libraries were sequenced with a HiSeq2500 (Illumina, San Diego, CA). The Genome Analysis Toolkit (GATK) was used for variant calling (GATK HaplotypeCaller) (McKenna et al., 2010). A total of >99% of reads were mapped to genomic targets, with 20× coverage for >95% of bases. In the proband, a total of 118,818 variants were identified in exonic and splice site regions. "Rare deleterious" mutations were defined as those that met the following criteria: 1) their alternative allele frequencies were ≤0.5% in gnomAD database and our local database; 2) the severity of the impact on the protein should be high, such as a stop-gain, stop-loss, nonsense, frameshift, or splice-site mutation. The standard of missense mutation is REVEL ≥0.75 or all the prediction tools score as Damaging; 3) the clinical manifestations of the patient should closely associate with the disease phenotype. All of the mutations were classified following the ACMG/AMP guidelines to define (Richards et al., 2015). We comprehensively evaluated the pathogenicity, frequency, and clinical manifestations of the mutation. Sanger sequencing was used to verify the authenticity of the mutations.

SEQUENCING RESULTS

We identified 11,287 variants existing in genes that matched with known phenotypes. Variants from 1,683 genes associated with epilepsy were subsequently extracted, leading to the identification of a novel homozygous frameshift variant (c.2873_c.2874delCT, p.Thr958Thrfs*17) in the *CNTN2* gene (RefSeq NM_005076) (**Supplementary Table 1**). Parental WES data and Sanger analysis of the mutation revealed that one copy of the variant was inherited from his unaffected mother; the other variant was not detected in the father's genome. He has a healthy little brother who carried no variant at this locus (**Figure 1**).

This variant is not in gnomAD. It is located in the second last exon but not within the last 50aa; this frameshift variant is expected to result in a null product due to nonsense-mediated decay. On investigation, only one loss-of-function variant of *CNTN2* has been reported in an individual with a similar presentation as our patient (Stogmann et al., 2013). Five loss-of-function variants (c.1241-1G>C; c.2432-2A>G; g. (?_205034083_205035624del; c.2587C>T; c.2731 + 1G > A) are reported in ClinVar as pathogenic or likely pathogenic (**Figure 2A**). In the HGMD database, six heterozygous variants including four missense, one splice, and one nonsense variant are recorded. The nonsense variant (p.Tyr585Ter) was reported to be associated with autosomal recessive intellectual disability (Harripaul et al., 2018). All other variants were not reported to be associated with a specific phenotype.

The frameshift variant detected in our patient can be classified as pathogenic following the ACMG/AMG guideline (PVS1, PM2_P, PM3_P). Given the atypical inheritance pattern in this case, possibilities including maternal UPD or a paternal deletion including the *CNTN2* locus (at least exon 22) were examined. WES-based copy number analysis of the father's

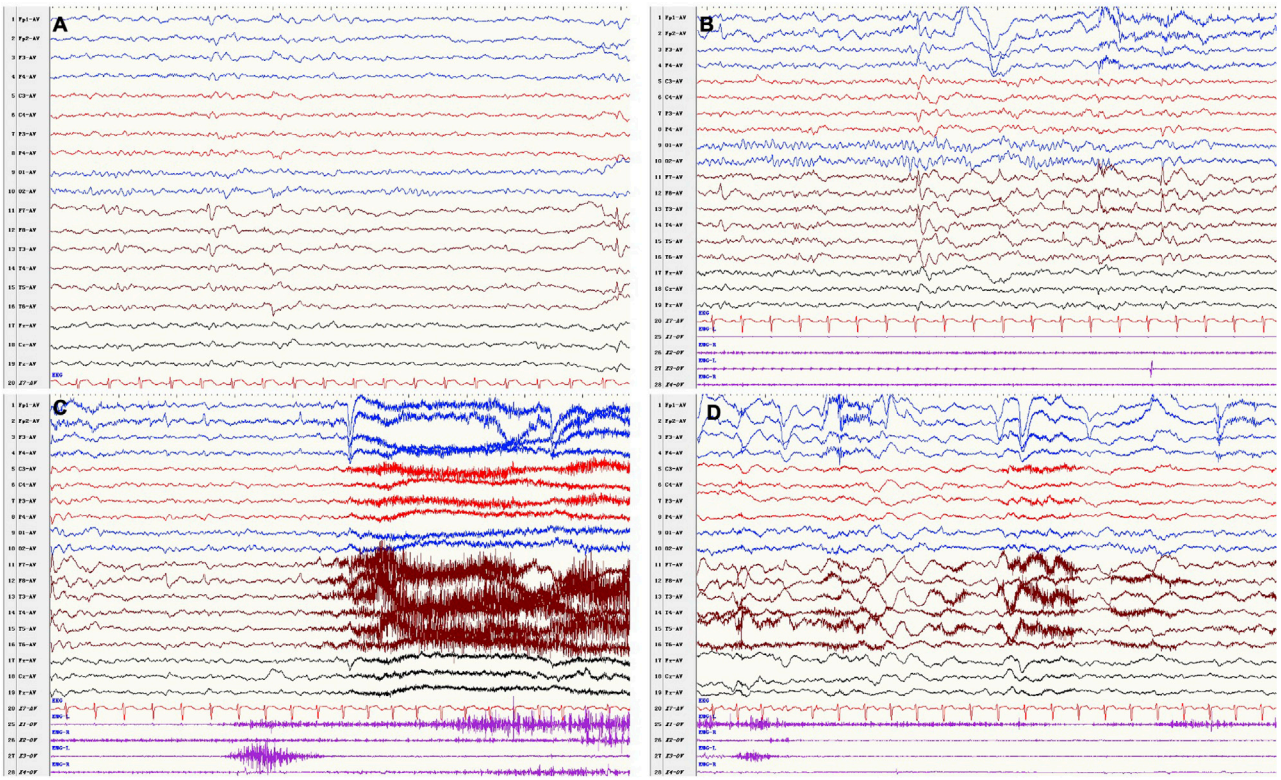

FIGURE 3 | VEEG after drug withdrawal at 10 years 8 months. Interictal **(A,B)**: bilateral frontal–temporal epileptiform discharges, **(B)** was the background a few seconds before the onset. Ictal **(C,D)** recorded a focal seizure (fear, closed eyes, vocalization, forward and backward movements of the hips, pedaling movements of lower limbs) in awake period.

genomic DNA yielded normal results and a further qPCR detecting genomic copy number abnormalities of exon 22 in *CNTN2* from his father.

As expected, SNP mutation ratio of Chr1 based on trios-WES showed the maternal UPD of chromosome 1 [UPD (1)mat] in the proband. It revealed the altered regions on chromosome one; maternal heterodisomy at chr1:1-26488019, chr1:79411951-150123132, and chr1:206230986-249250621; and maternal isodisomy at chr1: 26488019-49511248, chr1: 50957509-79411951, and chr1: 150123132-206230986 (**Figure 2B**). *CNTN2* is located on chromosome 1q32.1, from chr1: 205042937 to 205078289, exactly where the isodisomy of chr1: 150123132-206230986 occurred.

FOLLOW-UP

At the follow-up of 9 years old, he had been seizure free for 26 months since add-on therapy of VPA (9.3 mg/kg/day) with OXC remaining at 16.7 mg/kg/day, and LEV had been withdrawn 18 months earlier. The parents of the patient complained that the attack of behavior arrest occurred occasionally, which lasted for less than 10 s. However, EEG failed to monitor the ictal epileptiform discharges. By the last visit, the boy was 10 years 8 months; he had seizure relapse when his parents were trying to withdraw VPA and OXC. The seizure type and ictal EEG were similar as before (**Figure 3**), and a recurrent brain MRI did not show any abnormality. His seizure was under control with sufficient dose of VPA and OXC. He remained to have cognitive and behavioral deficits, as well as emotional regulation problem. He has normal growth.

DISCUSSION

We reported a non-consanguineous Han male with homozygous c.2873_c.2874delCT, p.T958Tfs*17 mutation in *CNTN2*, onset with generalized seizure and evolved into focal seizure (**Table 1**). At present, there was only one family reported worldwide with mutations in *CNTN2* and similar clinical presentation (Stogmann et al., 2013). According to the evidence accumulated from public databases such as HGMD, gnomAD, and ClinVar (**Figure 2A**), all the variants classified as pathogenic/likely pathogenic belong to loss-of-function.

This is a potentially important case for upgrading the gene–disorder relationship for this emerging seizure disorder. Similar to those patients reported by Stogmann et al. (2013), the patient showed focal seizures, which was indicative of a temporal origin in EEG, and cranial MRI revealing no abnormality. In addition, almost all patients demonstrated a non-progressive course on anti-epileptic therapy.

However, unlike previous patients with familial cortical myoclonic tremor with epilepsy (FCMTE) (Striano and Zara,

TABLE 1 | Summary of *CNTN2* mutations and main clinical features.

	Stogmann et al. (2013)					This report
Individual (sex)	1 (M)	2 (F)	3 (F)	4 (F)	5 (F)	6 (M)
Mutation (NM_005076.5)	p.Trp168fs					p.Thr958Thrfs*17
Age at seizure onset (years)	11	14	11	12	11	6
Age at follow-up (years)	39	37	29	24	21	10.7 (age at last follow-up)
Seizure type	GTCS, CPS	GTCS, CPS	GTCS, CPS	GTCS, CPS	GTCS, CPS	GTCS, CPS
Aura	—	—	—	—	—	–
Cortical tremor	+	+	+	+	+	–
Myoclonic jerks	–	+	+	+	–	–
Cognitive function	NA	IQ 85	IQ 86	IQ 79	IQ 78	Learning difficulties, memory deficits, ADHD traits
Mental disorder	—	—	—	Depressive symptoms	Depressive symptoms	Aggressive, impulsive
Cranial MRI/CT	Normal	Normal	Normal	Normal	MRI bilateral mS	Normal
EEG	—	Temporal IEDs	Normal	Tempoparietal IEDs	Temporal IEDs	T-F IEDs; ictal: T, F onset
AEDs	CBZ	CBZ	CBZ	CBZ, LTG	CBZ	VPA, OXC
Outcomes of AEDs	Good	Good	Good	Poor	Good	Good

M, male; F, female; GTCS, generalized tonic-clonic seizure; CPS, complex partial seizure; IQ, intelligence quotient; OXC, oxcarbazepine; VPA, valproate; LTG, lamotrigine; NA, not available; IED, interictal epileptic discharge; T, temporal; F, frontal; ADHD, attention-deficit hyperactivity disorder; mS, mesial sclerosis.

2016), the manifestation of myoclonus was not observed in our patient throughout the course of disease. It is unclear whether this symptom was an aspect of *CNTN2*-associated disorder or not.

Furthermore, by summarizing the clinical manifestation of the patients with homozygous mutation in *CNTN2*, we found that focal epilepsy is the main clinical feature, in conjunction with other neuropsychiatric symptoms, whereas our patient displayed more apparent cognitive impairment and emotional regulation problem than previous patients with FCMTE.

Evidence from Harripaul et al.'s study provide a suggestion that loss-of-function variants in *CNTN2* might be responsible for the neuropsychiatric symptoms. In that study, a nonsense variant (p.Tyr585Ter) of *CNTN2* was detected, although it was only supplemented as a candidate gene of autosomal recessive intellectual disability (Harripaul et al., 2018).

Rather than the only explanation of FCMTE, this spectrum of symptoms is more likely to be a consequence of clinical or genetic heterogeneity of *CNTN2*-associated disorder. Due to the limited number of such a rare disease, more cases will help to better understand the phenotype–genotype correlation.

The special autosomal recessive (AR) inheritance presenting in our case was finally confirmed to be a UPD (1)mat of *CNTN2* on 1q32.1. UPD is the presence of a chromosome pair derived only from one parent in a disomic cell line. So far, three types of UPD including isodisomy (UPiD, both copies of a single chromosome homolog are inherited from one parent), heterodisomy (UPhD, a pair of homologous chromosomes are inherited from one parent), and partial heterodisomy/partial isodisomy (segments of both isodisomy and heterodisomy are identified across the chromosome) have been reported (Benn, 2021).

UPD is rare in health populations. In fact, it could become a pathogenic event, when UPD involves imprinted chromosomal region or gene (chromosomes 6, 7, 11, 14, 15, or 20) (Eggermann, 2020), or results in the homozygosity of recessive mutation (Yamazawa et al., 2010). This occurs as a consequence of isodisomy, when one of the parents is a carrier for recessive disorder (Yamazawa et al., 2010).

Just in the case of our study, a mixture of partial heterodisomy and partial isodisomy was identified across the maternal chromosome one from the patient (**Figure 2B**). The homozygous state of *CNTN2* mutation was the result of maternal UPiD (1q32.1).

There are many possible mechanisms leading to UPD including meiotic non-disjunction with mitotic correction, gametic complementation, mitotic segregation error, or micronuclei (Conlin et al., 2010; Kearney et al., 2011; Benn P, 2020).

Mechanism for the formation of UPD in our case is supposed to be the initial chromosome segregation error during meiosis and a rescuing segregation error in the zygote (**Figure 2C**).

The occurrence of UPD in the inheritance of autosomal recessive disorder is not very rare (yet at least uncommon), and related studies have been reported since 1988 (Spence et al., 1988; Yamazawa et al., 2010; Soler-Palacín et al., 2018).

Based on the ChromosOmics Database (Liehr T., 2021), 32 records of maternal UPD (1) have been reported (clinical significance of seven cases are unavailable, one is irrelevant). Of the 24 cases with clinical findings, 20 have relevant phenotype with responsible genes located on the UPD, and almost of them are AR (19/20). The remaining four cases are neurodevelopmental disorders without associated pathogenic genes. Yet similar case of maternal UPD (1) of *CNTN2* has not been reported.

In brief, UPD (1) can cause disease not only through imprinting defects but also through homozygous exposure of recessive genes. For fetus with UPD (1) during pregnancy examinations, the recessive genes mapped on the chromosome should be analyzed with caution, and combined

with other important clinical features, appropriate management for the genetic diagnosis and counseling should be made.

In recent years, SNP array is recommended in the detection of UPD; it was proven to play an important role in disclosing the mechanisms of UPD (Conlin et al., 2010; Kearney et al., 2011). With the advance of next-generation sequencing, a late work demonstrated that WES-based copy number analysis could also reveal UPD (Soler-Palacín et al., 2018).

Collectively, our study suggested that loss-of-function variants in *CNTN2* may be responsible for temporal epilepsy accompanied with neurodevelopmental impairment. Reporting of this new case will help to upgrade the gene–disease relationship for this emerging *CNTN2*-related disorder. We also provided clinical experience for additional choice of appropriate AEDs for *CNTN2*-related epilepsy. This case revealed a rare a mixture of maternal isodisomy and heterodisomy of chromosome one that unmasked a heterozygous variant.

DATA AVAILABILITY STATEMENT

All of the data supporting the findings in this study are available upon reasonable request from the corresponding authors.

ETHICS STATEMENT

The studies involving human participants were reviewed and approved by The Ethical Review Committee (ERC) of Peking University People's Hospital (PKUPH). Written informed consent to participate in this study was provided by the participants' legal guardian/next of kin.

AUTHOR CONTRIBUTIONS

WC: writing—original draft and study designing. FC: conducting bioinformatics analysis and study designing. ZY: providing the data of VEEG. JQ and YS: writing—review and editing. All authors contributed to the article and approved the submitted version.

FUNDING

This study was funded by the Foundation of 2018 Beijing Key Clinical Specialty Construction Project-Pediatrics (2199000726), and the Key Research Project of the Ministry of Science and Technology of China (2016YFC0904400).

ACKNOWLEDGMENTS

We thank the patient's family for participation in the study. We acknowledge Dr. Zhang G for graph edition and sequencing data verification.

SUPPLEMENTARY MATERIAL

The Supplementary Material for this article can be found online at: https://www.frontiersin.org/articles/10.3389/fgene.2021.743833/full#supplementary-material

REFERENCES

Benn, P. (2021). Uniparental Disomy: Origin, Frequency, and Clinical Significance. *Prenatal Diagn.* 41, 564–572. doi:10.1002/pd.5837

Conlin, L. K., Thiel, B. D., Bonnemann, C. G., Medne, L., Ernst, L. M., Zackai, E. H., et al. (2010). Mechanisms of Mosaicism, Chimerism and Uniparental Disomy Identified by Single Nucleotide Polymorphism Array Analysis. *Hum. Mol. Genet.* 19 (7), 1263–1275. doi:10.1093/hmg/ddq003

Eggermann, T. (2020). Prenatal Detection of Uniparental Disomies (UPD): Intended and Incidental Finding in the Era of Next Generation Genomics. *Genes* 11, 1454. doi:10.3390/genes11121454

Harripaul, R., Vasli, N., Mikhailov, A., Rafiq, M. A., Mittal, K., Windpassinger, C., et al. (2018). Mapping Autosomal Recessive Intellectual Disability: Combined Microarray and Exome Sequencing Identifies 26 Novel Candidate Genes in 192 Consanguineous Families. *Mol. Psychiatry* 23 (4), 973–984. doi:10.1038/mp.2017.60

Kearney, H. M., Kearney, J. B., and Conlin, L. K. (2011). Diagnostic Implications of Excessive Homozygosity Detected by SNP-Based Microarrays: Consanguinity, Uniparental Disomy, and Recessive Single-Gene Mutations. *Clin. Lab. Med.* 31, 595–613. doi:10.1016/j.cll.2011.08.003

Liehr, T. (2021). Cases with Uniparental Disomy. Available at: http://cs-tl.de/DB/CA/UPD/0-Start.html. (Accessed 09, 2021).

McKenna, A., Hanna, M., Banks, E., Sivachenko, A., Cibulskis, K., Kernytsky, A., et al. (2010). The Genome Analysis Toolkit: a MapReduce Framework for Analyzing Next-Generation DNA Sequencing Data. *Genome Res.* 20 (9), 1297–1303. doi:10.1101/gr.107524.110

Richards, S., Aziz, N., Aziz, N., Bale, S., Bick, D., Das, S., et al. (2015). Standards and Guidelines for the Interpretation of Sequence Variants: a Joint Consensus Recommendation of the American College of Medical Genetics and Genomics and the Association for Molecular Pathology. *Genet. Med.* 17 (5), 405–423. doi:10.1038/gim.2015.30

Soler-Palacín, P., Garcia-Prat, M., Martín-Nalda, A., Franco-Jarava, C., Rivière, J. G., Plaja, A., et al. (2018). LRBA Deficiency in a Patient with a Novel Homozygous Mutation Due to Chromosome 4 Segmental Uniparental Isodisomy. *Front. Immunol.* 9, 2397. doi:10.3389/fimmu.2018.02397

Spence, J. E., Perciaccante, R. G., Greig, G. M., Willard, H. F., Ledbetter, D. H., Hejtmancik, J. F., et al. (1988). Uniparental Disomy as a Mechanism for Human Genetic Disease. *Am. J. Hum. Genet.* 42 (2), 217–226.

Stogmann, E., Reinthaler, E., Eltawil, S., El Etribi, M. A., Hemeda, M., El Nahhas, N., et al. (2013). Autosomal Recessive Cortical Myoclonic Tremor and Epilepsy: Association with a Mutation in the Potassium Channel Associated Gene CNTN2. *Brain* 136 (Pt 4), 1155–1160. doi:10.1093/brain/awt068

Striano, P., and Zara, F. (2016). Autosomal Dominant Cortical Tremor, Myoclonus and Epilepsy. *Epileptic Disord.* 18 (2), 139–144. doi:10.1684/epd.2016.0860

Striano, P., Zara, F., Striano, S., and Minetti, C. (2013). Autosomal Recessive Epilepsy Associated with Contactin 2 Mutation Is Different from Familial Cortical Tremor, Myoclonus and Epilepsy. *Brain* 136 (Pt 10), e253. doi:10.1093/brain/awt140

Yamazawa, K., Ogata, T., and Ferguson-Smith, A. C. (2010). Uniparental Disomy and Human Disease: An Overview. *Am. J. Med. Genet.* 154C, 329–334. doi:10.1002/ajmg.c.30270

Conflict of Interest: The authors declare that the research was conducted in the absence of any commercial or financial relationships that could be construed as a potential conflict of interest.

Publisher's Note: All claims expressed in this article are solely those of the authors and do not necessarily represent those of their affiliated organizations, or those of the publisher, the editors and the reviewers. Any product that may be evaluated in this article, or claim that may be made by its manufacturer, is not guaranteed or endorsed by the publisher.

frontiers in Genetics

CASE REPORT
published: 29 October 2021
doi: 10.3389/fgene.2021.750110

Case Report: Contiguous Xq22.3 Deletion Associated with ATS-ID Syndrome: From Genotype to Further Delineation of the Phenotype

*Jan Smetana[1], Vladimira Vallova[1,2], Marketa Wayhelova[1,2], Eva Hladilkova[2], Hana Filkova[2], Vera Horinova[3], Petr Broz[4], Aneta Mikulasova[5], Renata Gaillyova[2] and Petr Kuglík[1,2]**

[1]Department of Genetics and Molecular Biology, Institute of Experimental Biology, Faculty of Science, Masaryk University, Brno, Czech, [2]Department of Medical Genetics and Genomics, University Hospital Brno, Brno, Czech, [3]Genetic Ambulance and Counseling, Jihlava, Czech, [4]Department of Biology and Medical Genetics, 2nd Faculty of Medicine, Charles University Prague and Faculty Hospital Motol, Prague, Czech, [5]Biosciences Institute, Newcastle University, Newcastle upon Tyne, United Kingdom

OPEN ACCESS

Edited by:
Santasree Banerjee,
Beijing Genomics Institute (BGI), China

Reviewed by:
Yongyi Yuan,
PLA General Hospital, China
Andrea Accogli,
Istituto Giannina Gaslini, Italy

***Correspondence:**
Petr Kuglík
kugl@sci.muni.cz

Specialty section:
This article was submitted to Genetics of Common and Rare Diseases, a section of the journal Frontiers in Genetics

Received: 30 July 2021
Accepted: 27 September 2021
Published: 29 October 2021

Citation:
Smetana J, Vallova V, Wayhelova M, Hladilkova E, Filkova H, Horinova V, Broz P, Mikulasova A, Gaillyova R and Kuglík P (2021) Case Report: Contiguous Xq22.3 Deletion Associated with ATS-ID Syndrome: From Genotype to Further Delineation of the Phenotype. Front. Genet. 12:750110. doi: 10.3389/fgene.2021.750110

Alport syndrome with intellectual disability (ATS-ID, AMME complex; OMIM #300194) is an X-linked contiguous gene deletion syndrome associated with an Xq22.3 locus mainly characterized by hematuria, renal failure, hearing loss/deafness, neurodevelopmental disorder (NDD), midface retrusion, and elliptocytosis. It is thought that ATS-ID is caused by the loss of function of *COL4A5* (*ATS*) and FACL4 (ACSL4) genes through the interstitial (micro)deletion of chromosomal band Xq22.3. We report detailed phenotypic description and results from genome-wide screening of a Czech family with diagnosis ATS-ID (proband, maternal uncle, and two female carriers). Female carriers showed mild clinical features of microscopic hematuria only, while affected males displayed several novel clinical features associated with ATS-ID. Utilization of whole-exome sequencing discovered the presence of approximately 3 Mb of deletion in the Xq23 area, which affected 19 genes from *TSC22D3* to *CHRDL1*. We compared the clinical phenotype with previously reported three ATS-ID families worldwide and correlated their clinical manifestations with the incidence of genes in both telomeric and centromeric regions of the deleted chromosomal area. In addition to previously described phenotypes associated with aberrations in *AMMECR1* and *FACL4*, we identified two genes, members of tripartite motif family *MID2* and subunit of the proteasome PA700/19S complex (*PSMD10*), respectively, as prime candidate genes responsible for additional clinical features observed in our patients with ATS-ID. Overall, our findings further improve the knowledge about the clinical impact of Xq23 deletions and bring novel information about phenotype/genotype association of this chromosomal aberration.

Keywords: ATS-MR syndrome, trio-based whole exome sequencing, genotype-phenotype analysis, neurodevelopmental disorders, Xq22.3q23 deletions

INTRODUCTION

Alport syndrome with intellectual disability (ATS-ID, AMME complex; OMIM #300194) is classified as an X-linked contiguous gene deletion syndrome associated with an Xq22.3 locus. This syndrome is characterized by hematuria, progressive renal failure, progressive sensorineural hearing loss, ocular changes, intellectual disability (ID), midface hypoplasia, and elliptocytosis (Nozu et al., 2017). Genetic basis of the disease is traditionally associated with incidence of mutation and intragenic deletion of *COL4A5* gene (Lee et al., 2019). Several other studies showed that Xq22.3 locus contains more genes associated with ID and identified two additional genes *AMMECR1* and *FACL4* as important genetic markers of the disease (Lane et al., 1994; Jonsson et al., 1998; Meloni et al., 2002b; Bhat et al., 2006; Rodriguez et al., 2010; Gazou et al., 2013). In addition, *FACL4* (*ACSL4*) was identified as the candidate gene for nonspecific ID for ATS-ID patients (Meloni et al., 2002a).

The utilization of whole-exome sequencing (WES) approach was recently used for the detection of pathological genetic variants of various clinical syndromes and diseases (Zheng et al., 2018; Dai et al., 2019; Han et al., 2020; Zhang et al., 2020). In case of ATS-ID, exome sequencing analyses provided data connecting missense and nonsense pathogenic variants in *AMMECR1* with occurrence of elliptocytosis, cardiac and bone defects, ID, and midface hypoplasia (Andreoletti et al., 2017; Basel-Vanagaite et al., 2017; Moyses-Oliveira et al., 2018). Recently, Poreau et al. described unrelated patients with 70- and 146-kbp microdeletions in Xq22.3 affecting *TMEM164* and *AMMECR1*, providing novel evidence for involvement of *AMMECR1* in the ATS-ID phenotype (Poreau et al., 2019).

In this study, we report the clinical and genome-wide characterization of a Czech family with ATS-ID (proband, maternal uncle, and two female carriers). While karyotype assessed by conventional G-banding was normal in all four patients, oligonucleotide array-based comparative genome hybridization (array-CGH) and whole-exome sequencing in this family revealed a 3-Mb deletion including *TSC22D3* at the proximal breakpoint and *CHRDL1* at the distal breakpoint site. We compared the extent of the deleted region with previously published studies and performed a genotype/phenotype correlation study to further clarify the other associated clinical features within this contiguous deletion syndrome. In addition, based on our genome-wide approach, we speculate on potential candidate genes involved in the deleted chromosomal region.

CASE DESCRIPTION

A Caucasian Czech family with affected proband and maternal uncle (**Figure 1**: IV-1 and III-5) with ATS-ID syndrome and carrier mother and maternal grandmother (**Figure 1**: III-4 and II-4) were referred by the pediatrician to genetic counseling and diagnosis because of suspected neurodevelopmental disorder (NDD).

Proband

The proband (**Figure 1**: IV-1) was born at 37 weeks of gestation with birth weight of 3,200 g and length of 48 cm. He was conceived as the first child from uncomplicated gravidity to a 24-year-old mother with a 30-year-old father, both healthy and nonconsanguineous. Shortly after birth, intubation was needed because of respiration failure. The infant was born with sepsis, hypotonia, neonatal hepatitis of undefined etiology, duplicated left renal pelvis, hyperechogenic kidneys, diffuse axonal injury, pulmonary hypertension, valvular insufficiency, aortopulmonary collaterals, micropenis, and cryptorchidism. Dysmorphic features included brachycephaly and macrocephaly, midface retrusion, hypertelorism, antimongoloid eye slants, epicanthus, synophrys, anteverted nares, dysplastic low-set ears, downturned corners of mouth, and palmar crease on his hands (**Figures 2A,B**).

Examination at the age of 13 years confirmed most dysmorphic features (epicanthus, hypertelorism, synophrys,

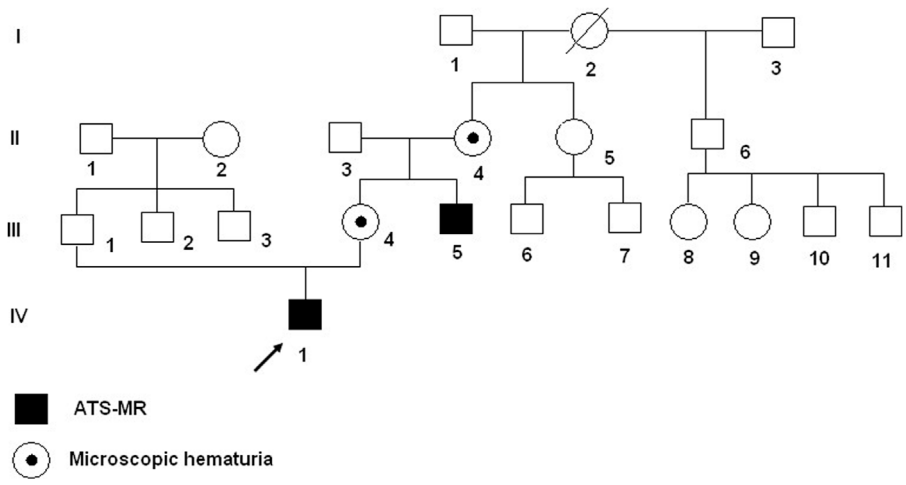

FIGURE 1 | Pedigree of the Czech family with ATS-ID syndrome. Proband (IV-1) and his maternal uncle (III-5) have hemizygous deletion in Xq22.3; the mother (III-4) and grandmother (II-4) are heterozygous for deletion Xq22.3.

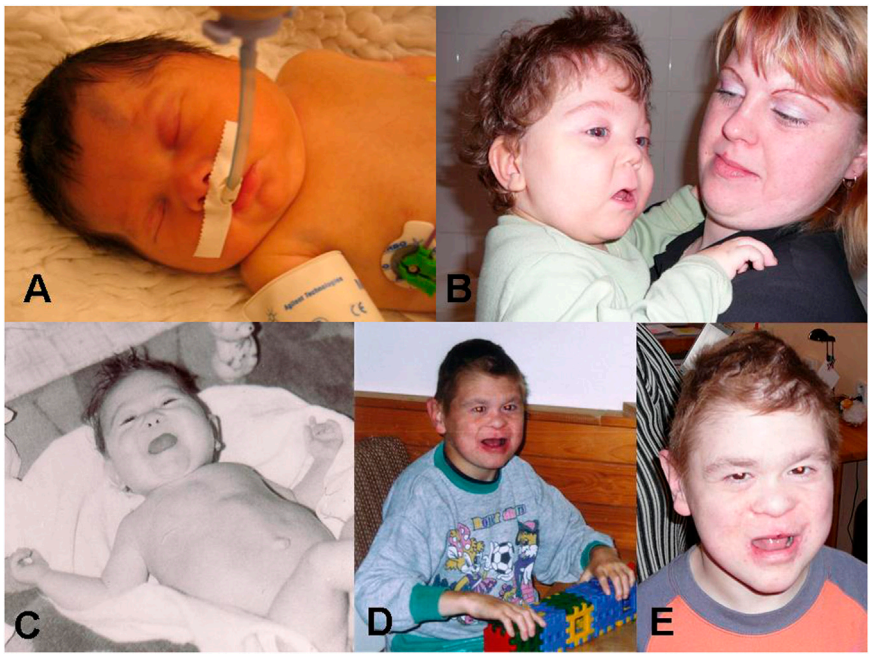

FIGURE 2 | Proband: **(A)** Short after birth. **(B)** At 2 years of age with mother. Maternal uncle: **(C)** At 10 months of age. **(D)** At 17 years of age. **(E)** At 20 years of age.

microcephaly, dysplastic low-set ears, downturned corners of mouth, palmar crease on both hands, widely spaced teeth, and caries) and showed severe NDD. There is no speech at all (his own few words and crooning); he is better receptive than expressive, and he is able to do simple tasks, but must be fed, spoon-food only. He is not able to keep cleanliness requirements and has fits of laughter. Also, attention deficit, instability, and mild aggressiveness were observed. He started to walk at 3 years; his walk is tentative with ataxic gait. At 13 years, the proband is approximately 140 cm in height with beginning puberty (pubic hair). Testes are *in situ* with normal male genitalia.

The proband has partial deafness (40%). He underwent cataract surgery (both lens implantation at 8 and 9 years of age). He is monitored at the cardiology (he underwent closing of arterial duct), neurology, and nephrology with no problems of the kidneys so far.

Maternal uncle

The maternal uncle (III-5) was born at 39 weeks of gestation (weight = 2,900 g, length = 49 cm) from second uncomplicated gravidity to a 25-year-old mother and a 28-year-old father, both healthy and nonconsanguineous. He was born with glucosuria, hyperbilirubinemia, pulmonary hypertension, and dysmorphic features, including flat midface, hypertelorism, antimongoloid slants, deep-set eyes, synophrys, anteverted nares, hypoplastic nasal bones, downturned corners of mouth, sparse hair, palmar crease, cutaneous syndactyly of two to three fingers, micropenis, cryptorchidism, cutis marmorata, and hypertrichosis (**Figures 2C–E**). In a later age, hepatopathy, decreased function of left kidney, hereditary glomerulopathy, short stature (150 cm in adultness), and severe developmental delay were described. He did not speak at all, and his walk was tentative. There also was attention deficit, instability, and mild aggressiveness, but no fits of laughter were noticed. He died at the age of 27 because of kidney failure.

The mother and maternal grandmother were heterozygous with manifested microscopic hematuria, but both were of normal intelligence.

Whole-Exome Sequencing

The proband and his parents were then examined by trio-based WES approach using commercially available Human Core Exome kit (Twist Bioscience) on Illumina NovaSeq 6000. Using our WES pipeline, we acquired a total of 226,580 genetic variants, of which we identified overall 151 filtered SNPs and indel variants, and all were classified as benign/likely begin or uncertain significance (see List 1 of **Supplementary Table S1**). In addition, two different segmentation algorithms for copy number variation (CNV) evaluation identified a Xq22.3q23 deletion of size approximately 2.91 Mb in the proband and his asymptomatic mother (**Figure 3**).

In order to confirm the WES results, we performed array-CGH in four family members (proband, mother, maternal grandmother, maternal uncle). The results showed loss of genetic material in the Xq22.3 locus [arr (hg19) Xq22.3q23 (107001860_110026871)x0] of size over 3.03 Mb, which affected the area comprised of 19 genes from *TSC22D3* to *CHRDL1*. Data from WES and array-CGH can be found in The European Genome-phenome Archive (EGA) (Lappalainen et al., 2015) under datasets IDs EGAD00001007740 and EGAD00001007743, respectively.

Cytogenetic and qPCR Analysis

Cultured metaphase chromosomes from peripheral blood lymphocytes were used for examination by standard

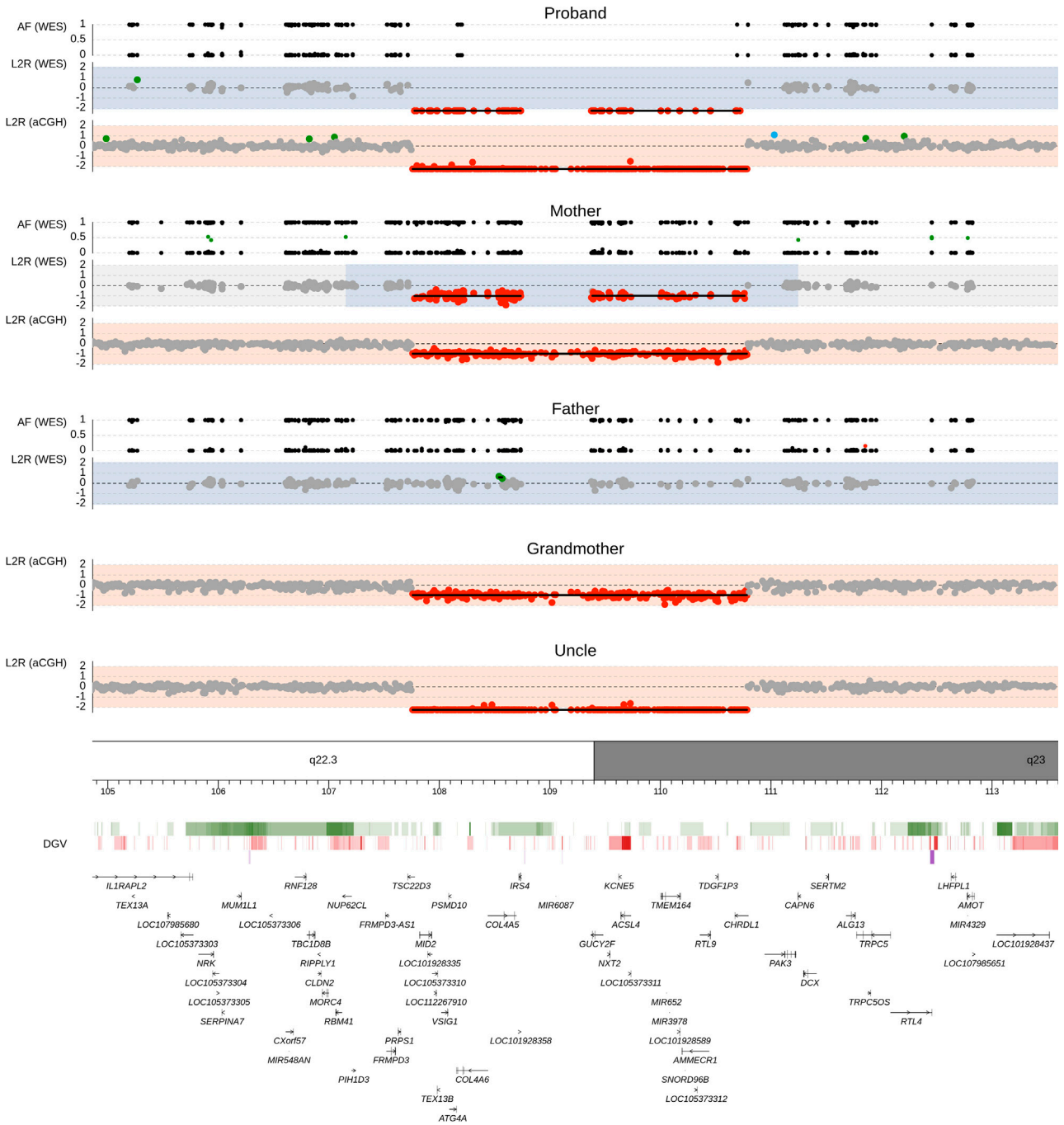

FIGURE 3 | Chromosomal deletion del(X) (q22.3q23) detected by whole-exome sequencing and array-comparative genome hybridization (CGH). Upper panel shows genomic profiles of the proband, father, and mother. Log2 ratio (L2R) track represents the copy-number profile indicating a maternally inherited hemizygous deletion in the male proband. Gray dots mark sequencing targets without any copy number abnormality. Red and green dots indicate the presence of losses and gains, respectively. Areas with light blue background show loss of heterozygosity regions predicted by zygosity status as shown in the allele frequency (AF) plot. In the AF track, black dots represent SNPs with a single allele detected in the sequencing reads, and green and red dots highlight SNPs with two alleles found in approximately 1:1 and another ratio, respectively. Lower panel contains the Database of Genomic Variants (DGV) and RefSeq gene annotation database. Color intensity within the DGV track corresponds to the level of population variability, green for losses, red for gains, and purple for complex regions.

G-banding karyotyping with normal results in the proband (IV-1) and his parents (III-1, III-4), maternal uncle (III-5), and grandmother (II-4).

FISH analysis using a probe RP1-31B8 (108,414,862–108,517,413), which spans the proximal region of *GUCY2F* gene, confirmed the deletion in the proband and in the affected

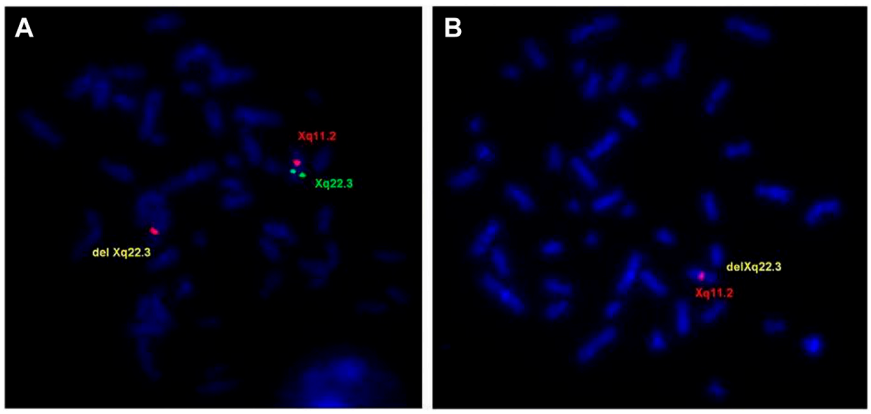

FIGURE 4 | FISH evaluations of the delXq22.3 region. **(A)** Metaphase chromosomes from the mother (III-4) showed FISH signal for the Xq22.3 region obtained using probe RP1-31B8 (green) on only one X chromosome. Probe for X chromosome centromeric region (RP13-34C21—red) showed FISH signals in both chromosomes. **(B)** Metaphase chromosomes from the proband (IV-I) showed no FISH signal for the Xq22.3 region and only one signal for the X chromosome centromeric region.

maternal uncle (IIII-5) (**Figure 4B**). The mother (III-4) and grandmother (II-4) were shown to be the carriers of the Xq22.3 deletion (**Figure 4A**), and the sister of the grandmother (II-5) was negative.

Deletion breakpoints were analyzed by qPCR together with a combination of WES and array-CGH results. Those breakpoints were detected between exon 1 and exon 2 of the *TSC22D3* gene (NM_198057.3) for the centromeric and between exon 2 and exon 3 of the *CHRDL1* gene (NM_001367204.1) for the telomeric one (see **Supplementary Methods**).

DISCUSSION

Alport syndrome with intellectual disability (ATS-ID, AMME complex; OMIM #300194) is an X-linked syndrome associated with the Xq22.3 loci. ATS-ID is a rare hereditary disorder with prevalence of about 1 in 50,000 live births (Kashtan et al., 2013). We reported the first Czech family affected with this congenital syndrome.

Comparison With Previously Reported ATS-ID Cases

A comparison of the deleted Xq22.3 area and clinical features in the reported family and three previously reported families with ATS-ID syndrome are shown in List 2 of **Supplementary Table S1**.

The 2.91-Mb region of loss of genetic material in our reported family is so far the largest of all described deletions in this region; it extended more telomerically and spans additional genes in comparison with the other previously described Xq22.3 deletions including *MID2*, *VSIG1*, *TEX13B*, *ATG4A*, *PSMD10*, *TDGF3*, *CHRDL1*. These findings could clarify the minor clinical differences observed in affected members of the Czech family and affected members of previously published families and bring novel information about the potential of candidate genes involved in the deleted segment. The clinical symptoms observed in our family, and not previously described in other families, included neonatal hepatitis, duplicated renal pelvis, aortopulmonary collaterals, palmar crease, growth retardation, micropenis, and cryptorchidism. We speculate that one or more of the genes found in our additional deleted region may be the causal gene for the symptoms, which were not described in previous families.

At present, the most interesting candidate gene is *MID2*, which encodes the protein midline 2 isoform 2, a member of the tripartite motif (TRIM) family. *MID2* is a member of E3 ubiquitin ligase subclass with a role in the microtubule stabilization in the cytoplasm (Short and Cox, 2006). *MID2* is closely related to the *MID1* with sequence similarity; *MID1* and *MID2* also share the same subcellular localization, but they have a different expression pattern during development (Buchner et al., 1999). To the best of our knowledge, there are no conclusive data connecting deregulation of *MID1* and *MID2* genes to the ATS-ID phenotype. However, *MID1* is the gene responsible for the Xp22-linked form of Opitz syndrome (OMIM 145410). This syndrome is a genetically and phenotypically complex disorder. It is defined by characteristic facial anomalies (hypertelorism, variably labiopalatine, laryngotracheo-esophageal clefting), structural heart defects, and anal and genital anomalies (Quaderi et al., 1997). Opitz syndrome also shares many anomalies with another X-linked disorder, FG syndrome (OMIM #305450), especially of midline structures. FG syndrome is characterized by multiple congenital anomalies (cleft palate, heart defects) and a broad range of central nervous system (CNS) dysfunctions (such as hypotonia, delay in motor development, speech delay) (Graham and Schwartz, 2013).

The clinical similarity between Opitz and FG syndromes, together with the sequencing homology between *MID1* and *MID2*, is probably the main reasons for considering *MID2* as a positional and functional candidate gene for FG syndrome (Jehee et al., 2005).

Both described syndromes are associated with congenital heart malformation, in case of Opitz syndrome additionally with genital anomalies. We speculate that *MID2* may play a role in the development and could be responsible for the heart defect (aortopulmonary collaterals) or genital anomalies (micropenis, cryptorchidism) or kidney defect (duplicated renal pelvis) and facial dysmorphism, including hypertelorism, in our family. This hypothesis must be verified by additional detailed analysis confirming the exact role of the *MID2* gene.

Until now, there is little information about the other genes, which were deleted in our case. The *VSIG1* gene is expressed in the normal testis and stomach, as well as in esophageal, ovarian, and gastric cancers (Oidovsambuu et al., 2011; Inoue et al., 2017), the *TEX13B* that is expressed in the testis during spermatogonia (Wang et al., 2001). *PSMD10* encodes 26S proteasome non-ATPase regulatory subunit (Gankyrin), which is essential for ubiquitin-dependent protein degradation (Hori et al., 1998). In addition, overexpression of *PSMD10* has been implicated in the development of many cancer types (Chattopadhyay et al., 2016). With the pivotal role in the ubiquitin–proteasome system (UPS), accumulation of this protein may be associated with the pathogenesis and phenotypic expression in several malignancies (Ermolaeva et al., 2015), cardiovascular, autoimmune, and neurodegenerative diseases including Alzheimer's disease, muscular dystrophies, and rare forms of neurodegenerative diseases associated with the development of dementia (Checler et al., 2000; Mathews and Moore, 2003; Mayer, 2003). While there are no conclusive data about degradation of synaptic proteins due to CNVs affecting *PSMD10* (Piton et al., 2011), we hypothesize that deregulation of *PSMD10* expression through loss of the genetic material in the locus could contribute to severe MR and developmental delay in our proband and maternal uncle. The effects of CNVs in *ATG4A*, *TDGF3*, and in the pathogenesis of MR have not been yet described.

A detailed comparison showed that patients in our study were similar in terms of clinical presentation. They shared similar major clinical characteristics with the previously reported ATS-MR phenotype. The difference in the phenotypes could be explained most probably due to deregulated expression of *MID2* and *PSMD10*. While evidence obtained from the literature indicate craniofacial abnormalities corresponding to midface retrusion seen in affected males, further functional, e.g., expression analysis of *MID2* and *PSMD10* need to be performed in order to verify the effect of deregulated expression on the phenotype. In addition, our detailed description of phenotype of the 20-year-old uncle might also be useful for future prediction of the development of the symptoms in other patients. Finally, the identification of CNVs in the Xq22.3 locus could be essential for genetic counseling strategies for other younger patients.

DATA AVAILABILITY STATEMENT

The datasets presented in this study can be found in online repositories. The names of the repository/repositories and accession number(s) can be found in the article/ **Supplementary Material**.

ETHICS STATEMENT

The studies involving human participants were reviewed and approved by Ethical committee of University Hospital Brno, Czech Republic. Written informed consent to participate in this study was provided by the participants' legal guardian/ next of kin. Written informed consent was obtained from the individual(s), and minor(s)' legal guardian/next of kin, for the publication of any potentially identifiable images or data included in this article.

AUTHOR CONTRIBUTIONS

JS wrote the article and supervised genetic analyses, VV participated article preparation and performed cytogenomic analyses, MW supervised sequencing analyses and qPCR, EH and HF were responsible for cytogenetic investigations, VH and RG were responsible for clinical investigations and data, PB. and AM performed WES data analyses, PK overlooked the article preparation process and made critical overview of the results.

FUNDING

This work was supported by the Ministry of Health of the Czech Republic, Grant No. NU20-07-00145 a Faculty hospital Brno PIG 5/19.

ACKNOWLEDGMENTS

We are grateful to the patients and their families for participating in this study.

SUPPLEMENTARY MATERIAL

The Supplementary Material for this article can be found online at: https://www.frontiersin.org/articles/10.3389/fgene.2021.750110/full#supplementary-material

REFERENCES

Andreoletti, G., Seaby, E. G., Dewing, J. M., O'Kelly, I., Lachlan, K., Gilbert, R. D., et al. (2017). AMMECR1: a Single point Mutation Causes Developmental Delay, Midface Hypoplasia and Elliptocytosis. *J. Med. Genet.* 54 (4), 269–277. doi:10.1136/jmedgenet-2016-104100

Basel-Vanagaite, L., Pillar, N., Isakov, O., Smirin-Yosef, P., Lagovsky, I., Orenstein, N., et al. (2017). X-linked Elliptocytosis with Impaired Growth Is Related to Mutated AMMECR1. *Gene* 606, 47–52. doi:10.1016/j.gene.2017.01.001

Bhat, S. S., Schmidt, K. R., Ladd, S., Kim, K. C., Schwartz, C. E., Simensen, R. J., et al. (2006). Disruption of DMD and Deletion of ACSL4 Causing Developmental Delay, Hypotonia, and Multiple Congenital Anomalies. *Cytogenet. Genome Res.* 112 (1-2), 170–175. doi:10.1159/000087531

Buchner, G., Montini, E., Andolfi, G., Quaderi, N., Cainarca, S., Messali, S., et al. (1999). MID2, a Homologue of the Opitz Syndrome Gene MID1: Similarities in Subcellular Localization and Differences in Expression during Development. *Hum. Mol. Genet.* 8 (8), 1397–1407. doi:10.1093/hmg/8.8.1397

Chattopadhyay, A., O'Connor, C. J., Zhang, F., Galvagnion, C., Galloway, W. R. J. D., Tan, Y. S., et al. (2016). Discovery of a Small-Molecule Binder of the Oncoprotein Gankyrin that Modulates Gankyrin Activity in the Cell. *Sci. Rep.* 6, 23732. doi:10.1038/srep23732

Checler, F., Alves da Costa, C., Ancolio, K., Chevallier, N., Lopez-Perez, E., and Marambaud, P. (2000). Role of the Proteasome in Alzheimer's Disease. *Biochim. Biophys. Acta (Bba) - Mol. Basis Dis.* 1502 (1), 133–138. doi:10.1016/s0925-4439(00)00039-9

Dai, Y., Liang, S., Dong, X., Zhao, Y., Ren, H., Guan, Y., et al. (2019). Whole Exome Sequencing Identified a Novel DAG1 Mutation in a Patient with Rare, Mild and Late Age of Onset Muscular Dystrophy-Dystroglycanopathy. *J. Cel Mol Med* 23 (2), 811–818. doi:10.1111/jcmm.13979

Ermolaeva, M. A., Dakhovnik, A., and Schumacher, B. (2015). Quality Control Mechanisms in Cellular and Systemic DNA Damage Responses. *Ageing Res. Rev.* 23 (Pt A), 3–11. doi:10.1016/j.arr.2014.12.009

Gazou, A., Riess, A., Grasshoff, U., Schäferhoff, K., Bonin, M., Jauch, A., et al. (2013). Xq22.3-q23 Deletion includingACSL4in a Patient with Intellectual Disability. *Am. J. Med. Genet.* 161 (4), 860–864. doi:10.1002/ajmg.a.35778

Graham, J. M., Jr., and Schwartz, C. E. (2013). MED12related Disorders. *Am. J. Med. Genet.* 161 (11), 2734–2740. doi:10.1002/ajmg.a.36183

Han, P., Wei, G., Cai, K., Xiang, X., Deng, W. P., Li, Y. B., et al. (2020). Identification and Functional Characterization of Mutations in LPL Gene Causing Severe Hypertriglyceridaemia and Acute Pancreatitis. *J. Cel Mol Med* 24 (2), 1286–1299. doi:10.1111/jcmm.14768

Hori, T., Kato, S., Saeki, M., DeMartino, G. N., Slaughter, C. A., Takeuchi, J., et al. (1998). cDNA Cloning and Functional Analysis of P28 (Nas6p) and p40.5 (Nas7p), Two Novel Regulatory Subunits of the 26S Proteasome. *Gene* 216 (1), 113–122. doi:10.1016/s0378-1119(98)00309-6

Inoue, Y., Matsuura, S., Yoshimura, K., Iwashita, Y., Kahyo, T., Kawase, A., et al. (2017). Characterization of V-set and Immunoglobulin Domain Containing 1 Exerting a Tumor Suppressor Function in Gastric, Lung, and Esophageal Cancer Cells. *Cancer Sci.* 108 (8), 1701–1714. doi:10.1111/cas.13295

Jehee, F. S., Rosenberg, C., Krepischi-Santos, A. C., Kok, F., Knijnenburg, J., Froyen, G., et al. (2005). An Xq22.3 Duplication Detected by Comparative Genomic Hybridization Microarray (Array-CGH) Defines a New Locus (FGS5) for FG Syndrome. *Am. J. Med. Genet.* 139A (3), 221–226. doi:10.1002/ajmg.a.30991

Jonsson, J. J., Renieri, A., Gallagher, P. G., Kashtan, C. E., Cherniske, E. M., Bruttini, M., et al. (1998). Alport Syndrome, Mental Retardation, Midface Hypoplasia, and Elliptocytosis: a New X Linked Contiguous Gene Deletion Syndrome? *J. Med. Genet.* 35 (4), 273–278. doi:10.1136/jmg.35.4.273

Kashtan, C. E., Ding, J., Gregory, M., Gross, O., Heidet, L., Knebelmann, B., et al. (2013). Clinical Practice Recommendations for the Treatment of Alport Syndrome: a Statement of the Alport Syndrome Research Collaborative. *Pediatr. Nephrol.* 28 (1), 5–11. doi:10.1007/s00467-012-2138-4

Lane, W., Robson, M., Lowry, R. B., and Leung, A. K. (1994). X-linked Recessive Nephritis with Mental Retardation, Sensorineural Hearing Loss, and Macrocephaly. *Clin. Genet.* 45 (6), 314–317. doi:10.1111/j.1399-0004.1994.tb04039.x

Lappalainen, I., Almeida-King, J., Kumanduri, V., Senf, A., Spalding, J. D., ur-Rehman, S., et al. (2015). The European Genome-Phenome Archive of Human Data Consented for Biomedical Research. *Nat. Genet.* 47 (7), 692–695. doi:10.1038/ng.3312

Lee, J., Nozu, K., Choi, D., Kang, H., Ha, I.-S., and Cheong, H. (2019). Features of Autosomal Recessive Alport Syndrome: A Systematic Review. *J. Clin. Med.* 8 (2), 178. doi:10.3390/jcm8020178

Mathews, K. D., and Moore, S. A. (2003). Limb-girdle Muscular Dystrophy. *Curr. Neurol. Neurosci. Rep.* 3 (1), 78–85. doi:10.1007/s11910-003-0042-9

Mayer, R. J. (2003). From Neurodegeneration to Neurohomeostasis: the Role of Ubiquitin. *Drug News Perspect.* 16 (2), 103–108. doi:10.1358/dnp.2003.16.2.829327

Meloni, I., Muscettola, M., Raynaud, M., Longo, I., Bruttini, M., Moizard, M.-P., et al. (2002a). FACL4, Encoding Fatty Acid-CoA Ligase 4, Is Mutated in Nonspecific X-Linked Mental Retardation. *Nat. Genet.* 30 (4), 436–440. doi:10.1038/ng857

Meloni, I., Vitelli, F., Pucci, L., Lowry, R. B., Tonlorenzi, R., Rossi, E., et al. (2002b). Alport Syndrome and Mental Retardation: Clinical and Genetic Dissection of the Contiguous Gene Deletion Syndrome in Xq22.3 (ATS-MR). *J. Med. Genet.* 39 (5), 359–365. doi:10.1136/jmg.39.5.359

Moysés-Oliveira, M., Giannuzzi, G., Fish, R. J., Rosenfeld, J. A., Petit, F., Soares, M. d. F., et al. (2018). Inactivation of AMMECR1 Is Associated with Growth, Bone, and Heart Alterations. *Hum. Mutat.* 39 (2), 281–291. doi:10.1002/humu.23373

Nozu, K., Minamikawa, S., Yamada, S., Oka, M., Yanagita, M., Morisada, N., et al. (2017). Characterization of Contiguous Gene Deletions in COL4A6 and COL4A5 in Alport Syndrome-Diffuse Leiomyomatosis. *J. Hum. Genet.* 62 (7), 733–735. doi:10.1038/jhg.2017.28

Oidovsambuu, O., Nyamsuren, G., Liu, S., Göring, W., Engel, W., and Adham, I. M. (2011). Adhesion Protein VSIG1 Is Required for the Proper Differentiation of Glandular Gastric Epithelia. *PLoS One* 6 (10), e25908. doi:10.1371/journal.pone.0025908

Piton, A., Gauthier, J., Hamdan, F. F., Lafrenière, R. G., Yang, Y., Henrion, E., et al. (2011). Systematic Resequencing of X-Chromosome Synaptic Genes in Autism Spectrum Disorder and Schizophrenia. *Mol. Psychiatry* 16 (8), 867–880. doi:10.1038/mp.2010.54

Poreau, B., Ramond, F., Harbuz, R., Satre, V., Barro, C., Vettier, C., et al. (2019). Xq22.3q23 Microdeletion Harboring TMEM164 and AMMECR1 Genes: Two Case Reports Confirming a Recognizable Phenotype with Short Stature, Midface Hypoplasia, Intellectual Delay, and Elliptocytosis. *Am. J. Med. Genet.* 179 (4), 650–654. doi:10.1002/ajmg.a.61057

Quaderi, N. A., Schweiger, S., Gaudenz, K., Franco, B., Rugarli, E. I., Berger, W., et al. (1997). Opitz G/BBB Syndrome, a Defect of Midline Development, Is Due to Mutations in a New RING finger Gene on Xp22. *Nat. Genet.* 17 (3), 285–291. doi:10.1038/ng1197-285

Rodriguez, J. D., Bhat, S. S., Meloni, I., Ladd, S., Leslie, N. D., Doyne, E. O., et al. (2010). Intellectual Disability, Midface Hypoplasia, Facial Hypotonia, and Alport Syndrome Are Associated with a Deletion in Xq22.3. *Am. J. Med. Genet.* 152a (3), 713–717. doi:10.1002/ajmg.a.33208

Short, K. M., and Cox, T. C. (2006). Subclassification of the RBCC/TRIM Superfamily Reveals a Novel Motif Necessary for Microtubule Binding. *J. Biol. Chem.* 281 (13), 8970–8980. doi:10.1074/jbc.M512755200

Wang, P. J., McCarrey, J. R., Yang, F., and Page, D. C. (2001). An Abundance of X-Linked Genes Expressed in Spermatogonia. *Nat. Genet.* 27 (4), 422–426. doi:10.1038/86927

Zhang, R., Chen, S., Han, P., Chen, F., Kuang, S., Meng, Z., et al. (2020). Whole Exome Sequencing Identified a Homozygous Novel Variant in CEP290 Gene Causes Meckel Syndrome. *J. Cel Mol Med* 24 (2), 1906–1916. doi:10.1111/jcmm.14887

Zheng, Y., Xu, J., Liang, S., Lin, D., and Banerjee, S. (2018). Whole Exome Sequencing Identified a Novel Heterozygous Mutation in HMBS Gene in a Chinese Patient with Acute Intermittent Porphyria with Rare Type of Mild Anemia. *Front. Genet.* 9, 129. doi:10.3389/fgene.2018.00129

Conflict of Interest: The authors declare that the research was conducted in the absence of any commercial or financial relationships that could be construed as a potential conflict of interest.

Publisher's Note: All claims expressed in this article are solely those of the authors and do not necessarily represent those of their affiliated organizations, or those of the publisher, the editors and the reviewers. Any product that may be evaluated in this article, or claim that may be made by its manufacturer, is not guaranteed or endorsed by the publisher.

frontiers in Genetics

ORIGINAL RESEARCH
published: 10 November 2021
doi: 10.3389/fgene.2021.738561

Genetic Analysis of Children With Unexplained Developmental Delay and/or Intellectual Disability by Whole-Exome Sequencing

Jingjing Xiang[1,2†], Yang Ding[1,2†], Fei Yang[1,2†], Ang Gao[1,2], Wei Zhang[1,2], Hui Tang[1,2], Jun Mao[1,2], Quanze He[1,2], Qin Zhang[1,2] and Ting Wang[1,2*]*

[1]Center for Reproduction and Genetics, The Affiliated Suzhou Hospital of Nanjing Medical University, Suzhou, China, [2]Center for Reproduction and Genetics, Suzhou Municipal Hospital, Suzhou, China

OPEN ACCESS

Edited by:
Anjana Munshi,
Central University of Punjab, India

Reviewed by:
Theresa V. Strong,
Foundation for Prader-Willi Research, United States
Santasree Banerjee,
Beijing Genomics Institute, China

***Correspondence:**
Ting Wang
biowt@njmu.edu.cn
Qin Zhang
zhangq110004@163.com

[†]These authors have contributed equally to this work

Specialty section:
This article was submitted to Genetics of Common and Rare Diseases, a section of the journal Frontiers in Genetics

Received: 09 July 2021
Accepted: 07 October 2021
Published: 10 November 2021

Citation:
Xiang J, Ding Y, Yang F, Gao A, Zhang W, Tang H, Mao J, He Q, Zhang Q and Wang T (2021) Genetic Analysis of Children With Unexplained Developmental Delay and/or Intellectual Disability by Whole-Exome Sequencing. Front. Genet. 12:738561. doi: 10.3389/fgene.2021.738561

Background: Whole-exome sequencing (WES) has been recommended as a first-tier clinical diagnostic test for individuals with neurodevelopmental disorders (NDDs). We aimed to identify the genetic causes of 17 children with developmental delay (DD) and/or intellectual disability (ID).

Methods: WES and exome-based copy number variation (CNV) analysis were performed for 17 patients with unexplained DD/ID.

Results: Single-nucleotide variant (SNV)/small insertion or deletion (Indel) analysis and exome-based CNV calling yielded an overall diagnostic rate of 58.8% (10/17), of which diagnostic SNVs/Indels accounted for 41.2% (7/17) and diagnostic CNVs accounted for 17.6% (3/17).

Conclusion: Our findings expand the known mutation spectrum of genes related to DD/ID and indicate that exome-based CNV analysis could improve the diagnostic yield of patients with DD/ID.

Keywords: whole-exome sequencing, developmental delay, intellectual disability, exome-based CNV analysis, variants

BACKGROUND

Developmental delay (DD) and intellectual disability (ID) are major manifestations of neurodevelopmental disorders (NDDs) with a global prevalence of 1%–3% (Thapar et al., 2017; Ismail and Shapiro, 2019). DD/ID shows phenotypic pleiotropy, and the underlying cause of DD/ID is heterogeneous, in which genetic factors such as copy number variations (CNVs) and variants in single genes have been recognized as major reasons (Savatt and Myers, 2021). With the advent of next-generation sequencing (NGS), the field of genetics was transformed; and the number of genes known to be associated with DD/ID has increased significantly. For example, over 700 genes have been identified in X-linked, autosomal-dominant, and autosomal-recessive ID until 2015 (Vissers et al., 2016).

Chromosomal microarray has been recommended as a first-tier clinical test to identify chromosomal CNVs and regions of homozygosity in individuals with DD/ID, autism spectrum disorders (ASDs), or multiple congenital anomalies with a diagnostic yield of 15%–20% (Manning et al., 2010; Miller et al., 2010). Whole-exome sequencing (WES) could detect single-nucleotide

TABLE 1 | Summary of patients' clinical manifestations and molecular diagnoses.

Patient ID/ sex/ age	Phenotype	Gene/ locus	Diagnosis (OMIM phenotype)	Variants	Zygosity	Variant type	Inheritance	Classification (ACMG)	References (PMID)
P1/ male/ 2 years	Global developmental delay, intellectual disability	*MED13L*	Developmental delay and distinctive facial features with or without cardiac defects (#616789)	NM_015335.4: c.1284_1,285 insTTTAAGCTTTT (p.Lys429Phefs*7)	Heterozygous	Frameshift	AD; *de novo*	P	—
P2/ male/ 8 years	Perinatal polyhydramnios, intellectual disability, global developmental delay, ataxia, anemia	—	—	—	—	—	—	—	—
P3/ male/ 5 years	Spastic cerebral palsy, febrile seizure, global developmental delay, mild intellectual disability, muscular hypertonia	—	—	—	—	—	—	—	—
P4/ male/ 6 years	Bilateral dislocation of hip joints, clubfoot, strabismus, global developmental delay, intellectual disability	—	—	—	—	—	—	—	—
P5/ male/ 6 years	Cerebral atrophy, seizure, global developmental delay, intellectual disability, muscular hypertonia	*CNPY3*	Developmental and epileptic encephalopathy 60 (#617929)	NM_006586.4: c.283C > G (p.Arg95Gly); c.834del (p.Ter279Gluext*8)	Compound heterozygous	Missense, frameshift	AR maternally inherited, paternally inherited	VUS, VUS	—
P6/ female/ 9 years	Intellectual disability, global developmental delay, hypermetropia	—	—	—	—	—	—	—	—
P7/ male/ 3 years	Global developmental delay, intellectual disability	*SCN2A*	Developmental and epileptic encephalopathy 11 (#613721); episodic ataxia, type 9 (#618924); seizures, benign familial infantile, 3 (#607745)	NM_021007.3: c.1117del (p.Ala373Profs*9)	Heterozygous	Deletion	AD; *de novo*	P	—
P8/ male/ 4 years	Global developmental delay, agenesis of the corpus callosum, low anterior hairline, strabismus	*ARID1B*	Coffin-Siris syndrome 1 (#135900)	NM_001374828.1: c.4194T > G (p.Tyr1398*)	Heterozygous	Nonsense	AD; *de novo*	P	—
P9/ male/ 6 years	Intellectual disability, seizure, autism, cerebral	*PRRT2*	Convulsions, familial infantile, with paroxysmal	NM_145,239.2: c.649dup (p.Arg217Profs*8)	Heterozygous	Insertion	AD; maternally inherited	P	22101681, 22870186, 22877996,

(Continued on following page)

TABLE 1 | (*Continued*) Summary of patients' clinical manifestations and molecular diagnoses.

Patient ID/ sex/ age	Phenotype	Gene/ locus	Diagnosis (OMIM phenotype)	Variants	Zygosity	Variant type	Inheritance	Classification (ACMG)	References (PMID)
	white matter atrophy		choreoathetosis (#602066); episodic kinesigenic dyskinesia 1 (#128200); seizures, benign familial infantile, 2 (#605751)						25667652, 22243967
P10/ female/ 5 years	Tetralogy of Fallot, autism, global developmental delay	7q11.23	Chromosome 7q11.23 duplication syndrome (#609757)	chr7:72649202-74191713dup, 1.54 Mb	Heterozygous	CNV	*De novo*	P	19249392, 26333794, 19752158
P11/ male/ 9 years	Moderate intellectual disability, global developmental delay	—	—	—	—	—	—	—	—
P12/ male/ 7 years	Mild intellectual disability, delayed speech and language development, low-set ears, downslanting palpebral fissures, short penis	*SETBP1*	Developmental delay, autosomal dominant 29 (#616078); Schinzel-Giedion midface retraction syndrome (#269150)	NM_015559.3: c.2311dup (p.Ser771Phefs*26)	Heterozygous	Frameshift	AD; unknown	LP	—
P13/ male/ 2 years	Premature birth, delayed speech and language development	—	—	—	—	—	—	—	—
P14/ male/ 7 years	Intellectual disability, global developmental delay	*GRIN2B*	Intellectual developmental disorder, autosomal dominant 6, with or without seizures (#613970); Developmental and epileptic encephalopathy 27 (#616139)	NM_000834.4: c.1711del (p.Ala571Profs*80)	Heterozygous	Deletion	AD; *de novo*	P	—
P15/ male/ 7 years	Prenatal hydrocephalus, global developmental delay, mild intellectual disability, retrognathia, strabismus	8p21.2p12	—	chr8:25184869-31641821del, 6.46 Mb	Heterozygous	CNV	*De novo*	P	—
P16/ male/ 6 years	Global developmental delay, moderate intellectual disability, neonatal feeding difficulties, strabismus	19p13.2	—	chr19:1,3044343-13227605del, 183.3 kb	Heterozygous	CNV	*De novo*	P	—

(Continued on following page)

TABLE 1 | (*Continued*) Summary of patients' clinical manifestations and molecular diagnoses.

Patient ID/ sex/ age	Phenotype	Gene/ locus	Diagnosis (OMIM phenotype)	Variants	Zygosity	Variant type	Inheritance	Classification (ACMG)	References (PMID)
P17/ male/ 4 years	Neonatal asphyxia, global developmental delay, muscular hypertonia	—	—	—	—	—	—	—	—

Abbreviations: CNV, copy number variation; AD, autosomal dominant; AR, autosomal recessive; P, pathogenic; LP, likely pathogenic; VUS, variant of uncertain significance.

variants (SNVs) and small insertions or deletions (Indels) by whole-exome capture and massively parallel DNA sequencing, which has a diagnostic advantage in situations of genetic heterogeneity or unknown causal genes compared with conventional tests of single gene or gene panels (Monroe et al., 2016). WES is also recommended as a first-tier clinical diagnostic test for individuals with NDDs with an overall diagnostic yield of 36%, including 31% for isolated NDD, and 53% for NDD plus associated conditions, which is greater than the diagnostic yield of CMA (15%–20%) (Srivastava et al., 2019). Recently, CNV calling has been performed by depth-of-sequence coverage analysis of WES data, which enables the detection of deletions and duplications at the exon level (Marchuk et al., 2018).

In this study, WES and exome-based CNV analysis were performed for 17 children with unexplained DD/ID, and a variety of diagnostic variants including SNVs/Indels and CNVs were identified, indicating that WES could help to identify their molecular etiology and the incorporation of CNV calling could improve the diagnostic rate.

METHODS

Patients

This study was approved by the institutional ethics committee of the Affiliated Suzhou Hospital of Nanjing Medical University. Written informed consent was obtained from each patient's parents. This study included 17 children with unexplained DD/ID referred to our center for reproduction and genetics, the affiliated Suzhou Hospital of Nanjing Medical University, Suzhou, Jiangsu, China, from January 2018 to March 2021. The characteristics of each patient including age, gender, and main phenotypes are listed in **Table 1**, and their clinical details are listed in **Supplementary Table S1**. Global DD is defined as a delay in two or more developmental domains of cognition, speech/language, gross/fine motor, social/personal, and activities of daily living (Mithyantha et al., 2017). Severity of ID was determined based on the intelligence quotient (IQ): severe ID (IQ < 40), moderate ID (IQ range 40–60), and mild ID (IQ range 60–70). In the absence of IQ, ID was diagnosed by the pediatric neurologist or geneticist.

Whole-Exome Sequencing and Data Analysis

Genomic DNA was extracted from the whole blood of the patients and their parents. WES was performed using the SureSelect Human All Exon Kit (Agilent, Santa Clara, CA, USA) and Illumina NovaSeq 6,000 platform (Illumina, San Diego, CA, USA). The sequencing reads were aligned to the human reference genome (hg19/GRCh37) using Burrows-Wheeler Aligner tool, and PCR duplicates were removed by Picard v1.57 (http://picard.sourceforge.net/). The fraction of target bases covered at least 20× should be over 96%, with an average sequencing depth on target bases of over 100×. GATK (https://software.broadinstitute.org/gatk/) was employed for identifying the SNVs and Indels. Variant annotation and interpretation were conducted by ANNOVAR (Wang et al., 2010). The variants were searched in the dbSNP (http://www.ncbi.nlm.nih.gov/SNP/), 1000 Genomes Project database (http://www.1000genomes.org/), Exome Aggregation Consortium (ExAC) (http://exac.broadinstitute.org/), and the Genome Aggregation database (gnomAD) (http://gnomad.broadinstitute.org/). The pathogenicity of mutations was predicted by PROVEAN (http://provean.jcvi.org), PolyPhen-2 (http://genetics.bwh.harvard.edu/pph2/), and MutationTaster (http://www.mutationtaster.org/). Disease and phenotype databases and published literature, such as OMIM (http://www.omim.org), ClinVar (http://www.ncbi.nlm.nih.gov/clinvar), HGMD (http://www.hgmd.org), and PubMed (http://www.ncbi.nlm.nih.gov/pubmed), were also searched. The variants were classified according to the Standards and Guidelines for the Interpretation of Sequence Variants released by the American College of Medical Genetics and Genomics (ACMG) and the Association for Molecular Pathology (Richards et al., 2015). Finally, the variants with minor allele frequency <0.05 were selected for further interpretation considering ACMG category, evidence of pathogenicity, clinical synopsis, and inheritance mode of associated disease.

Sanger Sequencing

To validate the WES results, the identified candidate variants were amplified by PCR using genomic DNA from the patients and their parents. The primers used for PCR are listed in **Supplementary Table S2**. The PCR products were purified

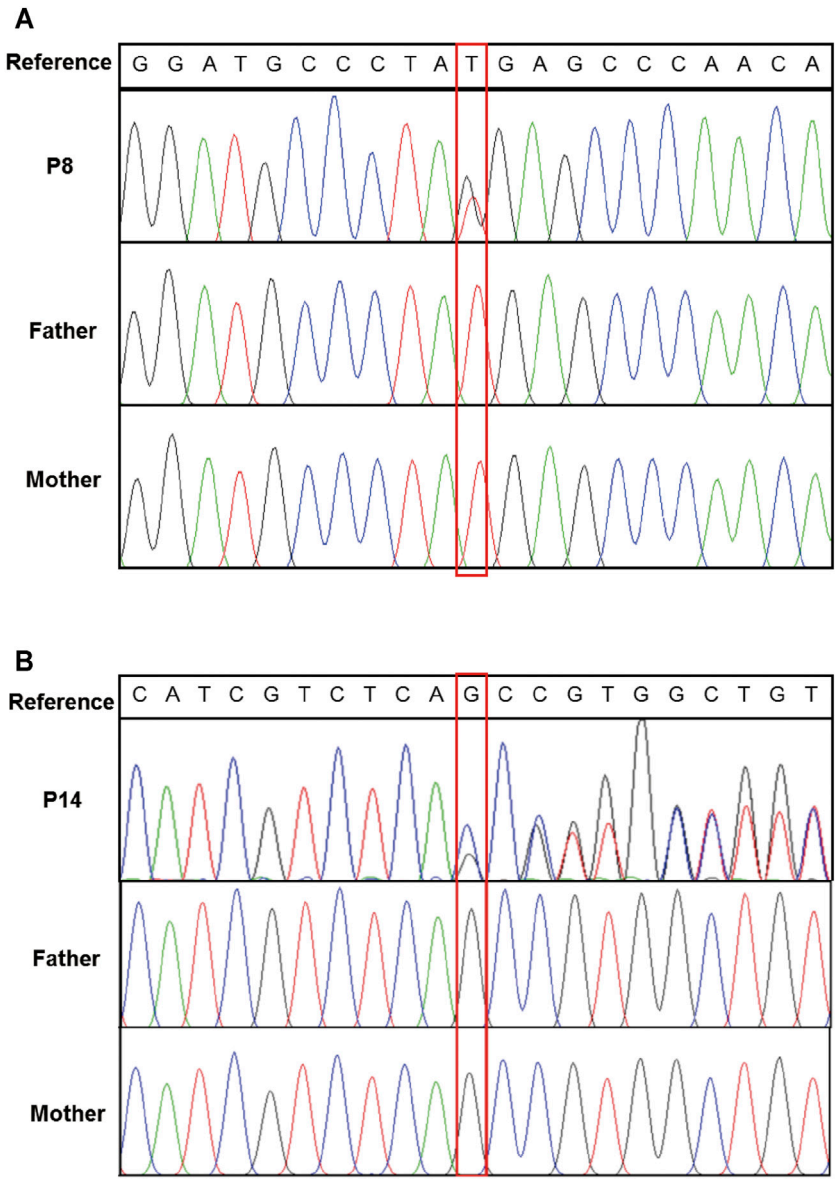

FIGURE 1 | Confirmation of *de novo* variants by Sanger sequencing. **(A)** Sanger sequencing of *ARID1B* in patient 8 and his parents. **(B)** Sanger sequencing of *GRIN2B* in patient 14 and his parents. Variants were indicated by red boxes.

and sequenced in two orientations using an ABI 3500 Genetic Analyzer (Applied Biosystems, Foster City, CA, USA). The mutation sites were analyzed by comparison with the GenBank reference sequences of each candidate gene.

Exome-Based CNV Detection and Validation

A comprehensive tool was used for CNV calling. It included XHMM (http://atgu.mgh.harvard.edu/xhmm) and PCA method to remove sequencing noise and CNVKit (https://github.com/etal/cnvkit) fix module to perform GC and bias correction; and then copy number calculation and CNV identification were performed in exons and long segment areas. The identified CNVs were interpreted according to the standards and guidelines for interpretation and reporting of postnatal constitutional CNVs released by the ACMG and the technical standards for the interpretation and reporting of constitutional copy-number variants recommended by the ACMG and the Clinical Genome Resource (ClinGen) (Kearney et al., 2011; Riggs et al., 2020). CNVs were further validated by multiplex ligation-dependent probe amplification (MLPA) or quantitative PCR (qPCR) or CNV sequencing (CNV-seq).

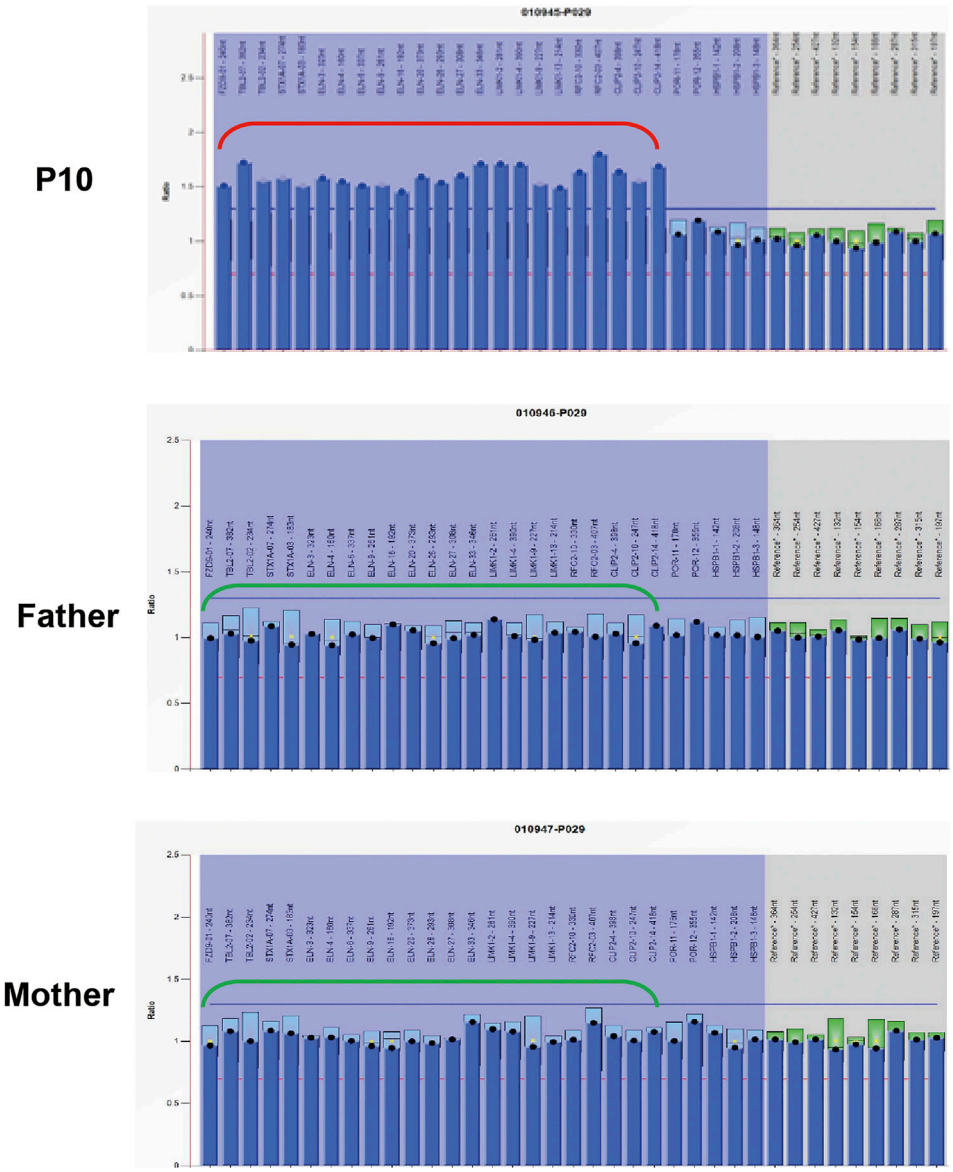

FIGURE 2 | MLPA results of patient 10 and her parents. MLPA was performed using SALSA MLPA Probemix P029 WBS kit, and the red bracket indicates the duplication region in patient 10.

RESULTS

A total of 17 children with DD/ID were enrolled and analyzed by WES. As shown in **Table 1**, the age of 17 probands in this study ranged from 2 to 9 years, with a mean age of 5.6 years. Male-to-female ratio was 15:2. The clinical characteristics of 17 probands include global DD (14/17) and ID (13/17) (**Table 1**, **Supplementary Table S1**).

Diagnostic Yields

Among the 17 probands, WES in family trios (Trio-WES) was performed for 14 patients (patients 1–11 and 15–17). Patient 12 and his father underwent WES as a father–proband duo, for the sample of the patient's mother was unavailable. And patients 13 and 14 had singleton WES. Analysis of WES data revealed that the coverage for over 97% of the targeted bases were over 20×, with an average sequencing depth of over 100×. An overall diagnostic rate of 58.8% (10/17) was achieved after analysis of SNV/Indel and CNV, of which diagnostic SNVs/Indels accounted for 41.2% (7/17) and diagnostic CNVs accounted for 17.6% (3/17) (**Table 1**).

A total of eight variants in seven genes were identified in seven probands by SNV/Indel analysis and confirmed by Sanger sequencing, including six variants in six genes associated with autosomal dominant disorders and two compound heterozygous variants in *CNPY3* gene related to an autosomal recessive

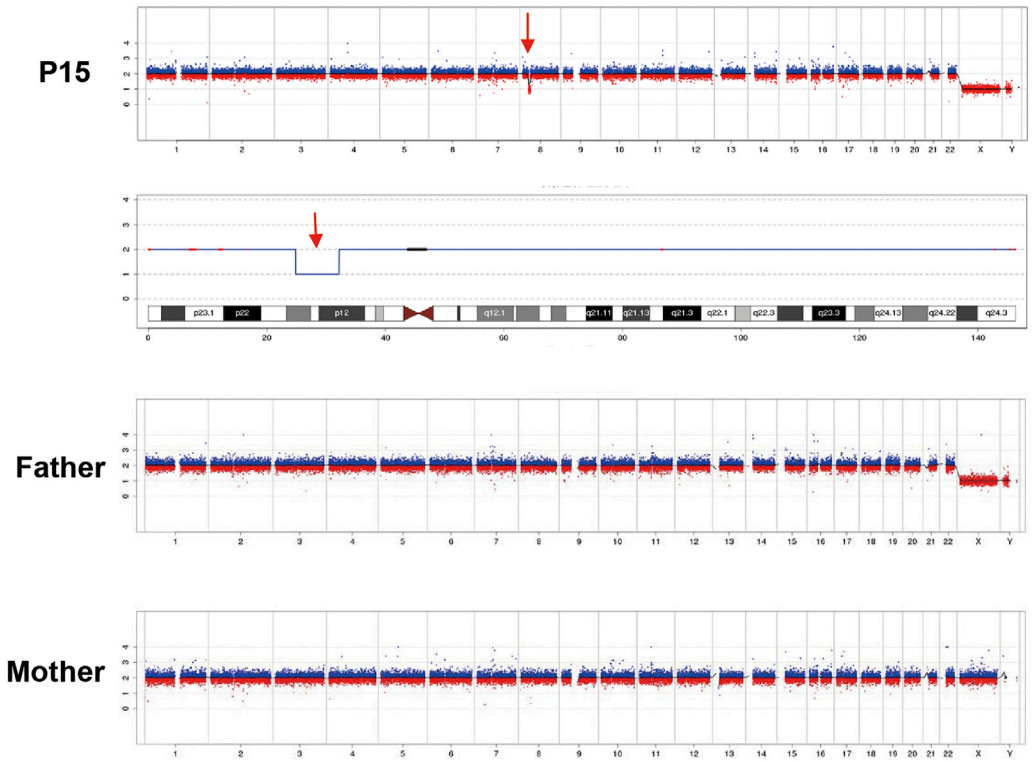

FIGURE 3 | CNV-seq results of patient 15 and his parents. A 6.46-Mb deletion on chromosome 8 of patient 15 is indicated by the red arrow.

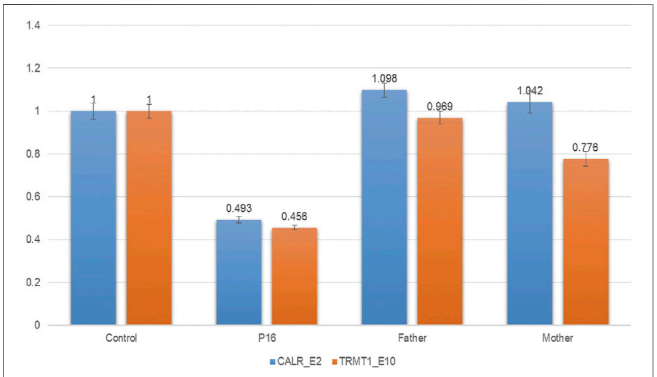

FIGURE 4 | qPCR results of patient 16 and his parents. To confirm the 183.3-kb deletion on chromosome 19p13.2, two pairs of primers for *CALR*_E2 and *TRMT1*_E10 were selected and used in the qPCR. Three replicates were performed, and the relative copy number was estimated by the comparative $2^{-\Delta\Delta CT}$ method using *ALB* gene as the internal control. The numbers in the *Y*-axis indicate the $2^{-\Delta\Delta CT}$ value. $2^{-\Delta\Delta CT} < 0.1$ is considered to be a homozygous deletion, $0.3 < 2^{-\Delta\Delta CT} < 0.7$ is considered to be a heterozygous deletion, $0.7 < 2^{-\Delta\Delta CT} < 1.3$ is considered to be normal, and $2^{-\Delta\Delta CT} > 1.3$ is considered to be a duplication.

disorder early infantile epileptic encephalopathy 60 (EIEE60). In autosomal dominant disorders, four variants detected in patients 1, 7, 8, and 14 occurred *de novo* (**Figure 1**); the origin of a variant in *SETBP1* gene of patient 12 is unknown, for his mother's sample is unavailable; and a variant in *PRRT2* gene of patient 9 was inherited from his unaffected mother. The two compound heterozygous variants in *CNPY3* gene of patient 5 were inherited from his mother and father (**Table 1**).

Exome-based CNV analysis revealed three *de novo* pathogenic CNVs. A 1.54-Mb duplication on chromosome 7q11.23 related to chromosome 7q11.23 duplication syndrome (MIM #609757) was identified in patient 10 and confirmed by MLPA (**Figure 2**). In patient 15, a 6.46-Mb deletion on chromosome 8p21.2p12 was detected and validated by CNV-seq (**Figure 3**). A 183.3-kb deletion on chromosome 19p13.2 was found in patient 16 and verified by qPCR (**Figure 4**).

Case Example

Patient 5 is a 6-year-old boy whose parents are healthy and non-consanguineous. He was born full term by natural delivery without abnormalities, weighing 2,900 g. He was bed ridden and presented with global DD, spastic quadriplegia, ID, and intractable seizure. He had multiple admissions for pneumonia and seizure. His first seizure started at age 6 months, and his electroencephalography (EEG) at 2 years of age showed diffuse sharp waves, spike waves, and multiple spike and slow wave complex. MRI of his brain at 6 years old revealed enlargement of the lateral ventricles and cerebral atrophy (**Figure 5A**).

WES in family trios (Trio-WES) was performed with DNA from patient 5 and his parents. For patient 5, the coverage for 97.87% of the targeted bases was over 20×. Ultimately, two compound heterozygous variants in *CNPY3* gene (c.283C > G

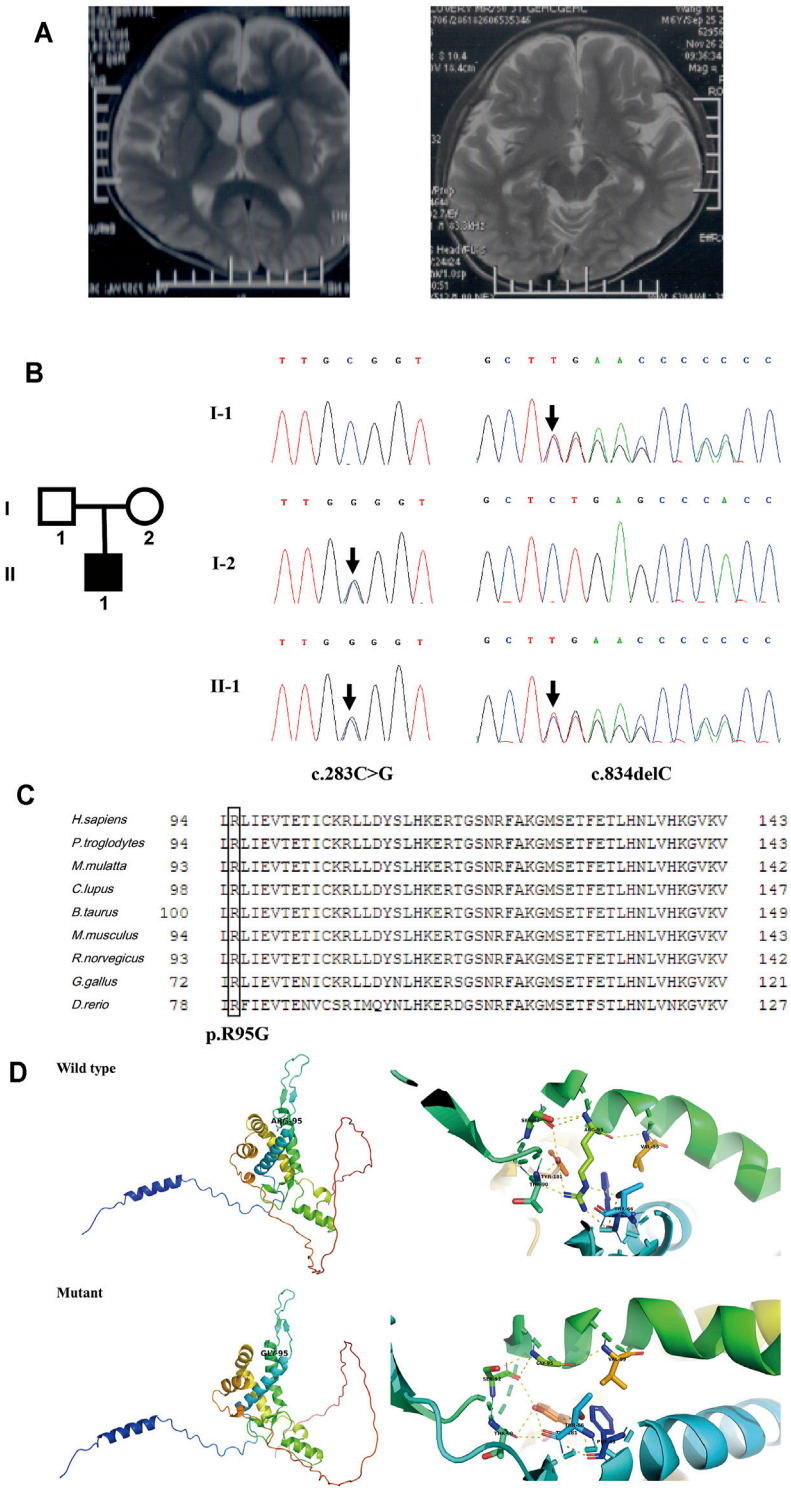

FIGURE 5 | Clinical information and genetic analysis of patient 5. **(A)** Brain MRI of the patient. The left panel shows enlarged lateral ventricles, and the right panel shows bilateral hippocampus. **(B)** Genetic analysis of the family. Left panel: the pedigree of the patient's family. Right panel: Sanger sequencing of *CNPY3* in family members demonstrated mutations in the proband and his parents. Mutations are indicated by black arrows. **(C)** Multiple sequence alignment of CNPY3 protein and its orthologs in different species. The arginine residue in position 95 is indicated by a black box. The protein and its orthologs were aligned using Clustal Omega (http://www.clustal.org/omega/). **(D)** Predicted structures of wild-type and mutated CNPY3 proteins using PyMOL (http://www.pymol.org). ARG-95 of wild-type protein may form hydrogen bonds with PHE-63, THR-66, THR-90, SER-92, VAL-99, and TYR-181, while GLY-95 of mutant protein may only form hydrogen bonds with SER-92 and VAL-99, which may affect the protein structure and function.

and c.834del) were detected. Sanger sequencing validated the two compound heterozygous variants in the patient. His mother was heterozygous for the c.283C > G variant in exon 3 of *CNPY3* gene, and his father was heterozygous for the c.834del variant in exon six of *CNPY3* gene (**Figure 5B**). These two variants were not recorded in the dbSNP, 1000 Genomes Project database, ExAC, or gnomAD. The c.283C > G variant was a novel missense mutation causing a substitution from arginine to glycine of CNPY3 protein (p.Arg95Gly), which is predicted to be deleterious by PROVEAN with a score of −6.62, probably damaging by PolyPhen-2 with a score of 1.0, and disease causing by MutationTaster with a probability value of 0.999. Furthermore, sequence alignment of human CNPY3 protein and its othologs in different species revealed that the R95 residue is highly conserved among species (**Figure 5C**). And protein structural analysis revealed that substitution from arginine to glycine of CNPY3 protein at position 95 may reduce the formation of hydrogen bonds, thus affecting the protein structure and function (**Figure 5D**). The c.834del variant is a novel frameshift deletion mutation, which results in a prolonged protein with the addition of eight amino acid residues (EPTQHPLS) to the C-terminal of CNPY3 protein (p.Ter279Gluext*8). According to the ACMG variant classification guideline (Richards et al., 2015), the c.283C > G variant could be classified as uncertain significance with two supporting (PM2_Supporting and PP3) evidences, and the c.834del variant could be classified as uncertain significance with one moderate (PM4) and one supporting (PM2_Supporting) evidences.

DISCUSSION

In this study, WES was performed for 17 probands with DD/ID with an overall diagnostic yield of 58.8% (10/17), which is consistent with a recent study that WES identified pathogenic variants in 53.5% (54/101) of patients with DD/ID (Hiraide et al., 2021). A total of eight *de novo* variants were detected, including five SNVs/Indels and three CNVs, corroborating the burden of *de novo* variants in DD/ID (Brunet et al., 2021). And further functional studies are needed to elucidate the effect of the identified variants at the transcriptional or translational level. In addition, exome-based CNV analysis revealed three pathogenic CNVs, increasing the diagnostic yield by 17.6% (3/17), which is consistent with a recent study that incorporation of exome-based CNV calling improved the diagnostic rate of trio-WES by 18.92% (14/74) in patients with NDDs (Zhai et al., 2021). However, WES analysis yielded negative results for seven patients in this study, possibly due to technical limitations of WES (e.g., deep intron mutations and structural variants).

SNV/Indel analysis identified eight variants of seven genes, including five novel heterozygous variants in patients 1, 7, 8, 12, and 14; one reported heterozygous variant in patient 9; and two compound heterozygous variants in patient 5. A novel *de novo* heterozygous variant c.1284_1285insTTTAAGCTTTT of *MED13L* gene was detected in patient 1, resulting in a frameshift and a premature stop codon (p.Lys429Phefs*7). The *mediator complex subunit 13-like* (*MED13L*) gene encodes a subunit of the mediator complex that functions as transcriptional regulation by physically linking DNA-binding transcription factors and RNA polymerase II in early development of the heart and brain (Utami et al., 2014). *MED13L* haploinsufficiency is involved in DD and distinctive facial features with or without cardiac defects (MIM #616789). In addition to DD/ID, patient 1 had mild dysmorphic facial features, but cardiac malformations were not observed, which is consistent with previous reports on variable penetrance of cardiac malformations (Adegbola et al., 2015; Cafiero et al., 2015).

For patient 7, a novel *de novo* heterozygous variant c.1117del of *SCN2A* gene was identified, leading to a frameshift and a premature termination (p.Ala373Profs*9). *SCN2A* encodes the voltage-gated sodium channel Nav1.2, which plays a role in the initiation and conduction of action potentials (Wolff et al., 2017). Mutations in *SCN2A* were related to a spectrum of epilepsies and NDDs with phenotypic heterogeneity, including developmental and epileptic encephalopathy 11 (MIM #613721); episodic ataxia type 9 (MIM #618924); and benign familial infantile seizures 3 (MIM #607745). Patient 7 is 3 years old with DD and ID, but he is seizure-free until now. He may have later-onset epilepsy, or he may show ID and/or autism without epilepsy as 16% (32/201) of previously reported cases with *SCN2A* mutations (Wolff et al., 2017).

WES identified a novel *de novo* heterozygous nonsense mutation (c.4194T > G, p. Tyr1398*) of *ARID1B* gene in patient 8. To date, nine genes have been reported to be related to Coffin-Siris syndrome, and mutations of *ARID1B* gene were the most common reason for Coffin-Siris syndrome. *ARID1B* encodes a small subset of SWI/SNF (SWItch/Sucrose Non-Fermentable) complexes that play an important role in chromatin remodeling (Sekiguchi et al., 2019). Agenesis of corpus callosum was detected prenatally and confirmed after birth in patient 8, but hypoplasia of the fifth digits/nails was not observed, which is consistent with a previous report that most patients with corpus callosum anomalies and *ARID1B* mutations (n = 8/11) had normal fingers and toes (Mignot et al., 2016).

For patient 9, a heterozygous variant (c.649dup, p. Arg217Profs*8) of *PRRT2* gene was identified, which was inherited from his mother. *PRRT2* encodes the proline-rich transmembrane protein 2 (PRRT2) and is highly expressed in the brain and spinal cord (Chen et al., 2011). *PRRT2* is associated with familial infantile convulsions with paroxysmal choreoathetosis (MIM #602066), episodic kinesigenic dyskinesia 1 (MIM #128200), and benign familial infantile seizures 2 (MIM #605751); and the penetrance of episodic kinesigenic dyskinesia 1 is estimated to be 60%–90% (van Vliet et al., 2012). The c.649dup variant was a mutation hotspot in families of different origins (Wang et al., 2011; Ono et al., 2012; Schubert et al., 2012), and a homozygous c.649dup mutation was detected in five individuals of an Iranian family with severe non-syndromic ID (Najmabadi et al., 2011). However, it was reported that only 0.6% (8/1,423) of individuals with heterozygous *PRRT2* mutations present ID (Ebrahimi-Fakhari et al., 2015), and *PRRT2* mutations are not related to increased susceptibility to ASD (Huguet et al., 2014),

suggesting that the maternally inherited c.649dup variant of *PRRT2* may not completely explain the phenotypes of ID and autism observed in patient 9.

A novel heterozygous variant c.2311dup of *SETBP1* gene was detected in patient 12, resulting in a frameshift and a premature termination (p.Ser771Phefs*26). *SETBP1* encodes the SET binding protein 1 expressed ubiquitously, but little is known about the function of *SETBP1* (Hoischen et al., 2010). *De novo* gain-of-function variants of *SETBP1* are associated with Schinzel-Giedion midface retraction syndrome (MIM #269150), while haploinsufficiency of *SETBP1* caused by loss-of-function (LoF) variant or a heterozygous gene deletion is related to DD, autosomal dominant 29 (MIM #616078). Patient 12 exhibited mild ID (IQ 65–70), consistent with a recent study that ID of various levels was observed in 77% (23/30) of patients with *SETBP1* haploinsufficiency disorder (Jansen et al., 2021). In addition, another study indicated that aberrant speech and language development are central to *SETBP1* haploinsufficiency disorder (Morgan et al., 2021), and patient 12 also showed impaired speech and language development.

For patient 14, a novel heterozygous variant c.1711del of *GRIN2B* gene was identified, leading to a frameshift and a premature stop codon (p.Ala571Profs*80). *GRIN2B* encodes the subunit NR2B of *N*-methyl-D-aspartate (NMDA) receptors, which are neurotransmitter-gated ion channels involved in the regulation of synaptic function in the central nervous system (Endele et al., 2010). *GRIN2B* is related to intellectual developmental disorder, autosomal dominant 6, with or without seizures (MIM #613970), and developmental and epileptic encephalopathy 27 (MIM #616139). A previous study of 58 individuals with *GRIN2B* encephalopathy revealed that 52% (30/58) of the patients have had seizures with a variable age of onset (0–9 years) (Platzer et al., 2017). Patient 14 is 7 years old, and he is seizure-free until now.

EIEE is a group of neurological disorders characterized by frequent epileptic seizures and development delay beginning in infancy (McTague et al., 2016). In 2018, biallelic variants in *CNPY3* gene (MIM *610774) have been identified to cause EIEE60 (MIM #617929) (Mutoh et al., 2018). *CNPY3* gene is located on chromosome 6p21.1, comprises six exons and five introns, and encodes a co-chaperone of 278 amino acid residues in the endoplasmic reticulum. In this study, two compound heterozygous variants of *CNPY3* gene were identified in patient 5. To date, three individuals with biallelic *CNPY3* variants have been reported, and their MRI showed diffuse brain atrophy and hippocampal malrotation (Mutoh et al., 2018). Brain MRI of patient 5 also showed cerebral atrophy, but hippocampal malrotation was not observed. And the other phenotypes of patient 5 were consistent with the three reported patients in the literature.

Three pathogenic CNVs were detected by exome-based CNV analysis in patients 10, 15, and 16. A 1.54-Mb heterozygous duplication on chromosome 7q11.23 was identified in patient 10; hence, he was diagnosed with chromosome 7q11.23 duplication syndrome (MIM #609757). 7q11.23 duplication syndrome is characterized by DD, speech delay, and congenital anomalies (Morris et al., 2015). To date, more than 150 individuals with 7q11.23 duplication syndrome have been reported (Mervis et al., 2015). Patient 10 was diagnosed with tetralogy of Fallot after birth and underwent surgical repair. And he showed delayed motor, speech, and autistic features at 3 years old, which are similar to the characteristics of 7q11.23 duplication patients reported in the literature.

For patient 15, a 6.46-Mb heterozygous deletion on chromosome 8p21.2p12 was detected, which overlaps with the deletion region of four cases recorded in the DECIPHER database (https://www.deciphergenomics.org). DECIPHER patient #390234 had attention deficit hyperactivity disorder, depressivity, expressive language delay, and mild ID. Patient #1557 had abnormality of the skin, blepharophimosis, fine hair, hearing impairment, hypothyroidism, ID, microtia, obesity, and short palm. Patient #415150 had mild ID, seizure. And patient #372147 had delayed speech and language development, generalized hypotonia, hypermetropia, short stature, and strabismus. A previous study reviewed 21 patients with deletions overlapping 8p21p12 region; and growth retardation, psychomotor retardation, and postnatal microcephaly were characteristics of most patients (Willemsen et al., 2009). Patient 15 also showed mild ID and DD, and he had hydrocephalus diagnosed prenatally, which was not reported in patients with deletion on 8p21.2p12. He underwent neurosurgical cerebrospinal fluid diversion after birth; afterwards, his follow-up CT scan was normal.

A 183.3-kb deletion on chromosome 19p13.2 encompassing *NFIX* gene was identified in patient 16. Haploinsufficiency of *NFIX* causes Sotos syndrome 2 (MIM #614753), which is characterized by postnatal overgrowth, macrocephaly, DD, and intellectual impairment (Malan et al., 2010). Patients with Sotos syndrome 2 will develop marfanoid habitus with age. The birth weight of patient 16 is 3.45 kg, and he had neonatal feeding difficulties. Now he is 6 years old with a weight of 21 kg (normal range) and height of 128 cm (+2 SD), consistent with a previous report that the median height of patients with Sotos syndrome 2 is 2.0 SD above the mean (range −0.5 to +3.8 SD) (Klaassens et al., 2015). He also had strabismus, DD, and moderate ID, similar to reported patients with 19p13.2 deletion encompassing *NFIX* gene (Klaassens et al., 2015; Jezela-Stanek et al., 2016).

In conclusion, WES could identify the underlying genetic causes for patients with unexplained DD/ID, and exome-based CNV analysis could detect clinically significant submicroscopic CNVs, thus improving the diagnostic yield. Our findings not only broaden the known mutation spectrum of genes associated with DD/ID but also indicate the potential of WES and exome-based CNV analysis in clinical diagnosis and discovery of disease-causing mutations and CNVs.

DATA AVAILABILITY STATEMENT

The datasets presented in this article are not readily available due to ethical concerns regarding patient privacy and consent. Requests to access the datasets should be directed to the corresponding authors.

ETHICS STATEMENT

The studies involving human participants were reviewed and approved by the institutional ethics committee of the Affiliated Suzhou Hospital of Nanjing Medical University. Written informed consent to participate in this study was provided by the participants' legal guardian/next of kin. Written informed consent was obtained from the individual(s), and minors' legal guardian/next of kin, for the publication of any potentially identifiable images or data included in this article.

AUTHOR CONTRIBUTIONS

JX, QZ, and TW are responsible for testing strategy design and manuscript preparation. Data analysis and interpretation were performed by JX, HT, JM, and QH. Genetic counselling was conducted by QZ, YD, FY, AG, and WZ. All authors read and approved the final manuscript.

FUNDING

This work is supported by Jiangsu Provincial Medical Innovation Team (CXTDB2017013), Suzhou Clinical Medical Expert Team (SZYJTD201708), Jiangsu Science and Technology Support Program (BE2019683), and Suzhou Science and Technology Support Program (SS2019066).

ACKNOWLEDGMENTS

We would like to thank the patients for participating in this research project. We also acknowledge all members of our center.

SUPPLEMENTARY MATERIAL

The Supplementary Material for this article can be found online at: https://www.frontiersin.org/articles/10.3389/fgene.2021.738561/full#supplementary-material

REFERENCES

Adegbola, A., Musante, L., Callewaert, B., Maciel, P., Hu, H., Isidor, B., et al. (2015). Redefining the MED13L Syndrome. *Eur. J. Hum. Genet.* 23 (10), 1308–1317. doi:10.1038/ejhg.2015.26

Brunet, T., Jech, R., Brugger, M., Kovacs, R., Alhaddad, B., Leszinski, G., et al. (2021). De Novo variants in Neurodevelopmental Disorders-Experiences from a Tertiary Care center. *Clin. Genet.* doi:10.1111/cge.13946

Cafiero, C., Marangi, G., Orteschi, D., Ali, M., Asaro, A., Ponzi, E., et al. (2015). Novel De Novo Heterozygous Loss-Of-Function Variants in MED13L and Further Delineation of the MED13L Haploinsufficiency Syndrome. *Eur. J. Hum. Genet.* 23 (11), 1499–1504. doi:10.1038/ejhg.2015.19

Chen, W.-J., Lin, Y., Xiong, Z.-Q., Wei, W., Ni, W., Tan, G.-H., et al. (2011). Exome Sequencing Identifies Truncating Mutations in PRRT2 that Cause Paroxysmal Kinesigenic Dyskinesia. *Nat. Genet.* 43 (12), 1252–1255. doi:10.1038/ng.1008

Ebrahimi-Fakhari, D., Saffari, A., Westenberger, A., and Klein, C. (2015). The Evolving Spectrum ofPRRT2-Associated Paroxysmal Diseases. *Brain* 138 (Pt 12), 3476–3495. doi:10.1093/brain/awv317

Endele, S., Rosenberger, G., Geider, K., Popp, B., Tamer, C., Stefanova, I., et al. (2010). Mutations in GRIN2A and GRIN2B Encoding Regulatory Subunits of NMDA Receptors Cause Variable Neurodevelopmental Phenotypes. *Nat. Genet.* 42 (11), 1021–1026. doi:10.1038/ng.677

Hiraide, T., Yamoto, K., Masunaga, Y., Asahina, M., Endoh, Y., Ohkubo, Y., et al. (2021). Genetic and Phenotypic Analysis of 101 Patients with Developmental Delay or Intellectual Disability Using Whole-exome Sequencing. *Clin. Genet.* 100, 40–50. doi:10.1111/cge.13951

Hoischen, A., van Bon, B. W. M., Gilissen, C., Arts, P., van Lier, B., Steehouwer, M., et al. (2010). De Novo mutations of SETBP1 Cause Schinzel-Giedion Syndrome. *Nat. Genet.* 42 (6), 483–485. doi:10.1038/ng.581

Huguet, G., Nava, C., Lemière, N., Patin, E., Laval, G., Ey, E., et al. (2014). Heterogeneous Pattern of Selective Pressure for PRRT2 in Human Populations, but No Association with Autism Spectrum Disorders. *PLoS One* 9 (3), e88600. doi:10.1371/journal.pone.0088600

Ismail, F. Y., and Shapiro, B. K. (2019). What Are Neurodevelopmental Disorders. *Curr. Opin. Neurol.* 32 (4), 611–616. doi:10.1097/WCO.0000000000000710

Jansen, N. A., Braden, R. O., Srivastava, S., Otness, E. F., Lesca, G., Rossi, M., et al. (2021). Clinical Delineation of SETBP1 Haploinsufficiency Disorder. *Eur. J. Hum. Genet.* 29, 1198–1205. doi:10.1038/s41431-021-00888-9

Jezela-Stanek, A., Kucharczyk, M., Falana, K., Jurkiewicz, D., Mlynek, M., Wicher, D., et al. (2016). Malan Syndrome (Sotos Syndrome 2) in Two Patients with 19p13.2 Deletion Encompassing NFIX Gene and Novel NFIX Sequence Variant. *Biomed. Pap.* 160 (1), 161–167. doi:10.5507/bp.2016.006

Kearney, H. M., Thorland, E. C., Brown, K. K., Quintero-Rivera, F., and South, S. T. (2011). Working Group of the American College of Medical Genetics Laboratory Quality Assurance, C. (American College of Medical Genetics Standards and Guidelines for Interpretation and Reporting of Postnatal Constitutional Copy Number Variants. *Genet. Med.* 13 (7), 680–685. doi:10.1097/GIM.0b013e3182217a3a

Klaassens, M., Morrogh, D., Rosser, E. M., Jaffer, F., Vreeburg, M., Bok, L. A., et al. (2015). Malan Syndrome: Sotos-like Overgrowth with De Novo NFIX Sequence Variants and Deletions in Six New Patients and a Review of the Literature. *Eur. J. Hum. Genet.* 23 (5), 610–615. doi:10.1038/ejhg.2014.162

Malan, V., Rajan, D., Thomas, S., Shaw, A. C., Louis Dit Picard, H., Layet, V., et al. (2010). Distinct Effects of Allelic NFIX Mutations on Nonsense-Mediated mRNA Decay Engender Either a Sotos-like or a Marshall-Smith Syndrome. *Am. J. Hum. Genet.* 87 (2), 189–198. doi:10.1016/j.ajhg.2010.07.001

Manning, M., Hudgins, L., Professional, P., and Guidelines, C. (2010). Array-based Technology and Recommendations for Utilization in Medical Genetics Practice for Detection of Chromosomal Abnormalities. *Genet. Med.* 12 (11), 742–745. doi:10.1097/GIM.0b013e3181f8baad

Marchuk, D. S., Crooks, K., Strande, N., Kaiser-Rogers, K., Milko, L. V., Brandt, A., et al. (2018). Increasing the Diagnostic Yield of Exome Sequencing by Copy Number Variant Analysis. *PLoS One* 13 (12), e0209185. doi:10.1371/journal.pone.0209185

McTague, A., Howell, K. B., Cross, J. H., Kurian, M. A., and Scheffer, I. E. (2016). The Genetic Landscape of the Epileptic Encephalopathies of Infancy and Childhood. *Lancet Neurol.* 15 (3), 304–316. doi:10.1016/S1474-4422(15)00250-1

Mervis, C. B., Morris, C. A., Klein-Tasman, B. P., Velleman, S. L., and Osborne, L. R. (2015). "7q11.23 Duplication Syndrome," in *GeneReviews®*. Editors M. P. Adam, H. H. Ardinger, R. A. Pagon, S. E. Wallace, L. J. H. Bean, G. Mirzaa, et al. (Seattle, WA: University of Washington, Seattle), 1993–2021. Available at: https://www.ncbi.nlm.nih.gov/books/NBK327268/

Mignot, C., Moutard, M.-L., Rastetter, A., Boutaud, L., Heide, S., Billette, T., et al. (2016). ARID1Bmutations Are the Major Genetic Cause of Corpus Callosum Anomalies in Patients with Intellectual Disability. *Brain* 139 (11), e64. doi:10.1093/brain/aww181

Miller, D. T., Adam, M. P., Aradhya, S., Biesecker, L. G., Brothman, A. R., Carter, N. P., et al. (2010). Consensus Statement: Chromosomal Microarray Is a First-Tier Clinical Diagnostic Test for Individuals with Developmental Disabilities or Congenital Anomalies. *Am. J. Hum. Genet.* 86 (5), 749–764. doi:10.1016/j.ajhg.2010.04.006

Mithyantha, R., Kneen, R., McCann, E., and Gladstone, M. (2017). Current Evidence-Based Recommendations on Investigating Children with Global Developmental Delay. *Arch. Dis. Child.* 102 (11), 1071–1076. doi:10.1136/archdischild-2016-311271

Monroe, G. R., Frederix, G. W., Savelberg, S. M. C., de Vries, T. I., Duran, K. J., van der Smagt, J. J., et al. (2016). Effectiveness of Whole-Exome Sequencing and Costs of the Traditional Diagnostic Trajectory in Children with Intellectual Disability. *Genet. Med.* 18 (9), 949–956. doi:10.1038/gim.2015.200

Morgan, A., Braden, R., Wong, M. M. K., Colin, E., Amor, D., Liégeois, F., et al. (2021). Speech and Language Deficits Are central to SETBP1 Haploinsufficiency Disorder. *Eur. J. Hum. Genet.* 29, 1216–1225. doi:10.1038/s41431-021-00894-x

Morris, C. A., Mervis, C. B., Paciorkowski, A. P., Abdul-Rahman, O., Dugan, S. L., Rope, A. F., et al. (2015). 7q11.23 Duplication Syndrome: Physical Characteristics and Natural History. *Am. J. Med. Genet.* 167 (12), 2916–2935. doi:10.1002/ajmg.a.37340

Mutoh, H., Kato, M., Akita, T., Shibata, T., Wakamoto, H., Ikeda, H., et al. (2018). Biallelic Variants in CNPY3, Encoding an Endoplasmic Reticulum Chaperone, Cause Early-Onset Epileptic Encephalopathy. *Am. J. Hum. Genet.* 102 (2), 321–329. doi:10.1016/j.ajhg.2018.01.004

Najmabadi, H., Hu, H., Garshasbi, M., Zemojtel, T., Abedini, S. S., Chen, W., et al. (2011). Deep Sequencing Reveals 50 Novel Genes for Recessive Cognitive Disorders. *Nature* 478 (7367), 57–63. doi:10.1038/nature10423

Ono, S., Yoshiura, K.-i., Kinoshita, A., Kikuchi, T., Nakane, Y., Kato, N., et al. (2012). Mutations in PRRT2 Responsible for Paroxysmal Kinesigenic Dyskinesias Also Cause Benign Familial Infantile Convulsions. *J. Hum. Genet.* 57 (5), 338–341. doi:10.1038/jhg.2012.23

Platzer, K., Yuan, H., Schütz, H., Winschel, A., Chen, W., Hu, C., et al. (2017). GRIN2B Encephalopathy: Novel Findings on Phenotype, Variant Clustering, Functional Consequences and Treatment Aspects. *J. Med. Genet.* 54 (7), 460–470. doi:10.1136/jmedgenet-2016-104509

Richards, S., Aziz, N., Aziz, N., Bale, S., Bick, D., Das, S., et al. (2015). Standards and Guidelines for the Interpretation of Sequence Variants: a Joint Consensus Recommendation of the American College of Medical Genetics and Genomics and the Association for Molecular Pathology. *Genet. Med.* 17 (5), 405–423. doi:10.1038/gim.2015.30

Riggs, E. R., Andersen, E. F., Cherry, A. M., Kantarci, S., Kearney, H., Patel, A., et al. (2020). Technical Standards for the Interpretation and Reporting of Constitutional Copy-Number Variants: a Joint Consensus Recommendation of the American College of Medical Genetics and Genomics (ACMG) and the Clinical Genome Resource (ClinGen). *Genet. Med.* 22 (2), 245–257. doi:10.1038/s41436-019-0686-8

Savatt, J. M., and Myers, S. M. (2021). Genetic Testing in Neurodevelopmental Disorders. *Front. Pediatr.* 9, 526779. doi:10.3389/fped.2021.526779

Schubert, J., Paravidino, R., Becker, F., Berger, A., Bebek, N., Bianchi, A., et al. (2012). PRRT2 Mutations Are the Major Cause of Benign Familial Infantile Seizures. *Hum. Mutat.* 33 (10), 1439–1443. doi:10.1002/humu.22126

Sekiguchi, F., Tsurusaki, Y., Okamoto, N., Teik, K. W., Mizuno, S., Suzumura, H., et al. (2019). Genetic Abnormalities in a Large Cohort of Coffin-Siris Syndrome Patients. *J. Hum. Genet.* 64 (12), 1173–1186. doi:10.1038/s10038-019-0667-4

Srivastava, S., Love-Nichols, J. A., Love-Nichols, J. A., Dies, K. A., Ledbetter, D. H., Martin, C. L., et al. (2019). Meta-analysis and Multidisciplinary Consensus Statement: Exome Sequencing Is a First-Tier Clinical Diagnostic Test for Individuals with Neurodevelopmental Disorders. *Genet. Med.* 21 (11), 2413–2421. doi:10.1038/s41436-019-0554-6

Thapar, A., Cooper, M., and Rutter, M. (2017). Neurodevelopmental Disorders. *The Lancet Psychiatry* 4 (4), 339–346. doi:10.1016/S2215-0366(16)30376-5

Utami, K. H., Winata, C. L., Hillmer, A. M., Aksoy, I., Long, H. T., Liany, H., et al. (2014). Impaired Development of Neural-Crest Cell Derived Organs and Intellectual Disability Caused ByMED13LHaploinsufficiency. *Hum. Mutat.* 35 (11), a–n. doi:10.1002/humu.22636

van Vliet, R., Breedveld, G., de Rijk-van Andel, J., Brilstra, E., Verbeek, N., Verschuuren-Bemelmans, C., et al. (2012). PRRT2 Phenotypes and Penetrance of Paroxysmal Kinesigenic Dyskinesia and Infantile Convulsions. *Neurology* 79 (8), 777–784. doi:10.1212/WNL.0b013e3182661fe3

Vissers, L. E. L. M., Gilissen, C., and Veltman, J. A. (2016). Genetic Studies in Intellectual Disability and Related Disorders. *Nat. Rev. Genet.* 17 (1), 9–18. doi:10.1038/nrg3999

Wang, J.-L., Cao, L., Li, X.-H., Hu, Z.-M., Li, J.-D., Zhang, J.-G., et al. (2011). Identification of PRRT2 as the Causative Gene of Paroxysmal Kinesigenic Dyskinesias. *Brain* 134 (Pt 12), 3493–3501. doi:10.1093/brain/awr289

Wang, K., Li, M., and Hakonarson, H. (2010). ANNOVAR: Functional Annotation of Genetic Variants from High-Throughput Sequencing Data. *Nucleic Acids Res.* 38 (16), e164. doi:10.1093/nar/gkq603

Willemsen, M. H., de Leeuw, N., Pfundt, R., de Vries, B. B. A., and Kleefstra, T. (2009). Clinical and Molecular Characterization of Two Patients with a 6.75Mb Overlapping Deletion in 8p12p21 with Two Candidate Loci for Congenital Heart Defects. *Eur. J. Med. Genet.* 52 (2-3), 134–139. doi:10.1016/j.ejmg.2009.03.003

Wolff, M., Johannesen, K. M., Hedrich, U. B. S., Masnada, S., Rubboli, G., Gardella, E., et al. (2017). Genetic and Phenotypic Heterogeneity Suggest Therapeutic Implications in SCN2A-Related Disorders. *Brain* 140 (5), 1316–1336. doi:10.1093/brain/awx054

Zhai, Y., Zhang, Z., Shi, P., Martin, D. M., and Kong, X. (2021). Incorporation of Exome-based CNV Analysis Makes trio-WES a More Powerful Tool for Clinical Diagnosis in Neurodevelopmental Disorders: A Retrospective Study. *Hum. Mutat.* 42, 990–1004. doi:10.1002/humu.24222

Conflict of Interest: The authors declare that the research was conducted in the absence of any commercial or financial relationships that could be construed as a potential conflict of interest.

Publisher's Note: All claims expressed in this article are solely those of the authors and do not necessarily represent those of their affiliated organizations, or those of the publisher, the editors, and the reviewers. Any product that may be evaluated in this article, or claim that may be made by its manufacturer, is not guaranteed or endorsed by the publisher.

frontiers in Genetics

ORIGINAL RESEARCH
published: 23 November 2021
doi: 10.3389/fgene.2021.741607

Familial Translocation t(2;4) (q37.3; p16.3), Resulting in a Partial Trisomy of 2q (or 4p) and a Partial Monosomy of 4p (or 2q), Causes Dysplasia

Jian Wang[1,2†], Shiyuan Zhou[3†], Fei He[2†], Xuelian Zhang[2], Jianqi Lu[4], Jian Zhang[2], Feng Zhang[4], Xiangmin Xu[2,5], Fang Yang[1] and Fu Xiong[1,2,5]**

[1]Department of Fetal Medicine and Prenatal Diagnosis, Zhujiang Hospital, Southern Medical University, Guangzhou, China, [2]Department of Medical Genetics, School of Basic Medical Sciences, Southern Medical University, Guangzhou, China, [3]Henan Provincial Research Institute for Population and Family Planning Zhengzhou China, Zhengzhou, China, [4]Obstetrics and Gynecology Hospital, NHC Key Laboratory of Reproduction Regulation (Shanghai Institute of Planned Parenthood Research), State Key Laboratory of Genetic Engineering at School of Life Sciences, Fudan University, Shanghai, China, [5]Guangdong Provincial Key Laboratory of Single Cell Technology and Application, Guangzhou, China

Background: Wolf-Hirschhorn syndrome, a well-known contiguous microdeletion syndrome, is caused by deletions on chromosome 4p. While the clinical symptoms and the critical region for this disorder have been identified based on genotype-phenotype correlations, duplications in this region have been infrequently reported.

Conclusion: Our case report shows that both deletions and duplications of the Wolf-Hirshhorn critical region cause intellectual disability/developmental delay and multiple congenital anomalies.

Keywords: balanced translocation of chromosomes, 4p16.3, wolf-hirschhorn syndrome, 4p16.3 microduplication syndrome, ID/DD

Case presentation: We report on a family presenting with a set of dysmorphic facial features, attention deficit hyperactivity disorders, learning difficulties, speech and cognitive delays, overgrowth/developmental delay, and musculoskeletal anomalies. Through karyotyping, chromosomal microarray, and PCR analyses, it was found that patients in this family had translocations on chromosomes 2q37 and 4p16. Patients with 2q duplications and 4p deletions showed clinical phenotypes typical of WHS syndrome. Family members with 2q deletions and 4p duplications similarly manifested distinct clinical phenotypes.

OPEN ACCESS

Edited by:
Santasree Banerjee,
Beijing Genomics Institute (BGI), China

Reviewed by:
Thomas Liehr,
Friedrich Schiller University Jena, Germany
Liang-Liang Fan,
Central South University, China
Chenming Xu,
International Peace Maternity and Child Health Hospital, China

****Correspondence:***
Fu Xiong
xiongfu@smu.edu.cn
Fang Yang
964175870@qq.com

[†]These authors have contributed equally to this work

Specialty section:
This article was submitted to Genetics of Common and Rare Diseases, a section of the journal Frontiers in Genetics

Received: *15 July 2021*
Accepted: *27 September 2021*
Published: *23 November 2021*

Citation:
Wang J, Zhou S, He F, Zhang X, Lu J, Zhang J, Zhang F, Xu X, Yang F and Xiong F (2021) Familial Translocation t(2;4) (q37.3;p16.3), Resulting in a Partial Trisomy of 2q (or 4p) and a Partial Monosomy of 4p (or 2q), Causes Dysplasia. Front. Genet. 12:741607. doi: 10.3389/fgene.2021.741607

BACKGROUND

Intellectual disability/developmental delay (ID/DD) is a common neuropsychiatric disorder with a complex etiology that includes external environmental factors and inherent genetic factors (Schalock et al., 2007). About 66.7% of ID is due to genetic factors. These can include mono- or polygenic diseases, abnormal gene copy numbers or chromosome counts, or structural abnormalities (Moeschler, 2008). Copy number variation (CNV) refers to the insertion, deletion, or amplification of DNA fragments from 1 kb to several Mb in size with resultant complex chromosomal structural variations when compared to reference sequences in the genome. Studies have shown that CNVs are found in 10–15% of patients with ID accompanied by congenital abnormalities (Kirov, 2015).

Wolf-Hirschhorn syndrome (WHS) syndrome is a classic example of a CNV-associated genetic condition. WHS is caused by differently sized deletions of the 4p chromosomal region. Notably, the deletion of the *WHSC1* gene is considered to be the cause of the facial appearance in WHS patients (Andersen et al., 2014). The core characteristics of WHS include delayed prenatal and postnatal growth, craniofacial hypoplasia, delayed development, and epilepsy (Bergemann et al., 2005; Engbers et al., 2009; Nevado et al., 2020). Typical craniofacial features include prominent glabellas, microcephaly, a "Greek warrior helmet appearance" of the nose, widely spaced and prominent eyes, a short philtrum, a broad nasal tip, and downturned corners of the mouth (Titomanlio et al., 2004). Identification of this condition strongly depends on recognition of the facial gestalt.

In this study, we report on a family in which several members have CNVs occurring on chromosomes two and 4. Their clinical phenotypes include ID, abnormal development, slow reactions, and abnormal skeletal development. Some patients presented with poor suction after birth. Therefore, a detailed survey of the family members was conducted, with karyotype analysis and CNV testing confirming the diagnoses.

MATERIALS AND METHODS

Patients

A detailed survey was conducted of all family members. The data were recorded and sorted according to the phenotypes of each member. Representative photos of the phenotype were obtained from some family members. Peripheral venous blood for DNA extraction was collected into evacuated EDTA tubes from most members of the family. Genomic DNA was prepared from peripheral blood leukocytes. This study was approved by the Zhujiang Hospital Ethics Committee, an affiliate of the Southern Medical University (Guangdong, China).

Karyotyping

Karyotyping was performed on phytohemagglutinin-stimulated peripheral blood lymphocytes according to standard clinical procedures. Karyotypes of the family members were analyzed using G-banding chromosome analysis (Zhang et al., 2020). The karyotypes were described according to the International System for Human Cytogenomic Nomenclature standards (ISCN 2016). Partial cell suspensions were stored at −20°C.

Chromosomal Microarray Analysis

To further understand if minor deletions were present on the chromosomes, comparative genomic hybridization experiments (array CGH) were performed on five samples using the Affymetrix Cytoscan® 750 k (Affymetrix, Santa Clara, CA, United States). This platform includes 200,000 SNP markers and 500,000 copy number variation (CNV) markers that are distributed across the human genome at an average density of about 1 marker/4 kb (Zhang et al., 2020). The arrays were strictly run according to the manufacturer's protocol and the data were visualized and analyzed using the Chromosome Analysis Suite software package (Affymetrix). The February 2009 human reference sequence (GRCh37/Hg19, http://genome.ucsc.edu/) was used as the reference sequence.

PCR Amplification

Primers were designed and the duplication or deletion of chromosome fragments was verified in different patients through PCR. To verify the balanced translocation through PCR analysis, two sets of primers were designed for the chromosome where the translocation occurred. PCR was performed with specific oligonucleotide primers as follows: chromosome 4 binding primer F: 5′- GTCCCGGTCCATAAC GCTTGC -3′ and R: 5′- GGAAGTTATGTGTACCGGAT -3' (amplified fragment length of 420bp); chromosome two binding primer F: 5′- GATCATTACCGAGTCTTTCTG -3′ and R: 5′- CGTCTGGGTTGCCACAGACGA -3' (amplified fragment length of 550 bp). The PCR products were analyzed by electrophoresis in 2% agarose gel, followed by ethidium-bromide staining.

RESULTS

Case Presentation

The proband was a 25-year-old woman who went to the hospital for medical examination due to ID. No abnormalities were found on electroencephalogram tests. It was learned through interviews that this phenomenon also existed in some of the family members of this woman's family. Among the family members, three had similar physical characteristics as the proband. These included tall, overweight, signs of dementia on the face, duck steps, and ID. In contrast, seven other family members had short, underweight statures, stunted growth, and were unable to restrict their behavior. The pedigree of this family is shown in **Figure 1**, while the detailed phenotypic records of family members are shown in **Table 1**. The differences among healthy, deletion, duplication, and translocation patients are shown in **Table 2**.

Among the surviving family members, the clinical details of the patients with more obvious symptoms are as follows:

IV-10: This 25-year-old female measured 163 cm in height, weighed 90 kg (overweight), and presented with small eyes, a drooping upper left eyelid, a full moon face, wide palms, lack of joints between the ring finger and metacarpal, a short ring finger, and large feet (wearing size 44 shoes on the European scale). Born at full term (40 weeks), she weighed 5 kg at birth with good post-natal feeding. Facial reaction dementia was noted 6–7 months after birth, but no abnormalities were found in the hospital following an EEG examination and other tests. Her intelligence test value was low. While she can take care of herself and communicate with people, she often gives irrelevant answers to questions. She was illiterate and lacked numeracy skills. She walks like a duck (**Figure 2A**).

IV-14: This 24-year-old female measured 157 cm in height and weighed between 90 and 95 kg. She weighed 3.2 kg at birth. She is married and was currently pregnant *in utero* for 7 + months (V-6). Except for typical hand bones and joints, the remaining clinical manifestations were the same as IV-10 (**Figure 2B**).

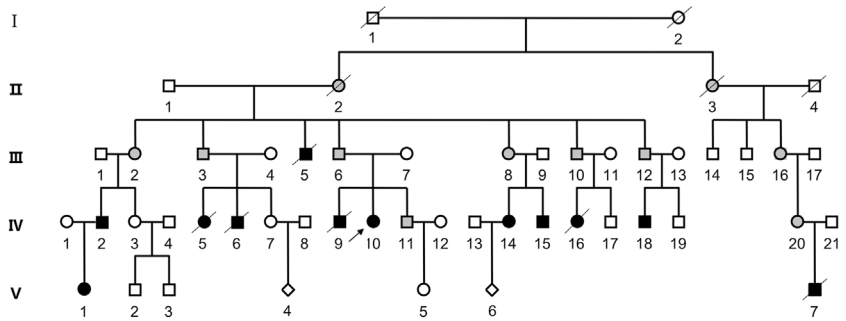

FIGURE 1 | Pedigree of the patient's family. Squares represent male family members, while circles represent female family members. The diamond symbol indicates unknown gender. Slash indicates that the family member is deceased. Black symbols represent individuals with ID/DD, and blank symbols represent unaffected family members. The gray filled symbols indicates balanced translocation carriers.

IV-15: This 17-year-old male measured 130 cm in height and weighed 25 kg (underweight). Born at full-term (40 weeks), he weighed 4 kg at birth. His suction was diminished, he ate less, and he developed slowly. The hospital diagnosed the patient with congenital malnutrition. While this patient is active, he is not good at communicating with others, is unable to pronounce words clearly, and cannot restrict his behavior. He was illiterate and had no numeracy skills (**Figure 2C**).

IV-18: This 13-year-old male measured 110 cm in height, was underweight, had big eyes and double eyelids, and a pointed chin. He weighed 2 kg at birth, had poor suction, ate less frequently when compared to the norm, and was stunted in growth. No abnormalities were seen during the hospitalization. While this patient is active, he cannot restrain his own behavior, is unable to pronounce words clearly, is not good at communicating with others, and often provides irrelevant answers to questions. He had no literacy or numeracy skills. His body posture and clinical manifestations were the same as for patient IV-15 (**Figure 2D**).

Karyotyping

In order to determine whether the patients of this family had intellectual disabilities due to chromosomal abnormalities, blood samples of some of the family members (patients and healthy control samples) were subjected to chromosome analysis. The results showed that the karyotypes of III-3, III-4, III-6, III-7, III-8, III-9, III-12, IV-7, IV-10, IV-11, IV-14, IV-15, IV-18, and IV-19 were normal.

Chromosomal Microarray Analysis

To further understand if there were minor deletions on the chromosomes, comparative genomic hybridization experiments (array CGH) were performed on five samples. The proband (IV-10) and IV-14 were found to harbor the same CNVs, with a 2.2 Mb 2q terminal deletion on chromosome two and a 4.6 Mb 4p terminal duplication on chromosome 4. The latter included the entire 4p16.3 region and part of 4p16.2. However, IV-18, who has a different phenotype, was found to have the opposite CNVs with a 2.2 Mb 2q terminal duplication noted on chromosome two and a 4.6 Mb 4p terminal deletion on chromosome 4. Besides there being a difference in length of less than 10bp, the deletion and duplication positions were the same as IV-10 and IV-14. The CNVs of chromosomes two and 4 of the above-mentioned patients originated from the same balanced translocation (**Figure 3A**). In addition, IV-10 not only possessed a 2.2 Mb 2q terminal deletion on chromosome two and 4.6 Mb 4p terminal duplication on chromosome 4, but also a 411 kb Xp duplication on her X chromosome. Among the family members, III-6 and IV-11 are in good health without any evidence of dysplasia. Except for congenital heart disease found in IV-11, all remaining family members are healthy.

Detection of Some Family Members by PCR Analysis

Based on the CGH results, it was speculated that a balanced translocation was present in the family members. To verify this, two sets of primers were designed for the chromosomes where the translocation occurred (**Figure 3B**). The forward and reverse primer binding positions of the first set of primers were for 2q and 4q respectively, that is, they could only bind to chromosome 4 with 2q fragments. The second set of primers were constructed in a similar way in that 4p fragments would bind to chromosome 2. The two sets of primers are used to amplify the patient's DNA. Banding noted on gel electrophoresis confirmed the presence of the translocation, while an absence of bands indicated normal chromosomal structure. Combining the two sets of results indicated the presence or absence of the translocation of chromosomes 2 and 4 in family members (**Figures 3C,D**).

DISCUSSION

In this study, a large family with an inherited balanced translocation between chromosomes two and 4 is described. This translocation resulted in either a 4.6 Mb deletion at chromosomal position 4p16.3 and a 2.2 Mb duplication at chromosomal position 2q37.3, or a 4.6 Mb duplication at 4p16.3 and a 2.2 Mb deletion at 2q37.3 in the offspring. By combining the patients' conditions, PCR amplification results, and CGH chip analysis results, a pedigree analysis could be

TABLE 1 | Details of the family members.

Clinical phenotype at diagnosis	Gender and age	Height (cm)	Weight (kg)	Development	Nerve state	Language skills	Nutritional status	Muscles and bones	Craniofacial features	Activity and gait	Other
II-1	M,85	153	61	good	normal	After tracheotomy	good	normal	normal	normal	\
III-3	M,59	168	74	good	normal	normal	good	normal	normal	normal	\
III-4	F,60	153	54.5	good	normal	normal	good	normal	normal	normal	\
III-5	M	170	\	\	Congenital dementia	Can communicate with others simply, but often give an irrelevant answer	\	\	\	Cannot restrain one's behavior	died of electric shock at the age of 44. Can take care of himself, can do simple housework, can't read, can't recognize numbers, and has no initiative
III-6	M,50	165	65	good	normal	normal	good	normal	normal	normal	\
III-7	F,50	158	62	good	normal	normal	good	normal	normal	normal	\
III-8	F,48	150	61	good	normal	normal	good	normal	normal	normal	\
III-9	M,46	172	132	good	normal	normal	good	normal	normal	normal	\
III-10	M	162		good	normal	normal	good	normal	normal	normal	\
III-11	F,43	162	56.5	good	normal	normal	good	Mild muscular atrophy in the left lower limb	normal	normal	The right eyeball is staring to the right slightly, with normal activities; the left limb is not flexible, and the calculation ability is poor
III-12	M,40	170	95	good	normal	normal	good	normal	normal	normal	\
IV-2	M,31	170	80	\	Slow response	\	\	\	Dull face, drooping upper left eyelid	\	3.3 kg at birth
IV-5	F	\	\	Stunting	\	\	Malnutrition	Weak sucking power	\	\	Weak sucking power, vomiting after eating, stunted physical development, discharge diagnosed as malnutrition.5–6 months after birth, convulsions occur, and the seizures gradually increase from small to large, Until the major attack, died of convulsions before the age of two
IV-6	M	\	\	Stunting	\	\	Malnutrition	Weak sucking power	\	\	Weak sucking power, vomiting after eating, stunted physical development, discharge diagnosed as malnutrition. Convulsions occurred 5–6 months after birth, and the seizures gradually increased from childhood to major seizures and died of convulsions before the age of two
IV-7	F,24	156	49	good	normal	normal	good	normal	normal	normal	Intrauterine pregnancy 40 + days (V4)

(Continued on following page)

TABLE 1 | (*Continued*) Details of the family members.

Clinical phenotype at diagnosis	Gender and age	Height (cm)	Weight (kg)	Development	Nerve state	Language skills	Nutritional status	Muscles and bones	Craniofacial features	Activity and gait	Other
IV-9	M	\	\	\	\	\	Severe malnutrition	\	\	\	Low birth weight, about 2.5 kg, no sucking power, died 1 month after birth
IV-10	F,25	163	90	good	Slow response	Can communicate with others, but often give an irrelevant answer	good	Flexion of the left knuckle of the two knuckles, no major knuckle of the hand, developmental defects of the index finger and ring finger of both hands; bilateral flat feet, large feet (wearing size 44 shoes)	Dementia face, dull expression, slightly drooping left eyelid	Walk like a duck	No abnormalities in EEG examination and low intelligence test value, no literacy, no numeracy
IV-11	M,21	172	63.5	good	normal	normal	good	normal	normal	normal	Congenital heart disease, diagnosed as ventricular septal defect, surgery at 7 years old, everything is normal after
IV-14	F,24	157	95	good	Slow response	Not very fluent in speaking, can communicate with others, but often give an irrelevant answer	good	Poor thumb development in both hands, shortened joint deformities; collapse of the bridge of the nose; flat feet on both sides	Dementia face, Stiff expression; small eyes, drooping upper left eyelid, full moon face	Walk like a duck	7 months pregnant
IV-15	M,17	130	30	Stunting	Slow response and naive behavior	Weak tongue, dysarthria, Slurred speech	Congenital malnutrition	Limited flexion and extension of the little fingers of both hands	Childish face	active, cannot restrain one's behavior	2 kg weight at birth, sucking power is acceptable, but small appetite: no literacy, no numeracy
IV-16	\	\	\	\	\	\	\	\	\	\	low weight at birth, about 2 kg, no suction, and died about a month after birth
IV-17	M,19	160	52.5	good	normal	normal	good	normal	normal	normal	Poor computing power
IV-18	M,13	110	20	Stunting	Slow response and naive behavior	Impossibility of tongue extension, dysarthria, slurred speech, often give an irrelevant answer	Malnutrition	lower than his peers, Flexion of both thumbs	Horror face, Head circumference 48 cm	active, cannot restrain one's behavior	weighs 2 kg at birth, has a weak sucking power, and eats less. No secondary sexual characteristics, no literacy, no numeracy
IV-19	M,8	128	24	good	normal	normal	good	normal	normal	normal	
V-1	F,2	\	\	\	Slow response	Slurred speech	\	\	\	\	Suspected mild intellectual disability
V-5	F,2.5		14.6	good	normal	normal	good	normal	normal	normal	\
V-7	\	\	87	\	\	\	\	\	\	\	Death at 12 years old, appearance and clinical manifestations are the same as IV18

TABLE 2 | Differences among healthy, deletion, duplication, and translocation patients.

Patient	Rearrangement	Development	Nerve state	Language skills	Nutritional status	Muscles and bones	Craniofacial features	Activity and gait	Other
III-7	46, (XX)	good	normal	normal	good	normal	normal	normal	\
IV-10	der (2) t (2; 4) (q37.3; p16.3)	good	Slow response	Can communicate with others, but often give an irrelevant answer	good	Flexion of the left knuckle of the two knuckles, no major knuckle of the hand, developmental defects of the index finger and ring finger of both hands; bilateral flat feet, large feet (wearing size 44 shoes)	Dementia face, dull expression, slightly drooping left eyelid	Walk like a duck	No abnormalities in EEG examination and low intelligence test value, no literacy, no numeracy
IV-14		good	Slow response	Not very fluent in speaking, can communicate with others, but often give an irrelevant answer	good	Poor thumb development in both hands, shortened joint deformities; collapse of the bridge of the nose; flat feet on both sides	Dementia face, Stiff expression; small eyes, drooping upper left eyelid, full moon face	Walk like a duck	7 months pregnant
IV-15	der (4) t (2; 4) (q37.3; p16.3)	Stunting	Slow response and naive behavior	Weak tongue, dysarthria, Slurred speech	Congenital malnutrition	Limited flexion and extension of the little fingers of both hands	Childish face	active, cannot restrain one's behavior	2 kg weight at birth, sucking power is acceptable, but small appetite; no literacy, no numeracy
IV-18		Stunting	Slow response and naive behavior	Impossibility of tongue extension, dysarthria, slurred speech, often give an irrelevant answer	Malnutrition	lower than his peers, Flexion of both thumbs	Horror face, Head circumference 48 cm	active, cannot restrain one's behavior	weighs 2 kg at birth, has a weak sucking power, and eats less. No secondary sexual characteristics, no literacy, no numeracy
III-3	t (2; 4) (q37.3; p16.3)	good	normal	normal	good	normal	normal	normal	\
III-12		good	normal	normal	good	normal	normal	normal	\
IV-11		good	normal	Z	good	normal	normal	normal	Congenital heart disease, diagnosed as ventricular septal defect, surgery at 7 years old, everything is normal after

performed for this family. Among the pedigrees developed from II-1 and II-2, it was noted that each family had an affected individual in the fourth generation, while balanced translocations were observed for family members III-3, III-12, and IV-11. It can be speculated that the offspring of II-1 and II-2 all possessed a balanced translocation. As their spouses demonstrated normal phenotypes, the fourth generation of patients and normal phenotypes appeared at the same time.

While the chromosomal phenotype of II-1 was completely normal, all offspring possessed balanced translocations. It is possible that germ cell mutations in II-2 resulted in homozygous translocations in the offspring. However, this hypothesis cannot explain the cause of the clinical presentation of III-5. As this patient had died, it was not possible to determine his chromosomal phenotype. It is therefore speculated that unknown, spontaneous changes occurred during the formation of gametes in both parents. Due to a lack of data, the family that extended from II-3 and II-4 could not be analyzed. It is theorized that it is possible that the clinical features of both III-16 and IV-20 are due to balanced translocations, and that patient V-7 harbors a dup2q + del4p variation due to having a clinical phenotype that is the same as

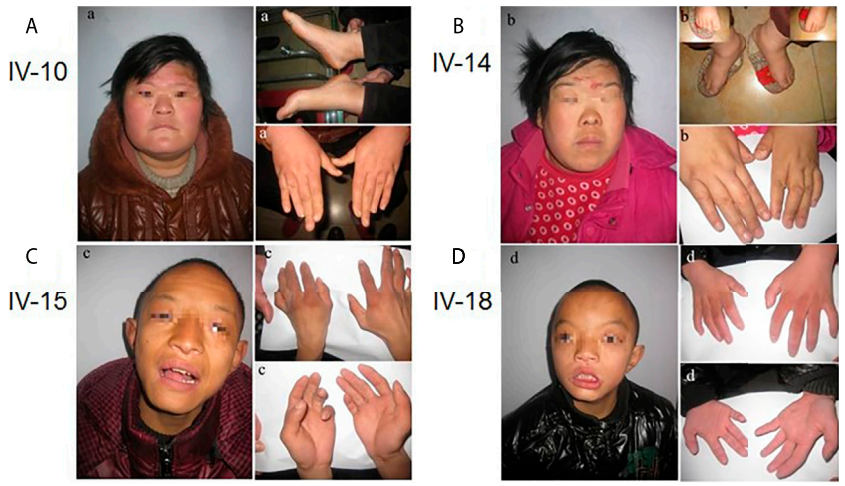

FIGURE 2 | Facial features, hand and foot characteristics of patients with more obvious symptoms in the family.

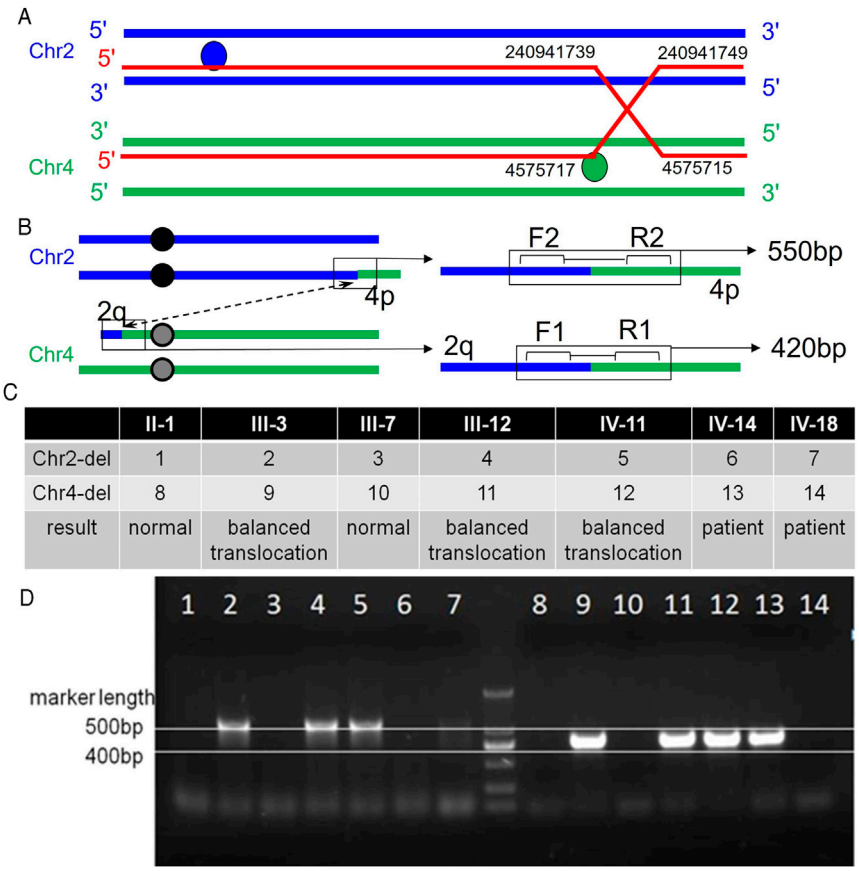

	II-1	III-3	III-7	III-12	IV-11	IV-14	IV-18
Chr2-del	1	2	3	4	5	6	7
Chr4-del	8	9	10	11	12	13	14
result	normal	balanced translocation	normal	balanced translocation	balanced translocation	patient	patient

FIGURE 3 | Primer position and agarose gel electrophoresis results. A: The breakpoint and binding position of the ectopic occurrence. Balanced translocation carriers have reciprocal and symmetric translocations, t (2; 4) (q37.1; p16.2). B: Primer position diagram. The forward and reverse primer binding positions of the first pair of primers are 2q and 4q respectively, that is, they can only bind to chromosome 4 with a 2q fragment. The second set of primers can also only bind to chromosome two and 4p fragments. C: Analysis of electrophoresis results. Bands are present in both primer pairs, indicating that the sample source represents a balanced translocation carrier. Neither band indicates that the sample source is normal. Only one pair of primers indicates that the sample source is that of a patient. D: Electrophoresis results.

patient IV-18. This scenario has a lower probability of being correct.

Based on the array CGH results, it is hypothesized that the cause of the disease in this family is mainly related to the deletion or duplication of 4p16.3. Microdeletions on the short arm of chromosome 4 are associated with WHS, which is a rare disease with an incidence of about 1/200 to 1/500,000. While the size of the deletion varies from person to person, studies have shown that larger deletions can lead to more severe ID and physical abnormalities (Akhtar, 2008; Dai et al., 2013; Battaglia et al., 2015). In this family, the 4p16.3 region of IV-18 was completely deleted. This included the deletion of the *WHSC1* gene. As the phenotype of this patient matched the core characteristics of WHS, it is believed that IV-18 suffers from WHS. The phenotypes of other affected family members may also be associated with WHS.

Similarly, duplications on chromosome 4 are likely to be pathogenic, with three cases having been reported to date (Hannes et al., 2010; Cyr et al., 2011; Palumbo et al., 2015). All three cases presented with the following clinical features: musculoskeletal abnormalities, psychomotor and speech delays, craniofacial abnormalities (frontal lobe protrusion, high forehead, short neck, hyperopia/blepharochalasis, epicanthal folds). These common features suggest that occult 4p16.3 replication leads to a novel recognizable microreplication syndrome; one patient was diagnosed with a form of giantism, while another patient was noted to present with overgrowth. In addition, a large study on 4p16.3 microdeletions and microduplications also provides evidence for 4p16.3 microduplication syndrome (Bi et al., 2016). The phenotypes of patients with duplicated 4p regions in this family, namely IV-10 and IV-14, are similar to those characteristics associated with 4p16.3 microduplication syndrome. SNP array analysis showed a 4p16.3 duplication of a maximum size of 413 kb, from nucleotide 1,390,388 to nucleotide 1,804,276, and a minimum duplication size of 393 kb, from nucleotide 1,405,662 to nucleotide 1,798,461. The repeated region contains the complete coding sequence of the 5′ ends of the *FAM53A*, *SLBP*, *TMEM129*, *TACC3*, and *FGFR3* genes. The *FAM53A*, *TACC3*, and *FGFR3* genes appear to play key roles in the etiology of the clinical phenotype (Palumbo et al., 2015). The deletions and duplications on 4p in this family include the entire 16.3 region. Therefore, it is believed that the cause of the illness in patients IV-10 and IV-14 is likely related to the duplication of 4p. Family members with phenotypes like that observed for patients IV-10 and IV-14 may similarly harbor this duplication.

The position of the deletions or duplications on chromosome two were found to be part of region 2q37.3. Deletions of this region have been the focus of studies targeting 2q37.3 deletion syndrome cases. This syndrome belongs to the chromosome 2q37 deletion disorder spectrum; some of its core phenotypes also manifest in this family. As for the duplication of 2q37.3, there is no definite report about the pathogenicity of this region, so the effect of it on patients is not clear. Duplications or deletions of 2q37.3 and their effects on human health therefore need further research.

Based on the analyses conducted in this study, we believe that the deletion or duplication of fragments on chromosome 4 resulted in patients with complex phenotypes within families. Deletions and duplications in the 4p16.3 region appeared to cause two reciprocal syndromes: WHS and 4p16.3 microduplication syndrome. In this report, we provide clinical and molecular evidence supporting the existence of 4p16.3 microduplication syndrome, expand the database related to both syndromes, and provide a new basis for the prenatal diagnosis of these two conditions.

DATA AVAILABILITY STATEMENT

The original contributions presented in the study are included in the article/supplementary material, further inquiries can be directed to the corresponding author.

ETHICS STATEMENT

The studies involving human participants were reviewed and approved by the Ethics Committee of Zhujiang Hospital, an affiliate of Southern Medical University (Guangdong, China). Written informed consent to participate in this study was provided by the participants' legal guardian/next of kin. Written informed consent was obtained from the individual(s), and minor(s)' legal guardian/next of kin, for the publication of any potentially identifiable images or data included in this article.

AUTHOR CONTRIBUTIONS

JW, XLZ, performed experiments. SYZ collected samples. JQL and FZ performed the Chromosomal Microarray Analysis. XMX and FX conceived the experiments, interpreted data and wrote the paper aided by FH and JW.

FUNDING

This work was supported mainly by a grant from the National Natural Science Foundation of China (31970558, 32170617), the Science and Natural Science Foundation of Guangdong Province (2020A1515010308), Research Grant of Guangdong Province Key Laboratory of Psychiatric Disorders (N201903), Science and Technology planning project of Guangdong Province, China (2016A020218010) and the Foshan Science and technology project (2020001003953).

ACKNOWLEDGMENTS

We thank the family members for their participation in the study.

REFERENCES

Akhtar, N. (2008). Wolf-Hirschhorn Syndrome. *J. Coll. Physicians Surg. Pak.* 18 (4), 254–256.

Andersen, E. F., Carey, J. C., Earl, D. L., Corzo, D., Suttie, M., Hammond, P., et al. (2014). Deletions Involving Genes WHSC1 and LETM1 May Be Necessary, but Are Not Sufficient to Cause Wolf-Hirschhorn Syndrome. *Eur. J. Hum. Genet.* 22 (4), 464–470. doi:10.1038/ejhg.2013.192

Battaglia, A., Carey, J. C., and South, S. T. (2015). Wolf-Hirschhorn Syndrome: A Review and Update. *Am. J. Med. Genet.* 169 (3), 216–223. doi:10.1002/ajmg.c.31449

Bergemann, A., Cole, F., and Hirschhorn, K. (2005). The Etiology of Wolf?Hirschhorn Syndrome. *Trends Genet.* 21 (3), 188–195. doi:10.1016/j.tig.2005.01.008

Bi, W., Cheung, S. W., Breman, A. M., and Bacino, C. A. (2016). 4p16.3 Microdeletions and Microduplications Detected by Chromosomal Microarray Analysis: New Insights into Mechanisms and Critical Regions. *Am. J. Med. Genet. A.* 170 (10), 2540–2550. doi:10.1002/ajmg.a.37796

Cyr, A. B., Nimmakayalu, M., Longmuir, S. Q., Patil, S. R., Keppler-Noreuil, K. M., and Shchelochkov, O. A. (2011). A Novel 4p16.3 Microduplication Distal to WHSC1 and WHSC2 Characterized by Oligonucleotide Array with New Phenotypic Features. *Am. J. Med. Genet.* 155 (9), 2224–2228. doi:10.1002/ajmg.a.34120

Dai, Y., Yang, J., Chen, Y., Bao, L., and Cheng, Q. (2013). Microarray Analysis of Unbalanced Translocation in Wolf-Hirschhorn Syndrome. *Pediatr. Int.* 55 (3), 368–370. doi:10.1111/j.1442-200x.2012.03684.x

Engbers, H., van der Smagt, J. J., van 't Slot, R., Vermeesch, J. R., Hochstenbach, R., and Poot, M. (2009). Wolf-Hirschhorn Syndrome Facial Dysmorphic Features in a Patient with a Terminal 4p16.3 Deletion Telomeric to the WHSCR and WHSCR 2 Regions. *Eur. J. Hum. Genet.* 17 (1), 129–132. doi:10.1038/ejhg.2008.168

Hannes, F., Drozniewska, M., Vermeesch, J. R., and Haus, O. (2010). Duplication of the Wolf-Hirschhorn Syndrome Critical Region Causes Neurodevelopmental Delay. *Eur. J. Med. Genet.* 53 (3), 136–140. doi:10.1016/j.ejmg.2010.02.004

Kirov, G. (2015). CNVs in Neuropsychiatric Disorders. *Hum. Mol. Genet.* 24 (R1), R45–R49. doi:10.1093/hmg/ddv253

Moeschler, J. B. (2008). Medical Genetics Diagnostic Evaluation of the Child with Global Developmental Delay or Intellectual Disability. *Curr. Opin. Neurol.* 21 (2), 117–122. doi:10.1097/wco.0b013e3282f82c2d

Nevado, J., Ho, K. S., Zollino, M., Blanco, R., Cobaleda, C., Golzio, C., et al. (2020). International Meeting on Wolf-Hirschhorn Syndrome: Update on the Nosology and New Insights on the Pathogenic Mechanisms for Seizures and Growth Delay. *Am. J. Med. Genet.* 182 (1), 257–267. doi:10.1002/ajmg.a.61406

Palumbo, O., Palumbo, P., Ferri, E., Riviello, F. N., Cloroformio, L., Carella, M., et al. (2015). Report of a Patient and Further Clinical and Molecular Characterization of Interstitial 4p16.3 Microduplication. *Mol. Cytogenet.* 8, 15. doi:10.1186/s13039-015-0119-6

Schalock, R. L., Luckasson, R. A., Shogren, K. A., Borthwick-Duffy, S., Bradley, V., Buntinx, W. H., et al. (2007). The Renaming ofMental Retardation: Understanding the Change to the TermIntellectual Disability. *Intellect. Dev. disabilities* 45 (2), 116–124. doi:10.1352/1934-9556(2007)45[116:tromru]2.0.co;2

Titomanlio, L., Romano, A., Conti, A., Genesio, R., Salerno, M., De Brasi, D., et al. (2004). Mild Wolf-Hirschhorn Phenotype and Partial GH Deficiency in a Patient with a 4p Terminal Deletion. *Am. J. Med. Genet.* 127A (2), 197–200. doi:10.1002/ajmg.a.20667

Zhang, R., Chen, S., Han, P., Chen, F., Kuang, S., Meng, Z., et al. (2020). Whole Exome Sequencing Identified a Homozygous Novel Variant in CEP290 Gene Causes Meckel Syndrome. *J. Cel Mol Med.* 24 (2), 1906–1916. doi:10.1111/jcmm.14887

Conflict of Interest: The authors declare that the research was conducted in the absence of any commercial or financial relationships that could be construed as a potential conflict of interest.

Publisher's Note: All claims expressed in this article are solely those of the authors and do not necessarily represent those of their affiliated organizations, or those of the publisher, the editors and the reviewers. Any product that may be evaluated in this article, or claim that may be made by its manufacturer, is not guaranteed or endorsed by the publisher.

frontiers in Genetics

CASE REPORT
published: 01 December 2021
doi: 10.3389/fgene.2021.761003

Case Report: Congenital Brain Dysplasia, Developmental Delay and Intellectual Disability in a Patient With a 7q35-7q36.3 Deletion

Liang-Liang Fan[1,2,3†], *Yue Sheng*[3†], *Chen-Yu Wang*[3], *Ya-Li Li*[2*] and *Ji-Shi Liu*[1,3*]

[1]Department of Nephrology, The Third Xiangya Hospital of Central South University, Changsha, China, [2]Departments of Reproductive Genetics, HeBei General Hospital, ShiJiaZhuang, China, [3]Department of Cell Biology, The School of Life Sciences, Central South University, Changsha, China

OPEN ACCESS

Edited by:
Santasree Banerjee,
Beijing Genomics Institute (BGI), China

Reviewed by:
Mohammed Ali Al Balwi,
King Saud bin Abdulaziz University for Health Sciences, Saudi Arabia
Thomas Liehr,
Friedrich Schiller University Jena, Germany
M. Anwar Iqbal,
University of Rochester, United States

***Correspondence:**
Ya-Li Li
lyl8703@sina.com
Ji-Shi Liu
jishiliuxy3yy@163.com

[†]These authors have contributed equally to this work

Specialty section:
This article was submitted to Genetics of Common and Rare Diseases, a section of the journal Frontiers in Genetics

Received: 19 August 2021
Accepted: 05 November 2021
Published: 01 December 2021

Citation:
Fan L-L, Sheng Y, Wang C-Y, Li Y-L and Liu J-S (2021) Case Report: Congenital Brain Dysplasia, Developmental Delay and Intellectual Disability in a Patient With a 7q35-7q36.3 Deletion. Front. Genet. 12:761003. doi: 10.3389/fgene.2021.761003

7q terminal deletion syndrome is a rare condition presenting with multiple congenital malformations, including abnormal brain and facial structures, developmental delay, intellectual disability, abnormal limbs, and sacral anomalies. At least 40 OMIM genes located in the 7q34-7q36.3 region act as candidate genes for these phenotypes, of which *SHH*, *EN2*, *KCNH2*, *RHEB*, *HLXB9*, *EZH2*, *MNX1* and *LIMR1* may be the most important. In this study, we discuss the case of a 2.5-year-old male patient with multiple malformations, congenital brain dysplasia, developmental delay, and intellectual disability. A high-resolution genome-wide single nucleotide polymorphism array and real-time polymerase chain reaction were performed to detect genetic lesions. A *de novo* 9.4 Mb deletion in chromosome region 7q35-7q36.3 (chr7: 147,493,985–156,774,460) was found. This chromosome region contains 68 genes, some of which are candidate genes for each phenotype. To the best of our knowledge, this is a rare case report of 7q terminal deletion syndrome in a Chinese patient. Our study identifies a rare phenotype in terms of brain structure abnormalities and cerebellar sulcus widening in patients with deletion in 7q35-7q36.3.

Keywords: 7q terminal deletion syndrome, 7q35-7q363 deletion, SNP array, cerebellar sulcus widening, congenital brain dysplasia, developmental delay

INTRODUCTION

The 7q deletion syndrome is a rare genetic disorder caused by the deletion of the long arm of chromosome 7 (Ayub et al., 2016). This 7q deletion was first described in patients with unusual facial structure and delayed mental and physical development, and was consequently defined as a syndrome in 1977 (Harris et al., 1977). The characteristic features of the 7q deletion include developmental delay, intellectual disability, behavioral problems, and distinctive facial features; penoscrotal transposition or ulnar ray deficiency, Kaposi sarcoma, oral malformations, mitral dysplasia, and scoliosis have also been reported (Lewis et al., 1996).

Relatively little is known regarding 7q terminal deletions in contiguous gene deletion syndrome. The typical clinical features of 7q terminal deletion syndrome include abnormal brain and facial structures, developmental delay, intellectual disability, abnormal limbs, and sacral anomalies (Rush et al., 2013; Jackson et al., 2017). At present, 7q terminal deletion syndrome has only been described in 28 patients, most of whom had 7q36 microdeletions

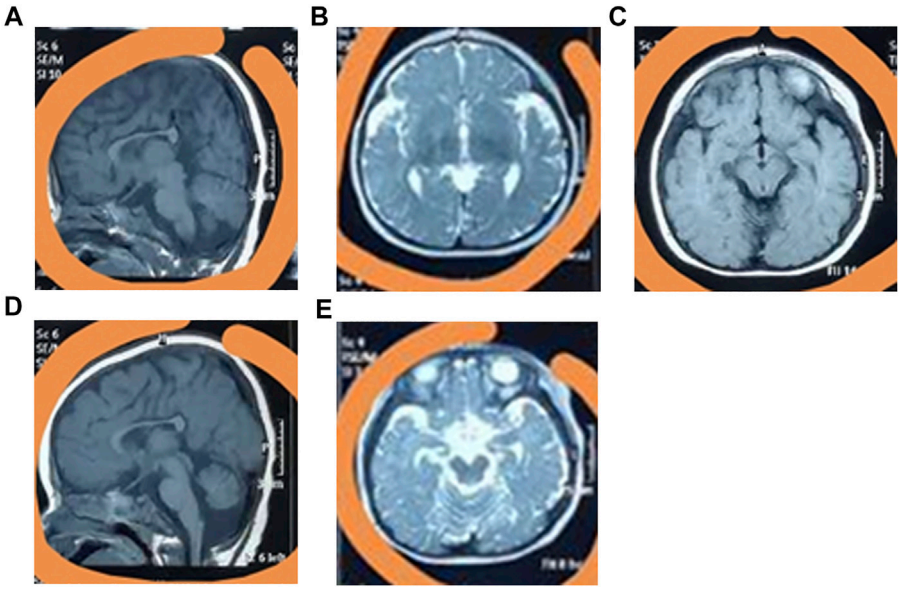

FIGURE 1 | The clinical phenotypes of the patient. The MRI testing identified the overt carcass dysplasia **(A)**, bilateral forehead subarachnoid space widening **(B)**, right iliac choroidal fissure cyst **(C)**, large cisterna magna **(D)**, and cerebellar sulcus widening **(E)**.

(Jackson et al., 2017). This region contains more than 40 OMIM genes, of which *SHH*, *EN2*, *KCNH2*, *RHEB*, *HLXB9*, *EZH2*, *MNX1* and *LIMR1* have been nominated as candidate dosage-sensitive key genes of clinical significance associated with this disorder (Rush et al., 2013; Coutton et al., 2014; Hyohyeon and Lee, 2015; Ayub et al., 2016; Jackson et al., 2017).

Majority of previous published cases were based on traditional G-banding resolution, which is inadequate to define cryptic interstitial deletion in the terminal region. With the development of SNP array technology, which can determine the precise breakpoints instead of terminal deletion, majority of these cases are found as *de novo* in origin. Here, we describe the case of a 2.5-year-old boy with multiple malformations, including congenital brain dysplasia, developmental delay, and intellectual disability, carrying a 9.4 Mb microdeletion in 7q35-7q36.3 (chr7: 147,493,985–156,774,460).

Case Presentation

The patient was a 2.5-year-old boy who first presented to the Department of Pediatrics of Hebei General Hospital due to developmental delay. Both his parents were healthy and were never exposed to undesirable substances, such as poisons and radiation. A family history of birth defects was absent. Pregnancy hypertension occurred at 34 weeks of pregnancy. At that time, B-mode ultrasound suggested that the fetus was 2 weeks less advanced and the head circumference was 3 weeks less advanced than the actual gestational age. Therefore, the mother underwent cesarean delivery.

The baby was bruised, and exhibited feeding difficulties after birth, with an Apgar score of 6. At six-months-old, he could sit with the help of external objects. At 9 months old, he could not crawl. The baby began to speak at 1.5 years old but could only enunciate simple words, and even now he cannot say full sentences. At present, the patient has a normal weight (11.5 kg) and height (90 cm), but a small head circumference (42 cm), eye crack, broad ears, and a pointed chin (**Supplementary Figure S1**). Furthermore, the patient cannot walk independently. Brain MRI revealed overt carcass dysplasia (**Figure 1A**), bilateral forehead subarachnoid space widening (**Figure 1B**), right iliac choroidal fissure cyst (**Figure 1C**), large cisterna magna (**Figure 1D**), and cerebellar sulcus widening (**Figure 1E**).

Banding cytogenetic results of the patient revealed a deletion of the long arm of chromosome 7, described as 46,XY,del (7)(q36). His parents' karyotypes were normal (**Supplementary Figure S2**). We subsequently performed single nucleotide polymorphism (SNP) array with Human660W-Quad Chip (Illumina Inc., San Diego, United States) to analyze any genetic lesions. A total of 173 CNVs were identified in the proband. Compared with the database of Genomic Variants, a *de novo* 9.4 Mb deletion ranging from 7q35 to q36.3 (chr7:147,493,985–156,774,460) (hg 38) was detected (**Figure 2**). This chromosome region contains approximately 68 genes, including *CNTNAP2*, *AGAP3*, *CDK5*, *CUL1*, *KMT2C*, *XRCC2*, *DPP6*, *HTR5A*, *EN2, SHH*, *LMBR1*, *KCNH2*, *PRKAG2,* and *EZH2*. The patient's parents did not carry this genomic lesion. Real-time quantitative polymerase chain reaction with part of the genomic DNA (SHH gene, the primers were as follows: forward: 5-GCAAGT GGCAACTCACCTA-3, reverse: 5-TTTATTTACCTCAGG CCCTAACC-3) of the trio (the proband and his parents) further confirmed this *de novo* deletion (**Supplementary Figure S3**).

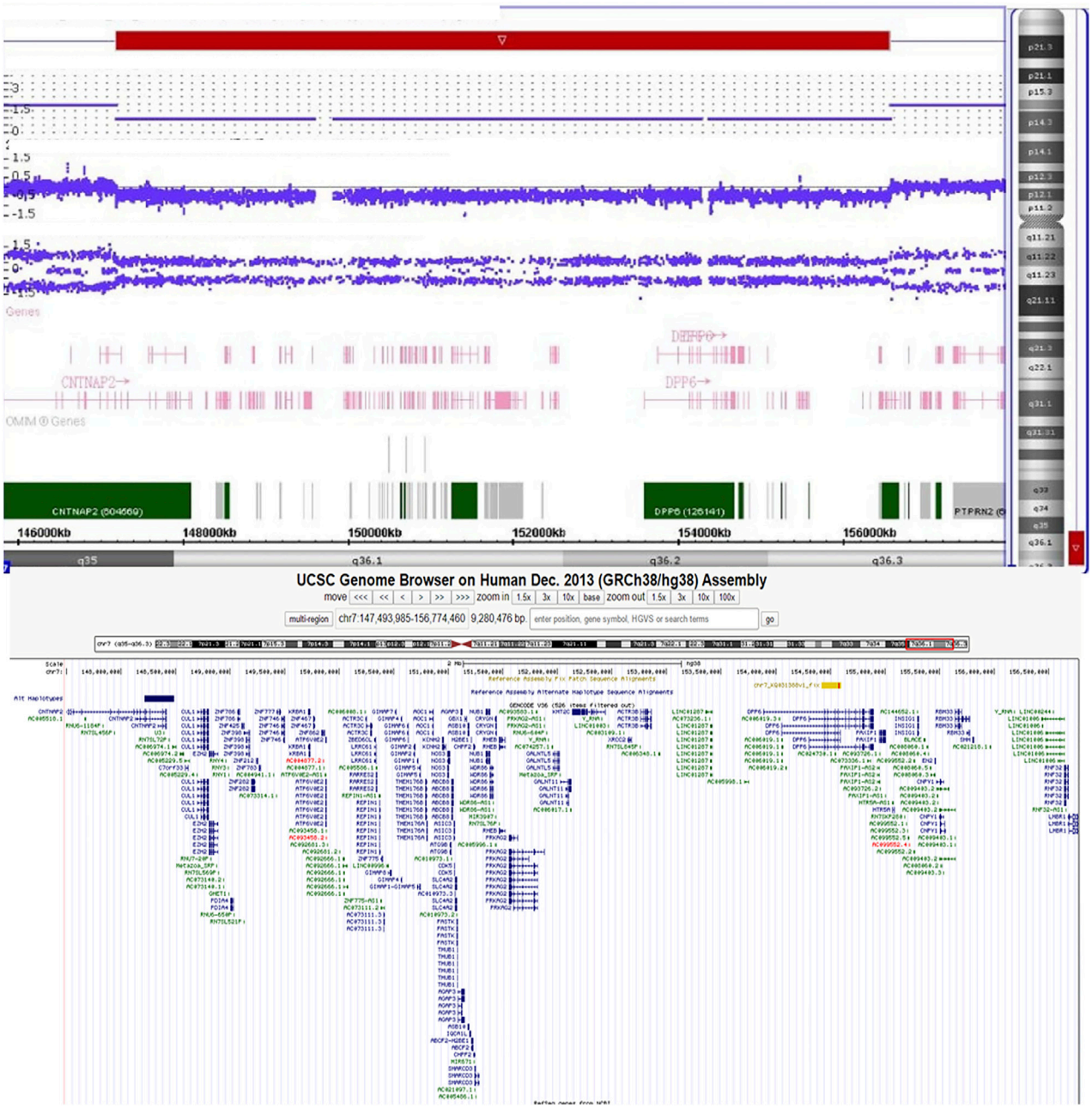

FIGURE 2 | The SNP array identified a 7q35-7q36.3 (chr7:147,493,985–156,774,460) deletion in the patient.

DISCUSSION

7q terminal deletion syndrome is a rare disorder worldwide. Currently, there have been very few reports in the Chinese population. In this study, we report a heterozygous 9.4 Mb microdeletion of 7q35-q36.3 (chr7:147,493,985–156,774,460) in a 2.5-year-old boy with congenital brain dysplasia, developmental delay, and intellectual disability. The findings of our study are consistent with those of previous studies and report that microdeletion in the 7q terminal may lead to abnormal brain and facial structures, developmental delay, and intellectual disability (Linhares et al., 2014; Busa et al., 2016).

There are several significant genes located in the region of 7q35-q36.3 (chr7:147,493,985–156,774,460). Previous studies have shown that mutations in *CNTNAP2*, *KMT2C*, *EN2* and *EZH2* can lead to intellectual disability and autism spectrum disorder (Penagarikano et al., 2011; Sundaram et al., 2014;

TABLE 1 | The summary of reported patients with 7q35-7q36 microdeletions.

Patient reported	Our patient	Suri and Dixit. (2017)	Jackson et al. (2017)	Busa et al. (2016)	Hyohyeon and Lee. (2015)	Coutton et al. (2014)	Rush et al. (2013)	Pelegrino et al. (2013)	
Sex	M	M	F	M	M	M	F	M	
Age	2.5 years	13 years	16 years	2 years	13 years	-	12 years	-	
Cytogenetic location	7q35-q36.3	7q36.1	7q34-q36.3	7q35–q36.3	7q36.1-q36.3	7q36	7q34-q36.1	7q36.1-q36.3	
Size of deletion	9.4 Mb	1.2 Mb	16 Mb	14 Mb	6.89 Mb	2.7 Mb	13.2 Mb	-	
Brain structure abnormalies	carcass dysplasia; bilateral forehead subarachnoid space widening; right iliac choroidal fissure cyst; cerebellar sulcus widening	-	-	-	-	-	-	hypoplasia of corpus callosum; white matter reduction	
Facial features	small head circumference; eye crack; broad ears; pointed chin	hypertelorism with downslanting palpebral fissures; coarse hair; full lips	dental malposition	bitemporal narrowing; upslanting palpebral fissures; bulbous nose; down turned corners of the mouth	downslanting palpebral fissures; a bulbous nasal tip	congenital nasal pyriform aperture stenosis	cleft lip and cleft palate; broad nasal bridge; bulbous nasal tip; deep-set eyes	bilateral epicanthal folds; upslanting palpebral fissures; bulbous nasal tip; enlarged columela; posteriorly rotated ears	
Growth retardation	+		+	+	+		+	+	
Intellectual disability	+	+	+	-	+	-	+		
Hearing loss	-	-	-	-			+		
Speech delay	+	+	+	+	+		+	+	
Seizures	-	-	-	-	+	-	+	+	
Short stature	-	-	-	-	+	-	+		
Poor attention	+	-	+	-	+	-	+	+	
Heart defect	-	-	+	-		-	-	-	
Limbs	-	Hypotonia	-	-	oligodactyly	-	-	Finger hyperconvex	
Urogenital anomalies	-	-	-	+	+	+	-	+	
Patient reported	Sehested et al. (2010) 1#	Sehested et al. (2010) 2#	Petrin et al. (2010)	Caselli et al. (2008)	Rossi et al. (2008)	Bisgaard et al. (2006)	Bisgaard et al. (2006)	Verma et al. (1992)	Fagan et al. (1994)
Sex	F	F	M	F	F	F	F	F	F
Age	42 years	34 years	-	-	-	-	-		
Cytogenetic location	7q34-q36.2	7q34-q36.2	7q33-q35	7q36.1-q36.2	7q33-q36.1	7q34-q36.2	7q34-q36.2	7q36.1-q36.2	7q35
Size of deletion	12.2 Mb	12.2 Mb	10 Mb	5.27 Mb	12 Mb	12.4 Mb	12.2 Mb	5.27 Mb	-
Brain structure abnormalies	-	-	cerebellar atrophy	hypoplasia of the corpus callosum	-	-	-	-	-
Facial features	hypertelorism; deep-set eyes; narrow palpebral fissures; bulbous nasal tip; broad nasal bridge; broad mouth; low-set ears	hypertelorism, deep-set eyes, narrow palpebral fissures, bulbous nasal tip, broad nasal bridge, broad	broad nasal root	prominent forehead; deep set eyes; posteriorly angulated ears; bilateral epicanthal folds; flat nasal bridge; bulbous nasal tip; flat malar region	bulbous nasal tip; deep-set eyes; broad nasal bridge	round face; deep-set eyes; narrow palpebral fissures; low set ears; bulbous nasal tip;	round face; deep-set eyes; narrow palpebral fissures; low set ears;	cleft lip, cleft palate	bulbous nasal tip

(Continued on following page)

TABLE 1 | (*Continued*) The summary of reported patients with 7q35-7q36 microdeletions.

Patient reported	Our patient	Suri and Dixit. (2017)	Jackson et al. (2017)	Busa et al. (2016)	Hyohyeon and Lee. (2015)	Coutton et al. (2014)	Rush et al. (2013)	Pelegrino et al. (2013)	
		mouth, and thick vermilion				smooth philtrum; narrow upper lip	bulbous nasal tip; smooth philtrum; narrow upper lip		
Growth retardation	+	+	-	+	+	+	+	+	+
Intellectual disability	+	+	-	+	+	+	+	+	+
Hearing loss	-	-	-			+	+	+, Conductive	
Speech delay	+	+	+	+	+			+	+
Seizures	+	+	-	+	+	+	+	+, Febrile	-
Short stature	+	+	-	-	+	-	-		
Poor attention	+	+	-	-	-	+	+	-	-
Heart defect	-	-	-	-	-				
Limbs	-	-	broad halluces	Small hands	-	-	-	-	-
Urogenital anomalies	+	+	-		-	-	-	-	-

M, male; F, female.

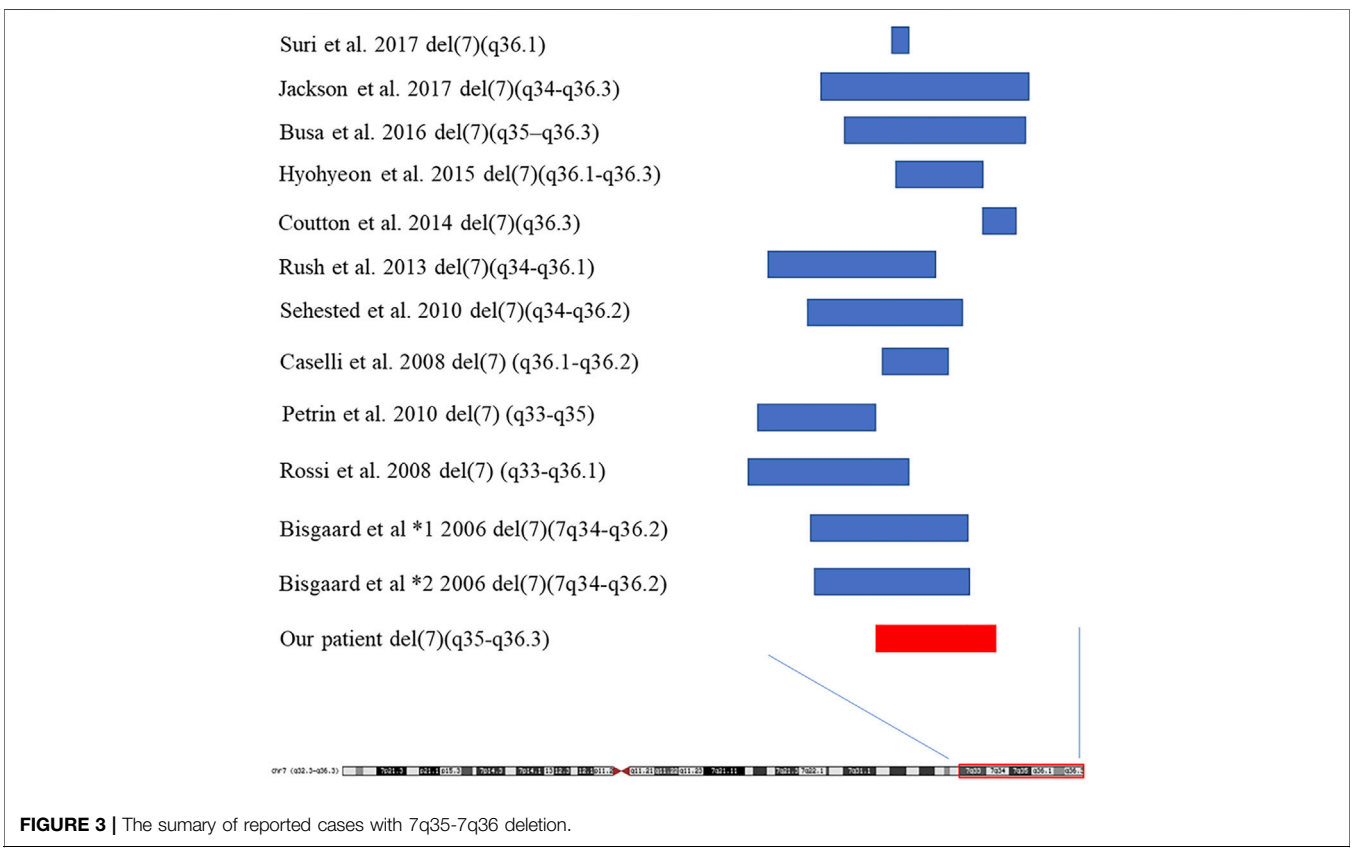

FIGURE 3 | The sumary of reported cases with 7q35-7q36 deletion.

Koemans et al., 2017; Suri and Dixit, 2017); *CDK5* is required for proper development of the mammalian central nervous system (Alvarez-Periel et al., 2018), *AGAP3* can regulate synaptic plasticity (Oku and Huganir, 2013), *XRCC2* is required for embryonic neurogenesis (Deans et al., 2000), DPP6 mutations may explain the lateral sclerosis (van Es et al., 2008), and *HTR5A* is a candidate gene for schizophrenia (Guan et al., 2016). These findings may explain congenital brain dysplasia and intellectual disability phenotypes. Furthermore, *DPP6* encodes a dipeptidyl-peptidase-like protein expressed predominantly in the brain, with very high expression in the cerebellum, which may explain the new phenotype of cerebellar sulcus widening (van Es et al., 2008). Finally, *CUL1* can regulate the β-catenin and Wnt pathways, which play a crucial role in body development (Wei et al., 2007).

In fact, another four genes (*SHH*, *LMBR1*, *KCNH2*, and *PRKAG2*) may also affect the phenotypes of 7q terminal deletion syndrome (Hyohyeon and Lee, 2015; Jackson et al., 2017). First, *SHH* and *LMBR1* are responsible for bone and tooth development; therefore, most 7q terminal deletion patients may show microcephaly, abnormal hand, and scoliosis (Rush et al., 2013). In our case, the head circumference was smaller than that in normal individuals, which may have been caused by the haploinsufficiency of the *SHH* and *LMBR1* genes. In addition, two other genes of interest were *KCNH2* and *PRKAG2*; *KCNH2* is a candidate gene of Long QT syndrome (Tuveng et al., 2018) and mutations in *PRKAG2* may lead to hypertrophic cardiomyopathy (Porto et al., 2016). However, most 7q terminal deletion patients show no obvious cardiovascular disorders. In our study, the patient also did not have cardiovascular disease, but we think 7q terminal deletion patients may have a high risk for the future development of cardiovascular disorders, and we will continue to follow the patient.

We summarized the 16 reported patients with 7q35-7q36 microdeletion, and found that facial deformities, growth retardation, intellectual disability, speech delay, and poor attention were the common phenotypes in 7q35-7q36 microdeletion patients (**Table1**; **Figure 3**), and the 7q36.1-7q36.3 including *EZH2*, *MNX1* and *SHH* may be the critical region of the 7q deletion syndrome which is responsible for facial malformation, developmental delay and intellectual disability (Coutton et al., 2014; Hyohyeon and Lee, 2015; Suri and Dixit, 2017). However, other phenotypes, including abnormal limbs, hearing loss, seizures, short stature, heart defects, and urogenital anomalies have been rarely reported. Meanwhile, most cases with 7q35-7q36 microdeletion have been reported in the United States population (Roessler et al., 1996). Compared to reported cases with 7q35-7q36 microdeletion, we did not observe any limb abnormalities, hearing loss, seizures, short stature, heart defect, or urogenital anomalies in our case. Simultaneously, brain structure abnormalities were only reported in three cases with 7q35-7q36 microdeletions. Caselli et al. reported the hypoplasia of the corpus callosum in a 9-year-old girl with a 5.27 Mb deletion in 7q36.1-q36.2 (Caselli et al., 2008). In 2010, Petrin et al. described cerebellar atrophy in a Brazilian stuttering case with a 10 Mb deletion of chromosome region 7q33-35 (Petrin et al., 2010). Afterwards, Pelegrino et al. reported the hypoplasia of corpus callosum and white matter reduction in a child with a deletion of 7q36.1–36.3 and duplication of 9p22.3–23 (Pelegrino et al., 2013). All the reported 7q35-7q36 microdeletions cases brain structure abnormalities were shown hypoplasia of the corpus callosum. Here, in our study, the case not only presented with hypoplasia of the corpus callosum, but also showed cerebellar sulcus widening, which has not been reported in previous 7q35-7q36 microdeletion patients.

In conclusion, we reported a *de novo* 9.4 Mb deletion ranging from 7q35 to q36.3 (chr7:147,493,985–156,774,460) in a patient with congenital brain dysplasia, developmental delay, and intellectual disability identified via SNP array analysis. Our study together with literature review indicated that 7q terminal deletion can be redefined as a contiguous 7q deletion syndrome, similar to other contiguous deletion syndromes, in which different regions and breakpoints gave an overlapping phenotype.

DATA AVAILABILITY STATEMENT

The raw data supporting the conclusions of this article will be made available by the authors, without undue reservation.

ETHICS STATEMENT

The studies involving human participants were reviewed and approved by Hebei General hospital. Written informed consent to participate in this study was provided by the participants' legal guardian/next of kin. Written informed consent was obtained from the individual(s), and minor(s)' legal guardian/next of kin, for the publication of any potentially identifiable images or data included in this article.

AUTHOR CONTRIBUTIONS

Y-LL enrolled the samples; YS and L-LF performed the SNP-array experiment and Real-time PCR. C-YW isolated the DNA; YS and L-LF wrote the draft; Y-LL and J-SL revised the manuscript and support the project. All authors read and approved the final manuscript.

FUNDING

This study was supported by the National Natural Science Foundation of China (82,000,427 and 82,070,738), Hunan Province Natural Science Foundation (2020JJ5785 and 2021JJ31015), Research Project of Hunan Provincial Health Commission (202,103,012,102, 202,103,050,563 and 202,104,022,248), 2020 Education Reform Project of Central South University (2020jy172) and the Fundamental Research Funds for Central Universities of Central South University (2021zzts0570).

ACKNOWLEDGMENTS

We thank all subjects for participating in this study. We thank Shuai Guo from University of Texas MD Anderson Cancer Center, the United States for editing the language.

SUPPLEMENTARY MATERIAL

The Supplementary Material for this article can be found online at: https://www.frontiersin.org/articles/10.3389/fgene.2021.761003/full#supplementary-material

REFERENCES

Alvarez-Periel, E., Puigdellívol, M., Brito, V., Plattner, F., Bibb, J. A., Alberch, J., et al. (2018). Cdk5 Contributes to Huntington's Disease Learning and Memory Deficits via Modulation of Brain Region-specific Substrates. *Mol. Neurobiol.* 55 (8), 6250–6268. doi:10.1007/s12035-017-0828-4

Ayub, S., Gadji, M., Krabchi, K., Côté, S., Gekas, J., Maranda, B., et al. (2016). Three New Cases of Terminal Deletion of the Long Arm of Chromosome 7 and Literature Review to Correlate Genotype and Phenotype Manifestations. *Am. J. Med. Genet.* 170 (4), 896–907. doi:10.1002/ajmg.a.37428

Busa, T., Panait, N., Chaumoitre, K., Philip, N., and Missirian, C. (2016). Esophageal Atresia with Tracheoesophageal Fistula in a Patient with 7q35-36.3 Deletion Including SHH Gene. *Eur. J. Med. Genet.* 59 (10), 546–548. doi:10.1016/j.ejmg.2016.09.001

Caselli, R., Mencarelli, M. A., Papa, F. T., Ariani, F., Longo, I., Meloni, I., et al. (2008). Delineation of the Phenotype Associated with 7q36.1q36.2 Deletion: Long QT Syndrome, Renal Hypoplasia and Mental Retardation. *Am. J. Med. Genet.* 146A (9), 1195–1199. doi:10.1002/ajmg.a.32197

Coutton, C., Poreau, B., Devillard, F., Durand, C., Odent, S., Rozel, C., et al. (2013). Currarino Syndrome and HPE Microform Associated with a 2.7-Mb Deletion in 7q36.3 ExcludingSHHGene. *Mol. Syndromol* 5 (1), 25–31. doi:10.1159/000355391

Deans, B., Griffin, C. S., Maconochie, M., and Thacker, J. (2000). Xrcc2 Is Required for Genetic Stability, Embryonic Neurogenesis and Viability in Mice. *EMBO J.* 19 (24), 6675–6685. doi:10.1093/emboj/19.24.6675

Guan, F., Lin, H., Chen, G., Li, L., Chen, T., Liu, X., et al. (2016). Evaluation of Association of Common Variants in HTR1A and HTR5A with Schizophrenia and Executive Function. *Sci. Rep.* 6, 38048. doi:10.1038/srep38048

Harris, E. L., Wappner, R. S., Palmer, C. G., Hall, B., Dinno, N., Seashore, M. R., et al. (1977). 7q Deletion Syndrome (7q32 Leads to 7qter). *Clin. Genet.* 12 (4), 233–238.

Hyohyeon, C., and Lee, C. G. (2015). A 13-Year-Old Boy with a 7q36.1q36.3 Deletion with Additional Findings. *Am. J. Med. Genet.* 167 (1), 198–203. doi:10.1002/ajmg.a.36792

Jackson, C. C., Lefèvre-Utile, A., Guimier, A., Malan, V., Bruneau, J., Gessain, A., et al. (2017). Kaposi Sarcoma, Oral Malformations, Mitral Dysplasia, and Scoliosis Associated with 7q34-q36.3 Heterozygous Terminal Deletion. *Am. J. Med. Genet.* 173 (7), 1858–1865. doi:10.1002/ajmg.a.38275

Koemans, T. S., Kleefstra, T., Chubak, M. C., Stone, M. H., Reijnders, M. R. F., de Munnik, S., et al. (2017). Functional Convergence of Histone Methyltransferases EHMT1 and KMT2C Involved in Intellectual Disability and Autism Spectrum Disorder. *Plos Genet.* 13 (10), e1006864. doi:10.1371/journal.pgen.1006864

Lewis, S., Abrahamson, G., Boultwood, J., Fidler, C., Potter, A., and Wainscoat, J. S. (1996). Molecular Characterization of the 7q Deletion in Myeloid Disorders. *Br. J. Haematol.* 93 (1), 75–80. doi:10.1046/j.1365-2141.1996.4841025.x

Linhares, N. D., Svartman, M., Salgado, M. I., Rodrigues, T. C., da Costa, S. S., Rosenberg, C., et al. (2014). Dental Developmental Abnormalities in a Patient with Subtelomeric 7q36 Deletion Syndrome May Confirm a Novel Role for the SHH Gene. *Meta Gene* 2, 16–24. doi:10.1016/j.mgene.2013.10.005

Oku, Y., and Huganir, R. L. (2013). AGAP3 and Arf6 Regulate Trafficking of AMPA Receptors and Synaptic Plasticity. *J. Neurosci.* 33 (31), 12586–12598. doi:10.1523/JNEUROSCI.0341-13.2013

Pelegrino, K. d. O., Sugayama, S., Catelani, A. L., Lezirovitz, K., Kok, F., and Chauffaille, M. d. L. (2013). 7q36 Deletion and 9p22 Duplication: Effects of a Double Imbalance. *Mol. Cytogenet.* 6 (1), 2. doi:10.1186/1755-8166-6-2

Peñagarikano, O., Abrahams, B. S., Herman, E. I., Winden, K. D., Gdalyahu, A., Dong, H., et al. (2011). Absence of CNTNAP2 Leads to Epilepsy, Neuronal Migration Abnormalities, and Core Autism-Related Deficits. *Cell* 147 (1), 235–246. doi:10.1016/j.cell.2011.08.040

Petrin, A. L., Giacheti, C. M., Maximino, L. P., Abramides, D. V. M., Zanchetta, S., Rossi, N. F., et al. (2010). Identification of a Microdeletion at the 7q33-Q35 Disrupting the CNTNAP2 Gene in a Brazilian Stuttering Case. *Am. J. Med. Genet.* 152A (12), 3164–3172. doi:10.1002/ajmg.a.33749

Porto, A. G., Brun, F., Severini, G. M., Losurdo, P., Fabris, E., Taylor, M. R. G., et al. (2016). Clinical Spectrum of PRKAG2 Syndrome. *Circ. Arrhythm Electrophysiol.* 9 (1), e003121. doi:10.1161/CIRCEP.115.003121.e003121

Roessler, E., Belloni, E., Gaudenz, K., Jay, P., Berta, P., Scherer, S. W., et al. (1996). Mutations in the Human Sonic Hedgehog Gene Cause Holoprosencephaly. *Nat. Genet.* 14 (3), 357–360. doi:10.1038/ng1196-357

Rush, E. T., Stevens, J. M., Sanger, W. G., and Olney, A. H. (2013). Report of a Patient with Developmental Delay, Hearing Loss, Growth Retardation, and Cleft Lip and Palate and a Deletion of 7q34-36.1: Review of Distal 7q Deletions. *Am. J. Med. Genet.* 161 (7), 1726–1732. doi:10.1002/ajmg.a.35951

Sundaram, S., Huq, A. H. M., Hsia, T., and Chugani, H. (2014). Exome Sequencing and Diffusion Tensor Imaging in Developmental Disabilities. *Pediatr. Res.* 75 (3), 443–447. doi:10.1038/pr.2013.234

Suri, T., and Dixit, A. (2017). The Phenotype of EZH2 haploinsufficiency-1.2-Mb Deletion at 7q36.1 in a Child with Tall Stature and Intellectual Disability. *Am. J. Med. Genet.* 173 (10), 2731–2735. doi:10.1002/ajmg.a.38356

Tuveng, J. M., Berling, B.-M., Bunford, G., Vanoye, C. G., Welch, R. C., Leren, T. P., et al. (2018). Long QT Syndrome KCNH2 Mutation with Sequential Fetal and Maternal Sudden Death. *Forensic Sci. Med. Pathol.* 14 (3), 367–371. doi:10.1007/s12024-018-9989-3

van Es, M. A., van Vught, P. W., Blauw, H. M., Franke, L., Saris, C. G., Van den Bosch, L., et al. (2008). Genetic Variation in DPP6 Is Associated with Susceptibility to Amyotrophic Lateral Sclerosis. *Nat. Genet.* 40 (1), 29–31. doi:10.1038/ng.2007.52

Wei, S., Lin, L.-F., Yang, C.-C., Wang, Y.-C., Chang, G.-D., Chen, H., et al. (2007). Thiazolidinediones Modulate the Expression of β-Catenin and Other Cell-Cycle Regulatory Proteins by Targeting the F-Box Proteins of Skp1-Cul1-F-Box Protein E3 Ubiquitin Ligase Independently of Peroxisome Proliferator-Activated Receptor γ. *Mol. Pharmacol.* 72 (3), 725–733. doi:10.1124/mol.107.035287

Conflict of Interest: The authors declare that the research was conducted in the absence of any commercial or financial relationships that could be construed as a potential conflict of interest.

Publisher's Note: All claims expressed in this article are solely those of the authors and do not necessarily represent those of their affiliated organizations, or those of the publisher, the editors and the reviewers. Any product that may be evaluated in this article, or claim that may be made by its manufacturer, is not guaranteed or endorsed by the publisher.

frontiers in Pediatrics

CASE REPORT
published: 26 January 2022
doi: 10.3389/fped.2021.805575

Case Report: A Relatively Mild Phenotype Produced by Novel Mutations in the *SEPSECS* Gene

Tingyu Rong [1,2,3†], Ruen Yao [4†], Yujiao Deng [1,2,3], Qingmin Lin [1,2,3], Guanghai Wang [1,2,3], Jian Wang [4], Fan Jiang [1,2,3] and Yanrui Jiang [1,2,3*]*

[1] Department of Developmental and Behavioral Pediatrics, Shanghai Children's Medical Center, School of Medicine, Shanghai Jiao Tong University, Shanghai, China, [2] Ministry of Education-Shanghai Key Laboratory of Children's Environmental Health, Xinhua Hospital, School of Medicine, Shanghai Jiao Tong University, Shanghai, China, [3] Shanghai Center for Brain Science and Brain-Inspired Technology, Shanghai, China, [4] Department of Medical Genetics and Molecular Diagnostic Laboratory, Shanghai Children's Medical Center, School of Medicine, Shanghai Jiao Tong University, Shanghai, China

Mutations in the human *O*-phosphoseryl-tRNA:selenocysteinyl-tRNA synthase gene (*SEPSECS)* are associated with progressive cerebello-cerebral atrophy (PCCA), also known as pontocerebellar hypoplasia type 2D (PCH2D). Early-onset profound developmental delay, progressive microcephaly, and hypotonia that develops toward severe spasticity have been previously reported with *SEPSECS* mutations. Herein we report a case with severe global developmental delay, myogenic changes in the lower limbs, and insomnia, but without progressive microcephaly and brain atrophy during infancy and toddlerhood in a child harboring the *SEPSECS* missense variant c.194A>G (p. Asn65Ser) and a novel splicing mutation c.701+1G>A. With these findings we communicate the first Chinese *SEPSECS* mutant case, and our report indicates that *SEPSECS* mutations can give rise to a milder phenotype.

Keywords: SEPSECS mutation, PCCA, PCH2D, milder phenotype, developmental delay

OPEN ACCESS

Edited by:
Chen Li,
Zhejiang University, China

Reviewed by:
Lorenzo Pavone,
University of Catania, Italy
Maurizio Elia,
IRCCS Oasi Maria SS, Italy

***Correspondence:**
Fan Jiang
fanjiang@shsmu.edu.cn
Yanrui Jiang
yanrui1027@126.com

[†] These authors have contributed equally to this work

Specialty section:
This article was submitted to Genetics of Common and Rare Diseases, a section of the journal Frontiers in Pediatrics

Received: *30 October 2021*
Accepted: *20 December 2021*
Published: *26 January 2022*

Citation:
Rong T, Yao R, Deng Y, Lin Q, Wang G, Wang J, Jiang F and Jiang Y (2022) Case Report: A Relatively Mild Phenotype Produced by Novel Mutations in the SEPSECS Gene. Front. Pediatr. 9:805575. doi: 10.3389/fped.2021.805575

INTRODUCTION

The *SEPSECS* gene encodes O-phosphoseryl-tRNA:selenocysteinyl-tRNA synthase (SepSecS), the final enzyme that catalyzes the Sep-tRNA to Sec-tRNA conversion, which is used in the synthesis of selenocysteine (1, 2). SepSecS is essential for the synthesis of selenoproteins, which are expressed unevenly and stably in the brain (3). The biallelic deletion of *Trsp* in mice (which impedes selenoprotein synthesis) resulted in cerebellar hypoplasia, seizure, and developmental delay (4)—phenotypes that are congruent with those described in previous clinical reports of *SEPSECS* mutations (5–11). Several investigators identified mutations in human *SEPSECS* as the cause of severe, early-onset neurological symptoms that were later characterized as causing pontocerebellar hypoplasia type 2D (PCH2D) (5–11)—with or without signs of mitochondrial deficiencies that include elevated blood lactate (7), visual impairment, and myopathy (9). Although harboring different mutant alleles, patients presented remarkably similar phenotypes typified by an autosomal recessive progressive microcephaly with profound developmental delay, progressive brain atrophy, and hypotonia (6, 7, 9). Repeated magnetic resonance imaging (MRI) of affected individuals revealed progressive cerebellar atrophy followed by cerebral atrophy involving both white and gray matter. Brain atrophy is recognized at various developmental stages, but principally within the first 18 months of life (6, 7, 9). However, *SEPSECS* mutations have been identified in three milder late-onset patients, with cerebellar atrophy first recognized by MRI at 9, 16, and 18 years of age (8, 10).

We hereby report on a mild phenotype without progressive microcephaly and brain atrophy up to 3 years of age in a Chinese pediatric patient who harbored biallelic *SEPSECS* mutations.

CASE PRESENTATION

Clinical Data and Laboratory Examinations

A 2-year-old girl was referred to the Department of Developmental and Behavioral Pediatrics due to severe global development delay and insomnia (case timeline presented in **Figure 1**). Clinical examination revealed left esotropia, severe muscle hypotonia, and decreased deep tendon reflexes, particularly with respect to both her lower limbs. The patient was born naturally at full-term by healthy non-consanguineous parents. Her birth weight was 3,750 g (86th percentile) and length was 52 cm (94th percentile); head circumference at birth was missing. The patient manifested low muscle tone and weak sucking upon birth, and was still unable to raise her head and turn over her body at 4 months of age. A developmental assessment at 4 months showed that the development quotients of gross motor control, fine motor control, language, reaction to objects, and reaction to people were 55, 66, 38, 28, and 28, respectively. No discomfort or malformation from heart, thorax, kidneys, genitourinary or extremities were mentioned or found. A brain MRI was performed at 5 months, which showed high signal intensities in the bilateral pallidum upon T2W1; her electroencephalography was normal. The patient was subsequently referred to the rehabilitation department for rehabilitation training.

At 15 months, the patient was brought to the outpatient unit for sporadic upper extremity high muscle tone with vocalization. Repeated EEG/video electroencephalogram (VEEG) at 15, 19, and 40 months exhibited no sign of epileptic seizure. The second brain MRI at 16 months revealed that the corpus callosum was slightly thin, and the lateral ventricle was plump, and we observed high-plaque signal intensity in the left frontal lobe (**Figure 2**). Electromyography (EMG) at 18 months showed a slight myogenic change in the tibialis anterior muscle and the peroneal muscle. Tandem mass spectrometry of blood and urine were normal. A follow-up brain MRI at 3 years of age revealed a slight enlargement of the ventricles bilaterally and a deepening of the bilateral frontotemporal sulci. Nevertheless, no obvious atrophy was found upon MRI. Electrocardiograph (ECG) result at 3 years was normal. Available head circumference data were within the normal range (42 cm at 6 months (42nd percentile) and 47.3 cm at 3 years (21st percentile)], as well as her weight [6.9 kg at 4 months (70th percentile) and 16 kg at 3 years (73rd percentile)] and lengths [68.3 cm at 4 months (>99th percentile) and 105 cm at 3 years (96^{th} percentile)] throughout the follow-ups.

Genetic Testing

Whole-exome sequencing was executed to ascertain a possible molecular cause for the patient's condition. Two variants in *SEPSECS* were subsequently identified: c.194A>G leading to the missense variant p.Asn65Ser, and a novel splice variant c.701+1G>A. Sanger sequencing confirmed these variants and a parental test revealed a compound heterozygous state for the pedigree. To determine the impact of the splice variant, mRNA was extracted from the patient's blood sample for reverse transcription polymerase chain reaction (RT-PCR) assay. We designed the PCR primers as follows: F, 5′-ATCACTGCAG GTTTTGAGCC-3′; R, 5′-ACGCAGACAATGACAACCAC-3′; amplification produced an abnormal cDNA fragment, proving the presence of an alternative splice product with retention of the fifth intron (**Figure 3**). According to the American College of Medical Genetics and Genomics (ACMG) guidelines for interpreting sequence variants, the c.701+1G>A variant was categorized as pathogenic.

DISCUSSION

Mutations in *SEPSECS* have now been found in individuals of several races and ethnicities—including Iraqi, Moroccan, Finnish, Arabic, Jordanian, and Japanese (6–9). Herein we reported the first case of pathogenic *SEPSECS* mutations in the Chinese population, which included the pathogenic splice variant c.701+1G>A.

Unlike previously reported cases, the patient in our study did not manifest the typical characteristics of PCH2D, and brain MRI results did not support obvious atrophy. There have been three cases reported of late-onset brain atrophy, either homozygous or heterozygous, and their mutation types are shown in **Table 1** (8, 10). The molecular structure of SepSecS includes three domains, two insertions, one pyridoxal phosphate-binding site, and one non-canonical N terminal (1). Van Dijk et al. reported a female patient who exhibited a mild phenotype, with cerebellar atrophy detected at 16 years of age (10). The authors argued that the late-onset phenotype might be the result of a mutation site in the last exon, and this may have allowed partial resumption of enzyme activity (10). Iwama et al. reported two patients with compound heterozygous mutations who shared the same c.356A>G mutation located in the 4th α-helix of SepSecS (8). However, our patient's mutations were located at the 1st insertion and between the 6th β-fold and 5th α-helix. Mutations related to milder phenotypes are located at various sites, and an *in vitro* test of enzymatic activity was not available to us due to technical reasons. Without sufficient evidence to infer prognosis, regular brain imaging and developmental evaluations are still required to determine whether cerebello-cerebral atrophy would occur in the future.

Epilepsy is a common comorbidity of encephalopathy, and evidence shows that it could exacerbate neurocognitive dysfunction (16). As a result, early diagnosis and treatment of epilepsy are required. Myoclonic or generalized tonic-clonic seizures were previously reported in most *SEPSECS* cases, primarily occurring during the first or second year of life (5, 7, 17). Absence of epilepsy or seizures has also been reported (8–11), especially for milder phenotypes where cerebello-cerebral atrophy was detected in children older than 9 years of age (8, 10). Our patient exhibited seizure-like symptoms at 15 months,

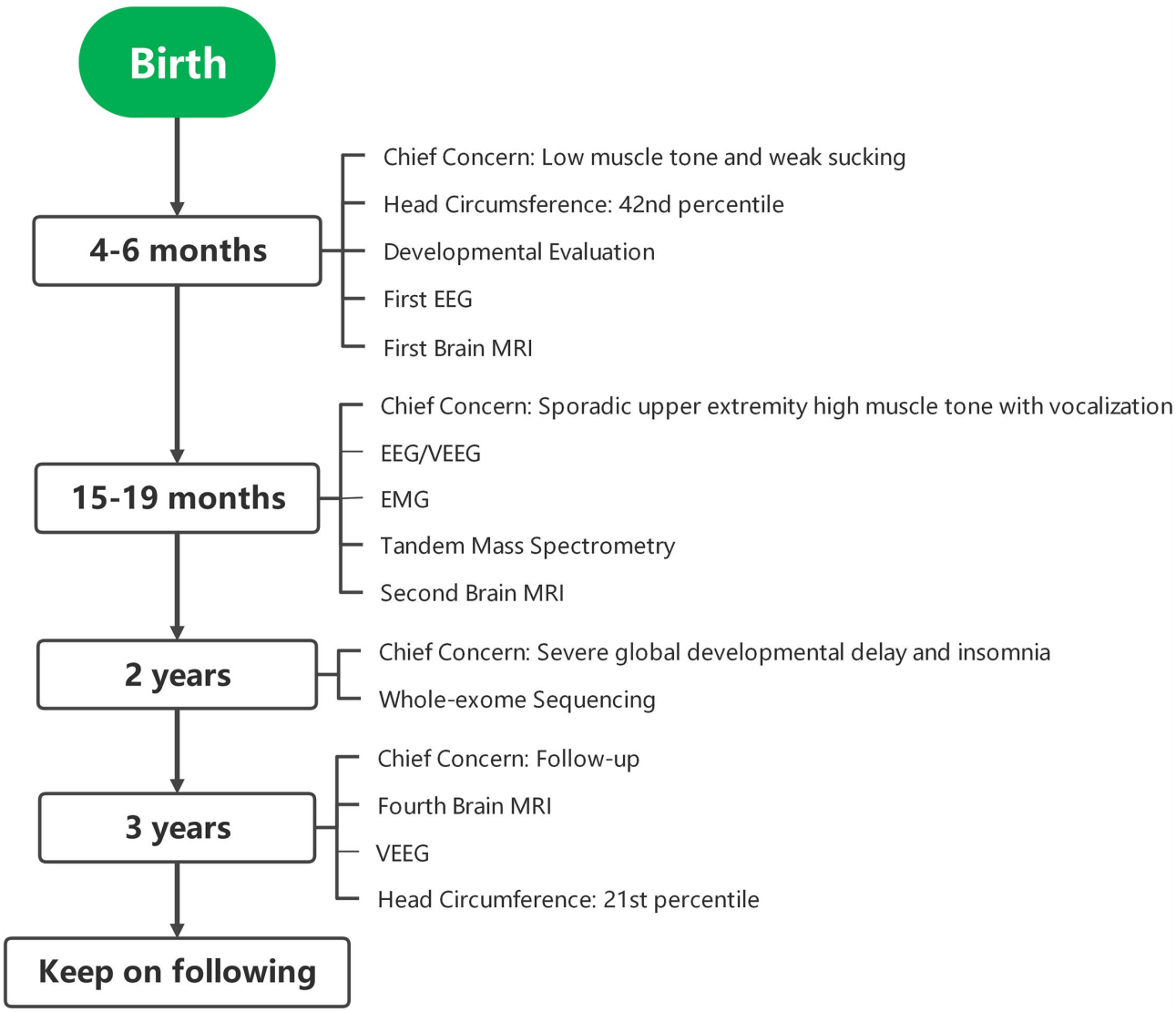

FIGURE 1 | Case timeline. EEG, electroencephalogram; MRI, magnetic resonance imaging; VEEG, video electroencephalogram; EMG, electromyography.

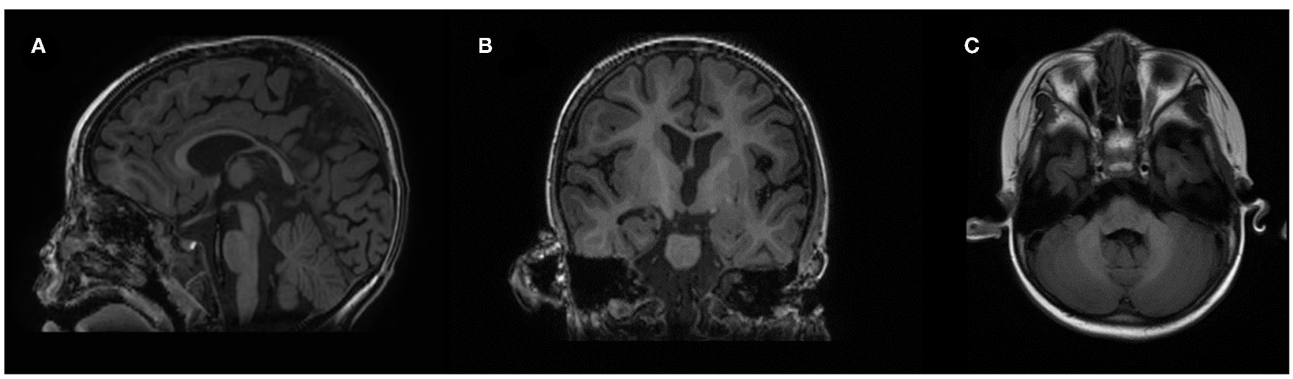

FIGURE 2 | Brain magnetic resonance imaging (MRI): **(A)** sagittal, **(B)** coronal, and **(C)** OAx planes.

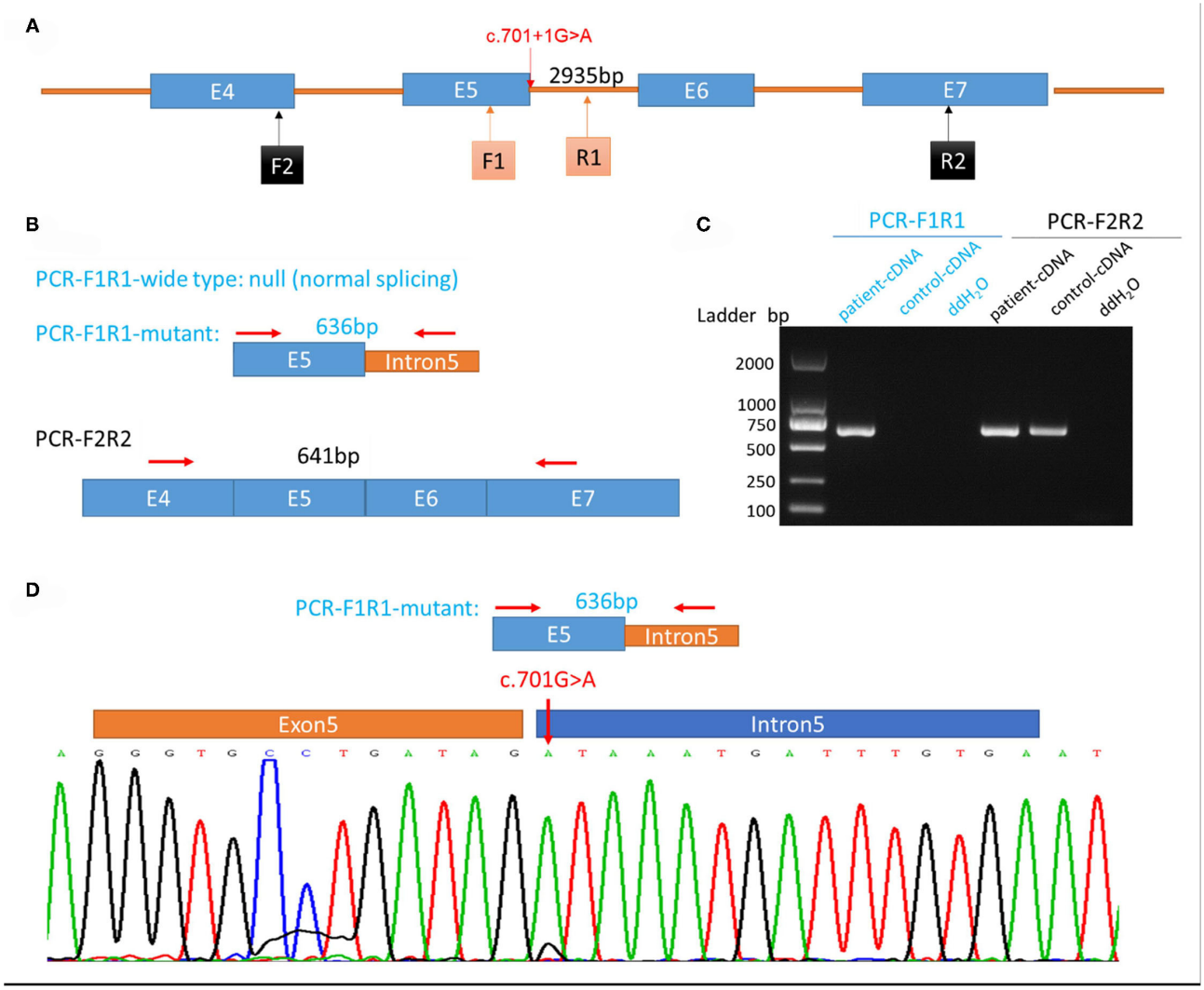

FIGURE 3 | Genetic testing of the patient and analysis of aberrant splicing. **(A)** Schematic diagram of primer design. **(B)** Schematic diagram of expected polymerase chain reaction (PCR) product. **(C)** Electrophoretogram of PCR product from the patient's and control's blood samples. **(D)** Sequence of aberrant splicing product with intron 5 retention (red arrow indicates the mutation site).

as she occasionally manifested upper-extremity high muscle tone together with monotone vocalizations; however, repeated EEG/VEEGs showed no epileptiform discharges at 15, 19, and 40 months. Ruling out epilepsy in our patient was congruent with her milder phenotype. However, with the potential of progressive encephalopathy, additional repeated measurements are essential once symptoms of epilepsy, such as focal or generalized seizures emerge.

Heterogeneous manifestations have been reported in cases with mutations of tRNA synthetase. For example, mutations in *HARS2* (which encodes the histidyl-tRNA synthetase) result in deafness in both genders and infertility in females (18); while mutations in *WARS* (which encodes the tryptophanyl-tRNA synthetase) result in distal hereditary motor neuropathy (19). The heterogeneity in different gene mutations is attributed to the complicated catalytic processes inherent to each tRNA, and the diverse functions of and mechanisms underlying the gene-encoded proteins. *SEPSECS* is essential for selenoprotein synthesis (1); most selenoproteins are oxidoreductases and participate in cellular redox regulation and antioxidant activities (20). Elevated blood lactate levels and visual impairment have been previously reported, suggesting potential mitochondrial impairment due to *SEPSECS* mutations (7–9). Our patient did manifest hypotonia and the EMG showed a slight myogenic change in the lower limbs, although metabolic products in blood and urine remained normal. Muscle biopsy is still an option if further diagnosis is needed.

In conclusion, we have identified a novel pathogenic mutation in the *SEPSECS* gene, which is the first case reported

TABLE 1 | Summary of *SEPSECS* mutations and related phenotypes.

Family	Ethnicity	Sex	Gene mutation	Protein change	Zygosity	Brain atrophy	Seizure	Hypotonia	Spasticity	Signs of mitochondrial dysfunction	References
1	Chinese	Female	194A>G	Asn65Ser	Compound heterozygous	–	–	+	–	Slight myogenic change in bilateral limbs; muscle biopsy unavailable	Current case
			701+1G>A								
2	Japanese	Female	77delG	Arg26Profs*42	Compound heterozygous	+(9 years)	–	+	+	High blood lactate	(8)
			356A>G	Asn119Ser							
3	Japanese	Female	356A>G	Asn119Ser	Compound heterozygous	+(18 years)	–	+ (3 months)	+ (18 years)	–	
			467G>A	Arg156Gln							
4	Dutch	Female	1321G > A	Gly441Arg	Homozygous	+(16 years)	–	–	–	–	(10)
5,6	Mixed Iraqi-Moroccan	Both sexes	715G>A	Ala239Thr	Compound heterozygous	+(12–28 months)	+ (5 in 7 patients)	–	+ (3–12 months)	–	(5, 6)
			1001A>G	Tyr334Cys							
7	Iraqi	Both sexes	1001A>G	Tyr334Cys	Homozygous						
8,9,10	Finnish	Both sexes	974C>G	Thr325Ser	Compound heterozygous	+(5–6 months)	+ (in 2 of 3 patients at 11–12 months)		+ (within 1 year)	High blood lactate in 2 of 3 patients	(7)
			1287C>A	Tyr429*							
11	Arabian	Male	1001A>G	Tyr334Cys	Homozygous	+(18 months)	–	+ (birth)	+	Borderline abnormal in mitochondrial biopsy; high blood CPK and urinary 3-hydroxyisovaleric acid	(9)
12	Moroccan	Female	114+3A>G		Homozygous	+(4 years)	–	–	+	+	(11)
13	N/A	Female	1A>G	Met1Val	Compound heterozygous	+	+	+	N/A	N/A	(12)
			388+3A>G								
14	Jordan	N/A	1466A>T	Asp489Val	Homozygous	+	N/A	N/A	N/A	N/A	(13)
15	N/A	N/A	1027_1120del	Glu343Leufs*2	Homozygous	N/A	N/A	+	+	N/A	(14)
16	N/A	Male	176C>T	Ala59Val	Homozygous	+	+ (3 weeks)	N/A	N/A	N/A	(15)

CPK, creatine phosphokinase.

in China, and it is associated with a mild phenotype that encompasses developmental delay, myogenic changes in the lower limbs, and sleep disorder but without progressive microcephaly and brain atrophy. According to other reported cases, disease progression in the future is not precluded, and thus a targeted and detailed follow-up is needed.

DATA AVAILABILITY STATEMENT

The original contributions presented in the study are included in the article/supplementary files, further inquiries can be directed to the corresponding author/s.

ETHICS STATEMENT

Ethical approval for this study was obtained from the Ethics Committee of Shanghai Children's Medical Center, School of Medicine, Shanghai Jiaotong University (SCMCIRB-W2021030). Written informed consent was obtained from the minor(s)' legal guardian/next of kin for the publication of any potentially identifiable images or data included in this article.

AUTHOR CONTRIBUTIONS

TR collected the clinical data and wrote the initial draft of the manuscript. RY determined the mutant gene and participated in writing and reviewing of the manuscript. YD, QL, GW, and JW participated in the diagnosis and critically reviewed the manuscript. FJ and YJ identified and followed up the patient, supervised data collection, and critically reviewed the manuscript. All authors contributed to the article and approved the submitted version.

FUNDING

The study was supported by National Natural Science Foundation of China (81773443; 81602868; 82073568; 82071493); Ministry of Science and Technology of China (2016YFC1305203); Science and Technology Commission of Shanghai Municipality (2018SHZDZX05; 18JC1420305; 21Y11907400; 19QA1405800; 19411968800).

ACKNOWLEDGMENTS

We are grateful to the patient and her parents to participate in the study and consent us to report on the case.

REFERENCES

1. Ganichkin OM, Xu XM, Carlson BA, Mix H, Hatfield DL, Gladyshev VN, et al. Structure and catalytic mechanism of eukaryotic selenocysteine synthase. *J Biol Chem.* (2008) 283:5849–65. doi: 10.1074/jbc.M709342200
2. Palioura S, Sherrer RL, Steitz TA, Soll D, Simonovic M. The human SEPSECS-tRNASec complex reveals the mechanism of selenocysteine formation. *Science.* (2009) 325:321–5. doi: 10.1126/science.1173755
3. Zhang Y, Zhou Y, Schweizer U, Savaskan NE, Hua D, Kipnis J, et al. Comparative analysis of selenocysteine machinery and selenoproteome gene expression in mouse brain identifies neurons as key functional sites of selenium in mammals. *J Biol Chem.* (2008) 283:2427–38. doi: 10.1074/jbc.M707951200
4. Wirth EK, Bharathi BS, Hatfield D, Conrad M, Brielmeier M, Schweizer U. Cerebellar hypoplasia in mice lacking selenoprotein biosynthesis in neurons. *Biol Trace Elem Res.* (2014) 158:203–10. doi: 10.1007/s12011-014-9920-z
5. Ben-Zeev B, Hoffman C, Lev D, Watemberg N, Malinger G, Brand N, et al. Progressive cerebellocerebral atrophy: a new syndrome with microcephaly, developmental relay, spastic quadriplegia. *J Med Genet.* (2003) 40:e96. doi: 10.1136/jmg.40.8.e96
6. Agamy O, Ben Zeev B, Lev D, Marcus B, Fine D, Su D, et al. Mutations disrupting selenocysteine formation cause progressive cerebello-cerebral atrophy. *Am J Hum Genet.* (2010) 87:538–44. doi: 10.1016/j.ajhg.2010.09.007
7. Anttonen AK, Hilander T, Linnankivi T, Isohanni P, French RL, Liu Y, et al. Selenoprotein biosynthesis defect causes progressive encephalopathy with elevated lactate. *Neurology.* (2015) 85:306–15. doi: 10.1212/WNL.0000000000001787
8. Iwama K, Sasaki M, Hirabayashi S, Ohba C, Iwabuchi E, Miyatake S, et al. Milder progressive cerebellar atrophy caused by biallelic SEPSECS mutations. *J Hum Genet.* (2016) 61:527–31. doi: 10.1038/jhg.2016.9
9. Pavlidou E, Salpietro V, Phadke R, Hargreaves IP, Batten L, McElreavy K, et al. Pontocerebellar hypoplasia type 2D and optic nerve atrophy further expand the spectrum associated with selenoprotein biosynthesis deficiency. *Eur J Paediatr Neurol.* (2016) 20:483–8. doi: 10.1016/j.ejpn.2015.12.016
10. van Dijk T, Vermeij JD, van Koningsbruggen S, Lakeman P, Baas F. A SEPSECS mutation in a 23-year-old woman with microcephaly and progressive cerebellar ataxia. *J Inherit Metab Dis.* (2018) 41:897–8. doi: 10.1007/s10545-018-0151-x
11. Arrudi-Moreno M, Fernández-Gómez A, Peña-Segura JL. A new mutation in the SEPSECS gene related to pontocerebellar hypoplasia type 2D. *Med Clin.* (2021) 156:94–5. doi: 10.1016/j.medcli.2019.10.005
12. Zhu X, Petrovski S, Xie P, Ruzzo EK, Lu YF, McSweeney KM, et al. Whole-exome sequencing in undiagnosed genetic diseases: interpreting 119 trios. *Genet Med.* (2015) 17:774–81. doi: 10.1038/gim.2014.191
13. Makrythanasis P, Nelis M, Santoni FA, Guipponi M, Vannier A, Béna F, et al. Diagnostic exome sequencing to elucidate the genetic basis of likely recessive disorders in consanguineous families. *Hum Mutat.* (2014) 35:1203–10. doi: 10.1002/humu.22617
14. Alazami AM, Patel N, Shamseldin HE, Anazi S, Al-Dosari MS, Alzahrani F, et al. Accelerating novel candidate gene discovery in neurogenetic disorders via whole-exome sequencing of prescreened multiplex consanguineous families. *Cell Rep.* (2015) 10:148–61. doi: 10.1016/j.celrep.2014.12.015
15. Olson HE, Kelly M, Lacoursiere CM, Pinsky R, Tambunan D, Shain C, et al. Genetics and genotype-phenotype correlations in early onset epileptic encephalopathy with burst suppression. *Ann Neurol.* (2017) 81:419–29. doi: 10.1002/ana.24883
16. Nickels KC, Zaccariello MJ, Hamiwka LD, Wirrell EC. Cognitive and neurodevelopmental comorbidities in paediatric epilepsy. *Nat Rev Neurol.* (2016) 12:465–76. doi: 10.1038/nrneurol.2016.98
17. Hady-Cohen R, Ben-Pazi H, Adir V, Yosovich K, Blumkin L, Lerman-Sagie T, et al. Progressive cerebello-cerebral atrophy and progressive encephalopathy with edema, hypsarrhythmia and optic atrophy may be allelic syndromes. *Eur J Paediatr Neurol.* (2018) 22:1133–8. doi: 10.1016/j.ejpn.2018.07.003
18. Tiosano D, Mears JA, Buchner DA. Mitochondrial dysfunction in primary ovarian insufficiency. *Endocrinology.* (2019) 160:2353–66. doi: 10.1210/en.2019-00441
19. Wang B, Li X, Huang S, Zhao H, Liu J, Hu Z, et al. A novel WARS mutation (p.Asp314Gly) identified in a Chinese distal hereditary motor neuropathy family. *Clin Genet.* (2019) 96:176–82. doi: 10.1111/cge.13563

20. Zhang Y, Roh YJ, Han SJ, Park I, Lee HM, Ok YS, et al. Role of selenoproteins in redox regulation of signaling and the antioxidant system: a review. *Antioxidants.* (2020) 9:383. doi: 10.3390/antiox9050383

Conflict of Interest: The authors declare that the research was conducted in the absence of any commercial or financial relationships that could be construed as a potential conflict of interest.

Publisher's Note: All claims expressed in this article are solely those of the authors and do not necessarily represent those of their affiliated organizations, or those of the publisher, the editors and the reviewers. Any product that may be evaluated in this article, or claim that may be made by its manufacturer, is not guaranteed or endorsed by the publisher.

frontiers in Genetics

STUDY PROTOCOL
published: 01 February 2022
doi: 10.3389/fgene.2021.766964

Genome Sequencing for Genetics Diagnosis of Patients With Intellectual Disability: The DEFIDIAG Study

Christine Binquet[1,2], Catherine Lejeune[1,2,3], Laurence Faivre[2,4,5], Marion Bouctot[1], Marie-Laure Asensio[1], Alban Simon[6], Jean-François Deleuze[7], Anne Boland[7], Francis Guillemin[8], Valérie Seror[9], Christelle Delmas[10], Hélène Espérou[10], Yannis Duffourd[2,4], Stanislas Lyonnet[11,12], Sylvie Odent[13], Delphine Heron[14], Damien Sanlaville[15], Thierry Frebourg[16,17], Bénédicte Gerard[18] and Hélène Dollfus[6,19] for the DEFIDIAG Study Group*

[1]Inserm, CHU Dijon-Bourgogne, CIC1432-Epidémiologie Clinique, Dijon, France, [2]CHU Dijon-Bourgogne, Fédération Hospitalo-Universitaire Médecine Translationnelle et Anomalies Du Développement (TRANSLAD), Dijon, France, [3]Inserm, Université de Bourgogne-Franche-Comté, UMR 1231, EPICAD, Dijon, France, [4]Inserm, Université Bourgogne-Franche-Comté, UMR1231, équipe GAD, Dijon, France, [5]Service de Génétique Clinique, Centre de Référence Anomalies Du Développement CLAD Est, CHU de Dijon, ERN ITHACA, Dijon, France, [6]Service de Génétique Médicale, Institut de Génétique Médicale D'Alsace, Hôpitaux Universitaires de Strasbourg, Strasbourg, France, [7]Université Paris-Saclay, CEA, Centre National de Recherche en Génomique Humaine (CNRGH), Evry, France, [8]CIC1433-Epidémiologie Clinique, Inserm, Centre Hospitalier Régional et Universitaire de Nancy, Université de Lorraine, Nancy, France, [9]Aix Marseille Université, IRD, APHM, SSA, VITROME, IHU-Méditerranée Infection, Marseille, France, [10]Inserm, Pôle de Recherche Clinique, Paris, France, [11]Université de Paris, INSERM, IHU Imagine–Institut des maladies génétiques, Paris, France, [12]Fédération de Génétique et Médecine Génomique, GHU APHP.centre-Université de Paris, Hôpital Necker-Enfants Malades, Paris, France, [13]Service de Génétique Clinique, Centre de Référence Anomalies Du Développement CLAD- Ouest, Université de Rennes, CNRS, IGDR (Institut de Génétique et Développement de Rennes), ERN ITHACA, Rennes, France, [14]Unité Fonctionnelle de Génétique Médicale et Centre de Référence « Déficiences Intellectuelles de Causes Rares », APHP Sorbonne Université, Groupe Hospitalier Pitié-Salpêtrière et Hôpital Trousseau, Paris, France, [15]Hospices Civils de Lyon, GHE, Service de Génétique, Université Claude Bernard Lyon 1, Lyon, France, [16]CHU de Rouen, Service de Génétique, Rouen, France, [17]Inserm, Université de Normandie, UMR1245, Centre de Génomique et de Médecine Personnalisée, Rouen, France, [18]Laboratoires de Diagnostic Génétique, Institut de Génétique Médicale D'Alsace, Hôpitaux Universitaires de Strasbourg, Strasbourg, France, [19]Inserm UMRS_1112, Institut de Génétique Médicale D'Alsace, Université de Strasbourg, France et CHRU, Strasbourg, France

OPEN ACCESS

Edited by:
Chen Li,
Zhejiang University, China

Reviewed by:
Taobo Hu,
Peking University People's Hospital, China
Santasree Banerjee,
Beijing Genomics Institute (BGI), China

***Correspondence:**
Christine Binquet
christine.binquet@u-bourgogne.fr

Specialty section:
This article was submitted to Genetics of Common and Rare Diseases, a section of the journal Frontiers in Genetics

Received: *30 August 2021*
Accepted: *28 December 2021*
Published: *01 February 2022*

Citation:
Binquet C, Lejeune C, Faivre L, Bouctot M, Asensio M-L, Simon A, Deleuze J-F, Boland A, Guillemin F, Seror V, Delmas C, Espérou H, Duffourd Y, Lyonnet S, Odent S, Heron D, Sanlaville D, Frebourg T, Gerard B and Dollfus H (2022) Genome Sequencing for Genetics Diagnosis of Patients With Intellectual Disability: The DEFIDIAG Study. Front. Genet. 12:766964. doi: 10.3389/fgene.2021.766964

Introduction: Intellectual Disability (ID) is the most common cause of referral to pediatric genetic centers, as it affects around 1–3% of the general population and is characterized by a wide genetic heterogeneity. The Genome Sequencing (GS) approach is expected to achieve a higher diagnostic yield than exome sequencing given its wider and more homogenous coverage, and, since theoretically, it can more accurately detect variations in regions traditionally not well captured and identify structural variants, or intergenic/deep intronic putatively pathological events. The decreasing cost of sequencing, the progress in data-management and bioinformatics, prompted us to assess GS efficiency as the first line procedure to identify the molecular diagnosis in patients without obvious ID etiology. This work is being carried out in the framework of the national French initiative for genomic medicine (Plan France Médecine Génomique 2025).

Methods and Analysis: This multidisciplinary, prospective diagnostic study will compare the diagnostic yield of GS trio analysis (index case, father, mother) with the French core minimal reference strategy (Fragile-X testing, chromosomal microarray analysis and Gene Panel Strategy of 44 selected ID genes). Both strategies are applied in a blinded fashion, in

parallel, in the same population of 1275 ID index cases with no obvious diagnosis (50% not previously investigated). Among them, a subgroup of 196 patients are randomized to undergo GS proband analysis in addition to GS trio analysis plus the French core minimal reference strategy, in order to compare their efficiency. The study also aims to identify the most appropriate strategy according to the clinical presentation of the patients, to evaluate the impact of deployment of GS on the families' diagnostic odyssey and the modification of their care, and to identify the advantages/difficulties for the patients and their families.

Ethics Statement: The protocol was approved by the Ethics Committee Sud Méditerranée I and the French data privacy commission (CNIL, authorization 919361).

Trial Registration: ClinicalTrials.gov identifier NCT04154891 (07/11/2019).

Keywords: genome sequencing, intellectual disability, cost-effectiveness, minimal reference strategy, diagnostic odyssey

INTRODUCTION

The advent of Next Generation Sequencing (NGS) technologies has revolutionized our approach to diagnosis and research in the field of rare diseases at an international level, prompting rapid efforts to deploy these technologies in many countries, and by the European Commission ("1 + Million Genomes Initiative", launched in 2018). In the same spirit, the 2016 launch of the French plan for genomic medicine (AVIESAN, 2016) was designed to serve a range of medical disciplines, including cancer and rare diseases. The France Genomic Medicine 2025 plan cited rare diseases as one of the key areas at the forefront of NGS implementation, to improve patient care, shorten their diagnostic odyssey and boost research. Indeed, genetic diagnosis is the first step towards appropriate care, follow-up and genetic counseling. Moreover, enhancing our understanding of pathogenesis could help to elaborate more specific therapies. The general goal of French Genomic Medicine plan is to implement the use of Genome Sequencing (GS) in France within the next 10 years, by creating national sequencing platforms (2 of which are now fully operational), and as a kick off, to implement four pilot studies, one of which is dedicated to rare diseases, namely the DEFIDIAG pilot study.

This DEFIDIAG pilot study focuses on intellectual disability (ID), as one of the most challenging models of rare disease. ID affects around 1–3% of the general population, with around 15 per 1,000 persons having mild ID and around 3 per 1,000 having severe ID. It is the most common cause of referral to pediatric genetic centers. ID results from abnormal brain development due to numerous possible cellular processes, including neuron proliferation and differentiation, neuron or astrocyte metabolism and maintenance, neurotransmitter synthesis, receptor or signal transduction, transcriptional and translational control. It is also well recognized that ID may result from non-genetic causes (neonatal anoxia, toxic effects, deprivation . . .) or from genetic causes. Gene and chromosomal variations involved in human ID are numerous and include recurrent chromosomal events from complete chromosomal duplication, segmental chromosomal duplication or deletion, or small genic variations altering the function one among more than 1,500 genes such as single nucleotide variants (SNV), insertions or deletions (indel), unbalanced (CNV) or balanced structural variants (SV) in coding or non-coding regions, or even rarer events such as repeat expansions, uniparental disomy, mobile element insertion etc., which are reported in the OMIM registry. Approximately 15% of ID is attributable to cytogenetically clear-cut abnormalities, with at least two-thirds of these cases accounted for by trisomy 21 (Ellison et al., 2013) and up to 40% to one variation in one of the 1500 ID gene when exome sequencing is performed (Han and Lee, 2020).

Before next generation sequencing methods, genetic testing was limited to traditional karyotype and fragile X analysis, sometimes with gene specific Sanger analysis, when a specific syndromic ID was suspected. In the past 10 years, microarray analysis (CMA) has been widely used for the genetic diagnosis of ID. NGS tests recently emerged, in the last 5 years, with gene panel approaches and Whole Exome Sequencing (ES) following CMA and fragile X syndrome screening. Today, the question arises about the input of whole genome sequencing as a first approach in such patients, as this may profoundly modify the testing process by replacing CMA and other sequencing approaches (specific genes, panel, ES) and in addition, may detect new molecular mechanisms not detectable by CMA and ES.

Nowadays, most patients with no clinical diagnosis in France still undergo basic investigation (Fragile X and CMA) with a diagnostic yield of less than 20%. This basic exploration is usually followed by additional analysis using gene panel approaches containing at the very least a minimal core of 44 genes, namely the 44GPS minimal list recommended by the French national association of molecular genetics practitioners (Association Nationale des Praticiens de Génétique Moléculaire, ANPGM). The panel sequencing in the proband gives an additional diagnostic yield of 10–12% (using the 44 gene panel), and up to 40% (Han and Lee, 2020) in case of ES. ES as the first line test for the diagnosis of rare genetic diseases has recently been shown in some countries to be cost-effective, tripling the diagnostic rate at one third of the cost, in children with suspected monogenic disorders (Stark et al., 2017; Schofield et al., 2019). There is also emerging evidence of the efficiency of GS over

standard testing (Alam and Schofield, 2018). However, the heterogeneity in clinical presentation, sample sizes and health economic evaluation standards makes it difficult to generalize the first published results (Schwarze et al., 2018) to other settings. A recent study in Ontario, Canada reported that GS might have a higher diagnostic yield than standard genetic testing, and could be a cost-effective strategy when used after standard testing or when used earlier in the diagnostic pathway (Ontario Health (Quality), 2020). However, these results need to be confirmed in the French setting since marked differences exist between countries in the technologies used, the costs, and the organization of clinical, biological and bioinformatics pathways.

Against this background, the DEFIDIAG study aims to evaluate the diagnostic performance and cost-effectiveness of GS as a systematic and unique molecular investigation for French patients with ID of unknown etiology, compared to the standard minimal protocol defined by the ANPGM, under conditions close to routine. Indeed, GS provides an opportunity to analyze a wider panel of molecular events, such as: 1) SNV and insertion/deletion (indel) in coding regions, even in CG rich regions, 5′ and 3′ UTR, promoter or intronic regions; 2) unbalanced chromosomal anomalies (CNV), with greater accuracy due to homogeneous coverage; 3) balanced structural variants, such as inversion and translocation, and lastly, 4) mechanisms observed very infrequently, such as uniparental disomy for imprinted chromosomal regions or insertion of mobile elements. Genome analysis was chosen because potential splice site mutations in deeper intronic regions are not enriched by exome analysis; CNV in exome enrichment strategies are still not 100% sensitive, specific and reliable; partial inversions or translocations affecting coding regions are not found by ES, and promoter or regulatory regions are not analyzed by ES.

This study also includes impact studies, aiming to assess the perceived impact for patients and their parents, for whom this technique may herald the end of their diagnostic odyssey. To this end, the DEFIDIAG study involves 15 medical genetics departments with strong clinical expertise in ID patients, as well as six diagnostic laboratories with a proven track record of competence in ID gene exploration, and the national sequencing platform of the National Center of Human Genomics Research (CNRGH), recognized for the high quality of its genomic sequence production and bioinformatics processes.

Specifically, the primary objective of this study is to compare the percentage of causal genetic diagnosis identified by GS performed on a trio (the patient and both parents) (GST), to the use of the current French reference minimal strategy (Fragile X + CMA + 44GPS) in ID patients attending a first genetics consultation. Secondary objectives focus on the diagnostic yield, and include the following:

- To compare the percentage of ID causal diagnosis identified by GST, to GS in the proband only (i.e., genome in solo, GSS) in a subgroup of randomized patients attending for a first genetic investigation. This evaluation is useful because in genetic counseling, both parents are not always available.
- To describe the estimated additional diagnostic yield that would be obtained at each step in sequential analysis of the GS data: for the minimal 44GPS gene panel, the list of genes known to be associated with disease from OMIM (referred to simply as OMIM), and ES, in patients attending for a first investigation (never-explored patients) and in patients who have already undergone investigations (previously-explored patients).
- To compare the percentage of causal diagnosis of ID identified by GST to that obtained with the French reference minimal strategy in various subgroups (defined according to age, severity of ID, presence of major non-cerebral manifestations or epilepsy), for patients with ID attending for a first genetic investigation (never-explored patients).
- To compare the percentage of causal structural changes (CNV, balanced structural variants) identified by GST versus CMA.
- The DEFIDAG study also aims to compare the reference strategy, GST and GSs, in terms of costs and effectiveness for the causal diagnosis of ID in patients with ID of unknown etiology, attending for a first genetic investigation.
- Finally, three impact studies are planned. The first will estimate the costs associated with searching for a molecular diagnosis that could potentially be avoided by performing GS as the first line approach. The second will evaluate the impact on the frequency and type of medical, medico-social and psychological care in the year following the release of GS results, compared to care during the year prior to inclusion, in particular in patients who were already engaged in a diagnostic process prior to being invited to participate in the DEFIDIAG study. The third impact study will be performed in two centers, and will use a qualitative approach, namely interviews with a sample of parents, to explore: 1) the burden experienced by the parents, 2) emotional adjustment of the patient and the parents to the results of genetic tests, and 3) the patient and parents' perception of the future.

METHODS AND ANALYSES

Study Setting

The DEFIDIAG study is a prospective multicenter diagnostic study comparing two main strategies (namely GST versus the minimal reference strategy) applied in a blinded fashion to consecutive patients with no obvious clinical diagnosis, referred to medical genetic departments. Each patient included serves as their own control, and will undergo both strategies being compared. In parallel, the percentage of ID causal diagnosis identified by GSS, as compared to GST, will be evaluated in a randomized subgroup of patients attending a first genetic investigation.

In addition to the prospective diagnostic study, we will also perform quantitative impact studies to collect data concerning management of patients before inclusion, during the genetic analyses process, and after the results are made known (**Figure 1**); as well as a qualitative substudy using interviews (one interview after inclusion, a second interview after the results

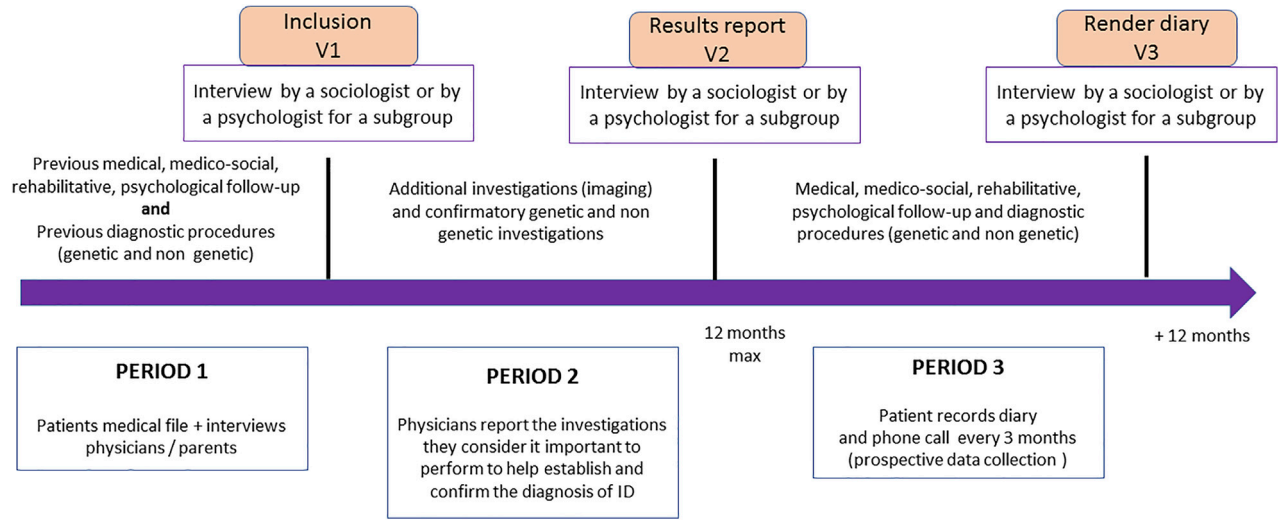

FIGURE 1 | Impact study procedures and schedule (DEFIDIAG study). The figure represents the key timepoints for patient visits in the inclusion centers (inclusion in the study, delivery of results, 12-months post-delivery visit), which also correspond to the time of the interviews between either a sociology or psychology researcher and the parents/patients who agreed to participate in the qualitative impact study. The figure also shows the three periods considered for cost estimation (period 1: before inclusion; period 2: waiting for results; period 3: during the 12 months following the results) and, for each of these periods, the different elements collected from the care teams and families in order to have the examinations carried out (for the three periods) and those envisaged with each of the strategies to confirm the diagnosis (period 2).

TABLE 1 | Correspondence between objectives and target population (DEFIDIAG study).

Eligible index cases (*n* = 1,275)	
Index cases with undiagnosed ID coming for the first time for a genetic investigation (*n* = 637)	**Index cases with undiagnosed ID already investigated (*n* = 637)**
Primary objective: Compare the percentage of genetic causal diagnosis identified in ID patients by performing trio GS analysis vs. the use of the current French reference minimal strategy	
Secondary objective: diagnostic yields •Compare the percentage of ID causal diagnosis identified by GST vs. the reference strategy in different subgroups (defined according to age, or clinical manifestations) •Compare the percentage of causal structural changes identified by GST vs. chromosomal microarray analysis •Compare the percentage of ID causal diagnosis identified by GST vs. GSS in a subgroup of randomized patients (*n* = 196)	
Secondary objective: Describe the estimated additional diagnostic yield that would be obtained at different steps of sequential analysis, for the 44 gene panels, OMIM and exome analysis	
Secondary objective: Assessing the efficiency of the three strategies (the reference minimal strategy; GSs; GS_T)	
	Secondary objective: Estimate the cost of the diagnostic odyssey that could be potentially avoided by first-line genomic analysis
Secondary objective: Estimate the frequency and nature of changes in medical follow-up of the patients, but also in medico-social, rehabilitation, and psychological follow-up in the first year after the reporting of GS analyses compared to the period before the inclusion	
Secondary objective: Evaluate the burden experienced by the parents, 2) the parents' emotional adjustment to the primary genetic tests results, and 3) the parents' perception of the future	

GS_T: genome sequencing—trio analysis; GS_S: genome sequencing—proband only.

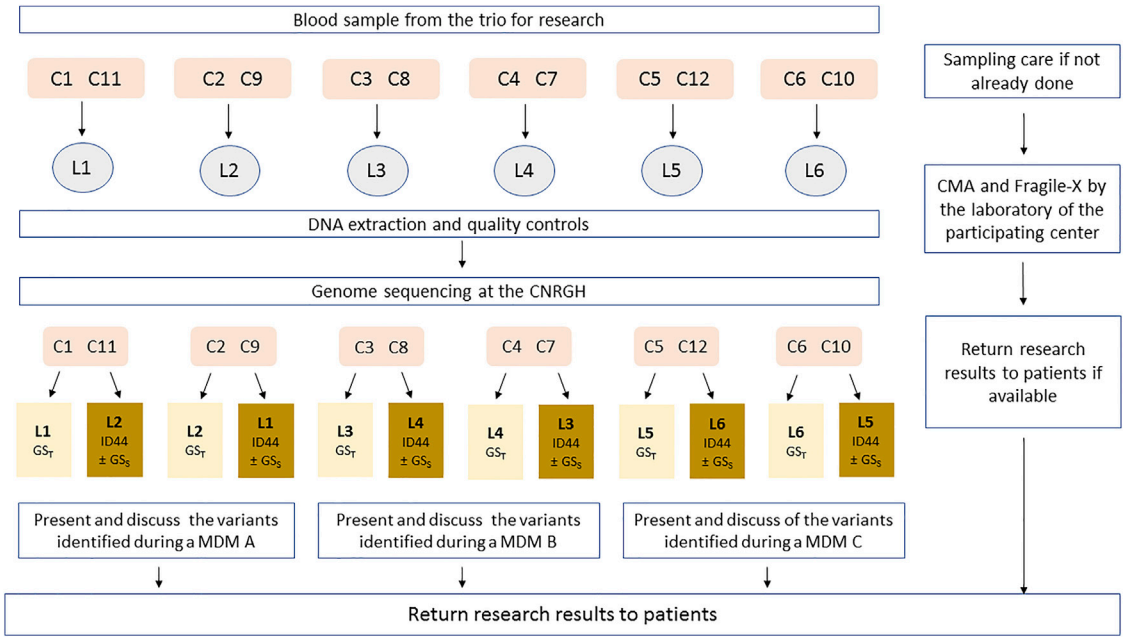

FIGURE 2 | Sample flow description (DEFIDIAG study). C: Clinical centers; L: Reference laboratory (highlighted in light yellow) and Mirror Laboratory (highlighted in dark yellow); MDM: MultiDisciplinary meeting; CNRGH: Centre National de Recherche en Génomique Humaine (National Centre for Human Genomic Research). Each clinical center (C, numbered 1–12) is affiliated to one reference laboratory (numbered 1–6) in charge of the analysis of trio-genome sequencing—GST; each laboratory (L) is affiliated to 2 clinical recruitment centers as a reference laboratory (for example: L1 will be the reference laboratory for patients from C1 and C2) and will work in pairs with another laboratory (mirror laboratories), in charge of ID44 and of the analysis of solo-genome sequencing (GSS) for patients randomized in the appropriate sub-group. This mirror laboratory is itself affiliated with two other recruitment centers (for example: L1 will be the mirror laboratory for patients from C3 and C4). The 4 clinical centers organize the multidisciplinary meeting (MDM) together with their 2 official laboratories.

are made known to the parents/patients, and a third and final interview 12 months after the results are made known) in a sample of parents. The target population for each objective is described in **Table 1**.

Strategies Compared

In order to avoid producing redundant sequences, for each patient included, one unique set of genomic data sequences will be produced by a unique sequencing platform (CNRGH, Evry, France). Analyses are then performed blindly by two independent mirror laboratories: one laboratory will analyze the genome with the parental inheritance information (GST), while the second will analyze only the 44 genes of the reference minimal strategy (44GPS), without parental inheritance information, as well as the proband genome (GSS) in a randomized selection of patients (**Figure 2**; **Supplementary Table S1**).

The results of the 44GPS will be withdrawn from the GS data for all patients, using a specific bioinformatics filtering procedure that mimics the results obtained using targeted capture analysis (exons ± 20 intronic bases, SNV and CNV analysis). Fragile-X and CMA (included in the reference strategy) follow the routine care circuit, which is mainly independent of the GS circuit.

GST analysis is performed following a harmonized, consensus protocol adopted by the six clinical laboratories involved in this study, and using a common web interface (Polyweb.fr, developed in-house at the Genetic diseases IMAGINE Institute, Paris, France). All genomic variations are called by standard callers (GATK and BWA) and are subsequently ranked using several factors to facilitate analysis (protein impact, inheritance model, ID known gene and control data bases, splice prediction effect . . .) in the Polyweb interface. For the SNV/small indel, the scheme contains a first minimal filtration step (for SNV/indel, elimination of the variations with over 1,000 hits in GnomAD, or 5 hits at homozygous state). All variations with a predicted protein impact are ranked at the top of the list and will be studied even when a first deleterious causative variation is detected. This broad approach ensures that co-occurring mutations in different genes will be identified [multi allelism is expected in about 5% of the cases (Yang et al., 2014)]. Additional bioinformatics modules such as repeat tracking, promoter and evolutionary conserved regions analysis, and mobile element insertion detection will be implemented and applied onto negative genome results during the ongoing protocol. Specific protocols for the proband GS data and 44GPS analysis are also developed and shared between the six laboratories. To limit time dedicated to GS proband analysis, SNV/indel analysis only focuses on exonic ± 20 bases of the known ID genes (SysID list) and OMIM disease-associated genes.

When the analysis is completed, variants of interest (highly suspected to be pathogenic) are recorded in a dedicated and secured electronic Case Report Form (e-CRF). Variant class (pathogenic as class 5 variant, probably pathogenic as class 4 variant or of unknown significance but highly suspected to be pathogenic as class 3 + variant) is validated during a Multi-

Disciplinary Meeting (MDM) before being communicated to the patient.

The results of the microarray analysis and Fragile X analysis will be communicated to families and collected in the dedicated e-CRF by the recruiting genetic team as soon as the results are obtained from the diagnostic laboratories. The laboratories in charge of the GS analyses will remain blinded to these results. The GS results will be available approximately 6–9 months after inclusion in the study. In the event of an emergency (such as pregnancy), the blinding can be lifted and the results delivered to families as soon as they become available.

Study Endpoint

Primary Outcome

The primary study endpoint is the identification of a causal diagnosis of ID, defined as the identification of one or more class 4 or 5 variant(s) that explain the symptoms presented by the patient, and validated during a specific MDM.

Secondary Outcomes

- Efficacy in terms of diagnostic yield: identification of causal structural changes
- Efficiency: estimation of the incremental cost-effectiveness ratio, expressed in terms of cost per additional positive diagnosis.
- Quantitative impact studies
- Cost of the diagnostic odyssey: mean cost related to the iterative search for a diagnosis in the previously investigated population.
- Change in follow-up: criteria will be the change in the number and type of medical, medico-social, rehabilitative, and psychological care induced by the results of the trio genomic analyses.
- Qualitative impact studies: A sociologist and a clinical psychologist will explore the consequences on the family, and on the personal, professional and social life of the parents who take care of a child or an adult with ID, as well as the emotional adjustment and possible information overload for the parents at the various stages of the study (inclusion, results rendering, 12 months after receiving results).

Population

The DEFIDIAG study will be conducted in 15 clinical genetic centers in France. All patients consulting a geneticist in one of the participating centers will be screened for eligibility. The study will include children or adults with ID of unknown etiology (index cases or probands), whatever the severity (but with proven ID by ad hoc neuropsychological testing in patients in whom ID is clinically questionable), and whatever the associated manifestations. Individuals with an obvious ID syndrome with a well-known molecular diagnosis will not be considered for inclusion. Children aged between 0 and 5 years will only be considered for inclusion in case of severely delayed development in terms of motor skills, language, and/or sociability. Patients and both biological parents are included if they confirm their willingness to comply with all the study procedures, their availability for the duration of the study, and sign the appropriate consent forms.

Non-inclusion criteria include: isolated learning disabilities; no possibility of obtaining a blood sample from both biological parents; any in the patient condition that, in the investigator's opinion, would jeopardize compliance with the protocol; one or both parents with ID; parent placed under judicial protection (guardianship, curatorship, tutorship).

The strategy based on GST is expected to yield a diagnosis in at least 60% of patients with ID versus 30% with the reference minimal strategy in the population of patients attending for a first genetic investigation (never-explored patients). However, the strategies will be compared in 7 subgroups: 1) 3 defined by age: children <2 years old/2–5 years/>5 years; 2) 4 subgroups of patients defined according the severity of ID, and/or 3) with associated manifestations:1) mild ID associated with another sign, 2) moderate to severe ID, 3) ID with major non-cerebral abnormality, and 4) ID associated with epilepsy The smallest sub-group (subjects with mild ID associated with another significant sign) should represent around 15% of the total population, and the difference between the GST and the reference strategy in this particular subgroup can be assumed to be less than 15%. In addition, it is assumed that fewer than 1% of diagnoses identified with the referral minimal strategy will not be identified by the GST. Finally, we will also compare GST and GSS in a subgroup of randomized patients referred for the first time. For this specific comparison, a difference of 7% is expected, and <0.1% of diagnoses identified by GSS and not by GST. Considering these 9 planned comparisons (8 comparisons between GST and the reference strategy and 1 between GST and GS), the one-sided alpha risk is fixed at 0.00278. Based on these hypotheses, and a power of 80%, among patients seen for a first genetic investigation (50% of the population to be recruited), 41 patients are required for the main comparison, and 91 patients with mild ID + other syndrome are necessary. To recruit this number of patients, we estimate that it will be necessary to screen 607 patients attending for a first referral. A subgroup of 196 patients will be randomized to undergo GSS in addition to GST plus the reference minimal strategy. The sample size for this subgroup will be sufficient to compare GST and GSS in terms of diagnostic yield, as well as in terms of efficiency (a sample size over 150 is usually deemed sufficient). As we intend to include 50% of patients attending for a first genetics evaluation (never-explored patients), and 50% of patients who have already been investigated (previously-explored patients), a total of 1,214 patients are necessary. Considering that approximately 5% of samples will not be analyzable, it will therefore be necessary to include 1,275 index cases plus both their parents, for a total of 3,825 participants.

The qualitative study will be performed in a sub-sample of the overall population, in two centres. In order to maximize the scientific rigor of the study and to alleviate the potential burden resulting from the interviews, whilst fostering discussions between the sociological and psychological sides, we chose to separate the interview procedures into two groups. For the psychological sub-study, 15 interviews with parents will be conducted at each assessment timepoint (T1, T2, T3), giving a

total of 45 interviews. For the sociological sub-study, 15 interviews with parents will be conducted at each assessment timepoint (T1, T2, T3), giving a total of 45 interviews. A total of 15 interviews per assessment timepoint was chosen to achieve data saturation, a key concept of qualitative analysis, namely the point beyond which further interviews do not yield any new information (Glaser and Strauss, 1967). As far as possible, the study populations of patients and parents will be stratified into two subgroups, namely never-explored, and previously-explored patients. The subgroups of parents will also be stratified according to the clinical profile of the patients (mild vs moderate or severe ID).

Study Conduct

Inclusion

During a genetics consultation and after verifying the inclusion and non-inclusion criteria, the patient and both parents will be informed about the study by the investigators and invited to participate. If they agree either during the visit or after a period of reflection, they will be invited to sign the consent form. During this visit, the history of the illness, family history, the examinations already carried out and the corresponding results will be collected with the assistance of a Clinical Research Technician (CRT) in the dedicated e-CRF prepared by the DEFIDIAG methodology and management center (INSERM Clinical Investigation Center—Clinical Epidemiology Unit CIC-EC1432), using CleanWEB software (Telemedecine technologies SAS, Boulogne-Billancourt, France). If necessary, the clinical geneticist will prescribe additional neuropsychological tests. A blood sample (5 ml -EDTA tubes) will be obtained from each participant (patients with ID as well as both biological parents). These blood samples will be sent to the reference DEFIDIAG laboratory of the center (**Figure 2**, **Supplementary Table S1**) in compliance with regulations for the shipment of diagnostic samples (category B). A diary will be given to the family where they will be asked to note the patients' use of healthcare and medico-social services until the return of the GS results. This diary makes it possible to collect the medical examinations, biological investigations, rehabilitation and psychological consultations as well as the medico-social follow-up. A follow-up by phone will be performed every 3 months by the CRT in order to guarantee the completeness of the collection.

For parents/patients willing to participate in the qualitative study in the two centers conducting this part of the study, additional data concerning the familial situation, the number of children, the social deprivation level and the existence of informal and/or professional caregivers at home will be collected, as well as the contact details and address of the participants, for the sociologist or psychologist to organize the interview.

Genomic Circuit

All blood samples received for the DEFIDIAG study by the reference laboratory are extracted using a method previously validated by the sequencing platform (Centre National de Recherche en Génomique Humaine, CNRGH). This validation step was performed on the same blood sample, and genomic sequences obtained after various DNA extraction methods were compared by the CNRGH in terms of global DNA quality, mean coverage and SNV/CNV detection. In all, five extractions methods were validated (three automatic and two manual). After blood extraction, 3 µg DNA aliquots labelled with an anonymous barcode are sent to the CNRGH *via* a courier at room temperature. Several quality controls are then performed before the sequencing step (fluorimetric DNA quantification, quality measurement using the DNA integrity number, PCR amplification test, and sex control). If DNA of the trio is accepted, 1.1 µg of DNA is fragmented using an optimized CNRGH GS protocol. The GS is optimized in order to reach a mean coverage of 30X for each sample; a minimum of 25X mean coverage is required. Below these specifications, the sequencing is considered as a failure and will not be repeated.

Variant Calling

Whole genomic sequences are analyzed by two separate SV and SNV/indel pipelines developed and validated by the CNRGH sequencing platform and IMAGINE bioinformatics team. Briefly, the raw data will be produced as compressed FASTQ files generated from the. bcl files by the CNRGH sequencing platform. The sequences are aligned to the human reference genome GRCh37 using the Burrows-Wheeler Aligner BWA software (Li and Durbin, 2010) and made available as BAM files. Aligned sequences are sorted, cleaned and the PCR duplicates are marked using the Sambamba software (Tarasov et al., 2015) in order to eliminate most of the NGS' well-known biases. A local realignment of the sequences around insertion and deletion sites and the base quality recalibration is performed using GATK (McKenna et al., 2010). After sequence quality control and alignment of the reference genome, the CNRGH performs the variant calling on the entire genome for the Single Nucleotide Variants (SNV), small insertion/deletions (indels) and structural variants (including Copy Number Variant, CNV). SNV and indel calling are performed using the Haplotype Caller from GATK software in "bp resolution" mode to produce gVCF files. Imbalanced SV (CNV) detection > 1 kb is performed using three different softwares: Wisecondor (Raman et al., 2019), Canvas (Roller et al., 2016) and Manta (Chen et al., 2016). Balanced SV (translocation, inversion) detection is done using Manta software. Results are produced in the format of a VCF file to match the common file standard format in NGS analysis. These files are then collected by the IMAGINE Polyweb platform: additional combined TRIO gVCF analysis (genotypeGvcf) and CNV Wisecondor analysis will also be performed.

Quality Controls

Several quality controls are carried out before biological analysis: genome mean coverage over 25X is required for the trio; sex verification (SRY detection) and trio concordance (<1% of Mendelian error transmission in trio using Plink software) are checked before interpretation.

Biological Analysis

The .vcf and .bam files are implemented in Polyweb software developed and previously validated by the IMAGINE

bioinformatics platform. This software makes it possible to annotate, analyse and visualise all the genomic variations in two different web interfaces Polyviewer (for SNV, small indel, exonic deletion or duplication) and Polycyto (for balanced and unbalanced SV) of all human genes in trio or solo analysis. Moreover, a specific ID44 bioinformatic gene panel will make it possible to study variations from this gene list. Read variations are visualized using IGV software (Robinson et al., 2011).

1) SNV/indel analysis

The polyviewer interface gives access to several annotations, such as patient and trio sequencing data (number of mutated and total reads), data from common free-access databases (GnomAD (Karczewski et al., 2020), Clinvar (Landrum et al., 2020), OMIM (Amberger et al., 2019), GenCode (Frankish et al., 2019) . . .), licensed database HGMDpro and also internal databases (Déjà Vu), gene or protein predicted impact, splice prediction [SpliceAI (Jaganathan et al., 2019)], and for trio analysis, inheritance status of the variation. Our objective is not to evaluate the value of GS for early detection of ID, but rather, to evaluate the risk/benefit of GS for the etiological diagnosis in already-identified ID. The internal database (Déjà Vu) contained over 20.000 exomes, 50.000 panels and 1,000 genomes for SNV/Indel variations with differentiation between ID and non-ID patients.

The following filtration keys are applied to focus on potentially pathogenic variations: GnomAD allele count<1,000, GnomAD homozygote count< 5, and predicted protein impact onto all gene transcripts (Stop gain, Stop loss, Start loss, frameshift, in frame deletions or insertions, missense, and predicted splice region, Déjà Vu for patients non ID < 1,000 and homozygote count < 5).

Ranking of identified variations is then performed based on internal Polyweb criteria: variation sequence quality, *de novo* status if available, known ID gene or OMIM gene, protein or splicing impact prediction, gene with AR inheritance and homozygous or compound heterozygous variations, male and X linked variation, known pathogenic variations in HGMDpro or ClinVar, frequency in GnomAD.

Those criteria will ensure that all variations are analyzed from all known human genes (OMIM or not) that are predicted to affect proteins.

2) SV analysis

The polycyto interface gives access to several annotations using AnnotSV software (Geoffroy et al., 2018), DGV, OMIM and internal Déjà Vu databases. The internal SV database (Déjà Vu) contained at the beginning of the project 200 Novaseq sequenced genomes from non-ID patients. The number of genomes in Déjà Vu is now up to 2000 (mostly ID patients).

Ranking of identified variations is based on calling quality and inheritance status. For balanced SV (translocation and inversion) a greater weight is given to variations whose break points are found in OMIM genes.

After filtering CNV already detected at least 10 times in the Déjà Vu database, all detected CNV are analyzed using standard criteria [ACMG recommendations (Riggs et al., 2020)]. For Déjà Vu count, two CNV are considered identical if they overlap over 75% of their reciprocal length. For balanced SV (translocation and inversion), break points must have an identical genomic position ± 50bp.

All imbalanced and balanced SV are checked in IGV software by visualizing paired read alignment anomalies (insert size, pair orientation and split read). In addition, for CNV, allele frequency plots ranked according to chromosomal positions are also available.

Biological Interpretation

Biological interpretation follows standard criteria [ACMG recommendations (Richards et al., 2015; Riggs et al., 2020)]. Briefly, balanced and imbalanced SV and SNV/Indel/Small exonic deletions, or duplications are all performed by two independent biologists. All variations are checked on. bam data and doubtful variations are confirmed using standard molecular analysis before biological analysis (less than 10 mutated reads for SNV, doubtful *de novo* status, doubtful deletion, duplication or translocation/inversion . . .).

For CNV (duplication, deletion), current cytogenetic analysis is performed based on DGV, inheritance mode, recurrency, and gene contents. For balanced SV, only variations disrupting a known ID gene are retained for interpretation. Small SNV/indel are analyzed following mendelian modes of transmission (*de novo* AD or X linked variations, transmitted AD variation in case of known incomplete penetrance or suspected parental mosaic, maternally X transmission in male patients, homozygous or compound heterozygous variations (SNV or CNV) in autosomal recessive hypothesis). This broad approach ensures that co-occurring mutations (expected in about 5% of cases) will be identified (Yang et al., 2014).

Variants of interest are then recorded in the e-CRF and discussed during the MDM.

Multidisciplinary Meeting

Each MDM includes clinician geneticists from the recruiting center, clinicians in charge of the patients' follow-up (i.e., neuropediatricians, neurologists, pediatricians, etc.), molecular and chromosomal geneticists (from the reference laboratory and its mirror laboratory). To ensure a reasonable number of cases to be reviewed by each MDM, three independent MDMs are organized in parallel, each of them grouping two laboratories and four clinical centers. Each MDM will thus review about 400 inclusions. In order to ensure consistency in decision-making between MDMs, all positive cases from the three MDMs will be validated in a general DEFIDIAG study review meeting.

Each MDM is organized according to the following format: discussion of the list of variants of interest obtained by the simplex 44GPS analysis; then by GSS analysis (for the 196 randomized patients); and finally, by GST. At each step, additional confirmation analysis that would be required in the course of standard care (Sanger, qPCR, FISH, analysis on mRNA, etc.) is recorded on the MDM report and in the e-CRF, for further medico-economic evaluation. The final conclusion concerning the pathogenicity of variant(s) identified by the different approaches will be reached during the session and recorded in

the e-CRF MDM conclusion. If additional confirmation methods are required, the reference laboratory will be in charge of this analysis and the case will subsequently be reviewed in a future MDM. The final results are recorded in a research report communicated to the clinical geneticist who included the index case.

Candidate genes or variations (new genes, or putative variations with no obvious pathogenic effect in known genes) are classified as class 3, of unknown significance until the end of the project. Potential reclassification will be managed using standard care procedures such as splice effect, epigenetic signature, functional studies, and cohorts of patients using international collaboration.

GS Results Visit and Subsequent 12 months Follow-Up

When the results become available, and regardless of the results (positive or negative), the clinical geneticist who included the patient (and parents) will inform patient/family about the results of the GS during a dedicated visit. These results will be made available approximately 9 months after inclusion in the study. If the study identifies one or several class 3+, 4, or 5 variation(s), the clinical geneticist will explain the type of associated medical condition, its mode of inheritance and the risk of recurrence for a future pregnancy, as well as the modalities of care. All information (examinations, medical or non-medical treatment, medico-social follow-up, etc.) will be collected by the geneticist, assisted by a CRT. The diary kept by the families will be retrieved and integrated into the e-CRF. A new diary will be given to the family for the subsequent 12 months, and the phone contact by the CRT is planned. If the parents or adult with mild ID agreed to participate in the qualitative study, the sociologist/psychologist will then contact them to check that they all still agree to continue the interviews and organize the second interview.

Twelve months after the GS results are made known to the patient, a final visit at the hospital will be organized (this visit can be replaced by a telephone contact, if necessary) to assess the medical condition, collect any results and retrieve the diary. If the parents agreed to participate in the qualitative study, once again, the sociologist/psychologist will then contact them to check that they all still agree to continue the interviews and organize the third interview.

Medico-Economic Evaluation

A cost-effectiveness analysis will be conducted over the estimated 9–12 months (maximum) required to perform the GS, interpret the data and return the results to the patient. Efficacy will correspond to the diagnostic yield of each of the three strategies being compared. In order to estimate costs from the perspective of the health service, patient management will be divided into three main periods of healthcare consumption (**Figure 2**). The costs in the medico-economic evaluation will be direct costs, corresponding to medical procedures carried out during period 2. They will include: 1) the costs of consultation with the clinical geneticist in the recruitment centers, 2) the costs of exams preceding the genetic analysis and inclusion in the DEFIDIAG project, and the cost associated with the first blood sample and its transport, 3) the costs associated with any new blood draws required; 4) the costs of genetic analyses, and 5) the costs of any additional and confirmatory tests. Most of these procedures will be valued using social security prices, except for GSS and GST, which will be valued using a micro-costing method (Drummond et al., 2005).

Impact Studies

Two impact studies will be conducted: the cost of the diagnostic odyssey will first be estimated. It will include the cost of all diagnostic procedures from the first genetics consultation, to inclusion in the DEFIDIAG project (period 1 of **Figure 1**). The impact of genomic analyses on follow-up will also be assessed. It will be based on a before-after study (period 3 compared to period 1) and will include treatment and diet as well as rehabilitation, psychological and medico-social follow-up.

Data Management and Data Analyses

Data Management

Clinical and paraclinical data as well as the results of the genetic analyses carried out will be entered directly into the dedicated e-CRF by the investigators, helped by CRTs and by biologists and bioinformatics specialists in charge of the GS analyses. The patient diary specific to microcosting and patient follow-up are in paper or electronic format (forms independent of the e-CRF). Each patient is identified by a unique code including: the number of the recruiting center, the inclusion rank, the initials of the patient (first letter of surname and first letter of first name) and a code corresponding to his/her sex. The use of the CleanWEB software makes it possible to carry out checks for missing and incoherent data, and to generate queries immediately after data entry. Requests for corrections may also be generated by the CIC-EC1432 and sent to the recruiting center and/or the reference laboratory. The corrections will be made directly in the e-CRF by the investigators and/or the biologists, assisted by the CRTs. Histories of changes are systematically recorded. A data management plan, specific to the study, integrating centralized monitoring (enabling, for example, comparative monitoring of the distribution of subpopulations between centers and indicators of the quality of sample processing) was prepared before initiating the study in the participating centers.

Statistical Analyses

The percentage of ID causal diagnosis identified will be compared between strategies (GST vs reference strategy) using a McNemar test in the overall first-investigation population, then in the seven subgroups of interest. To account for multiple testing, the unilateral alpha risk is set at 0.00278, and also for the secondary comparisons of the diagnostic yield of GST vs. GSS, which will be performed in the dedicated randomized subgroup.

McNemar tests (unilateral alpha risk set at 0.025) will also be used to compare the percentage of causal diagnoses identified by GS and reference strategies in the sub-groups of the individuals coming for a first genetic referral without major non-cerebral abnormality or without epilepsy. This test will also be used in the overall population (first-investigation patients and previously investigated patients) to compare the percentage of causal

diagnoses identified by GS strategies in patients with negative CMA. The percentage of causal structural changes identified by GST vs the reference minimal strategy will also be compared using McNemar tests in the first-investigation population (firstly considered all together, and then stratified by subgroups). The number and type of consistent and divergent variants identified with CMA and GS strategies will also be described. The frequency and characteristics of the situations where the causal diagnosis is identified by the reference strategy but not by the GS analyses will be described, as well as the frequency and characteristics of situations where the causal diagnostic is made by GSS and not by GST.

Cost-Effectiveness Study

The cost-effectiveness analysis will be performed in the population of randomized patients coming for a first genetic referral and for whom both GS strategies are performed in addition to the reference minimal strategy (i.e., 196 patients). The analysis will be based on the estimation of incremental cost-effectiveness ratios expressed in terms of cost per additional positive diagnosis. Deterministic analysis will take account of progress in technology. In order to manage the uncertainty associated with sampling, a non-parametric bootstrap analysis will be performed.

Impact Studies

The costs of finding a diagnosis will be described only in the population of patients who had previously had genetic investigations (50% of the 1,275 index cases), as the mean and standard deviation, if normally distributed, or as median and interquartile range otherwise.

The analysis of the impact of genomic analysis on medical, medico-social, rehabilitation and psychological follow-up after the results are made known, will be performed separately in the previously-explored population (50% of the 1,275 index cases) on the one hand, and in the population attending for a first genetics investigation on the other hand (never-explored patients). Frequencies of follow-up changes between the period prior to inclusion and the period following the results will be calculated with associated 95% confidence intervals. A global analysis will then be performed, regardless of the results of GST. Sub-analyses will be conducted according to the result of GST: positive, negative or uncertain.

Qualitative Study

The analysis of the interviews will be based on the following steps: 1) open coding of transcribed interviews, to identify as many topics as possible in the initial corpus; 2) categorization of codes; careful re-reading of the corpus as a whole will be performed to clearly define each category; 3) linking categories and writing of detailed memos and designing explanatory diagrams; 4) integration of the previous steps to identify the key points of the phenomenon; 5) theorization: meticulous and exhaustive construction of the "multidimensionality" and "multicausality" of the phenomenon of the relationships between needs, expectations and hopes, suffering, and the result of genetic analysis. For the psychological aspects, the interviews will be analyzed using the general inductive method (Thomas, 2006), which encompasses the first 3 steps mentioned above.

ETHICS AND DISSEMINATION

The study sponsor is the Institut National de la Santé Et de la Recherche Médicale (INSERM). DEFIDIAG study was supported by The French Ministry of Health in the framework of French initiative for genomic medicine (AVIESAN, 2016). An independent international scientific advisory board was constituted in order to make recommendations about the protocol and to evaluate and oversee the scientific and ethical integrity of the study. It is also tasked with evaluating potential sub-study proposals. The Ethics Committee Sud Méditerranée I approved the protocol in June 2019 (under the number 1955/19.05.29.60442). Authorization for detaining nominative databases was granted in March 2020 by the French data privacy commission (Commission Nationale de l'Informatique et des Libertés, CNIL, reference number: 919361). The protocol was registered with ClinicalTrials.gov under the identifier NCT04154891 in November 2019. The first patient was included in March 2020 and the study is expected to be completed by 2023.

We anticipate that the DEFIDIAG study will demonstrate an increase in performance of genetic testing performance in patients (children and adults) affected with ID of unknown etiology. This study will benefit the patient and the family, because it will identify a diagnosis, in turn providing the family with an explanation for the clinical condition, which will at last have a name (heralding the end of their diagnostic odyssey). Finding a diagnosis will enable initiation of appropriate medical therapy and ad hoc care if available, and help in the organization of follow up for the patient, prevent unnecessary medical biological and imaging investigations, authorize reproductive counseling for patient and/or family (prenatal diagnosis, preimplantation diagnosis), enable referral to ad hoc patient and support groups, and contribute to research protocols. Indeed, future perspectives include numerous research projects through the data collected concerning genotype-phenotype analyses, biological integrative analysis of pathways involved in brain development and functioning and last but not least, may help in the elaboration of targeted therapies.

In addition, it is expected that the cost-effectiveness and impact studies will show the efficiency of GST and also the cost-saving and the change in medical practice that can be expected from its implementation. To the best of our knowledge, no data has been published in France on the economic and medical impact of GS compared to the reference strategy or between trio and solo strategies. These arguments are essential to support the decision to implement the appropriate first line GS strategy in diagnostic routine practice, to help public health authorities to determine an adequate tariff with regard to the complete cost of GS, and also to demonstrate the impact of GS on improving patient care. Specifically, we believe it is important to determine the efficiency of a solo strategy, which is less costly in terms of sequencing, but also more pragmatic in many situations where biological relatives are not readily available.

However, it is potentially more time consuming to interpret than trio sequencing data. Comparing these two strategies from a medico-economic point of view therefore seems important. We made some important choices concerning the methodology of data collection. The completion of the DEFIDIAG study should enable the key stakeholders to decide on the implementation of GS in France as the first-line test in the care of patients with ID. It will help us to confirm the robustness of the results obtained with traditional data collection by providing GS diagnostic yield estimates in conditions close to routine.

DATASHARING

All requests for the study's data will be considered by the Defidiag trial steering committee. After the end of the study; and for participants who provide consent, data (excluding data corresponding to the image capture) will be transmitted to and stored at the "CAD" (Collecteur Analyseur de Données) of the French initiative for genomic medicine (AVIESAN, 2016), for potential re-use by other researchers including those not involved in the present study. The conditions for CAD data sharing are being implemented.

TRIAL STATUS

Recruitment is ongoing (955 patients included as of 09/06/2021).

FULL LIST OF CO-INVESTIGATORS OF THE DEFIDIAG STUDY GROUP:

Meyer Vincent, Centre National de Recherche en Génomique Humaine; Bonneau Dominique, Barth Magalie, Tessarech Marine, Ziegler Alban, CHU d'Angers; Goizet Cyril, Lacombe Didier, Legendre Marine, Margot Henri, Michaud Vincent, Naudion Sophie, Rooryck Thambo Caroline, CHU de Bordeaux; Bournez Marie, Bruel Ange-Line, Colin Estelle, Delanne Julian, Denomme-Pichon Anne-Sophie, Garde Aurore, Moutton Sébastien, Nambot Sophie, Philippe Christophe, Safraou Hana, Sorlin Arthur, Thauvin Christel, Tran-Mau-Them Fréderic, Vitobello Antonio, CHU Dijon-Bourgogne and Inserm UMR1231- Equipe GAD;Dietrich Klaus, Durand Chantal, Marey Isabelle, N'guyen-Morel Marie-Ange, Thevenon Julien, CHU Grenoble-Alpes; Boute Odile, Caumes Roseline, Colson Cindy, Dieux Anne, Ghoumid Jamal, Marsili Luisa, Petit Florence, Vanlerberghe Clémence, Vincent-Delorme Catherine, CHU de Lille; Armand Thibaud, Chatron Nicolas, Curie Aurore, Des Portes Vincent, Edery Patrick, Haye Damien, Labalme Audrey, Lesca Gaëtan, Monin Pauline, Pons Linda, Putoux Audrey, Rossi Massimiliano, Rougeot Christelle, Till Marianne, Hospices Civils de Lyon; Blanchet Patricia, Coubes Christine, Deiller Caroline, Genevieve David, Pinson Lucile, Wells Constance, Willems Marjolaine, CHU de Montpellier; Isidor Bertrand, Mercier Sandra, Nizon Mathilde, Vincent Marie, CHU de Nantes; Amiel Jeanne, Barcia Giulia, Baujat Geneviève, Cormier Valérie, Guimier Anne, Hadj Abdallah Hamza, Malan Valérie, Marlin Sandrine, Marzin Pauline, Michot Caroline, Ormieres Clothilde, Rio Marlène, Romana Serge, Hôpital Necker-Enfants Malades (AP-HP); Afenjar Alexandra, Burglen Lydie, Charles Perrine, Courtin Thomas, Heide Solveig, Keren Boris, Lehalle Daphné, Mignot Cyril, Mouthon Linda, Whalen Sandra, Groupe Hospitalier Pitié-Salpêtrière (AP-HP); Fradin Mélanie, Jean-Marcais Nolwenn, Lavillaureix Alinoë, Morel Godelieve, Pasquier Laurent, Quelin Chloé, Riou Audrey, Ugolin Mélissa, CHU de Rennes; Brehin Anne-Claire, Cassinari Kévin, Chambon Pascal, Goldenberg Alice, Guerrot Anne-Marie, Joly-Helas Géraldine, Lecoquierre François, Lemeur Nathalie, Nicolas Gaël, Saugier-Veber Pascale, Vera Gabriella, CHU de Rouen; El Chehadeh Salima, Calmels Nadège, Haushalter Virginie, Maillard Pierre-Yves, Muller Jean, Philippe Anaïs, Piton Amélie, Schaefer Elise, Scheidecker Sophie, Schluth-Bolard Caroline, Hôpitaux Universitaires de Strasbourg; Busa Tiffany, Philip-Sarles Nicole, Riccardi Florence, Sigaudy Sabine, Hôpital de la Timone (Hôpitaux Universitaires de Marseille); Nitschke Patrick, Institut Imagine.

AUTHOR CONTRIBUTIONS

CB: design of the diagnostic study methodology, drafting the protocol, supervision of the study, writing—original draft, CL: design and coordination of the medico-economic and impact studies, drafting the protocol, supervision of the study, writing—review and editing. LF: design and coordination of the patients circuit, drafting the protocol, supervision of the study, patient enrolment, writing—review and editing. MB: project administration, writing—original draft. M-LA: project administration, drafting the protocol, support to the coordination of the project, writing—review and editing. AS: project administration, drafting the protocol, support to the coordination of the project, writing—review and editing. J-FD: design and coordination of the genetic circuit in the CNRGH, drafting the protocol, supervision of the study, writing—review and editing. FG: design of the medico-economic and impact studies, drafting the protocol, supervision of the study, writing—review and editing. VS: design of the medico-economic and impact studies, drafting the protocol, supervision of the study, writing—review and editing. CD: project administration, drafting the protocol, Resources management, supervision of the study, writing—review and editing. YD: design and bioinformatics coordination, drafting the protocol, writing—review and editing. SL: drafting the protocol, supervision of the study, patient enrolment, writing—review and editing. SO: drafting the protocol, supervision of the study, patient enrolment, writing—review and editing. DH: drafting the protocol, supervision of the study, patient enrolment, writing—review and editing. DS: drafting the protocol, supervision of the study, patient enrolment, writing—review and editing. BG: design and coordination of the genetic circuit, drafting

the protocol, supervision of the study, writing—review and editing. HD: design and coordination of the study, drafting the protocol, supervision of the study, writing—review and editing.

FUNDING

This work was supported by The French Ministry of Health in the framework of the French initiative for genomic medicine (Plan France Médecine Génomique 2025; PFMG 2025; https://www.aviesan.fr/mediatheque/fichiers/version-anglaise/actualites-en/genomic-medicine-france-2025-web). This work was supported by government funding from the Agence Nationale de la Recherche under the "Investissements d'avenir" program (ANR-10-IAHU-01).

ACKNOWLEDGMENTS

The authors would like to thank the following clinical research technicians and genetic counsellors: Akloul Linda, Baudier Marie-Pierre, Baurand Amandine, Bellengier Laurence Bernard Céline, Borel Myriam, Consolino Emilie, Crantelle Laura, De Nadai Narimène, Dorian Virginie, El Amrani Lamia, Faudet Anne, Fournier Chloé, Galivel-Voisine Annastasia, Gaudillat Léa, Gauthier Marjolaine, Glazunova Olga, Goetz Nathalie, Gonde Delphine, Gourves-Noizet Lena, Guegan Caroline, Guyon Laura, Haquet Emmanuelle, Kastner Claire, Khalil Mirna, Laurent Manon, Lextreyt Barbara, Mallet Audrey, Moukossi Caroline, Oumessoum Amina, Ngom Ndeye-Fatou, Pellen Anne-Sophie, Pelletier Valérie, Poirel Elisabeth, Prouteau Clément, Rubeck Coralie, Staraci Stéphanie, Sawka Caroline, Tempe Laurine, Wyrebski Antoine, Zordan Cécile. We also thank the members of the Scientific Committee of the DEFIDIAG project: Beckmann Jacques, Fitzpatrick David, Matthijs Gert, Raymond Lucy, Riess Olaf, Abrahamowicz Michal, Buchanan James.Finally, the authors thank Fiona Ecarnot, PhD (University Hospital Besancon and EA3920, University of Burgundy Franche-Comté, Besancon, France) for editorial assistance.

SUPPLEMENTARY MATERIAL

The Supplementary Material for this article can be found online at: https://www.frontiersin.org/articles/10.3389/fgene.2021.766964/full#supplementary-material

REFERENCES

Alam, K., and Schofield, D. (2018). Economic Evaluation of Genomic Sequencing in the Paediatric Population: a Critical Review. *Eur. J. Hum. Genet.* 26 (9), 1241–1247. doi:10.1038/s41431-018-0175-6

Amberger, J. S., Bocchini, C. A., Scott, A. F., and Hamosh, A. (2019). OMIM.org: Leveraging Knowledge across Phenotype-Gene Relationships. *Nucleic Acids Res.* 47 (D1), D1038–D1043. doi:10.1093/nar/gky1151

AVIESAN (2016). *French Plan for Genomic Medicine 2025*. Available at: : https://www.aviesan.fr/mediatheque/fichiers/version-anglaise/actualites-en/genomic-medicine-france-2025-web (Accessed December 7, 2021).

Chen, X., Schulz-Trieglaff, O., Shaw, R., Barnes, B., Schlesinger, F., Källberg, M., et al. (2016). Manta: Rapid Detection of Structural Variants and Indels for Germline and Cancer Sequencing Applications. *Bioinformatics* 32 (8), 1220–1222. doi:10.1093/bioinformatics/btv710

Drummond, M. F., Schulpher, M. J., Torrance, G. W., O'Brien, B. J., and Stoddart, G. L. (2005). *Methods for the Economic Evaluation of Health Care Programme*. 3rd ed. Oxford, UK: Oxford University Press.

Ellison, J. W., Rosenfeld, J. A., and Shaffer, L. G. (2013). Genetic Basis of Intellectual Disability. *Annu. Rev. Med.* 64, 441–450. doi:10.1146/annurev-med-042711-140053

Frankish, A., Diekhans, M., Ferreira, A.-M., Johnson, R., Jungreis, I., Loveland, J., et al. (2019). GENCODE Reference Annotation for the Human and Mouse Genomes. *Nucleic Acids Res.* 47 (D1), D766–D773. doi:10.1093/nar/gky955

Geoffroy, V., Herenger, Y., Kress, A., Stoetzel, C., Piton, A., Dollfus, H., et al. (2018). AnnotSV: an Integrated Tool for Structural Variations Annotation. *Bioinformatics* 34 (20), 3572–3574. doi:10.1093/bioinformatics/bty304

Glaser, B., and Strauss, A. (1967). *The Discovery of Grounded Theory: Strategies for Qualitative Research*. Mill Valley, CA, USA: Sociology Press.

Han, J. Y., and Lee, I. G. (2020). Genetic Tests by Next-Generation Sequencing in Children with Developmental Delay And/or Intellectual Disability. *Clin. Exp. Pediatr.* 63 (6), 195–202. doi:10.3345/kjp.2019.00808

Jaganathan, K., Kyriazopoulou Panagiotopoulou, S., McRae, J. F., Darbandi, S. F., Knowles, D., Li, Y. I., et al. (2019). Predicting Splicing from Primary Sequence with Deep Learning. *Cell* 176 (3), 535–548. doi:10.1016/j.cell.2018.12.015

Karczewski, K. J., Francioli, L. C., Tiao, G., Cummings, B. B., Alföldi, J., Wang, Q., et al. (2020). The Mutational Constraint Spectrum Quantified from Variation in 141,456 Humans. *Nature* 581 (7809), 434–443. doi:10.1038/s41586-020-2308-7

Landrum, M. J., Chitipiralla, S., Brown, G. R., Chen, C., Gu, B., Hart, J., et al. (2020). ClinVar: Improvements to Accessing Data. *Nucleic Acids Res.* 48 (D1), D835–D844. doi:10.1093/nar/gkz972

Li, H., and Durbin, R. (2010). Fast and Accurate Long-Read Alignment with Burrows-Wheeler Transform. *Bioinformatics* 26 (5), 589–595. doi:10.1093/bioinformatics/btp698

McKenna, A., Hanna, M., Banks, E., Sivachenko, A., Cibulskis, K., Kernytsky, A., et al. (2010). The Genome Analysis Toolkit: a MapReduce Framework for Analyzing Next-Generation DNA Sequencing Data. *Genome Res.* 20 (9), 1297–1303. doi:10.1101/gr.107524.110

Ontario Health (Quality) (2020). Genome-Wide Sequencing for Unexplained Developmental Disabilities or Multiple Congenital Anomalies: A Health Technology Assessment. *Ont Health Technol. Assess. Ser.* 20 (11), 1–178.

Raman, L., Dheedene, A., De Smet, M., Van Dorpe, J., and Menten, B. (2019). WisecondorX: Improved Copy Number Detection for Routine Shallow Whole-Genome Sequencing. *Nucleic Acids Res.* 47 (4), 1605–1614. doi:10.1093/nar/gky1263

Richards, S., Aziz, N., Bale, S., Bick, D., Das, S., Gastier-Foster, J., et al. (2015). Standards and Guidelines for the Interpretation of Sequence Variants: a Joint Consensus Recommendation of the American College of Medical Genetics and Genomics and the Association for Molecular Pathology. *Genet. Med.* 17 (5), 405–424. doi:10.1038/gim.2015.30

Riggs, E. R., Andersen, E. F., Cherry, A. M., Kantarci, S., Kearney, H., Patel, A., et al. (2020). Technical Standards for the Interpretation and Reporting of Constitutional Copy-Number Variants: a Joint Consensus Recommendation of the American College of Medical Genetics and Genomics (ACMG) and the Clinical Genome Resource (ClinGen). *Genet. Med.* 22 (2), 245–257. doi:10.1038/s41436-019-0686-8

Robinson, J. T., Thorvaldsdóttir, H., Winckler, W., Guttman, M., Lander, E. S., Getz, G., et al. (2011). Integrative Genomics Viewer. *Nat. Biotechnol.* 29 (1), 24–26. doi:10.1038/nbt.1754

Roller, E., Ivakhno, S., Lee, S., Royce, T., and Tanner, S. (2016). Canvas: Versatile and Scalable Detection of Copy Number Variants. *Bioinformatics* 32 (15), 2375–2377. doi:10.1093/bioinformatics/btw163

Schofield, D., Rynehart, L., Shresthra, R., White, S. M., and Stark, Z. (2019). Long-term Economic Impacts of Exome Sequencing for Suspected Monogenic Disorders: Diagnosis, Management, and Reproductive Outcomes. *Genet. Med.* 21 (11), 2586–2593. doi:10.1038/s41436-019-0534-x

Schwarze, K., Buchanan, J., Taylor, J. C., and Wordsworth, S. (2018). Are Whole-Exome and Whole-Genome Sequencing Approaches Cost-Effective? A Systematic Review of the Literature. *Genet. Med.* 20 (10), 1122–1130. doi:10.1038/gim.2017.247

Stark, Z., Schofield, D., Alam, K., Wilson, W., Mupfeki, N., Macciocca, I., et al. (2017). Prospective Comparison of the Cost-Effectiveness of Clinical Whole-Exome Sequencing with that of Usual Care Overwhelmingly Supports Early Use and Reimbursement. *Genet. Med.* 19 (8), 867–874. doi:10.1038/gim.2016.221

Tarasov, A., Vilella, A. J., Cuppen, E., Nijman, I. J., and Prins, P. (2015). Sambamba: Fast Processing of NGS Alignment Formats. *Bioinformatics* 31 (12), 2032–2034. doi:10.1093/bioinformatics/btv098

Thomas, D. R. (2006). A General Inductive Approach for Analyzing Qualitative Evaluation Data. *Am. J. Eval.* 27 (2), 237–246. doi:10.1177/1098214005283748

Yang, Y., Muzny, D. M., Xia, F., Niu, Z., Person, R., Ding, Y., et al. (2014). Molecular Findings Among Patients Referred for Clinical Whole-Exome Sequencing. *JAMA* 312 (18), 1870–1879. doi:10.1001/jama.2014.14601

Conflict of Interest: The authors declare that the research was conducted in the absence of any commercial or financial relationships that could be construed as a potential conflict of interest.

frontiers in Genetics

ORIGINAL RESEARCH
published: 07 February 2022
doi: 10.3389/fgene.2022.781832

A Nonsense Variant of *ZNF462* Gene Associated With Weiss–Kruszka Syndrome–Like Manifestations: A Case Study and Literature Review

*Shaozhi Zhao, Chen Miao, Xiaolei Wang, Yitong Lu, Hongwei Liu and Xinwen Zhang**

Center of Medical Genetics, Xi'an People's Hospital (Xi'an Fourth Hospital), Xi'an, China

Objective: This study aims to explore the clinical characteristics and genetic basis of a patient with unilateral ptosis and unilateral hearing impairment in pedigree analysis.

Methods: The clinical data of the child and his father were collected. The genomic DNA of the patient and his relatives were extracted from their peripheral blood samples and subjected to trio-whole-exome sequencing (trio-WES) and copy number variation analysis. Sanger sequencing was used to verify the potential variant.

Results: The sequencing analysis identified a heterozygous nonsense variant c.6431C > A (p.Ser2144*) in the *ZNF462* gene (NM_021224.6) in the child and his father, whereas the locus in his asymptomatic mother, brother, and grandparents was found to be the wild type, which is an autosomal dominant inheritance. The new genetic variant has not been previously reported in the ClinVar and HGMD databases and the Genome Aggregation Database (gnomAD).

Conclusion: This is the first incidence of Weiss–Kruszka syndrome relating to the nonsense variant in the *ZNF462* gene in China. The finding from this study is novel in its expansion of the variant spectrum of the *ZNF462* gene and clarifies the genetic etiology of the patient and his father.

Keywords: *ZNF462* gene, Weiss–Kruszka syndrome, ptosis, hearing loss, craniofacial deformities

OPEN ACCESS

Edited by:
Anjana Munshi,
Central University of Punjab, India

Reviewed by:
Hasan Orhan Akman,
Columbia University Irving Medical Center, United States
Avinash Vijay Dharmadhikari,
Children's Hospital of Los Angeles, United States

****Correspondence:***
Xinwen Zhang
xianxinwen@163.com

Specialty section:
This article was submitted to Genetics of Common and Rare Diseases, a section of the journal Frontiers in Genetics

Received: *23 September 2021*
Accepted: *10 January 2022*
Published: *07 February 2022*

Citation:
Zhao S, Miao C, Wang X, Lu Y, Liu H and Zhang X (2022) A Nonsense Variant of ZNF462 *Gene Associated With Weiss–Kruszka Syndrome–Like Manifestations: A Case Study and Literature Review. Front. Genet. 13:781832. doi: 10.3389/fgene.2022.781832*

1 INTRODUCTION

Weiss–Kruszka syndrome (WSKA, MIM: 618,619) is a multiple congenital anomaly syndrome. WSKA is characterized by ptosis, growth restriction, craniofacial deformities, and corpus callosum hypoplasia (Weiss et al., 2017). Recent evidence revealed that WSKA is caused by the loss-of-function (LOF) variations in the *ZNF462* gene or deletions on chromosome 9 p 31.2 containing the *ZNF462* gene. Additionally, this genetic disease is inherited in an autosomal dominant manner, which often results from new variants. So far, only 27 cases of *ZNF462* gene variation have been reported globally (Weiss et al., 2017; Cosemans et al., 2018; Kruszka et al., 2019; González-Tarancón et al., 2020; Iivonen et al., 2021; Park et al., 2021), and the underlying mechanism of the syndrome has not been extensively studied. This study reported a family in which both the child and his father had WSKA with ptosis and hearing loss. The diagnosis was established based on clinical symptoms and gene tests. Through trio-whole-exome sequencing (trio-WES), a novel nonsense variant in the *ZNF462* gene was identified in the child and his father. With the first pedigree analysis of WSKA in

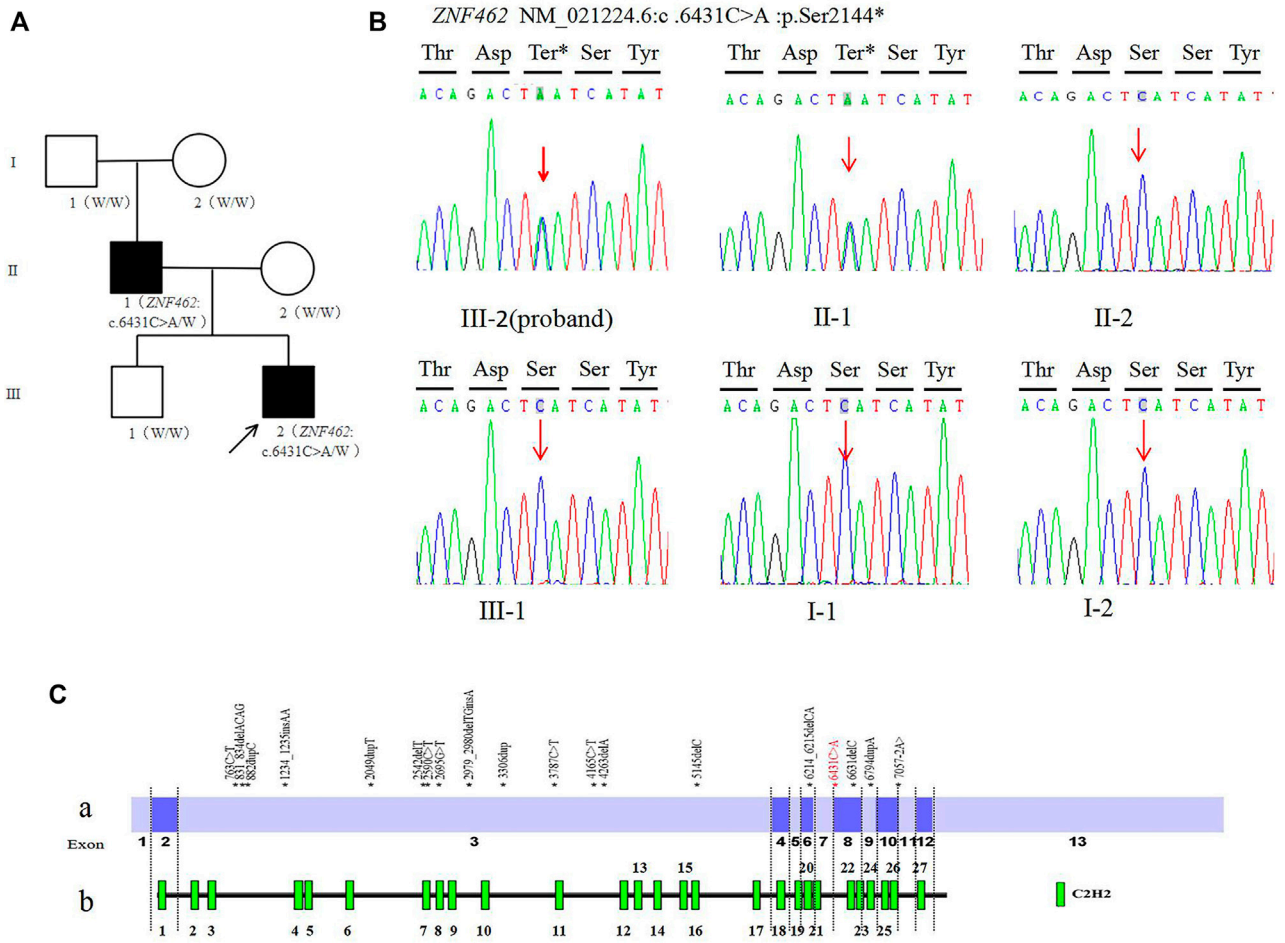

FIGURE 1 | (A). Family tree of this study (W: Wild type allele); **(B)**. Sanger sequencing of the *ZNF462:* c.6431C > A variant of family **(C)**. Distribution diagram of *ZNF462* gene variation (red fonts is the variant reported in this study) Ca. Distribution diagram of *ZNF462* gene variants reported in the HGMD database (numbers represent exons) Cb. Schematic diagram of C2H2 zinc finger structure distribution of ZNF462 protein.

China, the study enriched the variant spectrum of the *ZNF462* gene and enhanced the knowledge of clinical features, genetic characteristics, and diagnostic protocols for WSKA.

2 SUBJECTS AND METHODS

2.1 Subjects

The proband is a boy born prematurely (premature rupture of membranes at 36^{+5} weeks of gestation, G2P2, vaginal delivery, no asphyxia, Apgar score 10-10-10, and birth weight 3.08 kg). His parents are Chinese who are not close relatives. The child did not exhibit any abnormal breathing, vomiting, abdominal distension, or convulsions. His body temperature and reaction were normal, without the observance of yellow skin mucous membrane. His thoracic movements of both sides were the same, while the lungs were clear, the limbs were active, and the muscle tension was normal. He had no deformity in his skull, and the initial brain ultrasound showed that the triangular area of the bilateral ventricles had a slightly higher parenchymal echo. Furthermore, brain MRI showed no abnormalities. An echocardiogram detected a 1.2-mm patent ductus arteriosus. The boy exhibited an asymmetric crying face, and his left eyelid drooped significantly. The boy failed the hearing screening in the right ear. His father had a pathological droopy eyelid (the right eyelid) which was treated by surgery many years ago, while he has impaired hearing in the right ear. The proband's mother, brother, and grandparents have no clinical symptoms (**Figure 1A**).

Furthermore, the chromosomal karyotyping of the proband was normal. It is normal to use tandem mass spectrometry for analysis of samples extracted from dried blood spots (DBS) collected from infants, and this test is used for the screening of amino acid metabolic disorders, organic acidemia, and fatty acid oxidative metabolic disorders by detecting the levels of dozens of amino acids, free carnitine, and acylcarnitine in samples extracted from newborn DBS. The genome copy number variation sequencing (CNV-seq) did not reveal a pathogenic CNV (pCNV), and the CNV-seq is a high-resolution genome-wide method to identify pCNV(>100 kb)

based on low-coverage whole-genome sequencing. At 8 months old, the child manifested restriction in motor development and cannot sit alone or crawl with low muscle tone compared to his peers.

3 METHOD

3.1 Sample Collection

The study was approved by the Ethics Committee of Xi'an People's Hospital (Xi'an Fourth Hospital), and the written informed consent was granted by the parents of the patient. In total, 3 ml of the peripheral blood sample was collected from the child, his parents, brother, and grandparents, respectively, and stored in EDTA anticoagulant tubes. The genomic DNA was extracted from all the blood samples using a QIAamp DNA Blood Mini Kit and stored at -20°C for subsequent usage.

3.2 Trio Whole-Exome Sequencing Analysis

The genomic DNA was analyzed by trio-WES. The NanoWES probe was used for the whole-exome DNA hybridization and enrichment in high-throughput sequencing (Nova Seq 6,000). Sequencing data analysis was conducted by the Verita Trekker® mutation site detection system and Enliven® mutation site annotation interpretation system. The analysis filtered out the variants with mutation frequencies greater than 1‰ in the human exon database (ExAC), the 1000 Genomes Project, and the Genome Aggregation Database (gnomAD),and also filtered the nonfunctional variation site (such as synonymous variants and noncoding region variants.). The pathogenicity prediction was performed using multiple software packages including SIFT, Polyphen2, and CADD. The potential pathogenic variant was determined along with the related disease database and relevant clinical reports.

3.3 Sanger Sequencing and Family Analysis

The pathogenic variant was detected using trio-WES and Sanger sequencing in the proband and his parents, and then Sanger sequencing validation was used for family analysis. The PCR amplicons of the target sequences were verified by 1% agarose gel electrophoresis, and sequencing was performed on the ABI 3500DX. The pathogenicity classification and data interpretation of the variations in the gene are based on the guidelines of the American Society of Medical Genetics and Genomics (ACMG) guidelines (Richards et al., 2015)

4 RESULTS

4.1 Results of Genetic Analysis

The trio-WES analysis showed that both the proband and his father carried a novel heterozygous variant c.6431C > A (p.Ser2144*) in the *ZNF462* gene (NM_021224.6); however, no evidence of this variant was found in the other asymptomatic family members, including the proband's mother, brother, and grandparents. The results were validated using Sanger sequencing (**Figure 1B**). So, for his father, c.6431C > A (p.Ser2144*) is *de novo* by both maternity and paternity confirmed (PS2_moderate). The variant is a nonsense variant in the coding region of the *ZNF462* gene, which may generate a premature stop codon and induce a loss-of-function effect (PVS1). The variant was not present in ExAC, 1,000G, and the gnomAD database (PM2_Supporting). According to the ACMG guidelines, the variant c.6431C > A (p.Ser2144*) should be classified as pathogenic (PVS1+PS2_moderate + PM2_Supporting).

4.2 Results of Literature Review

Related keywords to the "*ZNF462* gene" and "Weiss–Kruszka syndrome" were used during the search in the Chinese Journal Full-text Database (CNKI), Wanfang Data Knowledge Service Platform, and Weipu Database (covering time to May 2021), and no relative case was reported. The same keywords were used in PubMed (covering time to May 2021), and six publications were found containing cases of WSKA associated with the *ZNF462* gene. The first reported case identified a new balanced translocation t (2; 9) (p24; q32), and the multiple phenotypes of this individual could be due to the disruption in the *ZNF462* gene and *ASXL2* gene as a consequence of chromosomal rearrangement (Ramocki et al., 2003; Talisetti et al., 2003; Kruszka et al., 2019); Weiss *et al.* reported that the dysfunctional variants of *ZNF462* gene were found in six patients from four families with significant deletions in two different regions of chromosome nine were detected in two patients from two unrelated families (Weiss et al., 2017). Cosemans *et al.* reported a case of WSKA that was associated with chromosomal balanced translocation t (9; 13) (q31.2; q22.1) (Cosemans et al., 2018). Kruszka P *et al.* updated 14 cases of WSKA patients caused by the LOF variants in the *ZNF462* gene and characterized the clinical phenotypes for the studied cases (Kruszka et al., 2019). González–Tarancón R *et al.* demonstrated that a new frameshift variant in the *ZNF462* gene could be associated with WSKA syndrome (González–Tarancón et al., 2020). Recently, Iivonen AP *et al.* found a case with WSKA and Kallmann syndrome due to the deletion of chromosome 9q31.2, and Park *et al.* reported a case involving WSKA and empty sella syndrome (ESS) associated with the deficiency in the growth hormone (GHD) (Iivonen et al., 2021; Park et al., 2021). The clinical characteristics of the WSKA cases from the cited studies are summarized in **Table 1**.

5 DISCUSSION

The *ZNF462* gene, consisting of 13 exons, is located on chromosome 9q31.2. It encodes a protein (2,506 amino acids) with 27 C2H2 zinc finger structures, which participates in transcriptional regulation and the remodeling of the chromosome by bonding with DNA molecules (Nagase et al., 2001; Massé et al., 2010; Eberl et al., 2013). The zinc finger protein is highly conserved in most mammals. It is localized in the nucleus and widely expressed in various human tissues (Fagerberg et al., 2014). While the specific function of the protein has not been established, some studies on animal models demonstrated that *ZNF462* could play a vital role in

TABLE 1 | Clinical phenotypes of 29 patients and the family patients of this study caused by *ZNF462* gene mutation.

Patients	Sex	Age	Variant type	Inheritance	DD	Ptosis	Hypotonia	Ear malformation/ Hearing loss	CHD	Down-slanting palpebral fissures	Arched eyebrows	Short upturned nose	Cupid's bow	Epicanthal folds	Cranio-synostosis/ Metopic ridging	Brain abnormalities	Feeding issues
1	M	16 months	c.2590C > T p.(Arg864*)	Maternal (Mosaic)	+	+	+	+		−	+	−	+	+	−	−	+
2	M	10 years	c.2542del p.(Cys848Valfs*66)	*De novo*	+	+	−	−		+	+	+	+	+	−	−	+
3	M	6 years	c.831_834del p.(Arg277Serfs*26)	*De novo*	+	−	+	+	+	−	−	+	−	−	−	−	+
4	M	2 years 7 months	c.6214_6215del p.(His2072Tyrfs*8)	*De novo*	+	+	−	+		−	−	−	+	+	+		+
5	F	14 years	c.763C > T p.(Arg255*)	Paternal	+	+	−	+		−	+	−	−	+	+		−
6	F	7 months	c.7057–2A > G	*De novo*	+	+	+	+	+	+	+	+	+	+	−	+	+
7	M	13 years	c.6794dup p.(Tyr2265*)	*De novo*	+	−	−	+		−	+	−	+	−	+		−
8	M	2 years	c.882dup p.(Ser295GLnfs*64)	*De novo*	+	+	−	−		+	−	−	−	−	−	+	−
9	M	15 years	c.4165C > T p.(Gln1389*)	*De novo*	+	+	+	+		+	+	−	+	−	−		+
10	M	8 years	c.1234_1235insAA p.(Ser412*)	Unknown	+	+	-	+		−	−	−	−		−	−	+
11	F	2 years 5 months	c.6214_6215del p.(His2072Tyrfs*8)	*De novo*	−	+	+			−	−	−	−		−		+
12	M	9 months	c.2049dup p.(Pro684Serfs*14)	*De novo*	+	+	+	−		+	+	+	+	+	−	−	−
13	M	8 years 7 months	c.6631del p.(Arg2211GLyfs*59)	*De novo*	−	+	−	−		+	−	−	+	−	−		−
14	F	8 years	c.2695G > T p.(Glu899*)	Mother negative Father unknown	+	−	+	−		−	+	+	−	−	−	−	+
15	F	2 years	c.3787C > T p.(Arg1263*)	Paternal	−	+	−	−		+	+	+	+	−	+	+	
16	F	4 years	c.3787C > T p.(Arg1263*)	Paternal	−	+	−	−		+	−	−	+	+	+	−	
17	M	34 years	c.3787C > T p.(Arg1263*)	Maternal	−	+	−	−		−	−	−	−	−	+		
18	M	2 years	c.2979_2980delinsA p.(Val994Trpfs*147)	*De novo*	+	+	−	+		+	+	+	−	+	+	−	+
19	M	32 months	c.4263del p.(Glu1422Serfs*6)	*De novo*	+	+	+	+	+	+	−	+	−	+	+	−	-
20	F	5 years	Chr9:g.(108940763-110561397)del (hg19)	*De novo*	−	−	+			+	+	+	+	+	−	+	
21	F	15 years	Chr9:g (108464368-110362345)del (hg19)	*De novo*	+	+	−		+	−	−	−	+	−	−		
22	M	9 years	c.5145delC p.(Tyr1716Thrfs*28)	*De novo*	+	+	+	−		-	−	−	−	−	−	−	
23	F	5 years	t (2; 9) (p24; q32) disrupting ZNF462 and ASXL2	*De novo*	+	+	+	+	+	+	+	+	+	−	−	+	+
24	M	24 years	t (9; 13) (q31.2; q22.1) disrupting ZNF462 and KLF12	*De novo*	+	+	+	+		+	−	−	−	+	+	+	+
25	F	3 years 4 months	c.3306dup p.(Gln1103Thrfs*10)	*De novo*	+	+	+			+	−	−	−	+	−		+

(Continued on following page)

TABLE 1 | (*Continued*) Clinical phenotypes of 29 patients and the family patients of this study caused by *ZNF462* gene mutation.

Patients	Sex	Age	Variant type	Inheritance	DD	Ptosis	Hypotonia	Ear malformation/ Hearing loss	CHD	Down-slanting palpebral fissures	Arched eyebrows	Short upturned nose	Cupid's bow	Epicanthal folds	Cranio-synostosis/ Metopic ridging	Brain abnormalities	Feeding issues
26	M	16 years	c.4185del	Mother negative	+	+	+	-	-	+	+	+	+	+	+	+	-
		9 months	p.(Met1396Ter)	Father unknown													
27	M	17 years 7 months	Chr9:g.(108331353–110707332)del (hg19)	*De novo*	+	+	-	+	+			+				+	
28	M	8 months	c.6431C > A p.Ser2144*	Paternal	+	+	+	+	+	-	-	-	-	-	-	-	-
29	M	31 years	c.6431C > A p.Ser2144*	*De novo*	–	+	–	+		–	–	–	–	–	–		–
Cohort prevalence					76%	86%	52%	51%	24%	52%	45%	41%	48%	45%	34%	28%	45%

Blank means no mention about the clinical features and/or no test results have been reported. Inheritance types were maternal 7% (2/29), paternal 14% (4/29), unknown 10% (3/29), de novo 69% (20/29).
Clinical characteristics were below: 76%(22/29) with DD, 86% (25/29) with ptosis, 52% (15/29) with hypotonia, 51%(15/29, six were hearing loss) with ear malformation/Hearing loss, 24%(7/29, 21 were not tested or not reported) with CHD, 52% (15/29) with down-slanting palpebral fissures, 45% (13/29) with arched eyebrows, 41% (12/29) with short upturned nose, 48% (14/29) with Cupid's bow, 45% (13/29) with epicanthal Folds, 34% (10/29) with metopic ridging, 52% (15/29) with hypotonia, 28% (8/29, 10 were not tested or not reported) with brain abnormalities and 45% (13/29) with feeding issues including our patient.
DD, developmental delay; CHD, congenital heart disease; MRI, magnetic resonance imaging; M, male; F, female.
Patient 1–26: Kruszka et al. (2019), Park et al. (2021), Patient 27: Iivonen et al. (2021), Patient 28: The proband of this study, Patient 29: The father of the patient 28.
In order to evaluate phenotype prevalence, we divided each positive phenotype report by the entire cohort (n = 29).

embryonic development. For instance, the downregulation of *Zfp462* (*ZNF462*) gene expression in *Xenopus laevis* could interfere with early embryonic development by altering the cell division at the cleavage stage; however, this phenotype could be compensated through the introduction of additional human *ZNF462* mRNA (Laurent et al., 2009). In another study, the *Zfp462* knockout mice showed prenatal lethality and the heterozygous ($Zfp462^{+/-}$) mice developed diverse symptoms including low body weight, delayed brain weight development, anxiety-like behavior, and hair loss (Wang et al., 2017).

Given the evidence obtained from previous articles, the haploinsufficiency of the *ZNF462* gene is the genetic cause of WSKA. In clinical studies, WSKA is characterized by the mild and overall developmental delay with variable craniofacial abnormalities (typically ptosis, abnormal skull shape, lower oblique eyelid fissure, epicanthus, arched eyebrows, and short nose, etc.), while hypotonia and feeding difficulty are usually observed. Furthermore, a few cases reported dysplasia of the corpus callosum on brain imaging (Kruszka et al., 2019). By summarizing the existing cases (27 patients in the published reports and two patients from this study, in **Table 1**), it was found that ptosis, developmental delay, and autism are common manifestations in WSKA patients. Also, four out of the 27 patients had hearing impairments. Most patients were studied individually. Out of the reported cases, two cases resulted from the paternal inheritance, with a case resulting from the maternal inheritance, while another case was found to be due to maternal low-proportion mosaic (the mosaic ratio was 17%). This study discovered a new case with paternal inheritance in the Chinese population: the child had a paternal inheritance, but his father was *de novo*. They carried a novel nonsense variant c.6431C > A (p.S2144*) in the *ZNF462* gene (NM_021224.6) found by using whole-exome sequencing, whereas the variant was not present in other tested family members. Both of them showed typical unilateral ptosis and unilateral hearing impairment. These findings indicated that the variant c.6431C > A (p.S2144*) in the *ZNF462* gene could be associated with WSKA. The child showed a mild asymmetrical crying face during the neonatal period, and further had mild hypotonia and developmental delay. Pathogenic CNV was undetectable. Therefore, it is speculated that the observed clinical feature of WSKA could be individually specific.

By January 2021, the HGMD® database has recorded 24 *ZNF462* gene variants, including five nonsense variants, 12 frameshift variants, three missense variants, one splicing variant, two large fragment deletion variants, and one chromosome balanced translocation. These reported variants are mostly found in exon 3 of the *ZNF462* gene (**Figures 1C,a**), which may be related to exon 3 is the largest exon of the gene. The variant c.6431C > A (p.S2144*) found in this study was located in exon 8 of the *ZNF462* gene, and there were several pathogenic nonsense variants reported in the downstream of c.6431C > A (p.S2144*). This point further confirms the pathogenicity of the variant. In addition, the variant may undergo nonsense-mediated decay (NMD), which may lead to heterozygous loss of *ZNF462* transcript and consequently result in the disease phenotype. Moreover, the variant c.6431C > A (p.S2144*) was located in the region between the 21st and 22nd C2H2 zinc finger structures, and it causes amino acid deletion from amino acids 2,144 (**Figure 1C,b**), leading to the absence of the last six zinc finger

structures. Hence, this variant was assumed to be responsible for DNA binding impairment and the subsequent protein dysfunction, which needs to be investigated in subsequent studies.

This is the first pedigree of WSKA in China. A novel nonsense variant c.6431C > A (p.S2144*) in the *ZNF462* gene was identified in the proband and his father; this finding enriched the variant spectrum of the *ZNF462* gene. The proband and his father showed unilateral ptosis and unilateral hearing impairment which were typical symptoms of WSKA (**Table 1**), so they were diagnosed combined with the sequencing result. The mild asymmetrical crying face during the neonatal period only showed in the proband could be individually specific, and the role of the pathogenic variant in this case required further investigation. The inheritance type of the proband was paternal, and *de novo* mutations were still the main way of inheritance in all the reported WSKA cases (**Table 1**). This study provided more clinical and genetic evidence to support the haploinsufficiency of the *ZNF462* gene proposed by earlier studies. The novel variant and phenotypes seen in this family contributed to understanding the clinical features, genetic characteristics, and diagnostic protocols for WSKA.

While WES has facilitated the identification of pathogenic gene variants for many rare diseases (Yang et al., 2014), the increasing knowledge will improve the diagnosis accuracy of rare diseases and contribute to the prediction or the prevention of birth defects. Combined with trio-WES analysis, the patients in this study were finally diagnosed. Besides the traditional diagnostic approach, the introduction of trio-WES can lead to the effective identification and differentiation of the variants, and thus offer feasible support for clinical diagnosis and treatment.

DATA AVAILABILITY STATEMENT

The datasets presented in this study can be found in online repositories. The names of the repository/repositories and accession number(s) can be found below: CNGB Sequence Archive (CNSA) of China National GeneBank DataBase (CNGBdb); accession number CNP0002511.

ETHICS STATEMENT

The studies involving human participants were reviewed and approved by the Ethics Committee of Xi'an People's Hospital (Xi'an Fourth Hospital). Written informed consent to participate in this study was provided by the participants' legal guardian/next of kin.

AUTHOR CONTRIBUTIONS

SZ, XW, HL, and XZ collected the study subjects and the clinical data and phenotyped the patients. CM and YL analyzed the next-generation sequencing data. SZ and YL performed Sanger sequencing data analyses. SZ and CM wrote the manuscript, and all authors critically revised the manuscript. XZ coordinated and managed the study.

FUNDING

This work was supported by the Youth training Project of Xi'an Health Commission (No. 2021qn04) and the Scientific and Technological Program of Xi'an city (No.2017117SF/YX011 (9)).

ACKNOWLEDGMENTS

Our sincere gratitude goes to Berry Genomics for their assistance with data collection and analysis. We also thank the patient and his family for their participation in this study.

REFERENCES

Cosemans, N., Vandenhove, L., Maljaars, J., Van Esch, H., Devriendt, K., Baldwin, A., et al. (2018). *ZNF462* and *KLF12* Are Disrupted by a De Novo Translocation in a Patient with Syndromic Intellectual Disability and Autism Spectrum Disorder. *Eur. J. Med. Genet.* 61 (7), 376–383. doi:10.1016/j.ejmg.2018.02.002

Eberl, H. C., Spruijt, C. G., Kelstrup, C. D., Vermeulen, M., and Mann, M. (2013). A Map of General and Specialized Chromatin Readers in Mouse Tissues Generated by Label-free Interaction Proteomics. *Mol. Cel* 49 (2), 368–378. doi:10.1016/j.molcel.2012.10.026

Fagerberg, L., Hallström, B. M., Oksvold, P., Kampf, C., Djureinovic, D., Odeberg, J., et al. (2014). Analysis of the Human Tissue-specific Expression by Genome-wide Integration of Transcriptomics and Antibody-Based Proteomics. *Mol. Cell Proteomics* 13 (2), 397–406. doi:10.1074/mcp.M113.035600

González-Tarancón, R., Salvador-Rupérez, E., Miramar Gallart, M., Barroso, E., Díez García-Prieto, I., Pérez Delgado, R., et al. (2020). A Novel Mutation in the *ZNF462* Gene c.3306dup; p.(Gln1103Thrfs*10) Is Associated to Weiss-Kruszka Syndrome. A Case Report. *Acta Clinica Belgica* 1, 1–4. doi:10.1080/17843286.2020.1780391

Iivonen, A.-P., Kärkinen, J., Yellapragada, V., Sidoroff, V., Almusa, H., Vaaralahti, K., et al. (2021). Kallmann Syndrome in a Patient with Weiss-Kruszka Syndrome and a De Novo Deletion in 9q31.2. *Eur. J. Endocrinol.* 185 (1), 57–66. doi:10.1530/eje-20-1387

Kruszka, P., Hu, T., Hong, S., Signer, R., Cogné, B., Isidor, B., et al. (2019). Phenotype Delineation of *ZNF462* Related Syndrome. *Am. J. Med. Genet.* 179 (10), 2075–2082. doi:10.1002/ajmg.a.61306

Laurent, A., Masse, J., Omilli, F., Deschamps, S., Richard-Parpaillon, L., Chartrain, I., et al. (2009). ZFPIP/Zfp462 Is Maternally Required for Proper Early *Xenopus laevis* Development. *Developmental Biol.* 327 (1), 169–176. doi:10.1016/j.ydbio.2008.12.005

Massé, J., Laurent, A., Nicol, B., Guerrier, D., Pellerin, I., and Deschamps, S. (2010). Involvement of *ZFPIP/Zfp462* in Chromatin Integrity and Survival of P19 Pluripotent Cells. *Exp. Cel Res.* 316 (7), 1190–1201. doi:10.1016/j.yexcr.2010.02.024

Nagase, T., Nakayama, M., Nakajima, D., Kikuno, R., and Ohara, O. (2001). Prediction of the Coding Sequences of Unidentified Human Genes. XX. The Complete Sequences of 100 New cDNA Clones from Brain Which Code for Large Proteins *In Vitro*. *DNA Res.* 8 (2), 85–95. doi:10.1093/dnares/8.2.85

Park, J., Ha, D. J., Seo, G. H., Maeng, S., Kang, S. M., Kim, S., et al. (2021). Empty Sella Syndrome Associated with Growth Hormone Deficiency: the First Case Report of Weiss-Kruszka Syndrome. *J. Korean Med. Sci.* 36 (18), e133. doi:10.3346/jkms.2021.36.e133

Ramocki, M. B., Dowling, J., Grinberg, I., Kimonis, V. E., Cardoso, C., Gross, A., et al. (2003). Reciprocal Fusion Transcripts of Two Novel Zn-finger Genes in a Female with Absence of the Corpus Callosum, Ocular Colobomas and a Balanced Translocation between Chromosomes 2p24 and 9q32. *Eur. J. Hum. Genet.* 11 (7), 527–534. doi:10.1038/sj.ejhg.5200995

Richards, S., Aziz, N., Bale, S., Bick, D., Das, S., Gastier-Foster, J., et al. (2015). Standards and Guidelines for the Interpretation of Sequence Variants: a Joint Consensus Recommendation of the American College of Medical Genetics and Genomics and the Association for Molecular Pathology. *Genet. Med.* 17 (5), 405–424. doi:10.1038/gim.2015.30

Talisetti, A., Forrester, S. R., Gregory, D., Johnson, L., Schneider, M. C., and Kimonis, V. E. (2003). Temtamy-like Syndrome Associated with Translocation of 2p24 and 9q32. *Clin. Dysmorphol.* 12 (3), 175–177. doi:10.1097/01.mcd.0000072161.33788.56

Wang, B., Zheng, Y., Shi, H., Du, X., Zhang, Y., Wei, B., et al. (2017). *Zfp462* Deficiency Causes Anxiety-like Behaviors with Excessive Self-Grooming in Mice. *Genes Brain Behav.* 16 (2), 296–307. doi:10.1111/gbb.12339

Weiss, K., Wigby, K., Fannemel, M., Henderson, L. B., Beck, N., Ghali, N., et al. (2017). Haploinsufficiency of *ZNF462* Is Associated with Craniofacial Anomalies, Corpus Callosum Dysgenesis, Ptosis, and Developmental Delay. *Eur. J. Hum. Genet.* 25 (8), 946–951. doi:10.1038/ejhg.2017.86

Yang, Y., Muzny, D. M., Xia, F., Niu, Z., Person, R., Ding, Y., et al. (2014). Molecular Findings Among Patients Referred for Clinical Whole-Exome Sequencing. *JAMA* 312 (18), 1870–1879. doi:10.1001/jama.2014.14601

Conflict of Interest: The authors declare that the research was conducted in the absence of any commercial or financial relationships that could be construed as a potential conflict of interest.

Publisher's Note: All claims expressed in this article are solely those of the authors and do not necessarily represent those of their affiliated organizations, or those of the publisher, the editors, and the reviewers. Any product that may be evaluated in this article, or claim that may be made by its manufacturer, is not guaranteed or endorsed by the publisher.

frontiers in Pediatrics

CASE REPORT
published: 18 February 2022
doi: 10.3389/fped.2022.799284

Case Report: Genetic Analysis of a Small Supernumerary Marker Chromosome in a Unique Case of Mosaic Turner Syndrome

Chao Li[1†], *Weiyao Luo*[2†], *Tingting Xiao*[1], *Xingkun Yang*[1], *Miaoling Ou*[1], *Linghua Zhang*[1], *Xiang Huang*[1*] *and Xiaodan Zhu*[1*]

[1] Department of Prenatal Diagnosis, Foshan Women and Children Hospital Affiliated to Southern Medical University, Foshan, China, [2] Department of Pediatric, Foshan Women and Children Hospital Affiliated to Southern Medical University, Foshan, China

OPEN ACCESS

Edited by:
Santasree Banerjee,
Beijing Genomics Institute (BGI), China

Reviewed by:
Jayesh J. Sheth,
Institute of Human Genetics, Foundation for Research in Genetics and Endocrinology, India
Shaobin Lin,
The First Affiliated Hospital of Sun Yat-sen University, China

***Correspondence:**
Xiaodan Zhu
343152753@qq.com
Xiang Huang
340382761@qq.com

[†]These authors have contributed equally to this work

Specialty section:
This article was submitted to Genetics of Common and Rare Diseases, a section of the journal Frontiers in Pediatrics

Received: 21 October 2021
Accepted: 10 January 2022
Published: 18 February 2022

Citation:
Li C, Luo W, Xiao T, Yang X, Ou M, Zhang L, Huang X and Zhu X (2022) Case Report: Genetic Analysis of a Small Supernumerary Marker Chromosome in a Unique Case of Mosaic Turner Syndrome. Front. Pediatr. 10:799284. doi: 10.3389/fped.2022.799284

Background: The aim of this study was to explore the source and morphology of a small supernumerary marker chromosome (sSMC) from karyotype analysis of a patient with a unique case of mosaic Turner syndrome. The study findings will provide technical reference and genetic counseling for similar cases.

Case Presentation: A female patient with 46,X,+mar karyotype was diagnosed by genetic karyotype analysis. Genetic methods including fluorescence *in situ* hybridization (FISH) and copy number variation sequencing (CNV-seq) based on low-depth whole-genome sequencing were used to explore the source and morphology of sSMC. FISH technology showed that 56.5% of the cells were X and 43.5% of the cells were XY. CNV-seq detection found that the sSMC was chrY, implying that the patient's karyotype was mos 45,X[58.6%]/46,XY[41.4%]. Retrospective karyotype analysis indicated that the female patient's sSMC was inherited from her father's small chrY. Customized FISH probe of Yq12 microdeletion was positive, indicating that the sSMC was a del(Y)(q12). Based on the results of genetic diagnosis, the specialist doctor gave a comprehensive genetic consultation and ordered regular follow-up examinations.

Conclusions: The findings of the current study showed that the chromosome description of the unique Turner case was mos 45,X[56.5%]/46,X,del(Y)(q12)[43.5%]. FISH technology played a key role in diagnosis of mosaicism. The terminal deletion of mosaic chrY provided a scientific and an accurate explanation for masculinity failure and abnormal sexual development of the current case.

Keywords: Turner syndrome, sSMC, FISH, CNV-seq, del(Y)(q12)

INTRODUCTION

Turner syndrome is a common sex-linked disease. It has the highest incidence of chromosomal abnormalities. The main clinical features of Turner syndrome include short stature, poorly developed secondary sexual characteristics, and infertility. Notably, intelligence of the patient is usually within the normal range. The most common karyotype of this type of patients is 45,X, which represents more than 50% of all cases. The mosaicism karyotype accounts for ∼30% of

all cases, whereas the mos 45,X/46,XX form accounts for most of the cases. The detection rate of 45,X/46,XY mosaicism, which is a rare chromosomal abnormality and usually not diagnosed in time, is 1.5/10,000 newborns (1). sSMCs refer to a type of extra chromosome fragment outside the normal karyotype. The source of sSMCs cannot be determined by conventional karyotype analysis. In most cases, sSMC's length is less than chr20, and may be derived from any chromosome. sSMCs are present in ∼3.3 million human beings currently (2). The other population (∼1.2 million) of sSMC carriers are clinically affected either by adverse effects of gained genetic material present on the sSMC or by uniparental disomy of the sSMC's sister chromosomes (2). Patients with sSMCs have variable clinical phenotypes owing to differences in the genetic material present in the marker chromosomes (3). These sSMCs cause uncertainty in clinical symptoms and make genetic diagnosis and counseling challenging. Therefore, it is important to accurately locate the source and morphology of sSMC. Currently, genetic diagnosis techniques are diverse. High-throughput sequencing methods have become more popular, such as CNV-seq and whole exome sequencing (WES). These methods are more comprehensive and accurate compared with traditional karyotyping and FISH probes. However, traditional technologies play irreplaceable roles. In the current study, an sSMC carried by a special mosaicism Turner syndrome was determined through a variety of mainstream molecular cytogenetic methods. Moreover, the source and morphology of the sSMC was successfully identified. The findings obtained through genetic analysis and interpretation of the current case provide scientific and technical reference for similar cases. Furthermore, the findings supplement effective genetic evidence and provide useful insights for abnormal sexual development.

MATERIALS AND METHODS

Study Subject

An 8-year-old patient showed stunted growth for more than 3 years. The patients visited the hospital for clinical consultation. The patient had no history of chronic diseases and had normal mental capacity. The height of the father of the patient was 170 cm and the height of the mother was 159 cm. The patient was born by cesarean section by a G2P2 mother. The patient did not have a history of asphyxia. The birth weight was 3.0 kg and the height was 52 cm. It showed that the patient was in good spirits and had normal reactions by physical examination. The patient has a childish face and a sharp voice, showed tanner stage I of vulva and genitalia, B1 breast score, and was in PH1 stage. Pelvic examination through B-ultrasound showed a uniform uterine muscular echo; only the right breast was developed, and no obvious ovarian echo was detected in the appendages on both sides. Pituitary MRI plain scan and enhanced scan did not show any abnormalities. GnRHa provocation test (including levodopa and arginine compound) was performed after the outpatient clinic. The initial diagnosis of endocrinology specialist was growth hormone deficiency and Turner syndrome. The female patient was then referred to the center of prenatal diagnosis for disease diagnosis and genetic counseling.

Methods

Karyotype Analysis of Peripheral Blood

Karyotyping is able to detect polyploidy, aneuploidy, translocations, inversions, rings, and copy number changes in the size range of 4–6 Mb. Lymphocyte culture medium was purchased from Da Hui Biology Company, Beijing. The patient signed an informed consent form, and peripheral blood was aseptically drawn and inoculated into the culture medium. Cell culture, harvest, G banding, and slide production were carried out in turn. G-banding slides were scanned and analyzed using the GSL120 platform, Leica Biosystems. The 5 karyotypes were analyzed under the microscope and 20 cells were counted. The count was expanded to 50 metaphase cells if mosaicism existed. Reporting of karyotype results was described based on the nomenclature system of human cytogenetics (ISCN-2016) (4).

Fluorescence *in situ* Hybridization

There are FISH probes for chromosomes 13, 18, 21, X, and Y, which may be used for rapid detection of aneuploidy prior to formal karyotyping. In addition, there are multiple FISH probes for areas associated with microdeletion. FISH probe was purchased from Jin Pu Jia Medical Technology Company, Beijing (5). Peripheral blood was drawn after the patient signed the informed consent. The experiment was performed following the manufacturer's instructions. After preparation of cell suspension, slide pretreatment, denaturation, and hybridization, slides were washed and sealed in turn. Samples were then analyzed by microscopy. Each set of probes randomly counted 50 cells. The count was expanded to 100 or 200 cells if more than one cell with abnormal signal was detected. If the proportion of abnormal cells in a certain indicator was ≥10%, it indicated that the indicator was abnormal. If the proportion of abnormal cells was between 10 and 60%, it indicated the presence of mosaicism (6).

Low-Depth Whole-Genome Sequencing

CNV analysis has become a first-tier clinical cytogenetics procedure in patients with unexplained developmental delay/intellectual disability. Peripheral blood was drawn after the patient signed the informed consent. DNA was extracted with an automatic nucleic acid extraction system. Library was prepared using the Ke Nuo An kit purchased from Bei Rui company, Beijing. Original read files were obtained by sequencing on the HiSeq3000 platform. Sequencing files were compared with the human reference genome GRCH37/hg19 using the bowtie2 package in Linux (7). Samtools package in Linux was used to sort and make index to obtain the bam intermediate file (8). The wisecondorx package in Linux was then used to calculate and visualize CNVs of each chromosome band of the samples (9). Genetic interpretation of the results on CNVs was performed following the 2020 version of ACMG and ClinGen's latest interpretation guidelines (10).

Screening for AZF Microdeletion of ChrY

PCR multiplex assays are the method of choice for quickly revealing genomic microdeletions in the large repetitive genomic sequence blocks on the long arm of the human chrY. They harbor the Azoospermia Factor (AZF) genes, which cause male

infertility when functionally disrupted. The ChrY microdeletion kit was purchased from Tou Jing Biotechnology Company, Beijing. The kit was used to qualitatively detect whether the AZF that affected sperm production on the chrY had a microdeletion. This fragment was located in the Yq band. Multiplex PCR-capillary electrophoresis technology was used for detection. A total of 15 sequence-tagged sites (STS) were selected following international guidelines. Primers were designed, and 4 tubes were used for multiplex PCR detection. In addition, the sex-determining region of chrY (SRY) (Yp11.3) was detected. All experiments and result interpretation were performed following the instructions in the kit.

RESULTS

Chromosome Karyotype Analysis

Karyotypes of the proband and her father were 46, X, +mar and 46, X, Yq-, respectively (**Figures 1A,B**). Analysis of family members showed that the morphology of +mar was probably inherited from the father's chrY. The chrY of the father occurred as a very small fragment, which may be due to normal shortening of the heterochromatin region of Yq12 or loss of pathogenicity of the other band of chrY. The social sex of the proband was female, and further analysis was needed to clarify the source and morphology of the +mar.

Fluorescence *in situ* Hybridization

Chromosome centromeric probes of FISH CSPX/CSPY (green/red) using uncultured peripheral blood sample showed that 56.5% of the cells had a single green signal (indicating X). Furthermore, 43.5% of the cells showed one green and one red signal (indicating XY) when 200 cells were counted (**Figure 2A**). Analysis of the cultured peripheral blood samples showed that 18.0% of the 200 cells had a green signal (indicating X) (**Figure 2B**). Notably, 82.0% of the 200 cells showed a green signal and a red signal (indicating XY) (**Figure 2C**). The FISH probe of Yq12 microdeletion showed that chrX only had a red signal, which was used as a normal positive control. In addition, all metaphase cells did not show a green signal, indicating that Yq12 was completely deleted (**Figure 2D**).

Detection of Microdeletion and Microduplication

Whole-genome high-throughput sequencing results showed that the sSMC was chrY (**Figure 3**), and the interval ratio of Yp11.3-Yq11.223 was ∼-0.5. Calculation and conversion indicated that the patient's karyotype was a mosaic deletion of 45,X[58.6%]/46,XY[41.4%]. Screening of the AZF of chrY did not show abnormality of microdeletion in the AZF region (Yq) and SRY gene region (Yp11.3).

Outcome and Follow-Up

Because Turner syndrome can involve multiple organ systems, the risk of occurrence of some complications increases with age. The patients face different neuropsychological problems at different age groups. According to the genetic detection results, the laboratory actively communicated with a clinical specialist. The specialist notified the family members to return to the outpatient clinic to further improve the relevant system examinations, and used estrogen and progesterone drugs to treat symptomatically in a timely manner in order to improve the patient's final height and maintain secondary sexual characteristics, so that the uterus can develop normally; various complications also can be prevented. Ask the patient for regular specialist follow-ups to monitor diseases of related systems or organs such as gonadotropin, cardiovascular, urinary system, liver and kidney function, eyes and ears, and autoimmunity. It was recommended that the patient maintained a healthy and active lifestyle and took medications actively. The specialist also informed her medical progress about the disease, including the possibility of prenatal diagnosis or assisted reproduction in later stages.

DISCUSSION AND CONCLUSION

The World Health Organization reports that the incidence of birth defects is ∼6.42% in low-income countries, 5.57% in middle-income countries, and 4.72% in high-income countries. Rapid development of molecular genetic technologies such as next-generation sequencing enables detection of more genomic abnormalities. Prevention and control of birth defects and genetic counseling have been widely advocated in the society.

In the current study, the morphology and source of sSMC carried by a rare mosaicism Turner syndrome were identified through a comprehensive application of various mainstream molecular cytogenetics techniques. Karyotyping technique was used to explore the sSMC of unknown origin. Family traceability was conducted to determine whether the sSMC's morphology was similar to the small chrY of the proband's father. FISH technology and advanced high-throughput sequencing technology were then used to confirm that the sSMC of the female proband was actually the chrY. High-throughput sequencing results showed that chrY was reduced. However, due to the limitations of the methods, it was not possible to determine the specific chromosome description. Therefore, it was not clear whether the reduction was due to mosaicism being X/XY or it was due to the Y band loss (11).

Moreover, the abnormality of the centromere and heterochromatin region of each chromosome was not detected owing to the presence of the detection blind band. Therefore, high-throughput sequencing could not detect the abnormality of the Yq12 region. Conventional normal FISH probe, which is a standard method for judging the specific proportion of mosaicism cells, confirmed the karyotype to be mosaicism X/XY. The findings of normal FISH demonstrated that chrY reduction was caused by mosaicism detected through high-throughput sequencing. Although sSMC was identified as the source of the chrY, its length was too short, and further analysis was performed to determine which bands were lost. Therefore, customized Yq12 probe of FISH was used to explore whether there was a deletion at the end of chrY. The findings showed that the mosaicism X/XY was a del(Y)(q12). We searched related literatures and found some research reports: 42.86% (6/14) of the mosaic

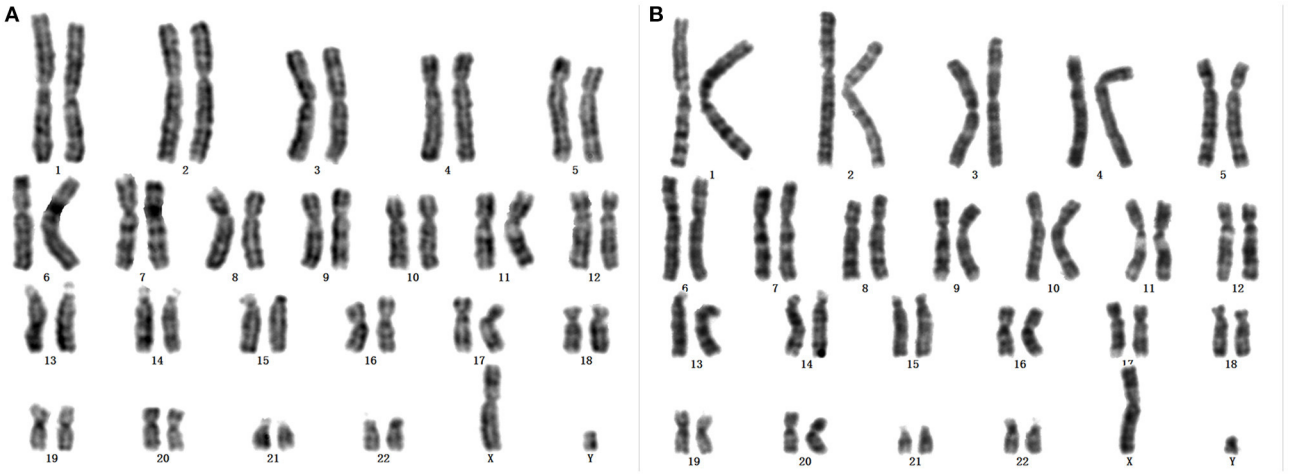

FIGURE 1 | (A) Karyotype of the proband: 46, X, +mar. **(B)** Karyotype of father to the proband: 46, X, Yq-.

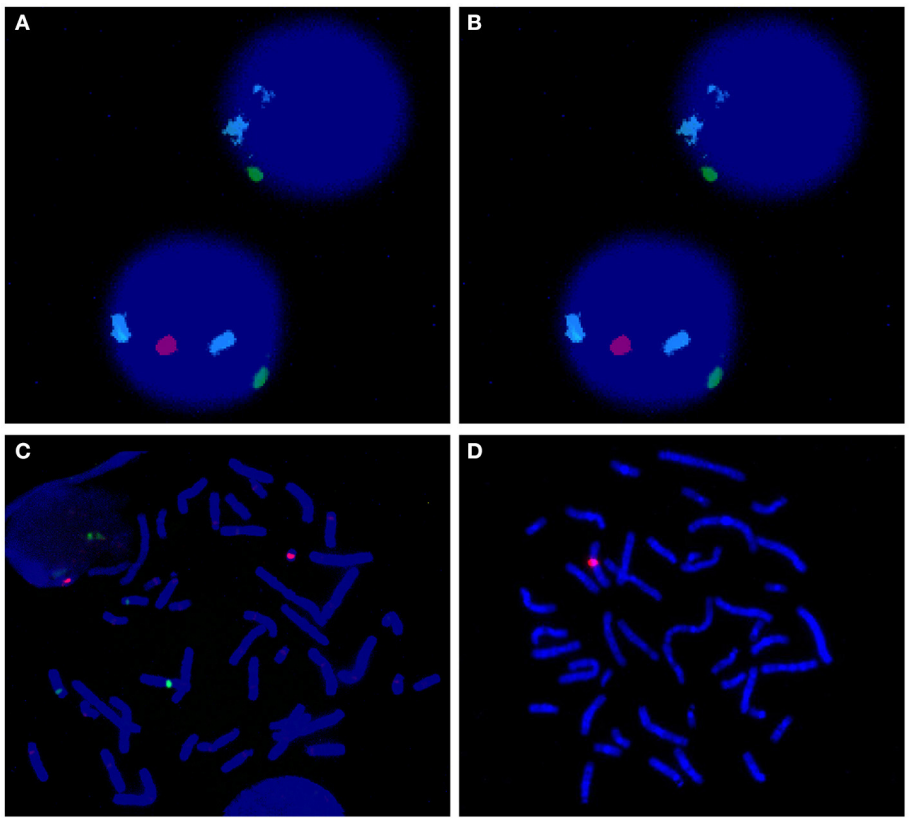

FIGURE 2 | (A) FISH of uncultured interphase cell; azure: chr18; green: chrX; red: chrY. The upper cell image shows no chrY whereas the lower cell image shows presence of chrY. **(B)** FISH of cultured metaphase cell; azure: chr18; green: chrX; red: chrY. These findings showed that no chrY was ppresent (implying that only X was present). **(C)** FISH of cultured metaphase cell; azure: chr18; green: chrX; red: chrY. These findings showed presence of chrY (implying presence of XY). **(D)** Yq12 FISH of cultured metaphase cell; red: chrX; green:chrY. The findings showed Yq12 deletion.

patients were mosaic for a structurally abnormal chrY in 46,XY cell lines; three with Yqh-, one with a Yq deletion, one with a Yp+, and the last with a dicentric Y. Four of these patients also presented with AZF microdeletions (12). The clinical phenotype of 45,X/46,XY individuals is very broad and includes Turner females, varying degrees of genital malformations, and men with

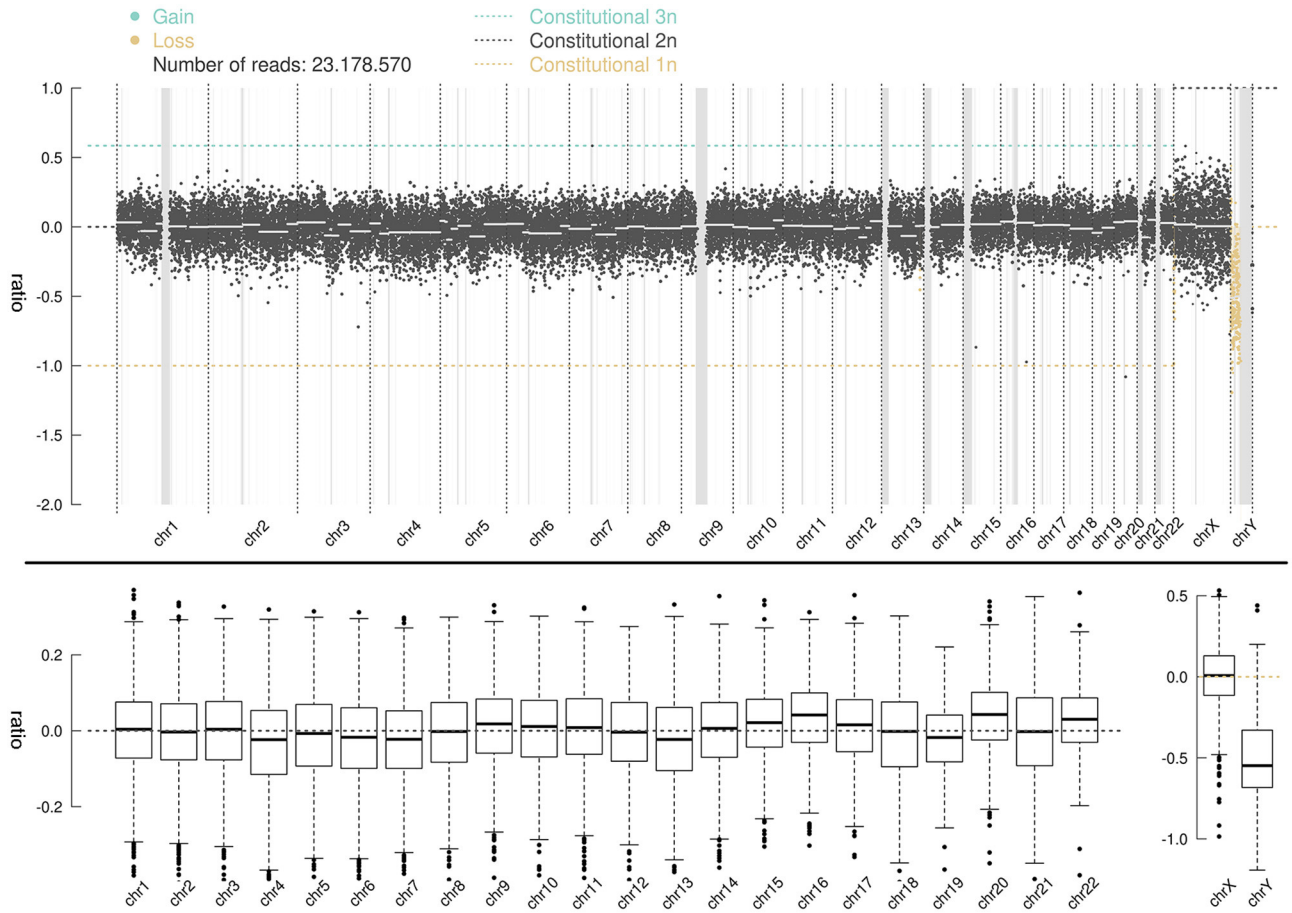

FIGURE 3 | CNV-seq distribution map for 46 chromosomes; the ordinate ratio represents $\log_2 \frac{test}{2}$; the test is the copy number of the corresponding band. The abscissa represents the chromosome band. A ratio of −1 indicates that one copy is lost; a ratio of 0 represents a normal value; a ratio of 0.58 indicates that one copy is gained; a ratio between −1 and 0 represents a mosaic deletion, and the ratio of abnormal cells is ∼2 ($1\text{-}2^{ratio}$).

normal phenotypes (13). The gonads of such patients have been reported as streak gonads, ovarian-like, and/or exhibiting other histopathological abnormalities in previous case reports, small studies, and large multicenter histological studies (14, 15).

These findings show that the nature of sex determination may be determined by expression and regulation of related genes of chrY. Defective chrY results in the person presenting a female phenotype even though that person possesses a karyotype of XY. This results in defective testicular development; thus, the infant may or may not have fully formed male genitalia internally or externally. Full range of ambiguity of structure may occur, mainly if mosaicism is present. The child is usually a girl with the features of Turner syndrome or mixed gonadal dysgenesis if the Y fragment is minimal and non-functional (16, 17). This is consistent with findings of the current study; thus, it explains the current case. However, the presence of small fragment variation and point mutations about sex determination-related genes in the sSMC in the case cannot be ruled out owing to the limitations of CNV-seq. Therefore, further studies should be performed. A genetic counselor carrying out genetic counseling of similar patients could include WES analysis based on the patient's wishes and economic conditions.

In summary, a comprehensive tracing analysis of an sSMC carried by a unique mosaicism Turner syndrome was explored through a variety of mainstream molecular cytogenetic methods, and the source and morphology of the sSMC was successfully identified. The findings of the current unique case provide scientific and accurate technical reference for similar cases. Furthermore, these findings supplement effective genetic evidence and provide useful insights into abnormal sexual development.

DATA AVAILABILITY STATEMENT

The original contributions presented in the study are included in the article/supplementary material, further inquiries can be directed to the corresponding author/s.

ETHICS STATEMENT

The study was approved by the Science and Technology Bureau of Foshan City, Guangdong Province, China. All subjects had signed an informed consent statement, agreeing that the data may be used for non-profit scientific research and teaching purposes. This study complies with the hospital's ethical review regulations.

AUTHOR CONTRIBUTIONS

The research idea was derived from XZ and XH. CL designed the experiments. XY participated in collecting the data. WL and LZ analyzed the data. CL and TX wrote the paper. All authors had read and approved the final manuscript.

FUNDING

This study was funded by the Engineering Technology Center of Precision Diagnosis of the Genetic Disease of Foshan City, Project Number: 2020001003953. The role of the funding was to support the cost of the experiment and language editing of the paper.

ACKNOWLEDGMENTS

We are grateful for the help provided by Foshan Women and Children Hospital Affiliated to Southern Medical University.

REFERENCES

1. Rosa RFM, D'Ecclesiis WFB, Dibbi RP, Rosa RCM, Trevisan P, Graziadio C, et al. 45, X/46, XY mosaicism: report on 14 patients from a Brazilian hospital. A retrospective study. *Sáo Paulo Med J.* (2014) 132:332–8. doi: 10.1590/1516-3180.2014.1326729
2. Liehr T, Al-Rikabi A. Mosaicism: reason for normal phenotypes in carriers of small supernumerary marker chromosomes with known adverse outcome. A systematic review. *Front Genet.* (2019) 10:1131. doi: 10.3389/fgene.2019.01131
3. Liehr T, Karamysheva T, Merkas M, Brecevic L, Hamid AB, Ewers E, et al. Somatic mosaicism in cases with small supernumerary marker chromosomes. *Curr Genomics.* (2010) 11:432–9. doi: 10.2174/138920210793176029
4. Stevens-Kroef M, Simons A, Rack K, Hastings RJ. Cytogenetic nomenclature and reporting. *Cancer Cytogenetics.* (2017) 2017:303–9. doi: 10.1007/978-1-4939-6703-2_24
5. Wray A, Landy H, Meck J. Patient decisions regarding prenatal aneuploid fluorescence in situ hybridization results. *Int J Gynecol Obstetrics.* (2007) 96:103–7. doi: 10.1016/j.ijgo.2006.11.005
6. Gozzetti A, Le Beau MM, editors. *Fluorescence in situ Hybridization: Uses and Limitations. Seminars in hematology*. Amsterdam: Elseiver (2020). doi: 10.1016/S0037-1963(00)90013-1
7. Salmi A, El Jadid S, Jamail I, Bensellak T, Philippe R, Blanquet V, et al. CNV-LDC: An optimized CNV detection method for low depth of coverage data. *Bioinformatics.* (2017) 2017:37–42. doi: 10.5220/0006111600370042
8. Li H, Handsaker B, Wysoker A, Fennell T, Ruan J, Homer N, et al. The sequence alignment/map format and SAMtools. *Bioinformatics.* (2009) 25:2078–9. doi: 10.1093/bioinformatics/btp352
9. Raman L, Dheedene A, De Smet M, Van Dorpe J, Menten B. WisecondorX: improved copy number detection for routine shallow whole-genome sequencing. *Nucleic Acids Res.* (2019) 47:1605–14. doi: 10.1093/nar/gky1263
10. Riggs ER, Andersen EF, Cherry AM, Kantarci S, Kearney H, Patel A, et al. Technical standards for the interpretation and reporting of constitutional copy-number variants: a joint consensus recommendation of the American College of Medical Genetics and Genomics (ACMG) and the Clinical Genome Resource (ClinGen). *Genet Med.* (2020) 22:245–57. doi: 10.1038/s41436-019-0686-8
11. Hayes J, Tzika A, Thygesen H, Berri S, Wood H, Hewitt S, et al. Diagnosis of copy number variation by Illumina next generation sequencing is comparable in performance to oligonucleotide array comparative genomic hybridisation. *Genomics.* (2013) 102:174–81. doi: 10.1016/j.ygeno.2013.04.006
12. Li L, Zhang H, Yang Y, Zhang H, Wang R, Jiang Y, et al. High frequency of Y chromosome microdeletions in male infertility patients with 45, X/46, XY mosaicism. *Brazil J Med Biol Res.* (2020) 53:8980. doi: 10.1590/1414-431x20198980
13. Lindhardt Johansen M, Hagen CP, Rajpert-De Meyts E, Kjærgaard S, Petersen BL, Skakkebæk NE, et al. 45, X/46, XY mosaicism: phenotypic characteristics, growth, and reproductive function—a retrospective longitudinal study. *J Clin Endocrinol Metabolism.* (2012) 97:E1540–9. doi: 10.1210/jc.2012-1388
14. Tosson H, Rose SR, Gartner LA. Description of children with 45, X/46, XY karyotype. *Eur J Pediatrics.* (2012) 171:521–9. doi: 10.1007/s00431-011-1600-9
15. Cools M, Pleskacova J, Stoop H, Hoebeke P, Van Laecke E, Drop S, et al. Gonadal pathology and tumor risk in relation to clinical characteristics in patients with 45, X/46, XY mosaicism. *J Clin Endocrinol Metabolism.* (2011) 96:E1171–80. doi: 10.1210/jc.2011-0232
16. Shinawi M, Cain MP, VanderBrink BA, Grignon DJ, Mensing D, Cooper ML, et al. Mixed gonadal dysgenesis in a child with isodicentric Y chromosome: Does the relative proportion of the 45, X line really matter? *Am J Med Genet Part A.* (2010) 152:1832–7. doi: 10.1002/ajmg.a.33475
17. Hatano M, Fukuzawa R, Hasegawa Y. The mosaicism ratio of 45, X may explain the phenotype in a case of mixed gonadal dysgenesis. *Sex Dev.* (2018) 12:175–9. doi: 10.1159/000489451

Conflict of Interest: The authors declare that the research was conducted in the absence of any commercial or financial relationships that could be construed as a potential conflict of interest.

Publisher's Note: All claims expressed in this article are solely those of the authors and do not necessarily represent those of their affiliated organizations, or those of the publisher, the editors and the reviewers. Any product that may be evaluated in this article, or claim that may be made by its manufacturer, is not guaranteed or endorsed by the publisher.

frontiers in Pediatrics

CASE REPORT
published: 04 March 2022
doi: 10.3389/fped.2022.806752

Compound Heterozygous Variants in a Surviving Patient With Alkuraya-Kučinskas Syndrome: A New Case Report and a Review of the Literature

Ling Yue[1], Mei Jin[2], Xin Wang[3], Jing Wang[3], Ling Chen[1], Rong Jia[1], Zuozhen Yang[4], Fan Yang[4], Jingman Li[1], Cuiying Chen[1], Huacheng Zheng[1] and Huafang Yang[1]*

[1] Department of Neurological Rehabilitation, Children's Hospital of Hebei Province, Hebei, China, [2] Electrophysiology Room, Children's Hospital of Hebei Province, Hebei, China, [3] Department of Neurology, Children's Hospital of Hebei Province, Hebei, China, [4] Cipher Gene LLC, Beijing, China

Background: Alkuraya–Kučinskas syndrome is an autosomal recessive disorder characterized by brain abnormalities associated with cerebral parenchymal underdevelopment, arthrogryposis, club foot, and global developmental delay. Most reported cases were cases of premature termination of pregnancies or neonatal deaths. To date, limited studies of nine surviving patients with global developmental delay and intellectual disability have been reported. In this study, we report another surviving patient.

Methods: Whole-exome sequencing was utilized for the proband, and variants were filtered, annotated, and classified. Candidate variants were validated by Sanger sequencing of the proband and his family. The literature was reviewed; the prognosis among different regions and the variant type was analyzed.

Results: A non-synonymous variant [NM_015312.3: exon29: c.4892C>G (p.Pro1631Arg)] was identified and validated in the patient's father. A frameshift duplication [NM_015312.3: exon62: c.10872dupA (p.Arg3625Lysfs*5)] that caused early translation termination was identified in his mother. The literature was reviewed, variants were classified into three regions of KIAA1109, and their survival status was summarized.

Conclusion: We reported another survival proband with Alkuraya–Kučinskas syndrome driven by KIAA1109. Our case expands the genotypic spectrum of Alkuraya–Kučinskas syndrome and explored the relationship between the variant region and survival.

Keywords: KIAA1109, Alkuraya-Kučinskas syndrome, compound heterozygous variants, survival, autosomal recessive, club foot

OPEN ACCESS

Edited by:
Anjana Munshi,
Central University of Punjab, India

Reviewed by:
Stephanie Efthymiou,
University College London, United Kingdom
Jingsi Luo,
Maternal and Child Health Hospital of Guangxi Zhuang Autonomous Region, China

***Correspondence:**
Mei Jin
jinmkx@163.com

Specialty section:
This article was submitted to Genetics of Common and Rare Diseases, a section of the journal Frontiers in Pediatrics

Received: *01 November 2021*
Accepted: *24 January 2022*
Published: *04 March 2022*

Citation:
Yue L, Jin M, Wang X, Wang J, Chen L, Jia R, Yang Z, Yang F, Li J, Chen C, Zheng H and Yang H (2022) Compound Heterozygous Variants in a Surviving Patient With Alkuraya-Kučinskas Syndrome: A New Case Report and a Review of the Literature. Front. Pediatr. 10:806752. doi: 10.3389/fped.2022.806752

INTRODUCTION

Alkuraya-Kučinskas syndrome (ALKKUCS) is a severe neurodevelopmental disorder characterized by global developmental delay, brain abnormalities, and arthrogryposis. Most probands die from the embryo suspension or soon after birth, and patients who survive always suffer from intellectual disabilities and epilepsy (1).

KIAA1109 was first cloned and sequenced using a size-fractionated adult brain cDNA (complementary DNA) library (2). Khuong et al. (3) demonstrated that tweek (the fly orthologue of KIAA1109) plays a crucial role in the growth of synapses at neuromuscular junctions (NMJs) by controlling both an Nwk (FCHSD2)-dependent pathway and phosphatidylinositol 4,5-bisphosphate [PI(4,5)P2] and Wsp-dependent pathways.

In 2015, another study identified a homozygous non-sense mutation in the KIAA1109 gene from a female infant in a consanguineous Saudi family (4). In 2018, Gueneau et al. (1) reported more homozygous or compound heterozygous mutations in 12 patients from nine unrelated families with ALKKUCS. Among the 13 patients reported by Gueneau et al. (1), only three patients from two families were alive at 7, 11, and 13 years of age. All patients had a global developmental delay from infancy and variable levels of intellectual disability. Besides, another two survival patients with severe phenotype were reported in 2019 (5). In 2020, Kumar et al. described four other surviving patients from two related families, similar to the cases reported by Gueneau et al. all of whom also suffered from global developmental delay and mild-to-severe intellectual disability (6).

To date, limited studies of surviving patients with global developmental delay and intellectual disability have been reported. In this study, we report another surviving patient carrying new variants in KIAA1109 and explore the potential relationship between the variant region and survival status.

MATERIALS AND METHODS

Proband

Informed consent was obtained from the patient's family members. This study was approved by the Institutional Review Board of the Children's Hospital of Hebei Province. The data on his clinical features, electroencephalogram (EEG), brain magnetic resonance imaging (MRI), malformations, and other examination results were collected.

WES and Sanger Sequencing

Genomic DNA was extracted from whole-blood samples. The IDT (Integrated DNA Technologies, USA) XGen Exome Research Panel was used to capture libraries, and the library was sequenced on the Novaseq 6,000 Sequencing platform. Finally, the paired end clean reads were mapped to the human reference genome (GRCh38/hg38). Variations were annotated using ANNOVAR software (7), and SNPs (Single Nucleotide Polymorphism) with a minor allele frequency $\leq$0.005 in the SNP database were obtained for further analysis. The pathogenic evaluation was performed according to the American College of Medical Genetics and Genomics (ACMG) guidelines (8). The Sanger sequencing of candidate variants was performed in the proband and his parents to validate the variation identified by whole-exome sequencing.

RESULTS

Case Presentation

The infant was a boy of the second pregnancy of a healthy 28-year-old mother. He was born at full term (39 weeks gestational age) natural delivery, weighing 3.7 kg. After birth, routine physical examination revealed a normal result. By about 3 months of age, failure to thrive was observed including failing to hold his head and turn over. At 4 months of age, he developed intermittent limb clonus and was admitted to a hospital.

Routine blood, homocysteine, genetic metabolism screening, and physical examination demonstrated normal results. Also, no abnormality was found in otolaryngology and ophthalmic examination. Cranial MRI showed that bilateral frontotemporal space was widened, the left ventricle was irregular, and the corpus callosum was short (**Figure 1A**). Video EEG revealed a normal result.

Convulsions could be observed in genetic metabolic disease, electrolyte disorder, and genetic disease. We excluded metabolic disease by negative results of genetic metabolic screening, excluded electrolyte disorder by the absence of typical clinical features including diarrhea, vomiting, poor eating, and other manifestations. Finally, we uncovered the candidate mutations in the KIAA1109 gene.

We treated the patient with oxiracetam (1 g/day for 10 days), cerebroside (2 ml/day for 10 days), and carnosine (0.1 g/day for 7 days); observed that the limb clonus disappeared; and then discharged him.

We followed up the patient when he was 2 years and 7 months old; he still showed global development delay, unstable walking, abnormal posture, foot valgus, poor balance ability, poor speech, and cognitive ability.

Exome Sequencing and Analysis

WES detected compound heterozygous variants in KIAA1109 (**Figure 1B**). The first variant [c.4892C>G (p.Pro1631Arg)] was a non-synonymous variant, causing amino acids from proline to arginine at 1,631st of the protein. The second variant was a frameshift duplication insertion at 3,625th of KIAA1109, causing amino acid translation from arginine to lysine, and terminating at 5th after the variant site. Both variants were absent in published databases, such as gnomeAD and Exome Aggregation Consortium (ExAC). c.4892C>G was predicted to cause damage to proteins (SIFT: Damaging, Polyphen2 _HDIV: Damaging, Mutation Taster: Disease-causing). Both variants were classified as VUS or LP according to the ACMG guidelines (**Table 1**). Both variants were validated from the father and mother, respectively, by Sanger sequencing (**Figure 1C**).

We reviewed all reported variants and survival information and defined three regions (Region I: 358–3,611 bp; Region II: 3,986 bp−5,873 bp; Region III: 9,149–14,564 bp) among full-length KIAA1109 (**Figure 1D**). We found that homozygous or compound heterozygous variants in regions I and III had a deteriorating effect on the patients, whereas compound heterozygous variants in region II showed a moderate effect on survival (**Figure 1D**). Interestingly, the variants for our survival

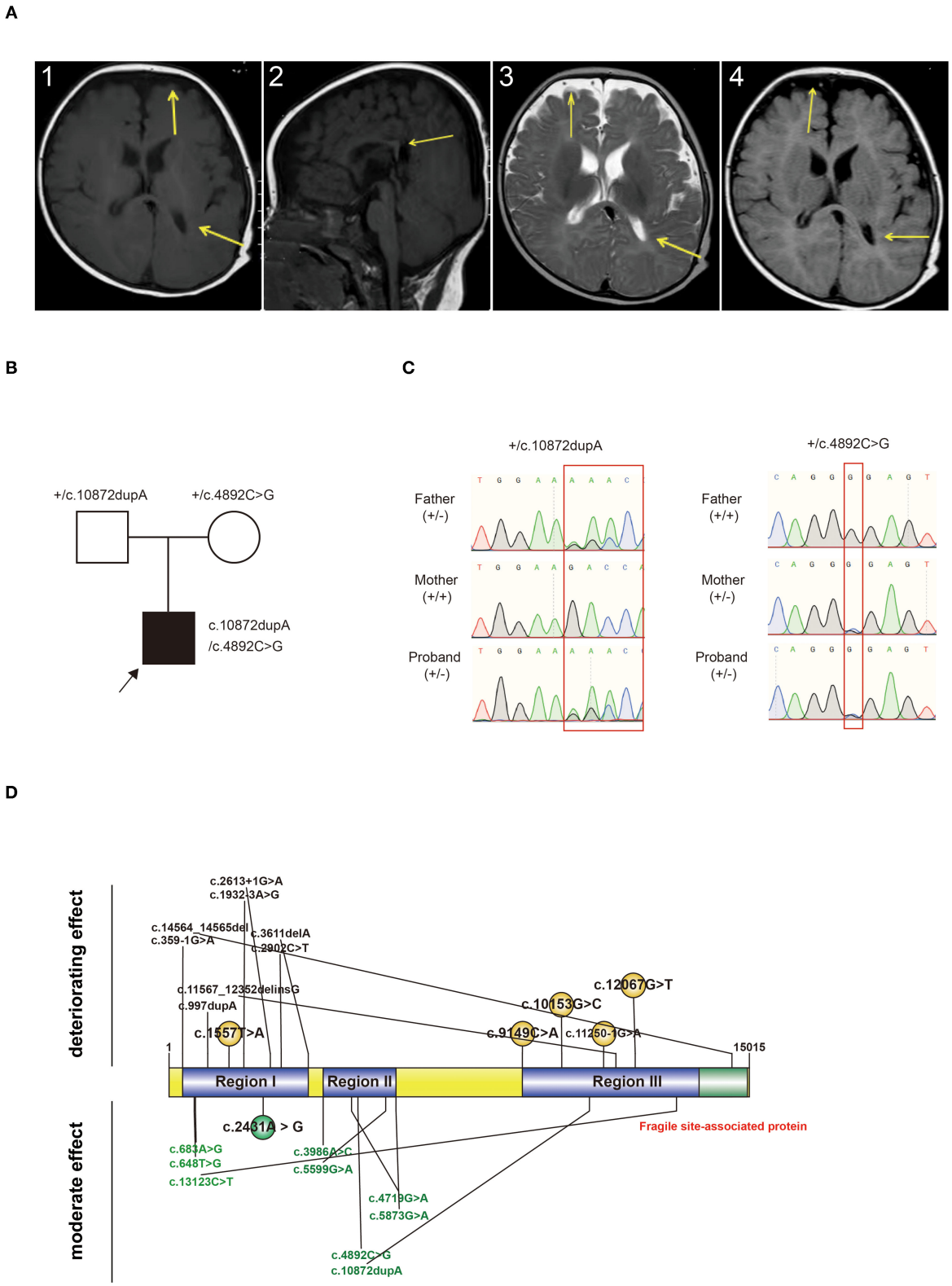

FIGURE 1 | (A) Characteristic changes in the MRI findings of the proband. MRI images revealed a widening of bilateral frontotemporal space, an irregular shape of the left ventricle, and a short corpus callosum. A.1 and A.2: T1W; A.3: T2W; A.4: FLAIR. Arrow: Change of sites. MRI: magnetic resonance imaging. **(B)** Pedigree chart and genotype information of the proband. Black arrow: proband. +: wildtype. **(C)** Genotype validated by Sanger sequencing. Compound heterozygous variants were

(Continued)

FIGURE 1 | inherited from both the father and mother. +: wildtype; -: variant type. **(D)** Variant-reported summary. Variants from one patient were labeled together. Variants written in black are those from dead probands. Variants written in green are those from probands who survived. Variants written in red are those discovered in our patient.

TABLE 1 | Analysis of variants detected in KIAA1109 (NM_015312.3).

No.	Variants	AA change	GnomeAD MAF	Inherit	Classification	Evidence
1	c.4892C>G	p.Pro1631Arg	Absent	Mother	VUS	PM2_Supporting+PM3 + PP3
2	c.10872dupA	p.Arg3625Lysfs*5	Absent	Father	LP	PVS1 + PM2_Supporting

MAF, minor allele frequency; VUS, variant of uncertain significance; LP, likely pathogenic.

TABLE 2 | Phenotype related to variant type.

	Moderate effect	Deteriorating effect
Missense + missense	60% (9/15)	40% (6/15)
Missense + structure	33.3% (1/3)	66.7% (2/3)
Structure + structure	0% (0/4)	100% (4/4)

case were compound heterozygous variants from regions II and III.

In order to explore a potential relationship between variant type (missense, non-sense, splice site, frameshift) and survival status, we combined non-sense, splicing, and frameshift as structure variants since they resulted in early premature termination and deletion exon or insertion intron. As an autosomal recessive disorder, bi-allelic variants were classified into three groups: missense+missense; missense+structure; and structure+structure. We reviewed all variants and the survival status of reported cases and found that 60% (9/15) (missense + missense) patients survived, and 40% (6/15) (missense + missense) patients died; 33.3% (1/3) (missense + structure) patients survived, and 66.7% (2/3) (missense + structure) patients died; and 100% (4/4) (structure+structure) patients died (**Table 2**). However, there was no significant relationship between the variant and survival status ($p > 0.05$).

Among 10 survival patients, 60 (6/10) presented severe global developmental delay, 20 (2/10) moderate delay, and 20% (2/10) mild delay. A certain proportion of organs exhibited dysfunction including 60 (6/10) in head and faces, 20 (2/10) in eyes, 20 (2/10) in mouth, 30 (3/10) in joints, 60 (6/10) in limbs, 40 (4/10) in gastrointestinal tract, 10 (1/10) in urogenital tract, 30 (3/10) in heart, 20 (2/10) in muscle, and 80% (8/10) in behavior. Development delay and abnormality in behavior, head, and face were widely observed in survival patients (**Supplementary Material Table**). Interestingly, our patient showed relative mild phenotype by only presenting development delay, limbs clonus, unstable walking, and foot valgus. Malfunctions in head and faces, eyes, mouth, gastrointestinal, urogenital, heart, and muscle were not observed.

DISCUSSION

Kiaa1109, located on the long arm of chromosome 4 (4q27), contains 84 exons and 15,592 base pairs in length (https://www.ncbi.nlm.nih.gov/nuccore/NM_015312.3). It is widely expressed in many different tissues in humans as viewed by BioGPS (9) and is predominantly expressed in the parathyroid, muscles, ears, eyes, mammary glands, lymph nodes, thymus, and 27 other tissues. KIAA1109 is also involved in various tumors such as bladder carcinoma, chondrosarcoma, glioma, leukemia, lymphoma, non-neoplasia, and retinoblastoma tissues.

KIAA1109 is conserved in many species. Orthologs have been found in many mammals and other vertebrates, and homologs have been identified in animals (such as insects). No human paralogs for KIAA1109 have been identified (10). The mRNA sequence identity in mammals ranges from 81.9 (platypus) to 99.5% (chimpanzees). In addition, the protein identity ranged from 93.2 in opossum to 99.8% in chimpanzees, and protein similarity was no less than 97% in all mammals. In addition, birds continue to show fairly high conservation with protein identities of ∼90 and protein similarities of 96%.

The NCBI conserved domain search identified two potential domains in KIAA1109 (11). The first is the fragile site around the C-terminus, which is associated with celiac disease susceptibility according to genome-wide association studies and may also be associated with polycystic kidney disease. The second conserved region is an uncharacterized conserved protein (DUF2246), whose function is unknown and conserved in various species, from humans to worms. It also contains one transmembrane domain from amino acids 26–46 (https://www.ncbi.nlm.nih.gov/protein/150378498). No signal peptides, mitochondrial targeting sequences, or chloroplast peptides were predicted; therefore, there was no localization to the secretory pathway, mitochondria, or chloroplast.

The correlation between variants and prognosis is not well-established as a severe neurodevelopmental and fetal disorder. In this study, we classified all reported patients and their variants and found that homozygous or compound heterozygous variants in region I or region III lead to deteriorating effects for the probands, whereas compound heterozygous variants in region II showed moderate effects on survival. The only exception is a proband carrying a homozygous variant of c.2431A>G in region I. Our cases carry one variant from regions II and III, conforming compound heterozygous variants. In order to understand the potential underlying mechanism between the region and survival status, we searched the domain information in SWISS-MODEL (https://swissmodel.expasy.org/repository/uniprot/Q2LD37), InterPro (https://www.ebi.ac.uk/interpro/protein/UniProt/Q2LD37/), and UniProt (https://www.uniprot.org/uniprot/Q2LD37), found a fragile site-associated region at C-terminal of KIAA1109 that shared 468 amino acids

with region III and a transmembrane helical from the 26th to 46th amino acid at N-terminal that does not share any overlap with our variants. Due to the limited domain information, it was hard to draw any conclusion from the relationship between a variant and functional domain.

Also, due to the limited number of reported cases with variants and prognoses, the region definition may be inaccurate. We believe it could be modified more accurate with additional cases in the future.

CONCLUSION

In this study, we report the eighth surviving patient with ALKKUCS who carries new variants in KIAA1109 and explore the potential relationship between variant regions and survival status. Our report extended the understanding of the ALKKUCS genotype and survival cases and provided more evidence of a better prognosis for ALKKUCS syndrome.

DATA AVAILABILITY STATEMENT

The original contributions presented in the study are included in the article/**Supplementary Materials**, further inquiries can be directed to the corresponding author/s.

ETHICS STATEMENT

The studies involving human participants were reviewed and approved by Institutional Review Board of the Children's Hospital of Hebei Province. Written informed consent to participate in this study was provided by the participants' legal guardian/next of kin.

AUTHOR CONTRIBUTIONS

LY: conceptualization, methodology, and data mining. XW, JW, JL, CC, HZ, and HY: writing—original draft preparation. LC and RJ: clinical data collection. ZY and FY: software, data mining, and investigation. MJ: supervision, writing—reviewing and editing. All authors contributed to the article and approved the submitted version.

FUNDING

This work was supported by the Hebei Medical Science Research Project (No. 20190785).

ACKNOWLEDGMENTS

We thank the Proband and his family for their kind cooperation. We also thank CipherGene LCC for data mining.

SUPPLEMENTARY MATERIAL

The Supplementary Material for this article can be found online at: https://www.frontiersin.org/articles/10.3389/fped.2022.806752/full#supplementary-material

REFERENCES

1. Gueneau L, Fish RJ, Shamseldin HE, Voisin N, Mau-Them FT, Preiksaitiene E, et al. KIAA1109 variants are associated with a severe disorder of brain development and arthrogryposis. *Am J Hum Genet*. (2018) 102:116–32. doi: 10.1016/j.ajhg.2017.12.002
2. Kikuno R, Nagase T, Ishikawa KI, Hirosawa M, Miyajima N, Tanaka A, et al. Prediction of the coding sequences of unidentified human genes. XIV. The complete sequences of 100 new cDNA clones from brain which code for large proteins *in vitro*. *DNA Res*. (1999) 6:197–205. doi: 10.1093/dnares/6.3.197
3. Khuong TM, Habets RL, Slabbaert JR, Verstreken P. WASP is activated by phosphatidylinositol-4,5-bisphosphate to restrict synapse growth in a pathway parallel to bone morphogenetic protein signaling. *Proc Natl Acad Sci USA*. (2010) 107:17379–84. doi: 10.1073/pnas.1001794107
4. Alazami AM, Patel N, Shamseldin HE, Anazi S, Al-Dosari MS, Alzahrani F, et al. Accelerating novel candidate gene discovery in neurogenetic disorders via whole-exome sequencing of prescreened multiplex consanguineous families. *Cell Rep*. (2015) 10:148–61. doi: 10.1016/j.celrep.2014.12.015
5. Kane MS, Diamonstein CJ, Hauser N, Deeken JF, Niederhuber JE, Vilboux T. Endosomal trafficking defects in patient cells with KIAA1109 biallelic variants. *Genes Dis*. (2019) 6:56–67. doi: 10.1016/j.gendis.2018.12.004
6. Kumar K, Bellad A, Prasad P, Girimaji SC, Muthusamy B. KIAA1109 gene mutation in surviving patients with Alkuraya-Kucinskas syndrome: a review of literature. *BMC Med Genet*. (2020) 21:136. doi: 10.1186/s12881-020-01074-2
7. Chang, X, Wang, wANNOVAR: annotating genetic variants for personal genomes via the web. *J Med Genet*. (2012) 49:433–6. doi: 10.1136/jmedgenet-2012-100918
8. Richards S, Aziz N, Bale S, Bick D, Das S, Gastier-Foster J, et al. Standards and guidelines for the interpretation of sequence variants: a joint consensus recommendation of the American college of medical genetics and genomics and the association for molecular pathology. *Genet Med*. (2015) 17:405–24. doi: 10.1038/gim.2015.30
9. Wu C, Jin X, Tsueng G, Afrasiabi C, Su AI. BioGPS: building your own mash-up of gene annotations and expression profiles. *Nucleic Acids Res*. (2016) 44:D313–6. doi: 10.1093/nar/gkv1104
10. Johnson M, Zaretskaya I, Raytselis Y, Merezhuk Y, McGinnis S, Madden TL. NCBI BLAST: a better web interface. *Nucleic Acids Res*. (2008) 36(Web Server issue):W5–9. doi: 10.1093/nar/gkn201
11. Marchler-Bauer A, Derbyshire MK, Gonzales NR, Lu S, Chitsaz F, Geer LY. et al. CDD: NCBI's conserved domain database. *Nucleic Acids Res*. (2015) 43: D222–6. doi: 10.1093/nar/gku1221

Conflict of Interest: ZY and FY were employed by CipherGene LLC.

The remaining authors declare that the research was conducted in the absence of any commercial or financial relationships that could be construed as a potential conflict of interest.

Publisher's Note: All claims expressed in this article are solely those of the authors and do not necessarily represent those of their affiliated organizations, or those of the publisher, the editors and the reviewers. Any product that may be evaluated in this article, or claim that may be made by its manufacturer, is not guaranteed or endorsed by the publisher.

frontiers in Genetics

CASE REPORT
published: 11 March 2022
doi: 10.3389/fgene.2022.729980

Case Report: Infantile Cerebellar-Retinal Degeneration With Compound Heterozygous Variants in *ACO2* Gene—Long-Term Follow-Up of a Sibling

Dong Jun Ha[1], *Jisun Park*[1,2], *Go Hun Seo*[3], *Kyoungyeul Lee*[3], *Young Se Kwon*[1,2], *Ji Eun Lee*[1,2] *and Su Jin Kim*[1,2]*

[1]Department of Pediatrics, Inha University Hospital, Inha University College of Medicine, Incheon, South Korea, [2]Northwest Gyeonggi Regional Center for Rare Disease, Inha University Hospital, Incheon, Korea, [3]3billion, Inc., Seoul, South Korea

Infantile cerebellar-retinal degeneration (ICRD) is an extremely rare, infantile-onset neurodegenerative disease, characterized by autosomal recessive inherited, global developmental delay (GDD), progressive cerebellar and cortical atrophy, and retinal degeneration. In 2012, a biallelic pathogenic variant in *ACO2* gene (NM_001098.3) was found to be causative of this disease. To date, approximately 44 variants displaying various clinical features have been reported. Here, we report a case of two siblings with compound heterozygous variants in the *ACO2* gene. Two siblings without perinatal problems were born to healthy non-consanguineous Korean parents. They showed GDD and seizures since infancy. Their first brain magnetic resonance imaging (MRI), electroencephalography, and metabolic workup revealed no abnormal findings. As they grew, they developed symptoms including ataxia, dysmetria, poor sitting balance, and myopia. Follow-up brain MRI findings revealed atrophy of the cerebellum and optic nerve. Through exome sequencing of both siblings and their parents, we identified the following compound heterozygous variants in the *ACO2*: c.85C > T (p.Arg29Trp) and c.2303C > A (p.Ala768Asp). These two variants were categorized as likely pathogenic based on ACMG/AMP guidelines. In conclusion, this case help to broaden the genetic and clinical spectrum of the *ACO2* variants associated with ICRD. We have also documented the long-term clinical course and serial brain MRI findings for two patients with this extremely rare disease.

Keywords: infantile cerebellar-retinal degeneration, ACO2 gene, aconitase hydratase, optic atrophy, global developmental delay

OPEN ACCESS

Edited by:
Muhammad Ayub,
Queens University, Canada

Reviewed by:
Sateesh Maddirevula,
King Faisal Specialist Hospital and Research Centre, Saudi Arabia
Olimpia Musumeci,
University of Messina, Italy

***Correspondence:**
Su Jin Kim
kimsjped@inha.ac.kr

Specialty section:
This article was submitted to Genetics of Common and Rare Diseases, a section of the journal Frontiers in Genetics

Received: *24 June 2021*
Accepted: *09 February 2022*
Published: *11 March 2022*

Citation:
Ha DJ, Park J, Seo GH, Lee K, Kwon YS, Lee JE and Kim SJ (2022) Case Report: Infantile Cerebellar-Retinal Degeneration With Compound Heterozygous Variants in ACO2 Gene—Long-Term Follow-Up of a Sibling. Front. Genet. 13:729980. doi: 10.3389/fgene.2022.729980

INTRODUCTION

Infantile cerebellar-retinal degeneration (ICRD, MIM #614559) is a rare, autosomal recessive, infantile-onset neurodegenerative disease. It is characterized by truncal hypotonia, epilepsy, developmental delay, progressive cerebellar and cortical atrophy, optic nerve atrophy, and retinal degeneration (Spiegel et al., 2012; Sharkia et al., 2019). In 2012, Spiegel et al. analyzed eight patients from two families and reported that homozygous variants of the 1-aminocyclopropane-1-carboxylic

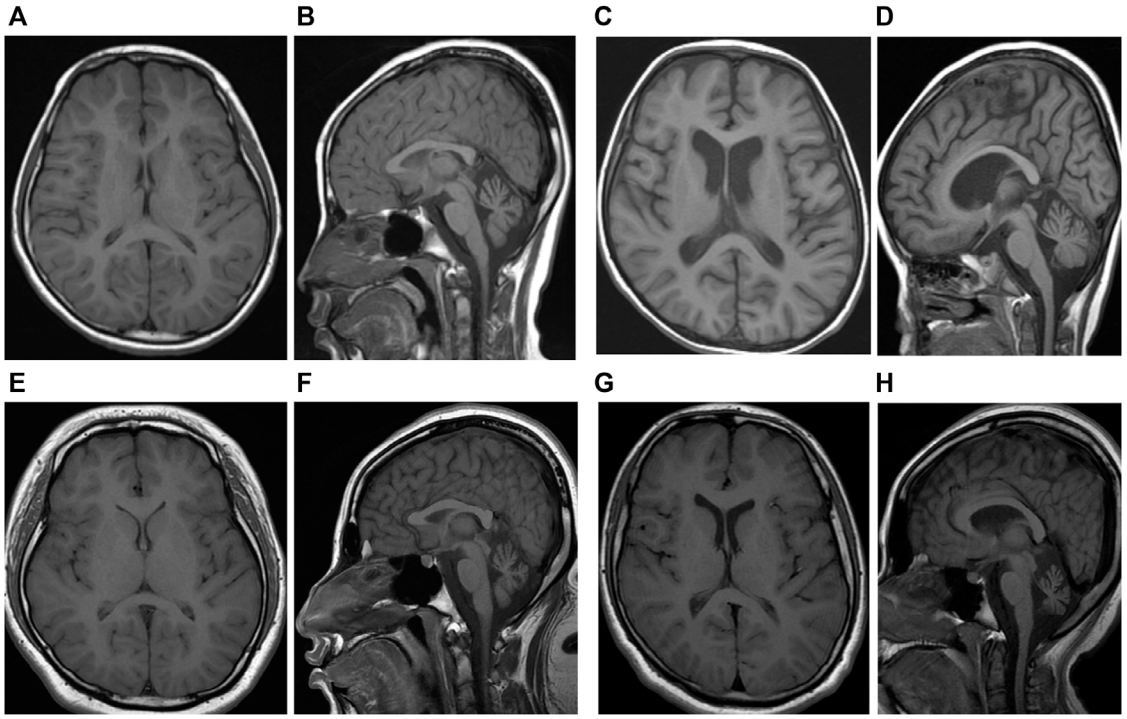

FIGURE 1 | (A) T1-weighted axial and **(B)** sagittal image of sibling one performed at 9 years of age show diffuse cerebral, cerebellar and brain stem atrophy and relatively normal ventricle. **(C)**T1-weighted axial and **(D)** sagittal image of sibling one performed at 18 years were not changed significantly. **(E)**T1-weighted axial and **(F)** sagittal image of sibling two performed at 4 years of age show diffuse cerebral, cerebellar and brain stem atrophy and mild hydrocephalus. **(G)**T1-weighted axial and **(H)** sagittal image of sibling two performed at 16 years were not changed significantly.

acid oxidase two gene (*ACO2*, NM_001098.3) were the cause of ICRD (Spiegel et al., 2012). To date, approximately 44 variants with varying clinical features have been reported. Here, we report a case of ICRD in two siblings cause by compound heterozygous variants in *ACO2*. This report can help expand the genomic and clinical spectrum of *ACO2*-related ICRD.

CASE DESCRIPTION

Two siblings without antenatal and perinatal problems were born to healthy non-consanguineous Korean parents. There was no family history of developmental delay, ataxia, or vision impairment.

Patient 1 (Older Sister)

She was a girl referred at the age of 30 months for occupational and physical therapies for delayed development from early infancy. The Bayley Scales of Infant Development II (BSID-II) test showed global developmental delay (GDD). She had been admitted to the hospital several times for febrile seizures. Her first brain magnetic resonance imaging (MRI) showed no significant abnormalities, and electroencephalography (EEG) suggested partial seizures. She did not take anticonvulsants because she had no partial seizures other than generalized tonic-clonic type convulsion accompanied by high fever. With age, she developed symptoms such as ataxia, dysmetria, poor sitting balance, strabismus, and myopia. Ophthalmic examination revealed atrophy of the bilateral optic nerves at age of 9 years. Follow-up brain MRI showed mild atrophy of the bilateral cerebellum (**Figures 1A,B**). At 9 years of age, her total intelligence quotient (TIQ), which was evaluating using the Korean Wechsler Intelligence Scale for Children-III was 31, indicating severe intellectual disability. A metabolic work-up, including blood lactic acid, pyruvic acid, amino acids, and urine organic acid tests, showed no abnormal findings. At 19 years of age, she speaks only a few words and can walk or lean against a wall. Further, she has severe vision impairment that allows her to only discern light. Follow-up brain MRI showed no significant changes (**Figures 1C,D**).

Patient 2 (Younger Sister)

She also showed GDD with BSID-II at 22 months of age. At 3 years of age, she was admitted to the intensive care unit with a diagnosis of status epilepticus. Her first brain MRI showed no significant abnormal findings, and electroencephalography showed epileptic discharges in the frontal and occipital lobes. She took anticonvulsants, including valproate and topiramate, until 7 years of age. At 4 years of age, she had a decreased response to visual stimuli, and a visual evoked potential study showed optic neuropathy, which led to complete blindness. Similar to her elder sibling, she demonstrated no abnormalities in the metabolic workup. However, her symptoms developed earlier and were more severe than her sister's symptoms. At

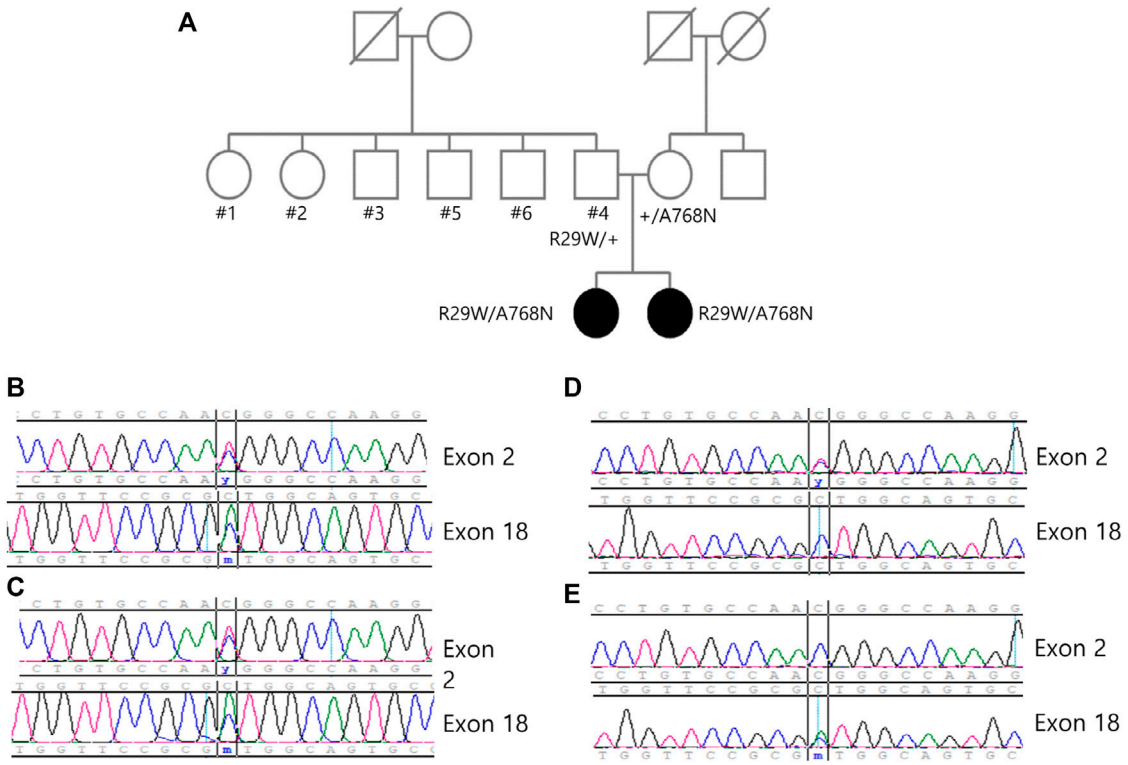

FIGURE 2 | (A) Pedigree of the family showing the two affected siblings and unaffected family members. The variants c.85 > T and c.2303C > A can be identified through the sanger sequence of **(B)** sibling 1, **(C)** sibling 2, **(D)** father and **(E)** mother, and each variant is carried from each parent.

9 years of age, her TIQ was 43, indicating severe intellectual disability. Follow-up brain MRI at 7 years of age revealed hydrocephalus and atrophies of the cerebellum, brain stem, and optic nerve (**Figures 1E,F**). At 17 years of age, she is unable to walk and cannot speak meaningful words. Follow-up brain MRI showed no significant changes (**Figures 1G,H**).

Exome Sequencing

We performed exome sequencing (ES) of DNA from the siblings. Genomic DNA was extracted from proband blood. All exon regions of all human genes (~22,000) were captured by Twist Human Core Exome Kit (Twist Bioscience, South San Francisco, CA, United States). The captured regions of the genome were sequenced using the sequencing ma-chine Novaseq 6,000 (Illumina, San Diego, CA, United States). The raw genome sequencing data analysis, including alignment to the GRCh37/hg19 human reference genome, variant calling, and annotation, was conducted using open-source bioinformatics tools and in-house software. We extracted evidence data on the pathogenicity of variants from previous studies and disease databases, including ClinVar (https://www.ncbi.nlm.nih.gov/clinvar/) and UniProt (https://www.uniprot.org/). The results of ES revealed the following compound heterozygous variants in *ACO2*: c.85C > T (p.Arg29Trp) and c.2303C > A (p.Ala768Asp). These variants were validated by paired-end Sanger sequencing. The variant segregation analysis of the unaffected parents demonstrated that they were heterozygous carriers of each variant (**Figure 2**). No other homozygous or compound-heterozygous pathogenic or likely pathogenic variants were identified in the known Mendelian disease genes in the exome sequencing data of the siblings.

Molecular Dynamic Stimulation

Both variants have been reported at an extremely low frequency in large population cohorts (https://gnomad.broadinstitute.org/). The heterozygous variant c.2303C > A on *ACO2* changes the amino acid Ala to Asp at codon 768 in exon 18. However, this has not been reported in large population cohorts (GenomAD). The programs MODELLER (https://salilab.org/modeller/) and GROMACS (https://www.gromacs.org/) were used to visualize and analyze the *ACO2* protein structure. The p. Ala768Asp variant showed probable damage to the protein structure/function (**Figure 3A**). Structural modeling was performed based on the protein data bank structure (1C96,pdb) of the taurus *ACO2* gene, which has a highly similar sequence (identity = 97%) to the human *ACO2* gene. The distance between two helices is predicted to be increased, and nearby residues (Asp 773, Arg 994) were dragged by charge changes due to the variant, resulting in the relocation of Asp773 and subsequently destabilizing loop structures. Molecular dynamic stimulation was performed to evaluate the effect of this variant on structural stability. The structure of the variant had a larger

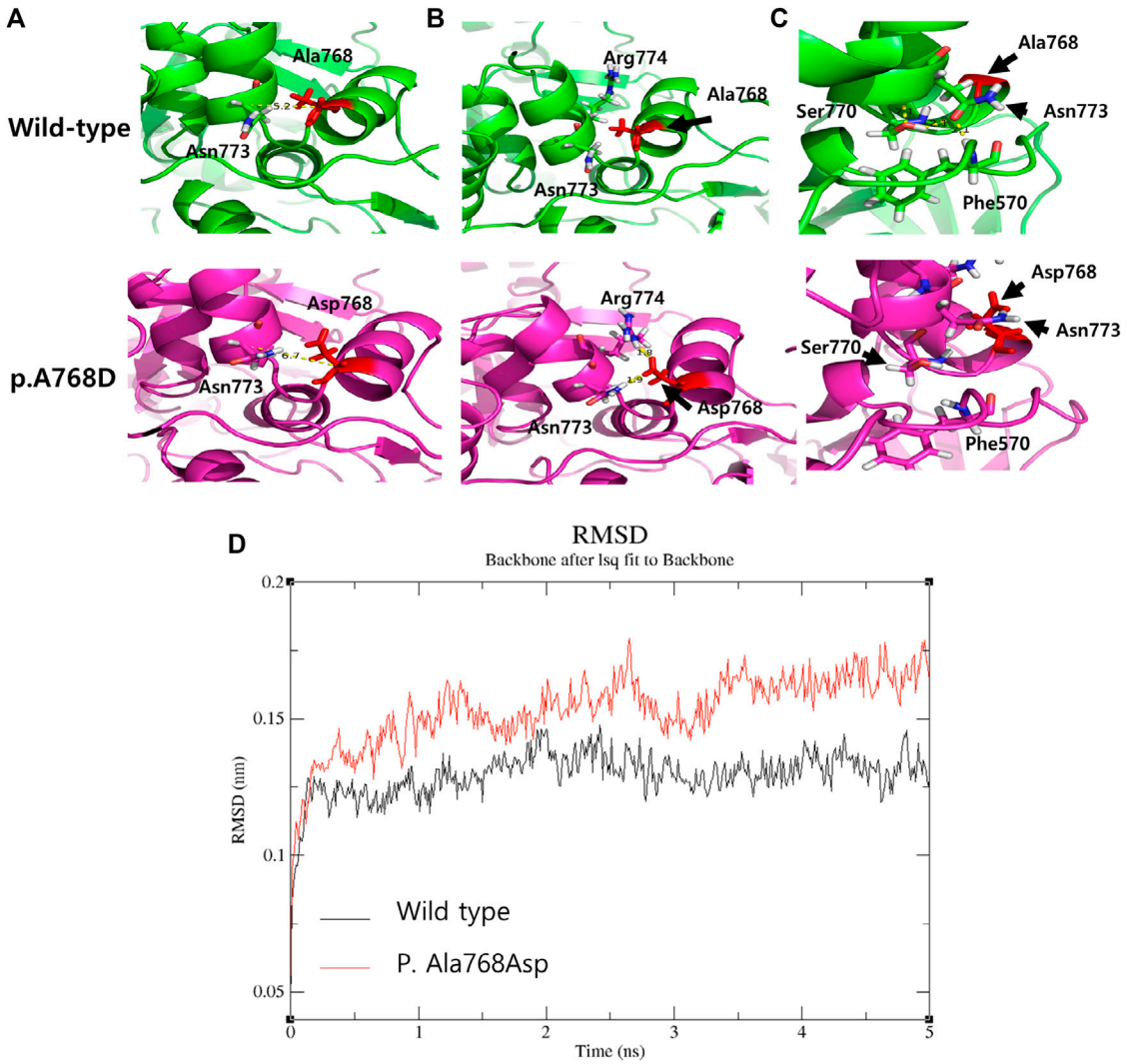

FIGURE 3 | The comparison of The three-dimensional structure between wild type and variant p. Ala768Asp. **(A)** The distance between two helices is predicted to be increased by 1.5 Å (measured by C-alpha distance between two residues). **(B)** Asparagine (773, polar) and Arginine (774, Positive) near the variant site are dragged into Asparagine (768) due to the negative charge of its side chain **(C)** Relocation of Asparagine (773) due to the variant triggers scattering of residues (Ser770 and Phe570) bonded by polar interaction (yellow dotted), thereby destabilizing loop structures. **(D)** The comparison of molecular dynamic (MD) stimulation between wild type and p. Ala768Asp. The Root-mean-square deviation (RMSD) of atomic positions indicated the change in structure over time, and the variant structure (red) shows a large change and unstable pattern compared to the normal structure (black).

variation in the root-mean-square deviation compared to the WT (**Figure 3B**). A missense variant is commonly associated with disease incidence, and the rate of benign missense variants is relatively low. The siblings' phenotypes were highly specific for this disease. This variant was categorized as likely pathogenic according to the American College of Medical Genetics and Genomics/Association for Molecular Pathology (ACMG/AMP) guidelines (PM2, PP1, PP2, PP3, and PP4) [3]. The heterozygous variant c.85C > T on *ACO2* changes the amino acid Arg to Trp at codon 29 in exon 2. It has been reported at an extremely low frequency in large population cohorts. The allele frequency in GenomAD is 0.00003. *In silico* prediction of this variant showed contradictory results. It is predicted to be disease-causing by Mutation Taster (http://www.muationtaster.org/) and Combined Annotation Dependent Depletion (score: 28.6, https://cadd.gs.washington.edu). Another *in silico* tool, REVEL (https://labworm.com/tool/revel) and MetaSVM (https://sites.google.com/site/jpopgen/dbNSFP) predicted this variant to be tolerated or benign. We could not predict the pathogenicity of this variation using protein structural modeling. However, the heterozygous variant c.85C > T on *ACO2* was co-segregated in affected family members and confirmed as trans with other likely pathogenic variants after the segregation analysis. Further, the phenotypes of the patients were consistent with ICRD. Thus, this variant was categorized as likely pathogenic according to the ACMG/AMP guidelines (PM2, PM3, PP1, PP2, and PP4) (Richards et al., 2015).

TABLE 1 | A review of the phenotype and genotype of patients with *ACO2* gene variant based on the present studies.

Reference	Our patients	Spiegel et al.	Metodiev et al.	–	–	Sadat et al. (2016)	Abela et al. (2017)	–	Srivastava et al. (2017)	Kelman et al.	Bouwkamp et al. (2018)	Marelli et al.	Sharkia et al.	–	–	–	Fukada et al. (2019)	Ji soo park et al.	Patrick R. et al.
No. of family	1	2	3	–	–	1	2	–	1	1	1	1	5	–	–	–	1	1	1
No. of patients	2	5 + 3	2	2	1	1	2	2	1	2	2	1	1	1	1	2	1	1	2
Onset age	30/22 mon	2–6 months	5/3 years	at birth	5 months	5 months	NA	NA	15 months	2/ 8 years	3/12 months	NA	7 months	1 day	5 weeks	2/ 12 months	6 months	2 months	12/ 20 months
Current age	19/ 17 years	0.5–18 years	41/ 36 years	Died at 57/ 61 days	10 years	3 years	17/ 14 years	Died at 46 months	18 years	5/ 9 years	28/14 years	56 years	8 years	Died at 14 years	5 years	8/6 years	Died at 5 years	7 months	12/ 15 years
Motor skills	Walk with assist	None ~ sit With support	Normal	NA	Wheelchair bound	Ataxic gait	NA	NA	Wheelchair bound	Normal	Walk with assist	Walk with assist	Walk with assist	None	None	Walk alone	None ~ sit with support	None	Impaired fine motor
Cognitive skills	A few words	None ~ smile	Normal	NA	Smile, recognize family	NA	NA	NA	Full sentence	Normal	A few words	Mild cognitive impairment	A few words	None	None	Some speech	None	None	Dysarthria
Hypotonia (69%)	+	+	–	+	+	+	+	+	+	–	–	–	+	+	+	+	+	+	–
Cerebellar ataxia (80%)	+	+	–	+	+	–	+	+	+	–	–	+	+	+	+	+	+	+	+
Seizures (78%)	+	+	–	+	–	–	+	+	+	–	+/–	–	–	+	+	+	+	+	-
Cortical atrophy (66%)	+	+	–	–	–	–	+	+	–	NA	–	–	–	+	+	–	+	+	+
Cerebellar atrophy (85%)	+	+	–	+	+	–	+	+	+	NA	+	+	–	+	+	+	+	–	+
Optic atrophy (85%)	+	+	+	+/–	+	-	+	+	+	+	–	+	+	+	+	–	–	+	–
Hearing loss (30%)	–	+	–	–	–	+	+	–	–	–	–	NA	–	–	–	–	+	–	–
Ethnicity	Northeast Asian	Arab	French	Algerian	NA	Afro-Caribbean	Arab	Caucasian	Mixed European	NA	Arab	Caucasian	Hispanic/ Caucasian	Caucasian	Caucasian	African/ Caucasian	Northeast Asian	Northeast Asian	Arab
Genotype	c.2303C > A c.85C > T	c.336C > G	c.220C > G c.1981G > A	c.776G > A	c.2208G > C c.2328_2331delGAAG	c.2135C > T c.1819C > T	c.336C > G	c.1859G > A c.2048G > T	c.2328_2331delGAAG c.1091 T > C	c.220C > G c.2208 + 1dup	c.1240 T > G	c.2135C > T c.940 + 5G > C	c.260C > T c.685–1 _685delinsAA	c.1181G > A c.1722G > A	c.172C > T c.590A > G	c.1787A > G c.2050C > T	c.1534G > A c.1997G > C	c.1179G > A c.1343G > C	c.2050C > T c.2153T > C
Enzyme activity	NA	12%	58/66%	5%	NA	20%	NA	NA	NA	NA	~20/20%	50%	12%	NA	NA	75/45% of control	15%	NA	NA

D, days; mo, months; wk, weeks; NA, not available; +, present; –, absent.

DISCUSSION AND CONCLUSION

In this study, we describe the clinical features of two siblings with two novel *ACO2* variants from infancy to adolescence through a long-term follow-up. *ACO2* (MIM #100850) encodes mitochondrial aconitase hydratase, which converts citrate to isocitrate in the tri-carboxylic acid (TCA) cycle (Mirel et al., 1998; Spiegel et al., 2012). The TCA cycle plays an important role in energy metabolism, and genetic defects in the TCA cycle are associated with various neurodegenerative disorders, including early-onset encephalopathies (Mirel et al., 1998; Briere et al., 2006). The biallelic variant of *ACO2* has rarely been reported and exhibits various clinical manifestations from severe neurodegenerative disorders, such as ICRD, to mild ones, such as isolated optic atrophy 9 (MIM #616289) (Kelman et al., 2018; Sharkia et al., 2019; Blackburn et al., 2020; Gibson et al., 2020). Both of the presented siblings had clinical features commonly seen in ICRD, such as intellectual disability, cerebellar atrophy, and optic nerve atrophy. Although their numbers are limited, patients with ICRD have a wide range of age of onset and severity of phenotype (Sharkia et al., 2019). **Table 1** shows the details of our and previously reported ICRD cases. Some reports state that residual aconitase activity in patient tissue or variant-specific assay *in vitro* is associated with clinical severity (Metodiev et al., 2014; Marelli et al., 2018; Blackburn et al., 2020). However, the methods of measuring aconitase activity differ across studies, hindering clinical application of aconitase activity measurement to the diagnosis of *ACO2*-related disorders. There are no useful metabolic biomarkers for the diagnosis of ICRD. Furthermore, sibling 2 demonstrated clinical symptoms, but characteristic radiologic findings, such as cerebellar atrophy on brain MRI, appeared several years later. Therefore, it is not easy for clinicians to suspect this extremely rare disease, ICRD.

To date, most of the known *ACO2* variations have been diagnosed based on ES, and most of them are missense variants that require attention for interpretation (Marelli et al., 2018; Sharkia et al., 2019; Blackburn et al., 2020; Park et al., 2020). To interpret a missense variant as pathogenic or likely pathogenic, it is helpful to prove through various web-based *in silico* prediction software applications or protein structure modeling that the variant can induce physicochemical differences or evolutionarily conserved amino acid modification. In this study, both variants in the patients were missense variants, and the heterozygous variant c.2303C > A on *ACO2* was predicted to modify the protein through homology modeling. However, for the other heterozygous variant c.85C > T on *ACO2*, we could not predict pathogenicity using *in silico* prediction tools or protein modeling. For the reasons mentioned above, we could not perform this variant-specific aconitase activity assay. Recently, it was reported that a 12-month-old infant with GDD and epilepsy had compound heterozygous missense variants in *ACO2* through ES, and the c.85C > T on *ACO2* variant was identical to ours (Bruel et al., 2019; Mau-Them et al., 2020). Aconitase activity could not be measured in this case as well. Lack of enzymatic activity measurement is our limitation in proving the pathogenicity of this variant. Nevertheless, the results of the segregation genetic analysis and patients' clinical manifestations consistent with ICRD offer the possibility that this variant is likely-pathogenic.

It has recently been established that the biallelic pathogenic *ACO2* variant is the genetic cause of ICRD, and although still a rare disease, publications on it are increasing. In patient who shared an identical variant with our case, no ophthalmic problems were found until the age of 2.3 years. In the previous reported literatures, the onset of ophthalmic symptoms varied, and our patient also began to develop ophthalmic problems after the age of 4 years. If *ACO2* variants are found in patients with GDD, regular follow-up for ophthalmic problems is required. In clinical practice, if patients with developmental delay with/without optic nerve atrophy and cerebellar dysfunction, further evaluations such as panel sequencing with *ACO2* genes should be performed. Furthermore, to assist diagnosing patients with mild phenotypes or those who cannot be confirmed through genetic testing, future research is required to determine the association between *ACO2* variants and ICRD and to explore biomarkers that can help obtain the diagnosis.

In conclusion, our cases could help broaden the genetic and clinical spectrum of *ACO2* variants associated with ICRD. In addition, we have shown the long-term clinical course and serial brain MRI findings of two patients with this extremely rare disease.

DATA AVAILABILITY STATEMENT

The datasets for this article are not publicly available due to concerns regarding participant/patient anonymity. Requests to access the datasets should be directed to the corresponding author.

ETHICS STATEMENT

The study was conducted according to the guidelines of the Declaration of Helsinki, and approved by the Institutional Review Board of Inha University Hospital (IRB No. 2020-05-032). All subjects provided written informed consent for clinical and molecular analyses. Written informed consent was obtained from the patient's parent for publication of this case report and any accompanying images.

AUTHOR CONTRIBUTIONS

SJK and JEL designed the experiments. DJH, YSK, and JP helped recruit the patients and their family members. GHS and KL performed the experiments and helped with the Molecular dynamic stimulation. DJH and SJK wrote the manuscript. All authors contributed to the article and approved the submitted version.

ACKNOWLEDGMENTS

We appreciate our patients and their family for their participation in this study. We are grateful to Han-Young Jeong of the Department of Rehabilitation Medicine at Inha University Hospital, and Seong-Mo Kang of the Department of Ophthalmology at Inha University Hospital, who took care of the patients in our study until they were diagnosed.

REFERENCES

Abela, L., Spiegel, R., Crowther, L. M., Klein, A., Steindl, K., Papuc, S. M., et al. (2017). Plasma Metabolomics Reveals a Diagnostic Metabolic Fingerprint for Mitochondrial Aconitase (*ACO2*) Deficiency. *PLoS ONE* 12, e0176363–15. doi:10.1371/journal.pone.0176363

Blackburn, P. R., Schultz, M. J., Lahner, C. A., Li, D., Bhoj, E., Fisher, L. J., et al. (2020). Expanding the Clinical and Phenotypic Heterogeneity Associated with Biallelic Variants in ACO2. *Ann. Clin. Transl Neurol.* 7, 1013–1028. doi:10.1002/acn3.51074

Bouwkamp, C. G., Afawi, Z., Fattal-Valevski, A., Krabbendam, I. E., Rivetti, S., Masalha, R., et al. (2018). *ACO2* Homozygous Missense Mutation Associated with Complicated Hereditary Spastic Paraplegia. *Neurol. Genet.* 4, e223. doi:10.1212/nxg.0000000000000223

Brière, J.-J., Favier, J., Gimenez-Roqueplo, A.-P., and Rustin, P. (2006). Tricarboxylic Acid Cycle Dysfunction as a Cause of Human Diseases and Tumor Formation. *Am. J. Physiology-Cell Physiol.* 291, C1114–C1120. doi:10.1152/ajpcell.00216.2006

Bruel, A.-L., Nambot, S., Nambot, S., Quéré, V., Vitobello, A., Thevenon, J., et al. (2019). Increased Diagnostic and New Genes Identification Outcome Using Research Reanalysis of Singleton Exome Sequencing. *Eur. J. Hum. Genet.* 27, 1519–1531. doi:10.1038/s41431-019-0442-1

Fukada, M., Yamada, K., Eda, S., Inoue, K., Ohba, C., Matsumoto, N., et al. (2019). Identification of Novel Compound Heterozygous Mutations in *ACO2* in a Patient with Progressive Cerebral and Cerebellar Atrophy. *Mol. Genet. Genomic Med.* 7, e00698. doi:10.1002/mgg3.698

Gibson, S., Azamian, M. S., Lalani, S. R., Yen, K. G., Sutton, V. R., and Scott, D. A. (2020). Recessive *ACO2* Variants as a Cause of Isolated Ophthalmologic Phenotypes. *Am. J. Med. Genet.* 182, 1960–1966. doi:10.1002/ajmg.a.61634

Kelman, J. C., Kamien, B. A., Murray, N. C., Goel, H., Fraser, C. L., and Grigg, J. R. (2018). A Sibling Study of Isolated Optic Neuropathy Associated with Novel Variants in the *ACO2* Gene. *Ophthalmic Genet.* 39, 648–651. doi:10.1080/13816810.2018.1509353

Marelli, C., Hamel, C., Quiles, M., Carlander, B., Larrieu, L., Delettre, C., et al. (2018). *ACO2* Mutations: A Novel Phenotype Associating Severe Optic Atrophy and Spastic Paraplegia. *Neurol. Genet.* 4, e225. doi:10.1212/nxg.0000000000000225

Metodiev, M. D., Gerber, S., Hubert, L., Delahodde, A., Chretien, D., Gérard, X., et al. (2014). Mutations in the Tricarboxylic Acid Cycle Enzyme, Aconitase 2, Cause Either Isolated or Syndromic Optic Neuropathy with Encephalopathy and Cerebellar Atrophy. *J. Med. Genet.* 51, 834–838. doi:10.1136/jmedgenet-2014-102532

Mirel, D. B., Marder, K., Graziano, J., Freyer, G., Zhao, Q., Mayeux, R., et al. (1998). Characterization of the Human Mitochondrial Aconitase Gene (*ACO2*). *Gene* 213, 205–218. doi:10.1016/s0378-1119(98)00188-7

Park, J. S., Kim, M. J., Kim, S. Y., Lim, B. C., Kim, K. J., Seong, M.-W., et al. (2020). Novel Compound Heterozygous *ACO2* Mutations in an Infant with Progressive Encephalopathy: A Newly Identified Neurometabolic Syndrome. *Brain Dev.* 42, 680–685. doi:10.1016/j.braindev.2020.07.003

Richards, S., Aziz, N., Bale, S., Bick, D., Das, S., Gastier-Foster, J., et al. (2015). Standards and Guidelines for the Interpretation of Sequence Variants: a Joint Consensus Recommendation of the American College of Medical Genetics and Genomics and the Association for Molecular Pathology. *Genet. Med.* 17, 405–424. doi:10.1038/gim.2015.30

Sadat, R., Barca, E., Masand, R., Donti, T. R., Naini, A., De Vivo, D. C., et al. (2016). Functional Cellular Analyses Reveal Energy Metabolism Defect and Mitochondrial DNA Depletion in a Case of Mitochondrial Aconitase Deficiency. *Mol. Genet. Metab.* 118, 28–34. doi:10.1016/j.ymgme.2016.03.004

Sharkia, R., Wierenga, K. J., Kessel, A., Azem, A., Bertini, E., Carrozzo, R., et al. (2019). Clinical, Radiological, and Genetic Characteristics of 16 Patients with *ACO2* Gene Defects: Delineation of an Emerging Neurometabolic Syndrome. *J. Inherit. Metab. Dis.* 42, 264–275. doi:10.1002/jimd.12022

Spiegel, R., Pines, O., Ta-Shma, A., Burak, E., Shaag, A., Halvardson, J., et al. (2012). Infantile Cerebellar-Retinal Degeneration Associated with a Mutation in Mitochondrial Aconitase, *ACO2*. *Am. J. Hum. Genet.* 90, 518–523. doi:10.1016/j.ajhg.2012.01.009

Srivastava, S., Gubbels, C. S., Dies, K., Fulton, A., Yu, T., and Sahin, M. (2017). Increased Survival and Partly Preserved Cognition in a Patient with *ACO2*-Related Disease Secondary to a Novel Variant. *J. Child. Neurol.* 32, 840–845. doi:10.1177/0883073817711527

Tran Mau-Them, F., Moutton, S., Racine, C., Vitobello, A., Bruel, A.-L., Nambot, S., et al. (2020). Second-tier Trio Exome Sequencing after Negative Solo Clinical Exome Sequencing: an Efficient Strategy to Increase Diagnostic Yield and Decipher Molecular Bases in Undiagnosed Developmental Disorders. *Hum. Genet.* 139, 1381–1390. doi:10.1007/s00439-020-02178-8

Conflict of Interest: GS and KL was employed by company 3 billion , Inc.

The remaining authors declare that the research was conducted in the absence of any commercial or financial relationships that could be construed as a potential conflict of interest.

Publisher's Note: All claims expressed in this article are solely those of the authors and do not necessarily represent those of their affiliated organizations, or those of the publisher, the editors and the reviewers. Any product that may be evaluated in this article, or claim that may be made by its manufacturer, is not guaranteed or endorsed by the publisher.

frontiers | Frontiers in Genetics

ORIGINAL RESEARCH
published: 23 June 2022
doi: 10.3389/fgene.2022.806190

Genomic, Proteomic, and Phenotypic Spectrum of Novel O-Sialoglycoprotein Endopeptidase Variant in Four Affected Individuals With Galloway-Mowat Syndrome

Malak Ali Alghamdi[1,2], Hicham Benabdelkamel[3], Afshan Masood[3], Narjes Saheb Sharif-Askari[4], Mahmood Y. Hachim[5], Hamad Alsheikh[6], Muddathir H. Hamad[6], Mustafa A. Salih[1], Fahad A. Bashiri[1,6], Khalid Alhasan[1,7,8], Tarek Kashour[9], Pilar Guatibonza Moreno[10], Sabine Schröder[10], Vasiliki Karageorgou[10], Aida M. Bertoli-Avella[10], Hisham Alkhalidi[11], Dima Z. Jamjoom[12], Ibrahim A. Alorainy[12], Assim A. Alfadda[3,13,14] and Rabih Halwani[15]*

[1]Pediatric Department, College of Medicine, King Saud University, Riyadh, Saudi Arabia, [2]Medical Genetics Division, Department of Pediatrics, King Saud University, Riyadh, Saudi Arabia, [3]Proteomics Resource Unit, Obesity Research Center, College of Medicine, King Saud University, Riyadh, Saudi Arabia, [4]Sharjah Institute for Medical Research, University of Sharjah, Dubai, United Arab Emirates, [5]College of Medicine, Mohammed Bin Rashid University of Medicine and Health Sciences, Dubai, United Arab Emirates, [6]Neurology Division, Department of Pediatrics, King Saud University, Riyadh, Saudi Arabia, [7]Nephology Division, Department of Pediatrics, King Saud University, Riyadh, Saudi Arabia, [8]Pediatric Kidney Transplant Division,Organ Transplant Center, King Faisal Specialist Hospital and Research Centre, Riyadh, Saudi Arabia, [9]Cardiology Department, College of Medicine, King Saud University, Riyadh, Saudi Arabia, [10]CENTOGENE GmbH, Rostock, Germany, [11]Pathology Department, College of Medicine, King Saud University, Riyadh, Saudi Arabia, [12]Radiology and Medical Imaging Department, College of Medicine, King Saud University, Riyadh, Saudi Arabia, [13]Department of Medicine, College of Medicine and King Saud Medical City, King Saud University, Riyadh, Saudi Arabia, [14]Strategic Center for Diabetes Research, College of Medicine, King Saud University, Riyadh, Saudi Arabia, [15]Department of Clinical Sciences, College of Medicine, Sharjah Institute for Medical Research (SIMR), University of Sharjah, Sharjah, United Arab Emirates

Galloway-Mowat syndrome is a rare autosomal recessive disease characterized by a unique combination of renal and neurological manifestations, including early-onset steroid-resistant nephrotic syndrome, microcephaly, psychomotor delay, and gyral abnormalities of the brain. Most patients die during early childhood. Here, we identified a novel homozygous O-sialoglycoprotein endopeptidase (OSGEP) variant, NM_017807.3: c.973C>G (p.Arg325Gly), in four affected individuals in an extended consanguineous family from Saudi Arabia. We have described the detailed clinical characterization, brain imaging results, and muscle biopsy findings. The described phenotype varied from embryonic lethality to early pregnancy loss or death at the age of 9. Renal disease is often the cause of death. Protein modeling of this OSGEP variant confirmed its pathogenicity. In addition, proteomic analysis of the affected patients proposed a link between the KEOPS complex function and human pathology and suggested potential pathogenic mechanisms.

Keywords: Galloway-Mowat syndrome, steroid-resistant nephrotic syndrome, GAMOS, proteomic, KEOPS complex

OPEN ACCESS

Edited by:
Santasree Banerjee,
Beijing Genomics Institute (BGI), China

Reviewed by:
Bixia Zheng,
Nanjing Children's Hospital, China
Ronen Schneider,
Boston Children's Hospital and Harvard Medical School, United States

****Correspondence:***
Malak Ali Alghamdi
malghamdi@ksu.edu.sa

Specialty section:
This article was submitted to Genetics of Common and Rare Diseases, a section of the journal Frontiers in Genetics

Received: *31 October 2021*
Accepted: *16 March 2022*
Published: *23 June 2022*

Citation:
Ali Alghamdi M, Benabdelkamel H, Masood A, Saheb Sharif-Askari N, Hachim MY, Alsheikh H, Hamad MH, Salih MA, Bashiri FA, Alhasan K, Kashour T, Guatibonza Moreno P, Schröder S, Karageorgou V, Bertoli-Avella AM, Alkhalidi H, Jamjoom DZ, Alorainy IA, Alfadda AA and Halwani R (2022) Genomic, Proteomic, and Phenotypic Spectrum of Novel O-Sialoglycoprotein Endopeptidase Variant in Four Affected Individuals With Galloway-Mowat Syndrome. Front. Genet. 13:806190. doi: 10.3389/fgene.2022.806190

INTRODUCTION

Galloway-Mowat syndrome (GAMOS) is a rare autosomal recessive renal–neurological disease characterized by early-onset steroid-resistant nephrotic syndrome, microcephaly, and brain anomalies (Galloway and Mowat, 1968; Cohen and Turner, 1994). It was first described in 1968 in two siblings with microcephaly, hiatal hernia, and kidney disease (Galloway and Mowat, 1968). In 2014, Colin et al. first identified that *WDR73* variants caused GAMOS in two unrelated families (Colin et al., 2014). During the last 5 years, several studies have described different variants in *WDR73* (Colin et al., 2014; Ben-Omran et al.,

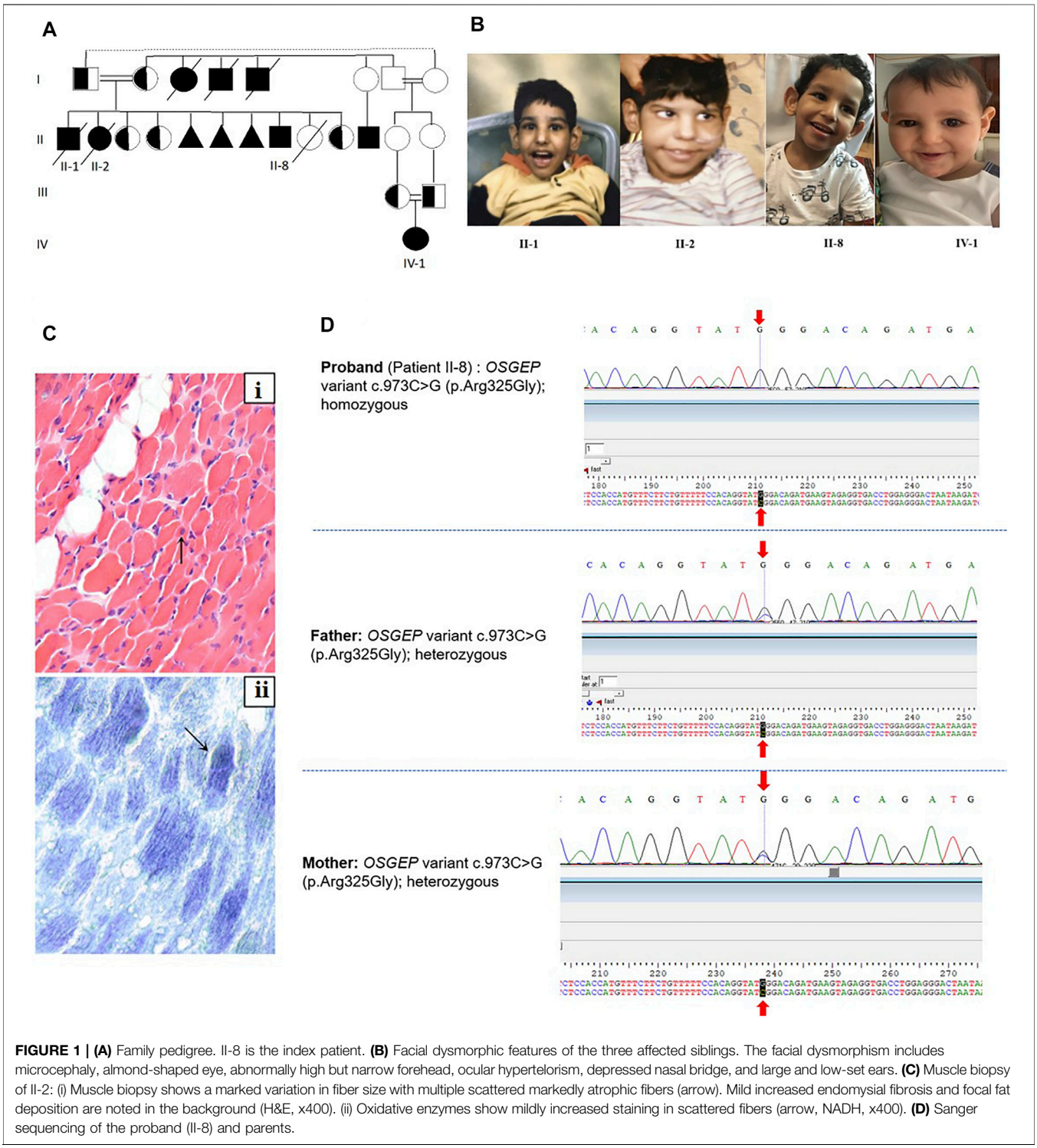

FIGURE 1 | (A) Family pedigree. II-8 is the index patient. **(B)** Facial dysmorphic features of the three affected siblings. The facial dysmorphism includes microcephaly, almond-shaped eye, abnormally high but narrow forehead, ocular hypertelorism, depressed nasal bridge, and large and low-set ears. **(C)** Muscle biopsy of II-2: (i) Muscle biopsy shows a marked variation in fiber size with multiple scattered markedly atrophic fibers (arrow). Mild increased endomysial fibrosis and focal fat deposition are noted in the background (H&E, x400). (ii) Oxidative enzymes show mildly increased staining in scattered fibers (arrow, NADH, x400). **(D)** Sanger sequencing of the proband (II-8) and parents.

TABLE 1 | Clinical features of affected individuals.

Case	II-1	II-2	II-8	IV-1
Gender	Male	Female	Male	Female
Age of death	9 years	6 years	Still alive	Still alive
Ethnicity	Arabic	Arabic	Arabic	Arabic
Neonatal Profile				
Gestational age	Full-term	Full-term	Full-term	Full-term
Apgar at 5 min	N/A	N/A	9	9
Pregnancy course	Uneventful, SVD	Uneventful, SVD	Uneventful, c/s	Uneventful, SVD
Birth length	N/A	N/A	48 cm	48 cm
Birth weight	3000 g	3500 g	2700 g	3000 g
Birth head circumference	N/A	N/A	30.5 cm	34.5 cm
Renal phenotypes				
Onset of nephrotic syndrome	4 years	1.5 years	1.5 years	1 year (still asymptomatic, documented in the laboratory)
Renal biopsy	Mesangial proliferative glomerulonephritis	NP	NP	NA
Urinary tract abnormalities	(–)	(–)	(–)	(–)
Neurological features				
Brain MRI	Cerebral and cerebellar atrophy with extensive high signal intensity in the periventricular deep white matter	Moderate cerebrum and cerebellum atrophy and mild brainstem atrophy. Increased signal intensity in the periventricular white matter	No cerebral or cerebellar atrophy Mild high signal intensity in the periventricular and deep white matter with sparing of the subcortical white matter	Mild cerebral and cerebellar atrophy with extensive high signal intensity in the periventricular deep white matter
Cerebellar atrophy	(+)	(+)	(–)	(+)
Others	Facial dysmorphism	Facial dysmorphism	Facial dysmorphism	Facial dysmorphism

2015; Jinks et al., 2015; Vodopiutz et al., 2015; Rosti et al., 2016; Jiang et al., 2017), *NUP107* (Rosti et al., 2017), *WHAMM* (Mathiowetz et al., 2017), and *PRDM15* (Mann et al., 2021) as a causal agent for GAMOS.

Recently, Braun et al. (2017) identified novel causative variants in four genes encoding the four "kinase, endopeptidase, and other proteins of small size" (KEOPS) subunits: *OSGEP*, *TP53RK*, *TPRKB*, and *LAGE3*, in 37 individuals from 32 families with GAMOS (Braun et al., 2017). *OSGEP* encodes the tRNA N6-adenosine threonylcarbamoyltransferase protein (OSGEP), a subunit of the highly conserved KEOPS complex. The KEOPS complex controls the universal chemical change of tRNAs essential for translational accuracy. It has been implicated in telomere-associated DNA damage response (DDR) signaling and exhibits intrinsic DNA binding ability (Braun et al., 2017). Braun et al. (2017) knocked down genes encoding KEOPS subunits in human podocytes, resulting in impaired cell proliferation, translational attenuation, endoplasmic reticulum stress, activation of DDR signaling, increased apoptosis, and defects in actin regulation, which are possible pathogenic features of GAMOS (Braun et al., 2017). Independently, another study by Edvardson et al. (2017) reported a familial case of GAMOS with a homozygous *OSGEP* variant.

Here, we report genetic and proteomic data and the clinical characterization of an extended family with four affected members with GAMOS.

CLINICAL REPORT

The parents of the patients were first cousins of Saudi origin. They have seven offsprings, three of whom exhibited strikingly similar phenotypes (II-1, II-2, and II-8) (**Figure 1**), and three spontaneous miscarriages. **Table 1** summarizes the clinical features of the affected individuals.

Patient II-1

The male baby was the first offspring of the family. No perinatal or neonatal problems were observed. The birth weight was 3.0 kg. He developed seizure and periorbital edema at 3 years of age and exhibited abnormal facial features (**Figure 1**). Considerable proteinuria was observed, and the patient was diagnosed with nephrotic syndrome and treated conservatively. MRI brain abnormalities are shown in **Figure 2**. He died at 9 years of age and had end-stage renal disease.

Patient II-2

The female baby was the second offspring of the family. No perinatal or neonatal problems were observed. The birth weight was 3.5 kg. She developed the same symptoms as her brother, starting at 2.5 years of age, and died at the age of 6 with respiratory insufficiency, pulmonary edema, and cardiac tamponade.

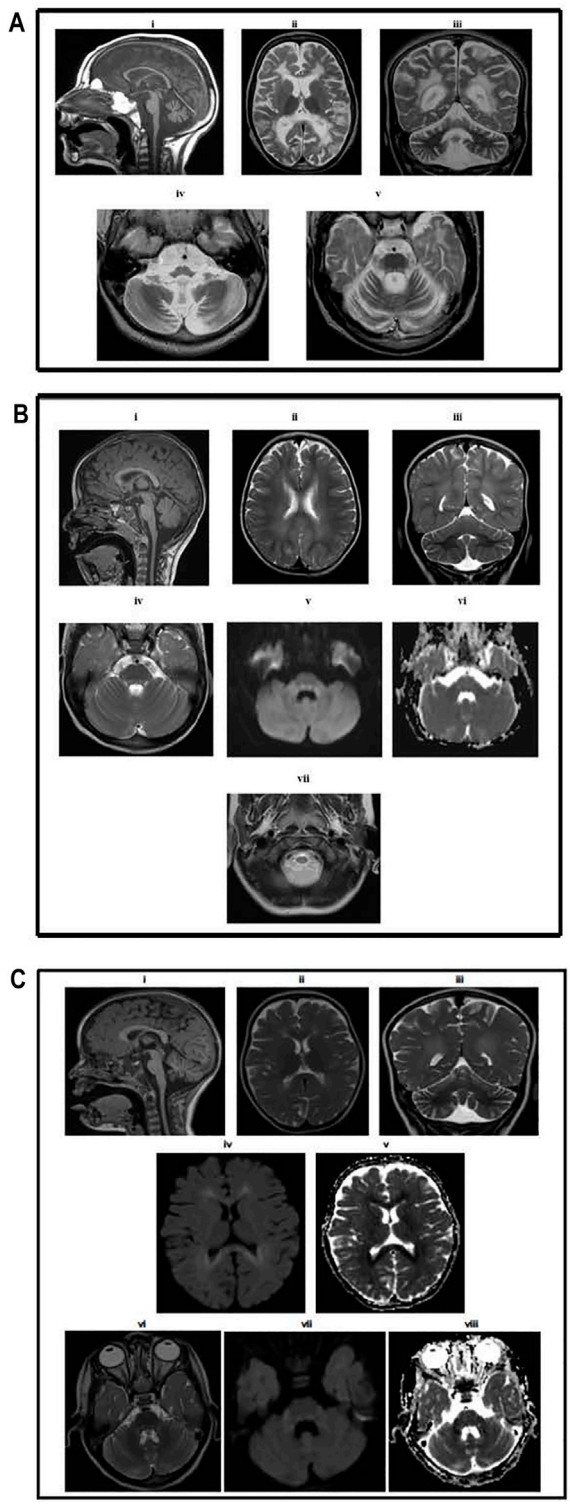

FIGURE 2 | (A) Brain MRI results for Patient II-1. MR examination of the brain at the age of 5. (i) T1-weighted image showing atrophy of the corpus callosum and cerebellum and medulla oblongata and upper cervical spinal cord with normal-sized pons and midbrain. Axial (ii) and coronal (iii) T2-weighted images demonstrating extensive high signal intensity in the periventricular and deep white matter with relative sparing of the subcortical white matter. The cerebral and cerebellar atrophy is evident by the large ventricular system, sulci, and folia. Axial T2-weighted images at the level of the medulla oblongata (iv) showing medullary atrophy and at the level of pons (v) showing signal alteration, mainly involving the dorsal and peripheral parts of the pons. **(B)** Brain MRI result for Patient II-8. MR examination of the brain at the age of 2 years. (i) T1-weighted image showing the normal corpus callosum, cerebellum, and brainstem. The upper cervical spinal cord is atrophic. Axial (ii) and coronal (iii) T2-weighted images demonstrating mild high signal intensity in the periventricular and deep white matter, sparing the subcortical white matter. There is no cerebral or cerebellar atrophy. Axial T2-weighted (iv), diffusion-weighted (v) images, and the apparent diffusion coefficient map (vi) at the level of pons showing signal alteration mainly involving the dorsal and peripheral parts of the pons with diffusion restriction in the dorsal pons (vii). **(C)** Brain MRI results for patient IV-1. MR examination of the brain at the age of 18 months. (i) T1-weighted image showing mild atrophy of the cerebellum normal corpus callosum, brainstem, and upper cervical spinal cord. Axial (ii) and coronal (iii) T2-weighted images demonstrating mild high signal intensity in the periventricular and deep white matter, sparing the subcortical white matter. There is mild cerebral and cerebellar atrophy. Axial diffusion-weighted (iv) images and apparent diffusion coefficient map (v) at the level of the lateral ventricles showing diffusion restriction in the periventricular and deep white matter. Axial T2-weighted (vi), diffusion-weighted (vii), and apparent diffusion coefficient map (viii) showing signal alteration involving the dorsal pons with diffusion restriction.

This patient underwent two muscle biopsies for diagnostic purposes. The first was performed during her third year. It showed mild variation in fiber size and rare degenerating fibers. NADH and SDH showed preservation of intermyofibrillar sarcoplasmic architecture. Few fibers showed some degree of increased activity of the oxidative enzymes. COX stain was reported to be negative in the majority of the myofibers. The second muscle biopsy (**Figure 1**) was performed at the age of six. The variation in this biopsy was prominent, with multiple small-sized muscle fibers and a focal increase of the perimysial connective tissue in the form of increased fat deposition or mild fibrosis. However, the endomysial fibrosis was mild and focal. Like the previous biopsy, the intermyofibrillar architecture using NADH and SDH stains was relatively preserved with a focal increase of the activity of oxidative enzymes. Electron microscopy was performed on the second sample and showed a slightly increased number of mitochondria. No structural changes, nemaline bodies, or intramitochondrial inclusions were documented. Both samples lacked evidence of inflammation or structural abnormalities. Trichrome staining did not reveal evidence of ragged red fibers. Fiber type grouping using ATPases showed a normal mosaic pattern of fiber types with no evidence of grouping or selective fiber type atrophy.

Patient II-8

This male patient was born at 37 weeks of gestation *via* emergency Cesarean section (C/S) due to previous C-section deliveries, with a birth weight of 2.7 kg, length of 48 cm, and head circumference (HC) of 30.5 cm (<3rd percentile). The Apgar scores at 1 and 5 min were 8 and 9, respectively. Soon after birth, the baby was admitted to the neonatal intensive care unit for hypoglycemia and respiratory distress, which was managed by Survanta® *via* an endotracheal tube. He was then extubated and treated with a continuous positive airway pressure

machine. After significant improvement, the patient was discharged in good health after 7 days. His mother noticed some dysmorphic facial features similar to those of his deceased siblings (**Figure 1**).

Initially, the patient did not have any symptoms, but the mother noticed delayed development. He started cruising at 1.5 years and walked with support at 1.8 years. He exhibited a delay in expressive language and communicated by pointing or facial/body gestures. He could say "mama" and "baba," using the words appropriately for the parents but could not speak more words. He was able to follow simple one-step commands. At 4 years of age, he developed generalized spasticity with impaired mobility. There were no seizures, abnormal movements, or changes in consciousness or behavior. He was able to self-feed.

Physical examination revealed that apart from the previously mentioned dysmorphic features, generalized spasticity occurred all over the body, more in the lower limbs. Along with central hypotonia, the lower limb showed fixed flexion at the knee and ankle joints and flattening of the foot arches. Brisk deep tendon reflexes were also observed. At this point, different specialties, including pediatrics, neurology, ophthalmology, genetics, and metabolism were involved in caring for this patient for further assessment and evaluation. Laboratory investigations revealed hypoalbuminemia and hypomagnesemia with normal calcium levels, normal total creatine kinase, thyroid panel, ammonia, lactic acid, and metabolic screening. Urinalysis showed 3 + proteinuria, no hematuria, normal cell counts in urine, and normal renal function. EEG was normal. The 46XY karyotype was normal. The renal ultrasonography findings were unremarkable.

Figure 2 shows brain MRI, which revealed bilaterally symmetrical T2/flair hyperintensity and diffusion restriction in the periventricular white matter and dorsal brain stem with normal spectroscopy, suggestive of metachromatic leukodystrophy. These findings were similar to the synthesis defect of T6 modification of tRNAs, addressed by Edvardson et al. (2017) and Braun et al. (2017).

Patient IV-1

She is the first baby of the young Saudi cousin-couple. She was an 18-month-old girl born at full term *via* normal spontaneous vaginal delivery (NSVD), with a birth weight of 3 kg, length of 48 cm, and HC of 34.5 cm. The Apgar scores at 1 and 5 min were 8 and 9, respectively. The patient was discharged in good health on the second day. She developed well, and her growth parameters at the age of 14 months were a weight of 11 kg (>75th centile), height 81 cm (>75th centile), and HC 44.5 cm (between the 10th and 25th centile). She received all the vaccines and follow-up care at a general pediatric clinic. Thereafter, her family started noticing some facial dysmorphic features similar to those of the affected cousins (**Figure 1**). However, she was asymptomatic at this age. Routine laboratory testing revealed proteinuria in urinalysis (++) (100–200), low albumin at 30 g/L, with normal prealbumin of 0.3 g/L, CBC differential, liver function test, electrolytes, blood gas, and renal profile. An MRI demonstrated similar imaging findings consisting of mild atrophy of the cerebellum normal corpus callosum, brainstem, and upper cervical spinal cord and also mild high signal intensity in the periventricular and deep white matter, sparing the subcortical white matter. There is mild cerebral and cerebellar atrophy (**Figure 2C**). Global parenchymal volume loss is seen in all patients.

MATERIALS AND METHODS

Human Subjects

All patients underwent complete clinical evaluation of the GAMOS phenotype. Standard clinical exome consent was used for whole-exome sequencing of the whole family in the clinical laboratory. The parents signed an informed consent form. Ethical approval for clinical and laboratory data collection was obtained from King Saudi University (KSU) in Riyadh, Saudi Arabia, under protocol number Ref. No.18/0093/IR. Blood was then collected from the subjects and the parents in EDTA-coated tubes for DNA extraction, and the skin biopsy sample was taken from the index patient (II-8) and a healthy sister for proteomic profiling. **Table 1** summarizes the clinical features of the affected individuals.

Whole-Exome Sequencing

Whole-exome sequencing was performed for Patient II-8 as there were no DNA samples from the deceased siblings, patients II-1 and II-2. Approximately, 37 Mb (214,405 exons) of the consensus coding sequences were enriched from fragmented genomic DNA by >340,000 probes that were designed against the human genome (Nextera Rapid Capture Exome, Illumina, CA, United States). The generated library was sequenced on an Illumina NextSeq or platform (Illumina) to an average coverage depth of 70–100 ×. An end-to-end, in-house bioinformatics pipeline, including base calling, primary filtering of low-quality reads, probable artifacts, and annotation of variants, was applied.

All the disease-causing variants reported in HGMD®, ClinVar and all variants with a minor allele frequency of less than 1% in the ExAc database were considered for this study. Our evaluation focused on the exons with intron boundaries of ±20. All relevant inheritance patterns were considered, and the family history and clinical information were used to evaluate the identified variants. Only variants related to the phenotype have been reported.

Computational Analysis of the Mutants

Protein modeling was performed to model the OSGEP amino acid variant exhibited by the patient. The crystal structure of the human probable tRNA N6-adenosine threonylcarbamoyltransferase (PDB accession number 6GWJ.1.C) was used as basis for modeling of the c.973C > G (p. Arg325Gly) variant using the Pymol program (pymol.org). Furthermore, *in silico* protein prediction algorithms (SIFT, PolyPhen, Mutation Taster) were used to predict the effect of selected mutation.

Tissue Collection and Fibroblast Culture

A dermal biopsy pinch was collected from each patient (GAMOS and control) and transferred to the research laboratory in a medium containing advanced RPMI (Gibco, 12633012, MA, United States) and 1% antibiotic–antimycotic solution (Gibco, 15240-062). The tissues were left in the medium for 1–2 h after collection. Skin mesenchymal stem cells were then isolated separately using the explant method, as previously described

(Alfares et al., 2020). In brief, fat was removed from the dermal biopsies, the tissues were chopped and plated in a six-well plate, and three pieces of tissue were collected in one well of a six-well plate. The cells were left undisturbed for 4–6 days in the conditioned medium (growth-specific medium) comprising advanced RPMI (Gibco, 12633012), 5% fetal bovine serum (FBS) (Gibco, 10099141), 20 pg recombinant human fibroblast growth factor (rh-FGF) (Lonza, CC-4065J), 0.1% insulin (Gibco, 51500056), and 1% antibiotic–antimycotic solution.

Protein Extraction From Patient Cells

Proteins were extracted from triplicate biological samples of -2×10^6 cells/mL from each patient (both GAMOS and control) directly in lysis buffer (0.5 ml, 30 mM Tris buffer pH 8.8 containing 7 M urea, 2 M thiourea, 4% Chaps, 1X protease inhibitor mix). The suspension was shaken for 1 h at room temperature and then sonicated using a microsonicator (Qsonica Sonicators, CT, United States) at 30% pulse and two intervals of 1 min each, separated by a minute's gap on ice. Fifty millimolar dithiothreitol was then added, and the protein extracts were centrifuged at 20,000 × g for 1 h at 4°C. The pellets were then removed, and the solubilized proteins in the supernatants were precipitated using a 2D clean-up kit, according to the manufacturer's protocol (GE Healthcare, IL, United States). The pellet was then solubilized in labeling buffer (7 M urea, 2 M thiourea, 30 mM Tris-HCl, 4% CHAPS, pH 8.5). The concentration of protein samples was determined in triplicate using a 2D-Quant Kit (GE Healthcare, IL, United States) (Galloway and Mowat, 1968).

Fluorescence Labeling and Two-Dimensional Difference in Gel Electrophoresis

The extracted proteins (50 μg) from the patient's sample and control were labeled with Cy3 and Cy5, respectively. Labeling was performed for 30 min on ice in the dark. The reactions were quenched by adding 1 μl of lysine (10 mM) for 10 min on ice in the dark. An equal amount of each sample was pooled, labeled with Cy2, and used as an internal standard. A dye-switching strategy was applied during labeling to avoid dye-specific bias (**Supplementary Table S1**). One-dimensional analytical gel electrophoresis was performed, followed by two-dimensional difference in gel electrophoresis on 12.5% fixed concentration gels, as previously described (Cohen and Turner, 1994; Alfadda et al., 2013). After two-dimensional difference in gel electrophoresis (2D-DIGE), the gels were scanned on a Typhoon 9410 scanner with Ettan DALT gel alignment guides using excitation/emission wavelengths specific for Cy2 (488/520 nm), Cy3 (532/580 nm), and Cy5 (633/670 nm).

Protein Identification by Matrix-Assisted Laser Desorption Ionization–Time of Flight Mass Spectrometry

Coomassie-stained gel spots showing a significant difference between the groups were excised from the preparatory gel, washed, and digested according to previously described methods (Colin et al., 2014; Ben-Omran et al., 2015). Briefly, a mixture of tryptic peptides (1 μl) derived from each protein was spotted onto a matrix-assisted laser desorption ionization (MALDI) target (384 MTP Anchorchip, 800 μm Anchorchip, Bruker Daltonics, Bremen, Germany). As previously described (Alfadda et al., 2013; Benabdelkamel et al., 2015), MALDI-MS(/MS) spectra were obtained using an UltraflexTerm time-of-flight (TOF) mass spectrometer (MS) equipped with a LIFT-MS/MS device (Bruker Daltonics) at reflector and detector voltages of 21 and 17 kV, respectively, as described previously (Galloway and Mowat, 1968; Colin et al., 2014; Jinks et al., 2015; Vodopiutz et al., 2015). Peptide mass fingerprints (PMFs) were calibrated against a standard (peptide calibration standard II, Bruker Daltonics). The PMFs were assessed using Flex Analysis software (version 2.4, Bruker Daltonics). MS data were interpreted using BioTools v3.2 (Bruker Daltonics). The peptide masses were searched against the Mascot search algorithm (v2.0.04, updated on 09/05/2019, Matrix Science Ltd., United Kingdom). The identified proteins were screened for Mascot scores higher than 56 and $p < 0.05$.

Bioinformatics Analysis: Pathway Analysis and Functional Classification of Proteins

The successfully identified proteins were uploaded into the ingenuity pathway analysis (IPA) software program (Ingenuity® Systems, http://www.ingenuity.com). This program helps identify proteins and annotates them with related functions and pathways. The annotations were carried out by overlaying the proteins with their most significant networks and biochemical pathways from previous publications. The identified proteins were additionally classified into different categories according to their function and location using the protein analysis through the evolutionary relationship (PANTHER) classification system (http://www.pantherdb.org).

Statistical Analysis

The 2D-DIGE gel images were uploaded into Progenesis SameSpots software (Nonlinear Dynamics, United Kingdom) and analyzed using an automated spot detection method. The analysis included comparing the samples from the GAMOS and control groups. Although an automatic analysis was performed to detect all the spots across all three gels, each selected spot was verified and manually edited wherever necessary. Normalized volumes were used to identify the differentially expressed spots. A cutoff ratio of ≥1.5-fold was considered significant. Student's t-test was used to calculate statistically significant differences between the groups ($p < 0.05$ considered statistically significant). Spots that fulfilled the previously mentioned statistical criteria were subjected to further MS analysis. Principal component analysis (PCA) of the log-transformed spot data was performed.

RESULTS

Whole-Exome Sequencing

The *OSGEP* variant NM_017807.3:c.973C>G (p.Arg325Gly) causing an amino acid change from Arg to Gly at position 325 was detected in the homozygous state in Patient II-8. This variant

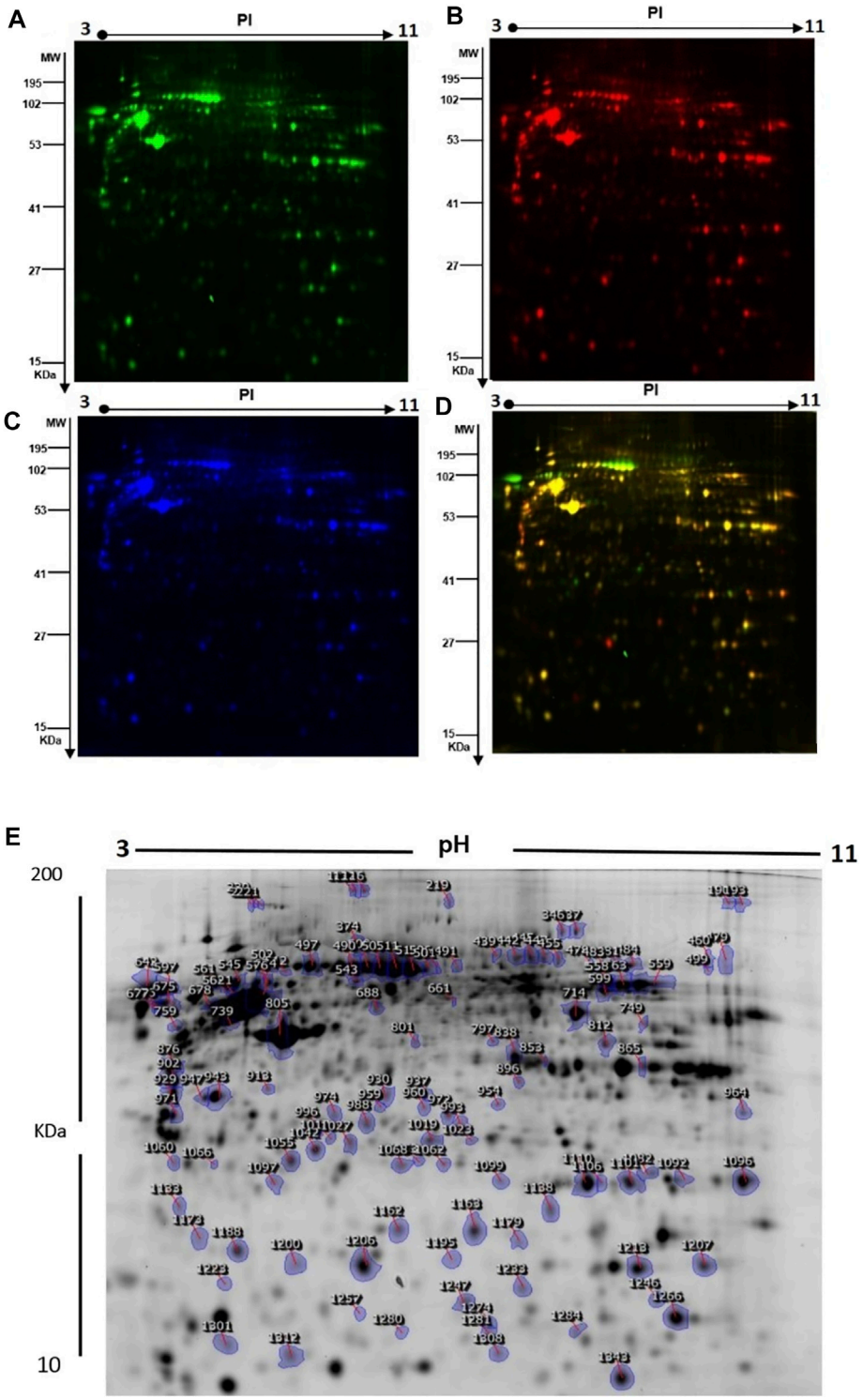

FIGURE 3 | (A) Representative fluorescent protein profiles of the 2D-DIGE containing Cy3-labeled control samples. **(B)** Cy5-labeled samples from patients with GAMOS. **(C)** Pooled Cy2-labeled internal control. **(D)** Cy3/Cy5-merged 2D-DIGE comparison. **(E)** Representative image of protein spots from the skin fibroblasts. Numbered spots indicate those identified to be differentially expressed (over 1.5-fold change, $p < 0.05$) and successfully identified with MALDI-TOF/TOF.

was detected in the parents in the heterozygous state. Variant segregation also showed that all healthy siblings were heterozygotes for the variant. Furthermore, other known monogenic causes of nephrotic syndrome or Galloway-Mowat syndrome have been excluded in the exome analysis.

Computational Analysis of the Mutants

The amino acid R325 of OSGEP is evolutionarily highly conserved across species (**Supplementary Figure S1**), suggesting critical functional implications for protein structure. OSGEP protein modeling was based on human probable tRNA N6-adenosine threonylcarbamoyltransferase (PDB accession number 6GWJ.1.C) crystal structure identity (**Supplementary Figure S1**). The amino acid changed from large-sized arginine (hydrophilic, positively charged) to small-sized glycine (hydrophobic, neutral) which is close by the main catalytic active sides of OSGEP and was predicted to affect its interaction with tRNA (Braun et al., 2018). The main catalytic active sides of OSGEP are present in the following residues: H109, H113, Y130, N266, G177, E181, N266, and D294 (The UniProt Consortium, 2021). The previously reported disease-causing variant, R325Q, demonstrates a change from arginine (hydrophilic, positively charged) to glutamine (hydrophilic, neutral) at the same amino acid position. These results strongly suggest the pathogenicity of the c.973C >G (p.Arg325Gly) variant in the *OSGEP* gene. Furthermore, based on the human genome 37 reference, this variant is presumed to be deleterious and "probably damaging," based on *in silico* protein prediction tools including SIFT and Mutation Taster. Using PolyPhen, the mutation predicted to be probably damaging with the score of 1.000, as well as Align-GVGD, revealed that this variant will most likely interfere with the function. Furthermore, MutationAssessor to assess the evolutionary conservation of the affected amino acid in protein homologs revealed a high score for this variant which suggests that it is likely to be deleterious. The mutation is present in the population gnomAD with an allele frequency of 0.0000040.

Fluorescence Labeling and Two-Dimensional Difference in Gel Electrophoresis

The differences in protein levels between the patients with GAMOS (n = 3) and controls (n = 3) were assessed by 2D-DIGE. Representative fluorescent protein profiles of 2D-DIGE containing Cy3-labeled control and Cy5-labeled GAMOS samples, Cy2-labeled pooled internal control, and a merged Cy3/Cy5 comparison are shown in **Figure 3A–D**. A total of 1,450 spots were identified on the gels, of which 150 were significantly different (ANOVA, $p \leq 0.05$; fold-change ≥1.5) between the GAMOS and control groups (**Figure 3E**). The spot patterns were reproducible across all three gels, leading to alignment and further analysis. Cy2-labeling (the internal standard) was included to permit normalization across the complete set of gels and quantitative differential analysis of the protein levels. The 150 spots showing significant difference between the two groups were then manually excised from the preparative gel for protein identification by MS.

Protein Identification by Mass Spectrometry

To further characterize the proteins differentially expressed between patients with GAMOS and controls, PMFs were used. We successfully identified 107 of the 150 protein spots excised from the preparative gel. MALDI-TOF MS identified 97 spots as unique protein sequences and were matched to the SWISS-PROT database entries by Mascot with high confidence scores (**Table 2**, **Supplementary Table S2**). The sequence coverage of the proteins identified by PMF ranged from 8 to 87%. In a few cases, variants of the same protein were found at several locations on the gel (**Table 2**, **Supplementary Table S2**, **Figure 3E**). Among the 107 proteins identified, 40 protein spots were upregulated and 67 were downregulated in the samples from patients with GAMOS compared to those in the control group (**Table 2**, **Supplementary Table S2**, **Figure 3E**). Among the significantly upregulated proteins were RNA-binding protein 6 (up 4.2-fold, p = 7.36E-05), actin, cytoplasmic-1 (up 4.17-fold, p = 0.004), tropomyosin alpha-4 chain (up 3.26-fold, p = 6.05E-04), C18orf34 protein (up 3.10-fold, p = 0.006), macrophage receptor MARCO (up 3.10-fold, p = 0.01), peroxiredoxin-1 (up 3.06-fold, p = 0.004), and the RNA polymerase II transcription subunit 9 (up 3.0-fold, p = 0.006). The significantly downregulated proteins included keratin, type I cytoskeletal 16 (down 5.70-fold, p = 2.86E-06), serpin B12 (down 5.36-fold, p = 9.02E-04), 4-trimethylaminobutyraldehyde dehydrogenase (down 4.08-fold, p = 7.97E-05), galectin-1 (down 3.98-fold, p = 5.00E-04), and TGFβ1-induced anti-apoptotic factor 1 (down 3.68-fold, p = 5.85E-05). A complete list of upregulated and downregulated proteins is presented in **Table 2**. Among the identified proteins, a few proteins, including hexokinase-3, annexin A2, glyceraldehyde-3-phosphate dehydrogenase, nuclear mitotic apparatus protein 1, zinc finger protein 74, and dynein heavy chain 3, were found in more than one spot on the gels, which could be attributed to posttranslational modifications, cleavage by enzymes, or the presence of different protein species.

Principal Component Analysis and Cluster Analysis

PCA was performed using Progenesis SameSpots software to determine and visualize the potential clustering of the proteins that were differentially expressed in the patients with GAMOS compared to the control group. PCA was performed on all 107 spots that exhibited statistically significant changes (ANOVA, $p <$ 0.05) in abundance as identified by MS. The analyses revealed that the two groups clustered distinctly based on different proteins with an 84.2% score (**Supplementary Figure S2**). The differentially abundant spots showed expression pattern clusters according to their abundant patterns based on a hierarchical clustering analysis (**Supplementary Figure S3**). The clustering pattern showed that the change in the protein

TABLE 2 | Identified proteins, with changes in abundance between the control and patients with GAMOS.

Spot no.	Protein name	*p*-value (ANOVA)	GAMOS/control ratio
1206	Keratin, type I cytoskeletal 16	2.86E-06	–5.7↓
960	TGFB1-induced anti-apoptotic factor 1	5.85E-05	–3.68↓
1019	RNA-binding protein 6	7.36E-05	4.2↑
1173	4-trimethylaminobutyraldehyde dehydrogenase	7.97E-05	–4.08↓
1163	Zinc finger protein 423	8.39E-05	–3.22↓
1138	Probable imidazolonepropionase	1.17E-04	–2.5↓
929	Egl nine homolog 1	3.55E-04	–1.86↓
193	Transcription initiation factor TFIID subunit 7	3.60E-04	–1.27↓
1312	Galectin-1	5.00E-04	–3.98↓
1097	Tropomyosin alpha-4 chain	6.05E-04	3.26↑
1200	Serpin B12	9.02E-04	–5.36↓
225	Endoplasmin	0.001	2.07↑
1233	Peptidyl-prolyl *cis–trans* isomerase A	0.002	–1.34↓
759	Baculoviral IAP repeat-containing protein 3	0.002	–1.61↓
512	Protein-tyrosine kinase 6	0.002	1.37↑
1042	Annexin A5	0.003	1.5↑
221	Src substrate cortactin	0.003	1.4↑
1188	Heterogenous nuclear ribonucleoprotein C-like 1	0.003	–1.09↓
497	OTU domain-containing protein 4	0.003	–1.21↓
972	Annexin A1	0.003	1.55↑
1179	Zinc finger MYM-type protein 1	0.003	–2.41
801	Actin, cytoplasmic 1	0.004	4.17↑
1082	Peroxiredoxin-1	0.004	3.06↑
838	Annexin A2	0.004	–1.19↓
1110	Putative annexin A2-like protein	0.004	–1.51↓
116	Lipase member I	0.004	–1.7↓
812	Glyceraldehyde-3-phosphate dehydrogenase	0.005	–1.31↓
675	Uncharacterized protein C1orf122	0.005	2.58↑
1101	Elongation factor 1-alpha 1	0.005	1.64↑
559	Nuclear mitotic apparatus protein 1	0.005	–1.29↓
749	Stress-associated endoplasmic reticulum protein 1	0.005	–1.29↓
478	Zinc finger protein 74	0.005	–1.26↓
1092	Cofilin-1	0.005	–2.32↓
947	Complement factor H–related protein 5	0.006	–1.95↓
677	Mediator of RNA polymerase II transcription subunit 9	0.006	3↑
1162	Pleckstrin homology domain-containing family A member 2	0.006	–1.39↓
913	40S ribosomal protein SA	0.006	–1.67↓
996	Integrator complex subunit 13	0.007	–1.32↓
1133	Calmodulin-1	0.007	–1.29↓
230	Ubiquitin carboxyl-terminal hydrolase 21	0.008	1.69↑
1207	Peptidyl-prolyl *cis–trans* isomerase B	0.008	–1.3↓
501	Transformation/transcription domain-associated protein	0.008	1.94↑
930	Zinc finger protein 28 homolog	0.009	–1.34↓
337	Poly (ADP-ribose) polymerase 1	0.009	–1.83↓
853	Annexin A2	0.009	–1.17↓
1266	Profilin-1	0.009	–1.18↓
1062	Spectrin beta chain, non-erythrocytic 4	0.009	-2.3↓
455	Syntaxin-binding protein 3	0.009	1.6↑
599	Dynein heavy chain 3, axonemal	0.01	–1.17↓
513	Macrophage receptor MARCO	0.01	3.1↑
122	Developmentally regulated GTP-binding protein 1	0.011	–1.6↓
1343	Beta-galactosidase-1–like protein 3	0.011	1.41↑
1099	Annexin A2	0.011	2.05↑
993	F-actin-capping protein subunit beta	0.013	–1.39↓
442	Zinc finger protein 74	0.013	1.84↑
483	Actin-related protein 2/3 complex subunit 2	0.015	–1.31
937	Protein maestro	0.016	–2.51
219	NADH dehydrogenase (ubiquinone) complex I, assembly factor 6	0.017	1.51↑
714	Pyruvate kinase PKM	0.017	–1.16↓
481	Piwi-like protein 4	0.018	–1.56↓
507	Nesprin-2	0.019	–2.3↓
563	Dynein heavy chain 3, axonemal	0.019	–1.45↓
374	Kelch repeat and BTB domain-containing protein 12	0.02	–1.78↓
1023	Polycomb protein SUZ12	0.021	1.45↑

(Continued on following page)

TABLE 2 | (*Continued*) Identified proteins, with changes in abundance between the control and patients with GAMOS.

Spot no.	Protein name	*p*-value (ANOVA)	GAMOS/control ratio
500	Hexokinase-3	0.021	2.16↑
491	Interferon regulatory factor 8	0.021	1.45↑
971	Macrophage receptor MARCO	0.021	–1.33↓
1246	Nucleoside diphosphate kinase B	0.023	–2.6↓
346	Regulating synaptic membrane exocytosis protein 1	0.023	–1.8↓
445	Allergin-1	0.023	1.88↑
543	Exocyst complex component 1	0.026	–1.32↓
555	Zinc finger protein Aiolos	0.027	–1.38↓
439	Poly (ADP-ribose) polymerase 1	0.027	1.755↑
964	Heterogenous nuclear ribonucleoprotein A1	0.028	–3.21↓
490	Hexokinase-3	0.029	1.67↑
1055	Probable ubiquitin carboxyl-terminal hydrolase MINDY-4	0.031	2.42↑
661	Carbohydrate sulfotransferase 7	0.034	–2.26↓
896	Receptor of activated protein C kinase 1	0.037	–1.28↓
739	Tubulin beta chain	0.039	–1.79↓
1106	Transgelin	0.039	–1.64↓
1096	Actin, cytoplasmic 1	0.041	–1.64↓
805	Actin, cytoplasmic 2	0.041	–1.22↓
1213	Destrin	0.043	–1.22↓
545	ATP-dependent RNA helicase TDRD9	0.049	1.74↑
865	Glyceraldehyde-3-phosphate dehydrogenase	0.049	–1.31↓
232	Heat shock protein HSP 90-beta	0.051	1.26↑
410	Nuclear mitotic apparatus protein 1	0.054	–1.52↓
813	Protein Shroom2	0.054	–1.28↓
738	Calumenin	0.054	1.71↑
554	Vascular endothelial growth factor C	0.06	–1.27↓
1059	14-3-3 protein zeta/delta	0.06	1.29↑
576	Apoptosis-inducing factor 3	3.12E-04	1.6↑
1280	Zinc finger protein with KRAB and SCAN domains 5	5.87E-04	1.51↑
1281	Putative E3 ubiquitin-protein ligase UBR7	0.001	1.97↑
943	Tropomyosin beta chain	0.003	–1.8↓
506	T-complex protein 1 subunit theta	0.005	2.54↑
642	C18orf34 protein	0.006	3.1↑
499	Non-POU domain-containing octamer-binding protein	0.006	1.42↑
1027	Basic immunoglobulin–like variable motif-containing protein	0.008	–1.35↓
1308	MICOS complex subunit MIC60	0.009	–1.31↓
988	Uncharacterized protein C2orf50	0.015	–1.34↓
132	Plasma kallikrein	0.017	–1.73↓
511	Synaptonemal complex protein 2	0.017	2.75↑
974	Elongation factor 1-delta	0.022	–1.21↓
621	Protein OSCP1	0.025	1.76↑
1060	Tropomyosin alpha-1 chain	0.041	–1.46↓
447	Heat shock cognate 71 kDa protein	0.049	1.67↑

The table shows average ratio values for control and GAMOS samples, with their corresponding levels of fold changes and one-way ANOVA (p-value < 0.05), using 2D-DIGE (Analysis type: MALDI-TOF; database: SWISS-PROT; taxonomy: Homo sapiens, *↓ Downregulated, ↑ Upregulated).*

intensities for the selected spots between the GAMOS and control samples was significantly different.

Protein–Protein Interaction Mapping

We next performed protein–protein interaction analysis for the 107 differentially regulated proteins in patients with GAMOS using IPA. The analysis revealed that among 107 proteins, 33 proteins interacted either directly or indirectly *via* protein networks (**Figure 4A**). The software computes a score based on the best fit obtained from the input data set of proteins and the biological functions database to generate a protein–protein interaction network. The generated network is preferentially enriched for proteins with specific and extensive interactions. The interacting proteins are represented as nodes and their biological relationships as a line. Based on the data, three interaction networks were identified for proteins exhibiting differential expression profiles. The highest scoring network (score = 50; **Figure 4**, **Supplementary Figure S4**) incorporated 29 proteins. The proposed highest-interaction network pathway was related to cellular assembly and organization, function and maintenance, and tissue development. Only the top pathways are shown in **Figure 4A**. The canonical pathways enriched in the current dataset are shown in **Figure 4B**. These canonical pathways are sorted down to a decreasing log (*p*-value) of enrichment. The three most interesting enriched canonical pathways included RhoA signaling, actin cytoskeleton signaling, and integrin signaling.

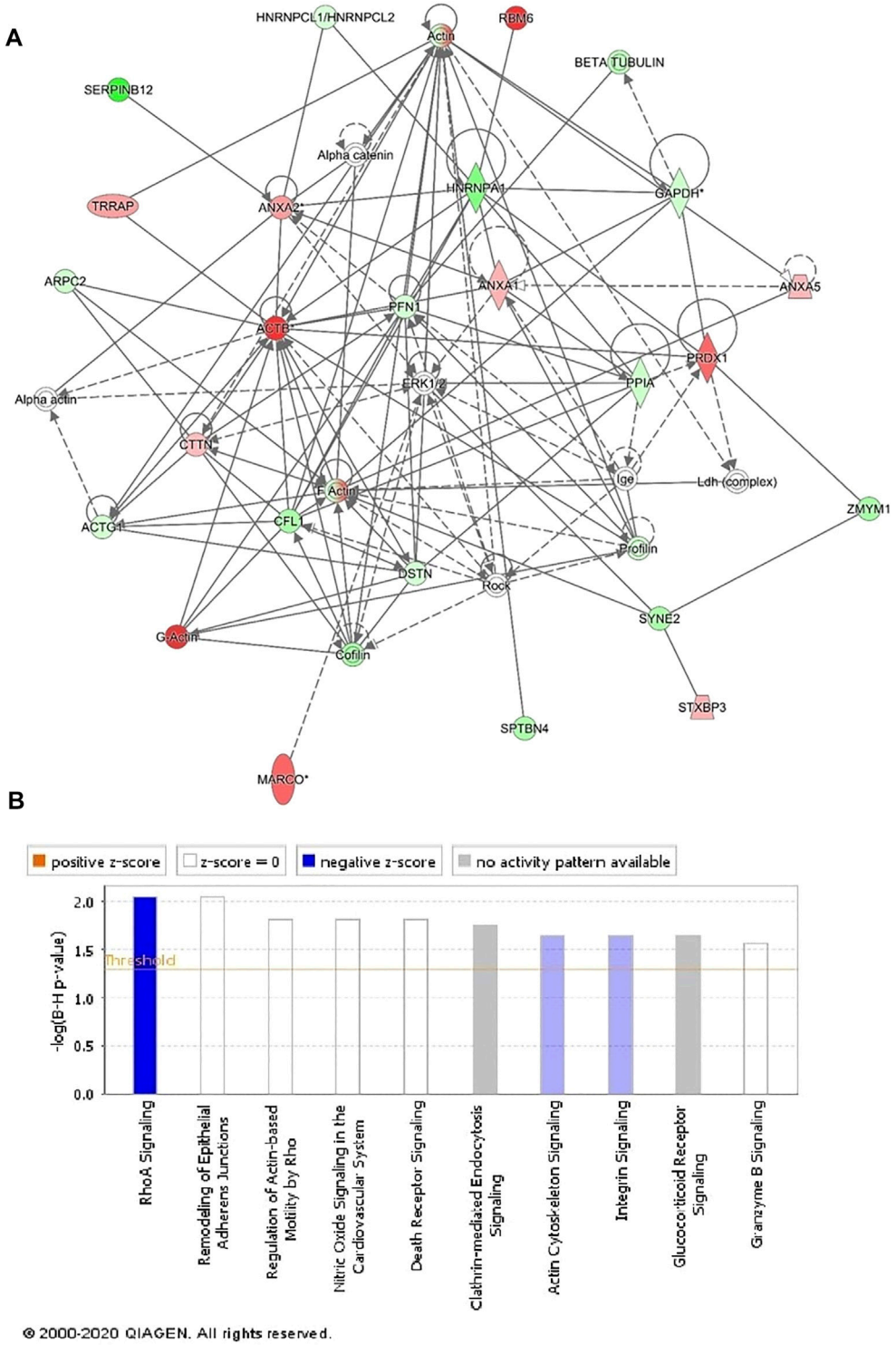

FIGURE 4 | Schematic representation of the most significant IPA networks involving the differentially regulated proteins between the GAMOS and control samples. IPA analysis found that the functional interaction network pathway with the highest score was related to "cellular assembly and organization, cellular function and maintenance, and tissue development." This pathway incorporated *PFN1*, *ERK1/2*, and *ACTB* as central nodes downregulated in patients with GAMOS. Nodes in green and red correspond to downregulated and upregulated proteins, respectively. **(A)** Colorless nodes were proposed by IPA and suggest potential targets functionally coordinated with the differentially abundant proteins. Solid lines indicate direct molecular interactions, and dashed lines represent indirect interactions. **(B)** Diagram shows the top canonical pathways ranked by the *p*-values obtained by the IPA.

Functional Characterization of the Differentially Expressed Proteins

Following MS analysis, all 107 differentially abundant proteins identified between the GAMOS and control samples were subjected to the PANTHER classification system (http://www.pantherdb.org) for classification according to their function (**Supplementary Figure S5A**) and location (**Supplementary Figure S5B**). The dominant functional categories identified were binding proteins (49%) and proteins involved in catalytic activity (28%) (**Supplementary Figure S5A**). Most proteins showed cellular localization (44%), followed by organelle-localized proteins (26%) (**Supplementary Figure S5B**).

DISCUSSION

GAMOS is a phenotypically heterogenous disease characterized by a combination of early-onset steroid-resistant nephrotic syndrome and microcephaly with brain anomalies (Galloway and Mowat, 1968; Cohen and Turner, 1994; Braun et al., 2017; Braun et al., 2018). The three siblings (II-1, II-2, and II-8) and their cousin from a consanguineous family share a similar phenotype, including dysmorphic facial features, respiratory distress, and nephrotic syndrome, resulting in massive proteinuria and brain abnormalities. Their phenotypes were similar to those of patients with *OSGEP* variants reported by Braun et al. (2017), which included microcephaly, severe deformation of the forehead, reduced gyration, diffuse cortical atrophy, focal segmental glomerulosclerosis, and foot process effacement resulting from massive proteinuria (Braun et al., 2017).

The homozygous variant, c.973C>G (p.Arg325Gly), in the *OSGEP* gene identified in Patient II-8 by whole-exome sequencing caused an amino acid change from arginine to glycine, which was presumed to be deleterious and probably damaging based on *in silico* protein prediction algorithms. While this particular variant has not been described previously in the literature, two different variants that affect the same amino acid residue have been published as disease-causing for Galloway-Mowat syndrome (Braun et al., 2017; Edvardson et al., 2017). Therefore, the variant detected here is classified as "probably pathogenic", according to the American College of Medical Genetics and Genomics (ACMG) recommendations. Retrospective clinical analysis revealed compatibility of the patient's phenotype with the identified variant, and variant segregation showed that all healthy siblings were heterozygotes for the variant.

We identified multiple differentially dysregulated proteins, indicating that OSGEP plays a role in multiple developmental pathways. Thereby, these dysregulated pathways might be involved in GAMOS pathology. For example, the downregulated proteins with the highest GAMOS/control ratio regulate supramolecular fiber organization, cyclic-nucleotide phosphodiesterase activity, modification by a host of symbiont morphology or physiology, and smooth muscle contraction (**Supplementary Figure S6**). Proteins that showed the highest GAMOS/control ratio were involved in the P2X7 receptor signaling complex, vesicle-mediated transport, translocation of *SLC2A4* (GLUT4) to the plasma membrane, and phagocytosis (**Supplementary Figure S7**). The renal–neurological presentation of GAMOS could be traced to the protein dysregulation found in this study. P2X7 signaling activation, which includes upregulation of ACTB, HSPA8, and HSP90AB1, has been shown to play a significant role in brain development and has been linked to many neurodegenerative, neuroinflammatory, and neurogenic diseases (Sharp et al., 2008; Andrejew et al., 2020). Furthermore, heat shock proteins (HSPA8 and HSP90B1), annexins (ANXA1, ANXA2, and ANXA5), and vesicle-mediated transport proteins (ACTB, CTTN, STXBP3, MARCO, and YWHAZ), which are essential for normal kidney development, are found to be dysregulated and to contribute to the observed nephrotic syndrome (Smoyer et al., 1996; Markoff and Gerke, 2005; Simsek et al., 2008; Chebotareva et al., 2018). Interestingly, none of the deferentially regulated genes described is a member of the KEOPS complex nor is it a known GAMOS-causing or NS-causing gene. Indeed, the deferentially regulated genes that are suggested to be involved in kidney pathology are important during development but are not a known cause of monogenic nephrotic syndrome.

Taken together, the data have suggested that the loss of tRNA N6-adenosine threonylcarbamoyltransferase protein function affects many other essential proteins required for protein folding, protein binding, transport, and catalytic activity.

DATA AVAILABILITY STATEMENT

The datasets for this article are not publicly available due to concerns regarding participant/patient anonymity. Requests to access the datasets should be directed to the corresponding author.

ETHICS STATEMENT

The studies involving human participants were reviewed and approved by KSU-IRB. Written informed consent to participate in this study was provided by the participants' legal guardian/next of kin. Written informed consent was obtained from the minor(s)' legal guardian/next of kin for the publication of any potentially identifiable images or data included in this article.

AUTHOR CONTRIBUTIONS

MA, RH, and TK conceived and designed the study. MA, MS, FB, and KA were involved in patient recruitment. HB, AM, and AA performed the proteomic laboratory work and data analysis. NS-A and MYH performed the proteomic data and analysis and protein modeling. PGM, SS, VK, and AB-A performed the genetic testing WES and Sanger sequencing and the analysis. MA, HAA, and MH performed full clinical characterization on the patients and wrote the manuscript. IA and DJ involved in neuroradiological description. HIA performed the analysis of the muscle biopsy and the histopathology figure. All authors have read and agreed to the published version of the manuscript.

FUNDING

This project was funded by the National Plan for Science, Technology, and Innovation MAARIFAH, King Abdul Aziz City for Science and Technology, Kingdom of Saudi Arabia, Award Number (5-18-03-001-0010).

ACKNOWLEDGMENTS

We are grateful to the family and study individuals for their contribution.

SUPPLEMENTARY MATERIAL

The Supplementary Material for this article can be found online at: https://www.frontiersin.org/articles/10.3389/fgene.2022.806190/full#supplementary-material

Supplementary Figure S1 | OSGEP protein 3D model. **(A)** Crystallized structure of the human probable tRNA N6-adenosine threonylcarbamoyltransferase (PDB accession number 6GWJ.1.C). **(B,C)** Protein structure is shown as teal ribbon, while the amino acids at the mutation site are displayed as red stick. The catalytic binding sites of OSGEP are mapped as blue spheres (Residues: H109, H113, Y130, N266, G177, E181, N266, and D294). **(D)** Surface electrostatic potential surrounding Arg325, with the protruding positive patch generated by the arginine, which is lost in the bottom–right picture **(E)** after the replacement for glycine. The amino acid substituted from large-sized arginine (hydrophilic, positively charged) to smaller-sized glycine (hydrophobic, neutral) at position 325 which is close by the main catalytic active sides of OSGEP and predicted to affect its interaction with tRNA.

Supplementary Figure S2 | PCA plot of the two first principal components.

Supplementary Figure S3 | Expression profiles.

Supplementary Figure S4 | Top canonical pathways.

Supplementary Figure S5 | Comparative depiction of location and function.

Supplementary Figure S6 | Top pathways of genes of the downregulated proteins.

Supplementary Figure S7 | Top pathways of genes of the upregulated proteins.

REFERENCES

Alfadda, A. A., Benabdelkamel, H., Masood, A., Moustafa, A., Sallam, R., Bassas, A., et al. (2013). Proteomic Analysis of Mature Adipo Cytes from Obese Patients in Relation to Aging. *Exp. Gerontol.* 48 (11), 1196–1203. doi:10.1016/j.exger.2013.07.008

Alfares, A., Alfadhel, M., Mujamammi, A., Alotaibi, B., Albahkali, S., Al Balwi, M., et al. (2020). Proteomic and Molecular Assessment of the Common Saudi Variant in ACADVL Gene through Mesenchymal Stem Cells. *Front. Cel Dev. Biol.* 7, 365. doi:10.3389/fcell.2019.00365

Andrejew, R., Oliveira-Giacomelli, Á., Ribeiro, D. E., Glaser, T., Arnaud-Sampaio, V. F., Lameu, C., et al. (2020). The P2X7 Receptor: central Hub of Brain Diseases. *Front. Mol. Neurosci.* 13, 124. doi:10.3389/fnmol.2020.00124

Ben-Omran, T., Fahiminiya, S., Sorfazlian, N., Almuriekhi, M., Nawaz, Z., Nadaf, J., et al. (2015). Nonsense Mutation in theWDR73gene Is Associated with Galloway-Mowat Syndrome. *J. Med. Genet.* 52, 381–390. doi:10.1136/jmedgenet-2014-102707

Benabdelkamel, H., Masood, A., Almidani, G. M., Alsadhan, A. A., Bassas, A. F., Duncan, M. W., et al. (2015). Mature Adipocyte Proteome Reveals Differentially Altered Protein Abundances between Lean, Overweight and Morbidly Obese Human Subjects. *Mol. Cell. Endocrinol.* 401, 142–154. doi:10.1016/j.mce.2014.11.021

Braun, D. A., Rao, J., Mollet, G., Schapiro, D., Daugeron, M. C., Tan, W., et al. (2017). Mutations in KEOPS-Complex Genes Cause Nephrotic Syndrome with Primary Microcephaly. *Nat. Genet.* 49 (10), 1529–1538. doi:10.1038/ng.3933

Braun, D. A., Rao, J., Mollet, G., Schapiro, D., Daugeron, M. C., Tan, W., et al. (2018a). Mutations in the Evolutionarily Highly Conserved KEOPS Complex Genes Cause Nephrotic Syndrome with Microcephaly. *Nat. Genet.* 49 (10), 1529–1538. doi:10.1038/ng.3933

Braun, D. A., Shril, S., Sinha, A., Schneider, R., Tan, W., Ashraf, S., et al. (2018b). Mutations in WDR4 as a New Cause of Galloway-Mowat Syndrome. *Am. J. Med. Genet.* 176, 2460–2465. doi:10.1002/ajmg.a.40489

Chebotareva, N., Bobkova, I., Lysenko, L., Neprinzeva, N., Vinogradov, A., and Moiseev, S. (2018). Heat Shock Protein 70 and Anti-heat Shock Protein 70 Antibodies in Patients with Chronic Glomerulonephritis. *Cell Stress and Chaperones* 23 (6), 1229–1235. doi:10.1007/s12192-018-0928-8

Cohen, A. H., and Turner, M. C. (1994). Kidney in Galloway-Mowat Syndrome: Clinical Spectrum with Description of Pathology. *Kidney Int.* 45, 1407–1415. doi:10.1038/ki.1994.184

Colin, E., Huynh Cong, E., Mollet, G., Guichet, A., Gribouval, O., Arrondel, C., et al. (2014). Loss-of-function Mutations in WDR73 Are Responsible for Microcephaly and Steroid-Resistant Nephrotic Syndrome: Galloway-Mowat Syndrome. *Am. J. Hum. Genet.* 95, 637–648. doi:10.1016/j.ajhg.2014.10.011

Edvardson, S., Prunetti, L., Arraf, A., Haas, D., Bacusmo, J. M., Hu, J. F., et al. (2017). tRNA N6-Adenosine Threonylcarbamoyltransferase Defect Due to KAE1/TCS3 (OSGEP) Mutation Manifest by Neurodegeneration and Renal Tubulopathy. *Eur. J. Hum. Genet.* 25, 545–551. doi:10.1038/ejhg.2017.30

Galloway, W. H., and Mowat, A. P. (1968). Congenital Microcephaly with Hiatus Hernia and Nephrotic Syndrome in Two Sibs. *J. Med. Genet.* 5, 319–321. doi:10.1136/jmg.5.4.319

Jiang, C., Gai, N., Zou, Y., Zheng, Y., Ma, R., Wei, X., et al. (2017). WDR73 Missense Mutation Causes Infantile Onset Intellectual Disability and Cerebellar Hypoplasia in a Consanguineous Family. *Clinica Chim. Acta* 464, 24–29. doi:10.1016/j.cca.2016.10.029

Jinks, R. N., Puffenberger, E. G., Baple, E., Harding, B., Crino, P., Fogo, A. B., et al. (2015). Recessive Nephrocerebellar Syndrome on the Galloway-Mowat Syndrome Spectrum Is Caused by Homozygous Protein-Truncating Mutations ofWDR73. *Brain* 138, 2173–2190. doi:10.1093/brain/awv153

Mann, N., Mzoughi, S., Schneider, R., Kühl, S. J., Schanze, D., Klämbt, V., et al. (2021). Mutations in *PRDM15* Are a Novel Cause of Galloway-Mowat Syndrome. *Jasn* 32, 580–596. doi:10.1681/asn.2020040490

Markoff, A., and Gerke, V. (2005). Expression and Functions of Annexins in the Kidney. *Am. J. Physiology-Renal Physiol.* 289 (5), F949–F956. doi:10.1152/ajprenal.00089.2005

Mathiowetz, A. J., Baple, E., Russo, A. J., Coulter, A. M., Carrano, E., Brown, J. D., et al. (2017). An Amish Founder Mutation Disrupts a PI(3)P-WHAMM-Arp2/3 Complex-Driven Autophagosomal Remodeling Pathway. *MBoC* 28, 2492–2507. doi:10.1091/mbc.e17-01-0022

Rosti, R. O., Dikoglu, E., Zaki, M. S., Abdel-Salam, G., Makhseed, N., Sese, J. C., et al. (2016). Extending the Mutation Spectrum for Galloway-Mowat Syndrome to Include Homozygous Missense Mutations in the WDR73 Gene. *Am. J. Med. Genet.* 170, 992–998. doi:10.1002/ajmg.a.37533

Rosti, R. O., Sotak, B. N., Bielas, S. L., Bhat, G., Silhavy, J. L., Aslanger, A. D., et al. (2017). Homozygous Mutation inNUP107leads to Microcephaly with Steroid-Resistant Nephrotic Condition Similar to Galloway-Mowat Syndrome. *J. Med. Genet.* 54, 399–403. doi:10.1136/jmedgenet-2016-104237

Sharp, A. J., Polak, P. E., Simonini, V., Lin, S. X., Richardson, J. C., Bongarzone, E. R., et al. (2008). P2x7 Deficiency Suppresses Development of Experimental Autoimmune Encephalomyelitis. *J. Neuroinflammation* 5 (1), 33–13. doi:10.1186/1742-2094-5-33

Simsek, B., Buyukcelik, M., Soran, M., Bayazit, A. K., Noyan, A., Seydaoglu, G., et al. (2008). Urinary Annexin V in Children with Nephrotic Syndrome: a New Prognostic Marker? *Pediatr. Nephrol.* 23 (1), 79–82. doi:10.1007/s00467-007-0606-z

Smoyer, W. E., Gupta, A., Mundel, P., Ballew, J. D., and Welsh, M. J. (1996). Altered Expression of Glomerular Heat Shock Protein 27 in Experimental Nephrotic Syndrome. *J. Clin. Invest.* 97 (12), 2697–2704. doi:10.1172/jci118723

The UniProt Consortium (2021). UniProt: the Universal Protein Knowledgebase in 2021. *Nucleic Acids Res.* 49, D480–D489. doi:10.1093/nar/gkaa1100

Vodopiutz, J., Seidl, R., Prayer, D., Khan, M. I., Mayr, J. A., Streubel, B., et al. (2015). WDR73Mutations Cause Infantile Neurodegeneration and Variable Glomerular Kidney Disease. *Hum. Mutat.* 36, 1021–1028. doi:10.1002/humu.22828

Conflict of Interest: Authors PGM, SS, VK, and AB-A as employees of CENTOGENE GmbH.

The remaining authors declare that the research was conducted in the absence of any commercial or financial relationships that could be construed as a potential conflict of interest.

Publisher's Note: All claims expressed in this article are solely those of the authors and do not necessarily represent those of their affiliated organizations, or those of the publisher, the editors, and the reviewers. Any product that may be evaluated in this article, or claim that may be made by its manufacturer, is not guaranteed or endorsed by the publisher.

Advantages of publishing in Frontiers

OPEN ACCESS
Articles are free to read for greatest visibility and readership

FAST PUBLICATION
Around 90 days from submission to decision

HIGH QUALITY PEER-REVIEW
Rigorous, collaborative, and constructive peer-review

TRANSPARENT PEER-REVIEW
Editors and reviewers acknowledged by name on published articles

Frontiers
Avenue du Tribunal-Fédéral 34
1005 Lausanne | Switzerland

Visit us: www.frontiersin.org
Contact us: frontiersin.org/about/contact

REPRODUCIBILITY OF RESEARCH
Support open data and methods to enhance research reproducibility

DIGITAL PUBLISHING
Articles designed for optimal readership across devices

FOLLOW US
@frontiersin

IMPACT METRICS
Advanced article metrics track visibility across digital media

EXTENSIVE PROMOTION
Marketing and promotion of impactful research

LOOP RESEARCH NETWORK
Our network increases your article's readership